Bootstrapping Quantum Field Theories

by

Alexandre Homrich

A thesis
presented to the University of Waterloo
in fulfillment of the
thesis requirement for the degree of
Doctor of Philosophy
in
Physics

Waterloo, Ontario, Canada, 2024

Examining Committee Membership

The following served on the Examining Committee for this thesis. The decision of the Examining Committee is by majority vote.

External Examiner:	Simon Caron-Huot Professor, Dept. of Physics, McGill University
Supervisor:	Pedro Vieira Adjunct Faculty, Dept. of Physics and Astronomy, University of Waterloo Research Chair, Perimeter Institute
Co-Supervisor:	Freddy Cachazo Adjunct Faculty, Dept. of Physics and Astronomy, University of Waterloo Research Chair, Perimeter Institute
Internal Member:	Niayesh Afshordi Professor, Dept. of Physics and Astronomy, University of Waterloo Research Associate, Perimeter Institute
Internal Member:	Davide Gaiotto Adjunct Faculty, Dept. of Physics and Astronomy, University of Waterloo Research Chair, Perimeter Institute
Internal-External Member:	Benoit Charbonneau Associate Professor, Dept. of Pure Mathematics, Cross Appointed Faculty, Dept. of Physics and Astronomy, University of Waterloo Affiliate, Perimeter Institute

Author's Declaration

This thesis consists of material all of which I authored or co-authored: see Statement of Contributions included in the thesis. This is a true copy of the thesis, including any required final revisions, as accepted by my examiners.

I understand that my thesis may be made electronically available to the public.

Statement of Contributions

Chapters (2-8) are adapted from the papers listed in this section. They represent equal contributions from the authors.

Chapter II - The S-matrix Bootstrap IV: Multiple Amplitudes

A. Homrich, J. Penedones, J. Toledo, B. van Rees, P. Vieira. [1]

Chapter III - S-matrix bootstrap: Supersymmetry, Z_2, and Z_4 symmetry

C. Bercini, M. Fabri, A. Homrich, P. Vieira. [2]

Chapter IV - Dual S-matrix bootstrap. Part I. 2D theory

A. Guerrieri, A. Homrich, P. Vieira [3]

Chapter V - The Wilson loop — large spin OPE dictionary

C. Bercini, V. Goncalves, A. Homrich and P. Vieira [4]

Chapter VI - Spinning Hexagons

C. Bercini, V. Goncalves, A. Homrich and P. Vieira [5]

Chapter VII - Structure Constants in $\mathcal{N} = 4$ SYM and Separation of Variables

C. Bercini, A. Homrich, P.Vieira. [6]

Chapter VIII - Complex Spin: The Missing Zeroes and Newton's Dark Magic

A. Homrich, D. Simmons-Duffin, P. Vieira [7]

Abstract

This thesis compiles a few developments on the S-matrix bootstrap, conformal field theory, and integrability in $\mathcal{N} = 4$ SYM. After an introduction contextualizing the various works that compose this thesis, we present a number of results in independent chapters, followed by a conclusion discussing some future directions. A lightning summary of each chapter is as follows:

- In chapter 2, we extend the S-matrix Bootstrap by considering the analyticity and unitarity of multiple amplitudes at once, and describe how to generalize the framework in order to study theories with a mass hierarchy in two space-time dimensions.
- In chapter 3 we consider a number of 2D bootstrap problems, uncovering a web of integrable theories at the boundary of theory space.
- In chapter 4 we develop an alternative formulation to the 2D S-matrix bootstrap that rules out quantum field theories by proving that there cannot exist analytic S-matrices with given physical properties.
- In chapter 5 we explore the multi-lightcone limit of six-point functions in a conformal gauge theory to estabilish precise formulas mapping structure constants of large spin operators and null-hexagonal Wilson loops in conformal gauge theory.
- In chapter 6 we consider the problem of computing structure constants of multiple spinning operators from integrability in $\mathcal{N} = 4$ SYM.
- In chapter 7 we develop a framework computing structure constants in $\mathcal{N} = 4$ SYM in terms of Baxter Q-functions to the first few orders in perturbation theory. At leading order, this reduces to the "Separation of Variables" framework of rational spin-chains.
- In chapter 8 we describe how analyticity in spin is compatible with the growth in the number of primary operators with spin in conformal field theory. We do so by introducing a technique that allows to compute complex spin CFT data from the Euclidean data.

Acknowledgements

It is hard to do justice to Pedro as an advisor. That he is an exceptionally creative scientist, with an endless enthusiasm and a terrific capacity to inspire is, I believe, obvious to anyone that interacted with him. Less obvious perhaps is his generosity towards students, his empathy and encouragement during challenging times, his commitment to lead by example. Some would say that you can't imagine a better advisor. I think he could improve on his jokes. Thank you so much, Pedro.

I am incredibly fortunate to have had David as a mentor and collaborator. I learned from him that properly turning over every rock in the simplest examples often leads to a much broader perspective. He also showed me that one can be as humble and kind as they are knowledgeable (and he knows a lot). I would also like to thank João for showing how one can go pretty far by asking the simplest questions. I am grateful to Carlos, Vasco, Andrea, Balt, Jon and Matheus for their collaboration in the various projects that form this thesis and for all that they thought me.

Perimeter is a fantastic place. I learned a huge amount of science from the faculty, postdocs and students here. Sometimes this happened in classrooms, sometimes in seminars, but most often in recycled bistro menus or random blackboards around the building. I will miss this atmosphere no matter where I end up at. This environment is only possible due to the fantastic effort of the non-scientific staff at Perimeter, to whom I am also very much in-debt. Special thanks to the members of my committee, Freddy, Benoit, Niayesh, for always having my best interest in mind.

My PhD would not have been nearly as rich and exciting without the Bootstrap community. I would like to thank all the researchers, many of which now friends, that helped to foster such a vibrant, collaborative environment.

I've had the opportunity to visit ICTP-SAIFR several times during my PhD. Having the opportunity to get completely immersed in a quantum field theory bootcamp every few terms was very productive. It was also inspiring and influential to see Nathan, Pedro and Jandira's efforts in bringing high-grade scientific events to South America, as well as their commitment to outreach. I thank them for this opportunity.

Despite common lore saying this is not possible, I had a lot of fun in Waterloo. This is in big part due to having great friends. A special thanks to my former housemates Bruno, Francisco, Fabian and Kasia for being awesome. I would also like to thank Benjamin, Laura and Antonio for being the best neighbours in Waterloo. Sorry new neighbours.

I could also count with friends back home. I am grateful to Tom, Corridinha and Rafa for always receiving me with open arms, and for remaining present in my life. In particular, their friendship made the harder days of the pandemic easier to withstand, and for that I am specially thankful.

Spending a good part of my PhD in Brazil allowed me to see my former-little brother grow into someone that makes me proud. I thank him for all the fun times together, and for his care.

I am very lucky to have Amalia in my life. Her never-ending joy makes happiness effortless, and I am extremely grateful for her amazing companionship and love.

At last, my parents, for their unconditional support, enabling me to follow my curiosity and live my dreams, and for teaching me the lessons that shaped who I am. This thesis is dedicated to them.

Dedication

Aos meus pais, Marli e Paulo.
To my parents, Marli and Paulo.

Table of Contents

Chapter 1

Introduction

Strongly interacting quantum field theories (QFTs) underlie some of the most awe-inspiring phenomena in nature. The large quantum fluctuations that give rise to their rich dynamics also make them notoriously challenging to study. QFTs come in all shapes and forms, and there is no one-size-fits-all strategy to analyse them. This thesis investigates various types of QFTs, most often exploring Lorentzian physics. In this introduction, we provide context for the various chapters that comprise this work.

An important class of quantum theories consists of those which admit asymptotic stable particles, allowing us to probe the theory's dynamics through particle scattering experiments. This class includes "gapped" theories, for which the vacuum is unique and long range interactions are absent, as well as theories with sufficiently "soft" low energy physics, such as theories of Goldstone bosons.

Not all results of these scattering experiments are consistent with a microscopic theory respecting fundamental principles such as causality, locality, and unitarity [8]. Indeed, systematic exploration of the consistency between these basic requirements leads to a rigid, constraining framework. This framework, known as the S-matrix Bootstrap [9], in turn, allows us to place powerful bounds on possible outcomes of collision experiments, even when the low energy dynamics is strongly coupled[1].

Locality and causality of the microscopic theory are reflected in the analytic structure of the scattering amplitudes as a function of kinematic invariants [2]. At the boundaries of the domain of analyticity the scattering amplitudes are constrained by (generalized) unitarity

[1] See [1,10–27] for a number of examples as well as [28–43] for a number of related technical developments.
[2] See reviews [44–46].

equations. One possible numerical realization of the S-matrix bootstrap is to parameterize the space of analytic functions, for example through some power series representation, or a dispersion relation, and numerically search this space, imposing the unitarity equations as constraints along the boundaries of the analyticity domain. One may then optimize over the value of certain physical observables, such as effective couplings or Wilson coefficients, thus deriving bounds on these objects as the numerical search converges. Inheriting nomenclature from convex optimization, this is often referred to as the "primal" S-matrix Bootstrap[3].

This strategy is easier to put in practice when considering the two-to-two scattering of the lightest particles in the field theory. In this case the boundaries of the domain of analyticity are simple to characterize: they correspond to regions of physical momenta in the complexified kinematic space, and are thus bounded by simple unitarity equations. When heavier stable particles exist, more powerful bounds on the space of quantum field theory can be obtained by requiring that *all* two-to-two amplitudes are consistent with the aforementioned fundamental principles.

In chapter 2 we extend the S-matrix bootstrap framework to the case of multiple two-to-two amplitudes. There are two main novelties. First, there are now singularities away from the physical scattering region. Their monodromies are given by "extended" unitarity equations, of a more complicated nature. Second, the unitarity equations now couple several amplitudes at once. After these challenges are overcome we observe powerful improvements over previous single amplitude bounds, and uncover rich physics sourced by the interplay of the various scattering processes. Our results are valid provided the heaviest scattered particles are not too heavy in units of the lightest mass in the theory. Extending our results to arbitrary mass spectrum is an important direction of future investigation.

An important experimental observation in these studies is that, when imposing the consistency of two-to-two scattering, theories on the boundary of the allowed S-matrix space *saturate* unitarity: the probability of two particles scattering into anything other than two particles is *zero*. Generically this is unphysical. Indeed, in higher dimensions, Aks theorem [47] shows that an interacting analytic and crossing symmetric two-to-two amplitude cannot saturate unitarity[4]. Vanishing particle production is possible in two dimensional integrable theories. The presence of higher-spin symmetries in these theories imply these selection rules as well as algebraic constrains on the two-to-two S-matrix, which must satisfy the Yang-Baxter equation: sequential scattering processes must lead to

[3]Haters might claim this strategy is also primitive. See chapter 4.

[4]This is not in contradiction with the numerics since they only asymptote to unitarity saturation, and Aks theorem does not set a lower bound on particle production at finite energies.

identical results irrespective of the order in which particles scatter. In chapter 3 we explore a number of 2D scattering setups involving multiple particle species. We find that in the boundary of the allowed space of theories live a number of remarkable integrable theories[5]. In these explorations, only analyticity and unitarity are imposed. At the boundary, Yang-Baxter *emerges*. In fact, through these numerical explorations we identify a previously unknown - to us, at least - integrable deformation of the supersymmetric sine-Gordon S-matrix. Thus integrable field theories not only serve as beacons in the space of S-matrices, but also can be uncovered by the bootstrap.

To exclude unphysical S-matrices on the boundary of the allowed space of previous studies one must impose constraints that forbid vanishing particle production. Unless something extraordinary happens, as does in integrable theories, this is ideally achieved by requiring the analyticity and unitarity of multiparticle amplitudes[6]. It is an ambitious goal to parametrize the domains of analyticity of multiparticle amplitudes. So far, this seems far from reach. Nevertheless, in [48] we will discuss the first multiparticle S-matrix bootstrap study. We consider the scattering of the Goldstone bosons of broken Poincare symmetry in long effective strings. In these theories, bundles of left- or right-moving Goldstones effectively behave as one-particle states. Requiring the consistency of the scattering of these effective "jets" thus allow us to probe physical theories with non-vanishing particle production. Fortunately, there is an ideal application to this technique: to study the dynamics of long chromodynamic fluxtubes. We study the multiparticle scattering on 3D Yang-Mills fluxtubes in [48], and leave the case of 4D Yang-Mills for future work.

The *primal* bootstrap strategy adopted in these works is unsatisfactory for two reasons. First, it is often computationally expensive to search the infinite-dimensional space of scattering amplitudes. Only when convergence of the numerical algorithm is achieved can one claim a bound on the space of theories. Second, once an S-matrix is constructed in the primal method, it is not guaranteed that this amplitude will remain valid once more physical principles are demanded, e.g. some of the S-matrices at the surface of the two-to-two S-matrix studies are incompatible with unitarity of two-to-many processes. It would be preferable to develop a *dual* strategy that rules out regions of theory space once and for all, and for which one can claim true bounds regardless of the convergence of numerical algorithms. This is the strategy adopted in the very successful numerical conformal bootstrap: there, one searches over functionals with certain properties, which once found exclude regions of conformal field theory space once and for all. In chapter 4

[5]Some had already been observed in chapter 2.

[6]Generically, higher point amplitudes contain singularities whose discontinuities are proportional to lower point amplitudes, and these do not vanish along the boundary of theory space of previous studies.

we develop the dual S-matrix bootstrap method in the case of two dimensional theories[7].

So far we have discussed quantum field theory that admit a basis of scattering states. More generally, in scenarios involving long range interactions, especially when these interactions are strong, measuring isolated asymptotic particles might not be possible due to the uncontrolled emission of massless excitations. Of course, we can still prepare states in these quantum field theories, perform asymptotic measurements, and require that the outcome of these measurements are compatible with microscopic local, unitary and causal physics, even if "particle detectors" are not well defined. A classical example of these can be found in [49], where the authors consider the consistency of energy-flux measurements in a unitary conformal field theory and derive bounds on the ratio of the conformal anomaly coefficients a/c.

What is the space of asymptotic measurements in these more general quantum field theories? In conformal field theory, a minimal set are null averages of local operators, known as "light-transforms". These includes the energy and charge flux measurements just discussed. One might ask, in analogy with local operators, if there exists a convergent expansion of two light-transforms in terms of effective non-local operators. The answer turns out to be positive [50, 51], but the objects that appear in this operator product expansion are not light-transforms of local operators but generalized continuous spin light-ray operators [52]. It is an open problem to determine whether the algebra of light-transforms closes on these generalized light-ray operators. Uncovering the algebra of asymptotic measurements in these theories could open the way to systematically bootstrap real-time observable in these theories. A crucial point to note is that correlation functions of these observable are, by construction, free of infrared divergences.

The structure of these generalized light-ray remains somewhat poorly understood, specially in the case of multi-twist trajectories, i.e. those composed of more than two operators[8]. In chapters 8 we address a few of these puzzles through analysis of related objects in $\mathcal{N} = 4$ SYM. In particular, we explain how analyticity in spin, see [55], is compatible with the growth of primary operators at large spin and develop technology to compute complex spin continuations of CFT correlators from the euclidean CFT data. In a longer article to appear along this thesis [56], we consider how the naive continuum of light-ray operators at weak coupling is quantized into a discrete set of operators corresponding to the discrete Reggee trajectories of the theory, explain how to compute CFT data in this theory directly at complex spin and analyse the fate of these infinite families of discrete trajectories as

[7] See [12] where this strategy was first developed in a single-component setup from a different perspective as well as [34, 35] for some developments in higher dimensions.

[8] This description makes sense in general CFT at large spin [53, 54].

they interact in the complex spin plane. We hope that the technology which we started to develop here might help in uncovering the structure of these light-ray operators more generally.

As the paragraph above illustrates, a common strategy in exploring QFTs is to examine in detail models that are simple enough to employ analytic methods in their study but rich enough to capture generic features. This is advantageous in two ways. First, from the explicit solution to the theory, one may uncover unexpected universal structures. Second, one can use these theories as a playground to explicitly test general conjectures. With this strategy in mind, $\mathcal{N} = 4$ SYM serves as an excellent laboratory to explore QFTs, being at once a conformal gauge theory, a theory of quantum gravity, and exactly solvable at large N_c.

Integrability of the large N_c dynamics in $\mathcal{N} = 4$ SYM is possible thanks to the AdS/CFT correspondence [57,58]. Observables in this gauge theory can be computed by a dual string theory, and it is the the dynamics on the two-dimensional string worldsheet that satisfy a more standard definition of integrability: the theory on the long-string admits an S-matrix description, and this S-matrix integrable - the multiparticle scattering is factorized, momentas are individually conserved, and the fundamental two-to-two amplitude satisfy the Yang-Baxter equation. The caveat is that the world-sheet S-matrix is not relativistic, and thus admits a much richer analyticity structure than those considered earlier in this introduction. Nevertheless, symmetry considerations paired with minimal physical assumptions are enough to completely fix the long-string scattering amplitudes in this theory at any value of the coupling [59,60].

With knowledge of the long-string S-matrix, a strategy can be developed to compute a large class of observables in the gauge theory such as exact conformal dimensions [61–65], correlation functions of local single trace operators [66–70], gluon scattering amplitudes and null Wilson loops [71–76], and others [77–79]. These computations can be summarized as follows. One starts from a world-sheet description of these observables. One then considers a "large geometry" expansion, in which one cuts open the world-sheet along some tesselation. The finite volume structure of the world-sheet is in this way replaced by a sum over excitations that propagate over the cut edges. Evaluating each patch of the world-sheet is now reduced to a generalized scattering problem - we have particles in asymptotic regions which now are decompactified. These generalized scattering problem can be completely solved by the "integrable" S-matrix bootstrap. One then recovers the field theory observable by re-summing these patches.

The main challenge lies on realizing this last step. Re-suming the large-geometry expansion is often too hard as one must consider contributions of any number of particle

excitations along cut edges and integrate over their phase-spaces. This strategy is thus of practical use only when subleading terms in this expansion are under control. This include, for example, correlations of heavy operators, scattering amplitudes in near collinear kinematics, or perturbative computations.

In the case of conformal dimensions, i.e the spectrum, this re-summation can be performed in general, thanks to special techniques under the name of "thermodynamic Bethe ansatz"[9] [61–65]. Careful investigation of the final results uncovers deep simplicity that is obscured in the very physical but complicated large volume expansion [83, 84]. Based on these observations, a beautiful reformulation of the spectral problem has been accomplished under the name of "Quantum Spectral Curve" [85, 86]. These are a set of finite difference and monodromy equations on a set of "Q-functions" living on an infinite genera Riemann surface whose solutions encode the complete spectrum of the planar gauge theory. They admit efficient numerical solution [87]. The spectrum problem in this gauge theory is thus solved.

Given the success of the Quantum Spectral Curve, and the hidden simplicity uncovered in the spectral problem, it is natural to ask if there exist a sort of Riemann-Hilbert problem for other observables in this gauge theory, such as local correlation functions and scattering amplitudes. Inspired by a number of related advancements [88–100], in chapter 7 we lay down the groundwork for such a formulation in the case of three-point correlators. At leading order in the coupling, this construction reduces to the "Separation of Variables" (SoV) framework of integrable rational spin-chains. We develop the first few "quantum corrections" to this formalism, and reproduce the first few finite volume effects associated to the closed world-sheet geometry describing these observables. To some problems, this new framework is already far more efficient than previous "tesselation based" methods, most notably for the investigations of light-ray operators in chapter 8. Hopefully it will be possible to lift the SoV structure to finite coupling in the coming years.

Computations of local correlators and of gluon amplitudes are not independent in this theory. The later are included in the former by considering correlation function with operators approaching cusps of null polygons [101]. The multi-lightcone singularities of these correlators are controlled by excitations propagating along the null separations which effectively source polygonal null Wilson loops. The latter are related by string dualities to scattering amplitudes [102, 103]. In chapter 5 we provide sharp formulas expressing these hexagonal Wilson loops/six gluon amplitudes in terms of three point functions of large spin operators. The kinematics of the scattering process are controlled by the spin polarisation of the spinning operators. The result is derived solely by analysing the six-point crossing

[9] See [78–82] for a few other notable exceptions.

equation in the multi-lightcone limit, and does not rely on integrability.

On the other hand, these results have clear implications for the integrability structure of $\mathcal{N} = 4$ SYM: it shows that different tesselations strategies - those applied to scattering amplitudes and those applied to local correlators - should provide the same answer. In particular, the manifest simplicity of the collinear expansion in the amplitudes side must imply huge hidden simplifications on the correlation computation, while this latter might simplify and reveal structure in a different kinematical region. In chapter 6 we investigate three-point functions of spinning operators from this perspective. Despite deriving all-loop formulas expressing the structure constants of large twist spinning operators in some particular polarizations through nice pfaffian formulas, we do not succeed in making direct contact with scattering amplitudes. Instead, we provide recursion relations capable of generating "analytic data" for these structure constants at finite values of spin. These should be important in the development of the SoV framework[10], which so far computes correlation functions with at most one spinning correlator[11].

In summary, this thesis tackles questions in quantum field theory from diverse perspectives. The various chapters can be read independently, and up to minor adaptations are equivalent to the papers listed in the Statement of Contributions of this thesis. The chapters are ordered with $+i\epsilon$.

[10]The SoV framework also seems more suitable to large spin applications than the hexagonalization/tesselation framework. It might thus be the better framework to investigate local correlator/scattering amplitudes dualities from the integrability perspective.

[11]With one minor exception, see chapter 7.

Chapter 2

The S-matrix Bootstrap: Multiple Amplitudes

2.1 Introduction

The bootstrap of the two-to-two S-matrix of the lightest particle in a relativistic unitarity quantum field theory was revived in [9, 10, 104] and extended to particles with flavour in [11, 13–15]. These works can be seen as gapped counterparts of the conformal bootstrap explorations in [105, 106] and [107] (without and with flavour respectively). In this chapter we discuss the bootstrap analysis of S-matrix elements involving different external particles in $\mathbb{Z}_2$ symmetric theories. This multiple amplitude study again mimics a similar development in the conformal bootstrap, namely the multiple correlator analysis of the Ising model which famously gave rise to the CFT islands in [108].

We will consider two-dimensional QFTs with exactly two stable particles of masses m_1 and m_2. We will assume the theory to be parity and time-reversal invariant and both particles to be parity even. For simplicity we will also postulate the existence of a $\mathbb{Z}_2$ symmetry, under which the first particle is *odd* and the second particle is *even*.[1] This means that the nonzero three-particle couplings are g_{112} and g_{222}, which can be defined non-perturbatively in terms of the residues of a pole in a suitable S-matrix element. In the first part of this chapter we will analyze all the two-to-two S-matrices of particles 1 and 2 and use crossing symmetry, analyticity and unitarity to explore the space of possible points in the (non-dimensionalized) (g_{112}, g_{222}) plane as a function of m_2/m_1 – see figure 2.8 on page 24 to get an idea. In order to avoid singularities or Coleman-Thun poles [109], which complicate the analytic structure of the scattering amplitudes, we will restrict ourselves to

$$m_2 \leq \sqrt{2} m_1 \,. \tag{2.1}$$

Note that we allow $m_2 < m_1$ also.

Under the stated assumptions there are five different physical two-to-two scattering processes as shown in figure 2.1. These can be grouped either according to the nature of

[1] In two dimensions theories with fermions and scalars are naturally $\mathbb{Z}_2$ symmetric theories so the setup here applies as well to any theories with scalars and fermions, not necessarily supersymmetric.

their intermediate states, which can be $\mathbb{Z}_2$ odd or even, or according to whether they are 'diagonal' or not. To wit, for a diagonal process the incoming and outgoing momenta are the same whereas for an off-diagonal process they are different.[2] As is also indicated in figure 2.1, we call the $12 \to 12$ diagonal process 'forward' scattering, and the $12 \to 12$ off-diagonal process 'backward'.

In section 2.2 we will state in detail the conditions of unitarity, analyticity, and crossing symmetry that these five processes must obey. To guide ideas let us mention two conspicuous facts. First, we note that crossing symmetry flips the s and t axes on the diagram. This relates the two off-diagonal processes and thereby reduces the number of independent amplitudes (*i.e.* functions of the Mandelstam invariant) to four. Of course, it also imposes a non-trivial constraint on the amplitudes for the diagonal processes. Second, we observe that particle 1 can appear as an intermediate state in all the odd processes and gives rise to a pole in these amplitudes with residue proportional to g_{112}^2, whereas particle 2 gives rise to poles in all the even amplitudes with residues proportional to g_{112}^2, $g_{112}g_{222}$ or g_{222}^2, depending on the process. These poles can be thought of as our definition of the corresponding couplings.[3]

2.1.1 Quick comparison with single-correlator bounds

As a warm up exercise let us first discuss the three diagonal processes in isolation and explain how the methods discussed in [9, 10, 110] already lead to some constraints on the couplings.

The analyticity and crossing symmetry of the diagonal processes in the Mandelstam s plane is pretty straightforward. For example, the odd process has a two-particle s-channel cut starting at $s = (m_1 + m_2)^2$ and a pole at m_1^2 with residue proportional to g_{112}^2, plus the crossed t-channel singularities obtained by swapping $s \to 2m_1^2 + 2m_2^2 - s$. The even processes $S_{11\to11}$ and $S_{22\to22}$ have their two-particle s-channel cuts starting at $\min(4m_1^2, 4m_2^2)$ and a pole with residue g_{112}^2 or g_{222}^2, again plus the crossed t-channel singularities obtained by swapping $s \to 4m_1^2 - s$ or $s \to 4m_2^2 - s$. As for unitarity, notice that the discontinuity across the cut is always positive, but it is bounded from *above* only for physical s, which means $s > 4m_1^2$ for $S_{11\to11}$ and $s > 4m_2^2$ for $S_{22\to22}$. Therefore only for the *lightest* of the two particles is the discontinuity everywhere bounded from above, whereas for the other particle the discontinuity can be arbitrarily large (but not negative) in the interval between $\min(4m_1^2, 4m_2^2)$ and $\max(4m_1^2, 4m_2^2)$.

We can bound the couplings as follows. First let us bound g_{112}^2 by using the maximum modulus principle for $S_{12\to12}^{\text{forward}}$ following [9, 10, 110]. We define

$$f_{12\to12}(s) \equiv S_{12\to12}^{\text{forward}}(s) / \frac{h_{12}(s) + h_{12}(m_1^2)}{h_{12}(s) - h_{12}(m_1^2)}\,, \tag{2.2}$$

[2] As explained further below, in two dimensions the scattering angle can take only two values by kinematical restrictions; the outgoing momenta are essentially 'locked' in terms of the incoming momenta. Unlike in higher dimensions, there is therefore no (analytic) function interpolating between forward and backward scattering.

[3] The astute reader will have noticed that this defines the couplings only up to an overall sign flip, leading to an obvious reflection symmetry in some of our plots.

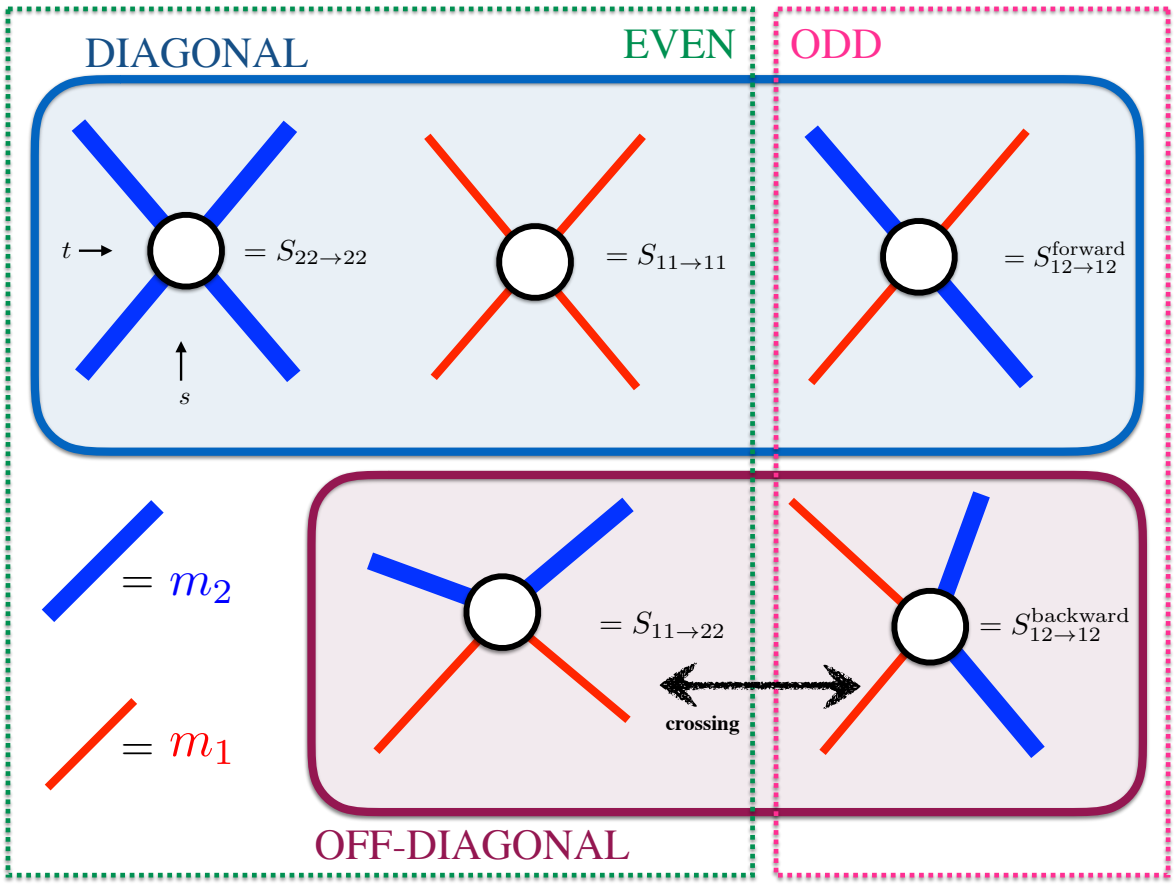

Figure 2.1: Diagonal processes are those where the incoming and outgoing particles have the same momenta as illustrated in the first row; they are all crossing invariant. The non-diagonal processes in the second row are those for which the final momenta are not the same as the initial momenta. Swapping space and time interchanges the odd and even off-diagonal processes so these off-diagonal processes play a crucial role in connecting these two sectors of different $\mathbb{Z}_2$ charge.

with $h_{ab}(s) \equiv \sqrt{(s-(m_a-m_b)^2)((m_a+m_b)^2-s)}$. The function $f_{12\to 12}$ is free of singularities (since we divided out by functions with poles at the pole location of the amplitudes) and is bounded at the s– and t– channel cuts (since the functions we divided by are phases at those cuts and the amplitude is bounded). Therefore $f_{12\to 12}(s)$ must have absolute value smaller or equal to 1 everywhere, and in particular at m_2^2 and m_1^2 where we can simply read off the maximally allowed couplings in these amplitudes. This leads to a universal upper bound on g^2_{112}, which is the solid line in figure 2.2.

The exact same analysis can be used for the elastic amplitude for the lightest of the two particles. If we denote this by ℓ, so $m_\ell = \min(m_1, m_2)$, then the maximum modulus principle for

$$f_{\ell\ell\to\ell\ell}(s) \equiv S_{\ell\ell\to\ell\ell}(s) \Big/ \frac{h_{\ell\ell}(s)+h_{\ell\ell}(m_2^2)}{h_{\ell\ell}(s)-h_{\ell\ell}(m_2^2)} \tag{2.3}$$

gives a bound on the coupling appearing on $S_{\ell\ell\to\ell\ell}$, which is $g^2_{\ell\ell 2}$. This is the dashed line for $m_2 > m_1$ in figure 2.2 and the solid line for $m_2 < m_1$ in figure 2.3.

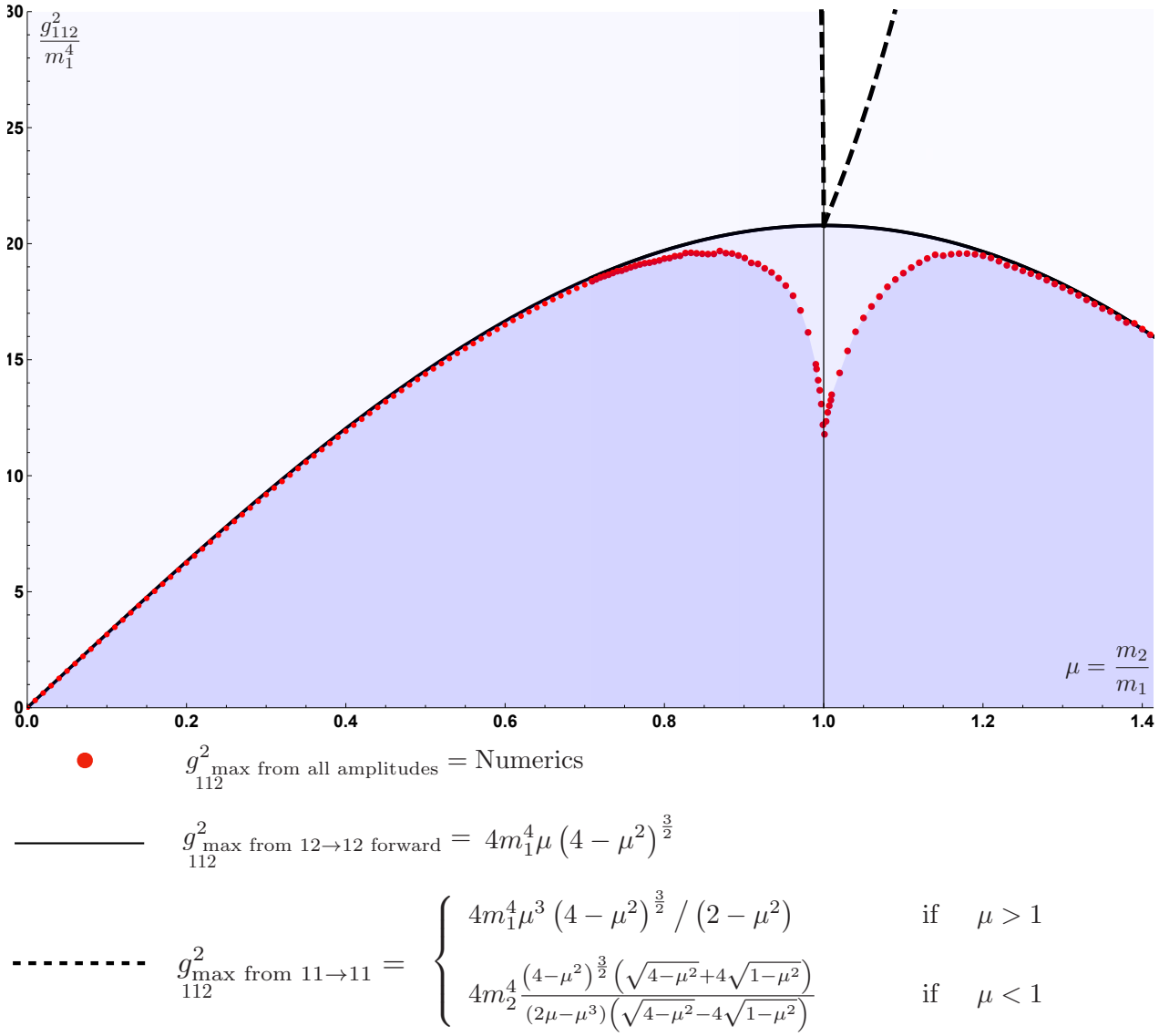

Figure 2.2: Upper bounds on the cubic coupling g_{112}^2 as a function of $\mu \equiv m_2/m_1$. *Dashed line:* Analytic bound based on the scattering of the lightest odd particle, from [9]. *Solid line:* Analytic bound arising from the forward (or transmission) scattering of the odd particle against the even particle; it is a much stronger bound. *Red dots:* The numeric bound obtained from *all* two-to-two processes as discussed in the main text. The shaded regions represent the allowed regions which nicely shrink as we include more constraints. Any relativistic, unitary, $\mathbb{Z}_2$ invariant theory theory with two stable particles (one odd with mass m_1 and one even with mass m_2) must lie inside the darkest blue region.

Finally we can use the techniques of [9] to also derive a bound on g_{222} from the amplitude $S_{22\to22}$ even when m_2 is not the lightest particle. In this case there is a cut which is not bounded directly by unitarity as depicted in figure 2.4. As we derive in appendix A.3, the

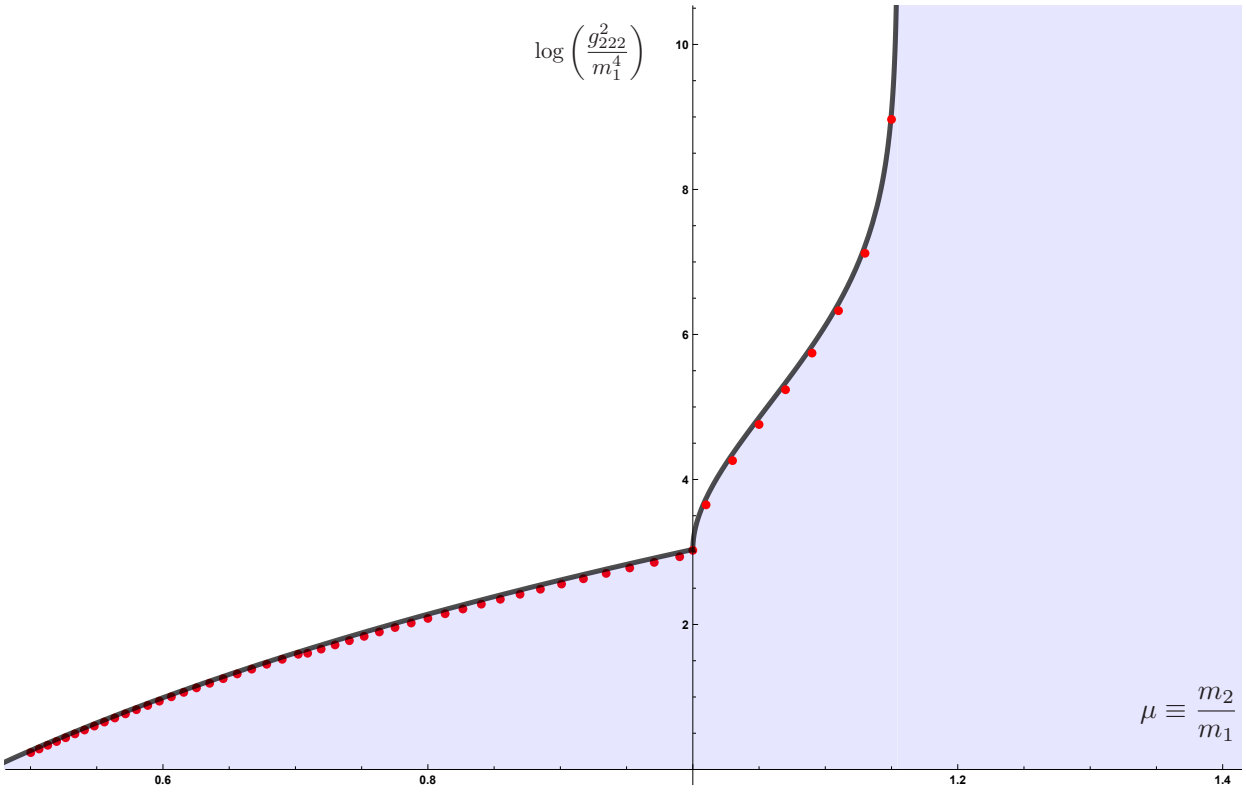

Figure 2.3: Upper bounds on the cubic coupling g_{222} as a function of $\mu \equiv m_2/m_1$. *Solid line:* Analytic bound based on the scattering of the lightest even particle, from [9]. *Red dots:* The numeric bound obtained from *all* two-to-two processes as discussed in the main text. The shaded region represent the allowed region. When the even particle is the lightest, we can solve analytically for the maximal coupling, even considering the full set of amplitudes. When the odd particle is the lightest, the coupling can be bigger, diverging when singularities of the amplitudes corresponding to physical processes collide. This happens at $m_2/m_1 = 2/\sqrt{3}$. After this mass ratio the upper bound disappears.

amplitude with maximal g_{222}^2 is given by

$$S_{22\to22}(s) = -\frac{h_{22}(s) + h_{22}(m_2^2)}{h_{22}(s) - h_{22}(m_2^2)} \times \frac{h_{22}(s) + h_{22}(4m_1^2)}{h_{22}(s) - h_{22}(4m_1^2)} \tag{2.4}$$

The corresponding bound on g_{222}^2 is plotted as the solid line in figure 2.3 for $m_2 > m_1$. As the figure shows, the bound actually disappears for $m_2 \geq \frac{2}{\sqrt{3}}m_1$, which is due the t-channel pole colliding with the s-channel cut in the $22 \to 22$ process at this mass ratio. This is

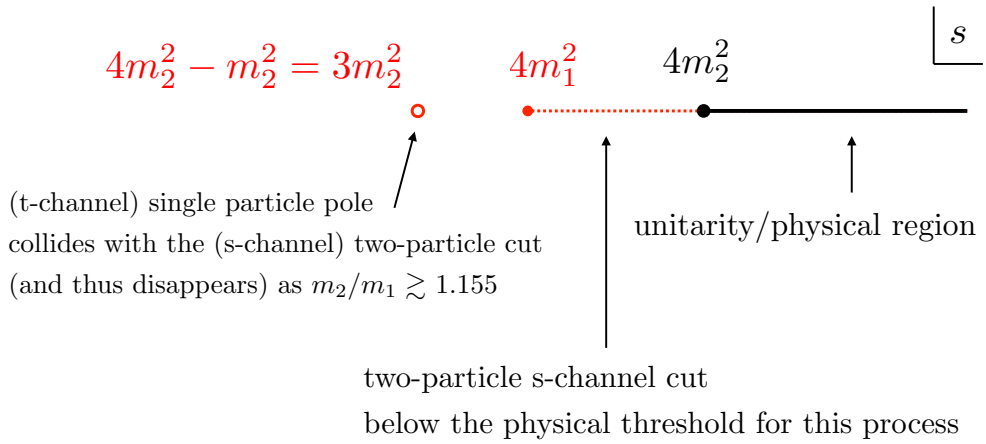

Figure 2.4: Analytic structure of the $S_{22\to22}$ amplitude (for clarity we do not show the left cut and s-channel pole following from crossing symmetry $S_{22\to22}(s) = S_{22\to22}(4m_2^2 - s)$). If m_2 is not the lightest particle, there is a new feature in the $S_{22\to22}$ amplitude: a two particle cut starting at $s = 4m_1^2$ corresponding to the contribution of two particles m_1. This cut appears before the cut for two particles m_2 at physical energies $s \geq 4m_2^2$ where regular unitarity is imposed and the amplitude needs to be bounded. As m_2 grows beyond $2/\sqrt{3}m_1$ the t-channel pole corresponding to the exchange of particle m_2 enters the new cut (by crossing symmetry the s-channel pole enters the t-channel cut) so we "lose" this pole. Beyond this point we can no longer bound g_{222} since it does not appear in any other diagonal amplitude. This is indeed what we observe in the numerics as illustrated in figure 2.3. Note that before the bound on g_{222} disappears it diverges. This divergence, arising from the collision of the t-channel pole with an s-channel cut is analogous to the divergences in bounds on couplings when s– and t– channel poles collide as already observed in [9]; the dashed line in figure 2.2 which was taken from [9] diverges at $m_2 = \sqrt{2}m_1$ for exactly this reason.

the simplest instance of a phenomenon we call *screening*. It is detailed in figure 2.4 and we will encounter it again below. In the same way we could obtain a bound on g_{112}^2 from the $11 \to 11$ process even when m_1 is the heaviest particle. This bound corresponds to the dashed line in figure 2.2 for $\mu < 1$, and is always less restrictive than the bound from $\mathcal{S}_{12\to12}^{\text{forward}}$.

This concludes our discussion of the single-amplitude results. As a preview for the more detailed numerical results presented below, we already marked in figures 2.2 and 2.3 in red dots our best numerical values of the coupling obtained from a simultaneous analysis of the full set of two-to-two amplitudes depicted in figure 2.1. Figure 2.2 displays a clear improvement over the quick single-amplitude analysis for $m_1/\sqrt{2} < m_2 < \sqrt{2}m_1$, with an intriguing kink at $m_2 = m_1$. It would be fascinating to find if this kink corresponds to a physical theory. On the other hand, in figure 2.3 we see no improvement over the single-amplitude results. In fact, in section 2.3 we will prove that the maximal value of g_{222} in the multi-amplitude analysis saturates the single-amplitude analytic bounds just derived. In the same section we will show a more complete picture by considering the entire (g_{112}, g_{222}) plane.

2.1.2 QFT in AdS

As shown in [104], there exists a completely orthogonal approach towards the problem of determining the maximal couplings in QFT. Rather than working from the S-matrix, which required analyticity assumptions that in general dimension D are not very well understood, the idea is to consider QFTs on an AdS background. The boundary correlators of such a QFT, which are defined in a similar way as in the AdS/CFT correspondence, behave much like conformal correlation functions in one lower dimension $d = D - 1$. By applying numerical conformal bootstrap methods of [105] one can put a universal upper bound on the three-point couplings of QFTs in AdS. One can then extrapolate this bound to the flat-space limit (by sending all scaling dimensions to infinity), resulting in putative bounds for flat-space QFTs. In [9, 104] this was shown to work extremely well for two-dimensional QFTs: a precise match was found between the *single-correlator* analysis using the conformal bootstrap, and the *single-amplitude* analysis that we partially reviewed above.

In this chapter we extend these explorations. As discussed further in section 2.4, the $\mathbb{Z}_2$ symmetric setup that we consider is easily translated to a multi-correlator conformal bootstrap problem for QFTs in AdS. In most cases we again find a very good match, and in particular we are able to recover the coupling of the 3-state Potts field theory from the conformal crossing equations. For large-ish mass ratios, however, we will see that the multi-correlator bootstrap appears to be less powerful than even the single-amplitude bootstrap.

2.1.3 Outline

The $\mathbb{Z}_2$ symmetric S-matrix bootstrap is fully spelled out in section 2.2 and analysed numerically in section 2.3 leading to various bounds on the allowed coupling space for various mass ratios as illustrated in figure 2.8. In section 2.3.3 we discuss integrable $\mathbb{Z}_2$ symmetric theories with $m_2 = m_1$ and how some of them nicely show up at the boundary of the allowed S-matrix space found in the numerical bootstrap. These include a massive deformation of the 3-state Potts model, the super-symmetric Sine-Gordon model and a SUSY breaking integrable elliptic deformation of the super-symmetric Sine-Gordon which seems to be novel as far as we know. Section 2.4 contains the results from the QFT in AdS analysis. Various appendices complement the main text with further extensions. (For example, the special role of the Tricritical Ising model as a kink in the space of S-matrices is discussed in appendix A.8.)

2.2 Multiple amplitudes

2.2.1 Kinematics of the various $\mathbb{Z}_2$ preserving processes

There are *six* two-to-two processes involving particles m_1 (odd) and m_2 (even) in a two dimensional $\mathbb{Z}_2$ symmetric theory. We also assume time-reversal and parity symmetry. Four of those six are even processes where we scatter either 11 or 22 into either 11 or 22.

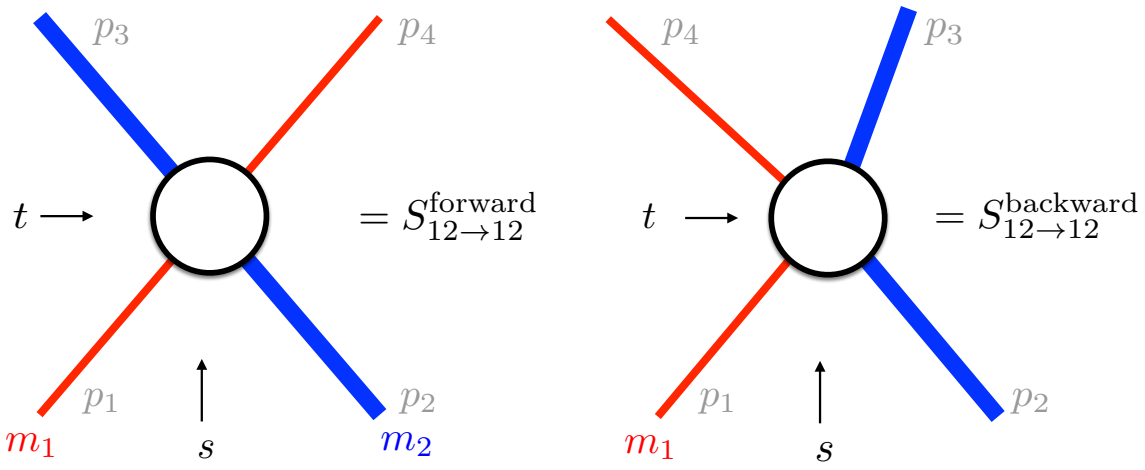

Figure 2.5: In two dimensions when we scatter two particles m_a and m_b from the infinite past with m_a to the left of m_b we can end up, in the infinite future with m_a to the right of m_b or vice-versa. If the particles are distinguishable these are two genuinely different processes denoted as the forward or backward process. (They are sometimes also called the transmission and reflection processes.) In higher dimensions, these two scenarios are limiting values of the a single amplitude when the scattering angle tends to $\theta = 0$ or $\theta = \pi$, but in two dimensions there is no scattering angle and these processes are described by independent functions. As we exchange time and space, i.e. as we analytically continue these processes by swapping t and s we see that the forward process is mapped to itself while the backward process as seen from its crossed channel describes the $m_a m_a \to m_b m_b$ event. This translates into equations (2.19) and (2.20) in the main text.

Of those four, two are trivially related by time-reversal,

$$M_{22\to11} = M_{11\to22} \tag{2.5}$$

so we can ignore one of them (say $22 \to 11$) in what follows. The remaining two processes are $\mathbb{Z}_2$ odd processes where we scatter the odd particle against the even particle obtaining those same two particles in the future. As explained in the introduction this process splits into two possibilities which we call the forward and the backward component, see figures 2.1 and 2.5.

In two dimensions, any process depends uniquely on the center of mass energy or equivalently on the Mandelstam invariant

$$s = (p_1 + p_2)^2 \,. \tag{2.6}$$

This in particular means that the other two Mandelstam invariants

$$t = (p_1 - p_3)^2 \,, \qquad u = (p_1 - p_4)^2 \,. \tag{2.7}$$

are completely determined in terms of s. It is important to find the precise relation because crossing symmetry permutes the three Mandelstam invariants and therefore leads

to symmetries of the amplitudes $M(s)$ that we need to impose. In a process[4] involving $m_a m_b \to m_c m_d$

$$0 = 8 \begin{vmatrix} p_1 \cdot p_1 & p_1 \cdot p_2 & p_1 \cdot p_3 \\ p_2 \cdot p_1 & p_2 \cdot p_2 & p_2 \cdot p_3 \\ p_3 \cdot p_1 & p_3 \cdot p_2 & p_3 \cdot p_3 \end{vmatrix} = \begin{vmatrix} 2m_a^2 & s - m_a^2 - m_b^2 & -t + m_a^2 + m_c^2 \\ s - m_a^2 - m_b^2 & 2m_b^2 & -u + m_b^2 + m_c^2 \\ -t + m_a^2 + m_c^2 & -u + m_b^2 + m_c^2 & 2m_c^2 \end{vmatrix} \tag{2.8}$$

The first equal sign is the two dimensional constraint: in two dimensions p_3 is always a linear combination of the two-vectors p_1 and p_2 and hence the determinant vanishes. In the second equal sign we used the on-shell conditions and momentum conservation. For example $2p_2 \cdot p_3 = -(p_2 - p_3)^2 + p_2^2 + p_3^2 = -(p_1 - p_4)^2 + p_2^2 + p_3^2 = -u + m_b^2 + d_c^2$ and so on. Evaluated explicitly and combined with the previous linear constraint on the Mandelstam invariants, this can be cast in a nice symmetric form:

$$0 = stu + s(m_a^2 + m_b^2)(m_c^2 + m_d^2) + t(m_a^2 + m_c^2)(m_b^2 + m_d^2) + u(m_a^2 + m_d^2)(m_b^2 + m_c^2) + C \tag{2.9}$$

where $C = -\frac{1}{6}(\sum m_i^2)^3 - \frac{1}{2}(\sum m_i^4)(\sum m_i^2) + \frac{2}{3}\sum m_i^6$.

Let us now specialize to the $\mathbb{Z}_2$ preserving cases mentioned above. For the simplest processes corresponding to all equal masses (i.e. for $11 \to 11$ and $22 \to 22$) the condition dramatically simplifies into $stu = 0$ which leads to $u = 0$ or $t = 0$ or $s = 0$. In fact, we can not set $s = 0$ since by definition we assume s to be constructed from two incoming particles and setting $u = 0$ or $t = 0$ is the same up to a simple relabelling of the final particles which we can always do for indistinguishable particles. Hence without loss of generality we can set $u = 0$ recovering the famous result that elastic scattering of identical particles in two dimensions has zero momentum transfer.

Next we have the processes involving two particles of mass m_1 and two particles of mass m_2. Here it matters whether the two particles of the same mass are both incoming or if one is incoming and the other is outgoing. Let us start first with the second case so that we can set $m_a = m_d = m_1$ and $m_b = m_c = m_2$ in agreement with the conventions of figure 2.5. Then we obtain a nice factorization of the constraint (2.9) into

$$0 = u\left(\left(m_1^2 - m_2^2\right)^2 - \left(2m_2^2 + 2m_1^2 + s\right)s + su\right) \tag{2.10}$$

with two clear solutions: $u = 0$ corresponding to forward scattering and $u = 2m_1^2 + 2m_2^2 - \left(m_1^2 - m_2^2\right)^2/s + s$ corresponding to the more complicated backward scattering. Note that in forward scattering the final momenta are equal to the initial momenta but this is not the case in backward scattering where the momentum transfer is non-zero as highlighted in figure 2.5.

Lastly we have the even process $11 \to 22$ where $m_a = m_b = m_1$ and $m_c = m_d = m_2$ which of course corresponds to a simple relabelling of the previous constraint in which $s \leftrightarrow u$ and thus leads, after discarding the $s = 0$ solution, to

$$0 = \left(m_1^2 - m_2^2\right)^2 - \left(2m_2^2 + 2m_1^2 + u\right)u + su \tag{2.11}$$

[4]In the convention $p_1^2 = m_a^2$, $p_2^2 = m_b^2$, $p_3^2 = m_c^2$ and $p_4^2 = m_d^2$.

whose solutions are $u = \frac{1}{2}(2m_1^2 + 2m_2^2 \pm \sqrt{(4m_1^2 - s)}\sqrt{(4m_2^2 - s)} - s)$. In fact, these two solutions are equivalent up to relabelling of the two outgoing particles. Of course, the $s \leftrightarrow u$ relation between $11 \to 22$ and backward $12 \to 12$ scattering is just crossing symmetry.

All in all we understood that all amplitudes can be thought of as functions of s with the other Mandelstam invariants given by

$$M_{11\to 11}(s): \qquad t = 4m_1^2 - s, \qquad u = 0, \tag{2.12}$$

$$M_{22\to 22}(s): \qquad t = 4m_2^2 - s, \qquad u = 0, \tag{2.13}$$

$$M^{\text{forward}}_{12\to 12}(s): \qquad t = 2m_1^2 + 2m_2^2 - s, \qquad u = 0, \tag{2.14}$$

$$M^{\text{backward}}_{12\to 12}(s): \qquad u + t = 2m_1^2 + 2m_2^2 - s, \qquad t = \frac{(m_1^2 - m_2^2)^2}{s}, \tag{2.15}$$

$$M_{11\to 22}(s): \qquad u - t = \sqrt{(4m_1^2 - s)}\sqrt{(4m_2^2 - s)}, \qquad u + t = 2m_1^2 + 2m_2^2 - s\,. \tag{2.16}$$

The above equations allow us to state the crossing symmetry equations which we will impose in the sequel. They are:

$$M_{11\to 11}(4m_1^2 - s) = M_{11\to 11}(s)\,, \tag{2.17}$$

$$M_{22\to 22}(4m_2^2 - s) = M_{22\to 22}(s)\,, \tag{2.18}$$

$$M^{\text{forward}}_{12\to 12}(2m_1^2 + 2m_2^2 - s) = M^{\text{forward}}_{12\to 12}(s)\,, \tag{2.19}$$

$$M_{11\to 22}(2m_1^2 + 2m_2^2 - \frac{(m_1^2 - m_2^2)^2}{s} - s) = M^{\text{backward}}_{12\to 12}(s)\,. \tag{2.20}$$

Note in particular that the last crossing relation plays quite an important role: it connects the even and the odd sectors.

For more on how the above discussion can be related to a similar analysis in higher dimensions see appendix A.1.

2.2.2 Analyticity, Unitarity and Extended Unitarity

The central hypothesis for the S-matrix bootstrap is that the scattering amplitudes are analytic for arbitrary complex values of s up to so-called Landau singularities [111] corresponding to on-shell intermediate processes. For the amplitudes and mass range discussed in this chapter, these singularities in the physical sheet correspond to the possibility of the full $a \to b$ scattering process to factorise into two scatterings, first $a \to c$ and then $c \to b$. Each on-shell state c of the theory will produce a singularity in the $a \to b$ process for s equal to the center of mass energy squared of the state c. This singularity will then proliferate according to its image under crossing transformations, see e.g. (2.17–2.20). The discontinuities around these singularities are governed by the generalized unitarity

equations [111],

$$M_{12\to 34}(s+i\epsilon) - M_{12\to 34}(s-i\epsilon) = 2\mathrm{Im}M_{12\to 34}(s+i\epsilon) = \sum_c \int \mathrm{d}\Pi_c M^*_{12\to c} M_{c\to 34} \quad (2.21)$$

(where the first equality assumes time reversal invariance.) Equation (2.21) is very powerful and reduces to a number of familiar examples in special cases:

- The contribution from one particle intermediate states corresponds to nothing but the usual bound-state poles: there the phase space integral reduces to the energy momentum delta function and the product of amplitudes to the physical three-point couplings, combining to the bound-state pole discontinuity $-2\pi i\delta(s-m_k^2)g_{12k}g_{34k}$.

- For real values of s for which there are no on-shell states, (2.21) reduces to the reality condition $\mathrm{Im}M_{12\to 34}=0$.

- If we are at physical energies, $s > \max\{(m_1+m_2)^2,(m_3+m_4)^2\}$, then (2.21) is just the physical unitarity condition $\langle \mathbf{34}|S^\dagger S - \mathbb{1}|\mathbf{12}\rangle = 0$.

- All of the above are very well known. Indeed, for the lightest two particle states in a given channel, there is nothing more to (2.21) than bound state poles, real analyticity and unitarity. For heavier external states, however, (2.21) extends the unitarity relation to the unphysical energy region $s < \max\{(m_1+m_2)^2,(m_3+m_4)^2\}$ by keeping the quadratic terms in the unitarity equation that correspond to physical intermediate states of energy $\sqrt{s}$. This is what is called *extended* unitarity.

  In our $\mathbb{Z}_2$ symmetric setup and for $\sqrt{s} < \min(3m_2, 2m_1+m_2)$,[5] we find

$$2\mathrm{Im}M_{11\to 11} = \frac{|M_{11\to 11}|^2}{2\sqrt{s(s-4m_1^2)}}\theta(s-4m_1^2) + \frac{|M_{11\to 22}|^2}{2\sqrt{s(s-4m_2^2)}}\theta(s-4m_2^2), \quad (2.22)$$

$$2\mathrm{Im}M_{11\to 22} = \frac{M_{11\to 22}M^*_{11\to 11}}{2\sqrt{s(s-4m_1^2)}}\theta(s-4m_1^2) + \frac{M^*_{11\to 22}M_{22\to 22}}{2\sqrt{s(s-4m_2^2)}}\theta(s-4m_2^2), \quad (2.23)$$

$$2\mathrm{Im}M_{22\to 22} = \frac{|M_{11\to 22}|^2}{2\sqrt{s(s-4m_1^2)}}\theta(s-4m_1^2) + \frac{|M_{22\to 22}|^2}{2\sqrt{s(s-4m_2^2)}}\theta(s-4m_2^2), \quad (2.24)$$

  and for $\sqrt{s} < \min(3m_1, 2m_2+m_1)$,

$$2\mathrm{Im}M^{\mathrm{Forward}}_{12\to 12} = \frac{|M^{\mathrm{Forward}}_{12\to 12}|^2 + |M^{\mathrm{Backward}}_{12\to 12}|^2}{2\sqrt{(s-(m_1-m_2)^2)(s-(m_1+m_2)^2)}}\theta(s-(m_1+m_2)^2), \quad (2.25)$$

$$2\mathrm{Im}M^{\mathrm{Backward}}_{12\to 12} = \frac{M^{*\mathrm{Forward}}_{12\to 12}M^{\mathrm{Backward}}_{12\to 12} + M^{*\mathrm{Backward}}_{12\to 12}M^{\mathrm{Forward}}_{12\to 12}}{2\sqrt{(s-(m_1-m_2)^2)(s-(m_1+m_2)^2)}}\theta(s-(m_1+m_2)^2), \quad (2.26)$$

[5] The bound corresponds to the first $\mathbb{Z}_2$ even three particle state.

where the denominators come from the phase space factors and θ is the Heaviside step function. For example, if $m_2 > m_1$ then equation (2.24) for $s > 4m_2^2$ is just unitarity for the $22 \to 22$ process, but for $4m_1^2 < s < 4m_2^2$ it is a "new" constraint over the $|\mathbf{11}\rangle$ production cut.

Of course, the scattering amplitudes also have cuts and poles corresponding to crossed intermediate processes. The discontinuities around those singularities are governed by the generalised unitarity equations for the crossed scattering, together with the crossing equations (2.17–2.20).

For energies above the three particle threshold, new terms corresponding to three-particle intermediate states should be introduced in the r.h.s. of equations (2.22-2.26) It is useful, however, to keep only the contributions from two-particle intermediate states and replace the full set of equations (2.22-2.26) by a positive semidefinite constraint on the amplitudes. For the $\mathbb{Z}_2$ even sector, by dropping the contributions from intermediate states with three or more particles in (2.21), we can write in matrix form

$$2\mathrm{Im}\mathbb{M} \succeq \mathbb{M}^\dagger \rho^2 \mathbb{M}, \qquad \mathbb{M} = \begin{pmatrix} M_{11\to 11} & M_{11\to 22} \\ M_{11\to 22} & M_{22\to 22} \end{pmatrix}, \qquad \rho = \begin{pmatrix} \rho_{11} & 0 \\ 0 & \rho_{22} \end{pmatrix}, \tag{2.27}$$

where $\rho_{ab}^2 = \frac{\theta\left(s-(m_a+m_b)^2\right)}{2\sqrt{s-(m_a+m_b)^2}\sqrt{s-(m_a-m_b)^2}}$ takes into account the phase space volume. Note that (2.27) is saturated for $\sqrt{s} < \min(3m_2, 2m_1 + m_2)$. As discussed in section 2.3, for the numerical implementation we impose (2.27) even before multiparticle thresholds, leaving for the computer to achieve saturation where (2.22-2.24) applies. A similar discussion holds for the $\mathbb{Z}_2$ odd sector.

In appendix A.2, we provide a direct derivation of (2.27) for $\sqrt{s} > 2\max(m_1, m_2)$. This derivation elucidates the physical meaning of the matrix $\mathbb{M}$ and its relation to transition probabilitues between initial and final states.

2.3 Numerics

2.3.1 Implementation

As discussed in section 2.2.2, the $\mathbb{Z}_2$ symmetric scattering amplitudes in the mass range (2.1) are analytic functions in the physical sheet of the the kinematical variable s up to poles corresponding to bound states. This sheet is defined by continuing the amplitudes away from physical kinematics respecting the $i\epsilon$ prescription and has as its boundaries cuts corresponding to two and higher particle production thresholds which may happen in the s, t and u channels. These can be summarised by expressing the amplitudes through

dispersion relations, as illustrated in figure 2.6. For the case $m_1 < m_2$, we obtain

$$M_{11\to11}(s) = C_{11\to11} - \frac{g_{112}^2}{s-m_2^2} - \frac{g_{112}^2}{t(s)-m_2^2} + \frac{1}{\pi}\int_{4m_1^2}^{\infty}\frac{\mathrm{Im}M_{11\to11}(s^*)}{s^*-s}\mathrm{d}s^* \tag{2.28}$$
$$+ \frac{1}{\pi}\int_{4m_1^2}^{\infty}\frac{\mathrm{Im}M_{11\to11}(t^*)}{t^*-t(s)}\mathrm{d}t^*,$$

$$M_{22\to22}(s) = C_{22\to22} - \frac{g_{222}^2}{s-m_2^2} - \frac{g_{222}^2}{t(s)-m_2^2} + \frac{1}{\pi}\int_{4m_1^2}^{\infty}\frac{\mathrm{Im}M_{22\to22}(s^*)}{s^*-s}\mathrm{d}s^* \tag{2.29}$$
$$+ \frac{1}{\pi}\int_{4m_1^2}^{\infty}\frac{\mathrm{Im}M_{22\to22}(t^*)}{t^*-t(s)}\mathrm{d}t^*,$$

$$M_{12\to12}^{\text{Forward}}(s) = C_{12\to12} - \frac{g_{112}^2}{s-m_1^2} - \frac{g_{112}^2}{t(s)-m_1^2} + \frac{1}{\pi}\int_{(m_1+m_2)^2}^{\infty}\frac{\mathrm{Im}M_{12\to12}(s^*)}{s^*-s}\mathrm{d}s^* \tag{2.30}$$
$$+ \frac{1}{\pi}\int_{(m_1+m_2)^2}^{\infty}\frac{\mathrm{Im}M_{12\to12}(t^*)}{t^*-t(s)}\mathrm{d}t^*,$$

$$M_{11\to22}(s) = C_{11\to22} - \frac{g_{112}g_{222}}{s-m_2^2} - \frac{g_{112}^2}{t(s)-m_1^2} - \frac{g_{112}^2}{u(s)-m_1^2} + \frac{1}{\pi}\int_{4m_1^2}^{\infty}\frac{\mathrm{Im}M_{11\to22}(s^*)}{s^*-s}\mathrm{d}s^* \tag{2.31}$$
$$+ \frac{1}{\pi}\int_{(m1+m2)^2}^{\infty}\frac{\mathrm{Im}M_{12\to12}^{Backward}(t^*)}{t^*-t(s)}\mathrm{d}t^* + \frac{1}{\pi}\int_{(m1+m2)^2}^{\infty}\frac{\mathrm{Im}M_{12\to12}^{Backward}(u^*)}{u^*-u(s)}\mathrm{d}u^*,$$

with $C_{a\to b}$ constant. Equations for the $m_1 > m_2$ case are obtained by replacing $4m_1^2 \to 4m_2^2$ in the lower limits of the integrals. Recall that these are the only independent amplitudes, since $M_{12\to12}^{\text{Backward}}(s) = M_{11\to22}(2m_1^2 + 2m_2^2 - \frac{(m_1^2-m_2^2)^2}{s} - s)$.

In deriving this relations, see figure 2.6, we assumed that the scattering amplitudes have no essential singularities at infinity, and in fact approach a constant in this limit, i.e. the S-matrix becomes free. This latter assumption is not crucial nor required: it can be lifted by introducing subtractions as discussed in [9] and the numerical problem of maximising the couplings is not sensitive to this. This is to be expected physically, since the low energy physics of bound state poles should not be much sensitive to the behaviour of the amplitudes at high energies.

To obtain a concrete numerical implementation to the problem, we proceed as follows. First, we define a dispersion grid $\{x_1, ..., x_M\}$ along the integration domains in (2.28-2.31). We then approximate the discontinuities $\mathrm{Im}M_{a\to b}(x^*)$ by splines $\sigma_{a\to b}(s)$ [6] linear in between the grid points up to a cutoff point x_M, after which we assume the discontinuities decay as $\mathrm{Im}M_{a\to b}(x^*) \sim 1/x^*$.[7] With this approximation we can analytically perform the integrals

[6] If $m_1 < m_2$, extended unitarity, equations (2.22-2.24), allows for $M_{22\to22}$ to diverge as $1/\sqrt{s-4m_1^2}$ close to the $4m_1^2$ threshold. Due to this, between the first two grid points, we approximate $\mathrm{Im}M_{22\to22} \propto 1/\sqrt{s-4m_1^2}$. If $m_1 > m_2$ we should replace $1 \leftrightarrow 2$ in this discussion.

[7] This is similar to the numerical implementation in [9]. We could have parametrised our amplitudes using the ρ variables defined in [10]. These variables provide a cleaner framework for the numerics but,

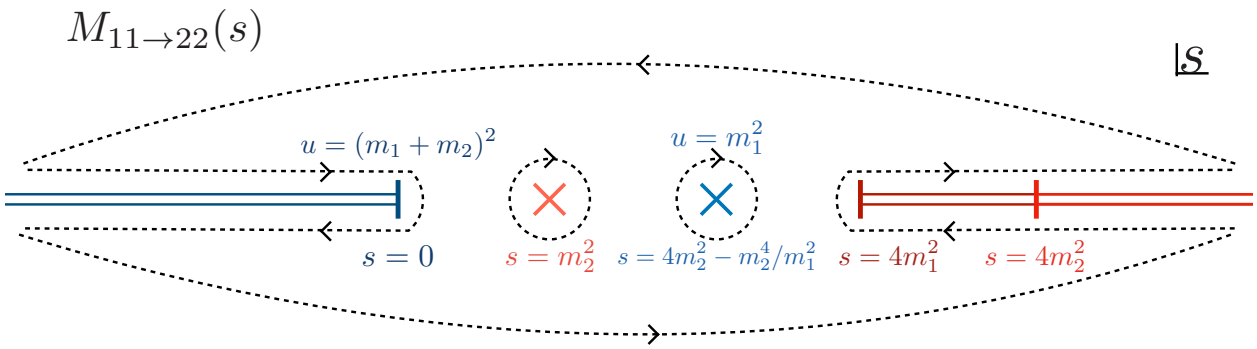

Figure 2.6: Analytic structure of $M_{11\to22}(s)$. According to the kinematics in equation (2.15), as we move in the s plane, we hit poles and two-particle (as well as multiparticle) thresholds in the s and u channel, but not in the t-channel. This is a consequence of our arbitrary definition of t and u (in the language of appendix A.1, this comes from choosing for each s a single point in the two-valued hyperbolas of figure A.2). To derive the dispersion (2.31) we start by assuming the amplitude approaches a constant at infinity (but see discussion in the main text) and write the identity $M_{11\to22}(s) = M_\infty + \frac{1}{2\pi i}\int_\gamma \frac{M_{11\to22}(s^*)-M_\infty}{s^*-s}\mathrm{d}s^*$, where γ is the dotted contour above. We can then neglect the arcs at infinity. The contribution from the arcs around the red singularities correspond to the s-channel pole and s^* integral in (2.31). After changing the integration variable in the remaining terms to $u^*(s^*)$ according to equation (2.15), we find the kernel transformation $\int_0^\infty \frac{\mathrm{d}s^*}{s^*-s} \to \int_{(m_1+m_2)^2}^\infty (\frac{1}{u^*-u}+\frac{1}{u^*-t})\mathrm{d}u^* + C_{11\to22}$, where we could relabel $u^* \to t^*$ in the second term. Then, after absorbing M_∞ into the constant $C_{11\to22}$ and using the crossing relation (2.20) and the discontinuity formula (2.21) for the pole terms, we obtain the dispersion relation (2.31).

in (2.28-2.31) obtaining, in the case $m_1 < m_2$ and for $M_{11\to11}$, as an example,

$$M_{11\to11}(s) \approx C_{11\to11} - \frac{g_{112}^2}{s-m_2^2} - \frac{g_{112}^2}{t(s)-m_2^2} + \sum_{i=1}^{M} \sigma_{11\to11}(x_i)(K_i(s)+K_i(t(s))), \quad (2.32)$$

where the functions K_i are defined in the appendix A of [9]. Next, we impose (2.27) along a fine grid over $s > \min\{4m_1^2, 4m_2^2\}$ (we impose analogous constraints over analogous ranges for the $\mathbb{Z}_2$ odd channels). Note that we leave for the computer to achieve saturation of (2.27) before the three-particles thresholds. As shown in appendix A.9, equation (2.27)is equivalent to the semidefiniteness constraint

$$\begin{pmatrix} \mathbb{I} & \rho\mathbb{M} \\ (\rho\mathbb{M})^\dagger & 2\mathrm{Im}\ \mathbb{M} \end{pmatrix} \succeq 0\,, \quad (2.33)$$

and a similar rewriting can be done for the $\mathbb{Z}_2$ odd sector. If we fix $\alpha = \frac{g_{222}}{g_{112}}$, as well as the masses, then the matrix in the l.h.s. of (2.33) is linear on the variables $\{C_{a\to b}, g_{112}^2, \sigma_{a\to b}(x_i)\}$. The problem of maximising g_{112}^2 in this space of variables under the positive semidefinite

in practice, we find that convergence with the ρ variables is much slower than with the use of discretized dispersion relations.

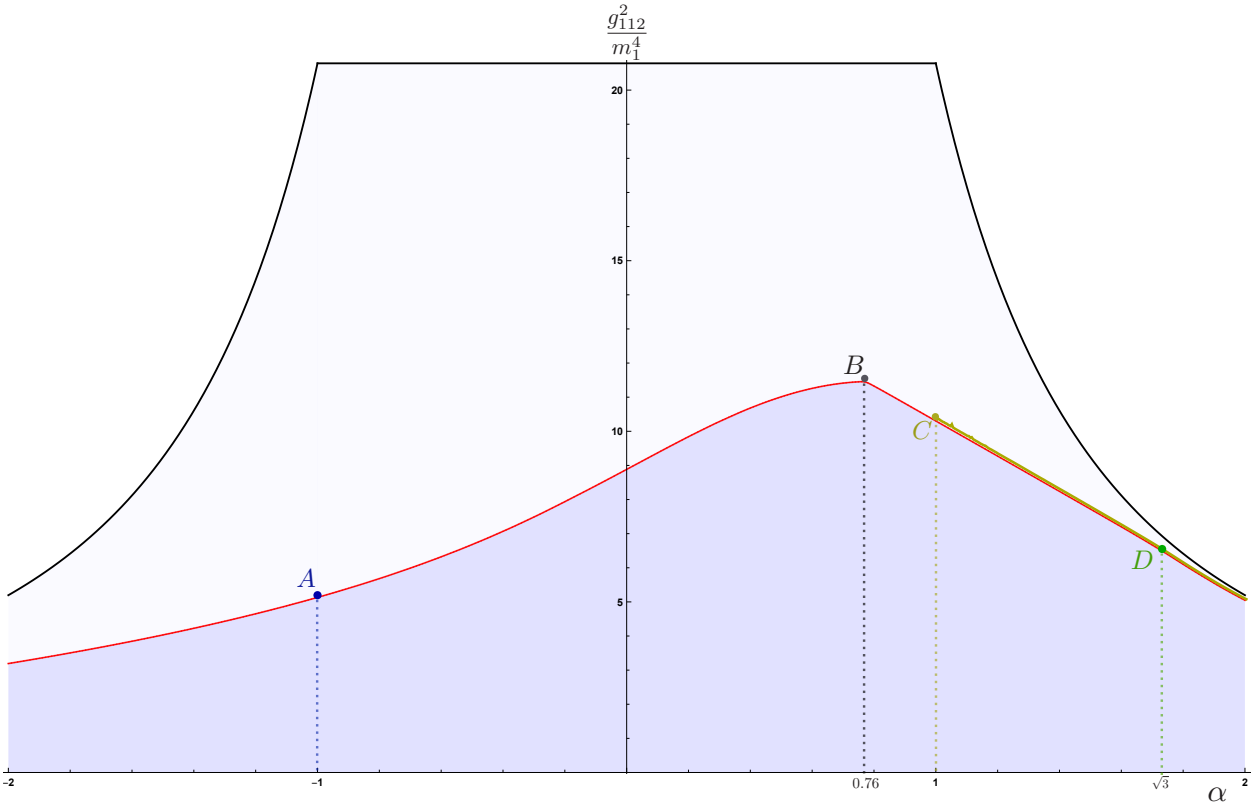

Figure 2.7: Maximum coupling g_{112} as a function of $\alpha = g_{222}/g_{112}$ for a $\mathbb{Z}_2$ symmetric theory with an odd and an even particle both with the same mass. Solid black: bounds from single amplitude analytics. Red: bounds from multiple amplitudes numerics. The interesting points A, B, C, D are discussed in more detail in the next section. Multiplying the α axis by g_{112} we convert this plot into a plot of the allowed coupling space (g_{112}, g_{222}), see figure 2.9.

constraint (2.27) (and equivalent for the $\mathbb{Z}_2$ odd sector) is therefore a semidefinite program and can be solved with, say, `SDPB` [112].

2.3.2 Results for any m_2/m_1

For each mass ratio m_2/m_1 and for each coupling ratio $\alpha \equiv g_{222}/g_{112}$ we can now look for the maximum value of g_{112}. By varying all parameters we obtain a nice 3D plot which is presented in appendix A.4; by contrast, in this section we will restrict ourselves to showing only 2D plots that each correspond to a fixed value of m_2/m_1. For example, at equal masses $m_2/m_1 = 1$ we have figure 2.7 which shows the upper bound as a function of α. Although holding α fixed is convenient for the numerics (as explained above), it is sometimes more useful to visualize the allowed space of couplings (g_{112}, g_{222}) instead. To do this we simply multiply the α axis in the numerics by g_{112}, and in this way we can represent the same $m_2/m_1 = 1$ data as in figure 2.9. Applying the same mapping to other mass ratios in

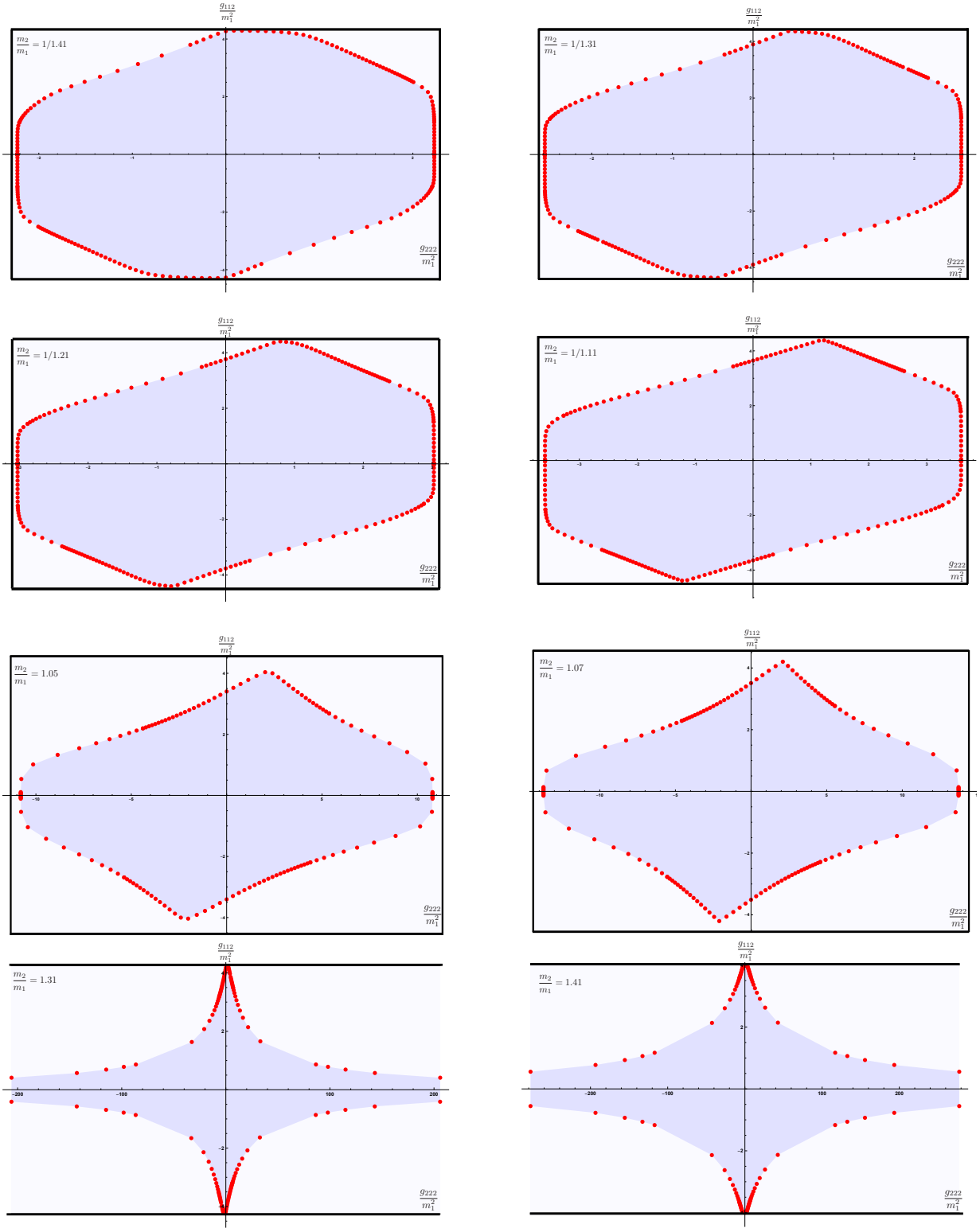

Figure 2.8: Space of allowed couplings for fixed mass ratios. *Horizontal and vertical solid lines:* Analytic bounds based on diagonal scattering derived in section 2.1. *Red dots:* The numeric bound obtained from *all* two-to-two processes. Features of the panels discussed in the main text.

the range $m_1/\sqrt{2} < m_2 < \sqrt{2}m_1$ we furthermore obtain the panels shown in figure 2.8. (As explained below, the results for $m_2 < m_1/\sqrt{2}$ are somehow trivial due to screening.) For the most part, the numerical bounds in these figures significantly improve the bounds single amplitude bounds derived in the introduction which set the box sizes.

The most remarkable feature of figures 2.7 and 2.8 is the existence of a pronounced maximum of g_{112}, which is attained for a non-trivial value of the ratio $\alpha = g_{222}/g_{112}$. In particular, for equal masses this maximum (point B in figure 2.7) is a clear kink in the boundary of the allowed region. It would be remarkable if there is a physical theory sitting close to this kink. As shown in figure 2.10, such a theory should not be integrable.

Sometimes the numerical red dots in figures 2.8 approach the solid black lines. When this happens the full numerical bounds saturate the analytically derived diagonal bounds. We see that this happens for very small g_{112}[8] and when we approach the boundaries of the mass range $m_1/\sqrt{2} < m_2 < \sqrt{2}$ (for some small values of α). This is not surprising: when $g_{112} \to 0$ we decouple the odd and even particles. Since there would be no poles in any amplitude but in $M_{22\to 22}$, the bound would reduce to the single amplitude bound coming from the $22 \to 22$ process and yielding

$$g_{222}^2|_{\max} = 12\sqrt{3}m_2^4 \qquad \text{for } m_2 < m_1 \text{ or} \tag{2.34}$$

$$g_{222}^2|_{\max} = 12m_1^4\mu^2\sqrt{3}\left(\frac{\mu^2\sqrt{3}+4\sqrt{\mu^2-1}}{\mu^2\sqrt{3}-4\sqrt{\mu^2-1}}\right) \qquad \text{for } \sqrt{2} > \mu \equiv m_2/m_1 > 1. \tag{2.35}$$

This explains the analytic bound in figure 2.3. In the second case, when we approach the boundary of the mass range, we expect screening to be very important since the extended unitarity region becomes quite large. The poles in the $M_{11\to 22}$ component can now be almost perfectly screened, see also appendix A.5.2, allowing for the diagonal amplitude bounds on g_{112} to be saturated. We omitted panels for $m_2 < m_1/\sqrt{2}$ since in this range we can have perfect screening for any value of g_{112}/g_{222}, so that the multiple amplitudes bounds in the (g_{112}, g_{222}) plane coincide with the rectangular frame derived from diagonal processes.

Note also that there are no vertical walls in the last row of panels in figure 2.8 since for $m_2 > \frac{2}{\sqrt{3}}m_1$ there are no longer analytic bounds on g_{222} from the $22 \to 22$ amplitude. As the extended unitarity region in $22 \to 22$ becomes bigger, it becomes increasingly more effective at screening the pole, until at $m_2/m_1 = 2/\sqrt{3}$ the s (t) channel $22 \to 11$ production threshold collide with the t (s) channel pole as discussed in figure 2.4. After this mass ratio, the discontinuity across the cut can completely screen the bound state pole implying that its residue can be arbitrary. This is indeed nicely backed up by our numerics as seen in the last two panels in figure 2.8 where we see that g_{222} becomes unbounded at this mass range.

Finally, we can also look for the maximum value of either coupling (g_{112} or g_{222}) leaving the other coupling arbitrary. In other words, how tall (g_{112}) and wide (g_{222}) are the darker allowed regions in (2.8) where the allowed coupling live. Once plotted for various mass

[8]The fact that the numerical points do not exactly touch the vertical lines in panels (a)-(d) in figure 2.8 when $g_{112} \simeq 0$ is due to numerical convergence. In that region it would be more sensible to ask for the computer to maximise g_{222} instead of g_{112}. This would lead to numerical saturation of the vertical lines.

ratios, this gives figures 2.2 and 2.3 in the introduction.

Each optimal S-matrix at the boundary of the allowed coupling space is numerically seen to *saturate* the extended unitarity equations (2.22-2.26). This means that the scattering of two particles of type 1 or 2 can never lead to multi-particle production. Processes such as $11 \to 222$ are forbidden. When dealing with 2D S-matrices, in particular extremal examples saturating unitarity such as the ones stemming from this numerical computation, we are commanded to look for integrable field theories. For $m_2 \neq m_1$, these are only possible if the inelastic amplitudes $M_{11\to 22} = M_{12\to 12}^{\text{Backward}} = 0$ but no S-matrices we found satisfy this condition[9] so the boundary S-matrices we find for $m_2 \neq m_1$ can at most be *close* to those describing good physical theories. This still leaves the possibility of finding interesting physical theories along the equal mass line $m_2 = m_1$.[10]

2.3.3 (Surprises at) the $m_2 = m_1$ line

Indeed, nice surprises are to be found in the $m_2 = m_1$ line depicted in the two equivalent figure 2.9 (depicting the space of allowed couplings) and figure 2.7 (for the maximum coupling g_{112} as a function of the coupling ratio $\alpha \equiv g_{222}/g_{112}$). Although equivalent these two figures highlight different aspects of this interesting line so it is worth having both in mind.

As concluded in the last section, the line $m_2 = m_1$ is where our hope lies if we are to match the S-matrices we obtained numerically with physical integrable theories. This necessary condition is *not* sufficient. For an extremal S-matrix to correspond to an integrable theory it should also obey the factorization conditions encoded in the so-called Yang-Baxter equations [113,114]. In figure 2.10 we see how our extremal S-matrices fail to satisfy these conditions as we move along the allowed coupling region (by sweeping α).

Before unveiling which analytic S-matrices we successfully identified along the $m_1 = m_2$ line let us go over these numerics in some detail: We observe that for large negative α Yang-Baxter is violated until we reach $\alpha = -1$ (i.e. when the couplings are equal up to a sign, $g_{222} = -g_{112}$) at which point Yang-Baxter is beautifully satisfied. This point is isolated; immediately to the right of $\alpha = -1$ Yang-Baxter fails again. It is curious to note that this special point – our first candidate for a physical integrable theory – marked with an A in figures 2.9 and 2.7 looks absolutely innocent there, without any apparent kink features. As we increase α further into positive values we reach point B for $\alpha \simeq 0.76$ where the coupling g_{112} is maximal. As seen in figures 2.9 and 2.7 this point is a nice kink. Since it does not obey Yang-Baxter, however, this can hardly correspond to a physical theory. As we increase α further we reach $\alpha = +1$ marked with a C in figures 2.9 and 2.7 where again something interesting happens. At that point something goes unstable as far as testing of Yang-Baxter goes indicated by the shower of points in figure 2.10 from $\alpha = 1$ until somewhere around $\alpha \simeq 1.2$. Once this mess settles we observe a nice line where Yang-Baxter is satisfied throughout! A particularly nice point along that line is point D

[9] This is not an accident, we knew this to be the case apriori since this could only happen if the bound state poles in these amplitudes collided and cancelled or if some extra Landau poles were present. This is not a possibility in the mass range (2.1).

[10] Actually, this line is a one-dimensional kink in the maximal coupling surface described in detail in appendix A.4.

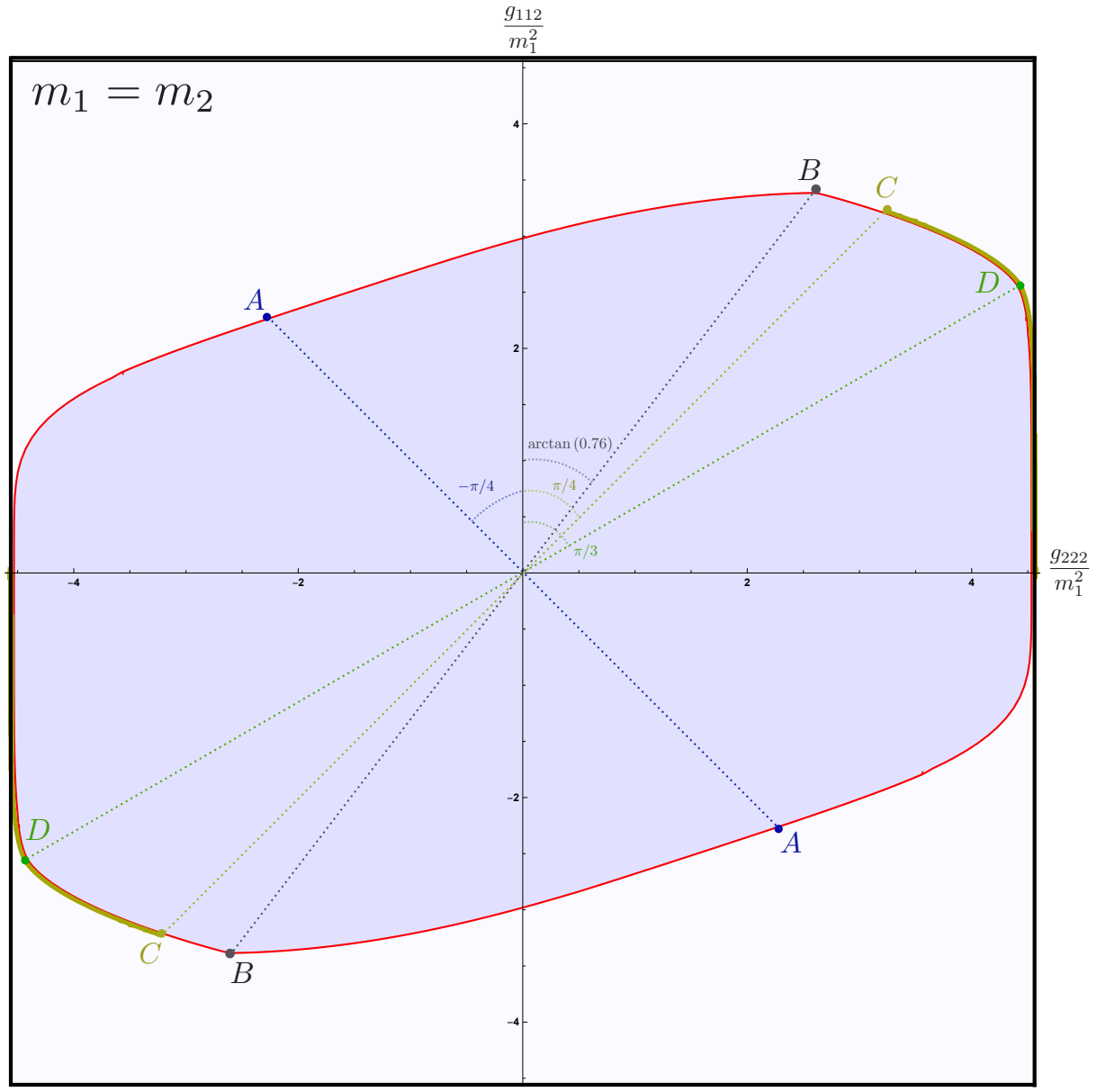

Figure 2.9: Allowed space of couplings for equal masses. A: Potts massive field theory, B: Maximum coupling g_{112}, C: Beginning of elliptic deformation line, D: Supersymmetric sine-Gordon (along the elliptic deformation line).

located at $\alpha = \sqrt{3}$. That point actually is the one furthest from the origin in figure 2.9, in other words, it maximizes $g_{112}^2 + g_{222}^2$ and as described below it corresponds to a nice known physical theory.

Now we unveil what we found about these points. In short (setting $m_1 = 1$ here):

- Point A is a massive deformation of the three state Potts Model.
  Here $g_{112}^{\max} = -g_{222}^{\max} = \sqrt{3\sqrt{3}} \simeq 2.28$.

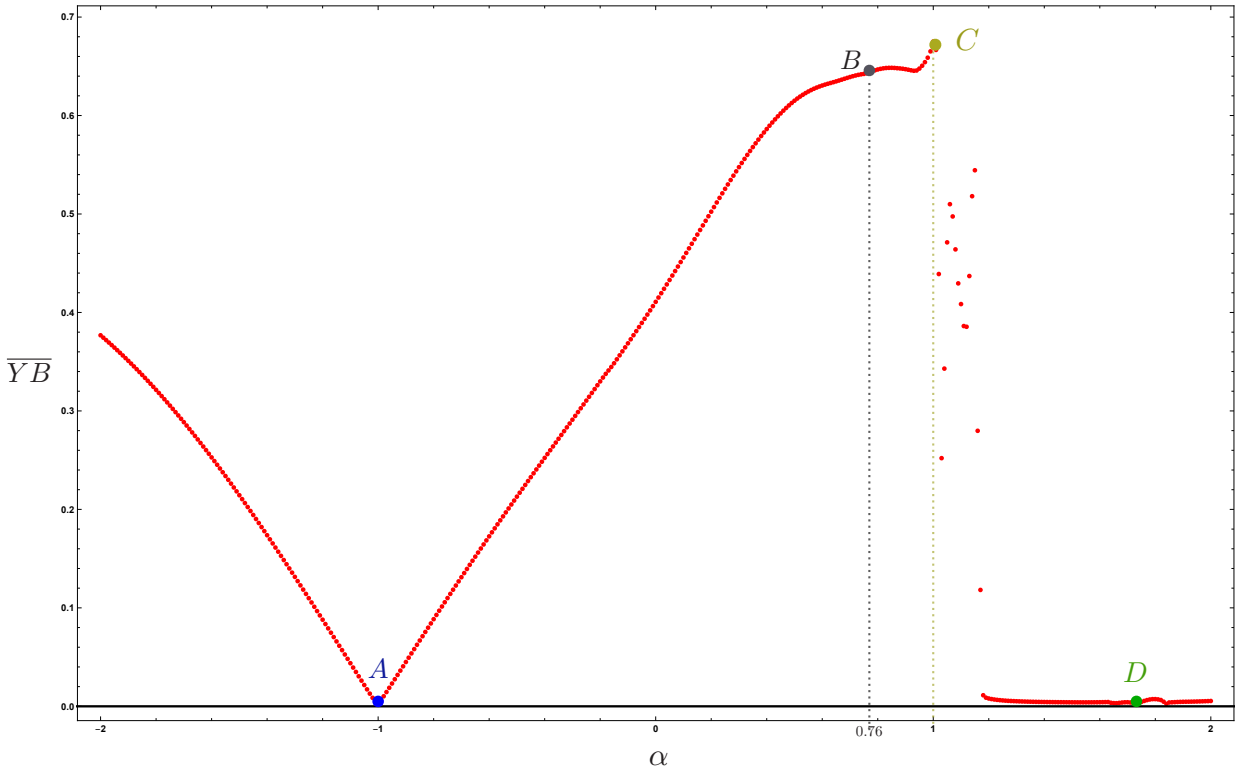

Figure 2.10: Because of $\mathbb{Z}_2$ symmetry, some Yang-Baxter equations are automatically satisfied. $\overline{YB}$ is an average over the non-trivial Yang-Baxter equations, with external rapidities at physical values. The qualitative features of the plot do not depend on averaging over the equations nor on the values of the external rapidities, taken here to be $\theta_1 = 1/2$, $\theta_2 = 0$, $\theta_3 = -1/3$. Once again, A: Potts massive field theory, B: Maximum coupling g_{112}, C: Beginning of elliptic deformation line, D: Supersymmetric sine-Gordon.

- Point B is yet to be identified. We do not know the analytic form of the corresponding S-matrix; Since it does not obey YB it can at most be close to a physical theory.

  Here $g_{112}^{\max} \simeq 1/0.76\, g_{222}^{\max} \simeq 3.38$.

- Point D is (an analytic continuation of the lightest breather S-matrix of) the super-symmetric Sine-Gordon model.

  Here $g_{112}^{\max} = -g_{222}^{\max} \simeq 2.56$.

- There is a line going from point C at $\alpha = 1$ all the way to $\alpha = \infty$ where the optimal S-matrix is given by an elliptic deformation of the super-symmetric Sine-Gordon. We are unaware of a physical theory with this S-matrix. Point C is the tip of the elliptic deformation where it becomes hyperbolic.

  Here $g_{112}^{\max} = -g_{222}^{\max} = \sqrt{6\sqrt{3}} \simeq 3.22$.

For comparison recall that the analytic diagonal bounds were $|g_{112}^{\max}| = |g_{222}^{\max}| = 4.56$.

We will now slowly build up towards those conclusions. The first observation, reviewed in appendix A.6, is that the full numerical optimization problem can actually be diagonalized and solved exactly for $\alpha = \pm 1$, that is when the two physical couplings are the same up to a sign. For $\alpha = -1$ the result is the S-matrix of the massive deformation of the three-state Potts model [115][11]

$$\begin{aligned} M_{11\to 11} = M_{22\to 22} = M_{12\to 12}^{\text{Forward}} =& 3m_1^4/(\sqrt{3}m_1^2 - \sqrt{(4m_1^2 - s)s}) - \sqrt{3}m_1^2 - 3\sqrt{(4m_1^2 - s)s} \\ M_{11\to 22} = -M_{12\to 12}^{\text{Backward}} =& \sqrt{3}(s - 2m_1^2)\sqrt{(4m_1^2 - s)s}/(\sqrt{3}m_1^2 - \sqrt{(4m_1^2 - s)s}) \,. \end{aligned} \tag{2.36}$$

From this solution we read off $g_{112} = -g_{222} = \sqrt{3\sqrt{3}}m_1^2$ which matches perfectly with point B in figures 2.9 and 2.7. In appendix A.7, we briefly review the 3 state Potts field theory.

As also explained in appendix A.6, the point $\alpha = +1$ is the other point where we can find a clever change of basis to diagonalize our problem and compute the maximal couplings analytically to find $g_{112} = +g_{222} = \sqrt{6\sqrt{3}}m_1^2$ which again matches perfectly with point C in figures 2.9 and 2.7. What we also observe in the process of deriving that analytic solution is that the S-matrix saturating this bound is not unique; there are zero modes. This is probably the explanation of the shower in figure 2.10. These zero modes are probably only present for $\alpha = +1$ but in the vicinity of this point there is probably still some small numerical remnant thereof. We thus expect the shower in figure 2.10 to be nothing but a zero-mode related numerical artifact; the true solution to the optimization problem probably obeys Yang-Baxter for any $\alpha > 1$. Yet, since this seems to be a zero mode issue, we expect the coupling as predicted by the numerics to still be correct. We will soon provide very strong evidence for these claims.

Point D for $\alpha = \sqrt{3}$ is a potentially interesting point if we interpret the $\mathbb{Z}_2$ symmetry as fermion number and think of particles 1 and 2 a Majorana fermion and a boson respectively. Then the condition $g_{222}/g_{112} = \sqrt{3}$ would follow for theories where these two particles are part of a $\mathcal{N} = 1$ supersymmetry multiplet, see also [2]. Inspired by this – and by [2] – we tried to compare the optimal S-matrices at $g_{222}/g_{112} = \sqrt{3}$ to those of the lightest breathers of the super-symmetric sine-Gordon theory.[12] Beautifully, although we only impose the

[11] Here we rotated the one particle basis from [115] as $|A\rangle = e^{i\pi/4}\frac{|2\rangle - i|1\rangle}{\sqrt{2}}$, $|A^\dagger\rangle = e^{-i\pi/4}\frac{i|2\rangle - |1\rangle}{\sqrt{2}}$, so that the charge conjugation operator is diagonalized. This operator is to be interpreted as the $\mathbb{Z}_2$ symmetry generator. In the $|A\rangle, |A^\dagger\rangle$ basis the S-matrix is diagonal and that is why we can solve this point exactly, see Appendix A.6.

[12] Strictly speaking we are comparing with an analytic continuation of that S-matrix since our bound-states have mass equal to the external particles while the next-to-lighests breathers of super-symmetric sine-Gordon have mass bigger than $\sqrt{2}$ times that of the external particles. In [9] the usual bosonic sine-Gordon S-matrix was identified as the theory with the largest coupling in the S-matrix of the lightest particle with a single bound-state of mass m_b. When $m_b > \sqrt{2}$ this is kosher but as $m_b < \sqrt{2}$ (and in particular for $m_b = 1$) we also need to extend the definition of the SG S-matrix beyond its original mass range. In that case it amounted to multiplying the S-matrix by -1. Here the situation is morally the same but the modification ends up a bit more complicated. This means that here – as there – we do not know a physical theory and we can only write an exact S-matrix that saturates the bound.

SUSY condition at the level of the couplings, we see that SUSY emerges at the level of the full S-matrix elements and indeed the optimal S-matrix saturating our bounds at point D is an analytical continuation of the lightest breather supermultiplet of the super-symmetric Sine-Gordon! Unfortunately, while we are able to check this to very convincing numerical accuracy we have no analytic derivation of this statement. For completeness, here are some super SG formulae [116].

The lightest breather supermultiplet SSG S-matrix $S_{SSG}^{(1,1)}(\theta)$ is equal to[13]

$$-\frac{\sinh(\theta)+i\sin(\gamma)}{\sinh(\theta)-i\sin(\gamma)}Y(\theta)Y(i\pi-\theta)\begin{pmatrix}\frac{i\sin(\gamma/2)}{\sinh\left(\frac{\theta}{2}\right)\cosh\left(\frac{\theta}{2}\right)}-1 & 0 & 0 & \frac{\sin(\gamma/2)}{\cosh\left(\frac{\theta}{2}\right)}\\ 0 & 1 & \frac{i\sin(\gamma/2)}{\sinh\left(\frac{\theta}{2}\right)} & 0\\ 0 & \frac{i\sin(\gamma/2)}{\sinh\left(\frac{\theta}{2}\right)} & 1 & 0\\ \frac{\sin(\gamma/2)}{\cosh\left(\frac{\theta}{2}\right)} & 0 & 0 & \frac{i\sin(\gamma/2)}{\sinh\left(\frac{\theta}{2}\right)\cosh\left(\frac{\theta}{2}\right)}+1\end{pmatrix}$$

where

$$Y(\theta)=\frac{\Gamma(-i\theta/2\pi)}{\Gamma(1/2-i\theta/2\pi)} \tag{2.37}$$
$$\times\prod_{n=1}^{\infty}\frac{\Gamma(\gamma/2\pi-(i\theta/2\pi)+n)\,\Gamma(-\gamma/2\pi-(i\theta/2\pi)+n-1)\,\Gamma^2(-(i\theta/2\pi)+n-1/2)}{\Gamma(\gamma/2\pi-(i\theta/2\pi)+n+1/2)\,\Gamma(-\gamma/2\pi-(i\theta/2\pi)+n-1/2)\,\Gamma^2(-(i\theta/2\pi)+n-1)}.$$

and where γ is fixed so that the bound state mass is equal to 1. That is $\gamma=2\pi/3$. Note that even though the overall scalar factor in the S-matrix is invariant under $\gamma=2\pi/3\leftrightarrow\gamma=\pi/3$, the matrix part is not. This is the sense in which our S-matrix is an analytic continuation of SSG. (compare with SG, in which picking $m_b=1$ instead of $m_b=\sqrt{3}$ only leads to an overall minus sign). More generally $m_b/m_1=2\cos\gamma/2$ and the physical mass range for SSG is $2>m_b>\sqrt{2}$.

Two-particle $\mathbb{Z}_2$ symmetric solutions of the Yang-Baxter equations are classified [117]. It is natural that if an extension of SSG exists with an extra parameter, that it is given by an elliptic solution of the Yang-Baxter equations. In fact, examining the classified solutions we see that the only good candidate for being promoted to an S-matrix with all the symmetry properties we have and that reduces to SSG in the trigonometric limit is solution 8VII of [117], which is equivalent to

$$\mathbf{ED}(\theta)\equiv\begin{pmatrix}\epsilon\frac{\mathrm{dn}(\theta\omega|\kappa)\mathrm{sn}(\gamma\omega|\kappa)}{\mathrm{cn}(\theta\omega|\kappa)\mathrm{sn}(\theta\omega|\kappa)}-\mathrm{dn}(\gamma\omega|\kappa) & 0 & 0 & \epsilon\frac{\mathrm{dn}(\theta\omega|\kappa)\mathrm{sn}(\gamma\omega|\kappa)}{\mathrm{cn}(\theta\omega|\kappa)}\\ 0 & 1 & \epsilon\frac{\mathrm{sn}(\gamma\omega|\kappa)}{\mathrm{sn}(\theta\omega|\kappa)} & 0\\ 0 & \epsilon\frac{\mathrm{sn}(\gamma\omega|\kappa)}{\mathrm{sn}(\theta\omega|\kappa)} & 1 & 0\\ \epsilon\frac{\mathrm{dn}(\theta\omega|\kappa)\mathrm{sn}(\gamma\omega|\kappa)}{\mathrm{cn}(\theta\omega|\kappa)} & 0 & 0 & \mathrm{dn}(\gamma\omega|\kappa)+\epsilon\frac{\mathrm{dn}(\theta\omega|\kappa)\mathrm{sn}(\gamma\omega|\kappa)}{\mathrm{cn}(\theta\omega|\kappa)\mathrm{sn}(\theta\omega|\kappa)}\end{pmatrix}, \tag{2.38}$$

where we normalised by the $12\to12$ forward component so that comparison with SSG is

[13] In the basis $|11\rangle,|12\rangle,|21\rangle,|22\rangle$ so that the second (third) element on the second row is the forward (backward) $12\to12$ component, for instance.

easier. $\epsilon = \pm 1$ from YB. The s-channel poles of $12 \to 12$ forward and backward correspond to the flow of a particle of type one, and therefore the residues of this two amplitudes at the $\theta = 2\pi i/3$ pole must coincide. This fixes $\epsilon\,\mathrm{sn}(\gamma\omega|\kappa) = \mathrm{sn}(\frac{2\pi i}{3}\omega|\kappa)$. Crossing symmetry together with the fact that in the trigonometric limit $\kappa \to 0$ we have to recover SSG fix $\omega = -\frac{i}{\pi}K(\kappa)$ where K is the complete elliptic integral of the first kind (more precisely, crossing gives $\omega = -\frac{i}{\pi}(2n+1)K(\kappa)$ with n an integer. The $\kappa \to 0$ limit fixes n). This completely fix a crossing symmetric matrix structure up to one free parameter, κ, which hopefully is unconstrained. There is a miracle going on. For our amplitudes, we have that

$$\operatorname*{res}_{\theta=2\pi i/3} M_{22\to 22} \operatorname*{res}_{\theta=2\pi i/3} M_{11\to 11} = \left(\operatorname*{res}_{\theta=2\pi i/3} M_{11\to 22}\right)^2 \tag{2.39}$$

and, moreover,

$$\operatorname*{res}_{\theta=2\pi i/3} M_{11\to 11} = \operatorname*{res}_{\theta=2\pi i/3} M^{\text{Forward}}_{12\to 12} \tag{2.40}$$

If (2.38) is a candidate of matrix structure of the S-matrices saturating the numerical bounds, we must have the same relation between the respective components. It turns out that this holds automatically for any κ after all the conditions above are imposed. Otherwise this would fix $\kappa = 0$ and we would conclude that there are no Yang-Baxter deformations respecting the symmetries and spectrum of our problem. So all we need to do now is to unitarize and introduce the poles. Note that

$$\mathbf{ED}\,(\theta)\,\mathbf{ED}\,(-\theta) = \left(1 - \frac{\mathrm{sn}\left(\frac{2K(\kappa)}{3}\middle|\,\kappa\right)^2}{\mathrm{sn}\left(\frac{i\theta K(\kappa)}{\pi}\middle|\,\kappa\right)^2}\right)\mathbb{I} \equiv g\,(\theta)\,\mathbb{I} \tag{2.41}$$

and $g(\theta) \geq 1$ for $\theta \in \mathbb{R}$. Therefore, as follows from [9], to unitarize **ED** we just need to multiply it by

$$U(\theta) = -i\sinh(\theta)\exp\left(-\int_\infty^\infty \frac{d\theta'}{2\pi i}\frac{\log\left(g^{-1}(\theta')/\sinh(\theta')\right)}{\sinh\left(\theta-\theta'+i\epsilon\right)}\right), \tag{2.42}$$

while to introduce the poles, we multiply by $\mathrm{CDD}_{\text{pole}}$ with direct channel pole at $2\pi i/3$,

$$\mathrm{CDD}_{\text{pole}}(\theta) = \frac{\sinh(\theta) + i\sin(2\pi/3)}{\sinh(\theta) - i\sin(2\pi/3)} \tag{2.43}$$

At the end of the day, a candidate for a unitary, crossing symmetric, integrable deformation of the supersymmetric sine-Gordon reads

$$\mathbb{S}_{\mathbf{ED}}(\theta) = -\mathrm{CDD}_{\text{pole}}(\theta)\,U(\theta)\mathbf{ED}\,(\theta) \tag{2.44}$$

Points D and C with $\alpha = \sqrt{3}$ and $\alpha = 1$ would now correspond to $\kappa \to 0$ and $\kappa \to 1$ respectively. As $\kappa \to -\infty$, $\alpha \to \infty$. We can now compute the couplings associated to the elliptic deformation (2.44), cross our fingers and compare those couplings with the numerics

of figures 2.9 and 2.7. The elliptic deformation analytic results are the solid chartreuse[14] lines in those figures. The agreement could not be better. Note that the agreement goes all the way to point C and since by construction the elliptic solution obeys Yang-Baxter, the shower in figure 2.10 should indeed be a simple zero-mode related numerical artifact. To make precise the elliptic notation used here, we present in appendix A.10 a representation of this S-matrix in Mathematica friendly notation, ready to be copy pasted so the reader can more easily explore this exotic solution.

An obvious question is whether this elliptic deformation corresponds to a nice physical theory.[15] Since the supersymmetric sine-Gordon we encountered here is not a totally kosher theory but an analytic continuation thereof, it is natural to first extend this analysis to the mass range were the super-sine Gordon breather lives and to study its elliptic deformation for those more physical set of parameters. This is investigated in chapter 3.

The $m_2 = m_1$ line was indeed full of surprises.

2.4 QFT in AdS

In the previous section we have numerically explored the space of scattering amplitudes that allow for a Mandelstam representation and we found examples of amplitudes that appear to maximize couplings subject to the unitarity constraints. These extremal coupling constants are not true 'upper bounds': although our numerical results appear to have converged, a numerically more refined ansatz will find slightly larger values. See also chapter 4 for an S-matrix resolution to this issue.

An orthogonal approach to the extremization of three-point couplings in field theories was developed in [104]. The idea is to consider a field theory in an AdS background and investigate the 'boundary' correlation functions that are so familiar from the AdS/CFT correspondence. In our setup gravity is non-dynamical and this translates into the absence of a stress tensor among the set of boundary operators. Nevertheless it is natural to claim [104] that these correlation functions obey all the other axioms of a unitary CFT, including crossing symmetry, making them amenable to a numerical bootstrap analysis as in [105]. In this way any general constraints on CFT data directly imply corresponding constraints for QFTs in AdS, and by extrapolating these results to the *flat-space limit* we can get constraints on flat-space QFTs as well. (For a gapped QFT in AdS_2 scaling dimensions and masses are related as $m^2R^2 = \Delta(\Delta - 1)$ and therefore the flat-space limit is typefied by sending all scaling dimensions $\Delta \to \infty$ whilst keeping ratios fixed, $\Delta_i/\Delta_j \to m_i/m_j$.)

The QFT in AdS approach uses CFT axioms to provide rigorous upper bounds, at least modulo our extrapolation procedures. It does not assume analyticity or any particular behavior at large complex energies, and the unitarity constraints are phrased in terms of reflection positivity rather than in terms of probabilities. And yet it was shown in [104] that it provides upper bounds on flat-space couplings that are numerically *equal* (up to three significant digits in some cases) to the extremal couplings obtained with the S-matrix

[14] Chartreuse, of selcouth beauty, is a colour half-way between yellow and green.

[15] We thank Davide Gaiotto for illuminating discussions on related topics.

bootstrap methods. In this section we demonstrate that this striking equivalence was not just a fluke by employing once more the QFT in AdS approach to reproduce some of the previous S-matrix bootstrap results from conformal crossing equations.

2.4.1 Setup

We will consider four-point functions of operators on the real line, which we think of as the boundary of an AdS_2 space with curvature radius R. There are two distinguished operators ϕ_1 and ϕ_2 of dimensions Δ_1 and Δ_2, which correspond to the two single-particle states of the setup described above – in particular it is understood that $\Delta_i(\Delta_i - 1) = m_i^2 R^2$ for $i = 1, 2$. Besides the assumed $\mathbb{Z}_2$ symmetry, under which ϕ_1 is odd and ϕ_2 is even, we will also assume that the QFT is parity invariant and that ϕ_1 and ϕ_2 are both parity even.[16] The OPEs are, schematically,

$$\begin{aligned}
\phi_1 \times \phi_1 &= \mathbf{1} + \lambda_{112}\phi_2 + (\text{parity and } \mathbb{Z}_2 \text{ even operators with } \Delta \geq 2\text{min}(\Delta_1, \Delta_2)) \\
\phi_2 \times \phi_2 &= \mathbf{1} + \lambda_{222}\phi_2 + (\text{parity and } \mathbb{Z}_2 \text{ even operators with } \Delta \geq 2\text{min}(\Delta_1, \Delta_2)) \\
\phi_1 \times \phi_2 &= \lambda_{112}\phi_1 + (\text{any } \mathbb{Z}_2 \text{ odd operators with } \Delta \geq \Delta_1 + \Delta_2)
\end{aligned} \tag{2.45}$$

Here the (non-)appearance of ϕ_1 and ϕ_2 on the right-hand sides is dictated by $\mathbb{Z}_2$ symmetry. The other operators are meant to correspond to multi-particle states for the QFT in AdS and their minimal scaling dimension mimicks the beginning of the two-particule cuts in the corresponding scattering amplitudes. The parity properties are dictated by the parity of the operators on the left-hand side. We should add that the OPE coefficients λ_{ijk} are related to bulk couplings g_{ijk} via

$$g_{123}/m_0^2 = \lambda_{123} C(\Delta_0; \Delta_1, \Delta_2, \Delta_3) \tag{2.46}$$

with the unsightly relative normalization coefficient [118]

$$C(\Delta_0; \Delta_1, \Delta_2, \Delta_3) = \frac{\pi 2^{4-\Delta_1-\Delta_2-\Delta_3}\sqrt{\Gamma[2\Delta_1]\Gamma[2\Delta_2]\Gamma[2\Delta_3]}}{\Delta_0^2\Gamma[\Delta_{123}/2]\Gamma[\Delta_{231}/2]\Gamma[\Delta_{312}/2]\Gamma[(\Delta_1+\Delta_2+\Delta_3-1)/2]} \tag{2.47}$$

where $\Delta_{ijk} = \Delta_i + \Delta_j - \Delta_k$. This relation was explained in [104].

In one dimension conformal transformations preserve operator ordering modulo cyclic permutations. This leads to the following non-equivalent four-point functions

$$\langle\phi_1\phi_1\phi_1\phi_1\rangle, \qquad \langle\phi_2\phi_2\phi_2\phi_2\rangle, \qquad \langle\phi_1\phi_1\phi_2\phi_2\rangle, \qquad \langle\phi_1\phi_2\phi_1\phi_2\rangle, \tag{2.48}$$

and we will numerically analyze the lot of them.[17] Our recipe follows that of [104] with

[16] It is often helpful to think of the parity odd operators as vectors. Indeed, they are equivalent in one dimension because the rotation group is reduced to the parity group $\mathbb{Z}_2$ and which has only one non-trivial irreducible representation.

[17] An interesting observation is that the $\langle\phi_1\phi_2\phi_1\phi_2\rangle$ correlator does not feature the identity operator. A conformal bootstrap analysis of this correlator *in itself* therefore does not give any bounds whatsoever because it lacks an overall normalization. This is completely different from the forward $12 \to 12$ amplitude which we have seen can give a meaningful bound on g_{112}. However we will shortly see that the ensemble

minor variations. Suppose that we wish to obtain a bound on g_{112}^2 (in units of m_1) for a given coupling ratio $\alpha = g_{222}/g_{112}$ and mass ratio $\mu = m_2/m_1$. We then proceed as follows:

1. Choose a Δ_1. Then set $\Delta_2 = \mu\Delta_1$ and also fix the ratio

$$\frac{\lambda_{222}}{\lambda_{112}} = \alpha \frac{C(\Delta_1;\Delta_1,\Delta_1,\Delta_2)}{C(\Delta_1;\Delta_2,\Delta_2,\Delta_2)}\,. \tag{2.49}$$

2. A single conformal bootstrap analysis of the four correlators listed above now yields a numerical upper bound on λ_{112}^2. Our multi-correlator bootstrap analysis is very similar to the one introduced in [108] where it was successfully applied it to the three-dimensional Ising model. The systematics of our analysis (normalizations, conformal block decompositions, functionals) can be found in appendix A.11. The bound so obtained also depends on the *number* of derivatives of the crossing equations that we analyze and this introduces a new parameter Λ, so we write

$$(g_{112}^2)^{\max}[\mu,\alpha,\Delta_1,\Lambda] \tag{2.50}$$

   where we use (2.46) to pass from $(\lambda_{112}^2)^{\max}$ to $(g_{112}^2)^{\max}$.

3. Upon repeating step 2 for various Λ one finds that $(g_{112}^2)^{\max}$ depends significantly on Λ. To obtain an estimate of the bound that we would obtain if we could analyze all the crossing equations, *i.e.*, if we possessed infinite computational resources, we extrapolate the results for various Λ to estimate

$$\lim_{\Lambda\to\infty} (g_{112}^2)^{\max}[\mu,\alpha,\Delta_1,\Lambda] \tag{2.51}$$

   In practice we do this by fitting a polynomial through data points ranging from $\Lambda = 32$ up to $\Lambda = 140$.[18] Examples of this extrapolation are shown in figure A.13 on page 212. This limit provides our estimate for the best possible upper bound for a QFT in AdS with two particles with masses determined by Δ_1 and μ and bulk coupling constant ratio given by α.

4. We view Δ_1 as a proxy for the AdS curvature radius. We therefore repeat steps 1 to 3 for a number of different values of Δ_1 and once more extrapolate to infinite Δ_1 to obtain a result on the flat-space coupling:

$$(g_{112}^2)^{\max}(\mu,\alpha) = \lim_{\Delta_1\to\infty}\left\{\lim_{\Lambda\to\infty}(g_{112}^2)^{\max}[\mu,\alpha,\Delta_1,\Lambda]\right\} \tag{2.52}$$

   This is the coupling we can compare with the flat-space S-matrix bootstrap analysis.

Appendix A.11.5 contains technical details of the extrapolation procedure.

of correlators does give numerical results that mostly agree with the ensemble of amplitudes.

[18] In [104] we were able to obtain results up to $\Lambda = 200$ or $\Lambda = 300$ for the different scenarios. The multi-correlator analysis of this chapter is numerically more demanding, even more so because the rho series expansion [119] for conformal blocks with large unequal dimensions converges much more slowly.

For finite Λ and Δ our results provide rigorous upper bounds on the three-point couplings for any QFT in AdS that obeys the stated assumptions. Once we begin the extrapolations we introduce errors that are hard to quantify and this is an unavoidable drawback of our method. Nevertheless we will soon see, as was the case in [104], that the extrapolated bounds appear to accurately reproduce the S-matrix bootstrap results in most cases.

2.4.2 Results

The numerical algorithm outlined above is computationally demanding. For a single μ and α we need about 10 different values of Δ_1 and for each of these we need about 15 different values of Λ, implying about 150 multi-correlator bootstrap runs. We have therefore chosen a few representative values of μ and α to demonstrate both the feasibility of the multi-correlator conformal bootstrap approach to scattering processes and the match with the flat-space S-matrix bootstrap results.

Results for equal masses

Our first plot is for $\mu = 1$ so we have two particles of equal masses. In figure 2.11 we overlay the QFT in AdS results (isolated data points) with the S-matrix bootstrap region shown before in figure 2.9. The black frame again indicates the single-amplitude bounds, which are in fact equal to the single-*correlator* bounds found in [104]. We have performed a multi correlator QFT in AdS analysis for ratios $\alpha = g_{222}/g_{112}$ equal to $+1$, 0, -1 and $-8/3$ and in all cases we find reasonably good agreement with the multiple amplitude S-matrix bootstrap result. For $\alpha = -8/3$ our bound comes out somewhat higher than the value reached by the S-matrix bootstrap. This might be due to our extrapolation procedure, which also makes it difficult to put error bars on the QFT in AdS points, but it might also be a consequence of the finite truncation level in the S-matrix bootstrap. It is of course reassuring that the S-matrix bootstrap always gives lower values than the conformal bootstrap.

For the ⊙ data points in figure 2.11 the extrapolation is standard, *i.e.*, as outlined above and elaborated on in appendix A.11, but the ◬ data point requires a comment. In that case we found that the maximal squared coupling $(g^2_{112})^{\max}[\mu, \alpha, \Delta_1, \Lambda]$ from the multi-correlator analysis is always numerically equal to one half of the corresponding maximal squared coupling obtained from the single-correlator analysis – even for finite Δ_1 and Λ so before any extrapolations. Therefore, rather than doing a detailed multi-correlator analysis, we just plotted one half the single-correlator result. This factor of one half is understandable: using a change of operator basis similar to the one described in appendix A.6, one finds that the multi-correlator problem effectively becomes that of two decoupled single-correlator problems which each feature a squared coupling that is rescaled by a factor 2.[19]

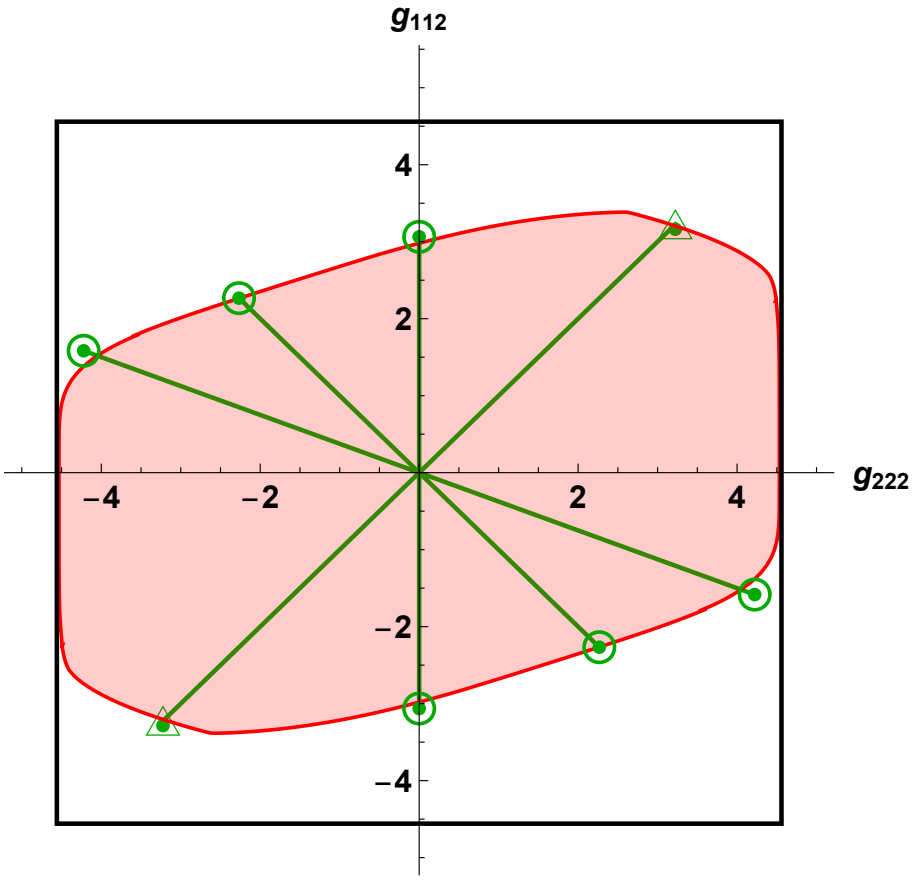

Figure 2.11: Overlaid on a repetition of figure 2.9, the green data points show the maximal values of $|g_{112}|$ as derived from the QFT in AdS analysis for fixed values of $\alpha = g_{222}/g_{112}$. (The green straight lines then indicate the allowed range in coupling space.) The conformal bootstrap agrees very well with the S-matrix bootstrap. The point with $\alpha = -1$ is point A in figure 2.9 which corresponds to the 3-state Potts model, which 'emerges' here from the conformal crossing equations in one dimension.

Results for $\alpha = -1$

Our next result is shown in figure 2.12, where we have assumed $g_{222}/g_{112} = -1$. We will discuss in turn the black curve, the red shaded region, and the green (new) data points.

The black curve corresponds to the best single-correlator bound for the given mass ratio. It is actually made up of two parts: for $m_2 > m_1$ it is the bound obtained from the $\langle 1111 \rangle$ four-point function, whereas for $m_2 < m_1$ it is the bound obtained from the $\langle 2222 \rangle$ four-point function. These single-correlator bounds were already obtained in [104] and were shown to agree with the single-amplitude analysis of [9].

In red we show the multi-amplitude results obtained with the methods discussed in section 2.3.1. It is again made up of different parts: for $1/\sqrt{2} < m_2/m_1 < \sqrt{2}$ we can use the numerical analysis and we take the $\alpha = -1$ slice from figure A.3. For $m_2/m_1 < 1/\sqrt{2}$

[19] It is essential here that $\alpha = 1$ so $\lambda_{222} = \lambda_{112}$.

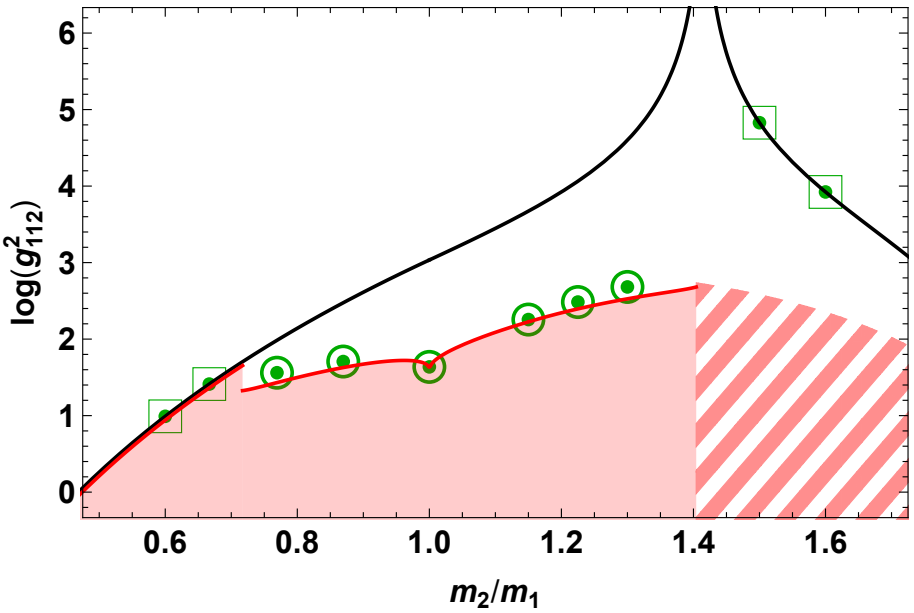

Figure 2.12: The green data points show the maximal values of $\log(g^2_{112})$ provided by the multi-correlator QFT in AdS analysis, now for $\alpha = g_{222}/g_{112} = -1$ and as a function of the mass ratio m_2/m_1. For comparison we have also added the single-correlator QFT in AdS bounds from [104], as solid lines, as well as the S-matrix bootstrap data, in red. The plot naturally splits into three regions. First of all, for $m_2/m_1 < 1/\sqrt{2}$ there is screening and the multi-amplitude bound reduces to the single-amplitude bound. As shown, the correlator bounds nicely follow this behavior. Moving rightward, for $1/\sqrt{2} < m_2/m_2 < \sqrt{2}$ we find a respectable match between the multi-correlator and the multi-amplitude data, in particular we again recover the three-state Potts field theory at $m_2 = m_1$. For $\sqrt{2} < m_2/m_1$ there are Landau singularities and the multi-amplitude analysis becomes complicated. However we know that the multi-amplitude bound must lie at or below the single-amplitude bound from $S^{\text{forward}}_{12\to 12}$, meaning that it must end up somewhere in the striped region. The multi-correlator analysis, on the other hand, appears unable to improve on the weaker $\langle 1111\rangle$ single-correlator bound.

we have screening and the multiple amplitude analysis does not give stronger results than the analysis of the single amplitude $S_{22\to 22}$ which, as we stated before, agrees with the $\langle 2222\rangle$ single-correlator bound. For $\sqrt{2} < m_2/m_1$ there are Landau singularities and a more sophisticated analysis is necessary to obtain multiple amplitude results, but we do know that the maximal coupling from the multiple amplitude analysis can only lie below the single amplitude bounds. In particular, it must lie below the bound obtained from $S^{\text{forward}}_{12\to 12}$, which was given as the solid line in figure 2.2 in the introduction and here yields the striped region in figure 2.12.[20]

Finally, the new data points obtained from the multi-correlator conformal bootstrap are indicated in green. The ⊙ data points are obtained from a standard extrapolation, as before, whereas for the ⊡ data points the numerical multi-correlator analysis gave identical

[20]We explain in appendix A.12 that Landau singularities do not appear in $M^{\text{forward}}_{12\to 12}$ for any mass ratio in the range $0 < m_2/m_1 < 2$, so the corresponding single-amplitude bound should be perfectly valid.

results to the numerical single-correlator analysis for all Δ and Λ. The extrapolation will therefore trivially equal the single-correlator result as is indicated in the plot.

For all points with $m_2/m_1 < \sqrt{2}$ our extrapolated QFT in AdS results lie at or just above the S-matrix results. As for the previous plot, the small finite difference might be either due to our extrapolation procedure but also due to the S-matrix bootstrap results not yet having converged. The points with $m_2/m_1 > \sqrt{2}$ are more puzzling. The striped domain, as we mentioned, arises from an analysis of $S^{\text{forward}}_{12\to 12}$ alone and so a multi-amplitude analysis (with Landau singularities and all) will only be able to land somewhere in that domain. Unfortunately this single-amplitude bound does not seem to be picked up by the multi-correlator analysis at all.[21] It would be nice to know why this is the case: are we missing constraints to be imposed for the QFT in AdS bootstrap?[22] Alternatively, is there maybe a 'phase transition' where by pushing to a very high number Λ of derivatives the single- and multi-correlator analysis begin to differ? Such a phenomenon would obviously invalidate our large Λ extrapolations and might therefore resolve the puzzle. It would be somewhat analogous to the observations discussed in appendix A.11.4, see in particular figure A.12, where we explain that taking different Λ's for different crossing equations leads to non-smooth behavior.

Of course, as we mentioned at the beginning of this section, at a technical level the conformal bootstrap analysis looks completely different from the S-matrix bootstrap. We are confident that both analyses yield valid constraints on three-point couplings, but besides physical intuition there was no a priori guarantee that these constraints had to be exactly the same. From this perspective the aspect most in need of an explanation in figure 2.12 is the quantitative *match* between the results for $m_2/m_1 < \sqrt{2}$ (and similarly for all points in figure 2.11 and the results of [104]) rather than the discrepancy in the other points. Either way, the precise connection between conformal correlators and scattering amplitudes warrants further investigation.

2.5 Discussion

We have demonstrated the feasibility of the multiple-amplitude bootstrap for the lightest two particles, and shown that it gives stronger bounds compared to the simpler S-matrix bootstrap of only the lightest particle. Clearly one expects to get increasingly stronger bounds by considering more and more scattering processes. It is interesting to consider how such results could converge to an 'optimal bound' that we would obtain by considering the entire S-matrix, as follows.

In all our numerical experiments it turns out that the unitarity condition at all energies is (numerically) *saturated* in the subspace we work on. To illustrate this, consider for example the various possible outcomes from scattering the lightest particle in our setup –

[21] See also footnote 17.

[22] At least the multi-correlator result, which is a hard upper bound, is above or equal to the S-matrix bootstrap results in all cases, so the results are not in direct conflict with each other.

let us say that it is the $\mathbb{Z}_2$ odd particle – against itself. Probabilities must add up to 1 so

$$1 = \underbrace{\overbrace{|S_{11\to 11}|^2}^{\geq 0}}_{\leq 1} + \underbrace{\overbrace{|S_{11\to 22}|^2}^{\geq 0}}_{\leq 1} + \underbrace{\overbrace{|S_{11\to 112}|^2}^{\geq 0}}_{\leq 1} + \overbrace{|S_{11\to 1111}|^2}^{\geq 0} + \dots \,. \tag{2.53}$$

where the red and blue inequalities follow trivially from probability positivity as indicated in dark green. In [9] we effectively considered only the weakest red inequality. The theories which lie on the boundary of this space turn out to saturate this inequality for all energies. This would mean that any other process has zero probability, and a theory saturating the bounds of [9] must therefore have zero particle creation or transmutation since the only allowed process is elastic scattering. This is possible for special cases like integrable theories, but generically it cannot be the case. Therefore, by including also the constraints of the other processes we should get better bounds and this is indeed what we have observed in this chapter: our improved bounds are due to the stronger constraint given by the lower blue inequality.

However, we once more found that the *optimal* solutions now saturate this *new* condition for all values of the energy, so the remaining processes for the extremal S-matrix are again all zero.[23] In other words, theories lying on the boundary of the new space are theories where particles 11 can continue into 11 or transmute into 22 but we still get zero probability for all other processes that have a different final-state particle content. We expect this pattern to continue by including more and more processes in the game, *i.e.* we will continue to observe unitarity saturation within the subspace we consider, no matter how large. As we increase the size of our truncation we will hopefully asymptotically approach an optimal bound, but we are unlikely to hit a non-integrable theory at our boundary if we consider only a finite number of processes.

Indeed, for our setup with two particles with mass m_1 and m_2 we find no integrable theories if the masses are different, whereas if they are equal then there are exciting physical theories at our boundary: the three-states Potts model and (an analytic continuation of) the super-symmetric sine-Gordon model. We also find a full segment around the supersymmetric sine-Gordon theory which seems to obey all the necessary factorisation requirements to be an integrable theory; it would be very interesting to see if that is the case.

We also discussed how the same bootstrap results can be obtained from AdS, using the setup first discussed in [104]. Putting a gapped $\mathbb{Z}_2$ symmetric theory into an AdS box induces a one dimensional $\mathbb{Z}_2$ symmetric conformal theory in its boundary which we can analyze by numerical conformal bootstrap methods. To make contact with flat space, we take this box to be large which corresponds to large scaling dimensions on the boundary. As it happens the numerical conformal bootstrap results become rather weak at large scaling dimensions and this makes it computationally quite challenging to obtain reliable results. This is the main drawback of the AdS approach. Fortunately there are interesting and potentially very helpful developments on this front: according to [120], convergence can be

[23] We do not know why this happens; it stands as an empirical observation.

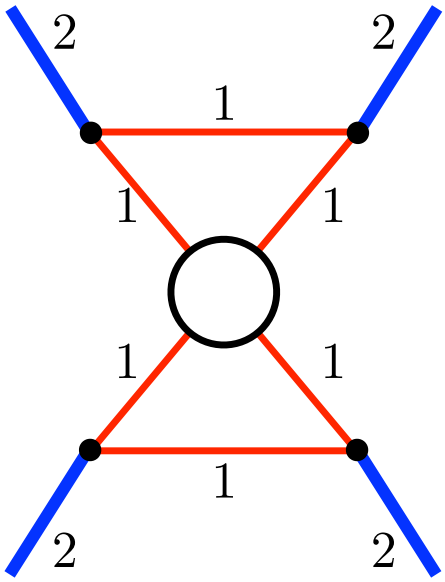

Figure 2.13: Landau diagram that gives rise to a double pole in $M_{22\to 22}$ if $m_2 > \sqrt{2}m_1$.

much improved by a smarter choice of functionals (see also [121, 122]). It would be very interesting to explore this further.

An important advantage of the AdS approach, on the other hand, is that it requires no subtle assumptions about the various analytic properties of scattering amplitudes. The AdS box is thus a literal black box from which we can get beautiful S-matrix bootstrap results even when the analytic properties of such amplitudes might be less obvious.

A good example of such a subtle assumption is extended unitarity, which we have seen is crucial for our multiple-amplitude bounds. Recall that this is a generalisation of usual unitarity which controls the analytic behaviour of scattering amplitudes for unphysical energies, below physical thresholds. For example, when we scatter the next-to-lightest particle against itself we have a two particle cut associated to the lightest particle starting at $s = (2m_{\text{lightest}})^2$, before the physical two particle cut at $s = (2m_{\text{next-to-lightest}})^2$, and extended unitarity governs the discontinuity of scattering amplitudes in the segment between those two values. Extended unitarity is built into perturbation theory [111] but it is not straightforwardly justified non-perturbatively. However, the fact that our QFT in AdS approach exactly reproduces the flat space results provides strong evidence for the validity of the extended unitarity assumption.

Relatedly, it is puzzling that the AdS bounds for $m_2 > \sqrt{2}m_1$ are so much weaker than the $12 \to 12$ forward flat space extremal coupling, see figure 2.12. Either the AdS numerics did not converge yet or perhaps there is something deeper to be learned there. It would be very interesting to extend our flat space analysis beyond the mass range (2.1) into the $m_2 > \sqrt{2}m_1$ domain. Here we would need to include so-called Coleman-Thun singularities in our setup. An example is shown in figure 2.13.

Another very important new ingredient which is not unrelated to the anomalous cuts arising in the extended unitarity region and which appeared in this chapter is the phenomenon of *screening*. Amplitudes involving heavier particles can sometimes produce dis-

continuities in some of these anomalous cuts which cancel, i.e. screen, other singularities such as physical poles corresponding to bound-state stable particles. That is, these discontinuities can be tuned so that the amplitudes can often be quite small in the physical energy region where experiments are done. This mechanism is not only possible but it is actually realised by some amplitudes which lie at the boundary of the truncated $2 \to 2$ multiple correlator S-matrix space. It is natural to expect that similar phenomena would also be realised at the boundary of the full S-matrix space. If this boundary is physically significant then screening would be an interesting way for nature to hide strong couplings from the observer.

Let us conclude with some interesting open problems and future directions.

One open problem for which we now have all tools to explore concerns the tricritical Ising field theory. This theory is obtained by deforming a conformal minimal model with two relevant deformations, see appendix A.8, and is integrable if one of the deformations is set to zero. It would be very interesting to bootstrap this theory when both parameters are non-zero. This is a particularly nice case study because the next to lightest particle here is well below $\sqrt{2}$ times the mass of the lightest particle – see table A.1 for its value at the integrable point – which means we can readily apply all the methods developed here. The only modification would be to include further poles in the ansatz corresponding to the other stable particles this theory has – see again table A.1. So here is a homework exercise: consider a line in the mass ratio parameter space which passes by the masses of the integrable theory. Something remarkable should happen: In the anomalous cut of the $22 \to 22$ amplitudes we should see a peak developing as we approach the integrable theory. This peak is going to become a new stable particle in the integrable theory with a mass we know. Seeing this peak show up in detail would be great, as it would constitute a "discovery" of a new particle through the S-matrix bootstrap. Of course, more interesting still would then be to move away from the masses of the integrable theory and explore the full tricritical Ising field theory, non-integrable and all. The previously discovered sharp peak – typical of an integrable theory – would now be smoothened out and correspond to a nearly stable resonance. Because there are so many masses and couplings this would be a challenge numerically, albeit a worthwhile one.

Another open problem which we could now easily address is the problem of multiple amplitudes without $\mathbb{Z}_2$ symmetry. We would now also include amplitudes such as $11 \to 12$ which have amusing 2D kinematics by themselves. The Ising field theory perturbed by both magnetic field and temperature would be a perfect case study for this case.

A much more challenging but very interesting open problem would be to extend the multiple amplitude analysis to higher dimensions (as in [10] and [15]). The $\mathbb{Z}_2$ spontaneously broken phase of the ϕ^4 model in 3D, for instance, seems to have a single stable bound state of mass $m_2 \simeq 1.8 m_1$ [123]; it would be fascinating to try to bootstrap this S-matrix.

Finally, another frontier in 2D would be to delve into the multiple particle S-matrix bootstrap. Can we tame scattering of 2 particles into $3, 4, \ldots$ final particles? There are two obvious obstacles. One is the analytic structure of these amplitudes. They depend now on more kinematical variables and have a huge plethora of Landau singularities; it is unclear if we can characterise them fully. The other challenge is even more basic: can we close up

the system of equations? Suppose we consider a basis of initial and final states with both two and three particles. Then we need to deal with the $3 \to 3$ amplitudes. But those, by crossing, are related to $2 \to 4$ (and much more! See [40].). By unitarity we would then need to include four particles in the final and initial states as well. But then we are forced to consider $4 \to 4$ processes which are now related by crossing to $3 \to 5$ and $2 \to 6$ scattering and so on. It seems we are suddenly obliged to consider any number of final particles at once which of course would be computationally completely infeasible. A suitable strategy in the case of massless scattering will be discussed in [48]. Along these lines, perhaps we could first try to get some inspiration from the AdS side. Some of the necessary higher point conformal blocks are well known in 1D [124], and some initial investigations of multipoint numerical bootstrap appeared in [125]. Can we use this to devise a 1D CFT bootstrap numerical problem dual to the very intimidating flat space multiple particle bootstrap? Even if very challenging numerically, this would prove of extreme conceptual value.

Chapter 3

The S-matrix Bootstrap: SUSY, $\mathbb{Z}_2$ and $\mathbb{Z}_4$ symmetry

3.1 Some beautiful sections

The S-matrix space can be very rich, with pointy structures such as edges and cusps. It is hard to visualize it since we are dealing with an infinite dimensional space so in practice we pick sections. If the theory has bound states, for instance, a natural set of variables to follow are the residues of S-matrix elements at their corresponding poles which physically correspond to the on-shell three particle couplings. While if the theory has no bound states we can measure the two-to-two S-matrix elements at some off-shell points, thus defining effective off-shell four point couplings. By picking appropriate linear functionals and S-matrix ansatze, we thus explore the possible S-matrix space sections compatible with crossing and unitarity following [1,9]. In this chapter we will consider a few simple sections which are two or three dimensional and thus can be nicely plotted. The physical setups we will consider are:

(A) Scattering of a massive real supermultiplet with and without bound states.

(B) A generic degenerate boson-fermion scattering where the previous case should sit in a special limit.

(C) $\mathbb{Z}_4$ symmetric models.

We will always be in two spacetime dimensions.

These examples are richer than the setup of [9, 10, 104] where the scattering of the lightest real bosonic particles in a gapped theory was considered but still simpler than the scattering of particles in the fundamental representation of a $O(N)$ flavour symmetry [11, 13], with $U(N)$ symmetry [14] or when we scatter the two lightest particles in $\mathbb{Z}_2$ symmetric 2D theories [1]. The great merit of the simpler examples considered herein is that they are simple enough to be able to be analytically described while rich enough to capture many of the intricate features of these other more elaborate examples. To generate all the plots here we followed the usual numerical algorithms in S-matrix bootstrap explorations, see appendix B.6 for a telegraphic summary.

3.1.1 The simplicity of supersymmetry

As the first example we consider a system with $\mathcal{N} = 1$ supersymmetry in which the lightest supermultiplet consists of a single real boson ϕ and a Majorana fermion ψ both of mass m. There are five possible two-to-two scattering amplitudes but SUSY relates most of them so that in the end only two channels are independent: the scattering of bosons $S^{\phi\phi}_{\phi\phi}(s)$ and the forward scattering of a boson against a fermion $S^{\phi\psi}_{\phi\psi}(s)$. These two amplitudes are crossing symmetric. They may have poles corresponding to bosonic or fermionic bound-states which would also be in an $\mathcal{N} = 1$ multiplet, hence with couplings all related by SUSY, see appendix B.3 for details. Evaluated at the crossing symmetric point $s_* = 2m^2$ these two amplitudes define a nice two dimensional section of effective four point off-shell couplings which we can use to probe the supersymmetric S-matrix space.

The space allowed for the two independent quartic off-shell couplings is depicted in figure 3.1. In purple, the smallest region, corresponds to the allowed coupling space for theories with no bound states. Then the S-matrix elements have no poles inside the physical strip. This purple football-like shape has two cusps corresponding to the free theories where $S = \pm\mathbb{I}$. At its boundary we find a remarkable well-known S-matrix: it's nothing but the lightest breather-breather S-matrix of the supersymmetric sine-Gordon theory (SSG) stripped out of the overall CDD-pole. This is also known as the breather S-matrix of the restricted sine-Gordon model (RSG) although this is quite a misnomer since the RSG model has no bound states. For a brief review of the so called RSG model see appendix B.4.2. The purple shape's boundary can actually be read off from the RSG S-matrices and possess a nice closed form

$$\left(S^{\phi\phi}_{\phi\phi}(s_*), S^{\phi\psi}_{\phi\psi}(s_*)\right)_{\texttt{boundary}} = \pm\frac{\exp\left(\frac{i}{\pi}\mathrm{Li}_2\left(\frac{i(1-2a\sqrt{1-a^2})}{2a^2-1}\right) - \frac{i}{\pi}\mathrm{Li}_2\left(\frac{i(2a\sqrt{1-a^2}-1)}{2a^2-1}\right) - \frac{2\mathcal{C}}{\pi}\right)}{(1\pm 2a, 1)^{-1}\sqrt{1-a^2}+a},$$

where $\mathcal{C} \simeq 0.915966$ is the Catalan's constant and $a > 0$. It is quite amusing to see such rich analytic structure arise from such a simple convex optimization problem. From an algebraic perspective, it is quite remarkable that all along the purple region we obtain S-matrices which obey the Yang-Baxter factorization condition although this condition was not imposed in any way.

In addition to the scattered boson and fermion we also consider a setup where there is a single bound state supermultiplet (b, f) of mass m_{bs} with b and f being the bosonic and fermionic bound states, respectively. This is implemented by allowing for simple poles in the physical sheet in the previous S-matrix elements at s and t equal to m^2_{bs}. As explained in appendix B.3 the bound state supermultiplet can transforms in the fundamental or the anti-fundamental representaion. These differ for slightly different relations between the couplings arising in the S-matrix elements, see equations (B.4). The allowed S-matrix space for both cases obtained from the numerical optimization is depicted in figure 3.1. The various red or blue regions correspond to the allowed S-matrix space for various bound state masses m_{bs} in either of the two possible representations. As the mass of the bound state increases these regions shrink. When $m_{\text{bs}} = 2m$, the bound state dissolves into the two-particle threshold and we recover the bound state free space depicted in purple at

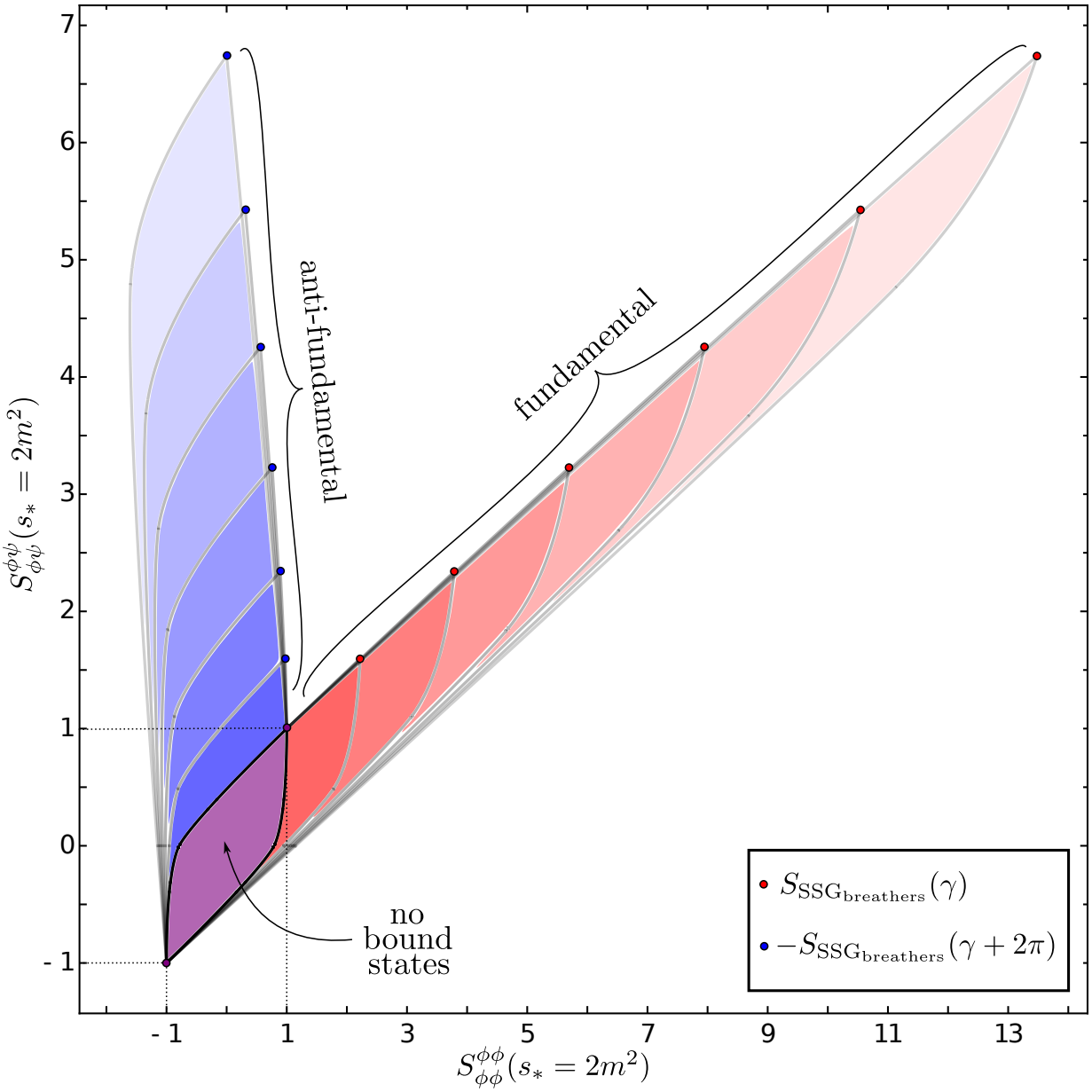

Figure 3.1: Allowed $\mathcal{N}=1$ S-matrix space with a single bound state of mass $m_{\mathrm{bs}}/m = \{1.73, 1.76, 1.80, 1.85, 1.90, 1.96\}$ transforming in the fundamental/anti-fundamental representation represented in red/blue. As we increase the mass of the bound state the allowed space shrinks.

figure 3.1.

The vertex at the top right corner of the red regions – corresponding to the S-matrix space with a single fundamental multiplet bound state – corresponds to the lightest breather S-matrix of the supersymmetric sine-Gordon model (SSG) [116]. We could also find that the S-matrix living at the top cusp of the blue regions – corresponding to the S-matrix space with a single anti-fundamental multiplet bound state – is an analytic continuation of the SSG S-matrix multiplied by an overall minus sign, see appendix B.4.4 for details. We

do not know of a Lagrangian theory which realizes this factorized S-matrix. Finally, we have the boundaries connecting to these red and blue vertices. We were able to find the exact S-matrices living at these boundaries, see appendix B.4.6. They saturate unitarity as usual but don't satisfy the Yang-Baxter factorization equations. These S-matrices are most likely not physical S-matrices but perhaps they are close enough to physical S-matrices with very little particle production. Finally, note that all this seems to be consistent with the classical intuition from [126] where it was found that the only supersymmetric model with a single real scalar boson and a Majorana fermion, with a Lagrangian description and without tree level particle production is the SSG model. Would be interesting to see if the blue cusps admits a Lagrangian description in terms of a fermion plus a pseudo-scalar.

3.1.2 How special is SUSY?

Supersymmetric theories are special instances of theories with bosons and fermions with further non-bosonic symmetries relating them. It is thus natural to look for generic theories with bosons and fermions *without* supersymmetry and see whether supersymmetry, with its extra structure, emerges naturally at special points in the allowed theory space. This is what we turn to next.

We consider a general $\mathbb{Z}_2$ symmetric system with an even (the boson ϕ) and an odd particle (the fermion ψ) with the same mass m, but a priori no symmetry relating them. To make contact with the previous bounds we also assume the existence of a boson (b), fermion (f) pair of bound states both with the same mass $m_{\rm bs}$ but, again, with no symmetry relating them. We then have a nice three dimensional section of the allowed S-matrix space parametrized by the three independent couplings $g_{\phi\phi b}$, $g_{\psi\psi b}$ and $g_{\phi\psi f}$. This space can be plotted following [1]; the result is the nice hourglass looking coupling space shown in figure 3.2. The supersymmetric sine-Gordon model beautifully appears as a special point (the green dot) on the boundary of the allowed space. At this point, all three couplings are related by supersymmetry. We also encounter an elliptic deformation of the SSG model (black curve) previously obtained in [1].[1] This elliptic deformation contains a parameter κ and varying it in the allowed range yields the bold curve in figure 3.2, in special when $\kappa = 0$ we recover SSG. This elliptic deformation preserves integrability, but breaks supersymmetry and its explicit form is given in appendix B.4.5.

This elliptic S-matrix is *not* the famous Zamolodchikov's $\mathbb{Z}_4$ S-matrix found in [114]; the $\mathbb{Z}_2$ S-matrix we found has a different matrix structure and contains a bound-state. Nonetheless, it does share many of its properties. Given that we encounter such rich elliptic solutions at the boundary of the allowed S-matrix space it is most natural to look for Zamolodchikov's $\mathbb{Z}_4$ S-matrix and see if that one can also be found in an appropriate bootstrap problem. This is what we discuss in the next section.

[1] Strictly speaking the elliptic deformation found in [1] is an analytic continuation of the one found here. Here we are taking $m_{\rm bs} > \sqrt{2}m$ to pass by the SSG in its physical domain where the second breathers are constrained to be in such mass range. There we took $m_{\rm bs} = 1$ so we were instead studying the elliptic deformation of an analytic continuation of the SSG beyond its physical regime. We expect the elliptic deformation encountered here to correspond to a proper physical theory; we suspect that this is not the case for the analytically continued version in [1].

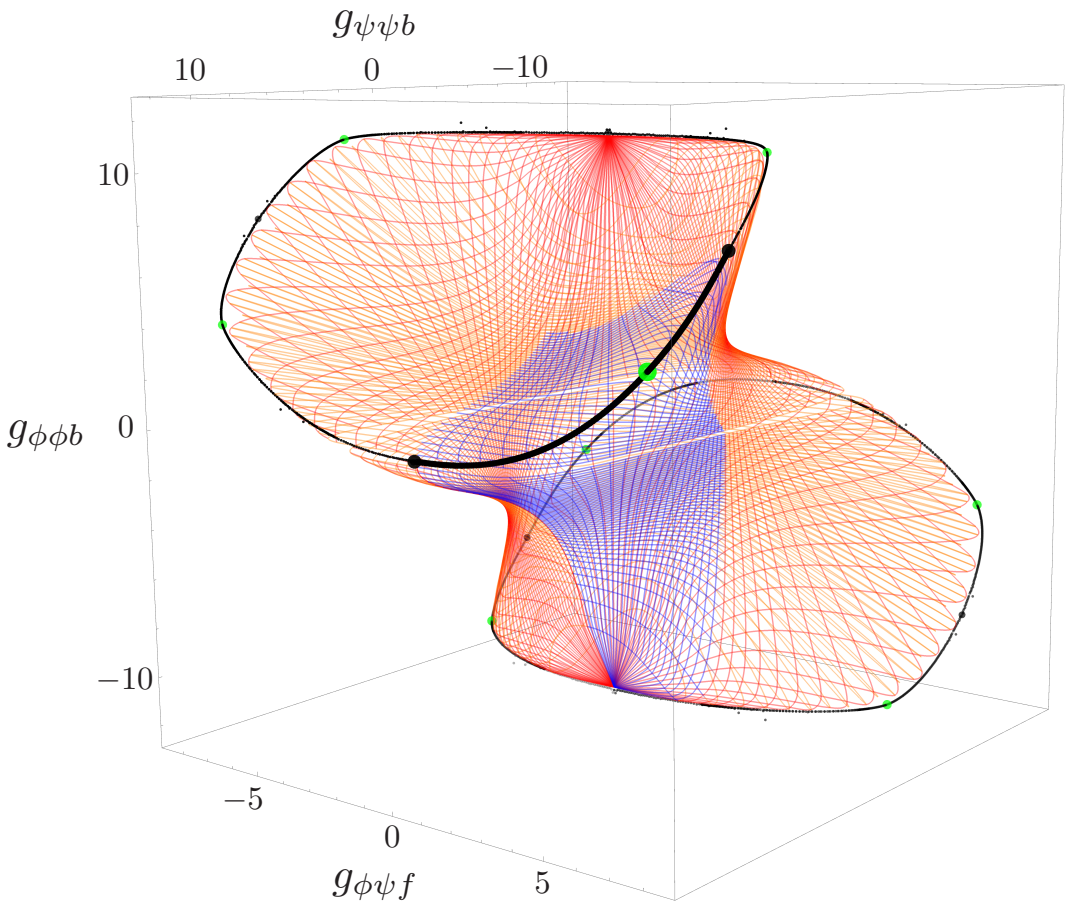

Figure 3.2: Coupling space for $\mathbb{Z}_2$ symmetric theories with a single bound state obtained from the S-matrix bootstrap. In this figure $m_{\rm bs} = \sqrt{3}m$ and all couplings are measured in units of m. The green point is the supersymmetric sine-Gordon theory, while the bold black line corresponds to an integrable elliptic deformation of SSG. The blue region is the fundamental domain: the rest of the 3D space can be obtained from it through trivial reflections corresponding to symmetries of the bootstrap problem.

3.1.3 The faces of $\mathbb{Z}_4$ symmetry

Inspired by the newly obtained elliptic S-matrix discussed in section 3.1.2, we consider a $\mathbb{Z}_4$ symmetric setup with a particle-antiparticle pair of mass m whose charges under $\mathbb{Z}_4$ are one and three. We assume that there are no further particles in the spectrum

After imposing selection rules from charge conservation and constraints from crossing, C, P and T, see details in appendix B.2, we are left with 3 independent amplitudes: S_{11}^{11}, S_{11}^{33} and S_{13}^{31}. In similar spirit to the scenario without bound states considered in the SUSY setup, section 3.1.1, we bootstrap the allowed space for the off-shell four point couplings defined by the values of these three independent amplitudes evaluated at the crossing symmetric point $s_* = 2m^2$.

The result is the smoothed rhombic dodecahedron displayed in figure 3.3. Yang-Baxter factorization once again makes an unexpected appearance: the *full* two dimensional surface[2] corresponds to Zamolodchikov's famous $\mathbb{Z}_4$ symmetric integrable S-matrix [114]. Edges connecting threefold vertices and fourfold vertices correspond, up to change of basis, to limits where the $\mathbb{Z}_4$ S-matrix degenerates into the sine-Gordon kinks S-matrix with $\gamma \geq \pi$, see section 3.2. In particular, fourfold vertices are equivalent to limits in which the $\mathbb{Z}_4$ or sine-Gordon S-matrix becomes free . The threefold vertices of the dodecahedron are smoothened resembling the pre-vertices of [12].

As far as Yang-Baxter is concerned we encountered this mysterious bonus factorization at special kinks in the supersymmetric setup (figure 3.1); at special lines in the $\mathbb{Z}_2$ bounds (figure 3.2) and now in full surfaces in the $\mathbb{Z}_4$ problem (figure 3.3). Would be great to understand mathematically where this additional physical factorization is coming from.

3.2 A web of relations

Both in this and in previews works [1, 9] a myriad of integrable two-component 2D S-matrices were found to be located along the boundary of the space of amplitudes allowed by consistency with UV completeness. The various S-matrices obtained in this way are not independent, but connected through an intricate web of relations, summarized in figure 3.4 and reviewed in this section. The expressions for the exact S-matrices can be found in appendix B.4 where more details are given.

We begin the web of relations with the Zamolodchikov's $\mathbb{Z}_4$ S-matrix, bootstrapped in figure 3.3. The most curious feature of this S-matrix, described in details in appendix B.4.3, is its periodicity for real values of the rapidity θ, defined by $s = 4m^2 \cosh(\theta/2)^2$, which at high energies amounts to periodicity in $\log s$. As pointed out by Zamolodchikov [114], this suggests a sort of RG-time periodicity, which may explain the current lacks of a Lagrangian description for this model. The S-matrix is described by two parameters: the elliptic modulus κ and the coupling γ. When we take $\kappa \to 0$ (arrow ①) the $\mathbb{Z}_4$ charge gets enhanced to a $U(1)$ topological charge, and the S-matrix gets reduced to the sine-Gordon kinks S-matrix. The remaining real parameter is the free parameter γ of the sine-Gordon model which controls the spectrum of the theory.

As a limit of the $\mathbb{Z}_4$ S-matrix (which has no bound-states) we land in the regime $\gamma > \pi$ where the only stable particles are the sine-Gordon solitons. Once we analytically continue into $\gamma < \pi$ we reach the regime where there are bound states called breathers. The scattering of these breathers can be obtained by fusing pairs of kinks in a multi-kink scattering process (arrow ②), detailed in appendix B.4.1. The lightest breather S-matrix, obtained in this way, is the simplest S-matrix one can bootstrap as analyzed in [9, 110].

As said previously, for $\gamma > \pi$ the only stable particles in the sine-Gordon spectrum are the solitons. However when $\gamma = \pi p$, with $p \geq 3$ and $p \in \mathbb{Z}$, some multi-soliton states decouple and the spectrum can be restricted (arrow ③). This process defines the restricted sine-Gordon theory, see appendix B.4.2. This theory has no free parameters and no bound

[2] More precisely, part of the surface corresponds to Zamolodchikov's $\mathbb{Z}_4$ S-matrix after charge conjugation of one of the particles, see appendix B.2.

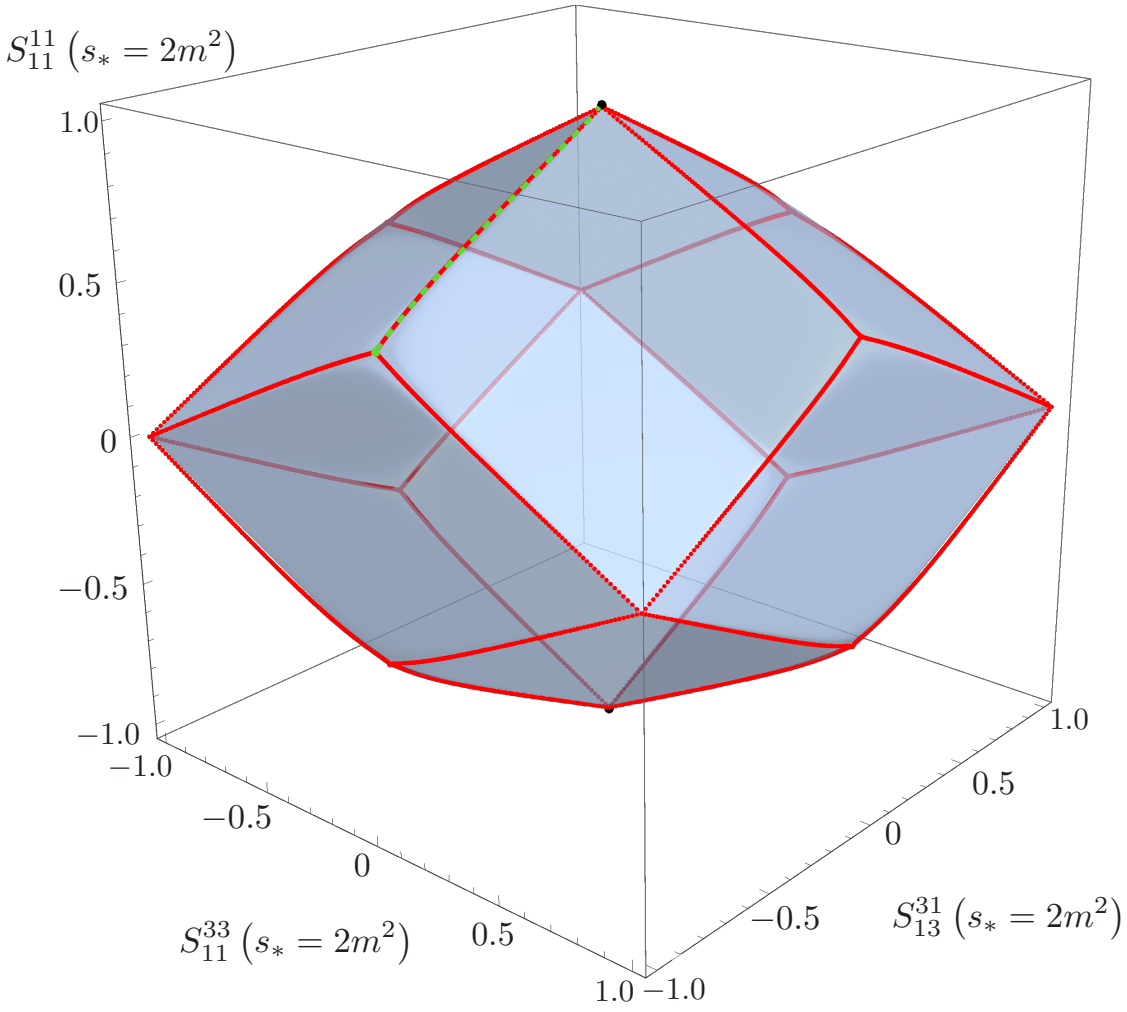

Figure 3.3: S-matrix space for the $\mathbb{Z}_4$ symmetric S-matrix bootstrap at $s_* = 2m^2$. The faces are equivalent to the Zamolodchikov's $\mathbb{Z}_4$ S-matrices (appendix B.4.3) and the edges to the sine-Gordon kinks S-matrices (appendix B.4.1).

states. The case of interest is $p = 4$, for which the restricted theory is supersymmetric.

The supersymmetric sine-Gordon solitons S-matrix is built in a nice factorized way (arrow ④) from the two S-matrices we just encountered as

$$S_{\mathrm{SSG}_{\mathrm{kinks}}}(\theta,\gamma) = S_{\mathrm{SG}_{\mathrm{kinks}}}(\theta,\gamma) \otimes S^{(p=4)}_{\mathrm{RSG}_{\mathrm{kinks}}}(\theta)\,,$$

where the SG soliton scattering matrix part takes care of the topological quantum numbers while the RSG matrix deals with the SUSY charges. Just like in SG we can fuse (arrow ⑤) the (supersymmetric) kinks to obtain the S-matrix of the (supersymmetric) breathers,

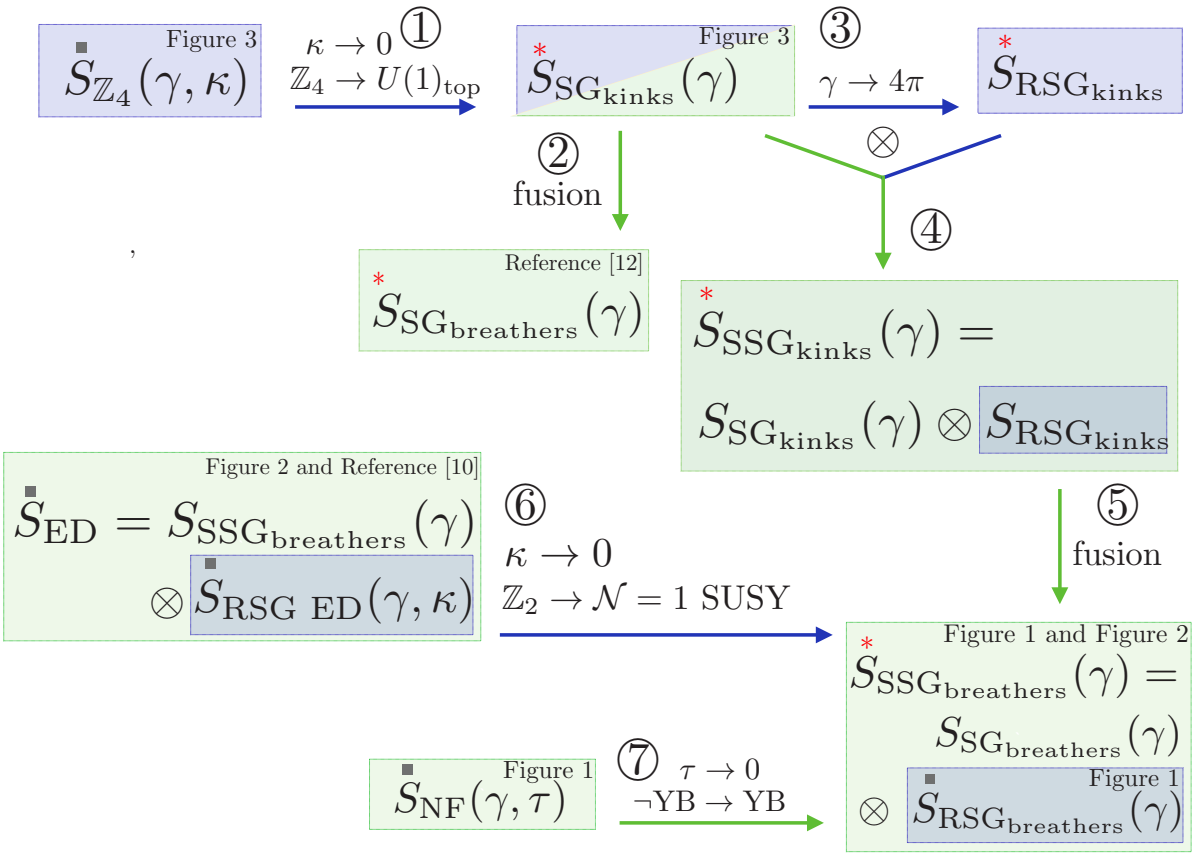

Figure 3.4: Connections between S-matrices showing up in this chapter as well as in [1,9]. *Green boxes*: S-matrices with bound-states. *Blue boxes*: S-matrices without bound states. $*$: Known corresponding Lagrangian field theory (LFT). ■: Unknown corresponding LFT.

which retains the factorized structure,

$$S_{\text{SSG}_{\text{breathers}}}(\theta,\gamma) = S_{\text{SG}_{\text{breathers}}}(\theta,\gamma) \otimes S^{(p=4)}_{\text{RSG}_{\text{breathers}}}(\theta,\gamma)\,.$$

This is the S-matrix at the vertex of figure 3.1.

Since the fusing momenta depend on γ, the fusion process introduces a γ dependence in the SUSY-related factor. However, this term does *not* correspond to a scattering process in the RSG theory. After all, as said before, the restricted model has no free parameter and no breathers. Nevertheless it is precisely this S-matrix factor by itself that shows up as as the boundary of the purple region in figure 3.1.

The SUSY factor in the SSG 1st breather supermultiplet S-matrix can be deformed into an elliptic integrable S-matrix S_{ED} controlled by an extra parameter κ, arrow ⑥. This deformation breaks supersymmetry but preserves the $\mathbb{Z}_2$ fermion number symmetry intact. We encounter it as the solid line in the more general $\mathbb{Z}_2$ setup of figure 3.2. Finally, it is also possible to deform the SSG 1st breather S-matrix preserving supersymmetry but breaking integrability, see arrow ⑦ and appendix B.4.6. Such S-matrix, S_{NF}, describes the full boundary of the space of theories in figure 3.1. It is a curious example of solution

which we can find analytically and yet does not obey Yang-Baxter. Would be nice if there was a physical theory which realizes (at least an approximate version) of this S-matrix.

The lower dimensional sections of various S-matrix spaces in figures 3.1, 3.2 and 3.3 – with a vast plethora of very rich S-matrices at their boundary as summarized in figure 3.4 – are the main results of this chapter. Some of the amazing features in these S-matrix spaces – such as unitarity saturation – are now somehow demystified [12] while others – such as emerge of factorization or exotic periodicities in the kinematical variables – remain as elusive as ever. Would be very interesting to explore other setups with different symmetries and space-time dimensions to better shed light over these puzzles and to best understand how universal they really are. One very concrete avenue for analytic progress is to zoom in on the vertices close to free theories and see if there is still some interesting Lagrangian games to be played a la [126, 127]. Would be nice to see if such simple perturbative games, combined with some important bootstrap intuition, could lead to the discovery of new interesting theories.

Chapter 4

The S-matrix Bootstrap: 2D Dual Theory

4.1 Introduction

Figure 4.1 is extracted from [10] and [15].

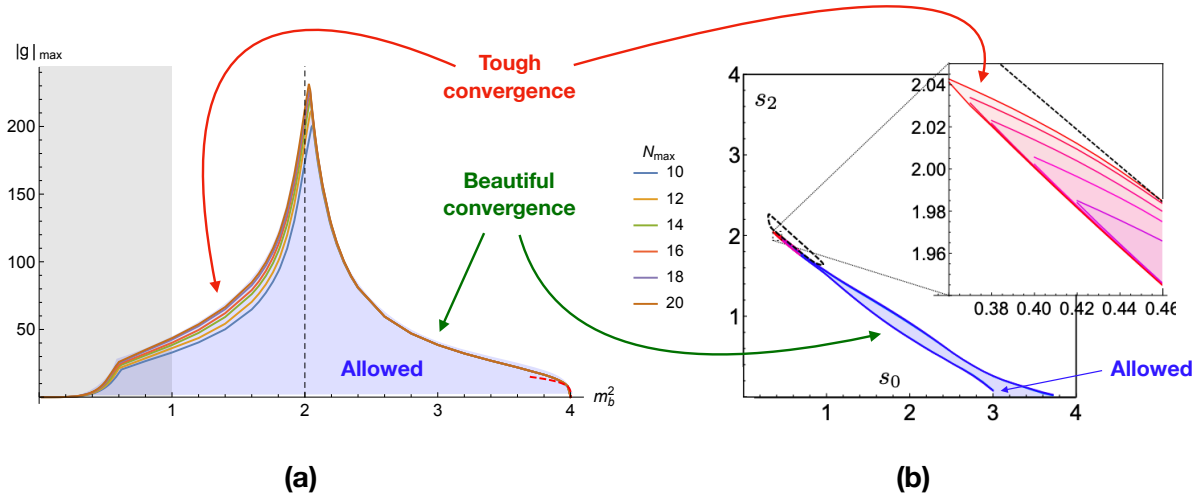

Figure 4.1: **a**) Maximal cubic coupling showing up in the scattering of the lightest particle in a gapped theory with a single bound-state (in this channel at least) [10]. Convergence is perfect when the bound-state mass (measured in units of the lightest mass) is bigger than $\sqrt{2}$ and quite painful otherwise. **b**) The allowed chiral zeroes space of putative pion S-matrices associated to an $SU(2)$ chiral symmetry breaking patterns draws a beautiful peninsula like object with a sharp tip [15].[1] Convergence is great almost everywhere except close to the tip where numerics struggle. In those cases where the primal problem struggles, having a dual rigorous bound would be a blessing. This chapter is about such dual bounds.

[1]There are, at least, other two structures would benefit a dual description. One is the "pion lake" [15], found imposing the presence of the physical ρ resonance only. Another interesting and recent structure is the "pion river" [128], found imposing additional constraints on the scattering lengths arising from χPT and monotonicity of the relative entropy. The dual formulation would allow to rigorously define these structures excluding theories not compatible with the assumed low energy QCD behavior.

These works explore the allowed space of physical 4D S-matrices. One parametrizes a vast family of S-matrices compatible with given physical and mathematical assumptions and maximize or minimize quantities within this ansatz to find the boundaries of what is possible. The more parameters the ansatz has, the better is the exploration. As the number of parameters become very large, one hopes that these boundaries converge towards the true boundaries of the S-matrix space.

Sometimes this works beautifully as illustrated in the figure; sometimes convergence is painful, to say the least, as also illustrated in the figure. In those cases where convergence is a struggle, what can we do? Sometimes, it is a simple matter of improving the ansatz; sometimes it is not clear what exactly is missing. And in either case, how can we ever tell how close to converging are we anyways?

A solution would be to develop a dual numerical procedure – called the dual problem – where instead of constructing viable S-matrices we would instead rule out unphysical S-matrix space.[2] Then we would approach the boundaries of the S-matrix space from two sides, dual and primal, and in this way rigorously bracket the true boundaries of the sought after S-matrix space. This was recently achieved in two dimensions for simple models with a single type of particle transforming in some non-trivial global symmetry group [12].[3]

This chapter concerns two dimensional multi-particle systems with arbitrary mass spectra from this dual perspective, clearly one step further in the complexity ladder, closer to the full higher dimensional problem.[4] We will also consider a different technical approach, complementary to [12], with some aspects which we hope can be more directly transposable to higher dimensions.

4.2 Dual optimization and the S-matrix bootstrap

To achieve the desired dual formulation, it is useful to revisit the S-matrix bootstrap with a slightly different perspective.

In the *primal* S-matrix bootstrap formulation one constructs scattering amplitudes consistent with a set of axioms, or constraints. Such amplitudes are said to be *feasible*, that is, they belong to the allowed space of theories. One then optimizes physical observables, such as the interaction strength between stable particles, in the space of feasible amplitudes. The prototypical example is [9, 110]: in a 2D theory with a single stable particle of mass m, what is the maximum cubic coupling g consistent with a $2 \to 2$ scattering amplitude M satisfying the constraints of unitarity, extended analyticity, and crossing?

In other words, we would like to solve the optimization problem

[2] Such dual bounds were attempted more than 50 years ago already in [129–132]. Would be very important to do some archeology work and revive/translate/re-discover/improve those old explorations in a modern computer friendly era. A beautiful first step is currently being pursued by Martin Kruczenski and Yifei He [34]. The conformal bootstrap bounds are also exclusion analysis of this sort [133].

[3] The primal version of these single particle studies with global symmetry was the subject of [11, 13, 14]; the case without global symmetry was considered in [9, 110].

[4] Multi-particle primal problems of this kind were pioneered in [1, 2].

Primal problem

$$\underset{\text{in } M(s),\, g^2}{\text{maximize}} \qquad g^2 \tag{4.1}$$

$$\text{constrained by} \quad \mathcal{A}(s) \equiv M(s) - \left(M_\infty - \frac{g^2}{s-m^2} + \int_{4m^2}^{\infty} \frac{dz}{\pi} \frac{\text{Im}M(z)}{s-z+i0} + \left(s \leftrightarrow 4m^2 - s\right)\right) = 0$$

$$\text{for } s > 4m^2, \tag{4.2}$$

$$\mathcal{U}(s) \equiv 2\ \text{Im}M(s) - \frac{|M(s)|^2}{2\sqrt{s-4m^2}\sqrt{s}} \geq 0 \qquad \text{for } s > 4m^2. \tag{4.3}$$

where we maximize over the space of analytic functions M, and emphasize that one parameter in this infinite dimensional space is the residue of such functions at $s = m^2$ which is equal to $-g^2$. The first constraint (4.2), an exact equality, imposes that feasible scattering amplitudes must respect crossing, real analyticity, and have singularities determined by physical processes: poles corresponding to one particle states, and cuts corresponding to multi-particle states.[5] We choose to impose this condition for $s > 4m^2$, but because we maximise over analytic functions, feasible amplitudes will have have this property for all s in the physical sheet.[6] The convenience of imposing this condition for $s > 4m^2$ will become clear in time. The second constraint (4.3) is the physical unitarity condition, equivalent to $|S(s)| \leq 1$.

Since the quantity we are maximising, the objective, is a linear map in the space of analytic functions, the map that evaluates the residue at a point, and since the constraints (4.2), (4.3) are affine and convex respectively, the optimization problem we aim to solve is an infinite dimensional convex optimization problem. For such a simple problem, there are now two directions that can be taken. The first option is to solve the infinite dimensional problem analytically. As is well known by now, this follows from a simple application of the maximum modulus principle [9,110]. The second option, available in more complicated situations, is to bring the problem to the realm of computers by maximizing our objective in some finite dimensional subspace of analytic functions. For example, one can consider analytic functions that are, up to poles, polynomial of at most degree N_{max} in some foliation variable ρ that trivializes the constraint (4.2), as done in [10]. This truncated problem can be efficiently solved by a convex optimization software, for example SDPB [112,134]. By choosing and increasing the finite dimensional subspace smartly, one obtains lower bounds to the solution of the primal problem that should converge to the correct bound with more expensive numerics.

The primal formulation suffers from two important shortcomings. First, for some problems it is hard to identify a simple ansatz, or truncation scheme, that allows for fast convergence. This is often the case in higher dimensional S-matrix bootstrap applications,

[5] It turns out that there is no loss of generality in omitting subtractions from (4.2), since a more careful analysis shows that the inclusion of those leads to the same result (4.15). We opt for not including subtractions in the main text for the sake of clarity – see appendix C.2.1 for a more detailed discussion.

[6] The physical sheet is defined as the first Riemann sheet encountered after analytically continuing from physical kinematics, $s > 4m^2$, using the $+i\epsilon$ prescription.

or when scattering heavy particles in 2D. Second, and perhaps more importantly, one may want to add extra variables and constraints to the primal problem. In the previous example, those variables and constraints could be, respectively, higher point amplitudes and higher point unitarity equations. It may be the case that a feasible $2 \to 2$ amplitude in the original primal problem may no longer be feasible in the enlarged space with extra constraints. In those cases, a point in theory space previously said to be allowed becomes forbidden. It would be more satisfying if bounds on the space of theories obtained by studying some scattering subsector remained true once the full set of QFT constraints were imposed.[7] To overcome both of this shortcomings, we introduce the dual formulation. We use the coupling maximization problem as a guiding example, before generalizing.

Consider the Lagrangian[8]

$$\mathcal{L}(M, w, \lambda) = g^2 + \int_{4m^2}^{\infty} ds\ w(s)\mathcal{A}(s) + \lambda(s)\mathcal{U}(s) \tag{4.4}$$

with $\lambda(s) \geq 0$ and define the dual functional

$$d(w, \lambda) = \sup_{\{M,g\}} \mathcal{L}(M, w, \lambda) \tag{4.5}$$

Notice that the supremum is taken over unconstrained analytic functions M.[9] The dual functional d is the central object in the dual formulation due to the following property:

Weak Duality

Let the solution of the primal problem be g_*^2. Then $d(w, \lambda) \geq g_*^2$. (4.6)

Weak duality holds due to two observations. First, note that since

$$\inf_{\{\lambda \geq 0, w\}} \mathcal{L}(M, w, \lambda) = \begin{cases} g^2 & \text{if } M \text{ is feasible} \\ -\infty & \text{otherwise,} \end{cases} \tag{4.7}$$

we have that

$$g_*^2 = \sup_{\{M,g\}} \left[\inf_{\{\lambda \geq 0, w\}} \mathcal{L}(M, w, \lambda) \right].$$

Weak duality then follows from the max-min inequality

$$d(w, \lambda) \geq \inf_{\{\lambda \geq 0, w\}} \left[\sup_{\{M,g\}} \mathcal{L}(M, w, \lambda) \right] \geq \sup_{\{M,g\}} \left[\inf_{\{\lambda \geq 0, w\}} \mathcal{L}(M, w, \lambda) \right] = g_*^2. \tag{4.8}$$

[7] Much in the same way that CFT data excluded by the numerical conformal bootstrap remains excluded once more crossing equations are included into the system.

[8] Note $\mathcal{A}(s)$ is actually real.

[9] It is useful to think of analytic functions as being defined through their independent real and imaginary parts along a line. Of course, if the dispersion (4.2) were to hold, then those would not be independent. However, since we maximise over generic analytic functions, we are free to treat Re M and Im M for $s > 4m^2$ as independent.

Exploring the $\{w, \lambda\}$ space, the space of dual variables, we therefore obtain upper bounds on the values of g allowed by the axioms and exclude regions in theory space. This, in turn, partially solves the first shortcome of the primal formulation: by providing upper limits on the coupling, it bounds how far from converging an ineffective primal truncation scheme may be. To find the best possible upper bound, we solve the

Dual problem (generic)

$$\begin{aligned} &\underset{\text{in } w(s),\, \lambda(s)}{\text{minimize}} && d(w,\lambda) \\ &\text{constrained by} && \lambda(s) \geq 0 \end{aligned} \tag{4.9}$$

The construction of dual functionals from a primal optimization problem is standard in optimization theory, but the particularities of the problems encountered in the S-matrix bootstrap lead to important simplifications. One of these is that the analyticity of the scattering amplitude is inherited by the dual variable $w(s)$, conjugate to the analyticity constraint. In fact, let's define a "dual scattering function", $W(s)$[10], odd under crossing and whose absorptive part is $w(s)$:

$$W(s) \equiv \frac{1}{\pi}\int_{4m^2}^{\infty} dz \frac{w(z)}{s-z+i0} - \left(s \leftrightarrow 4m^2 - s\right). \tag{4.10}$$

Then, swapping a few integrals in (4.4) and using $\frac{1}{(s-z\pm i0)} = \mp i\pi\delta(s-z) + \mathcal{P}\frac{1}{(s-z)}$ leads to a very simple representation for the lagrangian as

$$\mathcal{L}(M, W, \lambda) = g^2\left(1 + \pi W(m^2)\right) + \int_{4m^2}^{\infty} ds\ \mathrm{Im}\left(W(s)M(s)\right) + \lambda(s)\,\mathcal{U}(s). \tag{4.11}$$

Note that the Lagrangian density is now manifestly local in M as the Cauchy kernel from (4.2) has been nicely absorbed into W. This locality, together with the quadratic nature of the constraint equations[11] leads to the next simplification over generic dual optimization problems: we can perform both the maximization over M in (4.5) and the minimization over λ in (4.9) exactly. We now analyze those in sequence.

Before doing that, first notice, linearity of $\mathcal{L}$ under g^2 implies that

$$d(W, \lambda) = +\infty \quad \text{unless} \quad \pi W(m^2) = -1. \tag{4.12}$$

This means that unless W is properly normalized at m^2, the bounds obtained from the dual functional are vacuous. Hence, in solving the dual problem, there is no loss of generality in restricting ourselves to the space of W satisfying the constrain in (4.12).

[10] It is worth stressing that the introduction of an analytic function $W(s)$ is not mandatory. It is possible to work with real densities $w(s)$ and follow the argument presented in this section using the same logic. This possibility is particularly useful in higher dimensions if one wants to assume no more than the proven analyticity domains [132].

[11] Dispersions for higher point amplitudes are no longer expected to be quadratic in lower point functions due to the presence of Landau singularities.

The linear Lagrange equations with respect to variations of $M(s)$ for $s > 4m^2$ results in

$$M_{\text{critical}}(s) = \left[\text{Im}(W(s))/\lambda(s) + i\left(2\lambda(s) + \text{Re}(W(s))/\lambda(s)\right)\right]/(2\rho_{11}^2).$$

where $\rho_{11}^2 = 1/(2\sqrt{s-4m^2}\sqrt{s})$. Second order variations show that, indeed, this is a local maximum provided $\lambda(s) > 0$. It follows from the definition (4.5) that, provided $\pi W(m^2) = -1$,

$$d(W,\lambda) = \int_{4m^2}^{\infty} ds \left(\frac{|W(s)|^2}{4\lambda(s)} + \lambda(s) + \text{Re}W(s)\right)\Big/\rho_{11}^2. \tag{4.13}$$

Next, we minimize over λ leading to $\lambda = |W(s)|/2$. The result is $D(W) \equiv \inf_{\lambda\geq 0} d(W,\lambda))$ given by

$$D(W) = \int_{4m^2}^{\infty} ds \left(\text{Re}(W(s)) + |W(s)|\right)/\rho_{11}^2., \tag{4.14}$$

in which case[12]

$$M_{\text{critical}}(s) = \frac{i}{\rho_{11}^2}\left(1 + \frac{W^*}{|W|}\right).$$

In sum, the dual of (4.1) simplifies to

Dual problem (S-matrix bootstrap)

$$\underset{\text{in } W(s)}{\text{minimize}} \qquad D(W) = \int_{4m^2}^{\infty} ds \left(\text{Re}(W(s)) + |W(s)|\right)/\rho_{11}^2 \tag{4.15}$$

$$\text{constrained by} \qquad \pi W(m^2) = -1. \tag{4.16}$$

The dual problem can be tackled numerically through the same strategy used for the primal problem, that is, restricting our search to a finite dimensional subspace of analytic Ws. For example, one could use the ρ foliation variables to write the ansatz[13]

$$W_{\text{ansatz}}(s) = \frac{1}{s(4m^2-s)}\sum_{n=1}^{N_{\max}} a_n(\rho(s)^n - \rho(t)^n), \tag{4.17}$$

where

$$\rho(s) = \frac{\sqrt{2m^2} - \sqrt{4m^2-s}}{\sqrt{2m^2} + \sqrt{4m^2-s}}, \tag{4.18}$$

and minimize the functional (4.15) in the finite dimensional space parametrized by the a_n's. Note that the constraint (4.16) is a linear constraint in this space. The functional (4.14) is nonlinear, but it is convex in W. Performing such minimization, say, in `Mathematica` shows that, as one increases $N_{\max}$, the result of the problem (4.15) converges to the result of the primal problem (4.1). This is expected if our optimization problem satisfies

[12]Note that unitarity is automatically saturated once we minimize in λ.

[13]The Ansatz (4.17) is consistent with the dispersion (4.10). In particular, the poles in (4.17) correspond to a delta function contribution in $w(s)$.

Strong Duality

The solutions to the primal (4.1) and dual problem (4.15) are identical, i.e. $g_*^2 = \min_{\text{in } W} D(W)$. In other words, the $\geq$ symbol in (4.6) is actually an $=$ sign.

This property is argued for in appendix C.1.

To explain how the dual formulation solves the second shortcoming of the primal optimization, and in view of the applications in section 4.3, let's consider a slightly different class of S-matrix Bootstrap problems. Consider a gapped theory with two real stable particles of masses m_1 and m_2 respectively, $m_1 < m_2$, and suppose we were interested in maximizing the cubic coupling of particle m_1. Let $\mathbb{M}_{ab} = M_{a\to b}$. Assuming P and T symmetry, $\mathbb{M}$ is a symmetric matrix. We would like to solve the problem

Primal problem (matrix)

$$\begin{aligned} &\underset{\text{in } \mathbb{M}}{\text{maximize}} && g^2 && && (4.19)\\ &\text{constrained by} && \mathbb{A}(s) = 0 && \text{for } s > 4m_1^2, && (4.20)\\ &&& \mathbb{U}(s) \equiv 2\,\text{Im}\,\mathbb{M}(s) - \mathbb{M}^\dagger \rho\, \mathbb{M} \succeq 0 && \text{for } s > 4m_1^2. && (4.21) \end{aligned}$$

where $\mathbb{A}_{ab} \equiv \mathcal{A}_{a\to b}$ are analogous to (4.2) and impose the correct dispersion relations for the amplitudes $M_{a\to b}$ (see e.g. (4.36) in the next section). Here ρ are the phase space factors for the intermediate states (see e.g. (4.35) in the next section). To obtain the dual problem, we introduce the Lagrangian

$$\mathcal{L}(\mathbb{M}, \mathbb{w}, \mathbb{\Lambda}) = g^2 + \int_{4m_1^2}^{\infty} ds\ \text{Tr}\left(\mathbb{w}\cdot\mathbb{A}(s) + \mathbb{\Lambda}\cdot\mathbb{U}(s)\right), \tag{4.22}$$

where $\mathbb{w}$ and $\mathbb{\Lambda}$ are respectively symmetric and hermitian matrices of dual variables with $\mathbb{\Lambda}$ positive semi-definite. The new dual functional

$$d(\mathbb{w}, \mathbb{\Lambda}) = \sup_{\mathbb{M}} \mathcal{L}(\mathbb{M}, \mathbb{w}, \mathbb{\Lambda}) \tag{4.23}$$

satisfies weak duality by similar arguments as those in equations (4.7-4.8). The dual optimization problem is

Dual problem (matrix)

$$\begin{aligned} &\underset{\text{in } \mathbb{w}(s),\ \mathbb{\Lambda}(s)}{\text{minimize}} && d(\mathbb{w}, \mathbb{\Lambda}) && (4.24)\\ &\text{constrained by} && \mathbb{\Lambda}(s) \succeq 0. \end{aligned}$$

Note that an upper bound on the solution of the primal problem (4.1) is obtained by choosing minimizing d in the subspace $\mathbb{w}_{ab}(s) = \delta_a^{11}\delta_b^{11} w(s)$, $\mathbb{\Lambda}_{ab} = \delta_a^{11}\delta_b^{11}\lambda(s)$, $\lambda \geq 0$. This is equivalent to the dual problem obtained by including only the amplitude $M_{11\to 11}$ in the bootstrap system, or primal problem. Restricting to a scattering subsector in the dual

formulation provides true bounds to the more complete optimization problem. Conversely, bounds obtained by studying some restricted space of amplitudes and constrains remain valid once extra axioms and degrees of freedom are considered. We hope it is clear that the argument provided by means of an example is generic. This solves the second shortcoming of the primal formulation.

4.3 An application

4.3.1 The setup

We now turn our attention to much richer S-matrix bootstrap. We consider a theory with two particles of mass m_1 and $m_2 > m_1$. We will *not* assume any global symmetry. For concreteness, we will take[14]

$$m_1 = 1\,, \qquad m_2 = 3/2\,.$$

There are a priori four couplings involving these two particles: $g_{111}, g_{112}, g_{122}, g_{222}$. They would show up as s-channel residues in the various scattering amplitudes:

Amplitude	Exchange of particle 1	Exchange of particle 2
$11 \to 11$	g_{111}^2	g_{112}^2
$11 \to 12$	$g_{111}g_{112}$	$g_{112}g_{122}$
$12 \to 12$	g_{112}^2	g_{122}^2
$11 \to 22$	$g_{111}g_{122}$	$g_{112}g_{222}$
$12 \to 22$	$g_{112}g_{122}$	$g_{122}g_{222}$
$22 \to 22$	g_{122}^2	g_{222}^2

We will not consider the full coupled system of six amplitudes. Instead we will consider a nice closed subset involving the $11 \to 11$, $11 \to 12$ and (the forward) $12 \to 12$ processes only (that is, the first three lines in the table). As such we will be insensitive to g_{222}. We will furthermore consider a section of the remaining three-dimensional space where $g_{122} = 0$ so that the problem simplifies slightly to[15]

Amplitude	Exchange of particle 1	Exchange of particle 2
$11 \to 11$	g_{111}^2	g_{112}^2
$11 \to 12$	$g_{111}g_{112}$	0
$12 \to 12$	g_{112}^2	0

and our main goal here is to explore the allowed two dimensional (g_{112}, g_{111}) space. A convenient way to find the boundary of this space is by shooting radially. We fix an angle

[14]Setting $m_1 = 1$ simply sets our units. All $m_2 > \sqrt{2}$ would then give very similar plots/conclusions. We could also consider $m_2 < \sqrt{2}$; the plots are a little bit less eye pleasing in that case. The significance of the transition point $m_2^* = \sqrt{2}$ is that this is the crossing invariant point for the $11 \to 11$ process; on either sign of this point residues have different signs leading to quite different optimization results.

[15]The analysis for any other fixed value of g_{122} follows identically, see more at the end of this section.

β and define a radius R as

$$(g_{112}, g_{111}) = R(\cos\beta, \sin\beta)\,.$$

Then we find the maximum value of R for each β choice to plot the full two-dimensional space.

In the primal language we will get larger and larger R's as our ansatz is more and more complete. In the dual language we will rule out smaller and smaller R as we improve our ansatz. Sandwiched between the two will be the true (two dimensional section of the) boundary of the S-matrix space.

It is equally straightforward to fix g_{122} to any other value and analyze another 2d section in this way or even collect various values of g_{122} to construct the full $3D$ space. We leave such detailed scans for the future when we will have more realistic setups designed to bootstrap particular relevant physical theories such as the (regular and tricritical) Ising model (perturbed by thermal and magnetic deformations) as discussed in the conclusions.

4.3.2 Single Component Horn

Let us start our search for the two dimensional section of the allowed S-matrix space by focusing on the constraints arising from the single $M = M_{11\to 11}$ component alone.

This is a warm up section and many of the results here are not new: indeed, the primal formulation of single component scattering has been the subject of [9]; a minor new ingredient we will consider here is the radial search element. (The radial problem for the space of S-matrices with $O(N)$ symmetry and no bound states was introduced in [12].) In appendix H of [1] an almost identical primal problem was solved analytically; the analytic curves in figure 4.2 are obtained by trivially adapting the arguments therein. The dual formulation for these single component cases with several exchanges masses, however, will be novel and provide very useful intuition for the most general case.

The primal radial problem can be compactly formulated as

Primal Radial Problem for Single Component

$$\underset{\text{in } M,R^2}{\text{maximize}} \quad R^2$$

$$\text{constr. by} \quad \text{Res}_{m_1^2}(M) = R^2\sin^2\beta, \quad \text{Res}_{m_2^2}(M) = R^2\cos^2\beta \tag{4.25}$$

$$s \geq 4m_1^2 \qquad \mathcal{A}(s) = M(s) - M_\infty + \left(\frac{g_{111}^2}{s-m_1^2} + \frac{g_{112}^2}{s-m_2^2} - \frac{1}{\pi}\int_{4m_1^2}^{\infty} dz\, \frac{\text{Im}\, M(z)}{z-s} + (s\leftrightarrow t)\right) = 0$$

$$s \geq 4m_1^2 \qquad \mathcal{U}(s) = 2\text{Im}\, M(s) - \rho_{11}^2 |M(s)|^2 \geq 0. \tag{4.26}$$

We will now construct the dual problem. If it were not for the radial additional equality constraints (4.25) the corresponding dual problem would be given already in eq. (4.15). In this case we need to introduce additional Lagrange multipliers ν_1 and ν_2 to the la-

grangian (4.4)

$$\mathcal{L} = R^2 + \nu_1(\text{Res}_{m_1^2}(M) - R^2\sin^2\beta) + \nu_2(\text{Res}_{m_2^2}(M) - R^2\cos^2\beta) + \int_{4m_1^2}^{\infty} ds\, \mathcal{A}(s)w(s) + \mathcal{U}(s)\lambda(s). \tag{4.27}$$

Now we follow the logic of section 4.2 verbatin modulo a few small differences inherent to the radial nature of the primal problem which we will highlight. First of all note that the maximum of the Lagrangian with respect to R^2 yields a bounded result only when

$$1 - \nu_1 \sin^2\beta - \nu_2 \cos^2\beta = 0.$$

Next, identifying $w(s) = \text{Im}\, W(s)$ with $W(s)$ given by (4.10) as before will lead to a beautiful dual problem formulation with a totally local optimization target. Importantly

$$\int_{4m_1^2}^{\infty} ds\, \mathcal{A}(s)w(s) = \int_{4m_1^2}^{\infty} ds\, \text{Im}(M(s)W(s)) + \pi \text{Res}_{m_1^2}(M)W(m_1^2) + \pi \text{Res}_{m_2^2}(M)W(m_2^2)$$

so we see that the optimization with respect to the parameters $\text{Res}_{m_i^2}(M)$ identifies the lagrange multipliers ν_i with the normalization of the dual functional at the stable mass values $W(m_i^2)$. All in all we therefore obtain the simple dual problem radial generalization of (4.15) as

Dual Radial Problem for Single Component

$$\begin{aligned} &\underset{\text{in } W}{\text{minimize}} && D(W) = \int_{4m_1^2}^{\infty} ds\, (\text{Re}(W(s)) + |W(s)|)\, /\rho_{11}^2 \\ &\text{constrained by} && 1 + \pi\, W(m_1^2)\sin^2\beta + \pi\, W(m_2^2)\cos^2\beta = 0. \end{aligned} \tag{4.28}$$

Notice again the nice complementarity between the pole singularities associated to bound states in the physical amplitude and the absence of poles in the "dual scattering function" W given by (4.10), replaced instead by the simple normalization conditions (4.28). Conversely, when we maximize effective couplings in theories without bound-states the primal S-matrices have no bound-states and the dual functionals have poles [12].

In figure 4.2 we show the numerical results for both the primal (inner blue shaded regions) and the dual problem (outer red shaded regions).

4.3.3 Multiple Component Kinematics

Next we consider the full system with $11 \to 11$, $11 \to 12$ and *forward* $12 \to 12$ amplitudes.[16] The two dimensional kinematics of the $11 \to 11$ process and of the *forward* $12 \to 12$ process are reviewed in great detail in section 2 of [1] so here we will mostly focus on the new

[16] As reviewed in detail in [1] when a particle of type 1 scatters with a particle of type 2 it can either continue straight (*forward amplitude*) or bounce back (*backward amplitude*). Here we consider the forward process only. This process is nicely crossing symmetric. (The backward process is not; instead it is related by crossing to $11 \to 22$ scattering so considering this backward process would require more scattering processes to close the system of unitarity equations.)

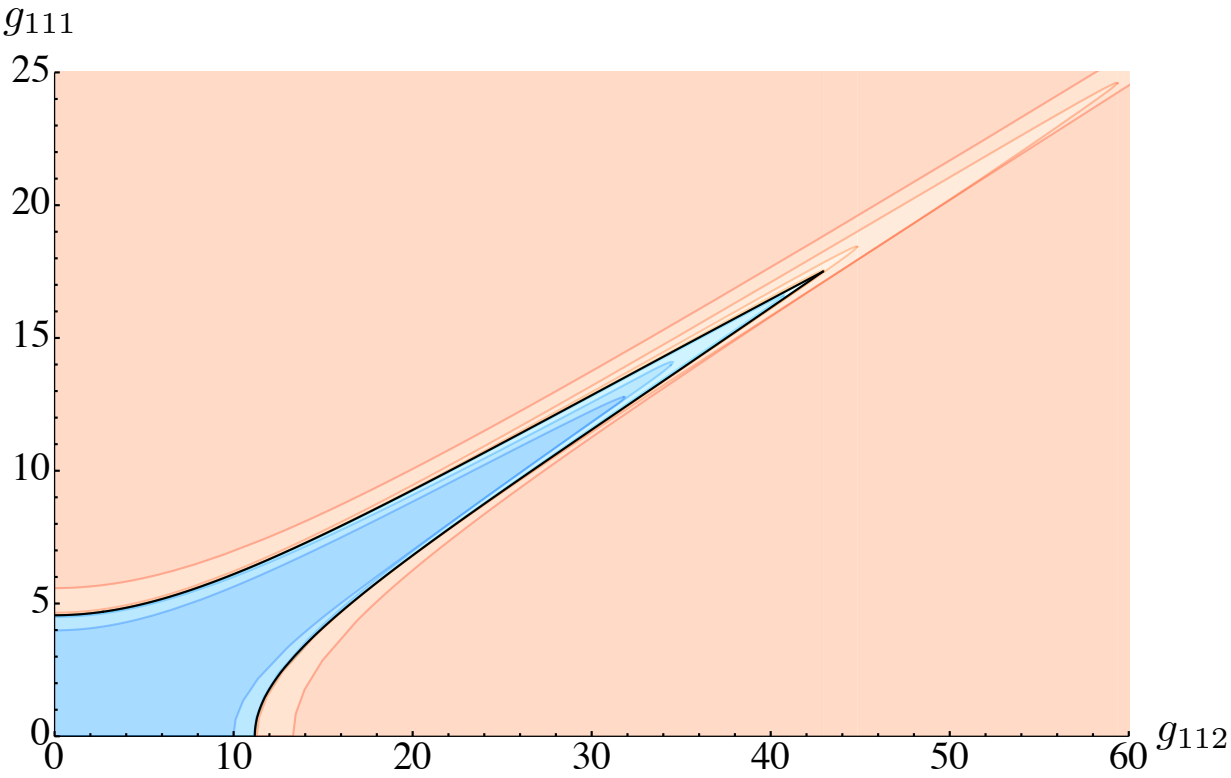

Figure 4.2: Numerical bounds on the coupling space $\{g_{111}, g_{112}\}$. The blue shaded regions enclose the allowed points for different $N_{\max}$ in our primal ansatz. The red shaded regions mark the points that are rigorously excluded. The thin black analytic curve is the boundary of the allowed region [1]. As we increase $N_{\max}$ from 1 to 5 in the primal problem, the blue regions enlarge, allowing for more and more points and eventually converging to touch the boundary of the permitted space (this is more evident in the "horn" region). In the dual strategy as we increase $N_{\max}$ from 1 to 5 we exclude more and more points. At convergence the excluded region touches the boundary of the allowed space. We restrict the plot to the first quadrant since it is symmetric under $g \leftrightarrow -g$.

$11 \to 12$ process.[17] This scattering process is a nice fully symmetric process. No matter which channel we look at it, it always describes two particles of type 1 (in the infinite future or past) scattering into a particle of type 1 and another of type 2. As such

$$M_{11\to 12}(s,t,u)$$

is fully symmetric under any permutation of the three Mandelstam variables s, t, u. Of course, they are not independent. Besides

$$s + t + u = 3m_1^2 + m_2^2 \tag{4.29}$$

[17]This process was not considered in [1] because it violates $\mathbb{Z}_2$ symmetry. Here we don't have $\mathbb{Z}_2$ symmetry so it is the first most natural process to consider after the lightest $11 \to 11$ scattering amplitude.

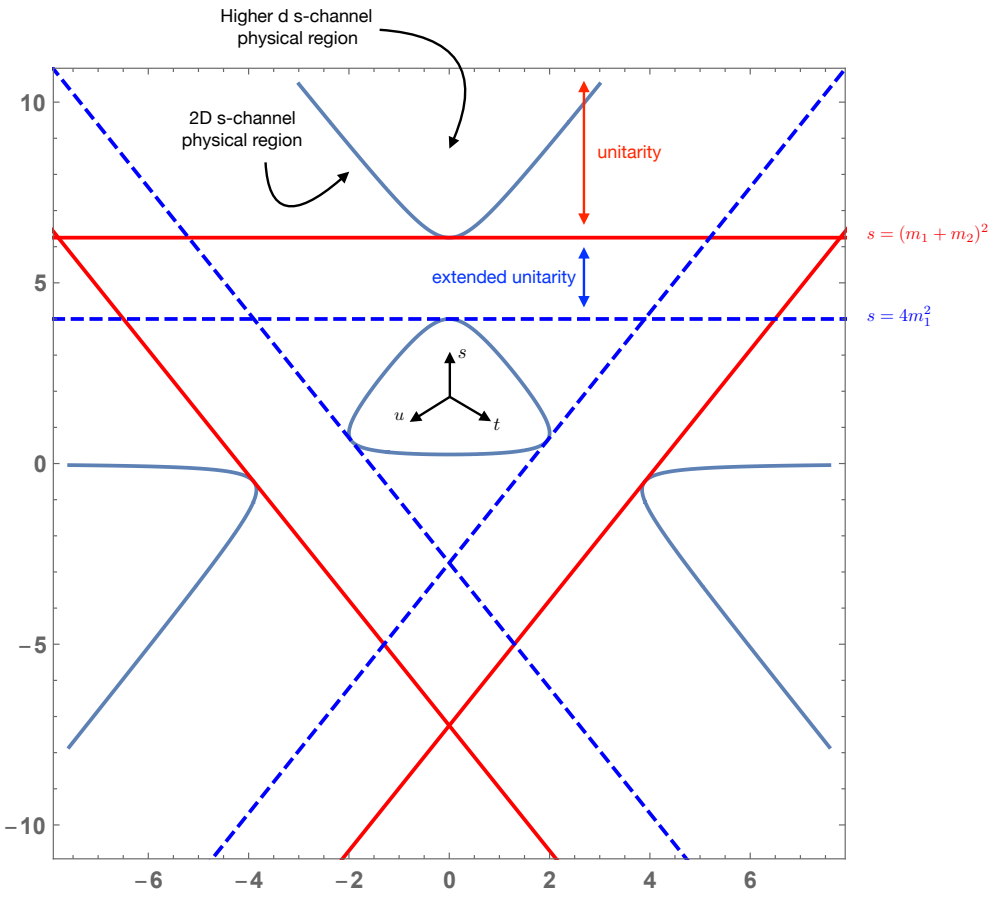

Figure 4.3: Maldelstam Triangle for $11 \to 12$ scattering. The x-axis is given by $x = (s + 2t - 3m_1^2 - m_2^2)/\sqrt{3}$. The $11 \to 12$ scattering if fully crossing invariant and indeed so is this picture. Physical processes in 2D lie on top of the blue solid lines and outside the red lines; in higher dimensions they fill in the interior of the regions delimited by the blue solid lines as one scans over physical scattering angles. Similar triangle for $12 \to 12$ scattering can be found in [1].

which holds in any dimension, we have the two dimensional constraint

$$stu = m_1^2 \left(m_1^2 - m_2^2\right)^2 \tag{4.30}$$

Equations (4.29) and (4.30) describe a curve. Its projection into real s, t, u is given by the solid curved blue lines in figure 4.3. There, we see four disconnected regions: three non-compact parabola like curves related by a rotation symmetry and a round triangle in the middle. The three outer curves are the three physical regions associated to the three scattering channels. The one in the top, for instance, corresponds to the s-channel. (Each outer curve has a left and right components which are equivalent; they are related to a simple parity transformation.) The s-channel outer curve start at $s = (m_1 + m_2)^2$ as indicated by the red solid line. That corresponds to the minimal energy necessary to produce a particle of type 1 and a particle of mass 2 at rest. (Recall that 2 is heavier than 1.) Another important energy marked by the blue dashed line in the figure occurs at $s = (2m_1)^2$

which would correspond to the minimal energy necessary to produce two particle of type 1 at rest. This is however *not* a physical energy for this process since physical energies are those for which we can produce *both* initial *and* final state. Nonetheless, the region between $s = 4m_1^2$ and $s = (m_1 + m_2)^2$ is very interesting because we know precisely what are the only possible physical states in that energy range: they can only be two particle states involving two particles of type 1. [111] The equation which reflects this is the so called *extended* unitarity relation which in this case reads

$$2\text{Im}\, M_{11\to 12} = \rho_{11}^2 M_{11\to 11} M_{11\to 12}^*, \qquad 4m_1^2 < s < (m_1+m_2)^2 \tag{4.31}$$

Here, since we are focusing on the top curve (which is crossing equivalent to any of the other two) we can think of M as a single function of s with

$$t(s) = \frac{1}{2}\left(3m_1^2 + m_2^2 - s - \sqrt{\frac{(s-4m_1^2)\left(-2m_2^2\left(m_1^2+s\right)+\left(s-m_1^2\right)^2+m_2^4\right)}{s}}\right) \tag{4.32}$$

$$u(s) = \frac{1}{2}\left(3m_1^2 + m_2^2 - s + \sqrt{\frac{(s-4m_1^2)\left(-2m_2^2\left(m_1^2+s\right)+\left(s-m_1^2\right)^2+m_2^4\right)}{s}}\right) \tag{4.33}$$

As a check, note that as $m_2 \to m_1$ we find $u \to 0$ and $t \to 4m_1^2 - s$ as expected for two dimensional elastic scattering of particles of equal mass.

The extended unitarity relation (4.31) is of course part of a coupled system of equations when we consider all components at once. They can all be nicely packed into matrix form by defining

$$\mathbb{U} \equiv 2\text{Im}\,\mathbb{M} - \mathbb{M}^\dagger \boldsymbol{\rho}\, \mathbb{M}\,, \tag{4.34}$$

where

$$\mathbb{M} \equiv \begin{pmatrix} M_{11\to 11} & M_{11\to 12} \\ M_{11\to 12} & M_{12\to 12} \end{pmatrix}, \quad \boldsymbol{\rho} \equiv \begin{pmatrix} \rho_{11}^2 = \frac{\theta\left(s-4m_1^2\right)}{2\sqrt{s-4m_1^2}\sqrt{s}} & 0 \\ 0 & \rho_{12}^2 = \frac{\theta\left(s-(m_1+m_2)^2\right)}{2\sqrt{s-(m_1+m_2)^2}\sqrt{s-(m_1-m_2)^2}} \end{pmatrix} \tag{4.35}$$

Then extended unitarity is the statement that $\mathbb{U} = \mathbf{0}$ for $s \in [4m_1^2, (m_1+m_2)^2]$. Above $s = (m_1+m_2)^2$ we are at physical energies and the extended unitarity relation is replaced by regular unitarity which is now nothing but the statement that $\mathbb{U}$ is a positive semi-definite matrix $\mathbb{U} \succeq 0$ for $s > (m_1+m_2)^2$.[18]

Finally we have poles. These correspond to the single particle exchanges when s or t or u are equal to either m_1 or m_2. The poles show up in the (rounded) triangle region in the Mandelstam triangle picture 4.3 in the $11 \to 12$ process as depicted in figure 4.4. For $12 \to 12$, we have $u = 0$ and the two t-channel poles lie in the extended unitarity

[18]Strictly speaking we can impose $\mathbb{U} = \mathbf{0}$ for a while longer in the unitarity region, more precisely until the energy where we can produce two particles of type 2 or three particles of type 1. In practice, bounds we will find will saturate unitarity so this will be automatic. Because of this, in all implementations, we will actually impose $\mathbb{U} \succeq 0$ even in the extended unitarity region, that is for any $s > 4m_1^2$. This is very convenient as it renders the problem convex.

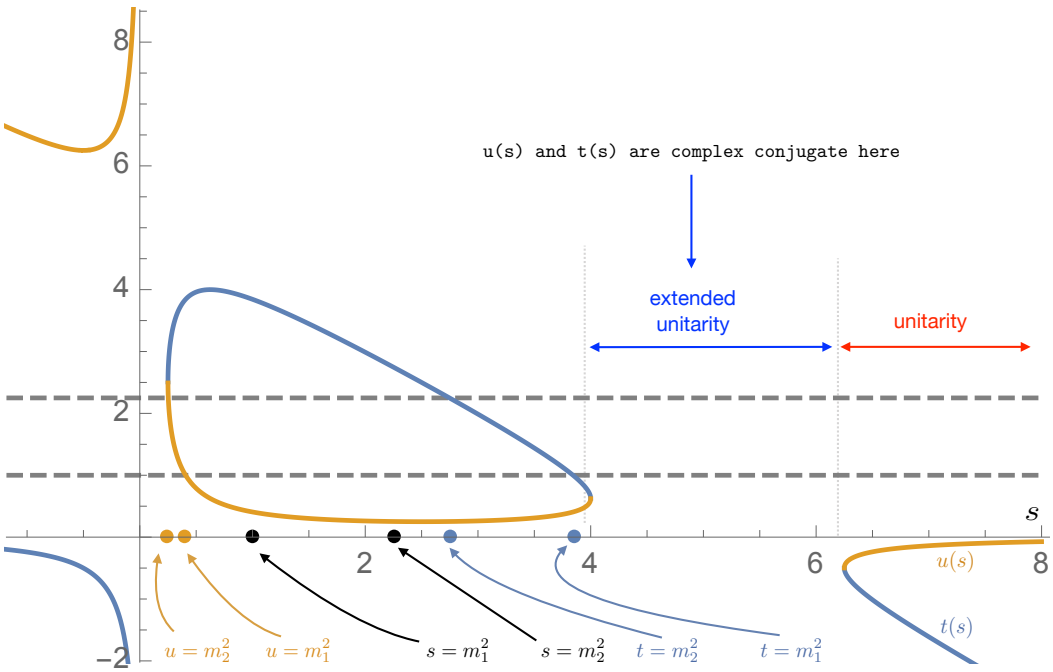

Figure 4.4: $t(s)$ (blue) and $u(s)$ (yellow) for $11 \to 12$ scattering and $m_2 = \frac{3}{2}m_1$. $u(s)$ and $t(s)$ are two branches of the same analytic function. In the extended unitarity region they are complex. As a function of s, all poles are located before the extended unitarity region. The grey horizontal dashed lines are equal to m_1^2 and m_2^2 and fix the position of the t– and u– channel poles.

region. Note here the important difference between unitarity and extended unitarity. In the unitarity region the amplitudes describe physical probability amplitudes, are bounded and can thus never have poles. In the extended unitarity region they can in principle. And here they do as we see in the figure.

All in all, we can summarize the analytic structure of our amplitudes with their cuts and poles by dispersion relations as usual. These can be conveniently packaged into a simple matrix statement $\mathbb{A} = \mathbf{0}$ with

$$\mathbb{A} \equiv \begin{pmatrix} \mathcal{A}_{11\to 11} & \mathcal{A}_{11\to 12} \\ \mathcal{A}_{11\to 12} & \mathcal{A}_{12\to 12} \end{pmatrix} \tag{4.36}$$

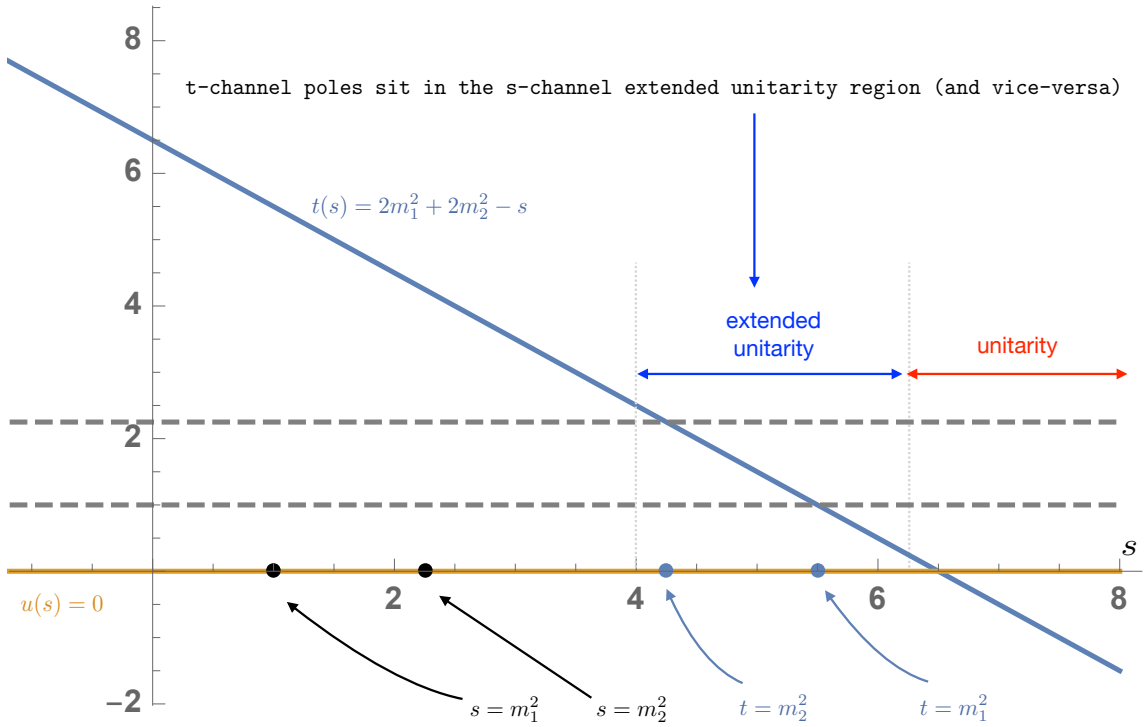

Figure 4.5: $t(s)$ (blue) and $u(s) = 0$ (yellow) for $12 \to 12$ forward scattering and $m_2 = \frac{3}{2}m_1$. In the s-channel extended unitarity sit t-channel poles (and vice-versa). The s-channel poles lie before the s-channel extended unitarity region. As in the previous figure, the grey horizontal dashed lines are equal to m_1^2 and m_2^2 determine the position of t-channel poles.

and

$$\mathcal{A}_{11\to11}(s) \equiv M_{11\to11}(s) - M^{\infty}_{11\to11} + g^2_{111}\left(\frac{1}{s-m_1^2} + \frac{1}{t(s)-m_1^2}\right) + g^2_{112}\left(\frac{1}{s-m_2^2} + \frac{1}{t(s)-m_2^2}\right) - \frac{1}{\pi}\int_{4m_1^2}^{\infty} \mathrm{Im}\, M_{11\to11}(z)\left(\frac{1}{z-s} + \frac{1}{z-t(s)}\right) dz\,, \tag{4.37}$$

$$\mathcal{A}_{11\to12}(s) \equiv M_{11\to12}(s) - M^{\infty}_{11\to12} + g_{111}g_{112}\left(\frac{1}{s-m_1^2} + \frac{1}{t(s)-m_1^2} + \frac{1}{u(s)-m_1^2}\right) - \frac{1}{\pi}\int_{4m_1^2}^{\infty} \mathrm{Im}\, M_{11\to12}(z)\left(\frac{1}{z-s} + \frac{1}{z-t(s)} + \frac{1}{z-u(s)}\right) dz\,, \tag{4.38}$$

$$\mathcal{A}_{12\to12}(s) \equiv M_{12\to12}(s) - M^{\infty}_{12\to12} + g^2_{112}\left(\frac{1}{s-m_1^2} + \frac{1}{t(s)-m_1^2}\right) - \frac{1}{\pi}\int_{4m_1^2}^{\infty} \mathrm{Im}\, M_{12\to12}(z)\left(\frac{1}{z-s} + \frac{1}{z-t(s)}\right) dz\,. \tag{4.39}$$

We hope there will be no confusing created by the fact that $t(s)$ signifies different things depending in which equation we are since crossing is implemented differently for different components. In (4.37) is it $t(s) = 4m_1^2 - s$; in (4.38) it is given by (4.32); and in (4.39) it is given by $t(s) = 2m_1^2 + 2m_2^2 - s$. In what follows, it should always be clear from the context which $t(s)$ we are talking about.

4.3.4 Multiple Component Dual Problem

The formulation of the dual problem for the multiple component scenario can be derived following the steps outlined in Sec. 4.2. There are, however, two practical obstacles: one is the complicated analytic structure of the $11 \to 12$ component, the other is the presence of the *extended* unitarity region. In this section we shall solve both problems if we want to arrive at an elegant and efficient dual numerical setup.

As always, we start from the primal radial problem

Primal Radial Problem for Multiple Component

$$
\begin{array}{lll}
\underset{\text{in } R^2,\mathbb{M}}{\text{maximize}} & R^2 & \\
\text{constr. by} & 0 = c_1 \equiv \text{Res}_{m_1^2}(M_{11\to 11}) - R^2 \sin^2\beta\,, & \\
& 0 = c_2 \equiv \text{Res}_{m_2^2}(M_{11\to 11}) - R^2 \cos^2\beta\,, & \\
& 0 = c_3 \equiv \text{Res}_{m_1^2}(M_{11\to 12}) - R^2 \sin\beta\cos\beta\,, & \\
& 0 = c_4 \equiv \text{Res}_{m_1^2}(M_{12\to 12}) - R^2 \cos^2\beta\,, & \\
s > 4m_1^2 & \mathbb{A} = 0 \qquad \text{where } \mathbb{A} \text{ is given in (4.36)}\,, & \\
s > 4m_1^2 & \mathbb{U} \succeq 0 \qquad \text{where } \mathbb{U} \text{ is given in (4.34)}\,. & (4.40)
\end{array}
$$

If not for the $c_i = 0$ equality constraints related to the radial problem, this setup would fit (4.19). Note also that the last constraint incorporate automatically unitarity and extended unitarity. Sometimes it is convenient to analyze it separately in the extended and regular unitarity regions corresponding to s bigger/smaller than $(m_1 + m_2)^2$ respectively.

We start our path towards the dual problem with the usual Lagrangian starting point

$$
\mathcal{L}{=}R^2 + \sum_{i=1}^{4} c_i\nu_i + \int_{4m_1^2}^{\infty} \text{tr}\ (\mathbb{w}\mathbb{A})\, ds + \int_{4m_1^2}^{\infty} \text{tr}\ (\mathbb{\Lambda}\mathbb{U})\, ds, \tag{4.41}
$$

with

$$
\mathbb{w} = \begin{pmatrix} w_1 & \frac{1}{2}w_2 \\ \frac{1}{2}w_2 & w_3 \end{pmatrix}
$$

and $\mathbb{\Lambda}$ semi-definite positive. Next we want to identify $\mathbb{w}$ as the discontinuities of full analytic functions $\mathbb{W}$ such that the resulting lagrangian becomes manifestly local. This is still possible here but turns out to be more interesting than before because of the richer $11 \to 12$ kinematics reviewed in the previous section. The final result is

$$
\mathbb{W} = \begin{pmatrix} W_1 & \frac{1}{2}W_2 \\ \frac{1}{2}W_2 & W_3 \end{pmatrix} \tag{4.42}
$$

with the dispersive representations of the three *dual scattering functions*

$$
W_1(s) = \frac{1}{\pi}\int_{4m_1^2}^{\infty} dz\, \text{Im}\, W_1(z) \left(\frac{1}{z-s} - \frac{1}{z-4m_1^2+s}\right), \tag{4.43}
$$

$$
W_2(s) = \frac{1}{\pi}\int_{4m_1^2}^{\infty} dz\, \text{Im}\, W_2(z) \left(\frac{1}{z-s} + \frac{J_t(s)}{z-t(s)} + \frac{J_u(s)}{z-u(s)}\right), \tag{4.44}
$$

$$
W_3(s) = \frac{1}{\pi}\int_{4m_1^2}^{\infty} dz\, \text{Im}\, W_3(z) \left(\frac{1}{z-s} - \frac{1}{z-(m_1+m_2)^2+s}\right). \tag{4.45}
$$

Note that the first and last lines here are pretty much as before: they correspond to anti-

crossing symmetric symmetric functionals W_1 and W_3. The middle line – with its Jacobians $J_t = dt/ds$ and $J_u = du/ds$ from (4.33,4.32) – is more interesting and more subtle. We explain its origin in full detail in appendix C.2.2.

Then we have the crucial relation required to render the Lagrangian local:

$$\begin{aligned}\int_{4m_1^2}^{\infty} \mathrm{tr}\ (\mathbb{w}\,\mathbb{A})\,ds \;\; &= \;\; \int_{4m_1^2}^{\infty} \mathrm{Im}\,\mathrm{tr}\ (\mathbb{W}\,\mathbb{M})\,ds + \pi\big(\operatorname*{Res}_{m_1^2}(M_{11\to 11})W_1(m_1^2) + \operatorname*{Res}_{m_2^2}(M_{11\to 11})W_1(m_2^2) \\ &\quad + \operatorname*{Res}_{m_1^2}(M_{11\to 12})W_3(m_1^2) + \operatorname*{Res}_{m_1^2}(M_{12\to 12})W_2(m_1^2)\big)\end{aligned}$$

Once we plug this relation into our lagrangian (4.41) the last line nicely combines with the first two terms there; these terms are the only terms where R, ν_i and the various residues appear.[19] Maximization with respect to the residues will relate the various functionals W evaluated at the stable particle masses to the lagrange multipliers ν_i as before while maximization with respect to R will lead to to a linear constraint involving all these functionals which plays the important role of our normalization condition. It reads:

$$1 + \pi(W_1(m_1)^2 \sin^2\beta + W_1(m_2^2)\cos^2\beta + W_2(m_1^2)\sin\beta\cos\beta + W_3(m_1^2)\cos^2\beta) = 0\,. \quad (4.46)$$

At this point we already got rid of the lagrange multipliers, the radius and the residues; our (partially extremized) Lagrangian is now a functional of the real and imaginary parts of the amplitudes $\mathbb{M}$ above $4m_1^4$ and of the functionals W_i also for $s > 4m_1^2$. Our dual functional d is therefore the maximization over the amplitudes $\mathbb{M}$ of

$$d(\mathbb{W}, \mathbb{\Lambda}) = \sup_{\mathbb{M}} \int_{4m_1^2}^{\infty} ds\Big(\mathrm{tr}\,(\mathrm{Im}\,\mathbb{W}\,\mathbb{M}) + \mathrm{tr}\ (\mathbb{\Lambda}\mathbb{U}(\mathbb{M}))\Big) \quad (4.47)$$

Since we are dealing with small 2×2 matrices we found it convenient to go to components at this point and also to separate the last integral into its extended and regular unitarity contributions separately.

For example, using

$$\mathbb{\Lambda} = \begin{pmatrix} \lambda_1 & \frac{1}{2}\lambda_2 \\ \frac{1}{2}\lambda_2^* & \lambda_3 \end{pmatrix} \succeq \mathbf{0}, \quad (4.48)$$

and evaluating the equations of motion for $\mathrm{Re}\,M_{12\to 12}$ and $\mathrm{Im}\,M_{12\to 12}$ in the extended unitarity region we get

$$\mathrm{Re}\,W_3 + 2\lambda_3 = 0, \qquad \mathrm{Im}\,W_3 = 0.$$

These two equations constrain the dual scattering function associated to the $12 \to 12$ to have a discontinuity starting at $(m_1 + m_2)^2$. Moreover, the semidefinite-positiveness condition on $\mathbb{\Lambda}$ implies[20] that

$$\lambda_3(s) \geq 0 \qquad \Longrightarrow \qquad \mathrm{Re}\,W_3(s) \leq 0, \qquad \text{for } 4m_1^2 < s < (m_1+m_2)^2.$$

[19] Recall that R, the residues and $M(s)$ for $s > 4$ are our primal variables, while ν_i and $W_i(s)$ are our dual variables.

[20] Second order variations show that the full positive semidefiniteness of $\mathbb{\Lambda}$ is required for the critical $\mathbb{M}_c$ to be a maximum.

We can solve all equations for all amplitude components in both the regular and extended unitarity region for the simple reason that $\mathbb{U}$ is quadratic in $\mathbb{M}$. In this way we get $d(\mathbb{W}, \mathbb{\Lambda})$ which we should now minimize. Its explicit expression is in appendix C.3.

We can now minimize first over positive semi-definite $\mathbb{\Lambda}$ to obtain our final dual functional $D(\mathbb{W})$. This step is quite non-trivial but leads to a very compact final result:

Dual Radial Problem for Multiple Component

$$\underset{\text{in } \mathbb{W}}{\text{minimize}} \qquad D^{\text{ext}}(\mathbb{W}) + D^{\text{phys}}(\mathbb{W}) \tag{4.49}$$

$$D^{\text{ext}}(\mathbb{W}) = -\int_{4m_1^2}^{(m_1+m_2)^2} ds\, \frac{|W_2|^2 - 4\text{Re}\, W_1 W_3 + |W_2^2 - 4W_1 W_3|}{4\rho_{11}^2 W_3}$$

$$D^{\text{phys}}(\mathbb{W}) = \int_{(m_1+m_2)^2}^{\infty} ds \left(\frac{\text{Re}\, W_1}{\rho_{11}^2} + \frac{\text{Re}\, W_3}{\rho_{12}^2} + \sqrt{\frac{|W_1|^2}{\rho_{11}^4} + \frac{|W_3|^2}{\rho_{12}^4} + \frac{|W_2|^2 + |W_2^2 - 4W_1 W_3|}{2\rho_{11}^2 \rho_{12}^2}} \right)$$

$$\text{const. by} \quad \text{Re}\, W_3 \leq 0, \quad \text{Im}\, W_3 = 0 \quad \text{for} \quad 4m_1^2 \leq s \leq (m_1+m_2)^2$$

$$\text{and by} \qquad 1 + \pi(W_1(m_1)^2 \sin^2\beta + W_1(m_2^2)\cos^2\beta + W_2(m_1^2)\sin\beta\cos\beta + W_3(m_1^2)\cos^2\beta) = 0$$

Here, the two contributions $D^{\text{phys}}(\mathbb{W})$ and $D^{\text{ext}}(\mathbb{W})$ correspond to the contributions of regular and extended unitarity. The last condition is the normalization condition (4.46) and the next-to-last line with the linear inequality constraint is in the end the only remnant of the positive semi-definiteness of the lagrange multiplier matrix $\mathbb{\Lambda}$. All these constraints can actually be trivialized as we explain in the next section. This will lead to a unconstrained (albeit non-linear) dual minimization problem which we will then solve numerically.

4.3.5 Numerical Results

Now we perform both a primal and a dual numerical exploration to check the correctness of problem (4.49).

It what follows we will propose ansatze to parametrize families of dual functionals W_j's. The cleverer the ansatze, the best will the bounds be and the fastest they will converge of course. Clever or not, it is of course important to stress that any ansatze for W_i leads to a totally rigorous exclusion bound.

The $11 \to 11$ dual ansatz is the same used to produce the rigorous dual bounds in figure 4.2

$$W_1(s) = \frac{1}{s(4m_1^2 - s)} \sum_{n=1}^{N_{\max}} a_n \left(\rho(s)^n - \rho(t)^n\right), \tag{4.50}$$

where $t = 4m_1^2 - s$, a_n are free variables and $\rho(s)$ is the usual ρ-variable foliation introduced in [10] – see eq. (4.18) with $m = m_1$. This ansatz has the right branch-point discontinuities and it is manifestly anti-crossing symmetric. At infinity it decays as $W_1 \sim s^{-5/2}$; in fact, this behavior ensures that the dual objective in (4.28) is integrable. The poles at $s = 4m_1^2$

and $s = 0$ are not necessary to obtain optimal bounds, but in practice they speed up the numerical convergence.[21]

For the $11 \to 12$ dual ansatz we use

$$W_2(s) = \frac{1}{\sqrt{4m_1^2 - s}\sqrt{4m_1^2 - t}\sqrt{4m_1^2 - u}} \sum_{n=1}^{P_{\max}} b_n \left(\rho(s)^n + J_t(s)\rho(t)^n + J_u(s)\rho(u)^n\right), \quad (4.51)$$

where t and u are respectively given in (4.32) and (4.33). Recall also that $J_t = dt/ds$ and $J_u = du/ds$. At infinity $W_2 \sim s^{-3/2}$, therefore the dual objective function (4.49) wouldn't be integrable at infinity. However, it is sufficient to fix two of the b_n's free variables to ensure the $W_2 \sim s^{-5/2}$ decay. Notice that eq. (4.51) has branch point singularities at $s = t = u = 4m_1^2$ where the extended unitarity discontinuity in the physical amplitude start. At the physical threshold $s = (m_1 + m_2)^2$ in principle we could add additional singularities such as a pole (similarly to (4.50)), however it turns out that numerically it makes no difference.

It is convenient to design the $12 \to 12$ dual ansatz such that it automatically satisfy the constraints $\operatorname{Im} W_3 = 0$ and $\operatorname{Re} W_3 < 0$ in the extended unitarity region so that our optimization is unconstrained. The former is easily achieved using a ρ-foliation with cut starting at $s = (m_1 + m_2)^2$ such as

$$\tilde{\rho}(s) = \frac{\sqrt{(m_1 + m_2)^2 - 2m_1^2} - \sqrt{(m_1 + m_2)^2 - s}}{\sqrt{(m_1 + m_2)^2 - 2m_1^2} + \sqrt{(m_1 + m_2)^2 - s}}.$$

The latter is more subtle: we could always impose linear constraints such as $\operatorname{Re} W_3(s) \equiv W_3(s) \leq 0$ on some grid of points in the $4m_1^2 < s < (m_1 + m_2)^2$ segment in our dual minimization problem, but this would make `Mathematica`'s basic `FindMinimum` slow and nearly unusable. Instead, we opt to write the ansatz

$$W_3(s) = (\tilde{\rho}(t) - \tilde{\rho}(s)) \left(\frac{1}{\sqrt{(m_1 + m_2)^2 - s}} + (s \leftrightarrow t)\right) \left(\sum_{n=0}^{Q_{\max}} c_n (\tilde{\rho}(s)^n + \tilde{\rho}(t)^n)\right)^2$$

where $t = 2m_1^2 + 2m_2^2 - s$. It is easy to check that W_3 has actually definite sign in a larger region than extended unitarity: $W_3 > 0$ in $t((m_1 + m_2)^2) = (m_1 - m_2)^2 < s < m_1^2 + m_2^2$ and $W_3 < 0$ in $m_1^2 + m_2^2 < s < (m_1 + m_2)^2$ which of course include the extended unitarity region. This may sound too restrictive, however this is one of the advantages of the dual formulation: as long as the dual scattering functions satisfy the dual constraints, the bounds obtained are rigorous. Of course, a legitimate question is whether our ansatz is able to attain the optimal value of the dual problem. It turns out that for the case we are studying

[21] We have numerical evidence to believe they are the right singularities the optimal dual scattering function should have. However, it is worth noticing they do not spoil integrability at threshold. We can look at eq. (4.11): the $\int_4^\infty \operatorname{Im}(M(s)W(s))\, ds$ is integrable if $W(s) \sim 1/(s-4)$ close to threshold because the amplitude vanishes as $M(s) \sim \sqrt{s-4}$.

[22] The dual curves, from outer to inner corresponds $(N_{\max}, P_{\max}, Q_{\max})$ equal to $(8,8,8)$, $(10,10,10)$ and $(10,20,20)$; the primal curves from inner to outer correspond to 136, 271 and 1111 degrees of freedom in the primal ansatz for the amplitude matrix. We used splines analogous to those used in [1].

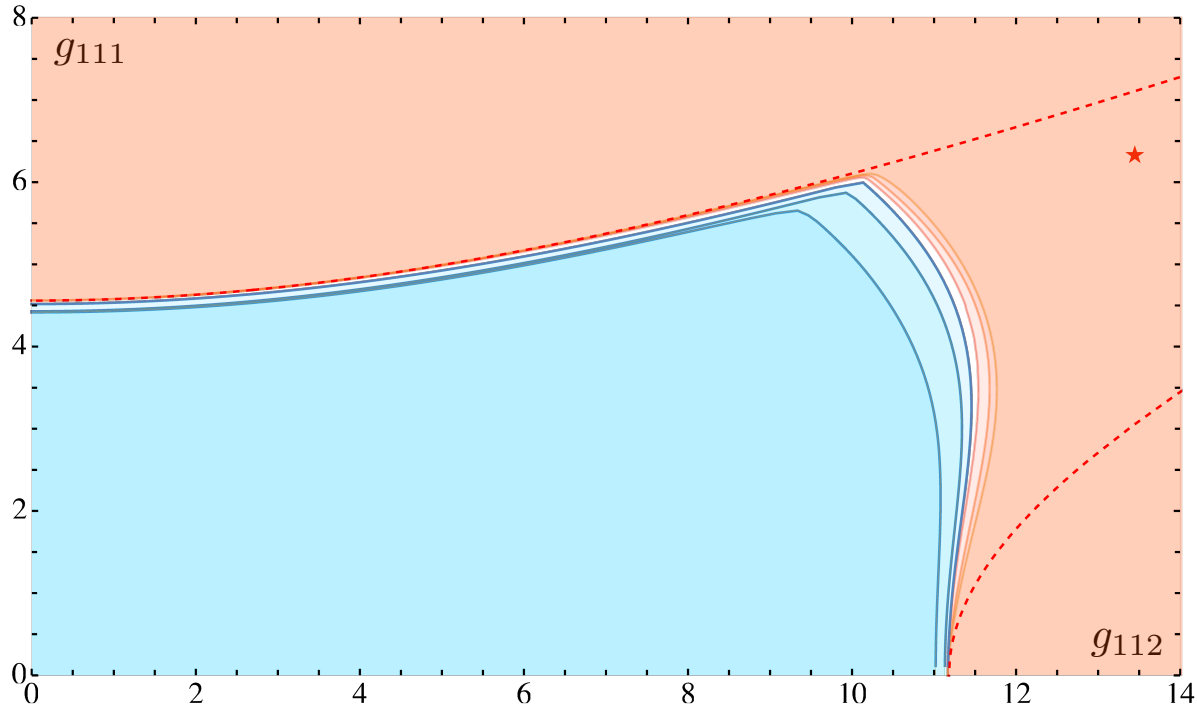

Figure 4.6: Dual (red) and Primal (blue) excluded/allowed regions once the full system of amplitudes is included.[22] The multi-component improved boundary is now rigorously trapped between the primal and dual bounds. The red dashed line is the previous single component boundary. As we now impose the full system constraints the bound improves dramatically excluding most of the horn like figure. The red star point, for instance, was allowed (feasible) before from the primal problem perspective (it was blue in figure 4.2) and is now excluded. Once again, we restrict the plot to the first quadrant due to $g \leftrightarrow -g$ symmetry.

this ansatz is also approximately optimal numerically.

Now we have all the ingredients to just code the objective in (4.49) and minimize it unconstrained. The result for the $\{g_{111}, g_{112}\}$ space is shown in figure 4.6 (red shaded regions). In the same figure, the blue shaded areas are determined running the primal problem eq. (4.40) – see [1] for details about primal multiple component numerics. The red dashed line marks the single component analytic bound. The white space in between the primal and dual areas is the uncertainty we have in the definition of the boundary for the full coupled system. Clearly the optimal bound is almost completely trapped!

4.4 Discussion

Icarus said that *all limits are self-imposed*. That is not totally true. Unitarity, crossing symmetry and analyticity clearly also impose very important bounds.

In this chapter we described the first steps towards a dual bootstrap program and applied it on the next-to-simplest S-matrix bootstrap scenario: Two dimensional amplitudes

with more than one particle type and more than one mass.[23]

One main goal of this chapter was to set up the theory behind this physical problem and connect it with the standard language of dual and primal maximization problems as optimization problems. Indeed, a great deal of section 4.2 can bet transported from math books [135–137].

In the S-matrix bootstrap studied here the primal problem is linear but constrained; the dual problem is non-linear but unconstrained.[24] For the primal problem, we used the powerful `SDPB` code to perform the optimizations. For the dual problem we used `Mathematica`'s basic `FindMinimum`.[25] Even so, the dual problem is orders of magnitude faster right now.[26] It would be very interesting to look for more tailor made algorithms for our kind of minimizations to speed the dual even more.

Of course, the main advantage of having a dual problem is not speed but the fact that the bounds whence generated are completely rigorous. What is once excluded can never be included back. This is in contradistinction with the primal formulation where more constraints will often rule out a previously feasible solution. In practice the best is to use both dual and primal problems at once. When they almost touch each other – meaning the so called duality gap is closing – we know we are reaching the very optimal bounds!

Having developed the theory and a very fast dual problem, we look forward to putting it to use in several interesting physical applications.

One goal would be to bootstrap the Ising model field theory with both thermal and magnetic deformations turned on. Let us recall why we think this is promising. The Ising field theory with pure magnetic deformation [138] is at the boundary of the single amplitude bound [9], see figure 12 there. What is more, it is precisely at the top of a sharp horn like 3D bound in the coupling space as depicted in figure 4.7.[27] Something we clearly learned in this chapter is how multiple amplitudes can truncate such horns; compare figures 4.2 and 4.6. At the magnetic Ising point this dramatic truncation can not happen. This theory exists after all, we can not rule it out. What happens is that the very special values of the masses of the stable particles of this theory allow for fine tuned cancelations in $11 \to 12$ and other amplitudes such that they completely vanish and thus do not affect the single component bound which produces the horn. In other words, the purely magnetic deformation, being precisely integrable, is very special. As soon as we move away from these special masses by turning a thermal deformation, the multiple amplitude bounds are now expected to strongly affect the single component analysis and this provides a strong

[23] The simplest example was kicked off in [12] for a single particle species transforming in some global symmetry group.

[24] The unconstrained nature of the dual problem is an extremely powerful and fortunate property which was not a priori guaranteed. It is the nature of the S-matrix Bootstrap problems considered up to now that allowed us to trivialize all dual constraints encountered thus far.

[25] `FindMinimum` is sometimes an art. It is not uncommon to ask for a minimization, give `Mathematica` a viable starting point and obtain a final result bigger than the starting value. Go figure. Of course, it is a price to pay when having a one size fits all algorithm. See also next footnote.

[26] The dual curves in figure 4.6 contain thousands of points and take about a day to generate in a regular laptop. The primal curves take a few days in a cluster. One reason why we did not use the cluster for the dual problem is that we found it useful to hotstart `FindMinimum` by starting the minimization search at a given point using the final result of the neighbouring point.

[27] In [9] only the maximum g_{111} coupling was plotted so it was not possible to see this cusp so sharply.

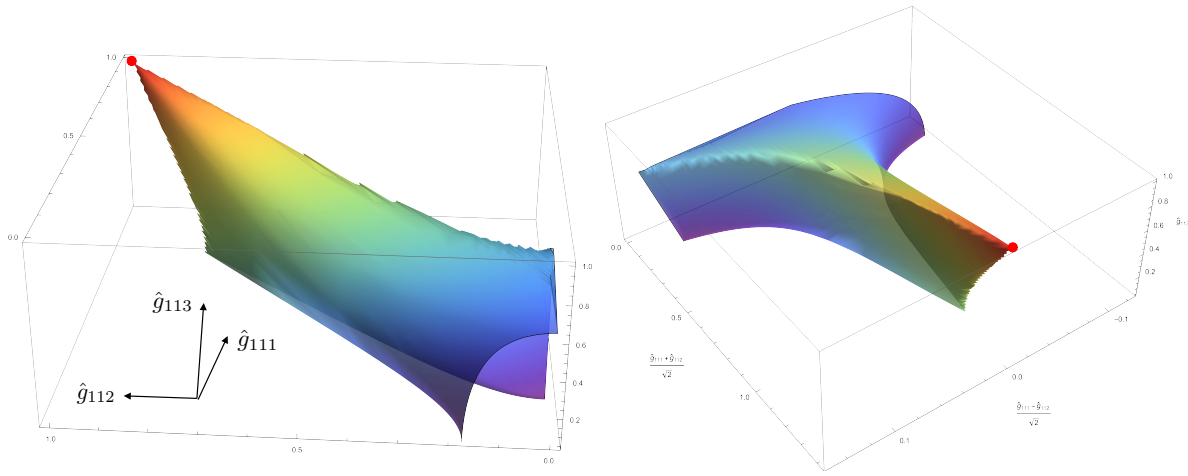

Figure 4.7: **Left:** Maximum couplings g_{11j} for a theory with the masses of the Ising field theory deformed by magnetic field depicted by normalizing those by the Ising couplings, $\hat{g}_{11j} \equiv g_{11j}/g_{11j}^{\texttt{Ising}}$ at this E_8 point. **Right:** The plot on the right is obtained by a simple rotation of the first by 45 degrees which magnify some of the nice features of the plot. (These plots were generated using the dual method developed in this chapter with $N = 20$; it might be possible to derive this shape analytically. We did it for one of the faces but did not pursue this further.) The Ising field theory, the red dot, lies beautifully at the very tip of these horn shaped single component plots.

improvement over the bounds in [9]. This is not totally trivial to implement because close to the magnetic point, the Ising field theory has three stable particles. Exploring the space of couplings g_{ijk} between these particles is hard because this space is ten dimensional. The trick here is to find a clever lower dimensional section of this multidimensional space, with good optimization targets, which could efficiently isolate the magnetic plus thermal Ising deformation.

Another interesting theory to explore would be the tri-critical Ising model. In the discussion section of [1] an S-matrix bootstrap homework exercise was proposed in relation to this model. With the great speed gains from the dual technology here developed this homework seems very doable. The deformation proposed there concerns a deformation preserving $\mathbb{Z}_2$ symmetry. The dual $\mathbb{Z}_2$ symmetric bootstrap is discussed in appendix C.4 for the case of equal masses; the uneven masses case should be a straightforward generalization of the analysis of the main text.

One step up in the complexity ladder of bootstrap problems are problems whose amplitudes depend on more than a single complex variable. One example is of course higher dimensions where we have both an energy and an angle even in two-to-two scattering processes.[28] Another example are higher point amplitudes, even in two dimensions. In fact, in a very roundabout way, we arrived at the class of problems presented in this chapter precisely while starting to tackle these multi-particle problems in work in progress with J.

[28]It is also in higher dimensions where the tension between absence of particle production and crossing symmetry is most striking [45, 47] which is another point a dual formulation should be very helpful in clarifying.

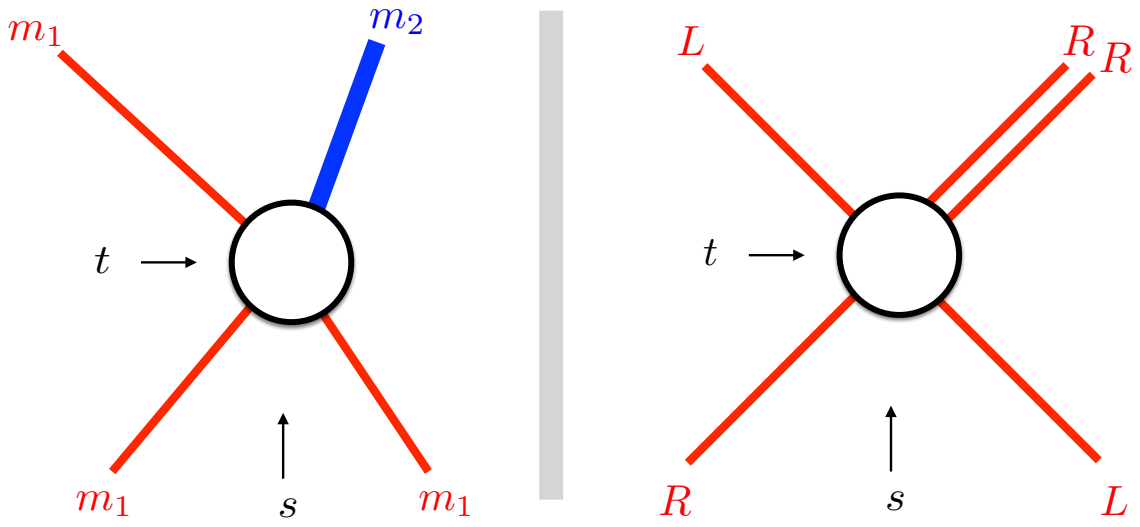

Figure 4.8: The kinematics of the two-to-two process $11 \to 12$ is very reminiscent of two-to-three scattering of massless particles as illustrated here. Both processes are fully crossing symmetric. Particle 2 on the left is analogous to the jet of two right-movers on the right. This two-to-three scattering process should show up in flux tube physics [139–141] where parity is broken. Extending the flux tube S-matrix boostrap program initiated in [142] to include such processes would be extremely interesting.

Penedones, [48]. The point is that the $11 \to 12$ amplitudes studied in this chapter are in a sense very similar to a sort of $2 \to 3$ scattering process of massless particles as illustrated in figure 4.8. The jet of the two right movers in the future is like particle 2. Of course, that jet can have any sub-energy. Nonetheless, this problem is within reach.

Chapter 5

The Wilson Loop – Large Spin OPE Dictionary

5.1 Introduction

In appendix B of [143] a duality was proposed between the n-point correlation functions of large spin single trace twist-two operators in planar $\mathcal{N} = 4$ SYM and the expectation value of null polygonal Wilson loops with $2n$ sides.[1] The simplest non-trivial example of such duality would relate three point functions and the null hexagon Wilson loop

$$\langle \mathcal{O}_{J_1}(x_1, \epsilon_1)\mathcal{O}_{J_2}(x_2, \epsilon_2)\mathcal{O}_{J_3}(x_3, \epsilon_3)\rangle \longleftrightarrow \mathbb{W}(U_1, U_2, U_3) \tag{5.1}$$

The goal of this chapter is to sharpen the arrow in this relation making it into a precise equation with an equal sign with all the appropriate normalizations and with a precise dictionary relating the variables on both sides of this equation: the spins J_j and polarization vector ϵ_j on the left hand side and the hexagon cross-ratios U_i on the right hand side.

This is (5.27).[2]

We got there in two steps. First we examined the OPE decomposition of six point functions in the so-called snowflake channel: we fuse adjacent pairs of external operators into spinning operators which are then glued together through a tensor structure parametrized by integer indices ℓ_i. The starting point is intimidating. It is given by 9 sums (3 are spin sums, 3 are sums over tensor structures indices and the last 3 appear in the representation of the relevant conformal block). When the external points approach the cusps of a

[1] This duality is one branch out of a rich web of dualities relating various seemingly distinct quantities in $\mathcal{N} = 4$ SYM such as Wilson Loops and Scattering Amplitudes [102] and Wilson loop and the null limit of correlation functions [101]. Indeed, null correlation functions are dominated by leading twist large spin operators which is one way to argue for the duality mentioned in the main text. The argument in [143] also uses some string theory intuition coming from the behavior of minimal surfaces of spinning strings and how they are expected to become related to the minimal surface describing null polygonal Wilson loops when their spin is taken to infinity. The argument was qualitative and no precise equality was spelled out in [143]. Our main result (5.27) fills in this gap.

[2] The reader might be frowning. In (5.27) there are ℓ_i's instead of ϵ_i's. Worry not, they are simply conjugate variables as reviewed in the next section and it is straightforward to change from one to the other. The map of kinematics using the spinors is given in (D.9).

null hexagon, six of these sums can be performed by saddle point. The location of the saddle point will fix the tensor structure indices ℓ_j to precise locations depending on the cross-ratios U_j of the null hexagon. This gives us the map $\ell(U)$ spelled out in equation (5.14) below. Next we analysed further the null six point correlator through an analytic bootstrap perspective (generalizing [144] – where this was carried over for small U_j in the so called origin limit [145] – to generic finite cross-ratios U_j). This allowed us to see how the correlators becomes Wilson loops and what are all the precise conversion factors showing up along the way.

Null hexagon Wilson loops have light-cone singularities when non-adjacent vertices become null. We conjecture how these singularities *emerge* from the discrete structure of the structure constants in the large spin limit. The limit (5.1) should be understood to hold *before* light-cones are crossed, i.e. in the "Euclidean" region of positive cross ratios. Configurations with time-like separations should then be achieved through analytic continuation from this safe region. These musings are backed up by explorations of novel one loop data we extract.

In sum, in this chapter we cleaned up the kinematics behind the duality (5.1) using bootstrap techniques.

5.2 Spinning Three Point Functions

The purpose of this section is to establish notation. A traceless symmetric, spin J, primary operator in a CFT can be represented through an homogenous polynomial of degree J on an auxiliary null polarization vector ϵ

$$\mathcal{O}_J(x,\epsilon) = \epsilon_{\mu_1}\dots\epsilon_{\mu_J}\mathcal{O}^{\mu_1\dots\mu_J}(x). \tag{5.2}$$

In a parity preserving 4D CFT, three point functions of traceless symmetric parity even operators can be parametrized as

$$\langle \mathcal{O}_{J_1}(x_1,\epsilon_1),\mathcal{O}_{J_2}(x_2,\epsilon_2),\mathcal{O}_{J_3}(x_3,\epsilon_3)\rangle = \frac{\sum\limits_{\ell_i} C^{J_1,J_2,J_3}_{\ell_1,\ell_2,\ell_3} V_{1,23}^{J_1-\ell_2-\ell_3} V_{2,31}^{J_2-\ell_3-\ell_1} V_{3,12}^{J_3-\ell_1-\ell_2} H_{23}^{\ell_1} H_{31}^{\ell_2} H_{12}^{\ell_3}}{(x_{12}^2)^{\frac{\kappa_1+\kappa_2-\kappa_3}{2}}(x_{23}^2)^{\frac{\kappa_2+\kappa_3-\kappa_1}{2}}(x_{31}^2)^{\frac{\kappa_3+\kappa_1-\kappa_2}{2}}}, \tag{5.3}$$

where κ_i is the conformal spin and

$$V_{i,jk} = \left(\epsilon_i\cdot x_{ik}x_{ij}^2 - \epsilon_i\cdot x_{ij}x_{ik}^2\right)\frac{1}{x_{jk}^2}, \qquad H_{ij} = \epsilon_i\cdot x_{ij}\epsilon_j\cdot x_{ij} - \tfrac{1}{2}x_{ij}^2\epsilon_i\cdot\epsilon_j,$$

are a basis of conformal covariant tensors [146], see appendix D.1. We sum over all non-negative integers ℓ's such that all exponents in (5.3) are non-negative.

Henceforth we will consider twist two operators in planar $\mathcal{N}=4$ SYM at weak coupling and use the short-hand notation $C^{\bullet\bullet\bullet} \equiv C^{J_1,J_2,J_3}_{l_1,l_2,l_3}$ for the structure constants of three

spinning operators. We also have

$$C^{\bullet\bullet\bullet} = \hat{C}^{\bullet\bullet\bullet} \times \underbrace{\prod_{i=1}^{3} \frac{J_i!^2}{(\ell_i!)^2\sqrt{(2J_i)!}(J_i+\ell_i-\sum_{j=1}^{3}\ell_j)!}}_{C^{\bullet\bullet\bullet}_{\text{tree level}}} \tag{5.4}$$

where $\hat{C}^{\bullet\bullet\bullet} \equiv C^{\bullet\bullet\bullet}/C^{\bullet\bullet\bullet}_{\text{tree level}}$ is given by an expansion in small 't Hooft coupling λ and captures all loop corrections.

5.3 Null Correlators and the $U(\ell)$ map

We consider the null polygonal limit of the six point correlator of the lightest single trace gauge invariant scalar operators as in [144]. This correlator is given by 9 cross-ratios carefully reviewed in appendix D.3. We will sequentially send 6 of them to zero when taking each x_i to be null separated from x_{i+1} to obtain in the end a function which depends on the remaining 3 cross-ratios. More precisely, the final result will depend on the three finite cross-ratios as well as logs of the six vanishing cross-ratios. The dependence on the latter will be through a factorized universal pre-factor which we can fix. The dependence on the finite cross-ratios will be related to the renormalized Wilson loop which is theory dependent.

As explained in [144] we can project into leading twist (i.e. two) in the 12, 34 and 56 channel in the snowflake decomposition by taking $u_1, u_3, u_5 \to 0$ or $x_{12}^2, x_{34}^2, x_{56}^2 \to 0$ as depicted in figure 5.1a. In this limit, in perturbation theory the six point function behaves as

$$G_6(u_1, u_2, u_3, u_4, u_5, u_6, U_1, U_2, U_3) \to u_1 u_3 u_5\, \hat{G}_6(u_2, u_4, u_6, U_1, U_2, U_3) \tag{5.5}$$

The function $\hat{G}_6$ has no powers of u_1, u_3 or u_5 but it implicitly contains arbitrarily many powers of $\ln(u_1), \ln(u_3)$ and $\ln(u_5)$ arising from the anomalous dimensions of the twist two operators. This function can be expanded as

$$G_6 = \sum_{J_1,J_2,J_3} \sum_{\ell_1,\ell_2,\ell_3} \underbrace{\hat{P}^{\bullet\bullet\bullet}(J_1, J_2, J_3, \ell_1, \ell_2, \ell_3)}_{\texttt{dynamic}} \int_{y_j\in[0,1]} dy_1 dy_2 dy_3 \underbrace{\mathcal{F}(J_i, \ell_i, y_i, u_i, U_i)}_{\texttt{kinematics}} \tag{5.6}$$

where $\hat{P}$ is a (theory dependent) normalized product of three point functions[3] and $\mathcal{F}$ is a (theory independent) conformal block integrand worked out in [144] and recalled in appendix D.4.

Series expanding the left and right hand side of relation (5.6) around $u_i, U_i = 1$ –

[3]It is given by a product of three three point functions of two scalar and one spinning operator (for the three OPE's of the 12, 34 and 56 OPE's of the external scalar operators) and a fully spinning three point function (the intersection of the three gray lines in figure 5.1),

$$\hat{P}^{\bullet\bullet\bullet}(J_1, J_2, J_3, \ell_1, \ell_2, \ell_3) = \hat{C}^{\bullet\bullet\bullet}(J_1, J_2, J_3, \ell_1, \ell_2, \ell_3)\hat{C}^{\circ\circ\bullet}(J_1)\hat{C}^{\circ\circ\bullet}(J_2)\hat{C}^{\circ\circ\bullet}(J_3)\,. \tag{5.7}$$

Here the hat $\hat{C}$ stands for tree-level normalized quantity $C/C_{\text{tree level}}$.

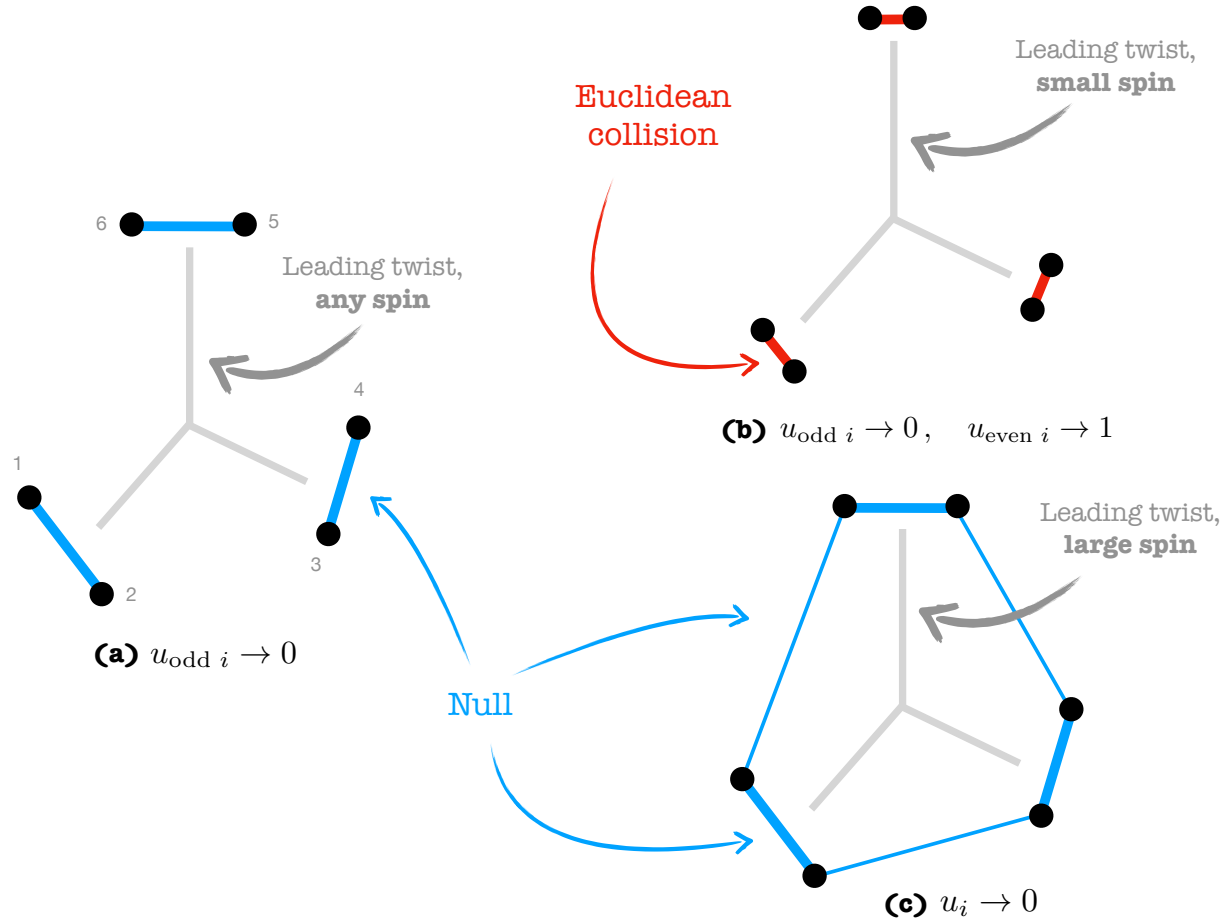

Figure 5.1: Various snow-flake OPE limits discussed in this chapter. The bottom right one is the double light-like OPE explored in this section. The top right one is the more conventional Euclidian OPE used in appendix D.5 to extract new one loop OPE data which is analysed in appendix D.6. We can get to both starting from the single light-like OPE on the left.

corresponding to the conventional Euclidean OPE limit depicted in figure 5.1b – allows us to extract structure constants $\hat{P}$ for the lowest spins J's and polarization integers ℓ's. This data extraction using the one loop result [147] for G_6 is described in appendices D.5, D.6. This one loop OPE data will be used in section 5.

In this section, we consider instead the limit $u_2, u_4, u_6 \to 0$ (at fixed U_j) – known as the Lorentzian null OPE limit depicted in figure 5.1c – which is realized when all external points approach the cusps of a null hexagon which in turn is parametrized by the finite cross-ratios U_i. In this limit

$$\hat{G}_6(u_2, u_4, u_6, U_1, U_2, U_3) \to u_2 u_4 u_6\, \widetilde{G}_6(U_1, U_2, U_3) \tag{5.8}$$

where $\widetilde{G}$ is a non-trivial function of the finite U_i which still contains arbitrary powers of $\ln(u_j)$ but no powers of u_j since these were by now all sent to zero. We find two important simplifications when computing the correlator (5.6) in this $u_j \to 0$ limit:

- The integral is dominated by large spins J_j and large polarization integers ℓ_j. We can thus transform

$$\sum_{J_1,J_2,J_3}\sum_{\ell_1,\ell_2,\ell_3} \to \frac{1}{8}\int_0^\infty dJ_1 dJ_2 dJ_3 d\ell_1 d\ell_2 d\ell_3$$

  in (5.6) being left with nine integrals in total. (The $8 = 2^3$ comes from the fact that the spins J are even.)

- Six of those nine integrals can be done by saddle point.

More precisely, we find that $0 = \partial \ln \mathcal{F}/\partial \ell_j = \partial \ln \mathcal{F}/\partial y_j$ leads to the saddle point location

$$y_1 = \frac{J_2}{J_2 + J_3\sqrt{\frac{U_2U_3}{U_1}}}\,, \tag{5.9}$$

$$y_2 = \frac{J_3}{J_3 + J_1\sqrt{\frac{U_1U_2}{U_3}}}\,, \tag{5.10}$$

$$y_3 = \frac{J_1}{J_1 + J_2\sqrt{\frac{U_1U_3}{U_2}}} \tag{5.11}$$

and more importantly

$$\ell_1 = \frac{J_2J_3}{J_2 + J_3 + J_1\sqrt{\frac{U_2}{U_1U_3}}}\,, \tag{5.12}$$

$$\ell_2 = \frac{J_1J_3}{J_1 + J_3 + J_2\sqrt{\frac{U_1}{U_2U_3}}}\,, \tag{5.13}$$

$$\ell_3 = \frac{J_1J_2}{J_1 + J_2 + J_3\sqrt{\frac{U_3}{U_1U_2}}} \tag{5.14}$$

which nicely relate the Wilson loop cross-ratios in the right hand side of (5.1) with the spin and polarization integers appearing in structure constant in the left hand side of this relation. They are the sought after dictionary between these two worlds. (If $J_i \gg \ell_i \gg 1$ then the U_i are very small; this was the limit studied in [144].)

The saddle point evaluation leads to

$$\widetilde{G}_6 = \frac{4u_2u_4u_6}{(U_1U_2U_3)^{\frac{1}{2}}}\int_0^\infty dJ_1\, dJ_2\, dJ_3\, \hat{P}^{\bullet\bullet\bullet}(J_1,J_2,J_3,\ell_1,\ell_2,\ell_3)e^{-\frac{J_1J_2}{J_3}\times\frac{u_2\sqrt{U_2}}{\sqrt{U_1U_3}}-\frac{J_2J_3}{J_1}\times\frac{u_4\sqrt{U_1}}{\sqrt{U_2U_3}}-\frac{J_1J_3}{J_2}\times\frac{u_6\sqrt{U_3}}{\sqrt{U_1U_2}}}$$
$$\times\, 2^{\gamma_1+\gamma_2+\gamma_3}\left(\frac{u_1}{J_1}\right)^{\frac{\gamma_1}{2}}\left(\frac{u_3}{J_2}\right)^{\frac{\gamma_2}{2}}\left(\frac{u_5}{J_3}\right)^{\frac{\gamma_3}{2}}\left(\frac{\ell_1}{U_1^{\frac{1}{2}}}\right)^{\frac{-\gamma_1+\gamma_2+\gamma_3}{2}}\left(\frac{\ell_2}{U_3^{\frac{1}{2}}}\right)^{\frac{\gamma_1-\gamma_2+\gamma_3}{2}}\left(\frac{\ell_3}{U_2^{\frac{1}{2}}}\right)^{\frac{\gamma_1+\gamma_2-\gamma_3}{2}}\,, \tag{5.15}$$

where ℓ_j depend on the integration variables J_j through (5.14). Implicit in this discussion is the assumption that the integral is dominated by the saddle point developed by the conformal block integrand. This should be valid for positive Us, see further discussion in section 5.5. One can nicely check that when $\lambda = 0$ (so that the full second line as well as $\hat{P}^{\bullet\bullet\bullet}$ can be set to 1) this expression indeed integrates into the free theory result $\widetilde{G}_6 = 1$.

We close this section with the inverse of the map (5.14):

$$\begin{aligned} U_1 &= \frac{J_1 J_3 \ell_1 \ell_3}{((J_2+J_3)\,\ell_1 - J_2 J_3)\,((J_1+J_2)\,\ell_3 - J_1 J_2)}\,, \\ U_2 &= \frac{J_2 J_3 \ell_2 \ell_3}{((J_1+J_3)\,\ell_2 - J_1 J_3)\,((J_1+J_2)\,\ell_3 - J_1 J_2)}\,, \\ U_3 &= \frac{J_1 J_2 \ell_1 \ell_2}{((J_2+J_3)\,\ell_1 - J_2 J_3)\,((J_1+J_3)\,\ell_2 - J_1 J_3)}\,. \end{aligned} \tag{5.16}$$

It is going to be used intensively below.

5.4 Multi-point Null Bootstrap and the $C_{123}/\mathbb{W}$ relation

We took a limit where all points approach the boundary of a null hexagon corresponding to all $u_j \to 0$. Because we did it in two steps (first $u_1, u_3, u_5 \to 0$ projecting to leading twist and then $u_2, u_4, u_6 \to 0$ projecting to large spin) the final result (5.15) is not manifestly cyclic invariant. In this section we follow [144] and impose the cyclic symmetry of our correlator under $u_i \to u_{i+1}$ and $U_i \to U_{i+1}$ to further constraint the structure constants $\hat{P}$. This will generalize the result in [144] from the origin kinematics to generic hexagon cross-ratios.

To kick this analysis off we start by converting the starting point (5.15) from the cross-ratios u_j to the more local cross-ratios v_j (both are reviewed in appendix D.3) since the expectation is that the Wilson loop should factorize into a universal prefactor depending on these variables alone times a renormalized Wilson loop [101, 144]. Beautifully, we see that this factorization is almost automatic once we convert to the v variables. Indeed, we find

$$\begin{aligned} \widetilde{G}_6 = 4\sqrt{v_2 v_4 v_6} \int_0^\infty dJ_1\, dJ_2\, dJ_3\, e^{-\frac{J_1 J_2}{J_3}\sqrt{\frac{v_2 v_6}{v_4}} - \frac{J_2 J_3}{J_1}\sqrt{\frac{v_2 v_4}{v_6}} - \frac{J_1 J_3}{J_2}\sqrt{\frac{v_4 v_6}{v_2}} + \frac{\gamma_1}{4}\ln\frac{16 v_1 v_5}{v_3 J_1^2} + \frac{\gamma_2}{4}\ln\frac{16 v_1 v_3}{v_5 J_2^2} + \frac{\gamma_3}{4}\ln\frac{16 v_3 v_5}{v_1 J_3^2}} \\ \times \hat{P}^{\bullet\bullet\bullet}(J_1, J_2, J_3, \ell_1, \ell_2, \ell_3) / \prod_{i=1}^{3} \ell_i^{\frac{\gamma_i - \gamma_{i+1} - \gamma_{i-1}}{2}} \end{aligned} \tag{5.17}$$

so that the first line is already only made out of v_j's while all U_j dependence arises from the second line through the $\ell_j(J_i, U_i)$ map (5.14). The problem at this point is how to constrain $\hat{P}$ so that the U_j and v_j dependence factorizes and so that the final result is cyclic invariant under $v_j, U_j \to v_{j+1}, U_{j+1}$. The factorization would be automatic as soon

as the ℓ_j dependence in $\hat{P}$ comes through a factor of the form

$$\texttt{factor} \equiv \prod_{i=1}^{3} \ell_i^{\frac{\gamma_i-\gamma_{i+1}-\gamma_{i-1}}{2}} \times \tag{5.18}$$

$$\times \mathbb{W}\left(\frac{J_1J_3\ell_1\ell_3}{((J_2+J_3)\ell_1-J_2J_3)((J_1+J_2)\ell_3-J_1J_2)}, \frac{J_1J_3\ell_1\ell_3}{((J_2+J_3)\ell_1-J_2J_3)((J_1+J_2)\ell_3-J_1J_2)}, \frac{J_1J_3\ell_1\ell_3}{((J_2+J_3)\ell_1-J_2J_3)((J_1+J_2)\ell_3-J_1J_2)}\right)$$

Indeed, the first factor would cancel precisely the factor in the denominator in the last line of (5.17) whereas – on the saddle point solution (5.14) – the arguments of the second function will become precise the U_j variables as indicated in (5.16). That is, if

$$\hat{P}^{\bullet\bullet\bullet}(J_1, J_2, J_3, \ell_1, \ell_2, \ell_3) = \texttt{factor} \times p(J_1, J_2, J_3)\,. \tag{5.19}$$

then we automatically find an explicit factorization

$$\widetilde{G}_6 = \mathbb{W}(U_1, U_2, U_3) \times \Big[4\sqrt{v_2v_4v_6} \int_0^\infty dJ_1\, dJ_2\, dJ_3\, e^{-\frac{J_1J_2}{J_3}\sqrt{\frac{v_2v_6}{v_4}}-\frac{J_2J_3}{J_1}\sqrt{\frac{v_2v_4}{v_6}}-\frac{J_1J_3}{J_2}\sqrt{\frac{v_4v_6}{v_2}}} \tag{5.20}$$

$$e^{\frac{f}{4}\ln(J_1)\ln\left(\frac{v_1v_5}{v_3}\right)+\frac{f}{4}\ln(J_2)\ln\left(\frac{v_1v_3}{v_5}\right)+\frac{f}{4}\ln(J_3)\ln\left(\frac{v_3v_5}{v_1}\right)+\frac{g}{4}\ln\left(\frac{16^3v_1v_3v_5}{J_1^2J_2^2J_3^2}\right)-\frac{f}{2}\sum_{j=1}^{3}\ln(J_j)\ln(J_j/4)} p(J_1, J_2, J_3)\Big]$$

where we have used the explicit form of the large spin anomalous dimension $\gamma_i = f\ln(J_i)+g$ to massage the second line. It is hard to imagine how anything else would lead to a factorization but we did not establish the uniqueness of (5.19); it is a conjecture which passes some non-trivial checks below and reduces to [144] in the origin limit.[4]

Next we have to impose cyclicity. For the first factor in (5.20) this simply means that $\mathbb{W}(U_1, U_2, U_3) = \mathbb{W}(U_2, U_3, U_1)$ but it does not constraint $\mathbb{W}$ any further. On the contrary, for the second factor, cyclicity is very powerful. It fixes p completely to all loop orders in perturbation theory, under very mild assumptions as explained below. The result is remarkably simple:

$$p(J_1, J_2, J_3) = \mathcal{N}\prod_{i=1}^{3}\left(\Gamma\left(1-\gamma_i\right)e^{\frac{f}{2}\ln(J_i)^2-f\ln 2\ln J_i}\right). \tag{5.21}$$

It is a nice and very instructive exercise to plug this proposal into (5.20), expand the integrand to any desired order in perturbation theory (corresponding to small cusp anomalous dimension f and small collinear anomalous dimension g), perform all the resulting integrations and realize that we only generate $\ln(v_j)$'s and that moreover the result non-trivially combines, order by order in perturbation theory, into a fully cyclic expression.

[4]The challenge is to relate (non-)factorization of integrands versus (non-)factorization of integrated expressions. Any extra ℓ_j dependence in (5.19) would show up inside the square bracket in (5.20) and thus generically lead to a U_j dependence once we integrate in J_j with (5.14). It might be that a very subtle ℓ_j dependence could integrate to zero or generate a factorized function of U_j which would renormalize $\mathbb{W}$. We were not imaginative enough to find any such example which made us confident that (5.19) is indeed unique.

It is an even more instructive exercise to simply plug a general perturbative ansatz for $p(J_1, J_2, J_3)$ as an infinite series of monomials made out of powers of $\ln(J_i)$'s in (5.20). Each such monomial will again integrate to simple polynomials in $\ln(v_j)$'s. Remarkably, imposing cyclicity at each order of perturbation theory will completely fix these polynomials and thus the full perturbative expansion up to an overall normalization constant. In this way, by considering a very large number of loops we could eventually recognize a simple pattern and arrive at (5.21). This brute force derivation is perfectly valid but was *not* how we originally arrived at (5.21).

We proceeded in a slightly more sophisticated way following similar ideas in the four point function analysis in [148]. This is explained in the box that follows; this discussion can be probably skipped in a first reading.

Deriving (5.21)

We first look for *an* integral transform for p such that ciclicity can be imposed at integrand level. We define

$$q\left(\ln J_1, \ln J_2, \ln J_3\right) = e^{-\frac{f}{2}\sum_{j=1}^{3}\ln(J_j)\ln(J_j/4)}\, p(J_1, J_2, J_3) \tag{5.22}$$

to absorb the last factor in the exponential in the second line in (5.20) and we change integration variables to

$$x_1 = \frac{J_2 J_3}{J_1}\sqrt{\frac{v_2 v_4}{v_6}}, \qquad x_3 = \frac{J_1 J_2}{J_3}\sqrt{\frac{v_2 v_6}{v_4}}, \qquad x_5 = \frac{J_1 J_3}{J_2}\sqrt{\frac{v_4 v_6}{v_2}}, \tag{5.23}$$

to trivialize the tree level measure. Then the previous expression (5.20) takes the very suggestive form

$$\begin{aligned}\widetilde{G}_6 =& \mathbb{W}(U_1, U_2, U_3) \times e^{\sum_i \frac{f}{16}\ln v_i \ln v_{i+3} - \frac{f}{8}\ln v_i \ln v_{i+1} + \frac{g}{4}\ln v_i} \times \\ &\times \int_0^\infty dx_1\, dx_3\, dx_5\, e^{-\sum_{i=1}^{3}\left(x_{2i-1} + \frac{g}{2}\ln(x_{2i-1}/4) - \frac{f}{4}\ln(x_{2i-1})\ln(v_{2i-1})\right)} \\ &\times q\left(\frac{\ln x_1 + \ln x_5 - \ln v_6}{2}, \frac{\ln x_3 + \ln x_1 - \ln v_2}{2}, \frac{\ln x_3 + \ln x_5 - \ln v_4}{2}\right)\end{aligned} \tag{5.24}$$

where we see the explicit appearance of the Sudakov factor [101, 144] in the first line. The lack of ciclicity is now quite striking in the very different way that the even and odd cross-ratios show up in the integral: The odd cross-ratios appear in the exponent in the form $\ln(x_i)\ln(v_i)$ while the even cross-ratios appear inside the arguments of the dressed structure constant $\hat{p}$. That asymmetry is trivial to fix: It suffices to write q itself as an integral transform introducing three new integration variables x_2, x_4, x_6 as

$$q(X, Y, Z) = \int_0^\infty dx_2\, dx_4\, dx_6\, e^{-\sum_{i=1}^{3}\left(x_{2i} + \frac{g}{2}\ln(x_{2i}/4)\right) - \frac{f}{2}\left(\ln(x_6)X + \ln(x_2)Y + \ln(x_4)Z\right)} \tilde{q}(x_4, x_5, x_6) \tag{5.25}$$

where the measure (first factor in the exponent) is written to mimic the already existing measure over x_1, x_3, x_5 to make sure the full result is properly symmetric. Similarly, the factor $f/2$ in the second factor in the exponential guarantees that the new $\ln(x_i)\ln(v_i)$ terms containing the even cross-ratios come with the same overall prefactor as their odd cousins in (5.24). Note also that $\ln(x_6)$ will multiply X which contains its two neighbors $\ln(x_{1=6+1})$ and $\ln(x_{5=6-1})$ and similarly for all other arguments. So in total we will get a beautiful symmetric chain of interactions and overall the only symmetry breaking term is $\tilde{q}(x_4, x_5, x_6)$! We should thus set it to a constant. Integrating (5.25) with $\tilde{q}$ equal to

a constant indeed leads to the anticipated simple result (5.21). This concludes our derivation.

Putting everything together we thus find the final result for the full correlator in the light-like limit (and for general hexagon kinematics) as

$$\widetilde{G}_6 = \underbrace{\mathbb{W}(U_1,U_2,U_3)}_{\texttt{Renormalized Wilson loop}} \times \underbrace{\exp\Big(\sum_i \frac{f}{16}\ln v_i \ln v_{i+3} - \frac{f}{8}\ln v_i \ln v_{i+1} + \frac{g-f\gamma_E}{4}\ln v_i\Big)}_{\texttt{Sudokov Factor}} \times \tag{5.26}$$

$$\times \underbrace{\mathcal{N}\left(\int_0^\infty \prod_{j=1}^6 dx_j e^{-\sum_{i=1}^6 (x_i + \frac{g}{2}\mathbf{ln}(x_i) - \frac{f}{4}\mathbf{ln}(x_i)\mathbf{ln}(x_{i+1}) - \frac{f}{4}\mathbf{ln}(x_i)\mathbf{ln}(v_i)) + \sum_i \frac{f\gamma_E}{4}\mathbf{ln}(v_i)}\right)}_{\texttt{Recoil } J},$$

where $\mathbf{ln}(x) = \ln(x) + \gamma_E$.

To obtain the full map between spinning three point functions and the Wilson loop we simply need to convert $\hat{P}$ to $\hat{C}$ using (5.7). In other words, we divide the result whence obtained by three large spin structure constants for a single spinning operator which were computed in [149]. This ratio nicely removes some of the gamma functions in (5.21) leading to our final main result

Structure Constant/Wilson Loop duality

$$\hat{C}^{\bullet\bullet\bullet}(J_i,\ell_i) = \underbrace{\mathcal{N}\prod_{i=1}^3 \Big(\frac{J_i\ell_i}{2\ell_{i+1}\ell_{i-1}}\Big)^{\frac{\gamma_i}{2}}}_{\texttt{conversion factor}} \times \mathbb{W}(U_1,U_2,U_3). \tag{5.27}$$

with the map between variables on both sides of this equation given by (5.14) or (5.16).

5.5 One-loop check and some speculative musings

The structure constant variables $(J_1,J_2,J_3,\ell_1,\ell_2,\ell_3)$ are mapped into the Wilson loop cross-ratios (U_1,U_2,U_3) through the map (5.16). The J_i are even non-negative integers and the ℓ_i are non-negative integers bounded by the condition that $\ell_i + \ell_j \leq J_k$ with i,j,k all different. For $J_1 = J_2 = J_3 = 30$ for instance we would have 7816 discrete ℓ_j choices, each with its own structure constant. The map (5.16) maps each one of these ℓ_j choices to a point in the cross-ratio space as depicted in figure 5.2.

The set of $\ell_k < J_iJ_j/(J_i+J_j)$ covers the full space of positive real cross-ratios U_j as represented in the figure 5.2 by the blue dots/region. The remaining ℓ_k's cover three disjoint regions in cross-ratio space where one cross-ratio is positive and two are negative. (In the large spin limit of course.) The region of all positive cross-ratios can be called the *space-like* region since it can be realized with all squared distances positive. The other three regions need some squared distances to be negative to get negative cross-ratios so we

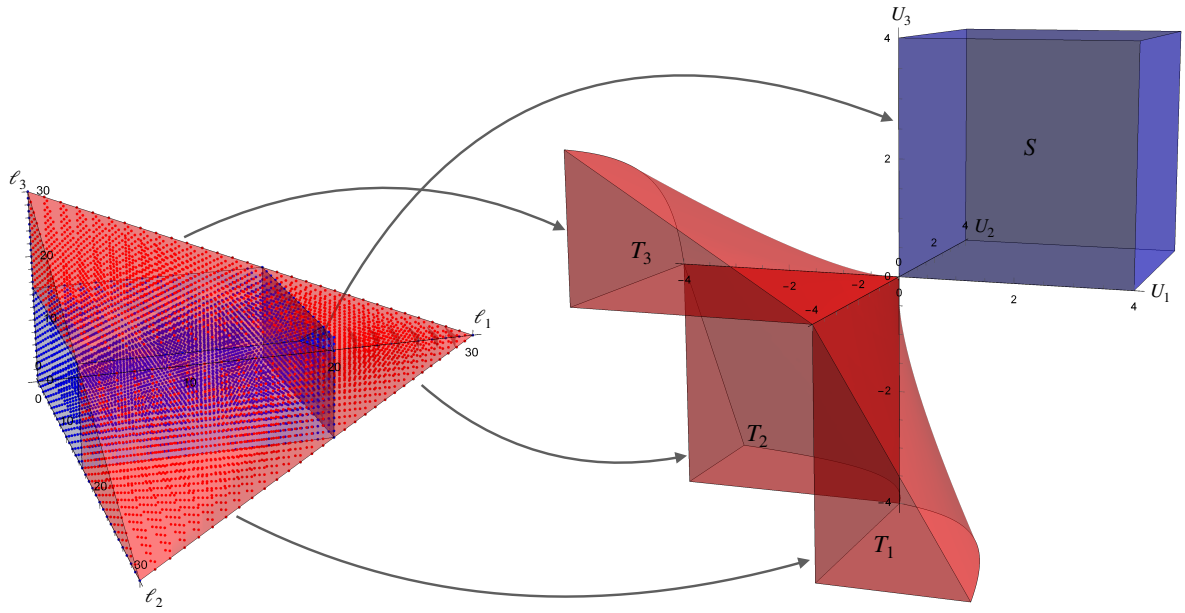

Figure 5.2: The OPE data $\hat{C}^{\bullet\bullet\bullet}(J_1, J_2, J_3, \ell_1, \ell_2, \ell_3)$ can be plotted in the cross-ratio space (U_1, U_2, U_3) if we map the ℓ_i and J_i variables to the U_i using (5.16). The one loop structure constants have a good $J_i \to \infty$ limit in the blue region perfectly matching with the Wilson loop in the Euclidean space-like (S) sheet. In contrast, the same structure constants blow up as $J_i \to \infty$ in the red region which would naively correspond to the Wilson loop in some Lorentzian time-like regions (T_i). To reach these regions we should instead start in the blue region and take the large spin limit so that an emergent analytic structure arises with new branch cuts. We can then cross them by analytically continuing away from the blue region and in this way obtain a match beyond the Euclidean regime. The structure constant/Wilson loop duality is a cute concrete example where expansions and analytic continuations do not commute.

call them *time-like regions*. (A beautiful detailed analysis of the geometry of the U_i space for hexagonal Wilson loops is given in [150].)

We propose that as we take the large J_k, ℓ_k limit the structure constants in the space-like region (S) will nicely match – according to (5.27) – with the Wilson loop in the space-like (or Euclidean) sheet, where we start with all cusps space-like separated and do not cross any light-cone. Let us discuss a non-trivial one loop check of this proposal.

In perturbation theory we have $\hat{C}^{\bullet\bullet\bullet}(J_i, \ell_i) = 1 + \lambda c + \dots$, `conversion factor` $= 1 + \lambda h + \dots$ and $\mathbb{W}(U_i) = 1 + \lambda w + \dots$ so that at one loop our prediction (5.27) simply translates into (up to an overall shift by a constant)

$$c(J_i, \ell_i) - h(J_i, \ell_i) = w\big(U_i(J_i, \ell_i)\big)\,. \tag{5.28}$$

The one loop Wilson loop is universal in any non-abelian gauge theory in the planar limit since it is given by a single gluon exchange from an edge of the hexagon to another. It

reads [145, 150–152]

$$w\big(U_1,U_2,U_3\big) = -4\pi^2 + 2\sum_{i=1}^{3} \mathrm{Li}_2\left(1-1/U_i\right). \tag{5.29}$$

This object – in the space-like region where all U_i are positive – should emerge from the one loop structure constant of large spin operators. These are extracted from the OPE of the one loop correlation functions of six $20'$ operators in planar $\mathcal{N}=4$ SYM, see appendix D.5.1.

A speculative detour

Before discussing the quantitative match of the structure constant and the Wilson loop we will open a speculative parentheses here. It can be skipped by the more orthodox readers.

Note that the analytic structure of the structure constant before taking the large spin and large polarizations limit is strikingly different to that of the Wilson loop.

The Wilson loop has a rich cut structure. In the physical sheet there are cuts at $U_i = 0$ which need to be crossed to go from space-like to time-like configurations. These are the only singularities of the Wilson loop in the physical space-like sheet [152]. If we cross the $U_i = 0$ cuts we go to other sheets and do see other singularities most notably at $U_i = 1$ but also at various other interesting locations, see e.g. [153–155].

Instead, the structure constant are meromorphic functions of ℓ_i and J_j with no cuts whatsoever – see appendix D.6.3 for explicit expressions full of Harmonic numbers, rational binomial sums and other similar meromorphic building blocks. They have poles at unphysical values of polarizations and spins. In the large ℓ_i and J_i limit these poles condense; seen from far away they become cuts as illustrated in figure 5.3. (This phenomenon of poles condensing into cuts is all over, most notably in Matrix model studies.) In other words, at finite ℓ_i, J_i there are no other sheets and no monodromies to be picked, only the space-like sheet exists. All other Lorentzian sheets are *emergent*. They only appear in the *semi-classical* limit of large ℓ_i, J_i. As such, what we expect is that if we stay in the Euclidean regime $\ell_k < J_iJ_j/(J_i+J_j)$ corresponding to the blue region in figure 5.2 we should obtain a match with the Wilson loop in the large spin limit. But if we want to access other regions in the Wilson loop, the order of limits is key: We *first* need to take the large spin and large polarization limit so cuts emerge; *then* we analytically continue our structure constant through those cuts.

When doing a numerical comparison of the Wilson loop and the structure constants we observe an interesting phenomenon which seems to back this up. In the space-like $\ell_k < J_iJ_j/(J_i+J_j)$ region the one loop structure constants c are $O(1)$ numbers; as we increase the spin we observe that these numbers do approach the expected Wilson loop expression (5.29). On the other hand, for $\ell_k > J_iJ_j/(J_i+J_j)$ the structure constants c become exponentially large real numbers which blow up as $J_j \to \infty$! This is in perfect synthony with the picture of the previous paragraph: to cross the cuts and reach the Lorentzian domain -encountering a complex valued finite Wilson loop - we must first

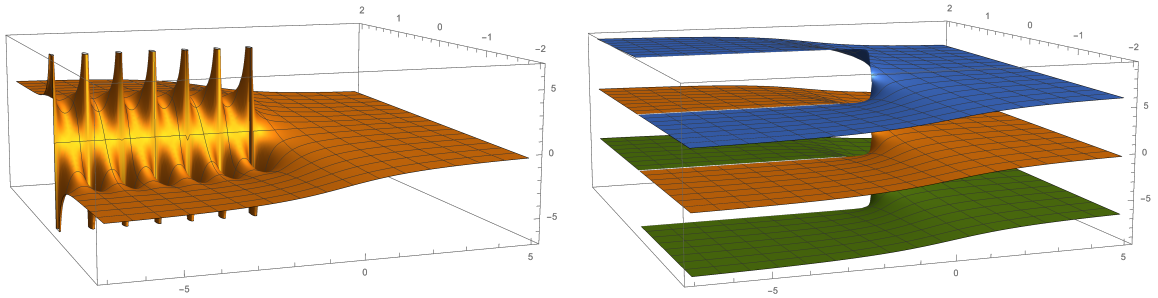

(a) (b)

Figure 5.3: **a)** (Imaginary part of) $H(z)$ where $H(z)$ are Harmonic numbers evaluate to rational numbers for z positive integer and has poles at negative integers. For large argument it behaves as $\log(z)$. In other words, seen from far away the poles condense into a cut. **b)** (Imaginary part of) $\log(z)$ lives in an infinite sheeted surface. The first one agrees with that of $H(z)$ for large arguments while the other sheets are *emergent*.

go to a safe region in the physical sheet and then take a classical limit so the cuts appear in the first place. If we go to the cuts *directly* in the structure constant side we encounter instead a divergence – we could call it a firewall in analogy with black holes. In this black hole analogy, the smooth cuts with emerge in the classical limit resemble the smooth black hole horizons while the poles in the structure constants which we would only see through very sensitive experiments would be the analogue of the quantum black hole micro-states inner structure; some kind of fuzzball.

A analytical toy model for this phenomenon is $\hat{C}^{\bullet\bullet\circ}$ in the large spin limit, discussed in detail in appendix D.6.2. In equation (D.34) we obtain nice $O(1)$ expressions valid for $\ell < J_1 J_2/(J_1+J_2)$ with emergent branch points at $\ell = J_1 J_2/(J_1+J_2)$ which should be thought of as analogues for the $U = 0$ light-cone singularities of the hexagonal Wilson loop. On the other hand, for $\ell > J_1 J_2/(J_1+J_2)$ the one-loop corrections become exponentially divergent, see equation (D.35). In fact, extending the black hole analogy, one must be careful when using these limits to compute observables that probe the "horizon" or "interior" regions. For example, the equal spins sum over ℓ of the three point function is finite in the large spin limit – given by (D.37) in the appendix – but it is not purely captured by the naive large ℓ, J limit with ℓ/J fixed. Indeed, if one first takes the large spin limit, a non integrable expression is obtained in the "interior" region. This singularity can be thought of as a "UV" divergence that is regulated by finer corrections coming from the microscopical structure of three point functions.

End of speculative detour.

We could not completely fix the analytic form of the one loop structure constants $c(J_i, \ell_i)$ and so we could not establish (5.28) fully. Instead we expanded the Wilson loop around the so-called origin limit [145] corresponding to small cross-ratios. Note that we have

$$w\big(U_1, U_2, U_3\big) = \sum_{i=1}^{3} \ln^2(U_i) + \sum_{i=1}^{3} \ln(U_i)\, \mathcal{A}_i + \mathcal{B} \tag{5.30}$$

where $\mathcal{A}_i$ and $\mathcal{B}$ have regular Taylor expansions around the origin $U_1 = U_2 = U_3 = 0$.[5] For instance

$$\mathcal{B} = -5\pi^2 + \frac{2}{1}\sum_i U_i + \frac{2}{4}\sum_i U_i^2 + \frac{2}{9}\sum_i U_i^3 + \frac{2}{16}\sum_i U_i^4 + \dots \tag{5.31}$$

The representation (5.30) makes manifest the branch-cuts at $U_i = 0$ of the Wilson loop. In the structure constant side, to make contact with the Wilson loop as an expansion around the origin we should consider the limit of very large spin and polarizations but very small ratios of the two,

$$\ell_i \gg 1\,, \qquad J_i \gg 1\,, \qquad \ell_i/J_j \ll 1\,, \tag{5.32}$$

indeed, in this regime we easily see that the cross-ratios obtained through (5.16) are very small, for example:

$$U_1 = \frac{\ell_1\ell_3}{J_2^2} + \frac{\ell_1^2\ell_3}{J_2^3} + \frac{\ell_1^2\ell_3}{J_2^2 J_3} + \frac{\ell_1\ell_3^2}{J_2^3} + \frac{\ell_1\ell_3^2}{J_1 J_2^2} + \dots\,, \ \ln(U_1) = \ln\left(\frac{\ell_1\ell_3}{J_2^2}\right) + \frac{\ell_1}{J_2} + \frac{\ell_1}{J_3} + \frac{\ell_3}{J_1} + \frac{\ell_3}{J_2} + \dots\,. \tag{5.33}$$

When matching the one-loop correlation function c with the Wilson loop w the various logs arising in the large spin limit of the structure constants should match the explicit logs in (5.30) while the powerlaw corrections in ℓ_j/J_k should be matched with the series expansion of $\mathcal{B}$ and $\mathcal{A}_i$ for small cross-ratios.[6] If we can match all terms in these Taylor expansions we would establish (5.28) completely. We almost did it. We matched all terms in the expansion of $\mathcal{A}_i$ (see discussion around (D.48) in the appendix D.6.3) and we matched the first 873 terms in the expansion of $\mathcal{B}$ once we translate (5.31) into small ratios expansions as (5.33) to more easily compare with the structure constants (see discussion around (D.49) in the appendix D.6.3). This is more than plenty to leave zero doubt in our mind that (5.28) holds. To fully establish it we would need to finish the full analytic determination of the structure constants which translate into finding a closed expression to the very simple remaining β constants discussed around (D.52) in appendix D.6.3. It would be very nice to find these constants. One reason is to conclude this analytic comparison but a perhaps even more interesting reason would be to analytically understand all the various speculative remarks about the behavior of the structure constants inside and outside the Euclidean regime which we mused about in the speculative detour above.

[5] Explicitly, $\mathcal{A}_i = 2\ln(1-U_i)$ and $\mathcal{B} = 2\mathrm{Li}_2(U_1) + 2\mathrm{Li}_2(U_2) + 2\mathrm{Li}_2(U_3) - 5\pi^2$.

[6] In the structure constant there are also terms like ℓ_1/J_2^3 and so on which have less powers of ℓ's in the numerator compared to powers of J's in the denominator; we call these terms *unbalanced*. The unbalanced terms vanish in the large spin/large polarization limit so we are insensitive to them when testing the WL/Correlation function duality. In other words, the structure constants contain way more information than the Wilson loop. We can think of them as an off-shell quantum version of the Wilson loop which reduced to the Wilson loop in a classical limit where we keep balanced terms only such as the ones in the expansions (5.33).

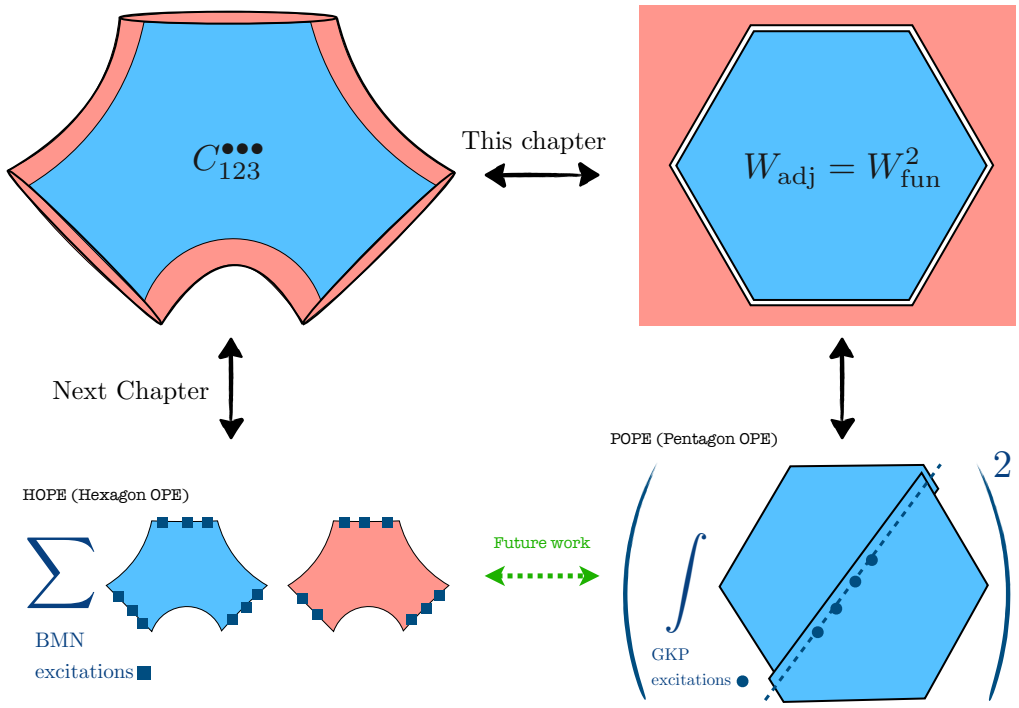

Figure 5.4: **Top arrow:** Large spin three-point function/hexagon Wilson loop duality [143]. **Left arrow:** Three point functions can be decomposed in terms of two hexagons [66]. For spinning operators the necessary formalism is cleaned up in [4]. **Right arrow:** Wilson loops can be decomposed in terms of two pentagons [71]. **Bottom arrow:** The top duality hints at a transmutation of hexagons into pentagons in the large spin limit. Would be fascinating to find out how this works. It might lead to a unified integrability description of open and closed strings in AdS/CFT.

5.6 Discussion

This chapter concerns the duality relation depicted at the top of figure 5.4. On the top left corner we have three point functions of three twist-two operators with large spins J_i and with polarizations tensor structures parametrized by ℓ_i. On the top right corner we have a renormalized Wilson loop parametrized by three finite conformal cross-ratios U_i. Our main result is (5.27) which precisely links these two quantities with a precise kinematical dictionary.[7]

Armed with a precise dictionary for the kinematics we can now attack the dynamics of this problem from an integrability perspective.

Three point functions of three excited two-two operators (each parametrized by J_i integrability magnon excitations) can be decomposed in terms of two hexagons [66]. When cutting each operator into two these excitations can end up on either hexagon; we must

[7]Key in deriving this result was the so-called snowflake decomposition of six point correlation function. It is an interesting open problem to use instead the comb decomposition of a six point correlation function and arrive at the Wilson loop limit. The method used in this chapter can also applied to derive a link between three point functions of two spinning operators and the expectaction value of a square Wilson loop and a local operator [156, 157].

sum over where they end up as indicated in the bottom left corner of figure 5.4.[8] The larger the spin, the more excitations we have and thus the scarier are these sums. In the large spin limit they ought to simplify and give rise to a Wilson loop (an adjoint Wilson loop or the square of a fundamental one). In turn, the Wilson loop can be obtained by gluing together two pentagons and summing over all possible virtual particles therein [71]. So the sum over hexagon's with their large number of BMN physical excitations should somehow transmute into a sum over pentagons with a sum over GKP virtual excitations. To attack this fascinating alchemy exercise, we need to understand how to polarize the hexagon OPE expansion for spinning operators (all examples so far were for scalar structure constants or spinning structure constants with a single tensor structure). This is the subject of chapter 6.[9]

[8] In principle we should also integrate over all possible mirror states at the three lines where the two hexagons are glued to each other. We are ignoring this extra contribution. We believe it is subleading at large spin when the effective size of all operators is very large. We are currently trying to check this by an explicit finite size computation.

[9] Related to that, in appendix D.6 we extract data for $C_{123}^{\bullet\bullet\bullet}$ at one loop in $\mathcal{N}=4$ SYM generalizing previous results by Marco Bianchi in [158]; as usual, this data will be very useful in testing any integrability based approaches.

Chapter 6

Spinning Hexagons

6.1 Introduction

Three point functions of single trace operators in planar $\mathcal{N} = 4$ SYM describe the scattering of three closed strings in AdS and are thus given by a pairs of pants. Pairs of pants can be obtained by stitching two hexagons together. That is how tailors make pants and it is also how one computes three point functions in this gauge theory using integrability [66]. This chapter is about spinning pair of pants where two or more operators have spin. In this case the 3pt function is given by a sum of conformal invariant tensor structures and we need to explain how the hexagons extract the coefficient multiplying each such structure. For three twist-two operators with spin 2, 4 and 6, for instance, we have the perturbative result (6.1), see [144], where $\langle ij \rangle$ is a scalar product involving a left spinor parametrizing operator i and a right spinor parametrizing operator j.[1] A main goal of this chapter is to develop the formalism to reproduce such results from integrability.

Not all terms are equally easy to get. The terms in blue, for instance, are the tree level contributions; we will develop an efficient recursion algorithm which will allow us to determine them all (and produce a plethora of new predictions for structure constants of larger twist operators). The boldfaced terms are what we call the *abelian* terms; these structure constants are very integrability friendly as they lack a complicated so-called *hexagon matrix part*; these abelian terms we can actually compute easily at one loop (in cyan here) or even at higher loops. The remaining non boldfaced orange terms are non-abelian one loop terms; we can also get them but it is quite painful to do so specially for operators of larger spin.

At the center of all these integrability based computations is a beautiful partition function represented in figure 6.1. We call it the *hexagon partition function*. The vertex in this partition function is Beisert's centrally extended $SU(2|2)$ R-matrix [59] while the open boundary conditions are given by contracting each boundary with a fixed two dimensional spinor. The various possible choices of such spinors parametrize the various tensor structures described above. (For some choice of boundary conditions this partition function trivializes – leading to the much simpler abelian contributions described above.) This

[1] These spinor variables render the various conformal invariant tensor structures into simple scalar products, recalled in appendix E.1.

hexagon partition function is the building block of all spinning correlators. It is an interesting object on its own right which we want to advertise. It has a beautiful very rich integrable structure, the surface of which we are barely starting to scratch.

$$
\begin{aligned}
C(2,4,6) = \frac{1}{84\sqrt{55}}\Bigg(& \langle 11\rangle\langle 13\rangle\langle 22\rangle^3\langle 23\rangle\langle 31\rangle\langle 32\rangle\langle 33\rangle^4\left(960-\frac{2400756}{385}g^2\right)+\langle 12\rangle^2\langle 21\rangle^2\langle 22\rangle^2\langle 33\rangle^6\left(15-\frac{88797}{770}g^2\right)+\\
& +\langle 11\rangle\langle 13\rangle\langle 23\rangle^4\langle 31\rangle\langle 32\rangle^4\langle 33\rangle\left(-2007-\frac{822990467}{34650}g^2\right)+\langle 13\rangle^2\langle 22\rangle\langle 23\rangle^3\langle 31\rangle^2\langle 32\rangle^3\langle 33\rangle\left(-7680-\frac{3113024}{231}g^2\right)+\\
& +\langle 12\rangle\langle 13\rangle\langle 21\rangle\langle 23\rangle^3\langle 31\rangle\langle 32\rangle^3\langle 33\rangle^2\left(-15360-\frac{13877312}{1155}g^2\right)+\langle 13\rangle^2\langle 22\rangle^4\langle 31\rangle^2\langle 33\rangle^4\left(23-\frac{7780337}{34650}g^2\right)+\\
& +\langle 12\rangle\langle 13\rangle\langle 21\rangle\langle 22\rangle\langle 23\rangle^2\langle 31\rangle\langle 32\rangle^2\langle 33\rangle^3\left(23040-\frac{12990112}{1155}g^2\right)+\langle 11\rangle^2\langle 22\rangle^4\langle 33\rangle^6\left(1-\frac{814939}{34650}g^2\right)+\\
& +\langle 11\rangle\langle 12\rangle\langle 21\rangle\langle 22\rangle^2\langle 23\rangle\langle 32\rangle\langle 33\rangle^5\left(576-\frac{5341948}{1925}g^2\right)+\langle 11\rangle^2\langle 23\rangle^4\langle 32\rangle^4\langle 33\rangle^2\left(327+\frac{128149187}{34650}g^2\right)+\\
& +\langle 13\rangle^2\langle 22\rangle^3\langle 23\rangle\langle 31\rangle^2\langle 32\rangle\langle 33\rangle^3\left(-1883-\frac{14853709}{4950}g^2\right)+\langle 11\rangle^2\langle 22\rangle^2\langle 23\rangle^2\langle 32\rangle^2\langle 33\rangle^4\left(360-\frac{3289708}{1155}g^2\right)+\\
& +\langle 12\rangle^2\langle 21\rangle^2\langle 22\rangle\langle 23\rangle\langle 32\rangle\langle 33\rangle^5\left(-567-\frac{3484307}{1650}g^2\right)+\langle 11\rangle^2\langle 22\rangle\langle 23\rangle^3\langle 32\rangle^3\langle 33\rangle^3\left(-640-\frac{5365984}{3465}g^2\right)+\\
& +\langle 12\rangle\langle 13\rangle\langle 21\rangle\langle 22\rangle^3\langle 31\rangle\langle 33\rangle^5\left(192+\frac{145072}{5775}g^2\right)+\langle 11\rangle\langle 12\rangle\langle 21\rangle\langle 22\rangle^3\langle 33\rangle^6\left(-16+\frac{2405402}{17325}g^2\right)+\\
& +\langle 11\rangle\langle 13\rangle\langle 22\rangle^4\langle 31\rangle\langle 33\rangle^5\left(-24+\frac{1432546}{5775}g^2\right)+\langle 11\rangle\langle 13\rangle\langle 22\rangle\langle 23\rangle^3\langle 31\rangle\langle 32\rangle^3\langle 33\rangle^2\left(7680+\frac{20817136}{1155}g^2\right)+\\
& +\langle 13\rangle^2\langle 23\rangle^4\langle 31\rangle^2\langle 32\rangle^4\left(960+\frac{272704}{231}g^2\right)+\langle 11\rangle\langle 12\rangle\langle 21\rangle\langle 22\rangle\langle 23\rangle^2\langle 32\rangle^2\langle 33\rangle^4\left(-2880+\frac{3467144}{1155}g^2\right)+\\
& +\langle 12\rangle\langle 13\rangle\langle 21\rangle\langle 22\rangle^2\langle 23\rangle\langle 31\rangle\langle 32\rangle\langle 33\rangle^4\left(-5760+\frac{1434656}{385}g^2\right)+\langle 12\rangle^2\langle 21\rangle^2\langle 23\rangle^2\langle 32\rangle^2\langle 33\rangle^4\left(1440+\frac{6762608}{1155}g^2\right)+\\
& +\langle 13\rangle^2\langle 22\rangle^2\langle 23\rangle^2\langle 31\rangle^2\langle 32\rangle^2\langle 33\rangle^2\left(8640+\frac{852608}{77}g^2\right)+\langle 11\rangle\langle 12\rangle\langle 21\rangle\langle 23\rangle^3\langle 32\rangle^3\langle 33\rangle^3\left(2560+\frac{46393456}{3465}g^2\right)+\\
& +\langle 11\rangle\langle 13\rangle\langle 22\rangle^2\langle 23\rangle^2\langle 31\rangle\langle 32\rangle^2\langle 33\rangle^3\left(-5760+\frac{19842568}{1155}g^2\right)+\langle 11\rangle^2\langle 22\rangle^3\langle 23\rangle\langle 32\rangle\langle 33\rangle^5\left(-48+\frac{1389824}{1925}g^2\right)+\\
& +\left(\langle 11\rangle^2\langle 23\rangle^4\langle 32\rangle^4\langle 33\rangle^2-\langle 11\rangle\langle 13\rangle\langle 23\rangle^4\langle 31\rangle\langle 32\rangle^4\langle 33\rangle\right)\left(-87+\frac{121910653}{34650}g^2\right)+\\
& +\left(\langle 13\rangle^2\langle 22\rangle^4\langle 31\rangle^2\langle 33\rangle^4-\langle 13\rangle^2\langle 22\rangle^3\langle 23\rangle\langle 31\rangle^2\langle 32\rangle\langle 33\rangle^3\right)\left(37+\frac{15349637}{34650}g^2\right)+\\
& +\left(\langle 12\rangle^2\langle 21\rangle^2\langle 22\rangle^2\langle 33\rangle^6-\langle 12\rangle^2\langle 21\rangle^2\langle 22\rangle\langle 23\rangle\langle 32\rangle\langle 33\rangle^5\right)\left(9+\frac{3091483}{11550}g^2\right)\Bigg)+\ldots
\end{aligned}
\tag{6.1}
$$

This chapter is naturally split into two main sections.

In section 6.2 we study the hexagon partition function mentioned above. This section might be interesting for hardcore integrabilists, even those with no interest in three point functions in SYM. We will study this partition function at weak coupling when it reduces to a rational vertex model partition function and at finite coupling where it is richer, of Hubbard type. Recursion relations, analytic continuations and several other tricks will play a key role in this analysis.

In section 6.3 we describe how to introduce polarizations into the hexagon formalism to compute spinning structure constants. We will do it mostly in the so called asymptotic regime where mirror particles can be ignored except in section E.6.1 where we perform some checks involving mirror particles at two loops. We will show how the triangle partition

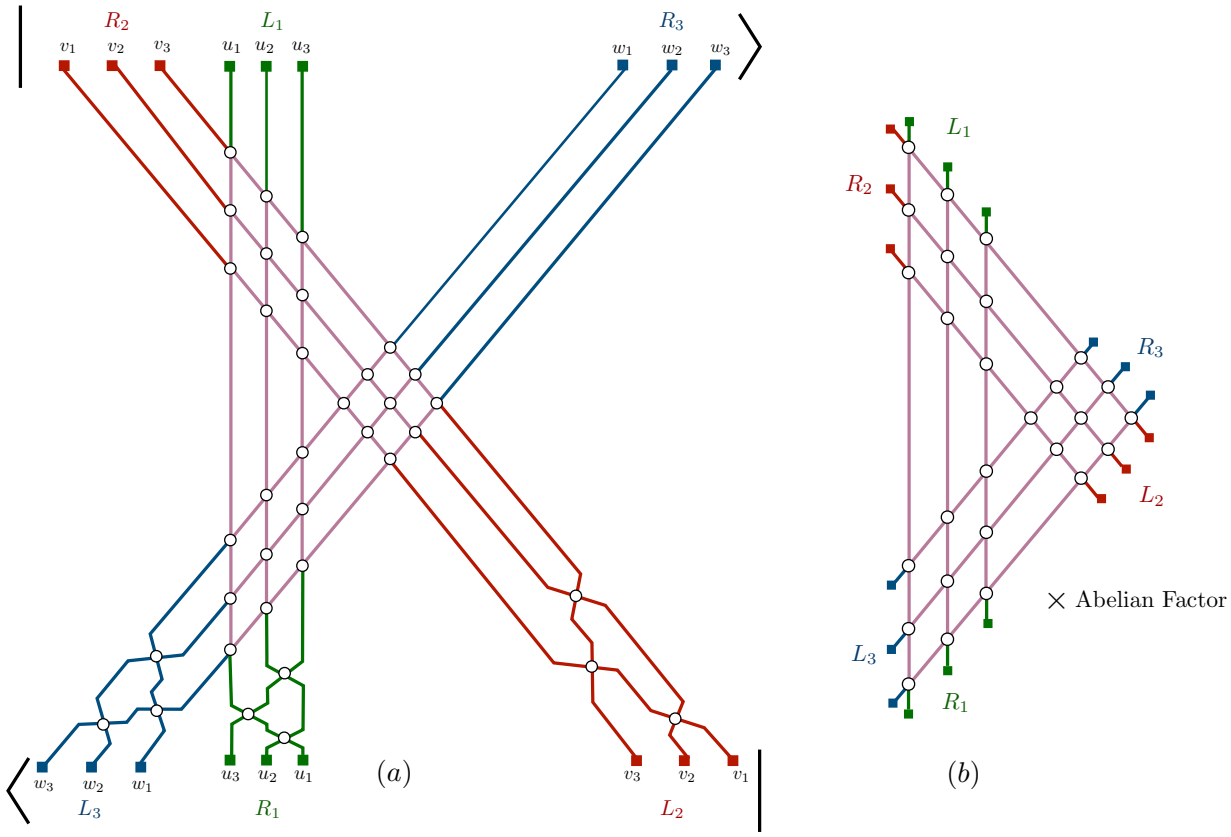

Figure 6.1: (a) The hexagon partition function Z_{J_1,J_2,J_3}, illustrated here in the case $Z_{3,3,3}$, describe the scattering of three sets of fermions, labelled by their rapidities v_i, u_j, w_k, in the $\mathcal{N} = 4$ SYM spin-chain. Each set starts polarized in a fixed direction labeled by the spinors R_2, L_1, R_3 respectively. The particles then scatter in all possible pairings according to Beisert's $PSU(2|2)$ vertex. The final state is then projected into fermions of definite polarization spinors L_2, R_1, L_3. In the gauge theory, the boundary conditions are set by the spacetime polarizations of spinning operators whose structure constants are governed by the hexagon partition function. Because the vertex is proportional to the identity when the incoming or outgoing particles are fermions with identical polarizations, the outer parts of the graph are trivial and result in a simple abelian factor. We represent these trivial scattering by the green red and blue colours. They can be factored out resulting in the equivalent representation (b). The interesting dynamics happens in the pink region in which particles from different sets interact.

function naturally shows up and the fundamental building block and we will test the hexagon construction against perturbative data for a few simple examples with low spins.

6.2 The Hexagon Partition Function

6.2.1 The Partition Function

The central object in this chapter is dubbed the **hexagon partition function** or simply the **hexagon**. It is defined in figure 6.1a. The name hexagon becomes clear when we realize it

is given by a simpler partition function depicted in figure 6.1b.

As usual, the partition function can be thought of as 2d classical statistical mechanical model where we sum over statistical weights at each vertex (more precisely the vertex is the Shastry R-matrix of the Hubbard model) and where at the edges we impose appropriate boundary conditions. For the hexagon partition function there are six different boundary conditions to impose each parametrized by its own two dimensional spinor.

Alternatively we can think of it as an integrable 1d quantum mechanical model. In this picture we start with three sets of fermions in an in-state and let them scatter – in a purely factorized fashion – into a final state also with three sets of fermions. (At intermediate time steps these fermions can scatter into bosons as well but in the initial and final states we only consider fermions.) These fermions have an $SU(2)$ flavour index and we contract each of the six sets of fermions (three in plus three out) with the same spinor; in other words, we scatter three groups of identical fermions. Because these fermions are identical scattering among the fermions of the same type will be trivial and this is why the big partition function in 6.1a ends up simplifying to the hexagon shape in figure 6.1b which gives the name to the partition function. In fact, this simplified shape is far from unique. Since the underlying model is integrable the order by which the particles scatter is imaterial so we can alternatively cast this partition function in a myriad of equivalent ways as illustrated in figure 6.2.

Each particle has a physical momenta which is conserved in each elastic scattering event; it is thus associated to each line in the figure. We parametrize it by a physical rapidity. Since we have three sets of momenta we will have three sets of rapidities which we label as v_i, u_j, w_k. What was before a valance four statistical mechanical weight is in this picture the two-to-two scattering matrix of two of the 1d particles:

$$S^{cd}_{ab}(z,z') \equiv$$

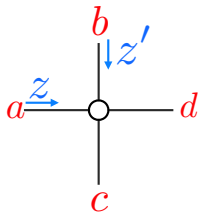

(6.2)

where each index can take four values (a fermion doublet and a boson doublet combined into an $SU(2|2)$ fundamental; for the external states we have fermions only but in intermediate states we will of course produce everyone in the multiplet.) This S-matrix is Beisert's PSU(2|2) S-matrix [59, 159] explicitly given by a simple combination of ten terms

$$\begin{aligned} S^{cd}_{ab}(z,z') = h(z,z')\Bigg(&\mathcal{A}(z,z')\frac{\Delta^c_a\Delta^d_b+\Delta^d_a\Delta^c_b}{2}+\mathcal{B}(z,z')\frac{\Delta^c_a\Delta^d_b-\Delta^d_a\Delta^c_b}{2}+\frac{1}{2}\mathcal{C}(z,z')\phi^{-1}_{\mathcal{Z}}(z,z')E_{ab}\epsilon^{cd}\\ &+\mathcal{D}(z,z')\frac{\delta^c_a\delta^d_b+\delta^d_a\delta^c_b}{2}+\mathcal{E}(z,z')\frac{\delta^c_a\delta^d_b-\delta^d_a\delta^c_b}{2}+\frac{1}{2}\mathcal{F}(z,z')\phi_{\mathcal{Z}}(z,z')\epsilon_{ab}E^{cd}+\mathcal{G}(z,z')\delta^c_b\Delta^d_a\\ &+\mathcal{L}(z,z')\delta^d_a\Delta^c_b+\mathcal{K}(z,z')\delta^d_b\Delta^c_a+\mathcal{H}(z,z')\delta^c_a\Delta^d_b\Bigg). \end{aligned} \tag{6.3}$$

The Beisert matrix elements $\mathcal{A},\mathcal{B},\mathcal{C},\mathcal{D},\mathcal{E},\mathcal{F},\mathcal{G},\mathcal{H},\mathcal{L},\mathcal{K}$ as well as the non-local markers $\phi_{\mathcal{Z}}$ are defined in appendix E.2 and depend on the rapidities z,z' through the Zhukovsky variables $x^{\pm}$ only. These are defined through

$$\frac{z+i/2}{g} = x^+(z) + \frac{1}{x^+(z)}, \qquad \frac{z-i/2}{g} = x^-(z) + \frac{1}{x^-(z)}. \tag{6.4}$$

where $g = \lambda/(4\pi)^2$ is the coupling.

The three particle sets are not on equal footing. In our conventions, u_j are **physical** rapidities while v_i and w_k are **crossed** kinematics. We can think of the corresponding excitations as anti-particles. Crossed parameters in the matrix elements are to be understood as analytically continued. The result of this analytic continuation is simple in this case: we should pick monodromies around the branch points of the Zhukovsky variables. This amounts to

$$x^{\pm}(v^{\circlearrowleft}) \to 1/x^{\pm}(v), \qquad x^{\pm}(w^{\circlearrowleft}) \to 1/x^{\pm}(w) \tag{6.5}$$

so that when we write, e.g.,

$$\mathcal{A}(z,z') \equiv \frac{x^+(z') - x^-(z)}{x^-(z') - x^+(z)},$$

we are simultaneously defining

$$\mathcal{A}(v,w) = \frac{1/x^+(w) - 1/x^-(v)}{1/x^-(w) - 1/x^+(v)}, \quad \mathcal{A}(v,u) = \frac{x^+(u) - 1/x^-(v)}{x^-(u) - 1/x^+(v)}, \quad \mathcal{A}(u,w) = \frac{1/x^+(w) - x^-(u)}{1/x^-(w) - x^+(u)}.$$

All other factors are treated in the same simple fashion; the exception is the overall factor $h(x,y)$ given by [66]

$$h(z,z') \equiv \frac{x^-(z) - x^-(z')}{x^-(z) - x^+(z')} \frac{1 - \frac{1}{x^-(z)x^+(z')}}{1 - \frac{1}{x^+(z)x^+(z')}} \sigma(z,z')^{-1}, \tag{6.6}$$

with σ the BES dressing phase [60] and which transforms nontrivial due to the non-trivial crossing transformation of σ under the $v^{\circlearrowleft}$ and $w^{\circlearrowleft}$ monodromies, see appendix E.3. In any case, this overall factor will lead to an overall factorized product sitting outside as an overall normalization; it is irrelevant for most of our discussion.

As emphasized above, each line segment in the partition function is a PSU(2|2) state $|x\rangle$ parametrized by two component polarizations c_α and d_a as

$$|x\rangle = \underbrace{c_\alpha |\psi^\alpha\rangle}_{\text{fermions}} + \underbrace{d_a |\phi^a\rangle}_{\text{bosons}} \equiv (c_1, c_2, d_1, d_2)^T.$$

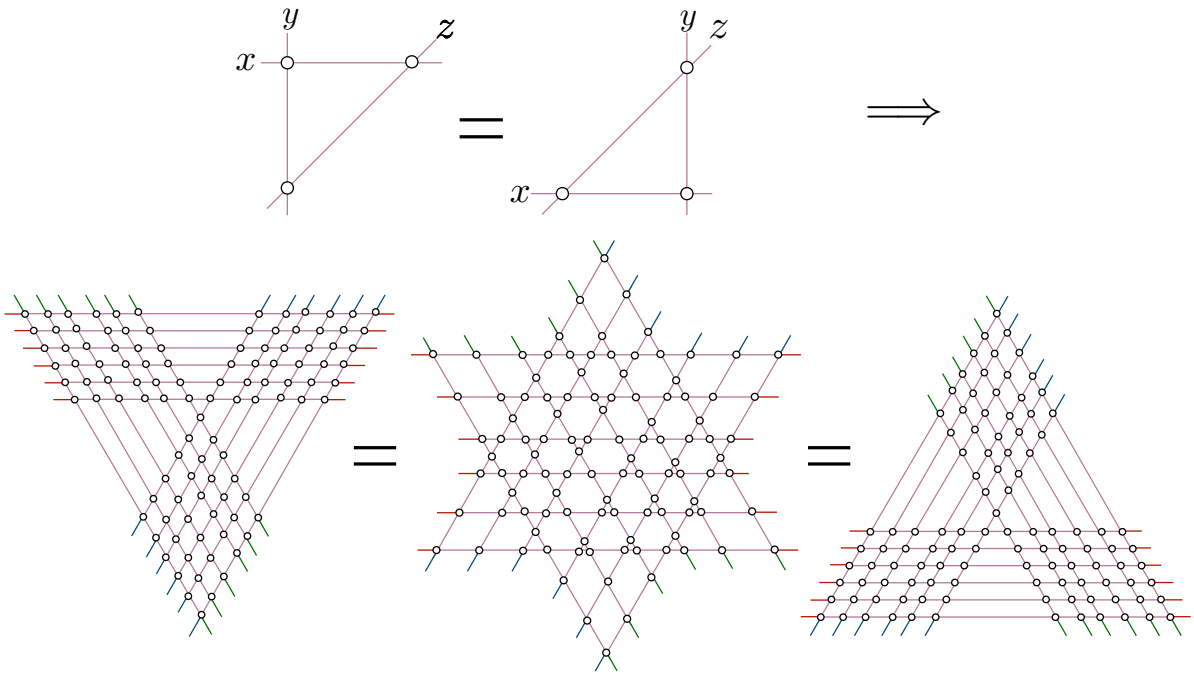

Figure 6.2: The PSU(2|2) vertex satisfies the Yang-Baxter relation illustrated in the first line. Simply put, the partition function is invariant under translating lines across vertices. These allows for many possible rewritings of the partition function, as expressed in the second line. The term on the left-hand side corresponds to the second line of (6.7). The next two terms give alternative representations whose explicit form we hope is clear from the picture. In particular, the middle shape relates the hexagon partition function to a Hubbard-type model in a Kagome-type lattice.

In this basis, the matrices $\delta, \Delta, \epsilon, E$ act as

$$\delta = \begin{pmatrix} 1 & 0 & 0 & 0 \\ 0 & 1 & 0 & 0 \\ 0 & 0 & 0 & 0 \\ 0 & 0 & 0 & 0 \end{pmatrix}, \quad \Delta = \begin{pmatrix} 0 & 0 & 0 & 0 \\ 0 & 0 & 0 & 0 \\ 0 & 0 & 1 & 0 \\ 0 & 0 & 0 & 1 \end{pmatrix}, \quad \epsilon = \begin{pmatrix} 0 & 1 & 0 & 0 \\ -1 & 0 & 0 & 0 \\ 0 & 0 & 0 & 0 \\ 0 & 0 & 0 & 0 \end{pmatrix}, \quad E = \begin{pmatrix} 0 & 0 & 0 & 0 \\ 0 & 0 & 0 & 0 \\ 0 & 0 & 0 & 1 \\ 0 & 0 & -1 & 0 \end{pmatrix}.$$

The boundary conditions are so that initial and final states are purely fermionic. Particles in the sets u, v, w have, respectively, incoming polarization spinors L_1, R_2, R_3 and outgoing polarization spinors R_1, L_2, L_3[2]. In the bulk of the partition function, coloured in pink in figure 6.1, the particles can transmute into scalars and explore the full PSU(2|2) dynamics.

Having defined all these elements, we can translate picture 6.1 into an equation for

[2]This weird choice of labels is made to simplify formulas in section 6.3, in which L_i and R_i will correspond to physical left and right space-time polarization spinors of local operators in $\mathcal{N} = 4$ SYM. Particle sets v_i and w_k, being crossed, have their right and left handed spinning components exchanged. It will also simplify some of the formulas to follow, see e.g. equation (6.16).

the partition function. This is equation (6.7). Note the vertex simplify dramatically for identical fermionic outgoing states, the matrix part being reduced to the element $\mathcal{D} = -1$. This was used to write the last three factors in equation (6.7).

$$Z_{J_1,J_2,J_3} \equiv \prod_{i=1}^{J_2}\prod_{j=1}^{J_1}\prod_{k=1}^{J_3} \underbrace{L_1{}^{b_j^1} R_2{}^{a_i^1} R_3{}^{c_k^1}}_{\text{incoming b.c.}} \times \underbrace{R_{1\,b_j^{J_2+J_3}} L_{2\,a_i^{J_1+J_3}} L_{3\,c_k^{J_1+J_2}}}_{\text{outgoing b.c.}} \times \underbrace{(-1)^{J_2+J_3}}_{\text{crossing factor}} \times \tag{6.7}$$

$$\underbrace{S^{a_i^{j+1} b_j^{i+1}}_{a_i^j b_j^i}(v_{J_2+1-i}, u_j)}_{v_i,\, u_j \text{ scattering}} \times \underbrace{S^{a_i^{J_1+k+1} c_k^{i+1}}_{a_i^{J_1+k} c_k^i}(v_{J_2+1-i}, w_k)}_{v_i,\, w_k \text{ scattering}} \times \underbrace{S^{b_j^{J_2+k+1} c_k^{J_2+j+1}}_{b_j^{J_2+k} c_k^{J_2+j}}(u_{J_1+1-j}, w_k)}_{u_j,\, w_k \text{ scattering}} \times$$

$$\prod_{i'<i} \underbrace{(-1)^{J_2(J_2-1)/2} h(v_{i'}, v_i)}_{v_{i'},\, v_i \text{ scattering}} \prod_{j'<j} \underbrace{(-1)^{J_1(J_1-1)/2} h(u_{j'}, u_j)}_{u_{j'},\, u_j \text{ scattering}} \times \prod_{k'<k} \underbrace{(-1)^{J_3(J_3-1)/2} h(w_{k'}, w_k)}_{w_{k'},\, w_k \text{ scattering}}.$$

6.2.2 Properties of the partition function

The $PSU(2|2)$ vertex enjoys four important properties which we will make use in the next few sections. First, it satisfies the Yang-Baxter relation

$$S^{\alpha\beta}_{bc}(z', z'') S^{d\gamma}_{a\alpha}(z, z'') S^{ef}_{\gamma\beta}(z, z') = S^{\beta\gamma}_{ab}(z, z') S^{\alpha f}_{\gamma c}(z, z'') S^{de}_{\beta\alpha}(z', z'') \tag{6.8}$$

which allows for many possible rewritings of the partition formula (6.7) as illustrated in figure 6.2. Second, it satisfies the unitarity relation

$$S^{\alpha\beta}_{ab}(z, z') S^{cd}_{\alpha\beta}(z', z) = h(z, z') h(z', z), \tag{6.9}$$

as follows from the unitarity of the Beisert PSU(2|2) S-matrix.

Note that unitarity immediately allows us to show that, up to a trivial overall factor, the hexagon partition function is an invariant function under swapping of any fermions of the same type as illustrated in figure 6.3. More precisely we can decompose any permutation of fermions within the same group as a sequence of neighbouring swaps, each of which simply generates an abelian S-matrix factor $S_0(z_i, z_{i-1}) \equiv h(z_i, z_{i-1})/h(z_{i-1}, z_i)$,

$$Z_{J_1,J_2,J_3}\Big|_{z_i \leftrightarrow z_{i-1}} = S_0(x_i, x_{i-1}) Z_{J_1,J_2,J_3} \tag{6.10}$$

This is the so-called Watson relation.[3]

The two properties above allow one to move lines around (Yang-Baxter) and collapse bubbles (Unitarity). The next two properties lead to situations which prepare the lines to be moved.

First, at equal rapidities, the scattering vertex degenerates. For example, when $v_i \to$

[3]Note that we could have redefined the partition function by a trivial product of h factors so that the symmetry relation (6.10) would simplify to full invariance under any swap of rapidities. We found it better *not* to do so to preserve some nice analytic properties.

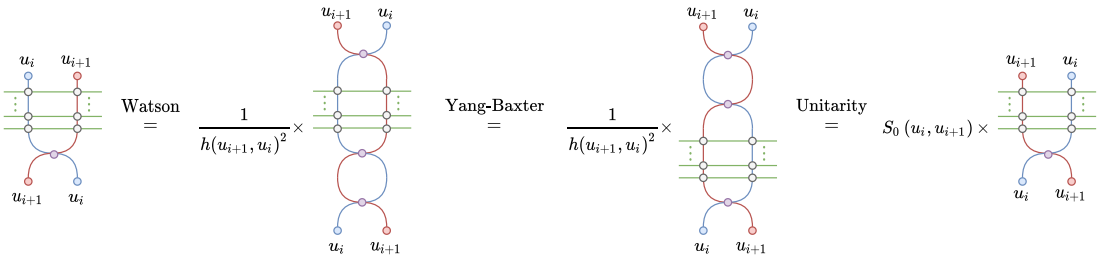

Figure 6.3: The Watson axiom imply that particles in the same external set can be exchanged through the action of the $SL(2,R)$ S-matrix $S_0(x,y) \equiv h(x,y)/h(y,x)$. This follows explicitly from the fact that for identical outgoing polarizations the vertex (6.3) projects into the $\mathcal{D}$ element. In equations, $R_{1c}R_{1d}S^{cd}_{ab}(u_i,u_{i+1}) = -R_{1a}R_{1b}h(u_i,u_{i+1}) = S_0(u_i,u_{i+1})R_{1c}R_{1d}S^{cd}_{ab}(u_{i+1},u_i)$.

w_k[4] we have, up to regular terms,

$$S^{cd}_{ab}(v_i,w_k) \sim \frac{i/\mu(w_k)}{v_i-w_k}\left(-\delta^c_a\delta^d_b - \delta^c_a\Delta^d_b - \Delta^c_a\delta^d_b - \Delta^c_a\Delta^d_b\right) = \tag{6.11}$$

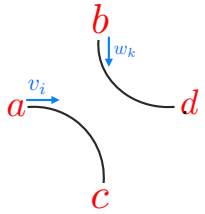

In the limit, the vertex develops a pole proportional to the index permutation operator, the residue of which defines the measure $\mu(w_k)$. Physically we can interpret this singularity as a a clustering property (two far away particles disconnect from the rest). As illustrated in the figure, at this point the two lines meeting at a vertex are now disentangled; they are thus ready to be moved around with unitarity and Yang-baxter in a sequence of moves which can dramatically simplify the partition function.

Finally, the vertex also simplifies in the infinite rapidity limit. We have, up to $1/u$ corrections

$$S^{cd}_{ab}(v,u) = S^{dc}_{ba}(u,w) \sim \left(-\delta^d_a\delta^c_b + \delta^d_a\Delta^c_b + \Delta^d_a\delta^c_b + \Delta^d_a\Delta^c_b\right) + O(1/u) = \tag{6.12}$$

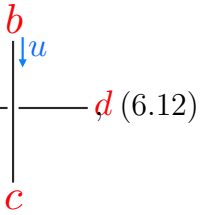

the minus sign in the first term corresponding to the trivial scattering of anticommuting fermions. Physically, when the rapidity is sent to infinity the particle has zero momenta and became a goldstone excitation which scatters trivially with other particles. After this limit the two lines also became two disentangled pairs, albeit a different choice of pairs compared to the decoupling example. In this case the particle whose root is sent to infinity scatters trivially with all other particles so the simplification of the partition function implies right away that in the $u_1 \to \infty$ limit, we simply have

[4]Here we mean to take w_k and v_i to be equal *after* performing the crossing monodromies $v_i^{\circlearrowleft}$ and $w_k^{\circlearrowleft}$.

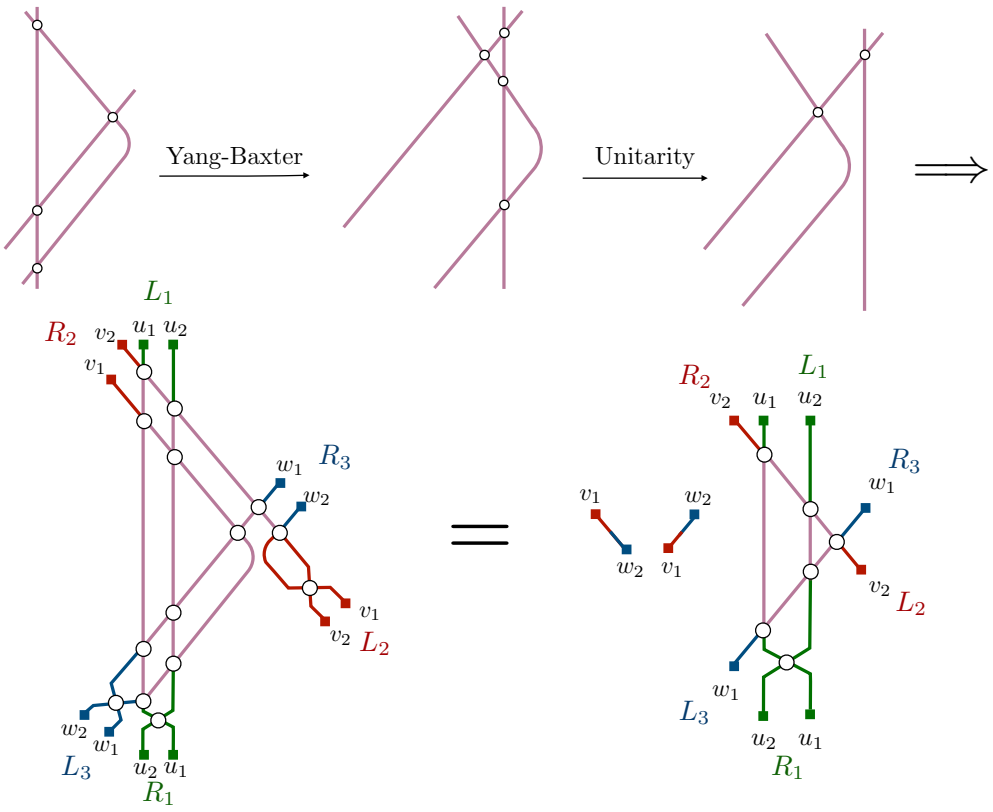

Figure 6.4: Decoupling limit in the $Z_{2,2,2}$ case. Top: lines can be disentangled through the basic Yang-Baxter and Unitarity moves. Bottom: When $v_1 \to w_2$ the vertex degenerate into the permutation operator, see equation (6.11). One can then use the basic moves (6.8, 6.9) to completely factorize the depende on v_1 and w_2, leading to equation (6.14). In doing so one makes use of the unitarity identities $h(v_i^{\circlearrowleft}, v_j^{\circlearrowleft})h(v_j^{\circlearrowleft}, v_i^{\circlearrowleft}) = h(w_j^{\circlearrowleft}, w_j^{\circlearrowleft})h(w_i^{\circlearrowleft}, w_j^{\circlearrowleft}) = h(v_i^{\circlearrowleft}, u_j)h(u_j, v_i^{\circlearrowleft}) = 1$,.

$$Z_{J_1,J_2,J_3} \sim (-1)^{J_1+J_2+J_3+1}\langle L_1, R_1\rangle Z^{u_1}_{J_1-1,J_2,J_3}, \qquad u_1 \to \infty \tag{6.13}$$

which is depicted in figure 6.6. Here and below, rapidities in a superscript in a partition function Z indicates that the rapidities in the superscript are *absent* from the partition function.

These four properties can be used to derive recursion formulas for the partition function. When a vertex degenerates into a permutation operator we can sequentially apply the Yang-baxter and unitarity properties to completely factorize the two decoupling particles from the rest of the partition function, as explained in figure 6.4. The result is that the singular term in the $v_1 \to w_{J_3}$ limit is

$$Z_{J_1,J_2,J_3} \sim -\frac{i}{\mu(w_J)}\frac{\langle L_2, R_3\rangle\langle L_3, R_2\rangle}{v_1 - w_{J_3}} Z_{J_1,J_2-1,J_3-1}\Big|_{v_a \to v_{a+1}}, \tag{6.14}$$

with $\langle L_a, R_b\rangle \equiv L_{ai}R^i_b$. This relation was particularly easy to visualize graphically because we decoupled neighboring particles, namely the last particle of type w with the first particle

of type v, see kets and bras in figure (6.1) where that is even more manifest. However, since we can rearrange any particles within any set using (6.10) we can immediately write down the decoupling between any v and any w particle,

$$Z_{J_1,J_2,J_3} \sim -\frac{i}{\mu(w_j)} \frac{\langle L_2, R_3\rangle\langle L_3, R_2\rangle}{v_i - w_k} \prod_{i'=1}^{i-1} S_0(v_{i'}, v_i) \prod_{k'=k+1}^{J_3} S_0(w_k, w_{k'}) Z_{J_1,J_2-1,J_3-1}\Big|_{v_a \to v_{a+1}}, \tag{6.15}$$

Decouplings for other pairs v_i, w_k can be obtained by moving the particle v_i to the position of v_1, and similar for w_k and w_{J_3}, by means of Watson equation, (6.10) .

Crossing symmetry relates different expressions for the partition function that exchange the various sets of particles. We illustrate this in figure 6.5. In particular, the expression (6.1) is invariant under $u \to v, v \to w, w \to u$ with $L_i \to L_{i+1}, R_i, \to R_{i+1}$:

$$Z_{J_1,J_2,J_3} = Z_{J_2,J_3,J_1}\Big|_{\substack{u\to v, v\to w, w\to u \\ (L_i,R_i)\to(L_{i+1},R_{i+1})}} . \tag{6.16}$$

Combining permutation invariance (6.16) with the $v \to w$ decoupling (6.14) provides $u \to v$ and $u \to w$ decoupling formulas

$$Z_{J_1,J_2,J_3} \sim -\frac{i}{\mu(v_i)} \frac{\langle L_1, R_2\rangle\langle L_2, R_1\rangle}{u_j - v_i} \prod_{j'=1}^{j-1} S_0(u_{j'}, u_j) \prod_{i'=i+1}^{J_2} S_0(v_i, v_{i'}) \times Z^{u_j,v_i}_{J_1-1,J_2-1,J_3}, \tag{6.17}$$

$$Z_{J_1,J_2,J_3} \sim \frac{i}{\mu(w_k)} \frac{\langle L_1, R_3\rangle\langle L_3, R_1\rangle}{u_j - w_k} \prod_{j'=j+1}^{J_1} S_0(u_j, u_{j'}) \prod_{k'=1}^{k-1} S_0(w_{k'}, w_k) \times Z^{u_j,w_k}_{J_1-1,J_2,J_3-1}. \tag{6.18}$$

Once again we write only the singular terms in the $u_j \to v_i$ and $u_j \to w_k$ limits respectively.

The equations (6.13) and (6.17, 6.18) in boxes are powerful constraints. They relate partition functions with a certain number of particles (lhs's) with partition functions with less particles (rhs's). An obvious question is whether we can turn them into recursion relations which completely determine the partition function in terms of trivial tiny partition functions with a vertex or two. We could not find a way to do it at finite coupling. The basic obstacle is that the partition function is not a simple rational function of the rapidities whose residues are simple, but instead a multi-sheeted object since the Zhukosky variables naturally take values in tori [160]. Before crossing cuts, all poles are of the type described in (6.13, 6.17, 6.18). However, in the second sheet there are extra poles capturing the fusion of the fundamental fermions into bound states. Correspondingly, the residues are no longer simple decoupled partition functions but instead partition functions with external bound-states. One could hope to bootstrap the complete system of partition functions including all possible external bound-states in a recursive way, but we did not achieve that. On the other hand, in perturbation theory the coupling goes to zero and these tori degenerate and simplify into simple (punctured) spheres. In more pedestrian terms, the square roots in the Zhukosky variables disappear and these become simply proportional to the Bethe roots so that the partition function becomes a nice rational function of the Bethe roots whose poles

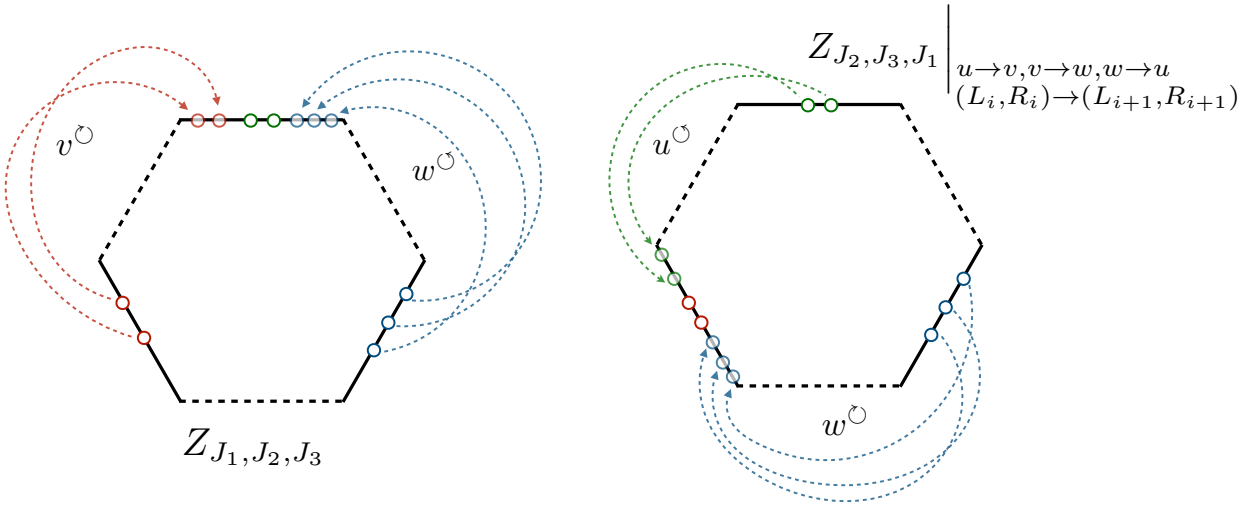

Figure 6.5: The $\mathcal{N}=4$ hexagon form factor [66] from which the hexagon partition function originates is symmetric in its three physical edges, represented here by solid lines. The expression (6.7) is obtained by moving all particles from the v and w edges to the top u edge, left picture. Moving particles to non-adjacent edges of the hexagon correspond to crossing transformations. Alternatively, the hexagon form factor could be evaluated through the prescription of the right figure, in which v particles remain physical while w is crossed clockwise and u crossed anticlockwise. The result is equation (6.16). An equivalent statement is that the hexagon form factor is invariant under crossing all particles in the same direction.

correspond to simple decouplings.[5] In that case we can indeed convert the above relations into powerful recursion relations. It is what we will do in section 6.2.3. After that we will consider a particular example where we can evaluate the full hexagon partition function at any value of the coupling.

6.2.3 Tree Level

When $g \to 0$ the Zhukovsky variables (6.4) become rational functions of the rapidities. More surprisingly, the full hexagon partition function becomes rational, the various square roots from the matrix elements (E.6 - E.7) cancelling out. In this section we use rationality to derive recursion relations that efficiently compute the hexagon partition function for any J_i.

Rational functions are completely fixed by their singularities and asymptotics. As a function of u_1, $Z(J_1, J_2, J_3)$ has two types of poles both of which with clear physical meaning. The first are poles corresponding to the fusion of two physical particles, u_1 and u_j, into a bound state. These are the singularities contained in the $h(u_1, u_j)$ factors in (6.7). All other singularities at tree level[6] are decoupling poles (6.17,6.18). We are immediately

[5] Even this is actually not totally trivial because of the non-local ϕ Z-markers with its own square roots. It turns out that these square roots can be simplify away.

[6] At $g \neq 0$ the physical particles may form bound states with the crossed particles, resulting in new

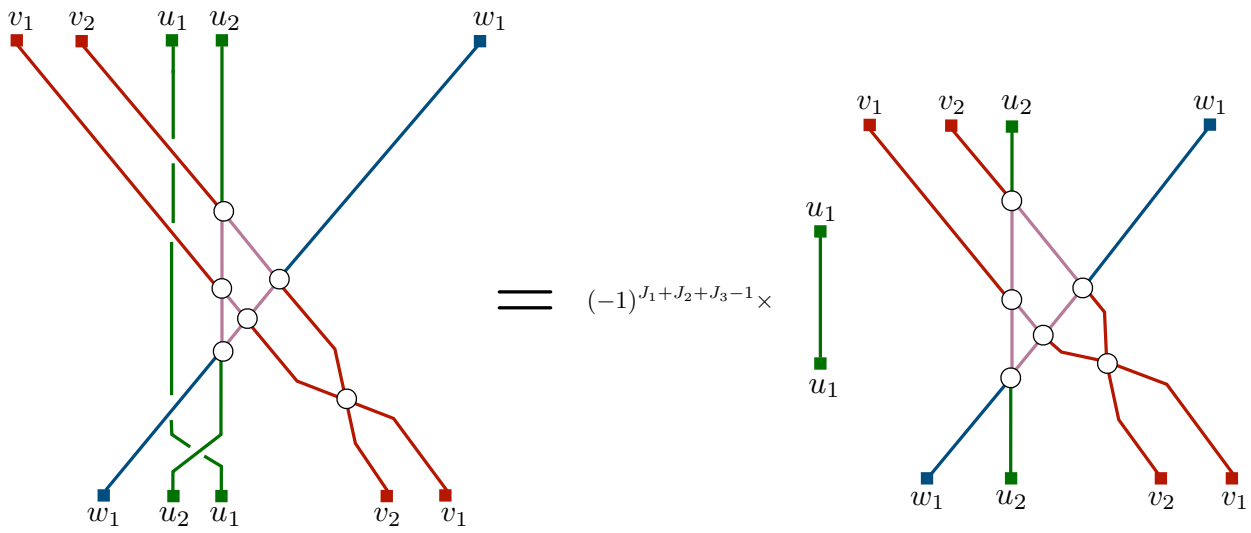

Figure 6.6: Decoupling when $u_1 \to \infty$ for $Z_{2,2,1}$. When one of the rapidities is sent to infinity the vertex reduces to the free S-matrix. All scatterings of particle u_1 are of the fermion-fermion type, resulting in the $(-1)^{J_1+J_2+J_3-1}$ factor of equation (6.13).

led to the recursion relation

$$\begin{aligned}\hat{Z}_{J_1,J_2,J_3} =&(-1)^{J_1+J_2+J_3+1}\langle L_1,R_1\rangle \hat{Z}^{u_1}_{J_1-1,J_2,J_3}+ \\ &-\sum_{i=1}^{J_2}\frac{i}{\mu(v_i)}\frac{\langle L_1,R_2\rangle\langle L_2,R_1\rangle}{u_1-v_i}\prod_{i'=i+1}^{J_2}S_0(v_i,v_{i'})\prod_{j=2}^{J_1}\hat{h}(v_i,u_j)^{-1}\ \times \hat{Z}^{u_1,v_i}_{J_1-1,J_2-1,J_3}+ \\ &+\sum_{k=1}^{J_3}\frac{i}{\mu(w_k)}\frac{\langle L_1,R_3\rangle\langle L_3,R_1\rangle}{u_1-w_k}\prod_{j'=2}^{J_1}S_0(u_1,u_{j'})\prod_{k'=1}^{k-1}S_0(w_{k'},w_k)\prod_{j=2}^{J_1}\hat{h}(w_k,u_j)^{-1}\times \hat{Z}^{u_1,w_k}_{J_1-1,J_2,J_3-1}\end{aligned} \tag{6.19}$$

with $\hat{Z}_{J_1,J_2,J_3} = Z_{J_1,J_2,J_3}\prod_{j<j'}h(u_j,u'_j)^{-1}$. Here $\hat{h} = h$ computed *without* performing crossing monodromies in the arguments, since in the decoupling limit u_j approaches v_i and w_k without going around Zhukovsky branch points[7]. Explicitly, at tree level

$$\hat{h}(x,y)=\frac{x-y}{x-y-i},\qquad \mu(x)=1,\qquad S_0(x,y)=\frac{x-y+i}{x-y-i}. \tag{6.20}$$

Repeated use of (6.19) reduces the computation of Z_{J_1,J_2,J_3} to that of Z_{0,J_2,J_3}. One could then use rationality in v_i and w_k to write further recursions that reduce the formula all the way to $Z_{0,0,0}=1$. One can skip this step, in practice, since the recursions for Z_{0,J_2,J_3}

singularities.

[7]These branch points disappear at tree level, the Zhukovsky variables becoming rational. This is an important point. The crossing transformations do not commute with the perturbative expansion. Crossing can only be performed at finite coupling. In a sense, the simplicity of the tree level result encode some of the finite coupling structure through the many properties derived from crossing and used to bootstrap (6.19).

can be solved explicitly. Through induction one finds the determinant formula

$$Z_{0,J_2,J_3} = (-1)^{A_{J_2J_3}} \frac{\prod_{i=1}^{J_2}\prod_{k=1}^{J_3}(v_i - w_k + i)}{(\prod_{i<i'} v_{i'} - v_i + i)(\prod_{k<k'} w_k - w_{k'} - i)} \det \mathrm{M},$$

where M is a square matrix of size $\max(J_2, J_3)$ whose elements are given by

$$M_{ij} = \begin{cases} \frac{\langle 23\rangle\langle 32\rangle}{v_i - w_j} + \frac{\langle 22\rangle\langle 33\rangle}{v_i - w_j + i} - \frac{\langle 23\rangle\langle 32\rangle}{v_i - w_j + i}\,, & \text{if } i \le J_2 \wedge j \le J_3 \\ -\frac{\langle 23\rangle\langle 32\rangle}{\langle 33\rangle v_i^{J_3 - j + 1}} - \frac{\langle 22\rangle}{(v_i + i)^{J_3 - j + 1}} + \frac{\langle 23\rangle\langle 32\rangle}{\langle 33\rangle (v_i + i)^{J_3 - j + 1}}\,, & \text{if } j > J_3 \\ \frac{\langle 23\rangle\langle 32\rangle}{\langle 22\rangle w_j^{J_2 - i + 1}} + \frac{\langle 33\rangle}{(w_j - i)^{J_2 - i + 1}} - \frac{\langle 23\rangle\langle 32\rangle}{\langle 22\rangle (w_j - i)^{J_2 - i + 1}}\,, & \text{if } i > J_2 \end{cases},$$

with $\langle ij\rangle \equiv \langle L_i, R_j\rangle$ and

$$A_{J_2J_3} = (J_2 + 1)(J_3 + 1) + \sum_{i=2}^{3}(J_i - 1)J_i/2 + \begin{cases} \frac{(J_3 - J_2)(1 + J_3 - J_2)}{2}\,, & \text{if } J_2 < J_3 \\ 0\,, & \text{otherwise} \end{cases}.$$

In section 6.3.2 the recursive formulas (6.19 ,6.21) will be used to produce three point structures data for operators of arbitrary twist at tree level. For convenience, we attach a ready to copy-and-paste Mathematica implementation of the tree level recursion. The SL(2) S-matrix and dynamical factor are

```
S0[z_, zp_] = (z - zp + I)/(z - zp - I);
h[z_, zp_] = (z - zp)/(z - zp - I);
```

We then write the recursive formulas for the partition function. As explained above, when applying the recursion to one of the three particle sets, it is useful to factor out the dynamical factors. We denote this procedure through "hats" which must be removed to recover Z. First we do recursions for "v's" starting with the trivial one-set answer:

```
Zhathat[0,J3_] := V[3]^J3 Product[(-1) h[w[k], w[kk]], {kk, J3}, {k, kk - 1}];
Zhathat[J2_,J3_]:= Zhathat[J2,J3] = (-1)^(J2+J3+1) V[2] (Zhathat[J2-1,J3] /.v[i_]:>v[i+1])-
    Sum[I H[2,3]/(v[1]-w[k])Product[S0[w[k],w[kk]],{kk,k+1,J3}] Product[h[w[k],v[i]]^-1,{i,2,J2}]
     (Zhathat[J2-1,J3-1] /.{v[i_]:>v[i+1],w[kkk_]/;kk>=k:>w[kkk+1]}),{k,J3}];
Zhat[0,J2_,J3_]:=Zhathat[J2, J3]Product[h[v[i], v[ii]],{ii,J2},{i,ii-1}];
```

Next, we perform recursions for the "u" particles to recover the full partition function,

```
Zhat[J1_,J2_,J3_]:= Zhat[J1,J2,J3]=(-1)^(J1+J2+J3+1)V[1](Zhat[J1-1,J2,J3] /.u[j_]:>u[j+1])-
     Sum[I H[1,2]/(u[1]-v[i])Product[S0[v[i],v[ii]],{ii,i+1,J2}]Product[h[v[i],u[j]]^-1,{j,2,J1}]
       (Zhat[J1-1,J2-1,J3]/.{u[j_]:>u[j+1],v[iii_]/;iii>=i:>v[iii+1]}),{i,J2}]+
          Sum[I H[3,1]/(u[1]-w[k])Product[S0[u[1],u[jj]],{jj,2,J1}]Product[S0[w[kk],w[k]],
            {kk,1,k-1}] Product[h[w[k],u[j]]^-1,{j,2,J1}](Zhat[J1-1, J2,J3-1]/.{u[j_]:>u[j+1],
```

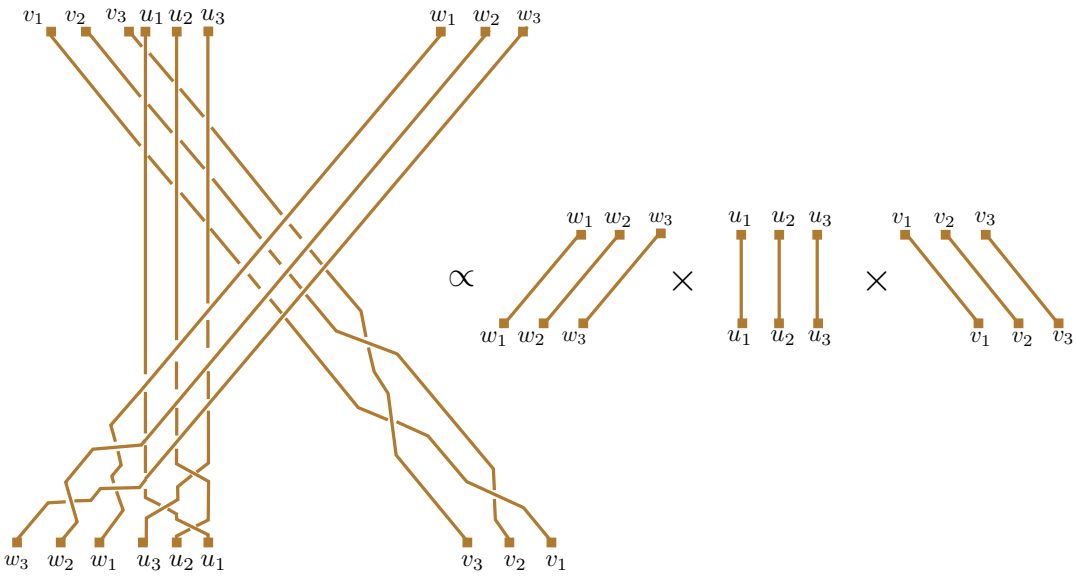

Figure 6.7: When the incoming state are fermions with parallel polarizations, the vertex becomes proportional to the identity, e.g. $R_2{}^a L_1{}^b S^{cd}_{ab}(u_i, u_{i+1}) = -R_2{}^c L_1{}^d h(v_2, u_1)$. This simplification happens at all vertices if $L_1 = R_2 = R_3$, the partition function reducing to the product of abelian factors times the inner product between incoming and outgoing polarizations, equation (6.21). Of course, the same simplification holds if instead we have $R_1 = L_2 = L_3$.

```
            w[kkk_]/;kkk>=k:>w[kkk+1]}),{k,J3}];
Z[J1_,J2_,J3_]:=Zhat[J1,J2,J3]Product[h[u[j],u[jj]],{jj,J1},{j,jj-1}];
```

as promised. In the code we denoted $V[i] \equiv \langle L_i, R_i \rangle$ and $H[i,j] \equiv \langle L_i, R_j \rangle \langle R_i, L_j \rangle$.

6.2.4 All Loop Abelian Simplifications

When $L_1 = R_2 = R_3$ the triangle partition function dramatically simplifies. In that case, only the terms proportional to the $\mathcal{D}$ matrix element in (6.3) survives. As shown in figure 6.7, the result is

$$Z^{\text{Abelian}}_{J_1,J_2,J_3} = \langle L_1, R_1 \rangle^{J_1} \langle L_2, R_2 \rangle^{J_2} \langle L_3, R_3 \rangle^{J_3} \times (-1)^{J_2+J_3+J(J-1)/2} \tag{6.21}$$
$$\prod_{i=1}^{J_2} \prod_{j=1}^{J_1} \prod_{k=1}^{J_3} h(v_i, u_j) h(u_j, w_k) h(v_i, w_k) \prod_{\substack{i'<i \\ j'<j \\ k'<k}} h(v_{i'}, v_i) h(u_{j'}, u_j) h(w_{k'}, w_k),$$

with $J = J_1 + J_2 + J_3$. We emphasize this result holds at finite coupling g.

Of course, from permutation invariance, the result also simplifies for $L_2 = R_1 = R_3$ and $L_3 = R_1 = R_2$. This is non-trivial from the expression (6.7) but can be made manifest

through crossing transformations. The vertices are also projected into the $\mathcal{D}$ element if $R_1 = L_2 = L_3$ or permutations, as can be seen from (6.3). The partition function for these polarizations also reduces to formula (6.21).

6.3 Spinning hexagons

6.3.1 Polarizing the Hexagon OPE

Now we shift gears by focusing on the computation of three point functions of primary operators in the SL(2|$\mathbb{R}$) sector of $\mathcal{N} = 4$ SYM. One important ingredient in our analysis, as we shall see below, is the hexagon partition function analysed in the previous section. Before delving into those details let us define the precise form of the operators that are being considered and summarize how the hexagon formalism can be used to compute three point functions.

The primary operators in the SL(2|$\mathbb{R}$) sector are traceless symmetric single traces made out of covariant derivative excitations $\mathcal{D}^{\alpha\dot{\alpha}}$ on top of a BPS "vaccum" of fundamental scalars, $\mathrm{Tr}(\vec{Y}\cdot\vec{\phi})^\tau$. To denote operators of spin J_i we use the index free notation in terms of polarization spinors

$$\mathcal{O}_{J_i}(x) \equiv \mathcal{O}_{J_i}(x, L_i, R_i) = \left(\prod_{j=1}^{J_i} L_{i\alpha_j} R_{i\dot{\alpha}_j}\right) \mathcal{O}_{J_i}^{\alpha_1\ldots\alpha_{J_i}\dot{\alpha}_1\ldots\dot{\alpha}_{J_i}}(x). \tag{6.22}$$

These operators are the same type of spinning operators we consider in the conformal bootstrap [4], being the only difference here that we do not need to consider leading twist, in fact, here they can have any twist τ, which we leave implicit.

By conformal symmetry, the full three point function can be recovered from its values in the conformal frame[8]. We place operators along the x_2 axis at 0, 1 and ∞. The rescaled correlator

$$C(J_1, J_2, J_3) \equiv \lim_{\mathcal{L}\to\infty} \mathcal{L}^{2\Delta_3} \langle \mathcal{O}_{J_1}(0)\rangle \mathcal{O}_{J_2}(1)\mathcal{O}_{J_3}(\mathcal{L}) \tag{6.23}$$

can then be expressed as a sum over tensor structures invariant under the residual unfixed symmetry [146, 161]. As defined in appendix E.1, these tensor structures can be written as inner products of the polarization spinors L_i and R_i, as follows

$$C(J_1, J_2, J_3) = \sum_{\ell_1,\ell_2,\ell_3} C_{\ell_1,\ell_2,\ell_3}^{J_1,J_2,J_3} \frac{\langle 1,1\rangle^{J_1-\ell_2-\ell_3}\langle 2,2\rangle^{J_2-\ell_1-\ell_3}\langle 3,3\rangle^{J_3-\ell_1-\ell_2}}{\langle 2,3\rangle^{-\ell_1}\langle 3,2\rangle^{-\ell_1}\langle 1,3\rangle^{-\ell_2}\langle 3,1\rangle^{-\ell_2}\langle 1,2\rangle^{-\ell_3}\langle 2,1\rangle^{-\ell_3}}. \tag{6.24}$$

where $\langle i, j\rangle = \langle L_i, R_j\rangle$. The goal is to reproduce this three point function – which at once captures all structure constants for any tensor structures – from the hexagon formalism.

The hexagon formalism has already been developed and tested thoroughly for spinless

[8] More generally, by superconformal symmetry, we can also fix the R-symmetry polarizations Y_i to point at fixed directions in $SO(6)$. The dependence on them is completely fixed by the Ward identities. In practice we use the twisted translated polarizations of [66]. The R-symmetry factors will not be important in our discussion and we mostly omit them.

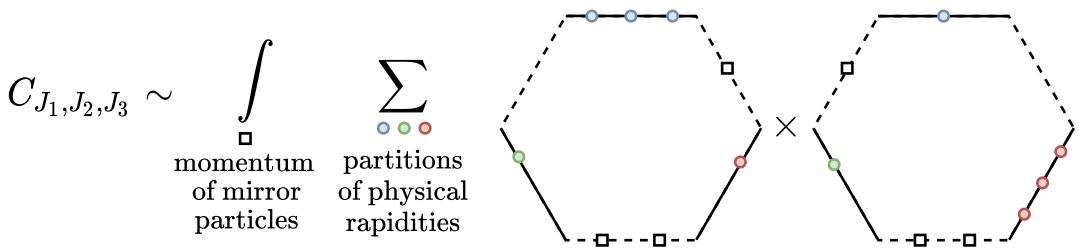

Figure 6.8: Each closed spin chain operator is split into two open chain operators. We sum over all the ways its excitations can end up in either one of the chains. Gluing the hexagons together amounts to integrating over all possible mirror states.

operators to very high perturbative orders (as well as for spinning correlators without non-trivial tensor structures) so the main novelty here is how to deal with the various spinor polarizations leading to the various terms summed in (6.24). Before presenting the relevant expressions with these spinor boundary conditions accounted for let us recall that the hexagon formalism entails two main components as illustrated in figure 6.8:

- One is a sum over partitions of physical rapidities for each external operator. When we cut the three point function pair of pants into two hexagons the excitations on each operator can end up on either hexagon so we must sum over ways of partitioning such excitations. These sums are often referred to as the asymptotic sums.

- The other are integrals over mirror rapidities along the three seams of the pair of pants. When we glue back the hexagons into a pair of pants we must sum over all possible quantum states along each edge where we glue. These mirror integrals are often referred to as wrapping effects.

In this chapter we completely ignore the second effect. Except for section E.6.1.

There are two simple reasons for doing so. The first is that wrapping corrections are delayed in perturbation theory. At tree level and one loop they do not show up even for the smallest twist two external operators for instance and for larger twist operators they are delayed even more in perturbation theory. So we better clean up the asymptotic part first – where all the subtleties related to the spinors already shows up – before addressing these finite size mirror corrections. The second reason is that even at loop level, sometimes we can drop the wrapping corrections altogether if the distances travelled by the mirror particles are very large. This happens for large operators with lots of R-charge but also for operators of small R-charge and very large spin. The intuition is that when the spin is very large the centripetal force effectively opens up the operator making it effectively very large; in this case sometimes these finite size corrections can be ignored. We thus suspect this to be the case for the case of three twist two operators with very large spin and generic polarizations. Evaluating this kind of correlator should beautifully connect to the remarkable Wilson loop dualities [4, 143, 162]. So if our goal is to eventually prove these dualities from integrability perhaps we can ignore wrapping for now.

With wrapping out of the window, we can then present our main formula for the spinning three point function. It is a long formula but fortunately most ingredients are

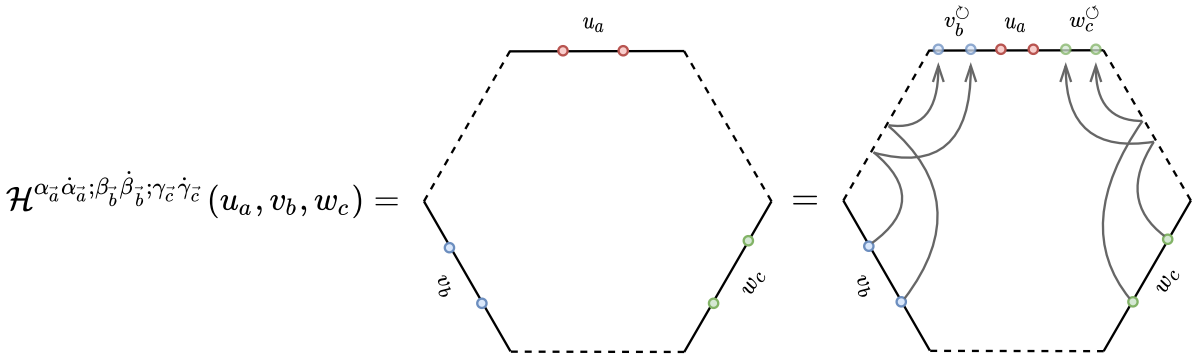

Figure 6.9: To obtain a correlator with all excitations on top we perform one crossing transformation in the left ($\circlearrowleft$) and another in the right ($\circlearrowright$). These monodromies will change the Zhukovsky variables as well as the indices of the excitations.

self-explanatory and have appeared before in several spinless studies. It reads

$$C(J_1, J_2, J_3) = \underbrace{\mathcal{N}(\mathbf{u})\mathcal{N}(\mathbf{v})\mathcal{N}(\mathbf{w})}_{\texttt{normalizations}} \times \sum_{\substack{a\cup\bar{a}=\mathbf{u}\\ b\cup\bar{b}=\mathbf{v}\\ c\cup\bar{c}=\mathbf{w}}} \underbrace{\omega_{\ell_{13}}(a,\bar{a})\omega_{\ell_{12}}(b,\bar{b})\omega_{\ell_{23}}(c,\bar{c})}_{\texttt{splitting factors}} \times \underbrace{\mathcal{H}(a,b,c)\times\mathcal{H}(\bar{a},\bar{c},\bar{b})}_{\texttt{hexagons}} \tag{6.25}$$

where the normalization and splitting factors are given by

$$\mathcal{N}(\mathbf{u})^2 = \frac{\prod_{i=1}^{J}\mu(u_i)}{\prod_{i\neq j}^{J} S(u_i,u_j)\det\left(\partial_{u_i}\phi_j\right)}\,, \qquad \omega_\ell(a,\bar{a}) = \prod_{u_j\in\bar{a}}(-e^{ip(u_j)\ell})\prod_{\substack{u_i\in a\\ i>j}} S(u_i,u_j)\,. \tag{6.26}$$

These are the same factors arising already in [66]; the notation and physical meaning of these factors is the same as there.

The most important objects in (6.25) – and where important novelty lies – are the hexagons form factors $\mathcal{H}$. We can relate either of them to a purely creation amplitude with all excitations in the top by applying a sequence of crossing transformations, see figure 6.9. This leads to a representation of the hexagon as

$$\begin{aligned}\mathcal{H}(a,b,c) = (-1)^{\frac{(a+b+c)(a+b+c-1)}{2}} \prod_{\substack{u_i\in a\\ v_j\in b\\ w_k\in c}} L_{1,\alpha_1}\ldots L_{2,\alpha_{2,j}}L_{3,\alpha_{3,k}}R_{1,\beta_{1,i}}R_{2,\beta_{2,j}}R_{3,\beta_{3,k}}\times\\ \times\langle\mathfrak{h}|\mathcal{D}^{\alpha_{2,j}\beta_{2,j}}(v_j^{\circlearrowleft})\mathcal{D}^{\alpha_{1,i}\beta_{1,i}}(u_i)\mathcal{D}^{\alpha_{3,k}\beta_{3,k}}(w_k^{\circlearrowleft})\rangle\end{aligned} \tag{6.27}$$

where the minus factor in front is the grading associated with the fermionic nature of the excitations.

This creation amplitude describes the scattering of three sets of fermions, labelled by their rapidities $\mathbf{u}$, $\mathbf{v}$ and $\mathbf{w}$ in the $\mathcal{N}=4$ SYM spin-chain. Each set starts polarized in a

fixed direction labeled by their correspondent left-hand spinors. The particles then scatter in all possible pairings according to Beisert's $PSU(2|2)$ vertex, with the final state being the projection into fermions of definite polarization defined by its right-hand spinors. The object that accounts for all these scatterings is the **hexagon partition function** (Z), defined as

$$\mathcal{H}(u_a, v_b, w_c) = (-1)^{\frac{(a+b+c)(a+b+c-1)}{2}} Z_{a,b,c}\,. \tag{6.28}$$

The particles entering this partition function are not on equal footing, since we used crossing transformations for the rapidities **v** and **w**. The first effect of these transformations is the exchange their left and right $PSU(2|2)$ indices

$$\mathcal{D}^{\alpha\beta} \overset{\circlearrowleft}{\to} -\mathcal{D}^{\beta\alpha} \text{ and } \mathcal{D}^{\alpha\beta} \overset{\circlearrowleft}{\to} -\mathcal{D}^{\beta\alpha}\,, \tag{6.29}$$

this will swap incoming and outgoing indices for particles **v** and **w**. More precisely, it will set L_1, R_2, R_3 to be the incoming boundary conditions and R_1, L_2, L_3 to be the outgoing boundary conditions for the scattering, see figure 6.1a.

Another implication of crossing is the introduction of **crossed** parameters in the S-matrix elements. This amounts to analytically continue these matrix elements when considering the crossed rapidities **v** and **w**. The effects of these analytical continuations are simple: we must pick monodromies around the branch point of the Zhukovsky variables (6.5) and mind the non-trivial factors introduced by the BES dressing phase, see appendix E.3.

In the next sections we use the properties of the **hexagon partition function** (6.7) discussed in section 6.2 to generate spinning three point functions data and compare it with the perturbative results such as (6.1).

6.3.2 Perturbative checks

As derived in (6.19) the tree-level hexagon partition function can be written as a recursion relation. The minus signs introduced by gradding slightly change the expression (6.28), but the physics behind it is still the same. One can fully determine the tree-level partition function by considering its decoupling poles and its behavior at infinity.

Both the recursion relation and its sum over partitions can be easily evaluated using for example `Mathematica`. Replacing the **u**, **v** and **w** by the Bethe roots for twist-2 operators with spins $J_1 = 2$, $J_2 = 4$ and $J_3 = 6$ we reproduce all the blue numbers in (6.1).

One nice aspect of the integrability formalism is that, even though the amount of terms in the recursion relation and in the sum over partitions grows exponentially with the spins of the operators they do not grow with the twist of these operators.

Therefore, the recursion relation above is a powerful tool to explore the corner of low spin and large twist three point functions. For example, the data for twist-10 operators with spins $J_1 = 2$, $J_2 = 4$ and $J_3 = 6$ can be easily evaluated. In particular for equal bridge

lengths ($\ell_{ij} = 5$) and Bethe roots

$$\begin{aligned}\mathbf{u} &= \{-0.0718891, 0.0718891\}\,,\\ \mathbf{v} &= \{0.164766, 0.327921, 0.844103, 1.31232\}\,,\\ \mathbf{w} &= \{0.296976, 0.491824, 0.756996, 1.13713, 2.62857, 3.91077\}\,,\end{aligned}$$

it reads

$$\begin{aligned}C(2,4,6) = {}& \langle 11\rangle\langle 13\rangle\langle 22\rangle^3\langle 23\rangle\langle 31\rangle\langle 32\rangle\langle 33\rangle^4\,(-0.0000297465) + \langle 12\rangle^2\langle 21\rangle^2\langle 22\rangle^2\langle 33\rangle^6\,(1.9812\times 10^{-6}) +\\ &+ \langle 11\rangle\langle 13\rangle\langle 23\rangle^4\langle 31\rangle\langle 32\rangle^4\langle 33\rangle\,(0.00491993) + \langle 13\rangle^2\langle 22\rangle\langle 23\rangle^3\langle 31\rangle^2\langle 32\rangle^3\langle 33\rangle\,(-0.00216325) +\\ &+ \langle 12\rangle\langle 13\rangle\langle 21\rangle\langle 23\rangle^3\langle 31\rangle\langle 32\rangle^3\langle 33\rangle^2\,(0.00999526) + \langle 13\rangle^2\langle 22\rangle^4\langle 31\rangle^2\langle 33\rangle^4\,(1.1861\times 10^{-6}) +\\ &+ \langle 12\rangle\langle 13\rangle\langle 21\rangle\langle 22\rangle\langle 23\rangle^2\langle 31\rangle\langle 32\rangle^2\langle 33\rangle^3\,(-0.00073364) + \langle 11\rangle^2\langle 22\rangle^4\langle 33\rangle^6\,(1.30467\times 10^{-7}) +\\ &+ \langle 11\rangle\langle 12\rangle\langle 21\rangle\langle 22\rangle^2\langle 23\rangle\langle 32\rangle\langle 33\rangle^5\,(-0.000071986) + \langle 11\rangle^2\langle 23\rangle^4\langle 32\rangle^4\langle 33\rangle^2\,(-0.00144007) +\\ &+ \langle 13\rangle^2\langle 22\rangle^3\langle 23\rangle\langle 31\rangle^2\langle 32\rangle\langle 33\rangle^3\,(-0.000092995) + \langle 11\rangle^2\langle 22\rangle^2\langle 23\rangle^2\langle 32\rangle^2\langle 33\rangle^4\,(0.000522219) +\\ &+ \langle 12\rangle^2\langle 21\rangle^2\langle 22\rangle\langle 23\rangle\langle 32\rangle\langle 33\rangle^5\,(0.0000727415) + \langle 11\rangle^2\langle 22\rangle\langle 23\rangle^3\langle 32\rangle^3\langle 33\rangle^3\,(0.000908203) +\\ &+ \langle 12\rangle\langle 13\rangle\langle 21\rangle\langle 22\rangle^3\langle 31\rangle\langle 33\rangle^5\,(-2.52289\times 10^{-6}) + \langle 11\rangle\langle 12\rangle\langle 21\rangle\langle 22\rangle^3\langle 33\rangle^6\,(-2.11167\times 10^{-6}) +\\ &+ \langle 11\rangle\langle 13\rangle\langle 22\rangle^4\langle 31\rangle\langle 33\rangle^5\,(-1.31656\times 10^{-6}) + \langle 11\rangle\langle 13\rangle\langle 22\rangle\langle 23\rangle^3\langle 31\rangle\langle 32\rangle^3\langle 33\rangle^2\,(-0.00342357) +\\ &+ \langle 13\rangle^2\langle 23\rangle^4\langle 31\rangle^2\langle 32\rangle^4\,(0.000683143) + \langle 11\rangle\langle 12\rangle\langle 21\rangle\langle 22\rangle\langle 23\rangle^2\langle 32\rangle^2\langle 33\rangle^4\,(-0.00146526) +\\ &+ \langle 12\rangle\langle 13\rangle\langle 21\rangle\langle 22\rangle^2\langle 23\rangle\langle 31\rangle\langle 32\rangle\langle 33\rangle^4\,(0.000215642) + \langle 12\rangle^2\langle 21\rangle^2\langle 23\rangle^2\langle 32\rangle^2\langle 33\rangle^4\,(0.00255232) +\\ &+ \langle 13\rangle^2\langle 22\rangle^2\langle 23\rangle^2\langle 31\rangle^2\langle 32\rangle^2\langle 33\rangle^2\,(0.00212987) + \langle 11\rangle\langle 12\rangle\langle 21\rangle\langle 23\rangle^3\langle 32\rangle^3\langle 33\rangle^3\,(0.000540332) +\\ &+ \langle 11\rangle\langle 13\rangle\langle 22\rangle^2\langle 23\rangle^2\langle 31\rangle\langle 32\rangle^2\langle 33\rangle^3\,(-0.00103067) + \langle 11\rangle^2\langle 22\rangle^3\langle 23\rangle\langle 32\rangle\langle 33\rangle^5\,(9.51785\times 10^{-6}) +\\ &+ \left(\langle 11\rangle^2\langle 23\rangle^4\langle 32\rangle^4\langle 33\rangle^2 - \langle 11\rangle\langle 13\rangle\langle 23\rangle^4\langle 31\rangle\langle 32\rangle^4\langle 33\rangle\right)(0.0020167) +\\ &+ \left(\langle 13\rangle^2\langle 22\rangle^4\langle 31\rangle^2\langle 33\rangle^4 - \langle 13\rangle^2\langle 22\rangle^3\langle 23\rangle\langle 31\rangle^2\langle 32\rangle\langle 33\rangle^3\right)(4.14448\times 10^{-6}) +\\ &+ \left(\langle 12\rangle^2\langle 21\rangle^2\langle 22\rangle^2\langle 33\rangle^6 - \langle 12\rangle^2\langle 21\rangle^2\langle 22\rangle\langle 23\rangle\langle 32\rangle\langle 33\rangle^5\right)(6.5287\times 10^{-6}) + \dots\,, \end{aligned} \tag{6.30}$$

Beyond tree-level, the hexagon partition function is not a simple rational function of the rapidities. Lack of control over the singularities in other Riemann sheets prevent us from writing a recursion relation akin to (6.19) at loop order. We are forced to evaluate the scattering of the hexagon form factor via the explicit form of the hexagon partition function (6.7).

For general boundary conditions the one-loop evaluation is computationally demanding. One of the problems is that structure constants are given by linear combinations of multiple

hexagons, which can be made explicit by combining (6.24) and (6.25) to write

$$\sum_{\ell_1,\ell_2,\ell_3} C^{J_1,J_2,J_3}_{\ell_1,\ell_2,\ell_3} \frac{\langle 1,1\rangle^{J_1-\ell_2-\ell_3}\langle 2,2\rangle^{J_2-\ell_1-\ell_3}\langle 3,3\rangle^{J_3-\ell_1-\ell_2}}{\langle 2,3\rangle^{-\ell_1}\langle 3,2\rangle^{-\ell_1}\langle 1,3\rangle^{-\ell_2}\langle 3,1\rangle^{-\ell_2}\langle 1,2\rangle^{-\ell_3}\langle 2,1\rangle^{-\ell_3}} =$$

$$= \mathcal{N}(\mathbf{u})\mathcal{N}(\mathbf{v})\mathcal{N}(\mathbf{w}) \times \sum_{\substack{a\cup\bar{a}=\mathbf{u}\\ b\cup\bar{b}=\mathbf{v}\\ c\cup\bar{c}=\mathbf{w}}} \omega_{\ell_{13}}(a,\bar{a})\omega_{\ell_{12}}(b,\bar{b})\omega_{\ell_{23}}(c,\bar{c}) \times \mathcal{H}(a,b,c) \times \mathcal{H}(\bar{a},\bar{c},\bar{b})\,. \quad (6.31)$$

When we fix the external polarizations L_i and R_i we must evaluate all the scaterrings, sum over partitions and in the end we obtain that a single glued hexagon is given by a combination of structure constants $C^{J_1,J_2,J_3}_{\ell_1,\ell_2,\ell_3}$. By considering several polarizations one can invert these relations obtaining single structure constants in terms of combinations of glued hexagons, see appendix E.5.

For simplicity we will consider a particular polarization where the computation of a single hexagon gives us a simple combination of structure constants. This is the configuration where all the operators have the same polarizations (i.e all the excitations are chosen to be the longitudinal modes $\mathcal{D}^{1\dot{2}}$). In terms of spinors, these means $L_1 = L_2 = L_3$ and $R_1 = R_2 = R_3$, making the inner products of (6.25) equal. The tensor structure factors out and we get that

$$\langle 1,1\rangle^{J_1+J_2+J_3} \sum_{\ell_1,\ell_2,\ell_3} C^{J_1,J_2,J_3}_{\ell_1,\ell_2,\ell_3} \quad (6.32)$$

is given by a single glued hexagon where all the excitations have the same polarization. Note that, this is **not** an abelian configuration, once we cross the rapidities $\mathbf{v}$ and $\mathbf{w}$ to the top operator we end up with distinct excitations that do not scatter trivially.

For twist-2 operators we were able to evaluate this sum for arbitrary values of spins in a close formula

$$\sum_{\ell_1,\ell_2,\ell_3} C^{J_1,J_2,J_3}_{\ell_1,\ell_2,\ell_3} = \frac{\Gamma\left(1+J_1+J_2\right)\Gamma\left(1+J_1+J_3\right)\Gamma\left(1+J_2+J_3\right)}{\Gamma\left(1+J_1\right)\Gamma\left(1+J_2\right)\Gamma\left(1+J_3\right)\sqrt{\Gamma\left(1+2J_1\right)\Gamma\left(1+2J_2\right)\Gamma\left(1+2J_3\right)}}\times$$

$$\times\, {}_4F_3\left[\begin{matrix}-J_1, & -J_2, & -J_3, & -1-J_1-J_2-J_3\\ & -J_1-J_2, & -J_1-J_3, & -J_2-J_3\end{matrix};1\right] \quad (6.33)$$

By computing the equal polarizations hexagon for twist-2 and spin $J_1 = 2$, $J_2 = 4$ and $J_3 = 6$ we recovered this tree-level value from the hexagon partition function (6.7) and also obtained the one-loop contribution

$$\sum_{\ell_1,\ell_2,\ell_3} C^{2,4,6}_{\ell_1,\ell_2,\ell_3} = \frac{75}{\sqrt{55}} - \frac{59077}{4620\sqrt{55}}g^2 + \dots\,. \quad (6.34)$$

which is reproduces the sum over all structure constants (all orange and cyan terms) appearing in the three point function (6.1).

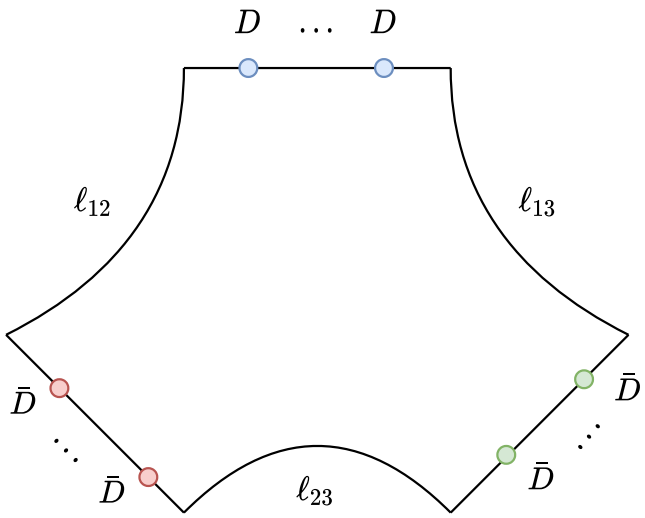

Figure 6.10: The first operator is orthogonal to the other two operators, once we perform crossing we end up with identical excitations in the physical edge, which scatter trivially. This configuration corresponds to the abelian configuration $\mathbb{A}_1$. By considering the other configurations where the operators two and three are the ones orthogonal to the other operators we get the abelian structures $\mathbb{A}_2$ and $\mathbb{A}_3$, respectively.

6.3.3 Abelian

As advertised in 6.2.4 there some polarizations which completely trivialize the scattering of the excitations. Since they are given by the abelian part of the hexagon partition function (6.7), we denote them by **abelian** components. They are associated with three-point functions where one operator has orthogonal polarization to the other two, see figure (6.10). By crossing these two operators we are left with three sets of excitations with identical polarizations in the same physical edge, which in turn scatter trivially.

One of such configurations can be obtained by considering $R_1 = L_2 = L_3$ and $L_1 = R_2 = R_3$, which sets the inner products of (6.24) to zero $\langle 12\rangle = \langle 13\rangle = 0$. Moreover, $\langle 23\rangle\langle 32\rangle = \langle 22\rangle\langle 33\rangle$, so the tensor structure factors out, resulting that the three point function

$$\langle 1,1\rangle^{J_1}\langle 2,2\rangle^{J_2}\langle 3,3\rangle^{J_3}\sum_{\ell_1,\ell_2,\ell_3} C^{J_1,J_2,J_3}_{\ell_1,0,0} \tag{6.35}$$

is given by an abelian hexagon. By permutation of the indices $1,2,3$ we have the other components

$$\mathbb{A}_1 = \sum_{\ell_1} C^{J_1,J_2,J_3}_{\ell_1,0,0}\,, \qquad \mathbb{A}_2 = \sum_{\ell_2} C^{J_1,J_2,J_3}_{0,\ell_2,0}\,, \qquad \mathbb{A}_3 = \sum_{\ell_3} C^{J_1,J_2,J_3}_{0,0,\ell_3} \tag{6.36}$$

which are structure constants given by hexagon form factors with purely abelian factors.

The scattering with these boundary conditions forces a trivial matrix part in (6.25) and yields the totally factorized contribution for the hexagon partition function shown in

(6.21) and reviewed here

$$\mathcal{H}(u_a, v_b, w_c) = \langle 1,1\rangle^a \langle 2,2\rangle^b \langle 3,3\rangle^c \times (-1)^{b+c} \prod_{v_i\in b} \prod_{u_j\in a} \prod_{w_k\in c} h(v_i,u_j)h(u_j,w_k)h(v_i,w_k)\times$$

$$\times \prod_{\substack{v_l\in b \\ l<i}} \prod_{\substack{u_m\in a \\ m<j}} \prod_{\substack{w_n\in c \\ n<k}} h(v_l,v_i)h(u_m,u_j)h(w_n,w_k)\,, \tag{6.37}$$

where the $h's$ above must be crossed according with their arguments, following (6.6).

These abelian form factors can be easily evaluated at any order in perturbation theory, in particular at one-loop and for twist-2 operators with spins $J_1 = 2$, $J_2 = 4$ and $J_3 = 6$ their sum over partitions reproduce the one-loop structure constants (colored in cyan) in expression (6.1).

It turns out that in the abelian case the sum over partitions can be performed analytically. The result (6.42) is a determinant formula for the three point function in the asymptotic regime valid for operators with arbitrary twist, which dependence enters only implicitly through the bridge lengths and the Bethe roots. This vastly reduces the computational effort required to evaluate the structure constants, and opens avenues to explore via integrability the large spin limit of the three point functions.

In this section we go over the result and derivation whose details and notation can be found in appendix E.6. The result for the case of one spinning operator was obtained in [163]. The key observation was that the sum over partitions of products of hexagon dynamical factors,

$$H(u_{\bar a}, u_{\bar a}) \equiv \prod_{i<j\in\bar a} h(u_i,u_j)h(u_j,u_i),$$

could be interpreted as the expansion of a Fredholm pfaffian,

$$\sum_{\bar a\subset \mathbf{u}} (-1)^{|\bar a|} w'(u_{\bar a}) H(u_{\bar a}, u_{\bar a}) = pf(I-\mathcal{K})_{2J_1\times 2J_1}. \tag{6.38}$$

We define the matrix $\mathcal{K}$ in appendix E.6. Crucial for our purposes is that this holds for **any** factorized function of the rapidities $w'(u_{\bar a}) = \prod_{i\in\bar a} w'(u_i)$.

The asymptotic structure constant for three spinning operators (6.31) can be rewritten in the abelian case as[9]

$$\begin{aligned}\mathbb{A}_1(J_1,J_2,J_3) =& \langle 11\rangle^{J_1}\langle 22\rangle^{J_2}\langle 33\rangle^{J_3}\mathcal{N}(J_1)\mathcal{N}(J_2)\mathcal{N}(J_3) h(\hat u,\hat u)h(\hat v,\hat v)h(\hat w,\hat w) \\ &\times \sum_{\substack{a\cup\bar a\subset\mathbf{u}\\ b\cup\bar b\subset\mathbf{v}\\ c\cup\bar c\subset\mathbf{w}}} (-1)^{|\bar a|+|\bar b|+|\bar c|} e^u_{\bar a} e^v_{\bar b} e^w_{\bar c} H(u_{\bar a},u_{\bar a}) H(v_{\bar b},v_{\bar b}) H(w_{\bar c},w_{\bar c}) \\ &\times h(v_b^{\circlearrowleft},u_a)h(u_a,w_c^{\circlearrowleft})h(w_{\bar c}^{\circlearrowleft},u_{\bar a},)h(u_{\bar a},v_{\bar b}^{\circlearrowleft})h(v_b^{\circlearrowleft},w_c^{\circlearrowleft})h(w_{\bar c}^{\circlearrowleft},v_{\bar b}^{\circlearrowleft}),\end{aligned} \tag{6.39}$$

[9] For the rest of this section we will be explicit about the crossing kinematics $\circlearrowleft$, $\circlearrowright$.

with $h(\hat{u},\hat{u}) \equiv \prod_{i<j} h(u_i,u_j)$,

$$e^u_{\bar{a}} \equiv \prod_{i\in\bar{a}} \frac{e^{iP(u_i)\ell_{13}}}{h(\hat{u},u_i)}, \qquad h(\hat{u},u_i) \equiv \prod_{j\neq i} h(u_j,u_i), \qquad h(v_b^{\circlearrowleft},u_a) \equiv \prod_{\substack{i\in a\\ j\in b}} h(v_j^{\circlearrowleft},u_i),$$

and similar for the other terms. The red terms depend explicitly on both sets $a,\bar{a}$. However, by completing the factors $h(v_b^{\circlearrowleft},u_a)h(u_a,w_c^{\circlearrowleft})$ to $h(v_b^{\circlearrowleft},\hat{u})h(\hat{u},w_c^{\circlearrowleft})$ and using the unitarity relation $h(x^{\circlearrowleft},y)h(y,x^{\circlearrowleft})=1$, it can be rewritten as

$$\begin{aligned}\text{red} &= h(v_b^{\circlearrowleft},\hat{u})h(\hat{u},w_c^{\circlearrowleft}) \sum_{a\cup\bar{a}\subset\mathbf{u}} (-1)^{|\bar{a}|} e^u_{\bar{a}} H(u_{\bar{a}},u_{\bar{a}}) \frac{h(w_{\bar{c}}^{\circlearrowleft},u_{\bar{a}})h(u_{\bar{a}},v_{\bar{b}}^{\circlearrowleft})}{h(v_b^{\circlearrowleft},u_{\bar{a}})h(u_{\bar{a}},w_c^{\circlearrowleft})}\\ &= h(v_b^{\circlearrowleft},\hat{u})h(\hat{u},w_c^{\circlearrowleft}) \sum_{\bar{a}\subset\mathbf{u}} (-1)^{|\bar{a}|}\omega'(u_{\bar{a}})H(u_{\bar{a}},u_{\bar{a}}),\end{aligned}$$

with $\omega'(u_{\bar{a}}) = e^u_{\bar{a}}/\left(h(v^{\circlearrowleft},u_{\bar{a}})h(u_{\bar{a}},w^{\circlearrowleft})\right)$, for which the pfaffian identity (6.38) applies.

Physically, from the point of view of O_1, the effect of the orthogonal operators O_2, O_3 is to create an effective background redefining the propagation factor $e^u_{\bar{a}}$ but leaving the interaction term $H(u_{\bar{a}},u_{\bar{a}})$ untouched. As we will see next, the same is true from the point of view of O_2, O_3 provided we interpret it as a larger operator with J_2+J_3 excitations.

Plugging this result in (6.39) leaves us with the blue terms,

$$\text{blue} = \sum_{\substack{b\cup\bar{b}\subset\mathbf{v}\\ c\cup\bar{c}\subset\mathbf{w}}} (-1)^{|\bar{b}|+|\bar{c}|} e^v_{\bar{b}} e^w_{\bar{c}} H(v_{\bar{b}},v_{\bar{b}})H(w_{\bar{c}},w_{\bar{c}})h(v_b^{\circlearrowleft},\hat{u})h(\hat{u},w_c^{\circlearrowleft})h(v_b^{\circlearrowleft},w_c^{\circlearrowleft})h(w_{\bar{c}}^{\circlearrowleft},v_{\bar{b}}^{\circlearrowleft}). \quad (6.40)$$

Once again completing to the overall factors and using the unitarity identity, we can reduce[10] the summand to functions of $\bar{b}$, $\bar{c}$ only,

$$\text{blue} = h(\hat{v}^{\circlearrowleft},\hat{w}^{\circlearrowleft})h(\hat{v}^{\circlearrowleft},\hat{u})h(\hat{u},\hat{w}^{\circlearrowleft}) \sum_{\substack{b\cup\bar{b}\subset\mathbf{v}\\ c\cup\bar{c}\subset\mathbf{w}}} (-1)^{|\bar{b}|+|\bar{c}|}\omega'(v_{\bar{b}}^{\circlearrowleft})\omega'(w_{\bar{c}})H(v_{\bar{b}}^{\circlearrowleft},v_{\bar{b}}^{\circlearrowleft})H(w_{\bar{c}},w_{\bar{c}})H(v_{\bar{b}}^{\circlearrowleft},w_{\bar{c}}), \quad (6.41)$$

with $\omega'(v_{\bar{b}}^{\circlearrowleft})$, $\omega'(w_{\bar{c}})$ defined in appendix (E.6). To conclude, one must reinterpret the double sum over partition as a single sum over the partition of the set $\mathbf{z}=\mathbf{v}^{\circlearrowleft}\cup\mathbf{w}$. One can then write

$$\text{blue} = h(\hat{v}^{\circlearrowleft},\hat{w}^{\circlearrowleft})h(\hat{v}^{\circlearrowleft},\hat{u})h(\hat{u},\hat{w}^{\circlearrowleft}) \sum_{d\cup\bar{d}\subset\mathbf{z}} (-1)^{|\bar{d}|}\omega'(z_{\bar{d}})H(z_{\bar{d}},z_{\bar{d}})$$

which can be cast as a pfaffian through (6.38).

The final result is

$$\begin{aligned}\mathbb{A}_1(J_1,J_2,J_3) = \langle 11\rangle^{J_1}\langle 22\rangle^{J_2}\langle 33\rangle^{J_3} &h(\hat{v}^{\circlearrowleft},\hat{u})h(\hat{u},\hat{w}^{\circlearrowleft})h(\hat{v}^{\circlearrowleft},\hat{w}^{\circlearrowleft})h(\hat{v},\hat{v})h(\hat{w},\hat{w})h(\hat{u},\hat{u})\times\\ &\mathcal{N}(J_1)\mathcal{N}(J_2)\mathcal{N}(J_3)\times pf\left(I-\mathcal{K}\right)_{2J_1\times 2J_1} pf\left(I-\mathcal{K}'\right)_{2(J_2+J_3)\times 2(J_2+J_3)}, \quad (6.42)\end{aligned}$$

[10] See appendix (E.6) for details.

with the matrices $\mathcal{K}$ and $\mathcal{K}'$ defined in appendix (E.6).

As discussed above, these formulas express the abelian three point functions at finite coupling in the asymptotic regime, that is, ignoring finite volume corrections coming from excitations wrapping around the seams of the pair of pants. These mirror corrections can be properly ignored at weak coupling when we consider three point functions of large twist operators so that all bridge numbers ℓ_{ij} are large. Due to the Boltzmann suppression of propagation over large distances ℓ_{ij}, mirror particles only start to contribute at $(\ell_{ij}+1)$ loops.

For example, when we consider operators of classical twist $\tau_1 = \tau_2 = \tau_3 = 6$ and bridge lengths $\ell_{ij} = 3$, equation (6.42) provides exact formulas up to three loops. As an example, for spins $J_1 = 6$, $J_2 = 4$, $J_3 = 2$ and bethe roots (at tree-level)

$$\begin{aligned}
\mathbf{u} &= \{-3.34538, -2.2266, -1.45396, -0.894775, -0.500817, -0.22559\}\,,\\
\mathbf{v} &= \{-2.18949, -1.24366, -0.66142, 0.163878\}\,,\\
\mathbf{w} &= \{-1.03826, 1.03826\}\,,
\end{aligned}$$

we obtain[11],

$$\begin{aligned}
C_{\text{abelian}}(6,4,2) =& 0.000087168875373411949253081221196521450200295689674319409\\
&-0.001094142375494603604370542121430802213283389165599208 1\, g^2\\
&+0.002463915063661158347872125956676178912367997715304497 5\, g^4\\
&+(0.151494665287313401721643382203859878814098570014594 63\\
&+0.009964497025595243027748841297370730499705378907494595 3 \times \zeta(3)) g^6.
\end{aligned}$$

We hope that the novel data generated through this result will be useful in future integrability explorations.

6.4 Discussion

This chapter reduces the computation of asymptotic three point functions of three spinning operators in $\mathcal{N}=4$ SYM to the statistical mechanical problem of computing the partition function of a system of the Hubbard type on a Kagome-like lattice whose boundary conditions are determined by the polarizations and quantum numbers of the spinning operators, equations (6.7, 6.25, 6.28). The analytic structure of this partition function is inherited from the vertex, Beisert's SU(2|2) extended S-matrix [59], and therefore is extremely rich. Its singularities are determined by the spectrum of the dual world-sheet theory and have clear physical interpretations: particles decoupling, annihilating, fusing into bound states, and others.

In the limit of weak coupling the vertex reduces to the rational type and the partition function can be solved. We do so in this chapter by exploiting the analyticity of the partition

[11] We keep the $\zeta(3)$ from the dressing phase explicit.

function. After stripping out overall factors, the partition function in the rational limit is a meromorphic function of the rapidities with no bound-state poles. It can be then solved recursively by concatenating the various decoupling poles in each of the rapidities. This is the result (6.19). From the point of view of the gauge theory, it provides an efficient way of generating tree-level structure constant data for spinning operators of arbitrary twist.

It would be fascinating to solve this partition function away from weak coupling. From the point of view of analyticity, we now have functions on a multi-sheeted Riemann surface with multiple additional fusion poles whose residues should be related to smaller partition functions involving bound-state lines. From the statistical mechanics viewpoint, similar integrable systems were solved in a more traditional fashion. For example, in [164] Baxter solves the thermodynamic partition function of a 8-vertex model defined on the faces of a Kagome lattice by matching it to the computation in the standard square lattice. His construction is the same behind the integrability of the fishnet model by Zamolodchikov [165]. Exploring solid-on-solids dualities of this type might lead to a direct solution in terms of the transfer-matrices and functional equations.

Once the statistical mechanics problem is solved, one must still resolve the sum over partitions (6.25), the complexity of which grows rapidly at large *but finite* spin[12]. Turns out this problem can be solved, at any value of the coupling, for certain boundary conditions of the partition function. When two operators are parallel and orthogonal to the third the hexagon becomes a simple abelian factor, the sum over partitions of which can be cast in pfaffian form. This is the result (6.42). It provides an efficient way of generating some high-loop data for structure constants of high twist spinning operators.[13] Note: for each generic three spinning operators, the pfaffian formulas provide three independent structure constants, one for each choice of orthogonal operator. The three point function must therefore interpolate between these three highly non-trivial pfaffian formulas involving matrices of different dimensionality as the polarization vectors vary. It would be great to identify non-trivial objects linear in the tensors structures (6.24) that performs such interpolation, as they might be relevant for describing the full three point function of spinning operators in $\mathcal{N} = 4$ SYM.

At large spin the asymptotic structure constant should provide the exact three point function of the gauge theory, finite size corrections being power-law suppressed in spin. In [4] we considered the null-hexagon limit of six point functions of $\mathbf{20}'$ operators and its respective snowflake OPE decomposition in terms of three large spin operators to derive a map between the expectation value of null hexagonal Wilson loops (WL) and the large spin limit of the three point functions considered in this chapter. Combining [4] and this chapter, we can write a sharp formula expressing the expectation value of the null WL in

[12] In the strict large spin limit we hope to have alternative techniques, see discussion below.

[13] Some corners of the cross ratios space parametrized by the null snowflake OPE limit of the 6-pt function should be controlled by the abelian structure constants. Having complete control over those, we could therefore generalize [163] to the higher point case and provide valuable boundary data for an eventual bootstrap approach to fix these correlators [80, 166, 167].

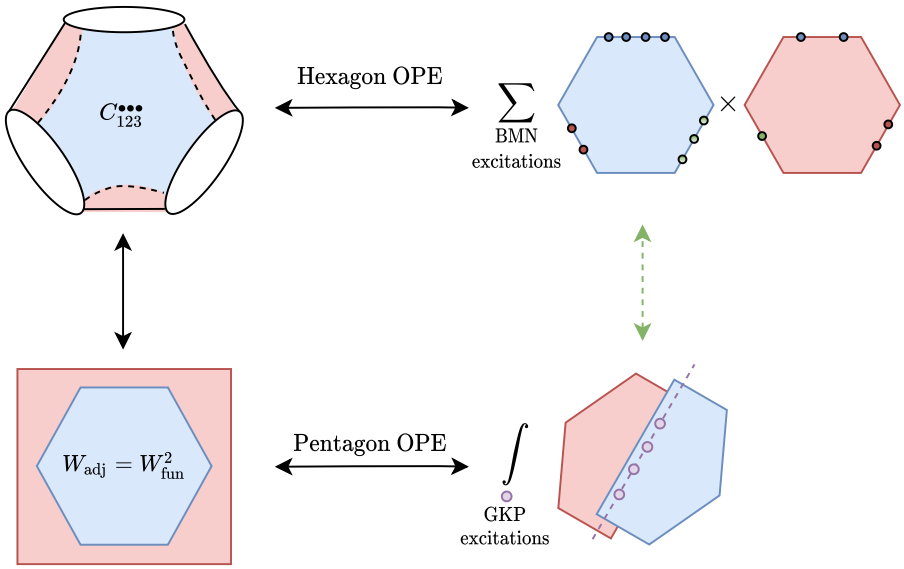

Figure 6.11: **Top arrow:** this chapter, decomposition of the spinning three point functions into polarized hexagons. **Left arrow:** large spin three-point functions duality with null Wilson loops [144]. **Bottom arrow:** decomposition of null Wilson loops into integrable pentagons [71]. **Right arrow:** future work, how the integrable hexagons and integrable pentagons are related in the large spin limit.

any geometrical configuration to the hexagons expansion:

$$\mathbb{W}(U_1,U_2,U_3) = \lim_{J_i,\ell_i\to\infty} \frac{\mathcal{N}_\lambda \mathcal{N}_{\mathbf{u}}\mathcal{N}_{\mathbf{v}}\mathcal{N}_{\mathbf{w}}}{\left(C^{\ell_1,\ell_2,\ell_3}_{J_1,J_2,J_3}\right)_{\text{tree}}} \times \prod_{i=1}^{3}\left(\frac{J_i\ell_i}{2\ell_{i+1}\ell_{i-1}}\right)^{-\frac{\gamma_i}{2}} \times \sum_{\substack{a\cup\bar{a}=\mathbf{u}\\ b\cup\bar{b}=\mathbf{v}\\ c\cup\bar{c}=\mathbf{w}}} \omega_{\ell_{13}}\omega_{\ell_{12}}\omega_{\ell_{23}} \times \mathcal{H}_{a,b,c}\mathcal{H}_{\bar{a},\bar{c},\bar{b}} \tag{6.43}$$

where the ratios of ℓ_i and J_i are kept fixed and determined in terms of the null hexagon cross ratios U_i through (10) of [4]; the boundary conditions of the hexagon partition function $\mathcal{H}$ are fixed in terms of U_i through (37) of [4]. Above, γ_i are the anomalous dimensions of operator O_i, while $\mathcal{N}_\lambda$ is a spin independent normalization constant to be determined.

Null WL can be decomposed as an expansion around the collinear limit by the Pentagon OPE, higher energy excitations of the GKP vacuum controlling the geometric expansion [71]. Equation (6.43) can therefore be understood as a map between hexagons and pentagons, see figure 6.11. Since the adjoint Wilson loop $\mathbb{W}$ is the square of the fundamental Wilson loop in the large N limit and since the latter is obtained gluing two pentagons $\mathcal{P}$ together we can cast the sharp equation (6.43) as the simplified slogan

$$\left(\sum \mathcal{P}\times\mathcal{P}\right)^2 = \lim_{\texttt{large spin}} \sum \mathcal{H}\times\mathcal{H}\,. \tag{6.44}$$

Explicitly uncovering this relation is a problem for the future which could lead to a more universal integrability framework for $\mathcal{N}=4$ SYM. More generally, one should ask if (6.43) could lead to an alternative effective way of computing WL physics and their dual gluon scattering amplitudes [102, 154]. The answer to this question depends on understanding

how to simplify the large spin limit of the computations discussed in this chapter. The thermodynamic limit of the hexagon partition function is therefore of special importance. The matrix-models inspired methods of [91, 168, 169] should also be useful.

It is also possible that instead of simplifying the building blocks arising in the summand in (6.43) we should discard all these partition functions and look for new tricks to compute directly the full sum over partitions. That would be bitter sweet, and naturally motivates the next chapter.[14]

[14]Even if that turns out to be the case, these (sums over) hexagon partition functions will always be useful to produce important data to test such scenario specially in perturbation theory.

Chapter 7

Structure Constants in $\mathcal{N} = 4$ SYM and Separation of Variables

7.1 Introduction

Solving planar $\mathcal{N} = 4$ SYM in a satisfactory way would mean efficiently computing both the spectrum as well as higher point correlation functions – starting with three points – at any value of the 't Hooft coupling.

A formalism for computing three point functions by means of integrability exists. It is the so called *hexagon* approach [66]. It is conjectured to hold for any coupling indeed but it is not easy to use, at least not by the remarkable standards of the spectrum quantum spectral curve approach [85, 86]. With *hexagons* one needs to go over infinitely many sums and integrals to produce such correlators. At weak coupling perturbation theory these sums and integrals truncate [69, 170, 171] and we can use hexagons to produce a wealth of data to test any putative new framework. We will do it all the time below.

In this chapter we suggest a new approach for correlation functions in $\mathcal{N} = 4$ SYM based on the Baxter Q-functions. The final representations are of so-called separation of variables (SoV) type where these Baxter functions are integrated against simple universal measures to produce the structure constants.

Q-functions play the central role in the quantum spectral curve, the top of the line tech for computing the dimension of any single trace operator in this conformal gauge theory so it is only natural to look for a similar central role for these objects in the context of other physical observables such as the OPE structure constants.

In the most conventional integrable spin chains, Q-functions are polynomials whose roots are the so called Bethe roots v_k. In SYM these polynomials are present at leading order at weak coupling but at higher coupling they get dressed by quantum non-polynomial factors. This is expected; as we crank up the coupling we are no longer dealing with a spin chain or with a classical string but something in between and so these Baxter polynomials get naturally deformed. For the so-called SL(2) sector of the theory which includes all

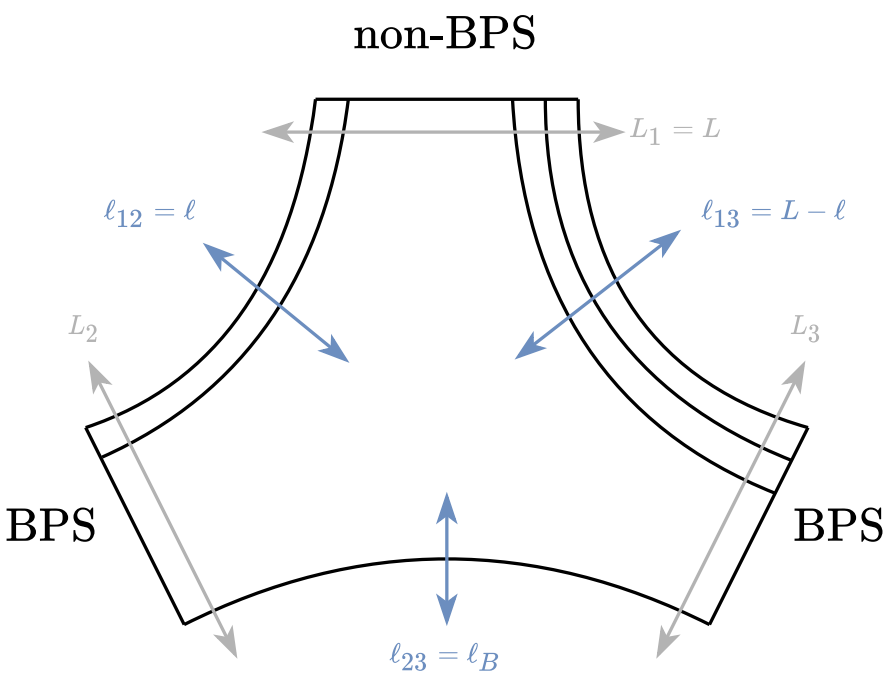

Figure 7.1: Three point functions of operators with sizes L_1, L_2 and L_3. At tree level there are $\ell_{ij} = (L_i + L_j - L_k)/2$ propagators between operators i and j; these integers ℓ_{ij} are called the bridge lengths. We will usually use $L \equiv L_1$ for the length of the non-BPS operator and $\ell \equiv \ell_{12}$ for its so-called left adjacent bridge (the right adjacent bridge will have length $L - \ell$); the bottom bridge we will often denote as $\ell_B \equiv \ell_{23}$.

operators of the schematic form $\mathrm{Tr}(D^J Z^L) + \texttt{permutations}$ we have

$$\mathcal{Q}(u) \equiv \left(\prod_{k=1}^{J} \frac{u - v_k}{\sqrt{x_k^+ x_k^-}}\right) \exp\left(\frac{g^2}{2} Q_1^+ H_1^+(u) + \frac{g^2}{2} Q_1^- H_1^-(u) + O(g^4)\right) \tag{7.1}$$

where the charges $Q_1^\pm$ are simple functions of the Zhukowsky variables $x_k^\pm = x^\pm(v_k)$ and $H_k^\pm$ are harmonic functions, see appendix F.1.1.

An operator is given by a Q-function (7.1). What we are after is thus a functional eating these functions and spitting out a number, the structure constant.

For the most part we will consider a single non-BPS operator and two BPS operators. The geometry of the three point function depends on the size of all these operators or – equivalently – on the so-called bridges that connect them as reviewed in figure 7.1.

The proposal is that (the square of) the structure constant is given by a ratio of SoV like scalar products

$$C^2_{\bullet\circ\circ} = \frac{(\mathbb{J}!)^2}{(2\mathbb{J})!} \frac{\langle \mathcal{Q}, \mathbf{1} \rangle_\ell^2}{\langle \mathcal{Q}, \mathcal{Q} \rangle_L} \tag{7.2}$$

Here $\mathbb{J} = J + g^2 Q_1^+$ and the scalar product

$$\langle \mathcal{Q}_1, \mathcal{Q}_2 \rangle_\ell \equiv \binom{\mathbb{J}_1 + \mathbb{J}_2 + \ell - 1}{\ell - 1} \int d\mu_{\ell-1} \prod_{i=1}^{\ell-1} \mathcal{Q}_1(u_i) \mathcal{Q}_2(u_i) \tag{7.3}$$

with a nice factorized measure

$$d\mu_\ell = \prod_{i=1}^{\ell} du_i \, \mu_1(u_i) \prod_{i=1}^{\ell-1} \prod_{j=i+1}^{\ell} \mu_2(u_i, u_j) \tag{7.4}$$

which is constructed out of the building blocks (using, s_u, c_u, t_u for $\sinh(\pi u), \cosh(\pi u), \tanh(\pi u)$)

$$\mu_1(u) = \frac{\pi}{2c_u^2} \left(1 + g^2\pi^2 \left(3t_u^2 - 1\right) + \ldots\right) \tag{7.5}$$

$$\mu_2(u,v) = \frac{\pi(u-v)s_{u-v}}{c_u c_v} \left(1 + g^2\pi^2 \left((t_u + t_v)^2 - \tfrac{4}{3}\right) + \ldots\right) \tag{7.6}$$

valid to leading order (LO) and next-to-leading order (NLO); the dots in the above expressions are NNLO corrections which start at $O(g^4)$. The structure of the result might be corrected at subleading orders as explained below. The contours in (7.2) are the real axis for all u_i.

We can *prove (7.2) by exhaustion* by comparing it with hexagon produced data for numerous L's and ℓ's and for different operators corresponding to different $\mathcal{Q}$-functions. We did it; (7.2) is correct. We can also establish it more honestly as discussed in the next section.

Representations like (7.2) are the main results of this chapter. In section 7.3 we present an SU(2) counterpart of this representation in (7.19); we managed to fully test it to LO, NLO *and* NNLO. We compare these two rank one sectors in section 7.4. In the discussion section 7.5 we discuss further generalizations such as multiple spinning operators and speculate on all loop structures we expect to find. Many appendices complement the main text.

7.2 SL(2)

At leading order, that is at tree level, correlation functions are given by Wick contractions. Each operator can be thought of as a spin chain and these Wick contractions are thus given by spin chain scalar products [172–174]. For the SL(2) sector such scalar products can be cast as SoV integrals [88] – see also [91] in the $\mathcal{N} = 4$ context. Once we properly normalize all these scalar products as in [174] to extract the structure constant we precisely end up with (7.2) for $g = 0$.

What we find remarkable is that this classical $g = 0$ expression seems to have a nice quantum lift as anticipated in the introduction.

Let us first discuss the simplest possible case where a twist two operator ($L = 2$) splits

evenly into two BPS operators ($\ell = 1$) so that the proposal (7.2) simply reads

$$C^2_{\bullet\circ\circ} = \frac{\mathbb{J}!^2}{(2\mathbb{J}+1)!}\left(\int du\, \mu_1(u)\mathcal{Q}(u)^2\right)^{-1} . \tag{7.7}$$

We derived the single-particle measure μ_1 as well as the quantum deformed Baxter functions $\mathcal{Q}$ in two ways. Both are based on looking for a measure such that, for two different twist-two states (i.e. with different spins J and J'), we have an orthogonality relation

$$\int \mu_1(u)\mathcal{Q}_J(u)\mathcal{Q}_{J'}(u) \propto \delta_{JJ'} , \tag{7.8}$$

a powerful relation which has been extensively exploited by [93–95] in numerous SoV studies, most of which for rational spin chains or for the fishnet reduction [175] of SYM, see most notably [96].

The first uses the fact that the Bethe roots v_k of twist two operators are given by the zeros of Hahn polynomials, a fact that persists at NLO. We have that $\prod_k(u - v_k)$ is proportional to the Hahn polynomial [176–178] $p_J(u|a, b, b, a)$ where $a - b = 2i\sqrt{2}g$ and $a+b = 1+4g^2H_1(J)$. Hahn polynomials are orthogonal with a simple measure as reviewed in appendix F.2.1 which allows us to derive (7.5) up to some simple tuning due to the mild J dependence in the polynomial parameters a, b, see appendix for details. It is the J dependence that renders the derivation non-trivial and which is responsible for the needed modification of the Baxter functions in (7.1).

The second derivation follows [94] closely (the novelty being the extension to g^2 corrections) and makes use of the Baxter equation [179]

$$\mathcal{B} \circ \mathbb{Q} = T(u)\mathbb{Q}(u) \tag{7.9}$$

where $\mathbb{Q}(u)$ are the Baxter polynomials (i.e. just the parentheses in (7.1)) and the Baxter operator

$$\mathcal{B} \equiv (x^+)^L\Big(1 - \frac{g^2}{x^-(u)}(Q_1^+ - iQ_1^-)\Big)e^{i\partial_u} + c.c. \tag{7.10}$$

Note that at $g = 0$ we have $x^+ = u + i/2$ and most importantly, $\mathcal{B}$ becomes a simple linear operator but as we turn on g corrections this is no longer true since the charges $Q_1^\pm$ depend on $\mathbb{Q}$. Consider first $g = 0$ and $L = 2$ so that the transfer matrix is $T(u) = 2u^2 + c_J$. Multiplying (7.9) by the sought after measure μ_1 and by another Baxter polynomial with a different spin, subtracting that to the same thing with the spin swapped and integrating yields

$$(c_J - c_{J'})\int \mu_1\mathbb{Q}_J\mathbb{Q}_{J'} = \int \mu_1\big(\mathbb{Q}_{J'}(\mathcal{B}\circ\mathbb{Q}_J) - (\mathcal{B}\circ\mathbb{Q}_{J'})\mathbb{Q}_J\big). \tag{7.11}$$

If we manage to make $\mathcal{B}$ self-adjoint we will thus have the required orthogonality. An i-periodic μ_1 would do the job since under shifts of contour the two terms of Baxter would swap and cancel in the right hand side. In detail, $\mathbb{Q}_{J'}(u)(u \pm \frac{i}{2})^2\mathbb{Q}_J(u \pm i)\mu_1(u)$ becomes $\mathbb{Q}_{J'}(u \mp i)(u \mp \frac{i}{2})^2\mathbb{Q}_J(u)\mu_1(u \mp i)$ under a shift of contour by $\mp i$ leading to an interchange (and thus cancellation) of the two terms in (7.11) once we use that the measure is periodic.

To make this manipulation kosher we need to make sure no singularities are picked when deforming the contour and to make the measure acceptable we need to make sure it decays fast enough at infinity so that it can be integrated against polynomials of arbitrary degree. Both this problems are solved at once with

$$\mu_1(u) = \frac{\pi/2}{\cosh^2(\pi u)} + O(g^2)\,. \tag{7.12}$$

The function decays faster than any polynomial and the double poles at $\pm i/2$ precisely cancel the double zeroes in the potential terms $(u \mp i/2)^L$ when $L = 2$ so that they lead to no extra contribution when deforming the contours. A periodic function without these double poles would not decay fast enough and a function with more than double poles would lead to extra contributions when deforming the contours; (7.12) is the sweet spot.

Turning on g corrections is not complicated. The redefinition (7.1) brings the Baxter operator to a linear operator again but introduces some further poles at $\pm i/2$ in the (no longer polynomial) Baxter $\mathcal{Q}$ functions so that the measure now needs some extra poles to cancel the contribution of these when deforming the contour. This explains (7.1) as well as (7.5); more details in appendix F.2.2.

Having derived the measure μ_1 and the Baxter polynomial dressing it remains to fix the overall normalization of the structure constant to be sure everything is in order. Evaluating the SoV integral using the loop corrected Bethe roots for various spins immediately leads to the cute result

$$\left(\int du\, \mu_1(u)\mathcal{Q}(u)^2\right)^{-1} = \frac{1 + g^2\big(4H_2(J) + \frac{8H_1(J)}{2J+1}\big) + \dots}{2J+1} \tag{7.13}$$

which is indeed almost the correct loop level structure constant computed in [180]. The prefactor in (7.7) with J deformed into $\mathbb{J}$ in a *reciprocity* reminiscent fashion [181, 182] neatly combines with this expression to give the full NLO structure constants for twist-two operators.

At this point it is straightforward to guess the general structure constant for any SL(2) operators of any twists by simply taking the tree level $g = 0$ result and deforming the new ingredient for higher twists – the two particle measure μ_2 – by a bunch of hyperbolic tangents following what was derived for twist two. The coefficients of these hyperbolic tangents are then fixed by requiring orthogonality between any two different Baxter solutions. The last line deformation of the Baxter functions in (7.1) – which was invisible for twist two operators for which odd charges vanish – is also fixed by imposing orthogonality. In the end, we just need to check that with a minimal reciprocity friendly prefactor as in (7.2) we precisely agree with perturbative data produced by hexagons. We do.

Even without matching with data, there is a nice self-consistency check of the full construction including the deformed pre-factor: The structure should be invariant under swapping left and right bridges $\ell \leftrightarrow L - \ell$; we checked that this is indeed realized by our expressions once the prefactors are deformed as in (7.2).

We made some progress at higher loops, in particular at NNLO (two loops) and for the smallest possible sizes and bridge lengths. For twist $L = 2$ operators for example we found

a Baxter function dressing as well as an orthogonal one-particle measure realizing (7.8) as

$$\mathcal{Q}(u) \equiv \prod_{k=1}^{J} \frac{u - v_k}{\sqrt{x_k^+ x_k^-}} \times e^{\frac{1}{2}g^2 Q_1^+ H_1^+ + \frac{1}{8}g^4 Q_1^+ Q_2^+ H_1^+ - \frac{1}{2}g^4 Q_1^+ H_3^+}$$

and

$$\mu_1(u) = \frac{\pi}{2c_u^2} \exp\Big(\pi^2 g^2 \big(3t_u^2 - 1\big) + \pi^4 g^4 \big(\tfrac{5}{6} - 7t_u^2 + \tfrac{11}{2}t_u^4\big) - \frac{g^4}{8} H_1^+ \big(Q_1^+(\mathbf{v}_1) Q_2^+(\mathbf{v}_2) + Q_1^+(\mathbf{v}_2) Q_2^+(\mathbf{v}_1)\big)\Big)\,, \tag{7.14}$$

where we use the fact that $Q_k^- = 0$ for twist-2 operators.

The last line is exotic as it depends now on the charges of the two operators in (7.8) with Bethe roots $\mathbf{v}_1$ and $\mathbf{v}_2$ respectively. Note, however, that when considering the pairings $\langle \mathcal{Q}, \mathbf{1} \rangle$ and $\langle \mathcal{Q}, \mathcal{Q} \rangle$ a single Baxter function shows up and thus this mixing term can be absorbed as new factor dressing $\mathcal{Q}$. One would then have different dressings in each pairing, a phenomenon we observe in the next section as well (in the SU(2) sector).

The first line in (7.14) is also not any random combination of trigonometric functions. Take the tree level measure $1/\cosh^2(\pi u)$ – which is periodic with period i and has poles at all the imaginary half integers – and promote it to a periodic function where all these poles are opened up into small cuts following [96], see figure 7.2,

$$\hat{\mu}_1 \equiv \oint \frac{dv}{2\pi i} \frac{\pi/2}{\cosh^2(\pi(u-v))} \frac{1}{x(v)}\,. \tag{7.15}$$

The integration contour encircles the Zhukowsky cut $v \in [-2g, 2g]$. Evaluating this integral in perturbation theory precisely reproduces the first line in (7.14) up to an overall normalization constant! It is tempting to conjecture that the finite coupling expression (7.15) might play an important role in an all loop SoV formulation. We make further comments on NNLO structure constants in the discussion.

Other sectors such as the SU(2) sector might also hint at other important structures in a putative all loop formulation. This is what we turn to now.

7.3 SU(2)

Up to NNLO the SU(2) magnon S-matrix does not receive corrections. Quantum effects do correct the propagation of scalar particles on top of the BMN vacuum. One could imagine mimicking this dressed propagation through appropriate deformations of the background vacuum by the insertions of inhomogeneities θ_i. This was made concrete in [183] where the authors determined NLO (one loop) structure constants in the SU(2) sector through the construction of a differential "θ-morphism" operator acting on the (θ-deformed) spin-chain scalar products defining the LO structure constants [173] and outputting the quantum three point functions.

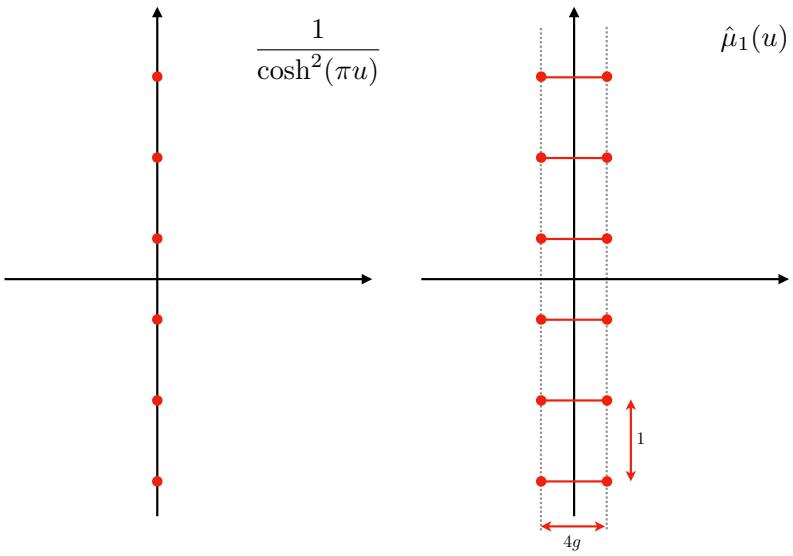

Figure 7.2: *Zhukowskization* of trigonometric functions opens up an infinite tower of poles into an infinite ladder of cuts.

Here we make two observations. First we note that there exists a θ-morphism that promotes $\mathrm{XXX}_{1/2}$ inhomogenous spin chain scalar products,

$$\begin{aligned}\mathcal{A}_\theta &= \sum_{\mathbf{u}=\alpha\cup\bar{\alpha}} (-1)^{|\bar{\alpha}|} \prod_{n=1}^{\ell} \prod_{i\in\bar{\alpha}} \frac{u_i-\theta_n+i/2}{u_i-\theta_n-i/2} \prod_{j\in\alpha} \frac{u_j-u_i+i}{u_j-u_i},\\ \mathcal{B}_\theta &= \det\left[\partial_{u_i}\log\left(\prod_{n=1}^{L}\frac{u_j-\theta_n+i/2}{u_j-\theta_n-i/2}\prod_{k\neq j}\frac{u_j-u_k-i}{u_j-u_k+i}\right)\right]\\ &\quad\times\prod_{i<j}\frac{(u_i-u_j)^2}{1+(u_i-u_j)^2},\end{aligned} \tag{7.16}$$

into $\mathcal{N}=4$ SU(2) structure constants all the way to NNLO:

$$C^2_{\bullet\circ\circ} = \left|\frac{(\mathcal{M}\circ\mathcal{A}_\theta)^2}{\Lambda_{\mathcal{B}}\,\mathcal{M}\circ\mathcal{B}_\theta}\right|\Bigg|_{\theta=0} + O(g^6), \tag{7.17}$$

where

$$\mathcal{M} = \exp\left[\sum_{i=1}^{L}\left(g^2(\partial_{i,i+1})^2 - \frac{1}{4}g^4(\partial_{i,i+1})^2(\partial_{i+1,i+2})^2\right)\right.$$
$$\left. - ig^2 Q_1^+(\partial_1 - \partial_L) + g^4\delta\mathcal{M}_{\text{NNLO-b}}\right], \tag{7.18}$$

with $\partial_i = \partial_{\theta_i}$ and $\partial_{i,i+1} = \partial_i - \partial_{i+1}$, see appendix F.3.1 for $\delta\mathcal{M}_{\text{NNLO-b}}$, and where $\Lambda_{\mathcal{B}}$ is a simple norm factor, (F.15). To NLO this is just the construction of [183]. We fix the NNLO part through comparison with the hexagons prediction, see appendix F.3.1 for details.

The second observation is that given the known integral representation for the scalar products in the inhomogeneous $\text{XXX}_{1/2}$ spin-chain, derived from Sklyanin's [89], Baxter's [93] and hexagon methods [90, 91], one can straightforwardly derive the functional SOV representation for the NNLO structure constants simply by acting with the θ-morphism operator on this classical measure.

The result is once again (the square of) a $\ell - 1$ dimensional integral over an $L - 1$ dimensional integral,

$$C^2_{\bullet\circ\circ} = \Lambda_\ell(\mathcal{Q}) \times \frac{(J!)^2}{(2J)!} \times \frac{\langle\langle \mathcal{Q}, \mathbf{1}\rangle\rangle^2_{\ell,L}}{\langle\langle \mathcal{Q}, \mathcal{Q}\rangle\rangle_{L,L}} + O(g^6), \tag{7.19}$$

with $\langle\langle f, g\rangle\rangle_{\ell,L} \equiv \langle f, g\rangle_{\ell,L}/\langle \mathbf{1}, \mathbf{1}\rangle_{\ell,L}$ and

$$\langle \mathcal{Q}_1, \mathcal{Q}_2\rangle_{\ell,L} \equiv \binom{\ell}{J_1 + J_2} \oint_\gamma d\mu_{\ell,L} \prod_{i=1}^{\ell-1} \mathcal{Q}_1(u_i)\mathcal{Q}_2(u_i). \tag{7.20}$$

The contour of integration is a circle wrapping the singularities of the measure (i.e. both Zhukowsky cuts), which once again is factorized:

$$d\mu_{\ell,L} = \prod_{i=1}^{\ell-1} du_i\, \mu^1_{\ell,L}(u_i) \prod_{j\neq i}^{\ell-1} \mu^2_{\ell,L}(u_i, u_j), \tag{7.21}$$

with

$$\mu^1_{\ell,L}(u) = \frac{\sinh(2\pi u)}{(x^+_u x^-_u)^2} e^{\delta_{\ell\neq L}\mathtt{A}_{\ell,L}(u)} \tag{7.22}$$

$$\mu^2_{\ell,L}(u, v) = \frac{\sinh(2\pi(u-v))(u-v)}{2x^+_u x^-_u x^+_v x^-_v} e^{\delta_{\ell\neq L}\mathtt{A}_{\ell,L}(u,v)} \tag{7.23}$$

$$\mathcal{Q}(u) \equiv \prod_{k=1}^{J} \frac{u - v_k}{\sqrt{x^+_k x^-_k}} e^{\delta_{\ell\neq L}\mathtt{B}(u)} \tag{7.24}$$

The scalar product in the denominator of (7.19) enters with $\ell = L$, and therefore the

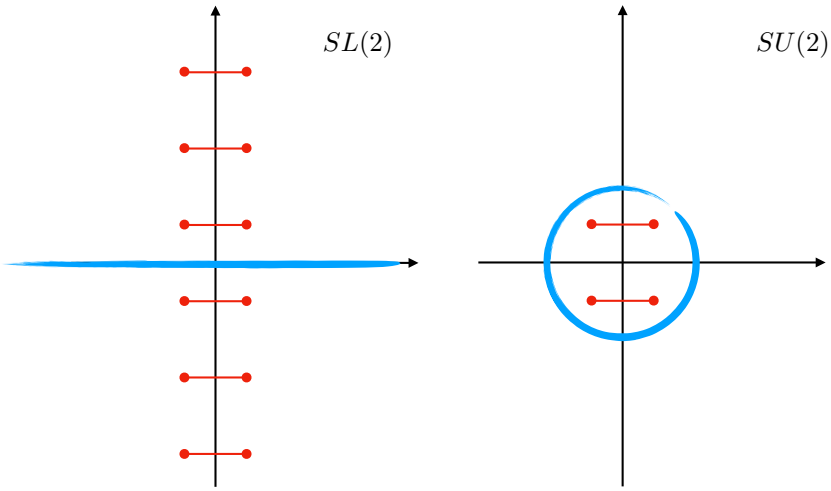

Figure 7.3: For SL(2) we integrate over the real axis; in SU(2) we have a contour integral encircling the Zhukowsky cuts.

exponential in all these expressions should be dropped in that case. For the numerator we need these extra quantum dressing factors. They read

$$\begin{aligned}
&\mathtt{A}_{\ell,L}(u) = g^2(q_1^-)^2 + g^4\left(\tfrac{1}{2}(q_2^+)^2 + 4\alpha(q_1^-)^2 - 6\pi^2 q_2^+\delta_{\ell=2}\right)\,,\\
&\mathtt{A}_{\ell,L}(u,v) = g^2 q_1^-\tilde{q}_1^- + g^4\left(\tfrac{1}{2}q_2^+\tilde{q}_2^+ + 2\alpha q_2^+ + 4\alpha q_1^-\tilde{q}_1^-\right)\,,\\
&\mathtt{B}(u) = g^2 q_1^- Q_1^- \qquad\qquad (7.25)\\
&+ g^4\Big(\tfrac{1}{2}q_2^+Q_2^+ + \alpha Q_2^+ + 4\alpha q_1^-Q_1^- - \pi^2 q_1^-Q_1^-\delta_{\ell=2} +\\
&+ \big(\big(\tfrac{1}{8}(Q_1^+)^2 - \tfrac{1}{4}Q_2^+ - Q_1^+ + \tfrac{3}{8}(Q_1^-)^2\big)q_2^+ - \tfrac{1}{2}q_3^-Q_1^-\big)\delta_{\ell,L-1}\Big)\,,
\end{aligned}$$

where the charges $q_k^\pm = q_k^\pm(u)$ and $\tilde{q}_k^\pm = q_k^\pm(v)$ are defined in appendix F.1 and $\alpha = \frac{2}{3}\pi^2 - 1$. Finally $\Lambda_\ell(Q)$ is a simple function of the higher conserved charges also given in appendix F.1.

Having expressed the results, a number of remarks are in order. The first is that (7.19) is an exact result capturing finite-volume effects around the seams adjacent to the NBPS operator[1]. These effects start at N^{3}LO in the SL(2) sector and therefore were not considered in the previous section, but for SU(2) they are present already at NNLO. Their effect in the SOV representation is encoded in the dressing of the Q-function through the $\delta_{\ell,L-1}$ factor, see appendix F.3.3 for a lengthy discussion on these finite volume effects. Here we emphasize that *the structure constant geometry dress the Q-function*: $\mathcal{Q}$ depends both on the state and ℓ.

[1]In this section we assume that $\ell_{23} \geq 2$ so that bottom mirror corrections can be neglected [170]. Otherwise, we expect its inclusion to follow a similar prescription as in the SL(2) case.

The second remark is the presence of the $\delta_{\ell=2}$ "anomaly" in (7.25). Its origin is not clear to us. Should it be put on foot with the $\ell = 1$ result (7.27) in the SL(2) sector at NNLO in which a new integral appears? Is it an indication that we are integrating out a simpler higher-dimensional integral for this short bridge overlap?

To a more basic point, in contrast to the SL(2) sector result (7.2), different measures and Q-dressings enter the numerator and denominator of (7.19) already at NLO. From the θ-morphism point of view, the mismatch is due to the boundary terms in the second line of (7.18) which cancel when acting on the denominator, a symmetric function of the θ_i, but do not on the numerator. It turns out that the denominator's *Gaudin* measure follows as in the SL(2) case from an orthogonality principle – see appendix (F.3.2). The numerator measure is more complicated and we could not identify an orthogonality principle that fixes it. Is there an alternative principle that generalizes to higher loops and allow us to move forward? We hope so. As usual, one can always rely on hexagons to compare any new proposal with data, as we did to confirm the correctness of (7.19).

7.4 SL(2) vs SU(2)

It is amusing to compare our results so far in the following summary table:

	SL(2)	SU(2)
Main result	(7.2) and (7.26)	(7.19)
Factorized measure	yes	yes
Same μ and $\mathcal{Q}$ for $\mathcal{A}$ and $\mathcal{B}$	yes	no
Contour	Real axis	Encircling $x^{\pm}(u)$ cuts
Manifest transcendentality	yes	no
Wrapping effects incorporated	Bottom: e.g. (7.27)	Adjacent: e.g. (7.25)
Derivation and guesswork tools	Hahn polynomials Baxter orthogonality Zhukowskization Hexagon data Bottom Wrapping Reciprocity	θ-morphism Baxter Hexagon data Adj. Wrapping Selection rules
Next step	Finish NNLO (& guess all loops)	Do NNNLO (& guess all loops)

Many things are common to both SU(2) and SL(2) correlators most notably both are given by a SoV like scalar products involving factorized quantum corrected measures and quantum dressed Baxter functions. As far as we checked, both are capable of capturing wrapping corrections.

There are also differences. Some seem minor: for example, the counting of transcendentality in the SU(2) expressions is a bit weird specially due to the mixed transcendentality

factor $\alpha = \frac{2}{3}\pi^2 - 1$ [2][3].

Some differences seem deeper: The contour of the non-compact SL(2) sector is non-compact while the contour for the SU(2) compact sector is a closed contour, see figure 7.3. (This was already observed before in rational SoV explorations, see e.g. [91, 93, 94]).

For states with two particles of opposite momenta $\{v, -v\}$, SL(2) three-point functions of length L and adjacent bride ℓ should match SU(2) correlators of length $L+2$ and bridge $\ell + 1$. We checked this by explicit evaluation but it is amusing that this type of relation – which follows from some SU(2) and SL(2) states being in the same supermultiplet – is manifest in the spectrum problem [184] but is totally obscure here. Would be desirable to make it more manifest; this might hint at an even more unified description of both sectors.

Let us conclude this section highlighting the beautiful appendix G of [91] by Jiang, Komatsu, Kostov and Serban. There the starting point are the hexagon sums over partitions for $\mathcal{A}$. These sums are cast as contour integrals and after several cleaver manipulations these contours end up being recast as new SoV like integrals. They do this for both SU(2) and SL(2). (The SL(2) derivation is more involved with some "straightforward (but complicated and tedious)" steps.) In other words, they *derive* SoV from hexagons. The drawback if that this derivation was done at tree level and there are a few steps (see previous quote) that don't seem to be obvious to lift to all loops. Revisiting this appendix in light of what we learned seems promising.

7.5 Discussion

We have initiated here a project for recasting correlators in $\mathcal{N} = 4$ SYM in a language closer to that of the spectrum quantum spectral curve. With all recent SoV related advances [93–100, 185] we believe the time is ripe for seeking out for such a new approach. We are probably scratching the tip of an iceberg as far as the full finite coupling structure goes but some elements are clearly emerging.

One is the central importance of SoV quantum corrected measures $\mu(u_1, \ldots, u_p)$ which can be found by combining a myriad of different approaches from orthogonality of quantum corrected Baxter equations, matching SoV integrals with hexagon combinatorics, converting hexagons sums into contour integrals which one then massages into SoV like integrals, $\theta-$morphism operations on in-homogeneous SoV integrals, re-summing wrapping corrections, extending orthogonality relations of known classical polynomials, Zhukowsky upgrades of trigonometric functions *etcetera*. (This *etcetera* often includes a good deal of *inspired guesswork*.)

These measures are then used to build scalar product like integrals which couple Baxter functions $\mathcal{Q}(u)$ for the various involved operators. The Baxter functions also are corrected

[2]It would be desirable to restore naive trascendentality counting, see also discussion at the end of appendix F.1.1.

[3]There is a fun fact about all the π's floating around in the SU(2) result – see the *anomaly* $\delta_{l,2}$ as well as α: they are there simply to cancel π's generated from the integrations so that the final result is a rational function of the Bethe roots. From a practical point of view we could drop these π's provided we also drop any π's generated when picking up residues. At higher loops the structure constants are no longer rational and such games would be dangerous.

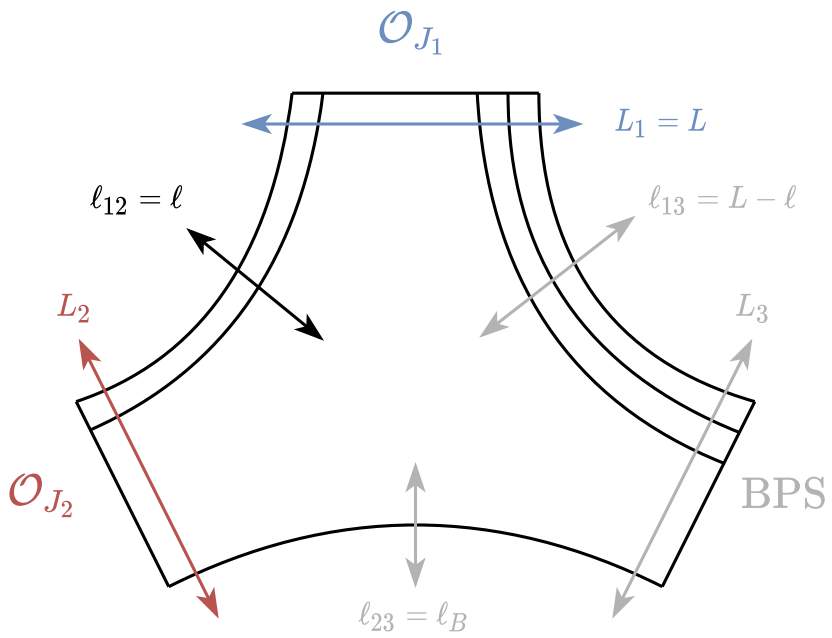

Figure 7.4: The NBPS operators have twists L_i and spins J_i. Their polarizations are orthogonal. In the conventions of [5] it is equivalent to $\sum_\ell C^{\bullet\bullet\circ}(J_1, J_2, \ell)$.

away from their tree level polynomial forms.

The most obvious question is then how to fix the measures and the Baxter Q-functions. Do these measures obey any sort of all loop bootstrap set of axioms? They must. It is crucial to work it out. Are these Q-functions some of the finite coupling solutions to the Quantum Spectral Curve? We hope so.

For the most part we considered a single non-trivial non-BPS operator but we could have considered correlation functions involving more than one non-BPS operators using the very same universal measures and Baxter functions. Take for the example the case of two spinning operators as studied in [5] and consider the so-called abelian polarization there, see figure 7.4. We found a compact representation of all such correlators at NLO as

$$\Big(\sum_\ell C_\ell^{\bullet\bullet\circ}\Big)^2 = \frac{(\mathbb{J}_1+\mathbb{J}_2)!^2}{(2\mathbb{J}_1)!(2\mathbb{J}_2)!}\frac{\langle \mathcal{Q}_1, \mathcal{Q}_2\rangle_\ell^2}{\langle \mathcal{Q}_1, \mathcal{Q}_1\rangle_{L_1}\langle \mathcal{Q}_2, \mathcal{Q}_2\rangle_{L_2}}\,. \tag{7.26}$$

Would be very interesting to find an SoV representation for the other spinning correlator tensor structures studied in [5]; a strategy could be to embed the external operator SL(2)'s into higher rank SL(N) where we could borrow recent SoV technology from [94].

Is the number of SoV integrals going to remain constant or at least grow in a controllable way? And if they grow, can we re-sum the full result into some kind of exotic infinite dimensional sort of scalar products? We have little to say about the last speculative question but as far as the growth of the number of integrals goes, we do seem to find some interesting structure. Take for example the SL(2) correlation function involving a single non-BPS operator with twist $L = 2$ and adjacent bridges $\ell = 1$. With $\ell = 1$ the numerator $\langle \mathcal{Q}, \mathbf{1}\rangle_1 = 1$ to LO and NLO since the scalar product in (7.3) is an $\ell - 1$ dimensional

integral. This is of course consistent with the hexagon approach where this numerator is given by the sum over partitions of magnons $\mathcal{A}_1$ weighted by the hexagon form factors – see (F.13) – and this sum over partitions normalized as in this chapter indeed evaluated to $1 + O(g^4)$. At NNLO $O(g^4)$, however, it is no longer unity. Instead it is given by a cute expression involving Bernouli numbers which we summarize in appendix F.2.3. Also, at this loop order, if the bottom bridge $\ell_{23} = \ell_B = 1$ there is a new wrapping correction to the structure constant [66]. Both these new effects can be compactly incorporated by simply modifying the trivial scalar product

$$\langle \mathcal{Q}, \mathbf{1} \rangle_1 \to 1 + \eta g^4 \int du\, \nu(u) \frac{\mathbb{Q}(u)}{\mathbb{Q}(i/2)} \\ + \texttt{simple contact terms}_\eta + O(g^6)\,, \tag{7.27}$$

with the various ingredients spelled out in appendix F.2.3 and where $\eta = 1$ for $\ell_B > 1$ (no wrapping effects) and $\eta = 2$ for $\ell_B = 1$ (wrapping effects included). It is very encouraging to see wrapping and asymptotic effects cast in such unified way. We see it as evidence that the number of integrals in this SoV approach should increase as we go to higher and higher loops but that increase is not directly related to wrapping effects which can be automatically incorporated (as seen in this bottom wrapping example and also in the SU(2) adjacent wrapping example, see appendix F.3.3). This growth of the number of SoV integrals is consistent with the picture that at finite coupling we are dealing with three quantum strings with infinitely many degrees of freedom and in the SoV approach the number of integrals is related to the number of such degrees of freedom [96].

As we go to higher loops, multiple wrapping effects come in at once and we should make contact with [186] where $PSU(2,2|4)$ transfer matrices are shown to appear. Again, our hope is that even in those cases, wrapping and no-wrapping are all cast in the same unified way.

We should fit strong coupling in this framework. For large operators there could be interesting semi-classical limits [90,168,187–189] where one might be able to make progress; for small operators we know very little about what to expect for the Baxter functions and we have nothing intelligent to say. A good starting point there might be [163] where important sets of wrapping corrections were beautifully resummed for structure constants involving one small operator and two large operators.

Another limit worth exploring is large spin. This is a particular limit where SoV should be quite powerful since the number of integrals does not grow with spin. Very interesting structures seem to emerge[4] which might also shed light on WL/correlator dualities [101,143] along the lines of chapters 5 and 6.

It would also be very interesting to think about how all this fits into a higher point function picture [67,68]. What is the SoV description of a four point function of BPS operators? Does it involve integrating over intermediate Baxter functions? Will the measures derived here play a role in this integration? A starting point for these explorations could be recasting the Coronado's all loop octagon correlator [80, 81] in this language, perhaps using its determinant representations [190]. The octagon is a large R-charge correlator

[4] Unpublished work with Benjamin Basso.

though so at the same time we should probably figure out what sort of simplifications take place on the SoV side when we consider large operators. (Another motivation for studying this limit.)

We explored the SU(2) and SL(2) sectors of $\mathcal{N} = 4$ SYM. There is life beyond it. We should look for it.

Chapter 8

Complex Spin: The Missing Zeroes and Newton's Dark Magic

8.1 Introduction

Certain CFT data can be analytically continued to complex values of spin S [55]. Specifically, for each four-point function $\langle \mathcal{O}_1 \mathcal{O}_2 \mathcal{O}_3 \mathcal{O}_4 \rangle$, Caron Huot's Lorentzian inversion formula produces functions $c^{\pm}_{1234}(\Delta, S)$ with the following properties. For integer S, they have simple poles at the locations of local spin-S operators $\mathcal{O}_i$ appearing in the OPE $\mathcal{O}_1 \mathcal{O}_2 \to \mathcal{O}_3 \mathcal{O}_4$:

$$c^{(-1)^S}_{1234}(\Delta, S) \sim \sum_i -\frac{f_{12i} f_{34i}}{\Delta - \Delta_i}, \quad (S \in \mathbb{Z}), \tag{8.1}$$

where f_{12i}, f_{34i} are OPE coefficients.[1] Furthermore, the $c^{\pm}_{1234}(\Delta, S)$ are analytic in S and bounded for $\mathrm{Re}(S) > 1$, when $\Delta = \frac{d}{2} + i\nu$ is on the principal series. The latter condition is crucially tied to the boundedness of correlators in the Regge limit and conformal Regge theory [55, 191].

Because the same local operators appear in every OPE (modulo global symmetries), different $c(\Delta, J)$-functions associated to different four-point functions have identical pole locations at integer S. We call this "local operator universality."

What happens at non-integer S is less clear. In [52], it was argued that singularities in Δ at non-integer S should be interpreted as matrix elements of light-ray operators. However, little is known about the structure of such singularities. Are there always single poles in Δ, or can there be higher poles, or cuts? Is there "light-ray operator universality," where the same light-ray operators appear in different $c(\Delta, S)$ functions, or do different four-point functions see completely different light-ray operators?

Perhaps the simplest hypothesis is that there is "light-ray operator universality" — that is, local operators live on discretely-spaced Regge trajectories, whose dimensions $\Delta(S)$ and structure constants $C(S)$ are analytic in S.[2] Furthermore, one should be able to construct the corresponding light-ray operators directly, without reference to a particular four-point

[1] In other words, $c^{\pm}_{1234}$ give analytic continuations of CFT data away from even-spin/odd-spin.

[2] Though there will be accumulation points in twist-space [53, 54].

function or $c_{1234}(\Delta, S)$ that they appear in. Some evidence for this idea can be found in perturbative constructions of certain classes of light-ray operators [192–202].

However, this idea raises an obvious puzzle:

There are usually many more local operators with large spin S than with small spin S. We illustrate this in figure 8.1, where we plot the leading-order dimensions and structure constants of twist 3 operators in planar $\mathcal{N} = 4$ SYM with even spin (up to spin sixty). As these figures clearly illustrate, the operators do seem to be nicely organized into smooth trajectories — or families — which we made more visible with colouring. This is consistent with analyticity in spin mentioned above. On the other hand, the contribution of the various families to physical observables is ostensibly non-analytic, given the disappearance of physical operators at small spin. How can these two facts be reconciled?

There is a simple possible solution to this puzzle:

Perhaps the analytically continued structure constants $C(S)$ of a higher family which starts at some large physical S_* will have zeroes at all integer spins below S_*, where a local operator is "missing". In other words, an infinite number of Regge trajectories of light-ray operators exist for complex S, but most of them have zeros at integer spins.[3]

In this chapter we confirm this picture. Using an extrapolation technique found in Newton's 1687 *Principia* we will continue physical[4] data at integer spins into the complex plane. What we will see can only be described as dark magic: these Newton series extrapolations will beautifully converge to functions with precisely these zeroes at the locations of "missing" operators.

8.2 The Twist 3 Data

Figure 8.1a contains the one loop anomalous dimensions $\gamma(S)$ for all primary operators of the form

$$\mathrm{Tr}(D_+^S Z^3) + \texttt{permutations} \tag{8.2}$$

with even[5] spin S. These operators have three units of R-charge and classical twist equal to three. Figure 8.1b depicts the three point functions $C(S)$ between these operators and two scalar BPS operators.[6]

[3] In [203] Regge trajectories of the $(2, 0)$ theory were studied. Several related puzzles were raised there and – for some of those (see *issue 2* there for instance) – one of the proposed decoupling mechanisms is identical to the one observed here. Could the Newton methods employed here help sharpen some of the conjectures in [203]?

[4] We use *physical* to refer to the data directly related to local operators. The continuation of the data is as physical as the local data once we consider null Wilson line operators [52, 196, 204, 205].

[5] We will consider even spin for the most part. It is well known that analytic continuation of even and odd spins are independent. We checked indeed that similar conclusions would be reached for odd spins.

[6] Any scalar BPS operators would lead to the same S-dependence of the three point function. These BPS operators are scalars with protected dimensions. We will not discuss them further.

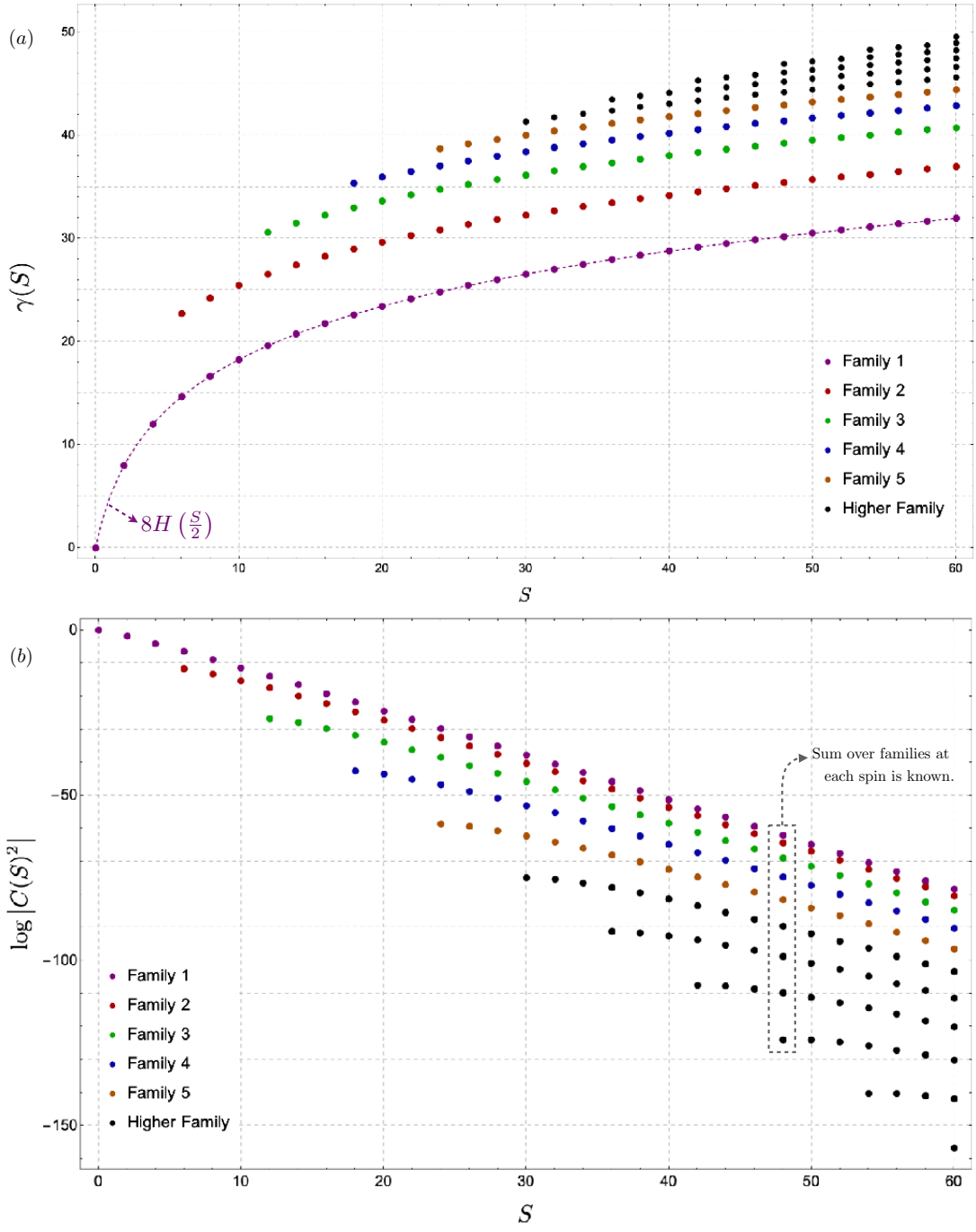

Figure 8.1: (a) Leading order anomalous dimensions $\gamma(S)$ where $\Delta(S) = 3 + S + g^2\gamma(S)$ and (b) square of structure constants $C(S)^2$ for the twist 3 operators of even spin. The energy of the lowest trajectory (8.5) as well as sum rules of all structure constants for fixed S (8.7) are known for any complex spin S; the structure constants for the lowest family (8.6) are derived here for even integer S.

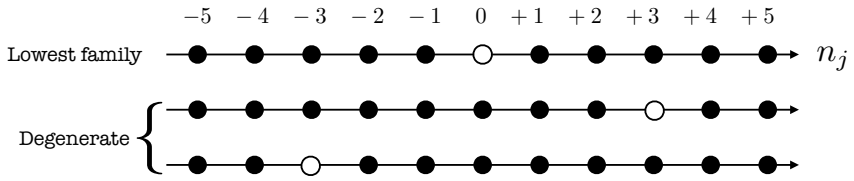

Figure 8.2: The u_j's need to be all distinct since these parametrize the momentum of the S excitations in the spin chain which behave as fermions. Since F and f vanish at the origin, solutions with distinct u_j require distinct external fields n_j. Since F and f are bounded functions these mode numbers must lie in the range quoted in the main text and since there are $S+1$ integers in this range we see that one of them – called the *hole* n_* – is not used. There is one additional selection rule on this n_*: It must generate a state of zero momentum (this is a gauge theory condition: the trace in (8.2) means we are only interested in cyclic symmetric quantum spin chain states). This requires $n_*/3$ to be an integer. There are $2\lfloor S/6\rfloor+1$ such choices which perfectly matches the counting of primaries. In the figure we illustrate the two possible choices for spin 10 corresponding to the lowest family and the second family; the black dots are the n_j and the white circle is the hole n_*.

The family of operators (8.2) will be central player in this note. These operators are the *second* simplest spinning operators in this conformal gauge theory. The simplest would be the twist two operators – simply replace Z^3 by Z^2 in (8.2) – which are however too simple for our purpose since there is a single lonely primary twist-two operator for each (even) spin S. The twist-two family is still very interesting, as reviewed in appendix G.4.

At weak coupling, the primary operators (8.2) can be thought of as eigenstates of an $\mathrm{SL}(2,R)$ quantum spin chain of length 3 with S excitations, the conformal dimension of the operators corresponding to the energy levels of the quantum spin chain [206, 207]. This energy, in turn, can be determined by solving a simple electrostatic problem of S charges in a line with real positions u_j given by

$$\sum_{j\neq k} f(u_j-u_k)+F(u_j)-2\pi n_j=0, \tag{8.3}$$

where the *external force* $F(u)=6\arctan(2u)$, the *interaction forces* $f=2\arctan(u)$ and the mode numbers[7] n_j are distinct integers taking all values from $-S/2$ to $S/2$, skipping one value which we call n_*. The twist three families depend on this missing mode number n_* also denoted as *the hole*, see figure 8.2. The lowest (dimension) family has $n_*=0$.[8] All other families are degenerate pairs with $n_*=\pm1,\pm2,\ldots$.

Solving the electrostatic equations (8.3) is trivial: `Mathematica`'s built-in `FindRoot` does the job.[9] Once we find a $\{u_1,\ldots,u_S\}$ we extract the energy – that is the dimension

[7] In the electrostatic picture we can think of them as an extra constant force felt by each particle. We can think that the particles have charge n_j and are acted by a constant electric field of magnitude 2π for instance to explain the last term in (8.3).

[8] Dimensions are monotonic as a function of $|n_*|$.

[9] We solved these equations all the way to spin 200 for all possible choices of n_*. We had to solve them

of the corresponding operator – by adding up the energies of each particle

$$\Delta = 3 + S + g^2\Big(\gamma \equiv \sum_{j=1}^{S} \frac{2}{u_j^2 + 1/4}\Big)\,. \tag{8.4}$$

This is how figure 8.1a was generated. Similarly, the structure constant $C(S)$ is also given by an expression in terms of the u_j from which we generated figure 8.1b. The explicit plug-in expressions are simple but not as simple the spectrum expression: $C(S)$ is given by a ratio of determinants of matrices of size S built out of these u_j or equivalently in terms of integrals of so called Baxter polynomials $Q(x) = \prod_{j=1}^{S}(x - u_j)$, as reviewed in appendix G.1.

Of course, this integrability description of the conformal data is tailored for physical operators: It is hard to put a non-integer number of particles on a line or make sense of determinants of matrices with non-integers sizes! We will soon discuss how to (partially) overcome this limitation.

This concludes the description of how we obtained all the physical twist three data. There are a few analytic things we know about it.

For the lowest family, we know Δ and S analytically for any even spin S. They are rational numbers. For even S, we have

$$\Delta(S)_{\texttt{lowest family}} = 3 + S + 8g^2 H(S/2) \tag{8.5}$$

$$C(S)^2_{\texttt{lowest family}} = \frac{4S!^2}{(2S+1)!}\left(\sum_{j=0}^{\infty}\left(\frac{\sqrt{1+4j}\,\Gamma\big(\frac{1}{2}+j\big)^2\Gamma\big(1+\frac{S}{2}+j\big)/\Gamma(j+1)^2}{\Gamma\big(\frac{1}{2}-\frac{S}{2}+j\big)\,\Gamma\big(1+\frac{S}{2}-j\big)\,\Gamma\big(\frac{3}{2}+\frac{S}{2}+j\big)}\right)^2\right)^{-1}. \tag{8.6}$$

The expression (8.5) for the energy of this lowest family was first found in [206, 208], see also appendix G.2.

The expression (8.6) for the structure constant is new. It is derived in appendix G.2 using the recently developed SoV representation of structure constants in this gauge theory [6]. We can use it to very efficiently produce physical data for spins as large as we want.[10] Evaluating (8.6) for $S = 10$, for instance, leads to $C(10)_{\texttt{lowest family}} = 1/84756$.

There is something unusual about (8.6): this expression holds for all even integers S – there is nothing wrong with it if we stick to physical operators – and it looks perfectly analytic in spin and yet it is *not* the correct analytic continuation of the physical data to complex spin S. Indeed, if we were to study this function in the complex plane we would find a myriad of unphysical poles in the right half-plane (RHP) (from zeroes of the big

with huge precision to make sure the corresponding energies and structure constants are accurately predicted. We found it very efficient to find the position of the particles u_j first with some reasonable precision (using `FindRoot` with `WorkingPrecision->100` digits say) and then using these locations as a starting point to solve the equations again with more precision (using `FindRoot` again with `WorkingPrecision->1000` digits say)

[10] Note that the sum in the second line of (8.6) can be truncated to $j \leq S/2$ since all terms with bigger j vanish. This sum in (8.6) can actually be trivially done: the result is a sum of two ${}_8F_7$'s.

parentheses in the last line), violating the expected Regge bahavior of this theory. The *correct* analytic continuation away from the even integers S is given to us by Newton as explained in the next section.

We also know [11] analytically the sum of all $C(S)^2$ is for each spin S. These sum rules appear in correlation functions, where all operators appear in the OPE. They evaluate to nice rational numbers [174]. Here, we find

$$\texttt{sum}(S) \equiv \sum_{\texttt{families}} C(S)^2 = \frac{S!^2}{(2S+1)!} \times \frac{(S+1)(S+3)}{3} \,. \tag{8.7}$$

For spin $S = 10$, for instance, we get $\texttt{sum}(10) = 1/81396$. At this spin, there are only two families and since we know the lowest one analytically we can read off the second family as[12] $C(10)^2_{\texttt{second family}} = 5/20532141$. Above spin $S \geq 12$, we have more than two families and only the lowest family is given by a rational number. All other solutions are given by more complicated algebraic numbers which we computed numerically with several hundreds of digits for all spins up to $S = 200$.

This concludes the study of the twist 3 data for physical integer spin. We now need to go to the complex spin plane. Enter Newton.

8.3 Newton's Magic

Given the CFT data at spins $S = 2, 4, 6, \ldots$, we want to go to the complex plane. Normally this is not a well posed problem; we can always add a bunch of simple (trigonometric) functions that vanish at the integers to any possible analytic continuation.

Here, however, physics come to the rescue to render the continuation unique. Conformal Regge theory ensures that the $c(\Delta, S)$ functions discussed in the introduction should be bounded and free of singularities in the complex S plane to the right of $S = 1$ [55, 191]. In a planar theory, this requirement is slightly weakened: singularities are excluded to the right of $S = 2$, as a consequence of the bound on chaos [209]. We hypothesize that this requirement extends to the individual structure constants $C(S)$ of each Regge trajectory

[11] We can derive this result in two trivial ways. We can construct this sum for various spins S from the solutions of the electrostatic problem and simply observe that they follow a nice sequence given by this expression; `Mathematica`'s `FindSequenceFunction` would give it right away. Alternatively we could simply decompose the leading twist contribution to the tree level BPS correlator (take (66) from [174] say)

$$G^{\texttt{tree}}_{2233}(z,\bar{z}) = \frac{(2z(\bar{z}-1)-2\bar{z}+3)(z\bar{z})^{3/2}}{(z-1)^2(\bar{z}-1)^2} \simeq \frac{(3-2z)z^{3/2}\bar{z}^{3/2}}{(z-1)^2}$$

$$= \bar{z}^{3/2} \sum_S \frac{\texttt{sum}(S)}{C^2_{233}} z^{S+\frac{3}{2}}\, {}_2F_1(S+2, S+2; 2S+3; z)$$

to read off (8.7) for even spin and $\texttt{sum}(S) = S!^2/(2S+1)! \times (S+1)(S-1)/3$ for odd spin. From a four point functions point of view we can only go beyond extracting such sum rules if we explore higher loops and/or multiple correlators otherwise all we access are these sums over classically degenerate operators.

[12] Recall that all higher families are double degenerate so that $\texttt{sum}(10)$ is equal to $C(10)^2_{\texttt{lowest family}} + 2\,C(10)^2_{\texttt{second family}}$.

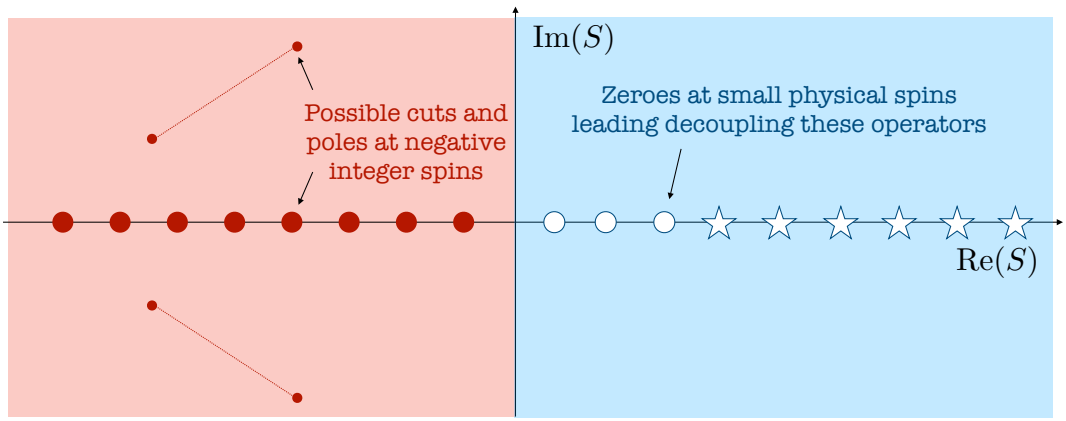

Figure 8.3: Cartoon for complex S plane behavior for $C(S)$. The main result of this note is the confirmation of the expected zeroes in the right half-plane.

(which are residues of $c(\Delta, S)$ at the locations of poles). A rough argument is that different $C(S)$ can be accessed as different residues of $c(\Delta, S)$ in Δ. As long as the Δ are not degenerate, these residues should be individually finite[13]. Finally, in our case, supersymmetry relates the twist-3 operators of interest to operators with higher spin by 2 units[14]. Thus, we expect that $C(S)$ should be bounded and free of singularities to the right of $S_* = 0$.

(At the same time, in the left half plane we do expect a host of singularities of various types as depicted in figure 8.3.)

Together, these conditions suffice for Carlson's theorem, which ensures the uniqueness of the analytic continuation of this data.[15]

What is perhaps less well-known is that the unique extension alluded to in Carlson's theorem can be explicitly constructed by a beautiful interpolation series written down by Newton in 1687's *Principia Mathematica*.[16] Newton's series

$$f_N(z) \equiv \sum_{j=0}^{N} \binom{z}{j} \sum_{i=0}^{j} \binom{j}{i} (-1)^{j-i} f(i)\,. \tag{8.8}$$

converges to the proper extension $f(z)$ as $N \to \infty$. For us, f could be either the energy of the structure constants and the argument would be $z = S/2 - S_n/2$ where S_n is the first value for which a given family exists. That is is $S_1 = 0$ for the lowest family, $S_2 = 6$ for the second family, $S_3 = 12$ for the third family etc. Then physical values correspond to $z = 0, 1, 2, \ldots$ and we include N of these in the interpolation. Newton's series is very powerful: it supposed to converge to the right of the first allowed singularity, so for us it

[13] We verify no such degeneracies occur in the RHP through an integrability based method in section 8.4. That the method presented in this section works suggests in itself the absence of degeneracies, as discussed in the main text.

[14] See [210, 211] for the precise Ward-identities in the twist 2 case.

[15] Carlson would require less. The function could grow exponentially along the imaginary direction provided the exponent is smaller than π (this is roughly speaking what rules out trigonometric functions like sin's and cos's while tan's and cot's are excluded by the absence of singularities.)

[16] It is Case 1 of Lemma V of Book III on the problem of *To find a curve line of the parabolic kind which shall pass though any given number of points.*

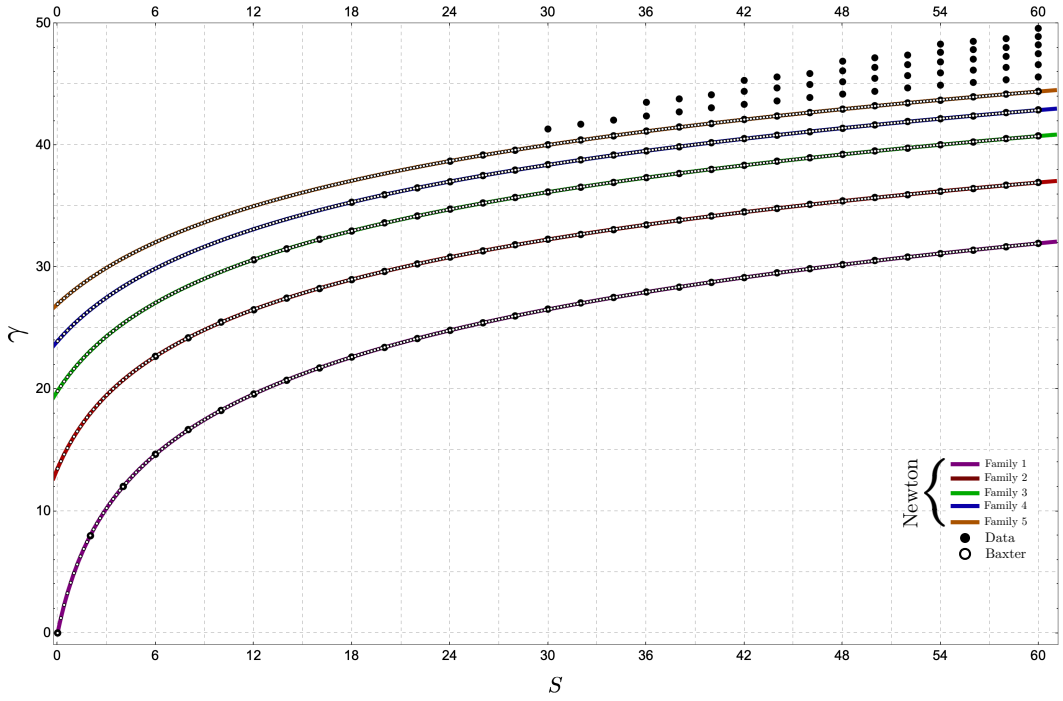

Figure 8.4: The Newton continuation of the operators dimensions is represented here for the lowest five families at $N = 88$. The white dots corresponding to an alternative integrability method described in section 8.4. They lie perfectly on top of the Newton continuations.

should converge in the full right half complex spin plane [212].

Applying this method to the anomalous dimensions of the various trajectories with $N = 88$ results in figure 8.4. Experimentally, the method quickly converges as N is increased. This confirms the picture that, indeed, each trajectory $\gamma(S)$ is free of singularities in the RHP, as otherwise the method would not have converged. Of course, given convergence, one could simply scan over the complex plane and observe that no degeneracies occur away from the real line. In section 8.4 we discuss an alternative integrability-based method that allows for the computation of the energies directly at complex spin. As shown in figure 8.4, it confirms the absence of operator mixing in the RHP and the numerical accuracy of the Newton series.

Having confirmed the lack of degeneracies, let us now jump to the most exciting application of this method: The study of the structure constants for the second family, which starts at spin $S = 6$. We first apply (8.8) using the first $N = 15$ physical spins; then we include more and more physical operators in the interpolation up to $N = 97$, see figure 8.5. As we increase N we see that the analytic continuation beautifully converges[17] and precisely predicts zeros at the lower spins $S = 4$ and $S = 2$ as mentioned in the introduction!

[17]To be precise, we continue $2^{\log(2)S}C(S)$ and later subtract the exponential. The reason for this is that the structure constants decay *too quickly*, which turns out to be an issue for the series convergence. Generically, once can always subtract the exponential behaviour of the interpolated sequence to obtain a convergent series representation provided there is no Stokes-like phenomena in the RHP. This is the case here due to Regge theory.

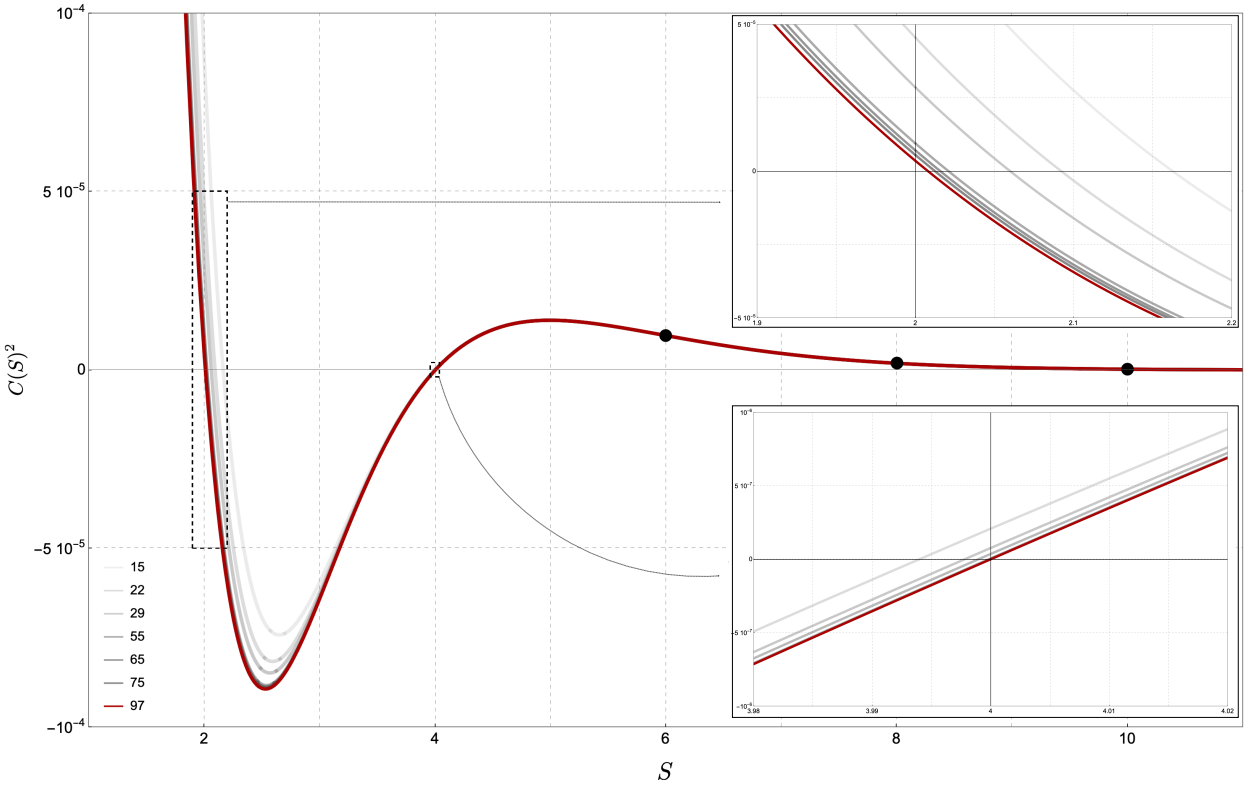

Figure 8.5: Newton's continuation of the structure constants for the second family converging as we include more and physical operators for $N = 15, \ldots, 97$. The outcome of Newton's interpolation is almost spooky: The physical structure constants are *growing* as we come from the right approaching $S = 6$ and the continuation reverses this growth and dives perfectly through zero surgically at (the even integer) 4 coming back up through zero again precisely at (the even integer) 2! If this is not dark magic, what is dark magic?

Repeating (a refinement of) this analysis for all families we end up with figure 8.6.[18] The picture put forward in the introduction with the decoupling of the various higher families at lower physical spins is neatly realized.

8.4 Baxter's Blessing

Can we cross-check the analysis of the last section and compute directly the CFT data at complex spin? We do not know how to do it for structure constants – as discussed below – but for the spectrum $\gamma(S)$ Baxter equations give an alternative method we can use which reduces to the previous electrostatic description for integer spin, but generalizes neatly for complex spin.

[18] We could in principle go all the way to $S = 0$ but it is harder to get convergence there; this is of course not surprising as $S = 0$ is the boundary of the RHP. We are agnostic about the expectation of (non) emergence zeroes at $S = 0$.

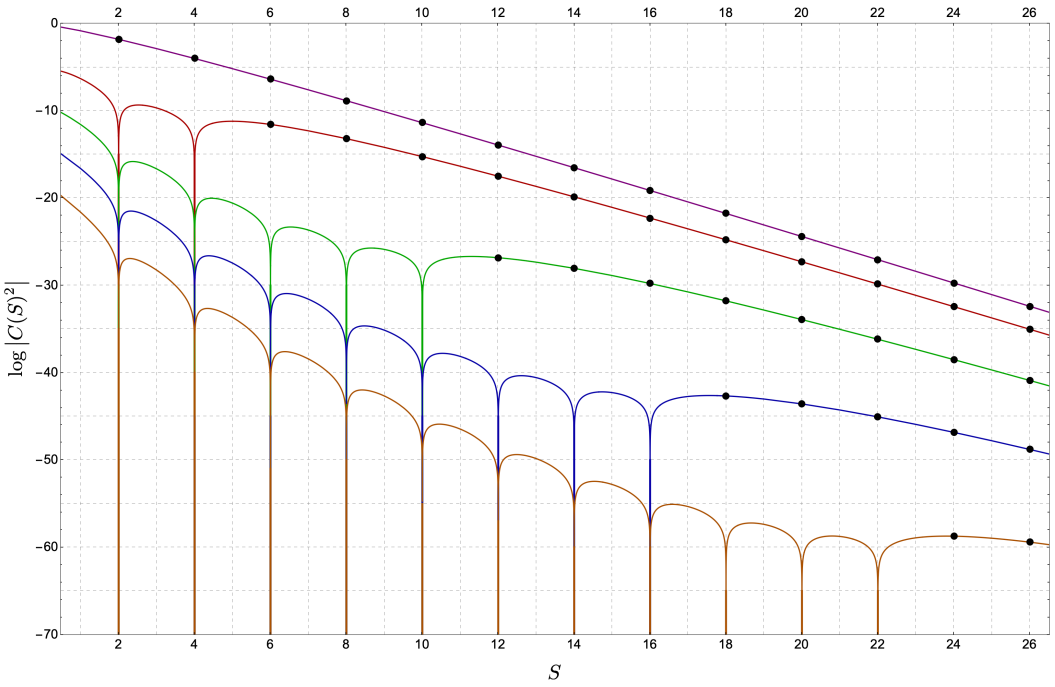

Figure 8.6: To extend the analytic continuation for all $S > 0$ we first run the interpolation for a family starting at S_n and check that a zero emerges dynamically as $S_n - 2$ as we increase N. Once this happens we can put it in by hand and continue instead the Newton's series interpolation of $C^2(S) \times (S - S_n + 2)$ and see if a zero at $S_n - 4$ emerges; If so we include it and interpolate $C^2(S) \times (S - S_n + 2) \times (S - S_n + 4)$ and so on, always checking for stability of the procedure.

The starting point is the Baxter twist three equation

$$Q(u+i)(u+i/2)^3 + Q(u-i)(u-i/2)^3 - Q(u)\big(2u^3 - (S^2+2S+\tfrac{3}{2})u + q\big) = 0.$$

For integer spin, this equation is equivalent to the electrostatic problem described above. Indeed, for integer S we look for polynomial solutions which we parametrize as $Q(u) = \prod_{j=1}^{S}(u - u_j)$. Evaluating this equation at $u = u_j$ we find that the second line vanishes and thus the ratio of the two terms in the first line must be equal to -1 when $u = u_j$. The logarithm of this statement is the electrostatic equation (8.3); the integers n_j correspond to the various possible log branches. From the Baxter point of view, the different trajectories are labelled through their $q \equiv q(S, n_*)$ eigenvalue, which is self-determined from (8.9) plus polinomiality.

What is beautiful about this equivalent Baxter formulation is that it now allows for an extension to complex spin S, once we relax the polynomiality property of the Baxter function $Q(u)$. The proposal is that we should look for the slowest growing entire solution of (8.9). We review this prescription in appendix G.3.

A numerical algorithm to obtain such solutions is as follows. Assume Q is given by a

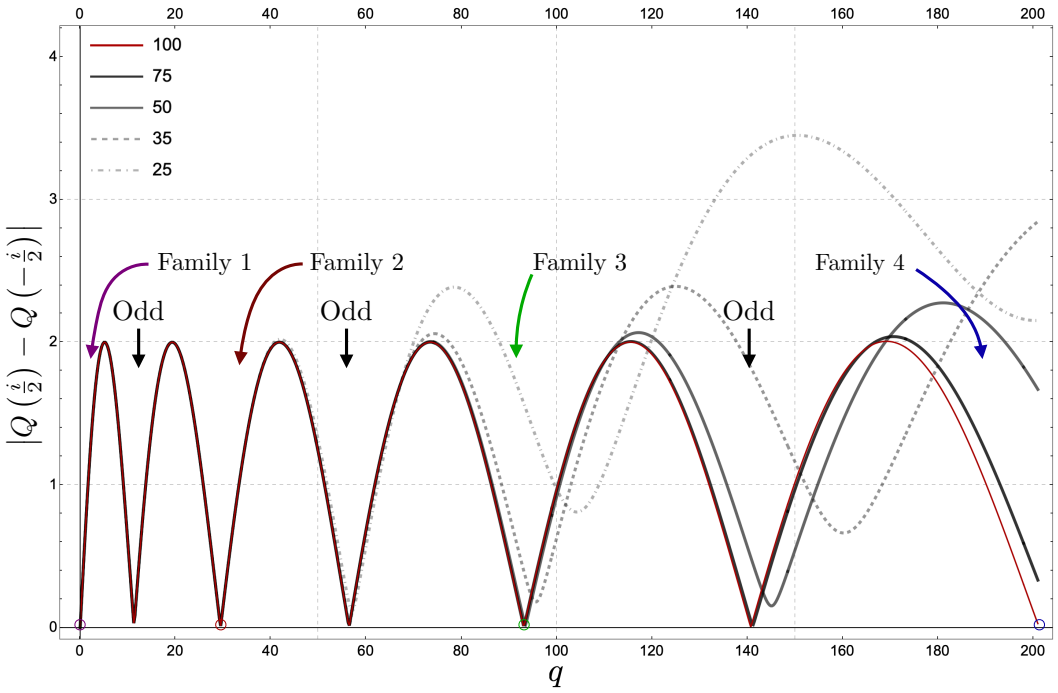

Figure 8.7: We can find the physical values of q by requiring that the continued Baxter solution preserves the zero momentum condition associated with single trace operators. More terms in the expansion (8.9) are needed to converge as we scan over higher values of q, corresponding to higher families, as indicated by the various $N_{\max}$ curves, which are evaluated at $S = 11/3$ here; to find the third family $N_{\max} = 35$ is almost enough for instance while $N_{\max} = 50$ is definitely plenty. The method identifies both even and odd spin trajectories, which come as alternating zeroes, since the same Baxter equation describes both sectors.

truncated power series normalized at $u = i/2$:

$$Q(u) = 1 + \sum_{k=1}^{N_{\max}} a_k (u - i/2)^k. \tag{8.9}$$

Plugging (8.9) in (8.9) and requiring that the first $N_{\max}$ orders of the expansion around $u = 0$ are satisfied completely fixes the coefficients a_k in terms of S and $q(S, n_*)$. The claim is that this procedure, in which we approximate the power series tail by zero, converges to the slowest growing entire solution as $N_{\max} \to \infty$. One is left with solving the quantization problem of determining $q(S, n_*)$ for complex S. This is achieved by requiring the cyclicity condition $Q(i/2) = Q(-i/2)$, see figure 8.2.

This procedure is illustrated in figure 8.7. Starting from integer spin, one can identify which local minimum of $|Q(i/2) - Q(-i/2)|$ corresponds to each family and adiabatically deform from there. Alternatively, one could determine $q(S, n_*)$ through the Newton's series of the physical data. Both methods show perfect agreement.

Having determined the power series (8.9) one can then simply extract the energies from

$$\gamma = 2i \left(Q'(\tfrac{i}{2}) - Q'(-\tfrac{i}{2}) \right), \tag{8.10}$$

which generalizes (8.4) to the non-polynomial case. The result for the first five families is presented in figure 8.4. It is in perfect agreement with the Newton's series continuation from the integer spin data.

8.5 Discussion

The complex spin plane is a formidable universe and planar $\mathcal{N} = 4$ SYM, being a solvable higher dimensional conformal field theory is a perfect laboratory for its exploration.

In this chapter, we focused on the right half-plane $\mathrm{Re}(S) > 0$. On this side, conformal Regge theory predicts controllable growth at large spin and no singularities at finite spin. As such, there is not much room for surprises in the RHP. The notable exception are the *missing zeroes* we explored here. We found that the analytic continuation of structure constants for higher trajectories develops zeroes at integer positive spins, explaining their decoupling from correlation functions and resolving the puzzle raised in the introduction.

We conjecture this decoupling picture to be a general mechanism for any higher dimensional conformal field theory. Of course, testing it is not easy. Here, the data obtained in planar $\mathcal{N} = 4$ SYM through integrability was precious. To convincingly observe these zeroes, we used about a hundred physical data points computed with hundreds of digits of precision and plugged those into a beautiful continuation formula by Newton. Of course, this is not a luxury we can afford in the 3D Ising model where we might have at most a few physical operators with a few digits of precision.

It would be very interesting to explore other theories where we might be able to compute large amounts of physical structure constants with great precision and look for the emergence of the missing zeroes there as well. We could also assume these zeroes to be there and use them to more efficiently continue physical data into the complex plane.

In $\mathcal{N} = 4$ SYM, we could also explore other sectors and learn about analyticity (or lack thereof) in several other parameters such as R-charges, mixed spins (S_1, S_2) for more complicated spinning operators, twist, etc. A very nice study of strong coupling double trace operator decoupling as one analytically continues their R-charge representations can be found in [213].

It is also an important open problem to understand how to directly compute the structure constants at any complex spin S from integrability without resorting to Newton's magic – as done for the spectrum in section 8.4 using Baxter's Q-functions. In [6] new formulae were put forward for structure constants in this theory in terms of Separation of Variables (SoV) like integrals [88, 91, 94] of Q-functions so one might wonder if we can not simply plug the Q-functions found in the spectrum study there. Sadly, we do not know how to do it. Take for example the simplest possible leading order structure constant in the $SL(2)$ sector corresponding to twist-two operators. There is no operator degeneracy and a single family of operators in this case for which Dolan and Osborn [180, 214] extracted $C(S)^2_{\texttt{twist-2 LO}} = \frac{S!^2}{(2S)!}$ many years ago already. In integrability terms this can be obtained

from chapter 7

$$C(S)^2_{\texttt{twist-2 LO}} = \frac{S!^2}{(2S+1)!} \frac{1}{\int_{-\infty}^{\infty} du \, \frac{\pi}{2} \frac{Q(u)^2}{\cosh(\pi u)^2}}\,, \tag{8.11}$$

see appendix G.4. For any even integer spin the Q function is a polynomial so that integral is perfectly convergent; it evaluates to $1/(2S+1)$ [6], see also appendix G.2.1 for a derivation. When S is not integer, the Baxter function Q grows as $e^{2\pi u}$ at infinity [215] however and the integral no longer converges. It would be interesting to generalize [6] so that it could apply not just for physical local operators of integer spin but also for analytically continued spins. One approach could be to try to make the SoV expressions manifestly gauge invariant under the symmetry $Q \to f_{\texttt{i-periodic}}\, Q$ of the Baxter equation.

A related question is whether we can explicitly write down the light-ray operators corresponding to the Regge trajectories we found in this chapter, in the spirit of [192–202]. Such light-ray operators should take the form

$$\int d\alpha_1 d\alpha_2 d\alpha_3 \psi(\alpha_1, \alpha_2, \alpha_3) \operatorname{Tr}(Z(\alpha_1) Z(\alpha_2) Z(\alpha_3)). \tag{8.12}$$

Here, $Z(\alpha)$ is an insertion of Z on a Wilson line lying along future null infinity, at retarded time α. The three Z insertions are integrated against a wavefunction $\psi(\alpha_i)$, which must be translationally-invariant in retarded time to describe a primary light-ray operator. The homogeneity of ψ is related to the spin S.[19]

In trying to directly construct such operators, we run into puzzles. Naively, at fixed S, the wavefunction ψ can depend in an arbitrary way on the translationally-invariant homogeneity-zero combination $\chi = \alpha_{12}/\alpha_{13}$. In other words, there seem to be a *continuous infinity* of primary light-ray operators we can write down at each spin S, parametrized by an arbitrary function of χ.

What reduces this continuous infinity of choices down to a discrete set of Regge trajectories? In our case, the mode number n_* gave a natural way to define trajectories. More generally, what mechanism could reduce the naive continuous infinity of light-ray operators (8.12) to a discrete set in non-integrable perturbative theories, like the Wilson-Fisher theory? Can we figure out the general mechanism by understanding operators in $\mathcal{N} = 4$ SYM well-enough?

A proposal will appear in [56]: we indeed manage to explicitly construct the light-ray operators appearing in this chapter in the form (8.12). These trajectories are selected out of the naive continuum by a smoothness criterion[20] on the wavefunctions $\psi(\alpha_1, \alpha_2, \alpha_3)$. We expect that similiar criterions apply in more general perturbative theories. The explicit expressions to appear in [56] also manifest the missing zeroes.

[19] In the case of integer spin, ψ should be a combination of δ-functions and their derivatives, and (8.12) becomes the light-transform [52] of a local operator.

[20] Let $\chi = \cos(x)/\cos(x - 2\pi/3)$. Then the light-ray operators which correspond to the trajectories considered in this chapter are such that the Fourier modes $a_n = \int_{-\pi}^{\pi} e^{inx} \psi(x, r) dx$ decay as $1/|n|$ as $|n| \to \infty$, where the $r = \sum_i \alpha_{ii+1}^2$ dependence is controlled by homogeneity. This can be translated as a smoothness condition in the variables α_i.

Everything we observed in this chapter at leading order in perturbation theory should hold at finite coupling.[21] Repeating the leading-order analysis at next-to-leading-order should be straightforward, for instance. More ambitiously, can the missing zeroes be useful in searching for a finite coupling version of chapter 7?

Finally, we have the left-half plane (LHP) of S, where there is a host of exciting physics to explore. In this left hand-side of the complex spin plane there will be dragons. In perturbation theory, we expect there a host of different singularities from poles at negative spins which would open up into cuts at finite coupling, creating an intricite infinitely-sheeted Riemann surface. This part of the plane contains so-called "horizontal trajectories" of BFKL type [197, 198, 217] whose tree-level spin S is fixed, but whose dimension Δ can vary. When the coupling is turned on, horizontal trajectories can recombine with the more traditional 45° trajectories discussed in this chapter [218].[22] In perturbation theory, such recombinations manifest as poles in anomalous dimensions and structure constants, which satisfy compatibility conditions between the two combining branches, see e.g. [191, 218]. A class of horizontal trajectories that should recombine with the twist-3 operators considered here was explored in [219]. It would be very interesting to describe the recombinations explicitly at the level of operators, using the techniques of [202]. We also expect branch cuts in perturbation theory where different twist-3 trajectories recombine, see figure 8.3. We will confirm this picture in [56].

[21] Confirming this picture is hard but it is not science fiction in planar $\mathcal{N} = 4$ SYM. In [87] and [216] beautiful finite coupling analysis of the spectrum of twist two operators was carried out with spectacular results. Our twist three setup is more complicated and for structure constants we do not have the powerful technology of the quantum spectral curve at our disposal yet despite recent advances such as [6] building on important previous works [88, 89, 91, 93, 94, 96, 97].

[22] The terminology "horizontal" and "45°" refers to the Chew-Frautschi plot, where we plot S vs. $\Delta - \frac{d}{2}$.

Chapter 9

Conclusion

Once upon a time, physicists realized that most of nature was described by relativistic quantum fields. This thesis is about quantum field theory. Yet, in a sense, quantum fields have not made an appearance in almost three hundred pages. There is not a single physical Lagrangian expressed in terms of local fields in this thesis; the word "Hamiltonian" does not appear. Instead, throughout we focused on discussing physical observable directly.

Some motivation to do so comes already from perturbation theory. Even at tree-level, computing scattering amplitudes of gluons from Feynman diagrams is an incredible laborious task that soon grows completely out of control. However, for example in the case of maximally helicity violating amplitudes, Park and Taylor observed that the end product of this computations takes a remarkable simple form [220]:

$$\mathcal{M}_{\text{c.o.}}\left(1^+2^+\dots i^-\dots j^-\dots n^+\right) = \frac{\langle ij\rangle}{\langle 12\rangle\dots\langle n1\rangle}. \tag{9.1}$$

Other tree-level amplitudes can be efficiently computed recursively [221]. This simplicity becomes clear only once one does away with Lagrangians, virtual particles, gauge redundancies, and what not, and focuses on the underlying physical principles[1].

This success story is not limited to perturbative computations. In the case of conformal field theory the bootstrap axioms, which directly encode underlying physical principles, have proven to be powerful enough to de-facto solve a number of second-order phase transitions. For example, in the 3D Ising model, the numerical conformal bootstrap is able to rigorously determine that the leading scaling dimensions Δ_σ, Δ_ϵ and OPE coefficients, $C_{\sigma\sigma\epsilon}, C_{\epsilon\epsilon\epsilon}$ live in a tiny island [222]:

$$(\Delta_\sigma, \Delta_\epsilon, C_{\sigma\sigma\epsilon}, C_{\epsilon\epsilon\epsilon}) = (0.5181489(10), 1.412625(10), 1.0518537(41), 1.532435(19))\,. \tag{9.2}$$

In the middle of the island known solutions to crossing involve hundreds of operators for which structure constants and scaling dimensions vary very little, allowing one to (non-rigorously) predict their values as well[2].

[1] To me, that is cinema.

[2] On the other hand, some observables such as the dimension of operators with very high twist are largely unconstrained by these studies.

A good fraction of this thesis was devoted to developing a strategy to constrain scattering observables in strongly coupled quantum field theories by appealing direly to physical principles. The hope is that, by tackling these observables heads on, we might encounter unexpected simplicity and enjoy some of the successes obtained in the perturbative amplitudes or conformal theories. In some aspects, we already have some humbly exciting successes. In others, there is clearly a lot of work to be done.

Let us describe one such success [48]. Consider a long flux tube in three dimensional[3] Yang-Mills theory sourced by external quarks. The low energy theory on the flux tube is that of a massless particle, the Goldstone boson of the 3D Poincare symemtry broken by the presence of the long string. We can describe the dynamics on this "QCD string" through the ~~Lagrangian~~ S-matrix of these particles. At low energies the S-matrix is constrained by the broken Poincare symmetry which is non-linearly realized. More interesting is the behaviour of the S-matrix at energies of order ℓ_s^{-1} where ℓ_s is the characteristic length of the flux tube. In this regime, the dynamics are strongly coupled. Can we say anything about the S-matrix at this energy scale? If so, how?

We can require that this S-matrix is unitary, analytic, etcetera and try to get something out of it. However, and here comes a twist, in this case we are not limited to $2 \to 2$ scattering! Let us see how. Because we are in two dimensions and the particles are massless, they must be either left or right movers. Consider a bundle of several left movers[4] with total energy p_L and energy fractions α_i distributed among the various partons:

$$\psi(\alpha_1, \ldots, \alpha_N) \equiv |\alpha_1 p_L, \ldots, \alpha_N p_L\rangle$$

with an analogous expression for right-movers. Suppose we integrate the state ψ against some wavefunction for the distribution of energy among the partons. This defines a *jet*. Kinematically, the jets behaves just like new massless one-particle states[5]. This means we can scatter left- and right- moving jets, and their S-matrices will satisfy standard analyticity (as a function of the energy), unitarity and crossing $2 \to 2$ properties[6]! Backtracking: what can we learn about the QCD string S-matrix by requring the consistency of the jet scattering? A first step towards the answer is described in figure 9.1. In sum, we can provide sharp bounds on the dynamics at order ℓ_s^{-1}: all $SU(N)$ 3D pure Yang-Mills theories must live in the small green island of figure 9.1.

Now, let us discuss some unsatisfactory features of these results - similar comments apply to most other S-matrix bootstrap studies. The first is that this small island is not so small: as emphasized, it includes all $SU(N)$ Yang-Mills theories, and is therefore a continent. A crucial question is whether we can do better and pinpoint each $SU(N)$ theory in an archipelago of sorts. This should be possible, as we do not expect to be able to continuously move between various $SU(N)$ theories in a parametric family of analytic and unitarity flux tube theories[7].

[3] There is no obstruction to repeating what follows in four dimensions.

[4] There are no collinear divergences due to the incredibly soft behaviour imposed by the symmetry breaking. To see this, boost the collinear particles to low energies.

[5] Note that this is very special to massless particles in 2D.

[6] Of course, all these properties are very non-trivially inherited from the full multi-particle S-matrix. Worry not, it works.

[7] It would be very interesting if this turned out to be false.

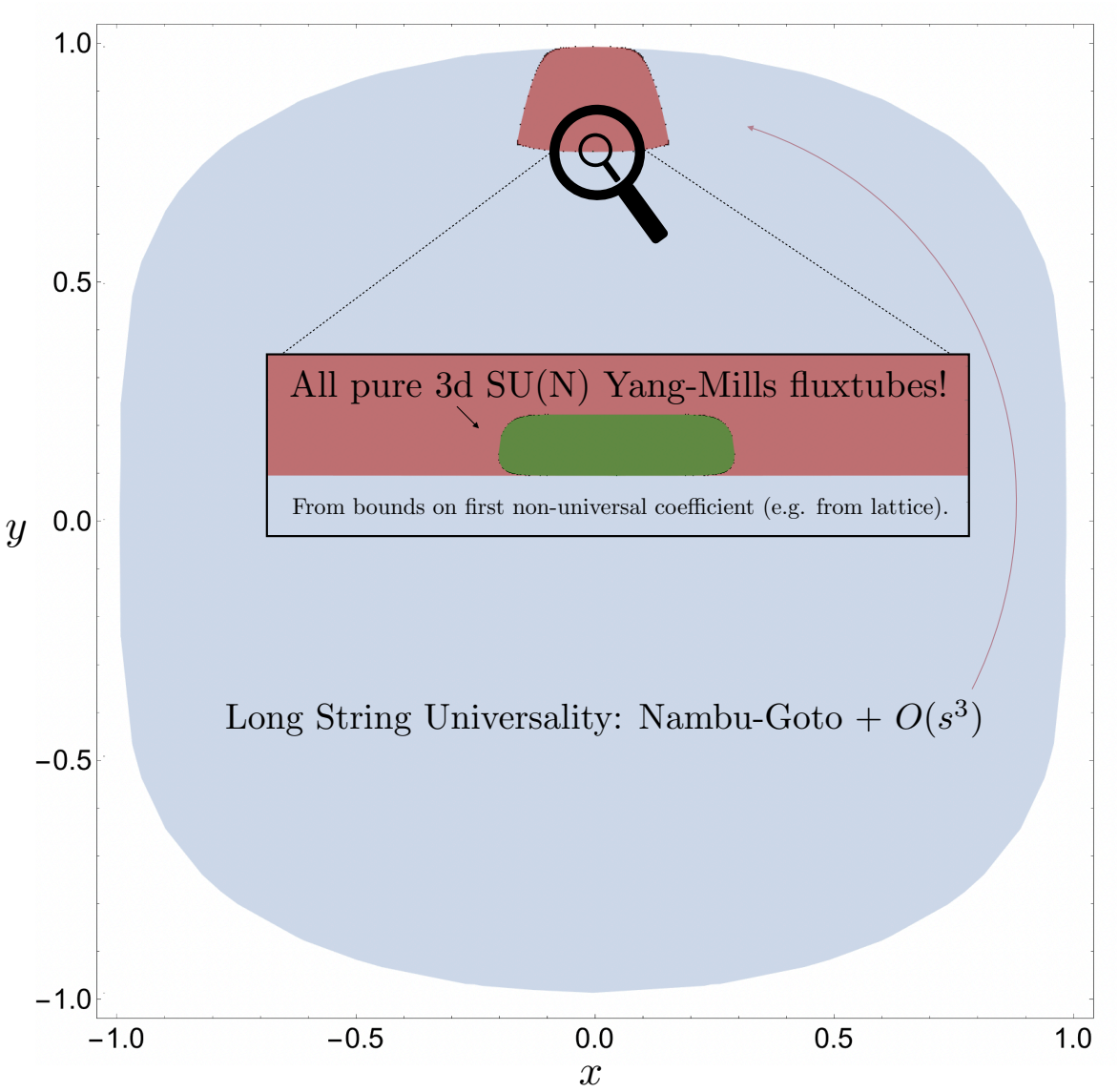

Figure 9.1: We consider all $2 \to 2$ processes involving the fundamental NGB $|f\rangle$ and the jet state $|\text{jet}\rangle \equiv \int_0^1 \mathrm{d}\alpha \left(\psi(\alpha, 1-\alpha)/\sqrt{8\pi\alpha(1-\alpha)}\right)$. Define $y = \frac{2}{\pi}\int_0^\infty \mathrm{d}s \mathrm{Re} S_{ff\to ff}(s)/(s^2+1)$ and $x = \frac{2}{\pi}\int_0^\infty \mathrm{d}s \mathrm{Re} S_{ff\to \text{jetjet}}(s)/(s^2+1)$, with the center-of-mass energy $\sqrt{s}$ measured in units of ℓ_s^{-1}. The specific form of the kernel is not essential and can be easily modified. The important point is that x and y are sum rules which capture the physics at order $s \sim \ell_s^{-2}$. They are not low energy sum rules. The blue bounds are obtained by requiring the analyticity, crossing (see figure 9.2) and unitarity of these processes. For the red region we additionally require that, up to order s^2 the S-matrix is universal and given by the Nambu-Goto action, as determined by the non-linearly realized symmetries. Finally, the green region is defined by requiring that the first non-universal operator in the EFT comes with a dimensionless coupling $\gamma_3 l_s^6 \leq 10^{-3}$, see [48, 142] for precise definition of γ_3. This assumption is conservative for pure $SU(N)$ flux tubes according to lattice QCD simulations. This allow us to place sharp bounds on the multiparticle S-matrix.

It is not expected that including more low energy constrains imposed by the broken Poincare effective field theory will change picture 9.1 much. Nor should considering more jet states[8] into the bootstrap system. What could we be missing then? Two speculative possibilities could be considered. The first is that isolating each $SU(N)$ theory is not a question about branons on the long flux tube, but about embedding this S-matrix in the richer framework of interacting strings: we should consider the physics of glueball emission and absortion by the long strings[9], and their interplay with glueball scattering[10]; or perhaps we should consider the consistency of the theory on finite volume[11]. The second possibility is that this is still a question that can be addressed by further exploring the scattering on the long string. For example, we have not explored analyticity on the energy fractions inside jets. Can we cross a single particle from inside a jet from the past to the future? It is not clear whether this is possible: it might be that no on-shell analytic path of continuation is available connecting these kinematics. If it is, then crossing is expected to take a more complicated form [40], see figure 9.2. These crossing constrains are highly non-linear, and seem to naturally break the convexity exploited in all bootstrap studies so far. This is exactly what is needed to break a convex island into a disjoint (and therefore non-convex) archipelago.

Perhaps a good laboratory to explore both of these proposals is the Ising field theory bootstrap. In that case, we know that the quantum field theories defined by pure magnetic or pure thermal deformations away from criticality define S-matrices at the boundary of the space of theories defined by consistent $2 \to 2$ scattering [9]. The one-parameter family of QFTs defined by arbitrary relevant deformations should then hopefully not be too far from the space defined by consistent $2 \to 2$ scattering. In contrast to the critical Ising island from the conformal bootstrap, the interior of the current S-matrix space contain theories whose physics are quite varied, making it impossible to make sensible predictions about the Ising field theory dynamics. How can we pin down the Ising theory? Once again, there are two suggestions: one is that we should impose much more information about the exactly solvable UV CFT than has been done so far [20]. The other is that the consistency of highly non-linear constrains will carve out large chunks of the current allowed space. In the case of Ising we do not need to go to multiparticle scattering to explore these ideas since the natural large hierarchy of masses for large magnetic deformations introduce non-convexities[12] at the $2 \to 2$ level through anomalous Landau diagrams, see chapter 2.

[8] A complete basis of jet states can be constructed.

[9] Related to this point, analyticity assumption on the S-matrix in quantum gravity are often quite speculative. The same is true in this flux tube problem since, after all, we are discussing a 1+1D quantum gravity theory. It would be very nice to examine these analyticity assumption more careful in this case. For example, what is the S-matrix for the scattering of two branons in critical bosonic string theory in the presence of a handle on the long-string? Sounds like a fun computation to think about.

[10] Against this proposal, one might ask about the large N theory first.

[11] We expect a Hagedorn transition at $R_H \sim l_s$. However one could imagine a scenario where, unless the S-matrix is fine-tuned -thus forming an archipelago- one obtains $R_H \gg l_s$. Recall this conclusion is a fairy tale.

[12] A baby example: consider an analytic function on the disk bounded in modulus by one at $|z| = 1$ and with a pole at the origin whose residue is $-4g^2 + g^4$. We interpret the first term as a t-channel pole and the second term as a Landau singularity. As follows from the maximus modulus principle, the allowed space for the "coupling" g is not connected, with a small island that is intrinsically strongly coupled at around $g = 2$. Of course, the real bootstrap system is much more elaborate than this.

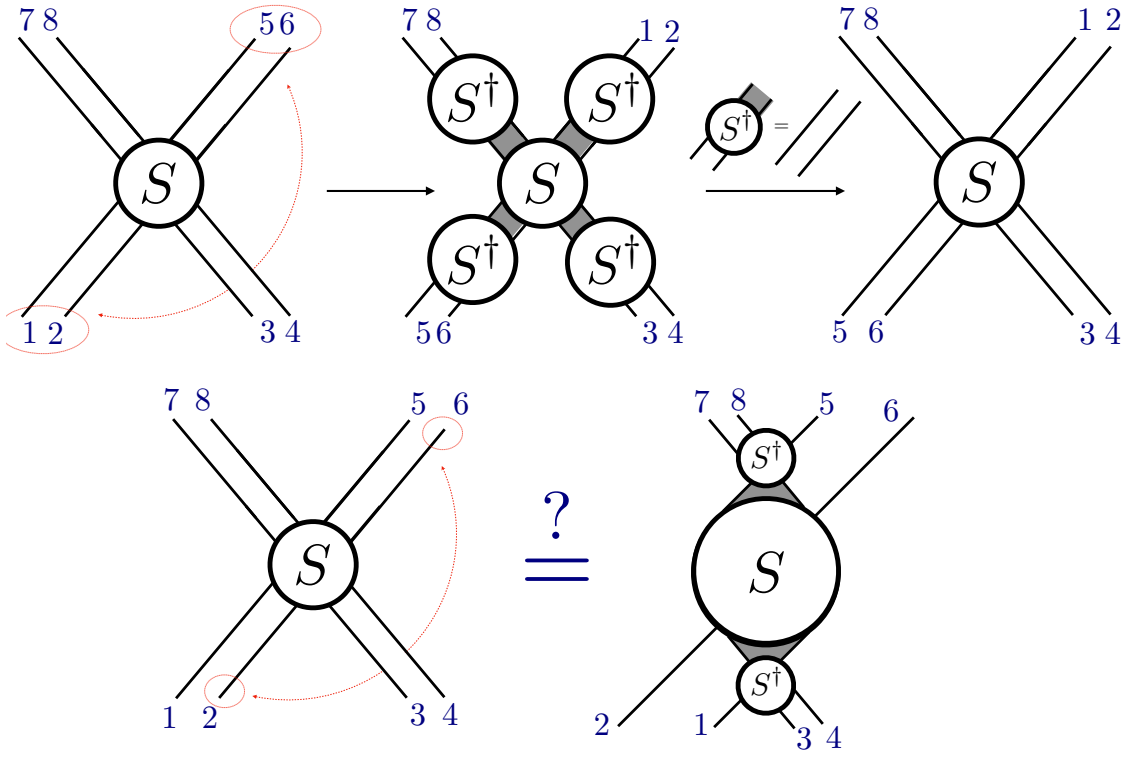

Figure 9.2: In this figure the direction of lines define left- or right- moving particles, and grey patches denotes a sum over a complete basis of states. A multiparticle crossing equation has been recently conjectured in [40]. **First row**: for example, the first arrow describes the (12) $\leftrightarrow$ (56) crossing in a $4 \to 4$ process. From the point of view of jets, this is just the standard $2 \to 2$ crossing. Indeed, since there is no left-left or right-right scattering in this theory, the crossing equation simplifies, as described in the second arrow. On the other hand, when crossing a single particle from inside a jet, the proposed crossing equation of [40] is given by the **second row**, and is a highly non-linear and non-trivial constrain.

Of course, we can't run from the central problem forever. Particle production is often the dominant outcome when particles are scattered. Except in the very particular case of flux tubes - soft massless two dimensional scattering - there are no known viable strategies to bootstrap multiparticle amplitudes. New ideas are urgent. Most likely one must develop techniques to bootstrap with limited knowledge on analyticity properties, much like in the jet's scenario where we used a single-variable dispersion on the total energy, but did not appeal to sub-energy analyticity. If this ancient problem is not overcome, the S-matrix bootstrap is likely to be saturated and die once again.

Before moving on to future questions beyond the S-matrix bootstrap, it is worth to mention a much less explored frontier which is to consider scattering in the presence of long-range topological order. It seems reasonable to expect that asymptotic states carrying topological lines are well-defined, but the standard crossing and analyticity assumptions are modified [32, 33, 223]. Uncovering the general structure would open another path to explore the very rich dynamics of non-abelian gauge theories coupled to matter which often exhibit rich IR topological phases [224].

In the case of a non-trivial IR CFT, a description of the quantum field theory in terms

of a basis of asymptotic particles is not available, and particle detectors are not good observables. On the other hand, nothing prevents us from preparing a state in the past, evolve it, and perform more general asymptotic measurements at future infinity. Requiring that the outcome of these Lorentzian measurements are consistent with a microscopic dynamics that is causal, local and unitary might reveal constrains that are deeply hidden in more microscopic definitions of the quantum field theory.

It is therefore crucial to uncover the space of asymptotic "detectors". Restricting to the IR CFT first, a minimal set of detectors are integrals of local operators at $\mathscr{I}^+$. But that is certainly not a complete basis, as can be seen from the OPE [49, 50] - one needs to add at least the light-ray operators of [52]. What else is needed to have a systematic description of these objects? A related question is to understand what controls correlation functions in various kinematical regions. For example, the leading contributions in the Regge limit are given by light-ray operators. Is there a physical interpretation for the complete expansion of correlators in the Regge sheet [225]? What about more complicated Lorentzian kinematics that can be accessed in higher-point correlators? Answering this questions should clarify the structure of non-local operators in CFT and beyond. As usual, we expect that planar $\mathcal{N} = 4$ SYM shall serve as a great laboratory to explore and test these ideas [56]. Of course, non-local operators are interesting regardless of what they can do for local correlators, and are effectively terra incognita compared to our understanding of local operators. The questions raised above should thus apply to and make contact with more general conformal defects investigations.

A particular type of defects relevant to this thesis are integrable line defects. For example, the transfer $\mathbf{T}$ and Baxter $\mathbf{Q}$ operators can be constructed explicitly in minimal 2D CFTs [226,227], realizing standard $\mathbf{TQ}$ and $\mathbf{QQ}$ relations[13]. In integrable planar gauge theories, such as $\mathcal{N} = 4$ SYM and its dual string theory, the construction of such operators remains elusive. In the case of 2D lattice theories whose continuum limit are integrable 2D CFTs the corresponding $\mathbf{T}$ and $\mathbf{Q}$ operators have recently been constructed from the point of view of 4D Chern-Simons theory [231–234]. It would be fascinating if this strategy could provide a operatorial derivation of the quantum spectral curve in planar gauge theories.

Possibly even more fascinating would be if this construction could shed light on how the integrability structure simplifies at strong coupling, making manifest the emergence of locality in the bulk. Even though integrability computations reproduce the correct results in this limit, it is often at a great cost and locality seems to be something that can only be observed a posteriori, once the results are at hand. Understanding whether there is a better way of thinking about the finite coupling integrability structure which clarify the relevant degrees of freedom at strong coupling could open the path to systematically study very quantum short strings in AdS/CFT.

Hopefully a top-down approach to the separation of variables framework for correlation functions will take off before any of these bottom-up approaches catch up. One direct frontier is to promote the weak coupling structure of chapter 7 to a $\mathrm{psu}(2,2|4)$ covariant framework. It is expected that some of the complicated structure that seem to be emerg-

[13] Let us point out that these structure allow for a description of these CFTs directly in terms of scattering states [228–230]. This directly contradicts the previous lore statement that this should not be possible. When can a CFT admit a scattering structure? Is this stricly limited to minimal models in 2D, or is this just the simplest case we have uncovered?

ing descends from privileging certain Q-functions associated to the rank-one sectors under consideration. Covariantizing the framework should reveal if this is correct and force us to exploit the full super-symmetry of the theory, which proven to be crucial both in the spectral problem as well as in the hexagonalization. It should also ease merging the separation of variables program with the quantum spectral curve, and point the way to finite coupling.

As in any thesis conclusion discussing solving $\mathcal{N} = 4$ SYM, I am legally obliged to mention how Onsager's solution of the 2D Ising model was crucial in the understanding of phase transitions, renormalization group, lattice field theories and so forth. The hope is that $\mathcal{N} = 4$ should play this role for gauge, conformal and string theory. In particular, Onsager's solution inspired numerical methods that allowed for the solution of more general non-integrable models. In the case of the holographic strings describing $\mathcal{N} = 4$ SYM, knowledge of the "long string" S-matrix was enough to compute the spectrum of short closed strings from the thermodynamic Bethe ansatz. Can we learn the right lessons from this computation, bootstrap the long string S-matrix in pure Yang-Mills, and numerically recover the spectrum of glueballs? *And they lived happily ever after.*

References

[1] Alexandre Homrich, João Penedones, Jonathan Toledo, Balt C. van Rees, and Pedro Vieira. The S-matrix Bootstrap IV: Multiple Amplitudes. *JHEP*, 11:076, 2019.

[2] Carlos Bercini, Matheus Fabri, Alexandre Homrich, and Pedro Vieira. S-matrix bootstrap: Supersymmetry, Z_2, and Z_4 symmetry. *Phys. Rev. D*, 101(4):045022, 2020.

[3] Andrea L. Guerrieri, Alexandre Homrich, and Pedro Vieira. Dual S-matrix bootstrap. Part I. 2D theory. *JHEP*, 11:084, 2020.

[4] Carlos Bercini, Vasco Gonçalves, Alexandre Homrich, and Pedro Vieira. The Wilson loop — large spin OPE dictionary. *JHEP*, 07:079, 2022.

[5] Carlos Bercini, Vasco Goncalves, Alexandre Homrich, and Pedro Vieira. Spinning hexagons. *JHEP*, 09:228, 2022.

[6] Carlos Bercini, Alexandre Homrich, and Pedro Vieira. Structure Constants in $\mathcal{N} = 4$ SYM and Separation of Variables. 10 2022.

[7] Alexandre Homrich, David Simmons-Duffin, and Pedro Vieira. Complex Spin: The Missing Zeroes and Newton's Dark Magic. 11 2022.

[8] Allan Adams, Nima Arkani-Hamed, Sergei Dubovsky, Alberto Nicolis, and Riccardo Rattazzi. Causality, analyticity and an IR obstruction to UV completion. *Journal of High Energy Physics*, 2006(10):014–014, oct 2006.

[9] Miguel F. Paulos, Joao Penedones, Jonathan Toledo, Balt C. van Rees, and Pedro Vieira. The S-matrix bootstrap II: two dimensional amplitudes. *JHEP*, 11:143, 2017.

[10] Miguel F. Paulos, Joao Penedones, Jonathan Toledo, Balt C. van Rees, and Pedro Vieira. The S-matrix bootstrap. Part III: higher dimensional amplitudes. *JHEP*, 12:040, 2019.

[11] Lucía Córdova and Pedro Vieira. Adding flavour to the S-matrix bootstrap. *JHEP*, 12:063, 2018.

[12] Lucía Córdova, Yifei He, Martin Kruczenski, and Pedro Vieira. The O(N) S-matrix Monolith. *JHEP*, 04:142, 2020.

[13] Yifei He, Andrew Irrgang, and Martin Kruczenski. A note on the S-matrix bootstrap for the 2d O(N) bosonic model. *JHEP*, 11:093, 2018.

[14] Miguel F. Paulos and Zechuan Zheng. Bounding scattering of charged particles in $1+1$ dimensions. *JHEP*, 05:145, 2020.

[15] Andrea L. Guerrieri, Joao Penedones, and Pedro Vieira. Bootstrapping QCD Using Pion Scattering Amplitudes. *Phys. Rev. Lett.*, 122(24):241604, 2019.

[16] Denis Karateev, Simon Kuhn, and João Penedones. Bootstrapping Massive Quantum Field Theories. *JHEP*, 07:035, 2020.

[17] Hongbin Chen, A. Liam Fitzpatrick, and Denis Karateev. Bootstrapping 2d ϕ^4 theory with Hamiltonian truncation data. *JHEP*, 02:146, 2022.

[18] Denis Karateev, Jan Marucha, João Penedones, and Biswajit Sahoo. Bootstrapping the a-anomaly in 4d QFTs. *JHEP*, 12:136, 2022.

[19] Hongbin Chen, A. Liam Fitzpatrick, and Denis Karateev. Nonperturbative bounds on scattering of massive scalar particles in d ≥ 2. *JHEP*, 12:092, 2022.

[20] Miguel Correia, Joao Penedones, and Antoine Vuignier. Injecting the UV into the bootstrap: Ising Field Theory. *JHEP*, 08:108, 2023.

[21] Yifei He and Martin Kruczenski. Bootstrapping gauge theories. 9 2023.

[22] Aditya Hebbar, Denis Karateev, and Joao Penedones. Spinning S-matrix bootstrap in 4d. *JHEP*, 01:060, 2022.

[23] Andrea Guerrieri, Joao Penedones, and Pedro Vieira. Where Is String Theory in the Space of Scattering Amplitudes? *Phys. Rev. Lett.*, 127(8):081601, 2021.

[24] Andrea Guerrieri, Harish Murali, Joao Penedones, and Pedro Vieira. Where is M-theory in the space of scattering amplitudes? *JHEP*, 06:064, 2023.

[25] Kelian Häring, Aditya Hebbar, Denis Karateev, Marco Meineri, and João Penedones. Bounds on photon scattering. 11 2022.

[26] Jan Albert and Leonardo Rastelli. Bootstrapping pions at large N. *JHEP*, 08:151, 2022.

[27] Jan Albert and Leonardo Rastelli. Bootstrapping Pions at Large N. Part II: Background Gauge Fields and the Chiral Anomaly. 7 2023.

[28] Barak Gabai and Xi Yin. On the S-matrix of Ising field theory in two dimensions. *JHEP*, 10:168, 2022.

[29] Piotr Tourkine and Alexander Zhiboedov. Scattering from production in 2d. *JHEP*, 07:228, 2021.

[30] Piotr Tourkine and Alexander Zhiboedov. Scattering amplitudes from dispersive iterations of unitarity. 3 2023.

[31] Miguel Correia, Amit Sever, and Alexander Zhiboedov. Probing multi-particle unitarity with the Landau equations. *SciPost Phys.*, 13(3):062, 2022.

[32] Barak Gabai, Joshua Sandor, and Xi Yin. Anyon scattering from lightcone Hamiltonian: the singlet channel. *JHEP*, 09:145, 2022.

[33] Umang Mehta, Shiraz Minwalla, Chintan Patel, Shiroman Prakash, and Kartik Sharma. Crossing Symmetry in Matter Chern-Simons Theories at finite N and k. *Adv. Theor. Math. Phys.*, 27:193–310, 2023.

[34] Yifei He and Martin Kruczenski. S-matrix bootstrap in 3+1 dimensions: regularization and dual convex problem. *JHEP*, 08:125, 2021.

[35] Andrea Guerrieri and Amit Sever. Rigorous Bounds on the Analytic S Matrix. *Phys. Rev. Lett.*, 127(25):251601, 2021.

[36] Kelian Häring and Alexander Zhiboedov. Gravitational Regge bounds. 2 2022.

[37] Sebastian Mizera. Bounds on Crossing Symmetry. *Phys. Rev. D*, 103(8):081701, 2021.

[38] Sebastian Mizera. Crossing symmetry in the planar limit. *Phys. Rev. D*, 104(4):045003, 2021.

[39] Simon Caron-Huot, Mathieu Giroux, Holmfridur S. Hannesdottir, and Sebastian Mizera. What can be measured asymptotically? 8 2023.

[40] Simon Caron-Huot, Mathieu Giroux, Holmfridur S. Hannesdottir, and Sebastian Mizera. Crossing beyond scattering amplitudes. 10 2023.

[41] Holmfridur Sigridar Hannesdottir and Sebastian Mizera. *What is the $i\varepsilon$ for the S-matrix?* SpringerBriefs in Physics. Springer, 1 2023.

[42] Sebastian Mizera. Natural boundaries for scattering amplitudes. *SciPost Phys.*, 14(5):101, 2023.

[43] Simon Caron-Huot, Yue-Zhou Li, Julio Parra-Martinez, and David Simmons-Duffin. Graviton partial waves and causality in higher dimensions. *Phys. Rev. D*, 108(2):026007, 2023.

[44] Richard John Eden, Peter V. Landshoff, David I. Olive, and John Charlton Polkinghorne. *The analytic S-matrix*. Cambridge Univ. Press, Cambridge, 1966.

[45] Miguel Correia, Amit Sever, and Alexander Zhiboedov. An analytical toolkit for the S-matrix bootstrap. *JHEP*, 03:013, 2021.

[46] Sebastian Mizera. Physics of the Analytic S-Matrix. 6 2023.

[47] Stanley O. Aks. Proof that Scattering Implies Production in Quantum Field Theory. *J. Math. Phys.*, 6(4):516–532, 1965.

[48] Andrea Guerrieri, Alexandre Homrich, Joao Penedones, and Pedro Vieira. Multiparticle S-matrix Bootstrap: Fluxtubes - to appear.

[49] Diego M. Hofman and Juan Maldacena. Conformal collider physics: Energy and charge correlations. *JHEP*, 05:012, 2008.

[50] Murat Kologlu, Petr Kravchuk, David Simmons-Duffin, and Alexander Zhiboedov. The light-ray OPE and conformal colliders. *JHEP*, 01:128, 2021.

[51] Cyuan-Han Chang, Murat Kologlu, Petr Kravchuk, David Simmons-Duffin, and Alexander Zhiboedov. Transverse spin in the light-ray OPE. *JHEP*, 05:059, 2022.

[52] Petr Kravchuk and David Simmons-Duffin. Light-ray operators in conformal field theory. *JHEP*, 11:102, 2018.

[53] A. Liam Fitzpatrick, Jared Kaplan, David Poland, and David Simmons-Duffin. The Analytic Bootstrap and AdS Superhorizon Locality. *JHEP*, 12:004, 2013.

[54] Zohar Komargodski and Alexander Zhiboedov. Convexity and Liberation at Large Spin. *JHEP*, 11:140, 2013.

[55] Simon Caron-Huot. Analyticity in Spin in Conformal Theories. *JHEP*, 09:078, 2017.

[56] Alexandre Homrich, David Simmons-Duffin, and Pedro Vieira. To appear.

[57] J. A. Minahan and K. Zarembo. The Bethe ansatz for N=4 superYang-Mills. *JHEP*, 03:013, 2003.

[58] Iosif Bena, Joseph Polchinski, and Radu Roiban. Hidden symmetries of the AdS(5) x S**5 superstring. *Phys. Rev. D*, 69:046002, 2004.

[59] Niklas Beisert. The SU(2|2) dynamic S-matrix. *Adv. Theor. Math. Phys.*, 12:945–979, 2008.

[60] Niklas Beisert, Burkhard Eden, and Matthias Staudacher. Transcendentality and Crossing. *J. Stat. Mech.*, 0701:P01021, 2007.

[61] Nikolay Gromov, Vladimir Kazakov, and Pedro Vieira. Exact Spectrum of Anomalous Dimensions of Planar N=4 Supersymmetric Yang-Mills Theory. *Phys. Rev. Lett.*, 103:131601, 2009.

[62] Nikolay Gromov, Vladimir Kazakov, Andrii Kozak, and Pedro Vieira. Exact Spectrum of Anomalous Dimensions of Planar N = 4 Supersymmetric Yang-Mills Theory: TBA and excited states. *Lett. Math. Phys.*, 91:265–287, 2010.

[63] Nikolay Gromov, Vladimir Kazakov, and Pedro Vieira. Exact Spectrum of Planar $\mathcal{N} = 4$ Supersymmetric Yang-Mills Theory: Konishi Dimension at Any Coupling. *Phys. Rev. Lett.*, 104:211601, 2010.

[64] Diego Bombardelli, Davide Fioravanti, and Roberto Tateo. Thermodynamic Bethe Ansatz for planar AdS/CFT: A Proposal. *J. Phys. A*, 42:375401, 2009.

[65] Gleb Arutyunov and Sergey Frolov. Thermodynamic Bethe Ansatz for the AdS(5) x S(5) Mirror Model. *JHEP*, 05:068, 2009.

[66] Benjamin Basso, Shota Komatsu, and Pedro Vieira. Structure Constants and Integrable Bootstrap in Planar N=4 SYM Theory. 5 2015.

[67] Thiago Fleury and Shota Komatsu. Hexagonalization of Correlation Functions. *JHEP*, 01:130, 2017.

[68] Thiago Fleury and Shota Komatsu. Hexagonalization of Correlation Functions II: Two-Particle Contributions. *JHEP*, 02:177, 2018.

[69] Benjamin Basso, Vasco Goncalves, and Shota Komatsu. Structure constants at wrapping order. *JHEP*, 05:124, 2017.

[70] Till Bargheer, Joao Caetano, Thiago Fleury, Shota Komatsu, and Pedro Vieira. Handling Handles: Nonplanar Integrability in $\mathcal{N} = 4$ Supersymmetric Yang-Mills Theory. *Phys. Rev. Lett.*, 121(23):231602, 2018.

[71] Benjamin Basso, Amit Sever, and Pedro Vieira. Spacetime and Flux Tube S-Matrices at Finite Coupling for N=4 Supersymmetric Yang-Mills Theory. *Phys. Rev. Lett.*, 111(9):091602, 2013.

[72] Benjamin Basso, Amit Sever, and Pedro Vieira. Space-time S-matrix and Flux tube S-matrix II. Extracting and Matching Data. *JHEP*, 01:008, 2014.

[73] Benjamin Basso, Amit Sever, and Pedro Vieira. Space-time S-matrix and Flux-tube S-matrix III. The two-particle contributions. *JHEP*, 08:085, 2014.

[74] Benjamin Basso, Amit Sever, and Pedro Vieira. Space-time S-matrix and Flux-tube S-matrix IV. Gluons and Fusion. *JHEP*, 09:149, 2014.

[75] Benjamin Basso, Joao Caetano, Lucia Cordova, Amit Sever, and Pedro Vieira. OPE for all Helicity Amplitudes. *JHEP*, 08:018, 2015.

[76] Benjamin Basso, Joao Caetano, Lucia Cordova, Amit Sever, and Pedro Vieira. OPE for all Helicity Amplitudes II. Form Factors and Data Analysis. *JHEP*, 12:088, 2015.

[77] Shota Komatsu and Yifan Wang. Non-perturbative defect one-point functions in planar $\mathcal{N} = 4$ super-Yang-Mills. *Nucl. Phys. B*, 958:115120, 2020.

[78] Yunfeng Jiang, Shota Komatsu, and Edoardo Vescovi. Exact Three-Point Functions of Determinant Operators in Planar $N = 4$ Supersymmetric Yang-Mills Theory. *Phys. Rev. Lett.*, 123(19):191601, 2019.

[79] Yunfeng Jiang, Shota Komatsu, and Edoardo Vescovi. Structure constants in $\mathcal{N} = 4$ SYM at finite coupling as worldsheet g-function. *JHEP*, 07(07):037, 2020.

[80] Frank Coronado. Bootstrapping the Simplest Correlator in Planar $\mathcal{N} = 4$ Supersymmetric Yang-Mills Theory to All Loops. *Phys. Rev. Lett.*, 124(17):171601, 2020.

[81] Frank Coronado. Perturbative four-point functions in planar $\mathcal{N} = 4$ SYM from hexagonalization. *JHEP*, 01:056, 2019.

[82] Troels Harmark and Matthias Wilhelm. Hagedorn Temperature of AdS_5/CFT_4 via Integrability. *Phys. Rev. Lett.*, 120(7):071605, 2018.

[83] Nikolay Gromov, Vladimir Kazakov, Sebastien Leurent, and Zengo Tsuboi. Wronskian Solution for AdS/CFT Y-system. *JHEP*, 01:155, 2011.

[84] Nikolay Gromov, Vladimir Kazakov, Sebastien Leurent, and Dmytro Volin. Solving the AdS/CFT Y-system. *JHEP*, 07:023, 2012.

[85] Nikolay Gromov, Vladimir Kazakov, Sebastien Leurent, and Dmytro Volin. Quantum Spectral Curve for Planar $\mathcal{N} = 4$ Super-Yang-Mills Theory. *Phys. Rev. Lett.*, 112(1):011602, 2014.

[86] Nikolay Gromov, Vladimir Kazakov, Sébastien Leurent, and Dmytro Volin. Quantum spectral curve for arbitrary state/operator in AdS_5/CFT_4. *JHEP*, 09:187, 2015.

[87] Nikolay Gromov, Fedor Levkovich-Maslyuk, and Grigory Sizov. Quantum Spectral Curve and the Numerical Solution of the Spectral Problem in AdS5/CFT4. *JHEP*, 06:036, 2016.

[88] Sergey E. Derkachov, G. P. Korchemsky, and A. N. Manashov. Separation of variables for the quantum SL(2,R) spin chain. *JHEP*, 07:047, 2003.

[89] Yoichi Kazama, Shota Komatsu, and Takuya Nishimura. A new integral representation for the scalar products of Bethe states for the XXX spin chain. *JHEP*, 09:013, 2013.

[90] Yunfeng Jiang, Shota Komatsu, Ivan Kostov, and Didina Serban. The hexagon in the mirror: the three-point function in the SoV representation. *J. Phys. A*, 49(17):174007, 2016.

[91] Yunfeng Jiang, Shota Komatsu, Ivan Kostov, and Didina Serban. Clustering and the Three-Point Function. *J. Phys. A*, 49(45):454003, 2016.

[92] Andrea Cavaglià, Nikolay Gromov, and Fedor Levkovich-Maslyuk. Quantum spectral curve and structure constants in $\mathcal{N} = 4$ SYM: cusps in the ladder limit. *JHEP*, 10:060, 2018.

[93] Nikolay Gromov, Fedor Levkovich-Maslyuk, Paul Ryan, and Dmytro Volin. Dual Separated Variables and Scalar Products. *Phys. Lett. B*, 806:135494, 2020.

[94] Andrea Cavaglià, Nikolay Gromov, and Fedor Levkovich-Maslyuk. Separation of variables and scalar products at any rank. *JHEP*, 09:052, 2019.

[95] Nikolay Gromov, Fedor Levkovich-Maslyuk, and Paul Ryan. Determinant form of correlators in high rank integrable spin chains via separation of variables. *JHEP*, 05:169, 2021.

[96] Andrea Cavaglià, Nikolay Gromov, and Fedor Levkovich-Maslyuk. Separation of variables in AdS/CFT: functional approach for the fishnet CFT. *JHEP*, 06:131, 2021.

[97] Simone Giombi and Shota Komatsu. Exact Correlators on the Wilson Loop in $\mathcal{N} = 4$ SYM: Localization, Defect CFT, and Integrability. *JHEP*, 05:109, 2018. [Erratum: JHEP 11, 123 (2018)].

[98] Simone Giombi and Shota Komatsu. More Exact Results in the Wilson Loop Defect CFT: Bulk-Defect OPE, Nonplanar Corrections and Quantum Spectral Curve. *J. Phys. A*, 52(12):125401, 2019.

[99] Simone Giombi, Shota Komatsu, and Bendeguz Offertaler. Large charges on the Wilson loop in $\mathcal{N} = 4$ SYM. Part II. Quantum fluctuations, OPE, and spectral curve. *JHEP*, 08:011, 2022.

[100] João Caetano and Shota Komatsu. Functional equations and separation of variables for exact g-function. *JHEP*, 09:180, 2020.

[101] Luis F. Alday, Burkhard Eden, Gregory P. Korchemsky, Juan Maldacena, and Emery Sokatchev. From correlation functions to Wilson loops. *JHEP*, 09:123, 2011.

[102] Luis F. Alday and Juan Martin Maldacena. Gluon scattering amplitudes at strong coupling. *JHEP*, 06:064, 2007.

[103] Nathan Berkovits and Juan Maldacena. Fermionic T-Duality, Dual Superconformal Symmetry, and the Amplitude/Wilson Loop Connection. *JHEP*, 09:062, 2008.

[104] Miguel F. Paulos, Joao Penedones, Jonathan Toledo, Balt C. van Rees, and Pedro Vieira. The S-matrix bootstrap. Part I: QFT in AdS. *JHEP*, 11:133, 2017.

[105] Riccardo Rattazzi, Vyacheslav S. Rychkov, Erik Tonni, and Alessandro Vichi. Bounding scalar operator dimensions in 4D CFT. *JHEP*, 12:031, 2008.

[106] Francesco Caracciolo and Vyacheslav S. Rychkov. Rigorous Limits on the Interaction Strength in Quantum Field Theory. *Phys. Rev. D*, 81:085037, 2010.

[107] Filip Kos, David Poland, and David Simmons-Duffin. Bootstrapping the $O(N)$ vector models. *JHEP*, 06:091, 2014.

[108] Filip Kos, David Poland, and David Simmons-Duffin. Bootstrapping Mixed Correlators in the 3D Ising Model. *JHEP*, 11:109, 2014.

[109] Sidney R. Coleman and H. J. Thun. On the Prosaic Origin of the Double Poles in the Sine-Gordon S Matrix. *Commun. Math. Phys.*, 61:31, 1978.

[110] M. Creutz. Rigorous bounds on coupling constants in two-dimensional field theories. *Phys. Rev. D*, 6:2763–2765, 1972.

[111] L. D. Landau. On analytic properties of vertex parts in quantum field theory. *Nucl. Phys.*, 13(1):181–192, 1959.

[112] David Simmons-Duffin. A Semidefinite Program Solver for the Conformal Bootstrap. *JHEP*, 06:174, 2015.

[113] Chen-Ning Yang and C. P. Yang. Thermodynamics of one-dimensional system of bosons with repulsive delta function interaction. *J. Math. Phys.*, 10:1115–1122, 1969.

[114] A. B. Zamolodchikov. Z(4) SYMMETRIC FACTORIZED S MATRIX IN TWO SPACE-TIME DIMENSIONS. *Commun. Math. Phys.*, 69:165–178, 1979.

[115] Luca Lepori, Gabor Zsolt Toth, and Gesualdo Delfino. Particle spectrum of the 3-state Potts field theory: A Numerical study. *J. Stat. Mech.*, 0911:P11007, 2009.

[116] Chang-rim Ahn. Complete S matrices of supersymmetric Sine-Gordon theory and perturbed superconformal minimal model. *Nucl. Phys. B*, 354:57–84, 1991.

[117] K. Sogo, M. Uchinami, Y. Akutsu, and M. Wadati. Classification of Exactly Solvable Two-Component Models. *Progress of Theoretical Physics*, 68(2):508–526, August 1982.

[118] Daniel Z. Freedman, Samir D. Mathur, Alec Matusis, and Leonardo Rastelli. Correlation functions in the CFT(d) / AdS(d+1) correspondence. *Nucl. Phys. B*, 546:96–118, 1999.

[119] Matthijs Hogervorst and Slava Rychkov. Radial Coordinates for Conformal Blocks. *Phys. Rev. D*, 87:106004, 2013.

[120] Miguel F. Paulos and Bernardo Zan. A functional approach to the numerical conformal bootstrap. *JHEP*, 09:006, 2020.

[121] Dalimil Mazac and Miguel F. Paulos. The analytic functional bootstrap. Part I: 1D CFTs and 2D S-matrices. *JHEP*, 02:162, 2019.

[122] Dalimil Mazac and Miguel F. Paulos. The analytic functional bootstrap. Part II. Natural bases for the crossing equation. *JHEP*, 02:163, 2019.

[123] M. Caselle, M. Hasenbusch, P. Provero, and K. Zarembo. Bound states in the 3-d Ising model and implications for QCD at finite temperature and density. *Nucl. Phys. B Proc. Suppl.*, 106:504–506, 2002.

[124] Vladimir Rosenhaus. Multipoint Conformal Blocks in the Comb Channel. *JHEP*, 02:142, 2019.

[125] David Poland, Valentina Prilepina, and Petar Tadić. The five-point bootstrap. *JHEP*, 10:153, 2023.

[126] Carlos Bercini and Diego Trancanelli. Supersymmetric integrable theories without particle production. *Phys. Rev. D*, 97(10):105013, 2018.

[127] Barak Gabai, Dalimil Mazávc, Andrei Shieber, Pedro Vieira, and Yehao Zhou. No Particle Production in Two Dimensions: Recursion Relations and Multi-Regge Limit. *JHEP*, 02:094, 2019.

[128] Anjishnu Bose, Parthiv Haldar, Aninda Sinha, Pritish Sinha, and Shaswat S. Tiwari. Relative entropy in scattering and the S-matrix bootstrap. *SciPost Phys.*, 9:081, 2020.

[129] L. Lukaszuk and A. Martin. Absolute upper bounds for pi pi scattering. *Nuovo Cim. A*, 52:122–145, 1967.

[130] Martin B Einhorn and Richard Blankenbecler. Bounds on scattering amplitudes. *Annals of Physics*, 67(2):480–517, 1971.

[131] C. Lopez. Rigorous Lower Bounds for the pi pi p-Wave Scattering Length. *Lett. Nuovo Cim.*, 13:69, 1975.

[132] B. Bonnier, C. Lopez, and G. Mennessier. Improved Absolute Bounds on the pi0 pi0 Amplitude. *Phys. Lett. B*, 60:63–66, 1975.

[133] David Poland, Slava Rychkov, and Alessandro Vichi. The Conformal Bootstrap: Theory, Numerical Techniques, and Applications. *Rev. Mod. Phys.*, 91:015002, 2019.

[134] Walter Landry and David Simmons-Duffin. Scaling the semidefinite program solver SDPB. 9 2019.

[135] David G. Luenberger. *Optimization by Vector Space Methods*. John Wiley & Sons, Inc., USA, 1st edition, 1997.

[136] Stephen Boyd and Lieven Vandenberghe. *Convex optimization*. Cambridge university press, 2004.

[137] D. Bertsekas, A. Nedic, and A. Ozdaglar. *Convex Analysis and Optimization*. Athena Scientific optimization and computation series. Athena Scientific, 2003.

[138] A. B. Zamolodchikov. Integrals of Motion and S Matrix of the (Scaled) T=T(c) Ising Model with Magnetic Field. *Int. J. Mod. Phys. A*, 4:4235, 1989.

[139] Sergei Dubovsky, Raphael Flauger, and Victor Gorbenko. Effective String Theory Revisited. *JHEP*, 09:044, 2012.

[140] Ofer Aharony and Zohar Komargodski. The Effective Theory of Long Strings. *JHEP*, 05:118, 2013.

[141] Sergei Dubovsky, Raphael Flauger, and Victor Gorbenko. Evidence from Lattice Data for a New Particle on the Worldsheet of the QCD Flux Tube. *Phys. Rev. Lett.*, 111(6):062006, 2013.

[142] Joan Elias Miró, Andrea L. Guerrieri, Aditya Hebbar, João Penedones, and Pedro Vieira. Flux Tube S-matrix Bootstrap. *Phys. Rev. Lett.*, 123(22):221602, 2019.

[143] Luis F. Alday, Davide Gaiotto, Juan Maldacena, Amit Sever, and Pedro Vieira. An Operator Product Expansion for Polygonal null Wilson Loops. *JHEP*, 04:088, 2011.

[144] Carlos Bercini, Vasco Gonçalves, and Pedro Vieira. Light-Cone Bootstrap of Higher Point Functions and Wilson Loop Duality. *Phys. Rev. Lett.*, 126(12):121603, 2021.

[145] Benjamin Basso, Lance J. Dixon, and Georgios Papathanasiou. Origin of the Six-Gluon Amplitude in Planar $N = 4$ Supersymmetric Yang-Mills Theory. *Phys. Rev. Lett.*, 124(16):161603, 2020.

[146] Miguel S. Costa, Joao Penedones, David Poland, and Slava Rychkov. Spinning Conformal Correlators. *JHEP*, 11:071, 2011.

[147] Nadav Drukker and Jan Plefka. The Structure of n-point functions of chiral primary operators in N=4 super Yang-Mills at one-loop. *JHEP*, 04:001, 2009.

[148] Luis F. Alday and Agnese Bissi. Crossing symmetry and Higher spin towers. *JHEP*, 12:118, 2017.

[149] Luis F. Alday and Agnese Bissi. Higher-spin correlators. *JHEP*, 10:202, 2013.

[150] Luis F. Alday, Davide Gaiotto, and Juan Maldacena. Thermodynamic Bubble Ansatz. *JHEP*, 09:032, 2011.

[151] Zvi Bern, Lance J. Dixon, and Vladimir A. Smirnov. Iteration of planar amplitudes in maximally supersymmetric Yang-Mills theory at three loops and beyond. *Phys. Rev. D*, 72:085001, 2005.

[152] Davide Gaiotto, Juan Maldacena, Amit Sever, and Pedro Vieira. Pulling the straps of polygons. *JHEP*, 12:011, 2011.

[153] Alexander B. Goncharov, Marcus Spradlin, C. Vergu, and Anastasia Volovich. Classical Polylogarithms for Amplitudes and Wilson Loops. *Phys. Rev. Lett.*, 105:151605, 2010.

[154] Lance J. Dixon, James M. Drummond, and Johannes M. Henn. Bootstrapping the three-loop hexagon. *JHEP*, 11:023, 2011.

[155] Daniel Parker, Adam Scherlis, Marcus Spradlin, and Anastasia Volovich. Hedgehog bases for A_n cluster polylogarithms and an application to six-point amplitudes. *JHEP*, 11:136, 2015.

[156] David Eliecer Berenstein, Richard Corrado, Willy Fischler, and Juan Martin Maldacena. The Operator product expansion for Wilson loops and surfaces in the large N limit. *Phys. Rev. D*, 59:105023, 1999.

[157] L. F. Alday, E. I. Buchbinder, and A. A. Tseytlin. Correlation function of null polygonal Wilson loops with local operators. *JHEP*, 09:034, 2011.

[158] Marco S. Bianchi. Three-point functions of twist-two operators at two loops. *Phys. Rev. D*, 105(8):086007, 2022.

[159] Niklas Beisert. The Analytic Bethe Ansatz for a Chain with Centrally Extended su(2|2) Symmetry. *J. Stat. Mech.*, 0701:P01017, 2007.

[160] Romuald A. Janik. The AdS(5) x S**5 superstring worldsheet S-matrix and crossing symmetry. *Phys. Rev. D*, 73:086006, 2006.

[161] Petr Kravchuk and David Simmons-Duffin. Counting Conformal Correlators. *JHEP*, 02:096, 2018.

[162] G. P. Korchemsky and G. Marchesini. Structure function for large x and renormalization of Wilson loop. *Nucl. Phys. B*, 406:225–258, 1993.

[163] Benjamin Basso and De-Liang Zhong. Three-point functions at strong coupling in the BMN limit. *JHEP*, 04:076, 2020.

[164] R. J. Baxter. Solvable eight vertex model on an arbitrary planar lattice. *Phil. Trans. Roy. Soc. Lond. A*, 289:315–346, 1978.

[165] A. B. Zamolodchikov. 'FISHNET' DIAGRAMS AS A COMPLETELY INTEGRABLE SYSTEM. *Phys. Lett. B*, 97:63–66, 1980.

[166] Enrico Olivucci and Pedro Vieira. Null Polygons in Conformal Gauge Theory. *Phys. Rev. Lett.*, 129(22):221601, 2022.

[167] Thiago Fleury and Vasco Goncalves. Decagon at Two Loops. *JHEP*, 07:030, 2020.

[168] Nikolay Gromov, Amit Sever, and Pedro Vieira. Tailoring Three-Point Functions and Integrability III. Classical Tunneling. *JHEP*, 07:044, 2012.

[169] Ivan Kostov. Classical Limit of the Three-Point Function of N=4 Supersymmetric Yang-Mills Theory from Integrability. *Phys. Rev. Lett.*, 108:261604, 2012.

[170] Benjamin Basso, Vasco Goncalves, Shota Komatsu, and Pedro Vieira. Gluing Hexagons at Three Loops. *Nucl. Phys. B*, 907:695–716, 2016.

[171] Burkhard Eden and Alessandro Sfondrini. Three-point functions in $\mathcal{N} = 4$ SYM: the hexagon proposal at three loops. *JHEP*, 02:165, 2016.

[172] Radu Roiban and Anastasia Volovich. Yang-Mills correlation functions from integrable spin chains. *JHEP*, 09:032, 2004.

[173] Jorge Escobedo, Nikolay Gromov, Amit Sever, and Pedro Vieira. Tailoring Three-Point Functions and Integrability. *JHEP*, 09:028, 2011.

[174] Pedro Vieira and Tianheng Wang. Tailoring Non-Compact Spin Chains. *JHEP*, 10:035, 2014.

[175] Ömer Gürdoğan and Vladimir Kazakov. New Integrable 4D Quantum Field Theories from Strongly Deformed Planar $\mathcal{N} = 4$ Supersymmetric Yang-Mills Theory. *Phys. Rev. Lett.*, 117(20):201602, 2016. [Addendum: Phys.Rev.Lett. 117, 259903 (2016)].

[176] L. D. Faddeev and G. P. Korchemsky. High-energy QCD as a completely integrable model. *Phys. Lett. B*, 342:311–322, 1995.

[177] Anatoly V. Kotikov, Adam Rej, and Stefan Zieme. Analytic three-loop Solutions for N=4 SYM Twist Operators. *Nucl. Phys. B*, 813:460–483, 2009.

[178] A. V. Belitsky. OPE for null Wilson loops and open spin chains. *Phys. Lett. B*, 709:280–284, 2012.

[179] B. Basso and A. V. Belitsky. Luescher formula for GKP string. *Nucl. Phys. B*, 860:1–86, 2012.

[180] F. A. Dolan and H. Osborn. Conformal four point functions and the operator product expansion. *Nucl. Phys. B*, 599:459–496, 2001.

[181] B. Basso and G. P. Korchemsky. Anomalous dimensions of high-spin operators beyond the leading order. *Nucl. Phys. B*, 775:1–30, 2007.

[182] Luis F. Alday, Agnese Bissi, and Tomasz Lukowski. Large spin systematics in CFT. *JHEP*, 11:101, 2015.

[183] Nikolay Gromov and Pedro Vieira. Tailoring Three-Point Functions and Integrability IV. Theta-morphism. *JHEP*, 04:068, 2014.

[184] Niklas Beisert and Matthias Staudacher. Long-range psu(2,2|4) Bethe Ansatze for gauge theory and strings. *Nucl. Phys. B*, 727:1–62, 2005.

[185] Nikolay Gromov and Fedor Levkovich-Maslyuk. Quantum Spectral Curve for a cusped Wilson line in $\mathcal{N} = 4$ SYM. *JHEP*, 04:134, 2016.

[186] Benjamin Basso, Alessandro Georgoudis, and Arthur Klemenchuk Sueiro. Structure Constants of Short Operators in Planar N=4 Supersymmetric Yang-Mills Theory. *Phys. Rev. Lett.*, 130(13):131603, 2023.

[187] Yoichi Kazama and Shota Komatsu. Three-point functions in the SU(2) sector at strong coupling. *JHEP*, 03:052, 2014.

[188] Ivan Kostov. Semi-classical scalar products in the generalised SU(2) model. *Springer Proc. Math. Stat.*, 111:87–103, 2014.

[189] Eldad Bettelheim and Ivan Kostov. Semi-classical analysis of the inner product of Bethe states. *J. Phys. A*, 47:245401, 2014.

[190] Ivan Kostov, Valentina B. Petkova, and Didina Serban. The Octagon as a Determinant. *JHEP*, 11:178, 2019.

[191] Miguel S. Costa, Vasco Goncalves, and Joao Penedones. Conformal Regge theory. *JHEP*, 12:091, 2012.

[192] Norman H. Christ, B. Hasslacher, and Alfred H. Mueller. Light cone behavior of perturbation theory. *Phys. Rev. D*, 6:3543, 1972.

[193] D. J. Gross and Frank Wilczek. Asymptotically Free Gauge Theories - I. *Phys. Rev. D*, 8:3633–3652, 1973.

[194] Howard Georgi and H. David Politzer. Electroproduction scaling in an asymptotically free theory of strong interactions. *Phys. Rev. D*, 9:416–420, 1974.

[195] John C. Collins and Davison E. Soper. Parton Distribution and Decay Functions. *Nucl. Phys. B*, 194:445–492, 1982.

[196] I. I. Balitsky and Vladimir M. Braun. Evolution Equations for QCD String Operators. *Nucl. Phys. B*, 311:541–584, 1989.

[197] E. A. Kuraev, L. N. Lipatov, and Victor S. Fadin. The Pomeranchuk Singularity in Nonabelian Gauge Theories. *Sov. Phys. JETP*, 45:199–204, 1977.

[198] I. I. Balitsky and L. N. Lipatov. The Pomeranchuk Singularity in Quantum Chromodynamics. *Sov. J. Nucl. Phys.*, 28:822–829, 1978.

[199] Alfred H. Mueller and Bimal Patel. Single and double BFKL pomeron exchange and a dipole picture of high-energy hard processes. *Nucl. Phys. B*, 425:471–488, 1994.

[200] I. Balitsky. Operator expansion for high-energy scattering. *Nucl. Phys. B*, 463:99–160, 1996.

[201] Simon Caron-Huot. When does the gluon reggeize? *JHEP*, 05:093, 2015.

[202] Simon Caron-Huot, Murat Kologlu, Petr Kravchuk, David Meltzer, and David Simmons-Duffin. Detectors in weakly-coupled field theories. *JHEP*, 04:014, 2023.

[203] Madalena Lemos, Balt C. van Rees, and Xiang Zhao. Regge trajectories for the (2, 0) theories. *JHEP*, 01:022, 2022.

[204] Ian Balitsky, Vladimir Kazakov, and Evgeny Sobko. Two-point correlator of twist-2 light-ray operators in N=4 SYM in BFKL approximation. *Nucl. Phys. B*, 993:116267, 2023.

[205] V. M. Braun, G. P. Korchemsky, and Dieter Müller. The Uses of conformal symmetry in QCD. *Prog. Part. Nucl. Phys.*, 51:311–398, 2003.

[206] Niklas Beisert. The Dilatation operator of N=4 super Yang-Mills theory and integrability. *Phys. Rept.*, 405:1–202, 2004.

[207] Matthias Staudacher. The Factorized S-matrix of CFT/AdS. *JHEP*, 05:054, 2005.

[208] Matteo Beccaria. Anomalous dimensions at twist-3 in the sl(2) sector of N=4 SYM. *JHEP*, 06:044, 2007.

[209] Juan Maldacena, Stephen H. Shenker, and Douglas Stanford. A bound on chaos. *JHEP*, 08:106, 2016.

[210] F. A. Dolan and H. Osborn. Superconformal symmetry, correlation functions and the operator product expansion. *Nucl. Phys. B*, 629:3–73, 2002.

[211] Miguel S. Costa, James Drummond, Vasco Goncalves, and Joao Penedones. The role of leading twist operators in the Regge and Lorentzian OPE limits. *JHEP*, 04:094, 2014.

[212] E. Norlund and ne Lagrange. *Lecons sur les series d'interpolation*. Gauthier-Villars, 1926.

[213] F. Aprile, J. M. Drummond, H. Paul, and M. Santagata. The Virasoro-Shapiro amplitude in $AdS_5 \times S^5$ and level splitting of 10d conformal symmetry. *JHEP*, 11:109, 2021.

[214] F. A. Dolan and H. Osborn. Conformal partial waves and the operator product expansion. *Nucl. Phys. B*, 678:491–507, 2004.

[215] Romuald A. Janik. Twist-two operators and the BFKL regime - nonstandard solutions of the Baxter equation. *JHEP*, 11:153, 2013.

[216] Mikhail Alfimov, Nikolay Gromov, and Vladimir Kazakov. QCD Pomeron from AdS/CFT Quantum Spectral Curve. *JHEP*, 07:164, 2015.

[217] L. N. Lipatov. Reggeization of the Vector Meson and the Vacuum Singularity in Nonabelian Gauge Theories. *Sov. J. Nucl. Phys.*, 23:338–345, 1976.

[218] Richard C. Brower, Joseph Polchinski, Matthew J. Strassler, and Chung-I Tan. The Pomeron and gauge/string duality. *JHEP*, 12:005, 2007.

[219] G. P. Korchemsky, J. Kotanski, and A. N. Manashov. Multi-reggeon compound states and resummed anomalous dimensions in QCD. *Phys. Lett. B*, 583:121–133, 2004.

[220] Stephen J. Parke and T. R. Taylor. Amplitude for n-gluon scattering. *Phys. Rev. Lett.*, 56:2459–2460, Jun 1986.

[221] Ruth Britto, Freddy Cachazo, Bo Feng, and Edward Witten. Direct proof of tree-level recursion relation in Yang-Mills theory. *Phys. Rev. Lett.*, 94:181602, 2005.

[222] Filip Kos, David Poland, David Simmons-Duffin, and Alessandro Vichi. Precision Islands in the Ising and $O(N)$ Models. *JHEP*, 08:036, 2016.

[223] Sachin Jain, Mangesh Mandlik, Shiraz Minwalla, Tomohisa Takimi, Spenta R. Wadia, and Shuichi Yokoyama. Unitarity, Crossing Symmetry and Duality of the S-matrix in large N Chern-Simons theories with fundamental matter. *JHEP*, 04:129, 2015.

[224] Jaume Gomis, Zohar Komargodski, and Nathan Seiberg. Phases Of Adjoint QCD_3 And Dualities. *SciPost Phys.*, 5(1):007, 2018.

[225] Simon Caron-Huot and Joshua Sandor. Conformal Regge Theory at Finite Boost. *JHEP*, 05:059, 2021.

[226] Vladimir V. Bazhanov, Sergei L. Lukyanov, and Alexander B. Zamolodchikov. Integrable structure of conformal field theory, quantum KdV theory and thermodynamic Bethe ansatz. *Commun. Math. Phys.*, 177:381–398, 1996.

[227] Vladimir V. Bazhanov, Sergei L. Lukyanov, and Alexander B. Zamolodchikov. Integrable structure of conformal field theory. 2. Q operator and DDV equation. *Commun. Math. Phys.*, 190:247–278, 1997.

[228] A. B. Zamolodchikov. From tricritical Ising to critical Ising by thermodynamic Bethe ansatz. *Nucl. Phys. B*, 358:524–546, 1991.

[229] Alexander B. Zamolodchikov and Alexei B. Zamolodchikov. Massless factorized scattering and sigma models with topological terms. *Nucl. Phys. B*, 379:602–623, 1992.

[230] P. Fendley and H. Saleur. Massless integrable quantum field theories and massless scattering in (1+1)-dimensions. In *Summer School in High-energy Physics and Cosmology (Includes Workshop on Strings, Gravity, and Related Topics 29-30 Jul 1993)*, pages 301–332, 9 1993.

[231] Kevin Costello, Edward Witten, and Masahito Yamazaki. Gauge Theory and Integrability, I. *ICCM Not.*, 06(1):46–119, 2018.

[232] Kevin Costello, Edward Witten, and Masahito Yamazaki. Gauge Theory and Integrability, II. *ICCM Not.*, 06(1):120–146, 2018.

[233] Kevin Costello and Masahito Yamazaki. Gauge Theory And Integrability, III. 8 2019.

[234] Kevin Costello, Davide Gaiotto, and Junya Yagi. Q-operators are 't Hooft lines. 3 2021.

[235] James D. Bjorken and Sidney D. Drell. Relativistic quantum fields. 1965.

[236] Steven Weinberg. *The Quantum theory of fields. Vol. 1: Foundations.* Cambridge University Press, 6 2005.

[237] M. Caselle, G. Delfino, P. Grinza, O. Jahn, and N. Magnoli. Potts correlators and the static three-quark potential. *J. Stat. Mech.*, 0603:P03008, 2006.

[238] A. B. Zamolodchikov. Exact Two Particle s Matrix of Quantum Sine-Gordon Solitons. *Pisma Zh. Eksp. Teor. Fiz.*, 25:499–502, 1977.

[239] M. Karowski. On the Bound State Problem in (1+1)-dimensional Field Theories. *Nucl. Phys. B*, 153:244–252, 1979.

[240] R. Shankar and Edward Witten. The S Matrix of the Supersymmetric Nonlinear Sigma Model. *Phys. Rev. D*, 17:2134, 1978.

[241] Kareljan Schoutens. Supersymmetry and Factorizable Scattering. *Nucl. Phys. B*, 344:665–695, 1990.

[242] N. Reshetikhin and F. Smirnov. Hidden Quantum Group Symmetry and Integrable Perturbations of Conformal Field Theories. *Commun. Math. Phys.*, 131:157–178, 1990.

[243] Denis Bernard and Andre Leclair. Residual Quantum Symmetries of the Restricted Sine-Gordon Theories. *Nucl. Phys. B*, 340:721–751, 1990.

[244] Vasco Gonçalves, Raul Pereira, and Xinan Zhou. $20'$ Five-Point Function from $AdS_5 \times S^5$ Supergravity. *JHEP*, 10:247, 2019.

[245] Alessandro Georgoudis, Vasco Goncalves, and Raul Pereira. Konishi OPE coefficient at the five loop order. *JHEP*, 11:184, 2018.

[246] Gabriel Francisco Cuomo, Denis Karateev, and Petr Kravchuk. General Bootstrap Equations in 4D CFTs. *JHEP*, 01:130, 2018.

[247] Burkhard Eden. Three-loop universal structure constants in N=4 susy Yang-Mills theory. 7 2012.

[248] F. A. Dolan and H. Osborn. Conformal partial wave expansions for N=4 chiral four point functions. *Annals Phys.*, 321:581–626, 2006.

[249] Yunfeng Jiang and Andrei Petrovskii. Diagonal form factors and hexagon form factors. *JHEP*, 07:120, 2016.

[250] Christian Marboe and Dmytro Volin. Fast analytic solver of rational Bethe equations. *J. Phys. A*, 50(20):204002, 2017.

[251] M. Beccaria, A. V. Belitsky, A. V. Kotikov, and S. Zieme. Analytic solution of the multiloop Baxter equation. *Nucl. Phys. B*, 827:565–606, 2010.

[252] Gleb Arutyunov, Sergey Frolov, and Matthias Staudacher. Bethe ansatz for quantum strings. *JHEP*, 10:016, 2004.

[253] Sergey E. Derkachov, G. P. Korchemsky, and A. N. Manashov. Evolution equations for quark gluon distributions in multicolor QCD and open spin chains. *Nucl. Phys. B*, 566:203–251, 2000.

[254] Vladimir M. Braun, Sergey E. Derkachov, G. P. Korchemsky, and A. N. Manashov. Baryon distribution amplitudes in QCD. *Nucl. Phys. B*, 553:355–426, 1999.

[255] Vladimir M. Braun, Sergey E. Derkachov, and A. N. Manashov. Integrability of three particle evolution equations in QCD. *Phys. Rev. Lett.*, 81:2020–2023, 1998.

[256] Amit Sever, Pedro Vieira, and Tianheng Wang. From Polygon Wilson Loops to Spin Chains and Back. *JHEP*, 12:065, 2012.

[257] A. V. Belitsky, V. M. Braun, A. S. Gorsky, and G. P. Korchemsky. Integrability in QCD and beyond. *Int. J. Mod. Phys. A*, 19:4715–4788, 2004.

[258] Giuseppe Mussardo. *Statistical field theory: an introduction to exactly solved models in statistical physics*. Oxford Univ. Press, New York, NY, 2010.

[259] G. Mack. All unitary ray representations of the conformal group SU(2,2) with positive energy. *Commun. Math. Phys.*, 55:1, 1977.

APPENDICES

Appendix A

Appendix: The S-matrix Bootstrap: Multiple Amplitudes

A.1 Two dimensions and higher dimensional kinematics

The Mandelstam plane provides us with a very useful depiction of the (real sections of the) interrelations between the three Mandelstam variables u, s, t. The first important object in this plane is the Mandelstam *triangle*.

Consider a two-to-two process involving particles with momenta p_a, p_b, p_c, p_d associated to particles of mass m_a, m_b, m_c, m_d. We define the three Mandelstam invariants $s = (p_a + p_b)^2$, $t = (p_a + p_c)^2$ and $u = (p_a + p_d)^2$. If particles p_a, p_b are the two incoming particles then $\sqrt{s}$ is the centre of mass energy of the scattering process. The same is true if the incoming particles are particles p_c, p_d. In either of these cases the process can only be physical if we have enough energy to produce both the initial and final state, so for $s \geq \max((m_a+m_b)^2, (m_c+m_d)^2)$. Of course, the same scattering amplitudes can describe other channels.[1] If p_a, p_c (or p_b, p_d) are the two incoming particles then $\sqrt{t}$ is the centre of mass energy of the scattering process and similarly for u so the physical conditions in those cases would read $t \geq \max((m_a + m_c)^2, (m_b + m_d)^2)$ and $u \geq \max((m_a + m_d)^2, (m_b + m_c)^2)$. The three inequalities are depicted by the shaded pink regions in figure A.1. The white region is the Mandelstam triangle.

To be in a physical region we thus need to be in the pink region. This is necessary but not sufficient. We need to have enough energy but we also need to scatter at a real angle. For instance for incoming particles p_a, p_b we can easily compute the scattering angle to find

$$\cos(\theta_{ab}) = \frac{(s + m_a^2 - m_b^2)(s + m_c^2 - m_d^2) + 2s(t - m_a^2 - m_c^2)}{\sqrt{((s - m_a^2 - m_b^2)^2 - 4m_a^2 m_b^2)((s - m_c^2 - m_d^2)^2 - 4m_c^2 m_d^2)}}\,. \tag{A.1}$$

For any left hand side between -1 and $+1$ corresponding to a real angle, and for any s

[1] To describe other channels we can either swap the masses and always keep s to the be the center of mass energy (as in the main text) or leave the masses untouched but reinterpret which Mandelstam invariant corresponds to the center of mass energy (as in this appendix). It is very simple (and very instructive) to go between these active/passive viewpoints.

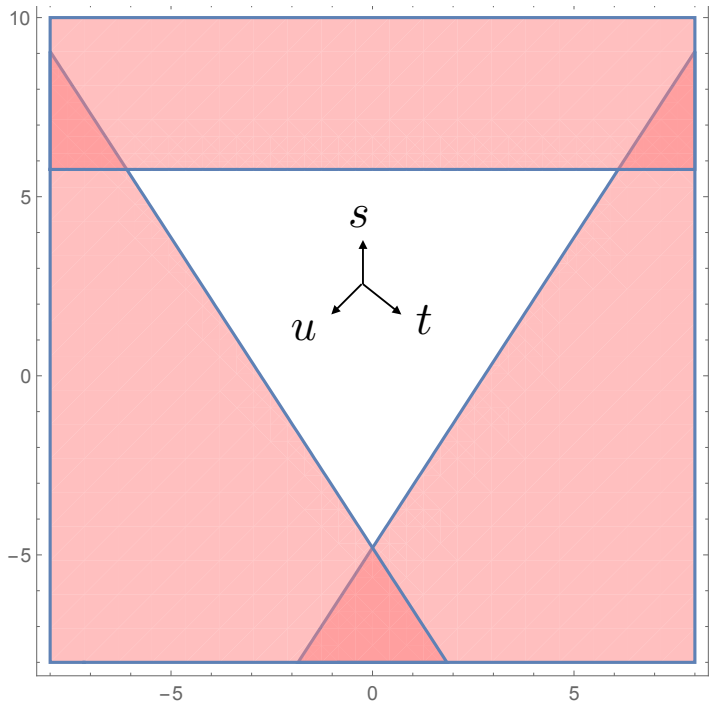

Figure A.1: The Mandelstam triangle is the region where all Mandelstam variables are below their corresponding two-particle threshold: $s < \max((m_a+m_b)^2,(m_c+m_d)^2) \wedge t < \max((m_a+m_c)^2,(m_b+m_d)^2) \wedge u < \max((m_a+m_d)^2,(m_b+m_c)^2)$ represented by the white region in this figure. (The y axis is s and the x axis is given by $x = (s+2t-m_a^2-m_b^2-m_c^2-m_d^2)/\sqrt{3}$ as in the next figures.)

in the physical range this equation determines a physical t. (Of course, $u = m_a^2+m_b^2+m_c^2+m_d^2-s-t$ is automatically fixed.) The set of physical s and t determined in this way determine the physical region in the s-channel. The other channels are treated similarly with

$$\cos(\theta_{ac}) = \text{RHS of (A.1)}_{m_b\leftrightarrow m_c,\, s\leftrightarrow t} \qquad , \qquad \cos(\theta_{ad}) = \text{RHS of (A.1)}_{m_b\leftrightarrow m_d,\, s\leftrightarrow u} \tag{A.2}$$

If all masses are equal (to m) then (A.1) reduces to the famous relation

$$\cos(\theta) = 1 - \frac{2t}{4m^2-s}\,. \tag{A.3}$$

so that the physical region in the s-channel is simply $s > 4m^2$ and $4m^2 - s \leq t \leq 0$ represented by the top blue region in figure A.2a. In two dimensions the angle ought to be 0 or π so that we have either $t = 0$ or $t = 4m^2 - s$, i.e. $u = 0$. These two conditions ($t = 0$ and $u = 0$) are equivalent if the external particles are indistinguishable so in that case we can pick either; in the main text we took $u = 0$. Note that these two conditions are nothing but the boundary of the darker blue region. Similarly we could study all other channels which we can simply obtain by relabelling the Mandelstam variables in (A.3). The two extra physical regions are the other two blue regions in the same figure A.2a. Note that

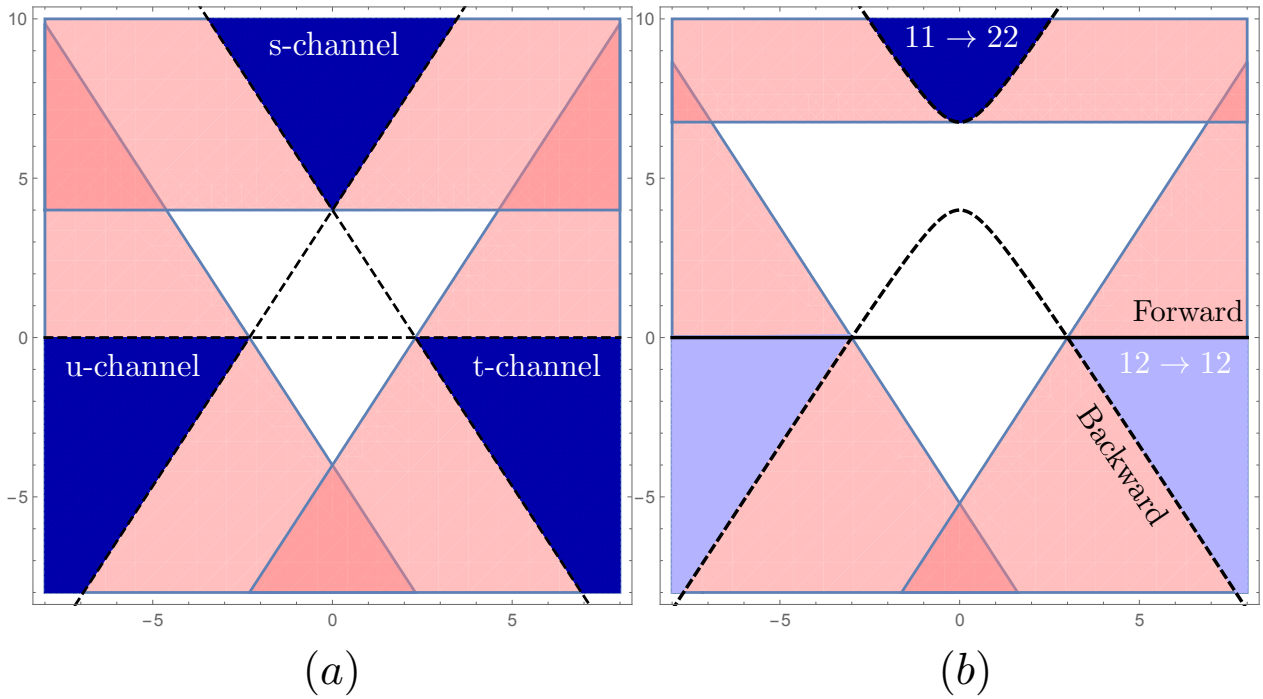

Figure A.2: (a) Physical regions (in dark blue) for a two-to-two process with all external particles of identical mass. The boundary of these regions correspond to scattering angle 0 or π and can thus also be identified with the physical scattering 'regions" (or better scattering lines) in two dimensions. (b) Physical regions for a process where the masses are equal in pairs. The darker blue region is the process $m_1 m_1 \to m_2 m_2$ while the two lighter regions (which are equivalent for identical particles) correspond to the $m_1 m_2 \to m_1 m_2$ channels. The boundary of these regions are again the two dimensional physical lines. The boundaries of the lighter blue regions are not identical: one corresponds to forward scattering; the other to backward scattering.

the boundary of all these blue regions can be written concisely as $stu = 0$ which is nothing but the constraint obtained in the main text from the two dimensional constraint (2.9) and represented by the dashed lines in figure A.2a.

Finally, we come to the more interesting case where the external masses are only pairwise equal: $m_a = m_b = m_1$ and $m_c = m_d = m_2$. This same configuration can describe the $11 \to 22$ process (with $\sqrt{s}$ being the centre of mass energy), and the $12 \to 12$ processes (with $\sqrt{t}$ being the centre of mass energy). For the first case we use (A.1) to get

$$\cos(\theta_{11\to 22}) = \frac{-2m_1^2 - 2m_2^2 + s + 2t}{\sqrt{(s-4m_1^2)\,(s-4m_2^2)}}\,. \tag{A.4}$$

The physical region corresponding to $-1 \leq \cos\theta_{11\to 22} \leq +1$ is now a more interesting curved region, represented by the darker blue region in figure A.2b. Again, in two dimensions we can only have backward or forward scattering so t must saturate one of these inequalities. If the particles of the same mass are indistinguishable then both solutions are

equivalent as before. We can thus take $\theta_{11\to 22} = 0$ without loss of generality leading to

$$t, u = m_1^2 + m_2^2 - \frac{s}{2} \pm \frac{1}{2}\sqrt{(s-4m_1^2)(s-4m_2^2)}\,. \tag{A.5}$$

and reproduce in this way the results below (2.11) in the main text. In the t-channel particles $m_a = m_1, m_c = m_2$ are incoming so we are scattering a odd particle against an even particle. Then we use the first relation in (A.2) which now reads

$$\cos(\theta_{12\to 12}) = 1 + \frac{2ts}{-2m_1^2\,(m_2^2+t) + (m_2^2-t)^{\,2} + m_1^4} \tag{A.6}$$

Note that in our convention it is $\sqrt{t}$ (and not $\sqrt{s}$) who is the center of mass energy in this channel.[2] The physical region corresponding to $|\cos(\theta_{12\to 12})| \leq 1$ is now represented by the lighter blue region in figure A.2b. The two dimensional conditions that the angle is 0 or π are now quite different. The former corresponds to forward scattering and is obtained by $s = 0$ (obtained by equating the RHS of (A.6) to $+1$) while the later corresponds to backward scattering and yields the more involved relation

$$s = 2\left(m_1^2 + m_2^2\right) - t - \frac{(m_1^2 - m_2^2)^{\,2}}{t} \tag{A.7}$$

(obtained by equating the RHS of (A.6) to -1.) Note that this relation is nothing but (A.5) if we solve for s. In other words, these two configurations are simply related by crossing symmetry $s \leftrightarrow t$.

To summarize: the boundary of the physical regions are now given by the black solid line and by the black dashed curve in figure A.2b. Crossing $u \leftrightarrow t$ at $s = 0$ relates the left to the right of the straight line – leading to condition (2.19). Crossing symmetry also relates the top to the bottom branch of the hyperbolic looking curve – reflected in equation (2.20). In two dimensions these two curves (the hyperbola and the straight line) are independent while in higher dimensions they are smoothly connected (by moving in angle space).

A.2 Unitarity and final state probabilities

The S-matrix is defined by the expansion of in-states in terms of out-states

$$|A\rangle_{\text{in}} = \sum_B S_{A\to B}|B\rangle_{\text{out}}\,. \tag{A.8}$$

The in-states and the out-states are both a complete basis of the Hilbert space. Let us start by discussing the physical meaning of the diagonal unitarity equations (2.22) and (2.24). These follow from the statement that the state $|A\rangle_{\text{in}}$ above is normalized. However, due to the continuum of states this is a bit subtle. The trick is to contract the state with

[2]Recall footnote 1 when comparing the results that follow to the main text.

itself but with different momenta

$$ {}_{\rm in}\langle A'|A\rangle_{\rm in} = \sum_B \sum_{B'} S_{A\to B} S^*_{A'\to B'}\ {}_{\rm out}\langle B'|B\rangle_{\rm out}\,. \tag{A.9}$$

Here, the state $|A'\rangle_{\rm in}$ represents a state with the same particle content but different momenta. We use the standard normalization for the inner products:

$$ {}_{\rm out}\langle C|B\rangle_{\rm out} = {}_{\rm in}\langle C|B\rangle_{\rm in} = \delta_{B,C} \prod_{i\in B} 2E_i 2\pi\delta(p_i^B - p_i^C)\,, \tag{A.10}$$

where the product runs over each particle in the state $|B\rangle_{\rm in}$. Unitarity then reads

$$ 1 = \sum_B |S_{A\to B}|^2 \mathcal{J}_{A,B}\,, \tag{A.11}$$

where $\mathcal{J}_{A,B}$ is the jacobian defined by

$$ {}_{\rm out}\langle B'|B\rangle_{\rm out} = \mathcal{J}_{A,B}\ {}_{\rm in}\langle A'|A\rangle_{\rm in}\,. \tag{A.12}$$

The natural physical interpretation is that

$$ P_{A\to B} = |S_{A\to B}|^2 \mathcal{J}_{A,B} \tag{A.13}$$

is the probability of the in-state $|A\rangle_{\rm in}$ end up in the out-state $|B\rangle_{\rm out}$.

For two particle states $|A\rangle_{\rm in} = |12\rangle_{\rm in}$ and $|B\rangle_{\rm out} = |34\rangle_{\rm out}$, equation (A.12) reduces to

$$ E_3E_4\delta(p_3 - p_3')\delta(p_4 - p_4') = \mathcal{J}_{12,34} E_1E_2\delta(p_1 - p_1')\delta(p_2 - p_2')\,, \tag{A.14}$$

with $E_i = \sqrt{m_i^2 + p_i^2}$ and

$$ p_1 + p_2 = p_3 + p_4\,, \qquad E_1 + E_2 = E_3 + E_4 = \sqrt{s}\,, \tag{A.15}$$

$$ p_1' + p_2' = p_3' + p_4'\,, \qquad E_1' + E_2' = E_3' + E_4'\,. \tag{A.16}$$

This gives

$$ \mathcal{J}_{12,34} = \frac{\sqrt{s-(m_3-m_4)^2}\sqrt{s-(m_3+m_4)^2}}{\sqrt{s-(m_1-m_2)^2}\sqrt{s-(m_1+m_2)^2}} = \frac{\rho_{12}^2}{\rho_{34}^2}\,. \tag{A.17}$$

We conclude that, for two particle states, the transition probabilities are given by

$$ P_{12\to 34} = |S_{12\to 34}|^2 \frac{\rho_{12}^2}{\rho_{34}^2}\,. \tag{A.18}$$

For example, for the initial state $|11\rangle_{\rm in}$, we can write

$$ |S_{11\to 11}|^2 + |S_{11\to 22}|^2 \frac{\sqrt{s-4m_2^2}}{\sqrt{s-4m_1^2}} = 1 - P_{11\to(N\geq 3\,\text{particles})}\,. \tag{A.19}$$

This equation is equivalent to (2.22) in the energy range

$$\max(2m_1, 2m_2) < \sqrt{s} < \min(3m_2, 2m_1 + m_2) \tag{A.20}$$

where only 2 particle states are available. To show this we contract (A.8) with a generic out-state ${}_{\rm out}\langle C|$, to find

$${}_{\rm out}\langle C|A\rangle_{\rm in} = \sum_B S_{A\to B}\ {}_{\rm out}\langle C|B\rangle_{\rm out}\,, \tag{A.21}$$

and use the standard definition of the amplitude M:

$${}_{\rm out}\langle C|A\rangle_{\rm in} = {}_{\rm in}\langle C|A\rangle_{\rm in} + i(2\pi)^2\delta^{(2)}(P_C - P_A)\, M_{A\to C}\,, \tag{A.22}$$

where P_A denotes the total momentum of the state $|A\rangle_{\rm in}$. This relates S with M. In the particular case of two particle states one finds

$$S_{12\to 34} = \delta_{12,34} + \frac{iM_{12\to 34}}{2\sqrt{s-(m_3-m_4)^2}\sqrt{s-(m_3+m_4)^2}} = \delta_{12,34} + i\rho_{34}^2 M_{12\to 34}\,, \tag{A.23}$$

where the first term is present (and equal to 1) if and only if the initial and final states are the same. This allows us to rewrite (A.19) in terms of M,

$$2{\rm Im}M_{11\to 11} = \rho_{11}^2|M_{11\to 11}|^2 + \rho_{22}^2|M_{11\to 22}|^2 + \frac{P_{11\to(N\geq 3\,\text{particles})}}{\rho_{11}^2}\,, \tag{A.24}$$

which should be compared with (2.22). Notice that the physical derivation given here is not valid for $2\min(m_1, m_2) < \sqrt{s} < 2\max(m_1, m_2)$ because the two particle state of the heavier particle is not available. This is the regime of extended unitarity where we must use (2.22).

There is also a more intuitive derivation of the full matrix form of the unitarity constraints (2.27). Consider the $\mathbb{Z}_2$ even sector for simplicity. The matrix of inner products of the states $\{|11\rangle_{\rm in}, |22\rangle_{\rm in}, |11\rangle_{\rm out}, |22\rangle_{\rm out}\}$:

$$\begin{array}{c} \\ {}_{\rm in}\langle 11| \\ {}_{\rm in}\langle 22| \\ {}_{\rm out}\langle 11| \\ {}_{\rm out}\langle 22| \end{array} \begin{array}{c} \begin{array}{cccc} |11\rangle_{\rm in} & |22\rangle_{\rm in} & |11\rangle_{\rm out} & |22\rangle_{\rm out} \end{array} \\ \begin{pmatrix} {}_{\rm in}\langle 11|11\rangle_{\rm in} & {}_{\rm in}\langle 11|22\rangle_{\rm in} & {}_{\rm in}\langle 11|11\rangle_{\rm out} & {}_{\rm in}\langle 11|22\rangle_{\rm out} \\ {}_{\rm in}\langle 22|11\rangle_{\rm in} & {}_{\rm in}\langle 22|22\rangle_{\rm in} & {}_{\rm in}\langle 22|11\rangle_{\rm out} & {}_{\rm in}\langle 22|22\rangle_{\rm out} \\ {}_{\rm out}\langle 11|11\rangle_{\rm in} & {}_{\rm out}\langle 11|22\rangle_{\rm in} & {}_{\rm out}\langle 11|11\rangle_{\rm out} & {}_{\rm out}\langle 11|22\rangle_{\rm out} \\ {}_{\rm out}\langle 22|11\rangle_{\rm in} & {}_{\rm out}\langle 22|22\rangle_{\rm in} & {}_{\rm out}\langle 22|11\rangle_{\rm out} & {}_{\rm out}\langle 22|22\rangle_{\rm out} \end{pmatrix} \end{array} \tag{A.25}$$

must be positive semi-definite. In fact, for the range of energies (A.20) where there are only two particle states, the rank of this matrix must be 2 because both the in and the out states are complete basis. This is a very intuitive way to derive the unitary constraints. However, one must be careful with Jacobian factors that relate different delta-functions. Factoring out ${}_{\rm in}\langle 11|11\rangle_{\rm in}$ and using (A.8) and (A.12), we can define a positive semi-definite

matrix (without delta-functions)

$$\begin{array}{c} \\ \langle 11|_{\rm in} \\ \langle 22|_{\rm in} \\ \langle 11|_{\rm out} \\ \langle 22|_{\rm out} \end{array} \begin{array}{c} \begin{array}{cccc} |11\rangle_{\rm in} & |22\rangle_{\rm in} & |11\rangle_{\rm out} & |22\rangle_{\rm out} \end{array} \\ \begin{pmatrix} 1 & 0 & S^*_{11\to 11} & \frac{\rho_{11}^2}{\rho_{22}^2} S^*_{11\to 22} \\ 0 & \frac{\rho_{11}^2}{\rho_{22}^2} & S^*_{22\to 11} & \frac{\rho_{11}^2}{\rho_{22}^2} S^*_{22\to 22} \\ S_{11\to 11} & S_{22\to 11} & 1 & 0 \\ \frac{\rho_{11}^2}{\rho_{22}^2} S_{11\to 22} & \frac{\rho_{11}^2}{\rho_{22}^2} S_{22\to 22} & 0 & \frac{\rho_{11}^2}{\rho_{22}^2} \end{pmatrix} \end{array} \tag{A.26}$$

It is convenient to rescale the states $|22\rangle \to \frac{\rho_{22}}{\rho_{11}}|22\rangle$ so that all diagonal entries become 1. This leads to the following positive semi-definite matrix:

$$\mathbb{V} = \begin{array}{c} \\ \langle 11|_{\rm in} \\ \frac{\rho_{22}}{\rho_{11}}\langle 22|_{\rm in} \\ \langle 11|_{\rm out} \\ \frac{\rho_{22}}{\rho_{11}}\langle 22|_{\rm out} \end{array} \begin{array}{c} \begin{array}{cccc} |11\rangle_{\rm in} & \frac{\rho_{22}}{\rho_{11}}|22\rangle_{\rm in} & |11\rangle_{\rm out} & \frac{\rho_{22}}{\rho_{11}}|22\rangle_{\rm out} \end{array} \\ \begin{pmatrix} 1 & 0 & S^*_{11\to 11} & \frac{\rho_{11}}{\rho_{22}} S^*_{11\to 22} \\ 0 & 1 & \frac{\rho_{22}}{\rho_{11}} S^*_{22\to 11} & S^*_{22\to 22} \\ S_{11\to 11} & \frac{\rho_{22}}{\rho_{11}} S_{22\to 11} & 1 & 0 \\ \frac{\rho_{11}}{\rho_{22}} S_{11\to 22} & S_{22\to 22} & 0 & 1 \end{pmatrix} \end{array} \tag{A.27}$$

Notice that using (A.23), the 4×4 matrix $\mathbb{V}$ can be written as

$$\mathbb{V} = \begin{bmatrix} \mathbb{I} & \mathbb{S}^\dagger \\ \mathbb{S} & \mathbb{I} \end{bmatrix}, \qquad \mathbb{S} = \mathbb{I} + i\rho\mathbb{M}\rho \tag{A.28}$$

where $\mathbb{M}$ and ρ are the 2×2 matrices defined in (2.27). We will now show that the condition $\mathbb{V} \succeq 0$ is equivalent to (2.27) for $\sqrt{s} > 2\max(m_1, m_2)$. First notice that the eigenvalues of the hermitian matrix $\mathbb{I} - \mathbb{V}$ take the form $(-\lambda_2, -\lambda_1, \lambda_1, \lambda_2)$.[3] Then, the condition $\mathbb{V} \succeq 0$ implies that $\lambda_i^2 < 1$. On the other hand, if we compute explicitly the square of $\mathbb{I} - \mathbb{V}$, we find

$$(\mathbb{I} - \mathbb{V})^2 = \begin{bmatrix} \mathbb{S}^\dagger\mathbb{S} & 0 \\ 0 & \mathbb{S}\mathbb{S}^\dagger \end{bmatrix}. \tag{A.29}$$

Therefore, the eigenvalues of $\mathbb{S}^\dagger\mathbb{S}$ must be less than 1. Equivalently, we can say that

$$\mathbb{I} - \mathbb{S}^\dagger\mathbb{S} = \mathbb{I} - (\mathbb{I} - i\rho\mathbb{M}^\dagger\rho)(\mathbb{I} + i\rho\mathbb{M}\rho) = \rho\left(2{\rm Im}\mathbb{M} - \mathbb{M}^\dagger\rho^2\mathbb{M}\right)\rho \succeq 0 \tag{A.30}$$

and (2.27) follows.[4] In the extended unitarity region $2\min(m_1, m_2) < \sqrt{s} < 2\max(m_1, m_2)$ this derivation does not apply but we can still use (2.27).

A.2.1 Bounding Im$M_{11\to 22}$

The discontinuity of the amplitude $M_{11\to 22}$ does not have well defined sign. Furthermore, in the region $2\min(m_1, m_2) < \sqrt{s} < 2\max(m_1, m_2)$ below the physical regime, one could worry that the discontinuity could be very large and lead to screening. However, the

[3] It is easy to see that the characteristic polynomial $\det(\mathbb{I} - \mathbb{V} - x\mathbb{I})$ is an even function of x.

[4] If a matrix $\rho\mathbb{X}\rho \succeq 0$ then $\mathbb{X} \succeq 0$. This follows from the fact that if $u^\dagger\rho\mathbb{X}\rho u \geq 0$ for any vector u then $v^\dagger\mathbb{X}v \geq 0$ for any vector v (just choose $u = \rho^{-1}v$).

generalized unitarity equations (2.22)-(2.24) forbid this phenomena in the range of masses we consider.

For $2\min(m_1, m_2) < \sqrt{s} < 2\max(m_1, m_2)$, equations (2.22-2.24) reduce to

$$2\text{Im}M_{11\to 11} = \rho_{\ell\ell}^2 \left|M_{11\to\ell\ell}\right|^2 \tag{A.31}$$

$$2\text{Im}M_{11\to 22} = \rho_{\ell\ell}^2 M_{22\to\ell\ell} M_{11\to\ell\ell}^* \tag{A.32}$$

$$2\text{Im}M_{22\to 22} = \rho_{\ell\ell}^2 \left|M_{22\to\ell\ell}\right|^2 \tag{A.33}$$

where the label $\ell = 1$ or $\ell = 2$ stands for the lightest particle. Taking the modulus square of equation (A.32) and using the other two equations, we find

$$|\text{Im}M_{11\to 22}|^2 = \text{Im}M_{11\to 11}\text{Im}M_{22\to 22} \tag{A.34}$$

Therefore the size of $\text{Im}M_{11\to 22}$ is related to the positive discontinuities $\text{Im}M_{11\to 11}$ and $\text{Im}M_{22\to 22}$, which for this reason are bounded. In fact, in our numerical procedure we impose unitarity as the set of inequalities (2.27), which in particular implies

$$\text{Im}\mathbb{M} \succeq 0\,. \tag{A.35}$$

This leads to

$$\det \text{Im}\mathbb{M} \geq 0 \qquad \Leftrightarrow \qquad |\text{Im}M_{11\to 22}|^2 \leq \text{Im}M_{11\to 11}\text{Im}M_{22\to 22} \tag{A.36}$$

which bounds $\text{Im}M_{11\to 22}$ in our setup.

A.2.2 Phase shifts

In the $\mathbb{Z}_2$ even sector, it is trivial to define diagonal phase shifts

$$S_{11\to 11}(s) = e^{2i\delta_{11}(s)}\,, \qquad\qquad S_{22\to 22}(s) = e^{2i\delta_{22}(s)}\,. \tag{A.37}$$

The $\mathbb{Z}_2$ odd sector is slightly more interesting. In this sector, it is convenient to use states of definite parity,

$$|12\rangle^{\pm} = \frac{1}{\sqrt{2}}\left(|12\rangle \pm |21\rangle\right)\,. \tag{A.38}$$

Then, we define the phase shifts by

$$e^{2i\delta_{12}^{\pm}} \equiv {}^{\pm}_{\text{out}}\langle 12|12\rangle^{\pm}_{\text{in}} = S_{12\to 12}^{\text{Forward}} \pm S_{12\to 12}^{\text{Backward}} = 1 + i\rho_{12}^2\left(M_{12\to 12}^{\text{Forward}} \pm M_{12\to 12}^{\text{Backward}}\right)\,. \tag{A.39}$$

In our numerical algorithm, we impose unitarity in the odd sector by the following positive semi-definite condition

$$2\text{Im}\tilde{\mathbb{M}} \succeq \rho_{12}^2 \tilde{\mathbb{M}}^{\dagger}\tilde{\mathbb{M}}, \qquad \tilde{\mathbb{M}} = \begin{bmatrix} M_{12\to 12}^{\text{Forward}} & M_{12\to 12}^{\text{Backward}} \\ M_{12\to 12}^{\text{Backward}} & M_{12\to 12}^{\text{Forward}} \end{bmatrix}\,, \qquad s > (m_1 + m_2)^2\,. \tag{A.40}$$

It is instructive to see what this implies for the phase shifts $\delta_{12}^{\pm}$. Using (A.39), we conclude

that

$$\left|e^{2i\delta_{12}^{\pm}(s)}\right|^2 = 1 - \rho_{12}^2\,(a \pm b)\ , \tag{A.41}$$

where

$$\begin{bmatrix} a & b \\ b & a \end{bmatrix} = 2\mathrm{Im}\tilde{\mathbb{M}} - \rho_{12}^2\tilde{\mathbb{M}}^\dagger\tilde{\mathbb{M}} \succeq 0\,. \tag{A.42}$$

Thus $|b| \leq a$ and we recover the usual unitarity inequality for the phase shifts

$$\left|e^{2i\delta_{12}^{\pm}(s)}\right|^2 \leq 1\,, \qquad\qquad s > (m_1+m_2)^2\,. \tag{A.43}$$

A.3 Analytic upper bound on g_{222}^2

The goal of this appendix is to prove that (2.4) is the amplitude with maximal coupling g_{222}^2 compatible with crossing symmetry and unitarity. To this end, it is convenient to define

$$q(s) = -S_{22\to22}(s)\frac{h_{22}(s)-h_{22}(m_2^2)}{h_{22}(s)+h_{22}(m_2^2)}\frac{h_{22}(s)-h_{22}(4m_1^2)}{h_{22}(s)+h_{22}(4m_1^2)} \tag{A.44}$$

such that

$$q(s) = q(4m_2^2 - s)\,, \tag{A.45}$$

$$|q(s)|^2 \leq 1\,, \qquad\qquad s > 4m_2^2\,, \tag{A.46}$$

and

$$q(m_2^2) = \frac{g_{222}^2\left(\sqrt{3}m_2^2 - 4m_1\sqrt{m_2^2-m_1^2}\right)^2}{12\sqrt{3}m_2^4\,(4m_1^2-3m_2^2)\,(4m_1^2-m_2^2)}\,. \tag{A.47}$$

Furthermore, $q(s)$ is analytic in the s-plane minus the s-channel cut $(4m_1^2, +\infty)$ and the t-channel cut $(-\infty, 4m_2^2 - 4m_1^2)$. In the extended unitarity region $4m_1^2 > s > 4m_2^2$, we have [5]

$$\mathrm{Im}\,q(s) = -\frac{\mathrm{Im}M_{22\to22}(s)}{2h_{22}(s)}\frac{h_{22}(s)-h_{22}(m_2^2)}{h_{22}(s)+h_{22}(m_2^2)}\frac{h_{22}(s)-h_{22}(4m_1^2)}{h_{22}(s)+h_{22}(4m_1^2)} \leq 0\,, \tag{A.48}$$

where we assumed $m_1^2 < m_2^2 < \frac{4}{3}m_1^2$. We conclude that maximizing g_{222}^2 is equivalent to maximizing $q(m_2^2)$ subject to $q(s) = q(4m_2^2 - s)$, $\mathrm{Im}\,q(s) \leq 0$ for $4m_1^2 > s > 4m_2^2$ and $|q(s)|^2 \leq 1$ for $s > 4m_2^2$.

To prove that the optimal solution is given by $q(s) = 1$ it is useful to change to the coordinate

$$z(s) = \frac{h_{22}(m_2^2)-h_{22}(s)}{h_{22}(m_2^2)+h_{22}(s)}\,, \tag{A.49}$$

such that the unit disk $|z| < 1$ covers (the half $\mathrm{Re}\,s > 2m_2^2$ of) the physical sheet (see figure 1 of [10] for more details). In these coordinates, the optimization problem translates to maximizing $q(z=0)$ subject to $|q(z)| \leq 1$ for $|z| = 1$ and $\mathrm{Im}\,q(z) \leq 0$ for $0 < z(4m_1^2) \equiv z_0 < z < 1$, with $q(z)$ analytic on the unit disk minus the cut from z_0 to 1. Then Cauchy's

[5] Recall that $S_{22\to22}(s) = 1 + \frac{M_{22\to22}(s)}{2h_{22}(s)}$.

theorem leads to

$$q(0) = \frac{1}{2\pi i}\oint_0 \frac{dz}{z} q(z) = \frac{1}{\pi}\int_{z_0}^{1} \frac{dz}{z} \mathrm{Im}\, q(z) + \frac{1}{2\pi}\int_0^{2\pi} d\theta\, q(z = e^{i\theta})\,. \tag{A.50}$$

Clearly, the optimal solution is given by $q(z) = 1$ (and $\mathrm{Im}\, q(z) = 0$ inside the unit disk).

A.4 3D Plots

Figure A.3 presents the numerical results for the maximum value of g_{112} for each mass ratio m_2/m_1 and for each coupling ratio $\alpha = g_{222}/g_{112}$. By changing axes and looking at different sections we obtain figures 2.8 and 2.9 from the main text. Many of its features were discussed in section 2.3.2. The black and red surface correspond to the bounds coming from diagonal processes and are, respectively, the translated versions of the horizontal and vertical solid lines in figure 2.8.

Figure A.3 has a ridge where the coupling g_{112} is maximal for each mass ratio. That maximal value set an upper bound for the question: how big can the coupling g_{112} be in a $\mathbb{Z}_2$ symmetric theory with only two stable particles? In figure 2.2 we depict this maximum $g_{112}^{\max}(m_2/m_1)$ (a similar analysis can be done for g_{222}, leading to figure 2.3). We see that this maximal coupling approaches the analytic bound derived from the diagonal $12 \to 12$ component as the mass approaches the boundary of the mass range (2.1) and is otherwise significantly stronger, specially when the particles are mass degenerate where we observe a nice kink feature in figure 2.2.

This kink has a cute geometrical interpretation in the full 3d plot in figure A.3: The top of the ridge meets a valley at $m_1 = m_2$. The valley is a kink for any α. For equal masses there is no extended unitarity region and that renders the numerics way more manageable. This is why we can afford to have so many points along the valley as clearly seen in the figure.

There is one more motivation for resolving this valley region very finely: It is the natural place to look for interesting physical theories. Indeed, each optimal S-matrix in the surface of figure A.3 saturates the extended unitarity equations (2.22-2.26). This means that the scattering of two particles of type 1 or 2 can never lead to multiparticle production. Processes such as $11 \to 222$ are forbidden. When dealing with 2D S-matrices, in particular extremal examples saturating unitarity such as the ones stemming from this numerical computation, we are commanded to look for integrable field theories. For $m_2 \neq m_1$, these are only possible if $M_{11\to 22} = M_{12\to 12}^{\text{Backward}} = 0$. It turns out that no point in the surface (A.3) satisfies this condition.[6] This leaves the possibility of having physical theories along the equal mass line $m_2 = m_1$. This line is an one-dimensional kink in the maximal coupling surface described in detail in section 2.3.3.

[6]This is not an accident, we knew this to be the case a priori since this could only happen if the bound state poles in these amplitudes collided an cancelled or if some extra Landau poles were present. This is not a possibility in the mass range (2.1).

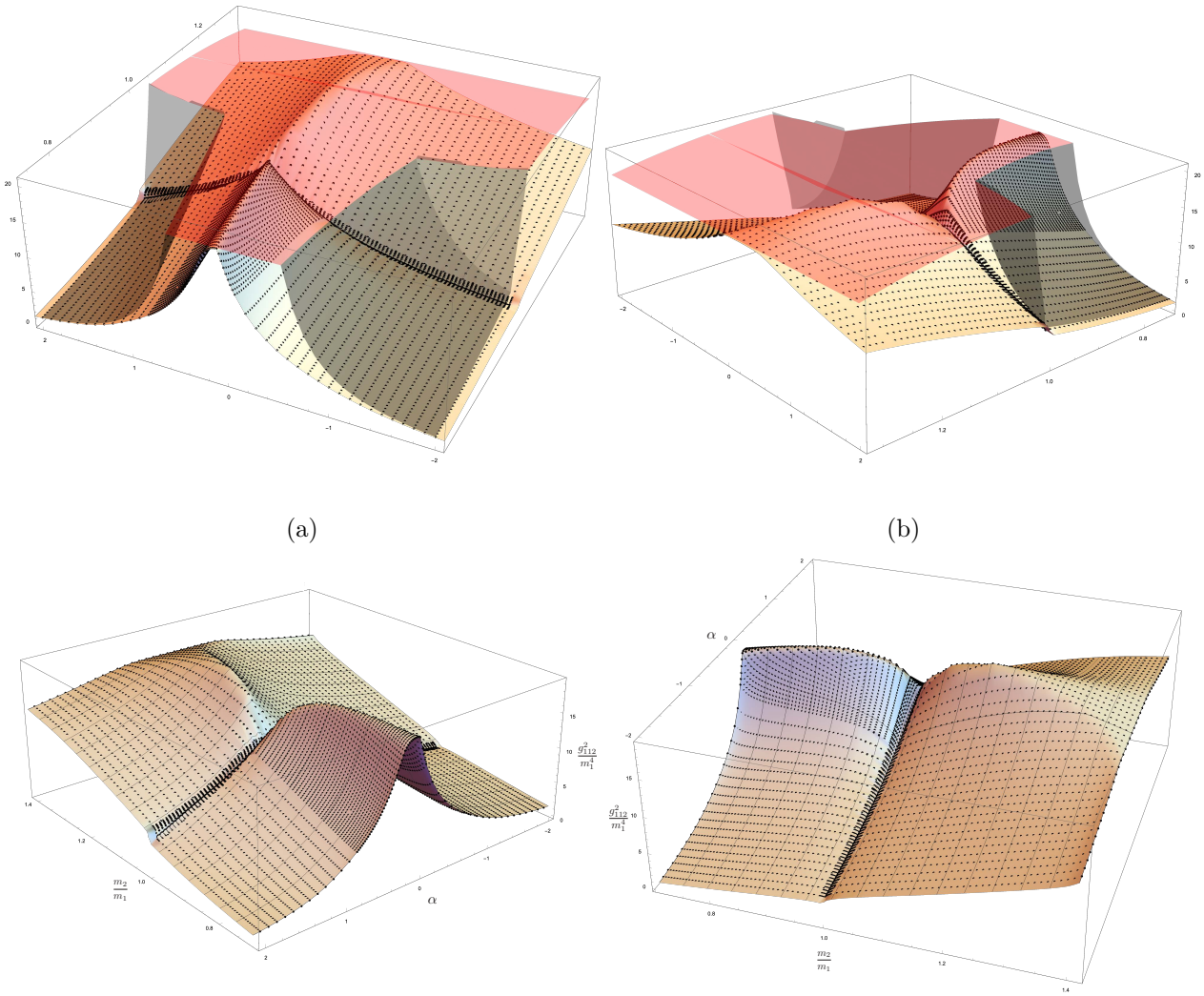

(a) (b)

(c) (d)

Figure A.3: Bounds on g^2_{112} following from the multiple amplitudes analysis, as a function of α and m_2/m_1. These bounds should hold for any $\mathbb{Z}_2$ symmetric quantum field theory with two particles in the spectrum, 1 being odd and 2 being even. They improve the bounds derived from individual amplitudes, corresponding to the red and black surfaces. As can be seen from the various angles (a)-(d), the bound surface has many interesting features that are described in the main text.

A.5 Screening

A.5.1 Invisibility Cloak Toy Model

In this appendix we highlight the importance of not leaving any densities unconstrained as they can lead to very efficient screening thus invalidating any possible bounds. To this

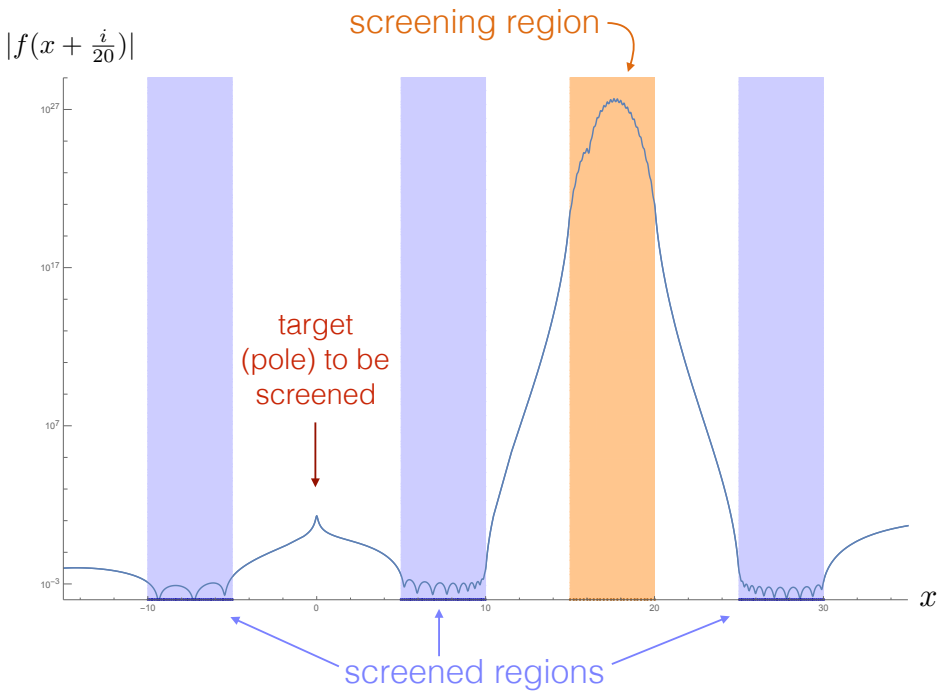

Figure A.4: Absolute value of the function $f(x)$ defined in the main text. The pole at the origin can be screened anywhere to any desired accuracy by a simple density in the orange region. The price to pay is that the density there is pretty extreme, fluctuating wildly and of huge magnitude. If we have regions where amplitude discontinuities are unbounded, we might expect such screening phenomena to produce such strange behaviour at unphysical regions leading to no bounds.

purpose consider as a toy model the function

$$f(x) = \frac{1}{x} + \int_a^b \frac{\rho(y)}{x-y} \tag{A.51}$$

where $0 < a < b$. We think of the first term, the pole at the origin, as a target which we would like to screen. The region $[a, b]$ where the density term is defined is denoted as the screening region and that second term is denoted as the screening term. We can think of it as an invisibility cloak whose role is to make the full function small in pre-defined regions. To make it concrete suppose we want the target to be screened in a region to the right of the screening region (as we would usually associate to an invisibility cloak *a la Harry Potter*) but also – thus making it much more challenging – in a region between the target and the screening region and even in another region to the left of the target! The point we want to make here is that this screening is trivial to achieve if we put no bounds on the density ρ. For that purpose it suffices to consider a discretized version of the problem $f(x) = \frac{1}{x} + \sum_{\text{grid}} \frac{c_i}{x-x_i}$ and show that by tuning the c_i's we can indeed screen the function remarkably well. Here is an example in Mathematica:

```
grid=Range[15, 20, 1/5];
screening=Range[25,30,1/10]~Join~Range[-10,-5,1/10]~Join~Range[5,10,1/10];
```

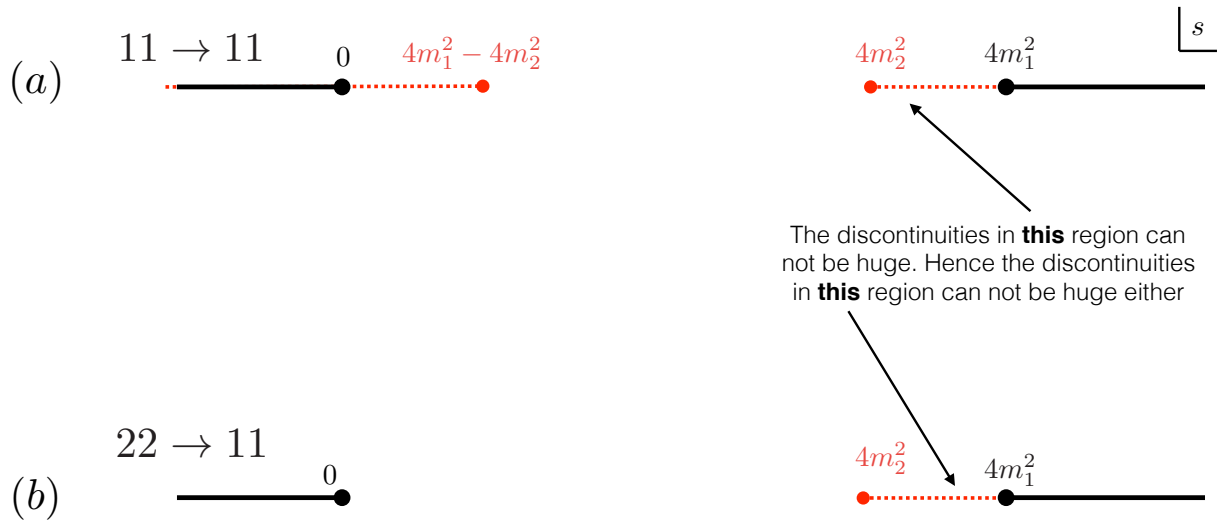

Figure A.5: If $m_2 < m_1$ then the amplitude $M_{22\to 11} = M_{11\to 22}$ contains an extended unitarity region which is bounded by the extended unitarity region in $M_{11\to 11}$. That, in turn, can not be too large or unitarity will be violated in the physical regions (in solid black).

```
f[x_]= 1/x + Sum[c[y]/(x - y), {y, grid}];
Total[f[screening]^2]//FindMinimum[#,Variables[#],WorkingPrecision->500]&
```

leading to the plot in figure A.4. Of course this only works because the density is unconstrained here otherwise the amount of possible screening is limited. In the screening region between a and b the function we get is pretty huge and wild. In other words, the invisibility cloak is working hard so that spectators in the blue screened regions see nothing.

A.5.2 Screening in our setup

The phenomenon of screening happens in our setup for $m_2 < m_1/\sqrt{2}$. In this case, the optimal bounds on the couplings g_{112} and g_{222} are just the same as the ones obtained from the single amplitude analysis. In fact, the off-diagonal amplitudes $M_{11\to 22}$ that saturate these bounds vanish in the physical region. To understand how this is possible it is convenient to first understand why the bounds improve in the region $m_1/\sqrt{2} < m_2 < m_1$.

For $m_1/\sqrt{2} < m_2 < m_1$, the amplitude $M_{11\to 22}$ can not vanish generically so the diagonal amplitude $M_{22\to 22}$ can not saturate unitarity since some production of 11 is inevitable. To see this more precisely note that $M_{11\to 22}$ has poles and an extended unitarity region where the discontinuity is bounded by the diagonal $M_{11\to 11}$ and $M_{22\to 22}$ components as in (A.36). On the one hand, $M_{22\to 22}$ is bounded by unitarity because this amplitude has no extended unitarity region. On the other hand, the discontinuity of the $11 \to 11$ amplitude is positive in the extended unitarity region and therefore is bounded by unitarity in the

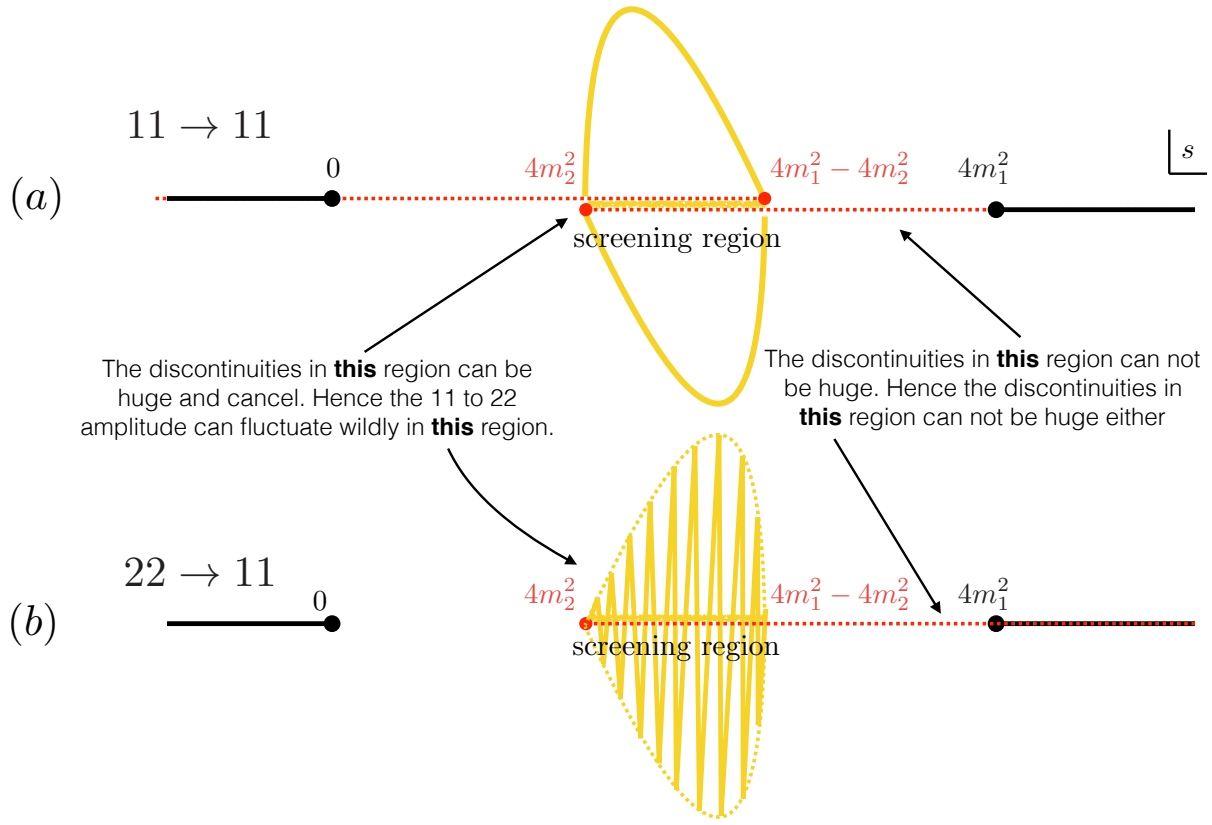

Figure A.6: The s- and t- channel discontinuities come with opposite signs. As such, when there is an overlapping region as in the $11 \to 11$ amplitude represented at the top, they can both be very large as long as their sum remains bounded and does not lead to violation of unitarity in the physical region represented by the black solid lines at the top. Furthermore the discontinuity of $M_{11\to 22}$ (at the bottom) in that same kinematical region is bounded by the $\text{Im}M_{11\to 11}$ and has no definite sign. Therefore, in the region where $\text{Im}M_{11\to 11}$ is unbounded, the amplitude $M_{11\to 22}$ can take advantage of screenning.

physical region. This is depicted in figure A.5. To summarize: we see that some screening is possible but it can not lead to a vanishing $11 \to 22$ amplitude in the physical region and thus to unitarity saturation for $11 \to 11$. This is why the multiple amplitude analysis *had* to improve the bound obtained from a purely diagonal analysis.

This same analysis also explains why for $m_2 < \frac{m_1}{\sqrt{2}}$ the diagonal bound is optimal in our setup. This is because in this range we have a collision between the s-channel and t-channel cuts corresponding to intermediate production of two of the lightest particles in the scattering of the heaviest particle $11 \to 11$, see figure A.6a. The s– and t– channel discontinuities can now be huge as long as they cancel each other and do not lead to a violation of unitarity for the $11 \to 11$ component in the physical region. If they are unbounded, then there is a region in the $11 \to 22$ non-diagonal component where this amplitude can also be unbounded. (Note that if the cuts overlap then the imaginary part in the right hand side of (2.22) should be understood as the s-channel discontinuity.) If the

amplitude can be huge with both signs in a finite segment then it can screen as illustrated in the previous section and can thus kill $11 \to 22$ in the physical region (the backward $12 \to 12$ amplitude, related by analytic continuation to the $11 \to 22$ process can also be killed of course). In other words, for $m_2 < \frac{m_1}{\sqrt{2}}$ we can set to zero all non-diagonal processes without violating any of our physical constraints! Therefore the full numerical plots are expected to coincide with the analytical diagonal bounds. This is indeed what we observed in our numerics.

Would be great to find a way to improve our bounds for $m_2 < \frac{m_1}{\sqrt{2}}$. The following section contains a toy model of this screening phenomena which might help elucidate what kind of physics could produce it.

For $m_2 > \sqrt{2}m_1$ there is a similar screening phenomena that occurs. Furthermore, in this mass range there are other Landau singularities known in two dimensions as higher pole Coleman-Thun singularities [109]. Indeed, if the mass $m_2 > \sqrt{2}m_1$ an on-shell diagram as in figure 2.13 will produce a double pole. Its residue, as seen in the figure, is governed by the coupling (to the fourth power) and by the $2 \to 2$ on-shell S-matrix of the lightest particle. These are all objects which we are already manipulating and it should thus be possible to tame these singularities if we properly understand how to deal with the inherent non-linearities. We look forward to reporting on this interesting problem in the future.

A.5.3 Multiple resonance toy model

One might wonder if the screening mechanism is a numerical artifact or could actually be realized in a reasonable QFT. Here we provide an example pointing towards the later provided we accept some fine tuning.

Consider a theory where $m_1 > \sqrt{2}m_2$. The dangerous screening region is the region where the s and t channel cuts overlap in the $11 \to 11$ amplitude, i.e. for $s \in [4m_2^2, 4m_1^2 - 4m_2^2]$ as described in the previous section. Suppose we have many extra $\mathbb{Z}_2$ even particles $m_3, m_4, \ldots, m_{2N}$ with m_A^2 in that screening region range[7] and suppose further that for each particle with mass squaredm_A^2 in that region there is a particle with mass squared

$$m_{A+1}^2 = 4m_1^2 - m_A^2 + O(\epsilon^2)\,, \tag{A.52}$$

where ϵ is a small parameter. Assume further that the couplings scale with this small parameter as

$$g_{22A} = O(\epsilon) \qquad , \qquad g_{11A} = O(1/\epsilon)\,, \tag{A.53}$$

while $g_{12A} = 0$ since the extra particles are even. Finally, assume that the couplings g_{11A} for two particles related as in (A.52) are the same up to small ϵ corrections. In this scenario, several interesting things might happen, including screening:

- The particles would not appear in the $22 \to 22$ channel since they would come as

[7]Strictly speaking these can not be stable particles since their mass is above $2m_1$ so we should think of them as long lived resonances. In other words, we should think of the corresponding poles as coming with a small imaginary part. Our cavalier analysis ignores these subtleties; the conclusions should remain the same since these small imaginary parts are important mostly for the $11 \to 11$ amplitude and for this amplitude we will see that these particles do not show up.

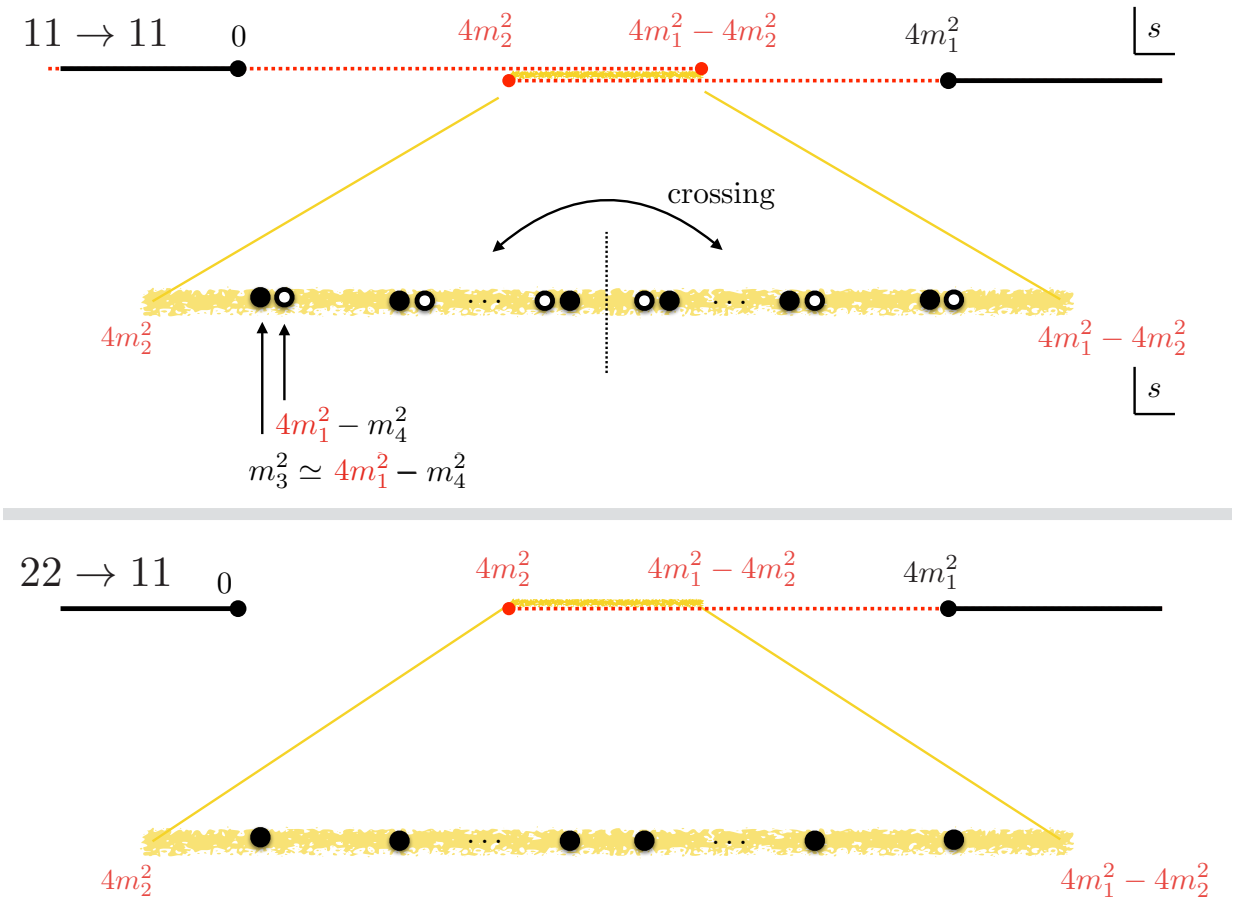

Figure A.7: We can realize the screening mechanism with a large number of resonances with masses $m_A^2 \in [4m_2^2, 4m_1^2 - 4m_2^2]$ in crossing related pairs so that their contribution is moderate in the diagonal channels due to s- and t-channel pair-wise cancelations while, at the same time, having the potential to screen the non-diagonal processes where no t-channel poles show up (since the resonances are taken to be $\mathbb{Z}_2$ even) and where the s-channel poles can have arbitrary sign as this is not a reflection symmetric process.

poles with residues of order $\epsilon^2 \to 0$ or in the $12 \to 12$ channel since they are $\mathbb{Z}_2$ even.

- The particles would appear in the $11 \to 11$ amplitude. Each particle contributes a huge amount since each coupling is of order $1/\epsilon^2$. However, because of the condition (A.52), for each s-channel pole there is a corresponding nearby t-channel pole which nearly cancels it, leading to a finite $O(\epsilon^0)$ result, see figure A.7a. If the mass degeneracy if very tiny the couplings could be huge and still lead to a very good cancelation, compatible with unitarity for this $11 \to 11$ amplitude.

- The particles would also appear as s-channel poles in the $11 \to 22$ amplitude since $g_{11A}g_{22A} = O(\epsilon^0)$, see figure A.7b. Note that this product could be very large and can take any sign. Hence it could lead to screening if N is large as explained in the toy example in section A.5.1. This screening could then lead to $11 \to 22$ being very

small in the physical region.

Of course we could ask: "who ordered these extra particles?" No one did but since it is a priori consistent to add them, the numerics will take advantage of them and add them whenever useful for the optimization goal.

A.6 Solvable Points at $m_1 = m_2$

For $m_1 = m_2$ it is sometimes possible to rotate the one-particle basis as

$$|1'\rangle = \delta|1\rangle + \beta|2\rangle, \qquad |2'\rangle = \bar{\beta}|1\rangle - \bar{\delta}|2\rangle, \qquad \text{with } |\delta|^2 + |\beta|^2 = 1 \tag{A.54}$$

so that the off-diagonal amplitudes have no poles. If that is the case, we can consistently set these amplitudes to zero and allow for the diagonal processes to saturate unitarity. For the spectrum considered in chapter 2, the poles terms in the $\mathbb{Z}_2$ basis are

$$\text{Poles}_{\mathbb{Z}_2} = \begin{pmatrix} \frac{-g_{112}^2}{s-m_2^2} + \frac{-g_{112}^2}{t-m_2^2} & 0 & 0 & \frac{-g_{112}g_{222}}{s-m_2^2} + \frac{-g_{112}^2}{t-m_1^2} \\ 0 & \frac{-g_{112}^2}{s-m_1^2} + \frac{-g_{112}^2}{t-m_1^2} & \frac{-g_{112}^2}{s-m_1^2} + \frac{-g_{112}g_{222}}{t-m_2^2} & 0 \\ 0 & \frac{-g_{112}^2}{s-m_1^2} + \frac{-g_{112}g_{222}}{t-m_2^2} & \frac{-g_{112}^2}{s-m_1^2} + \frac{-g_{112}^2}{t-m_1^2} & 0 \\ \frac{-g_{112}g_{222}}{s-m_2^2} + \frac{-g_{112}^2}{t-m_1^2} & 0 & 0 & \frac{-g_{222}^2}{s-{m_2}^2} + \frac{-g_{222}^2}{t-{m_2}^2} \end{pmatrix}. \tag{A.55}$$

A straightforward brute force analysis in Mathematica shows that a change of basis as in equation (A.54) can diagonalise (A.55) only if

$$\frac{g_{222}}{g_{112}} = -1 \qquad \Longrightarrow \qquad \delta = 1/\sqrt{2}, \qquad \beta = -i/\sqrt{2}, \tag{A.56}$$

in which case the rotated poles terms become of the form $\textbf{Diag}\left(\frac{-2g_{112}^2}{s-m_1^2}, \frac{-2g_{112}^2}{t-m_1^2}, \frac{-2g_{112}^2}{t-m_1^2}, \frac{-2g_{112}^2}{s-m_1^2}\right)$, or

$$\frac{g_{222}}{g_{112}} = 1 \qquad \Longrightarrow \qquad \delta = 1/\sqrt{2}, \qquad \beta = -1/\sqrt{2}, \tag{A.57}$$

where now the poles terms reduce to $\textbf{Diag}\left(\frac{-2g_{112}^2}{s-m_1^2} + \frac{-2g_{112}^2}{t-m_1^2}, 0, 0, \frac{-2g_{112}^2}{s-m_1^2} + \frac{-2g_{112}^2}{s-m_1^2}\right)$. In both cases, the S-matrix in the rotated basis (A.54) is schematically of the form

$$\begin{pmatrix} a & c & c & b \\ c & e & d & c \\ c & d & e & c \\ b & c & c & a \end{pmatrix}. \tag{A.58}$$

It is then straightforward to apply the maximum modulus principle as in section 2.1 to obtain bounds the optimal couplings. For the (A.56) scenario, we conclude that a and e are fixed while $b = c = d = 0$, since the diagonal processes must saturate unitarity. This solution corresponds to the S-matrix of the 3-states Potts model at $T \neq T_c$. Note that in the rotated basis we no longer have $s \leftrightarrow t$ symmetry for diagonal processes in this case, since

the external particles no longer diagonalise the charge conjugation operator, see appendix A.7. On the other hand, for (A.57) we conclude only that a is fixed and $b = c = 0$ (note that after changing basis b is no longer related to d by crossing), while d and e correspond to a zero modes that do not affect the optimal coupling. A particular choice of d and e lead to the hyperbolic limit of the elliptic deformation of the supersymmetric Sine-Gordon model, discussed in section 2.3.3.

A.7 3-state Potts field theory

The 3-state Potts model in two dimensions has a continuous phase transition described by a non-diagonal minimal model with central charge $c = 4/5$ and a global permutation symmetry S_3. This conformal field theory (CFT) contains 3 relevant scalar operators invariant under $\mathbb{Z}_2 \subset S_3$ (see [258] for a nice introduction to this topic). This allows us to define a family of $\mathbb{Z}_2$ symmetric QFTs with action

$$A_{QFT} = A_{CFT} + \tau \int d^2x\, \epsilon(x) + h \int d^2x\, \sigma_+(x) + h' \int d^2x\, \Omega_+(x)\,, \tag{A.59}$$

where τ, h and h' are relevant couplings and we used the notation of [115]. The scaling dimensions of the relevant operators are $\Delta_\epsilon = \frac{4}{5}$, $\Delta_\sigma = \frac{2}{15}$ and $\Delta_\Omega = \frac{4}{3}$. The purely thermal deformation ($\tau \neq 0$ and $h = h' = 0$) preserves the S^3 symmetry and leads to an integrable QFT. This theory has only two stable particles with the same mass m transforming as a doublet of S^3. These particles are usually described in a basis $|A\rangle, |A^\dagger\rangle$ where the $\mathbb{Z}_2$ acts as charge conjugation $C|A\rangle = |A^\dagger\rangle$ with $C^2 = 1$ [115, 237]. In this basis, the S-matrix is diagonal, *i.e.* $S_{AA\to A^\dagger A^\dagger} = S^{\text{Backward}}_{AA^\dagger \to AA^\dagger} = 0$ and

$$S_{AA\to AA} = S_{A^\dagger A^\dagger \to A^\dagger A^\dagger} = \frac{\sinh\left(\frac{\theta}{2} + \frac{i\pi}{3}\right)}{\sinh\left(\frac{\theta}{2} - \frac{i\pi}{3}\right)}\,, \qquad S^{\text{Forward}}_{AA^\dagger \to AA^\dagger} = -\frac{\sinh\left(\frac{\theta}{2} + \frac{i\pi}{6}\right)}{\sinh\left(\frac{\theta}{2} - \frac{i\pi}{6}\right)}\,, \tag{A.60}$$

where we used the rapidity θ to parametrize the Mandelstam invariant $s = 4m^2 \cosh^2 \frac{\theta}{2}$. Notice that, in this basis, the Yang-Baxter equations are trivially satisfied.

In chapter 2, we work in the eigenbasis of the $\mathbb{Z}_2$ global symmetry generated by charge conjugation,

$$|1\rangle = e^{i\pi/4} \frac{|A\rangle - |A^\dagger\rangle}{\sqrt{2}}\,, \qquad |2\rangle = e^{-i\pi/4} \frac{|A\rangle + |A^\dagger\rangle}{\sqrt{2}}\,. \tag{A.61}$$

In this basis, we find

$$S_{11\to 11} = S_{22\to 22} = S^{\text{Forward}}_{12\to 12} = -\frac{i \sinh\theta}{2i\sinh\theta + \sqrt{3}}\,, \tag{A.62}$$

$$S_{11\to 22} = -S^{\text{Backward}}_{12\to 12} = \frac{\sqrt{3}\cosh\theta}{2i\sinh\theta + \sqrt{3}}\,. \tag{A.63}$$

Using equation (A.23) we can obtain the expressions (2.36) for the connected scattering amplitudes that maximize g^2_{112} for $m_1 = m_2$ and $g_{222} = -g_{112}$ (point A in figure 2.9).

The magnetic deformations h and h' in (A.59) preserve $\mathbb{Z}_2$ and therefore must be compatible with our bounds, at least for small magnetic deformations $h\tau^{-\frac{14}{9}} \ll 1$ and $h'\tau^{-\frac{10}{9}} \ll 1$ that do not give rise to more stable particles. In fact, the mass spectrum of these theories (with $h \neq 0$ and $h' = 0$) has been studied in [115] using the Truncated Conformal Space Approach. The authors observed that the degeneracy between the two particles is lifted for $h \neq 0$. It would be interesting to study the cubic couplings and the S-matrices of this 2-parameter family of $\mathbb{Z}_2$ symmetric QFTs and compare them to our bounds.

A.8 Tricritical Ising (cusp)

The tricritical Ising model in two dimensions has a continuous phase transition described by a diagonal minimal model with central charge $c = 7/10$ and a $\mathbb{Z}_2$ (spin flip) symmetry. This conformal field theory (CFT) contains 2 relevant scalar operators invariant under $\mathbb{Z}_2$ (see [258] for a nice introduction to this topic). This allows us to define a family of $\mathbb{Z}_2$ symmetric QFTs with action

$$A_{QFT} = A_{CFT} + \tau \int d^2x\, \epsilon(x) + \tau' \int d^2x\, \epsilon'(x)\,, \tag{A.64}$$

where τ, τ' are relevant couplings. The scaling dimensions of the relevant operators are $\Delta_\epsilon = \frac{1}{5}$ and $\Delta_{\epsilon'} = \frac{6}{5}$. The purely thermal deformation ($\tau \neq 0$ and $\tau' = 0$) leads to an integrable QFT. This theory has seven particles but only four of them have masses below the continuum of multi-particle states. The masses of these particles are given in table A.1.

In chapter 2 we constrained the space of 2D S-matrices with $\mathbb{Z}_2$ symmetry by requiring unitarity and analyticity for the two-to-two S-matrix elements involving only the two lightest particles $\{m_1, m_2\}$ as external states. We restrained ourselves to study the subset of theories for which only m_1 and m_2 themselves appeared as bound states in these matrix elements. This excludes the tricritical Ising field theory from our analysis in chapter 2. However, one can easily relax this restriction. We shall not do a full numerical study of the multiple amplitude bootstrap in this more general setup. We will just derive the analytic bounds that follow from the amplitudes $S_{11\to11}$ and $S^{\text{Forward}}_{12\to12}$. For concreteness, we consider a theory with $\mathbb{Z}_2$ symmetry and a mass spectrum as in the table A.1.[8]

With this setup there is a richer structure of couplings to play with. For example, in the $11 \to 11$ amplitude we have bound state poles corresponding to particles m_2 and m_4:

$$S_{11\to11}(s) = -\mathcal{J}(m_2^2)\frac{g_{112}^2}{s-m_2^2} - \mathcal{J}(m_4^2)\frac{g_{114}^2}{s-m_4^2} + \text{t-channel poles} + \text{cuts} \tag{A.65}$$

[8] Any masses within the range $0 < 4m_1^2 - m_4^2 < m_2^2 < 2m_1^2$ and $m_1^2 < 2m_1^2 + 2m_2^2 - m_3^2 < m_1^2 + m_2^2$ would lead to qualitatively the same conclusions regarding single amplitude bounds as below but the precise locations of cusps and edges on the bounds does depend on the masses. If we deviate away from these mass constraints then we we would have to redo the analysis. This is the same discontinuous nature of the bounds already observed in [9], see e.g. figures 10 and 11 therein.

Particle	Mass	$\mathbb{Z}_2$ charge
m_1	m	odd
m_2	$2m\cos 5\pi/18 \approx 1.29\,m$	even
m_3	$2m\cos \pi/9 \approx 1.88\,m$	odd
m_4	$2m\cos \pi/18 \approx 1.97\,m$	even
+ possibly extra particles with masses bigger than $m_1 + m_2$.		

Table A.1: Spectrum assumed for the analysis in this appendix.

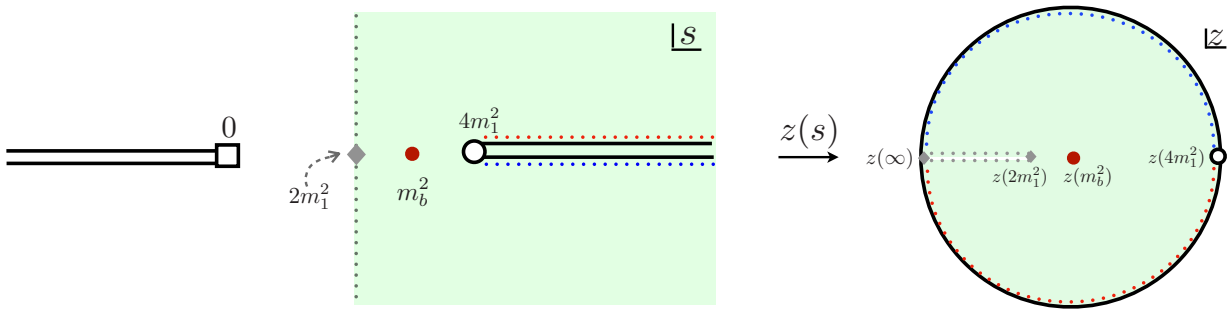

Figure A.8: The change of variables from s to z trivialises the crossing symmetry of the S-matrix and maps the cut half-plane $s > 2m_z^2$ to the unit disk by "opening" the cut and mapping it to the boundary of the unit disk. In doing so, it maps $s = m_b^2$ to $z = 0$, $s = \infty$ to $z = -1$ and the imaginary axis $s \in [2m_1^2 - i\infty, 2m_1^2 + i\infty]$ to a segment in the real z axis.

where $\mathcal{J}(s) = \frac{1}{2\sqrt{s(4m_1^2-s)}}$. One question that could be asked is: what values for the pair (g_{112}^2, g_{114}^2) are allowed by the unitarity constraint $|S_{11\to 11}| \leq 1$?

To answer this question, it is useful to introduce the variables

$$z(s) = \frac{m_b\sqrt{4m_1^2 - m_b^2} - \sqrt{s}\sqrt{4m_1^2 - s}}{m_b\sqrt{4m_1^2 - m_b^2} + \sqrt{s}\sqrt{4m_1^2 - s}}, \tag{A.66}$$

$$z_a \equiv z(m_a^2) \tag{A.67}$$

$$w_a \equiv w(z, m_a) = \frac{z - z_a}{1 - \bar{z_a} z}, \qquad |z_0| \leq 1 \tag{A.68}$$

where we take $m_b^2 = 2m_1^2$ for convenience. This choice of m_b maps $s \in [2m_1^2, 4m_1^2]$ to $z \in [0, 1]$ and the imaginary axis $s \in [2m_1^2 - i\infty, 2m_1^2 + i\infty]$ to $z \in [-1, 0]$. See figures A.8 and A.9 for an illustration of such maps.

As a function of the z variable, $S_{11\to 11}$ has poles at $z(m_2^2)$ and $z(m_4^2)$. Therefore the function

$$f(z) = -S(z)w_2 w_4 \tag{A.69}$$

is a holomorphic function on the unit disk which satisfies, as a consequence of unitarity, $|f(z)| \leq 1$. Moreover, from the fact that $S(s)$ has a negative residue at $s = m_2^2$ and a positive residue at $s = m_4^2$, we find that $f(z)$ is positive at z_2 and z_4.

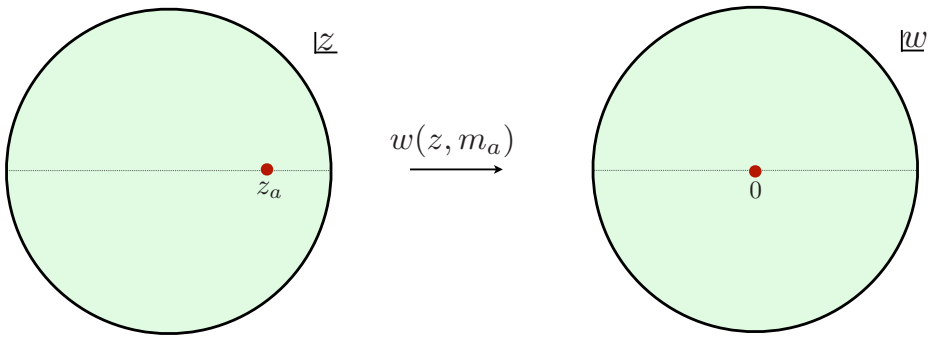

Figure A.9: The map w_a is an automorphism of the unit disk. It maps z_a to the origin. When z_a is real, it preserves the real segment $[-1, 1]$.

Suppose we want to maximise g^2_{112}. This is equivalent to maximising $f(z^* = z(m_2^2))$. But by the maximum modulus principle, $|f(z)| \leq 1$ everywhere inside the unit disc and, moreover, the optimal value $|f(z^*)| = 1$ is only achieved when $|f(z)| = 1$. From the fact that f is positive at z_2 and z_4 we conclude that a maximal g^2_{112} is obtained for $f(z) = 1$ and

$$(g^{max}_{112})^2 = \text{res}_{s=m_2^2} \frac{1}{\mathcal{J}(s) w_2 w_4}. \tag{A.70}$$

Note that this solution also maximises g^2_{114} so that

$$(g^{max}_{112})^2 = \text{res}_{s=m_4^2} \frac{1}{\mathcal{J}(s) w_2 w_4}. \tag{A.71}$$

Now we maximise g^2_{112} under the extra constraint that $g^2_{114} = \alpha (g^{max}_{114})^2$ with $\alpha \in [0, 1]$. This maximisation problem (together with the equivalent problem of maximising g^2_{114} with g^2_{112} fixed) completely determines the subspace of (g^2_{112}, g^2_{114}) compatible with $|S_{11\to 11}| \leq 1$, since this space is convex.

Under this extra constraint, we know that $f(z_4) = \alpha$ and so the solution $f(z) = 1$ is no longer possible. Consider, however, the function

$$g(w_4) = w(f(z(w_4), \alpha) = \frac{f(z(w_4)) - \alpha}{1 - \alpha f(z(w_4))}, \tag{A.72}$$

where we now think of f as a function of w_4 by inverting equation A.68. Since $w(f, \alpha)$ is an increasing function of f, to maximise $f(w_4(z_2)) = \frac{g^2_{112}}{(g^{max}_{112})^2}$ is equivalent to maximise $g(w_4(z_2))$. Moreover, since g is an automorphism of the disk, unitarity implies $|g(w_4)| \leq 1$ for w_4 on the unit disc. Finally, $g(0) = 0$. Now recall Schwartz Lemma:

Lemma 1 ***Schwartz Lemma****: Let* $\mathbf{D}$ *be the unit disk and* $g : \mathbf{D} \to \mathbf{D}$ *be a holomorphic map such that* $g(0) = 0$ *and* $|g(w)| \leq 1$ *on* $\mathbf{D}$*. Then* $|g(w)| \leq |w|$*. Moreover, if the inequality is saturated for any non-zero point in* $\mathbf{D}$*, then* $g(w) = aw$ *with* $|a| = 1$*.*

We conclude that under the extra constraint $g^2_{114} = \alpha (g^{max}_{114})^2$, the maximal value for

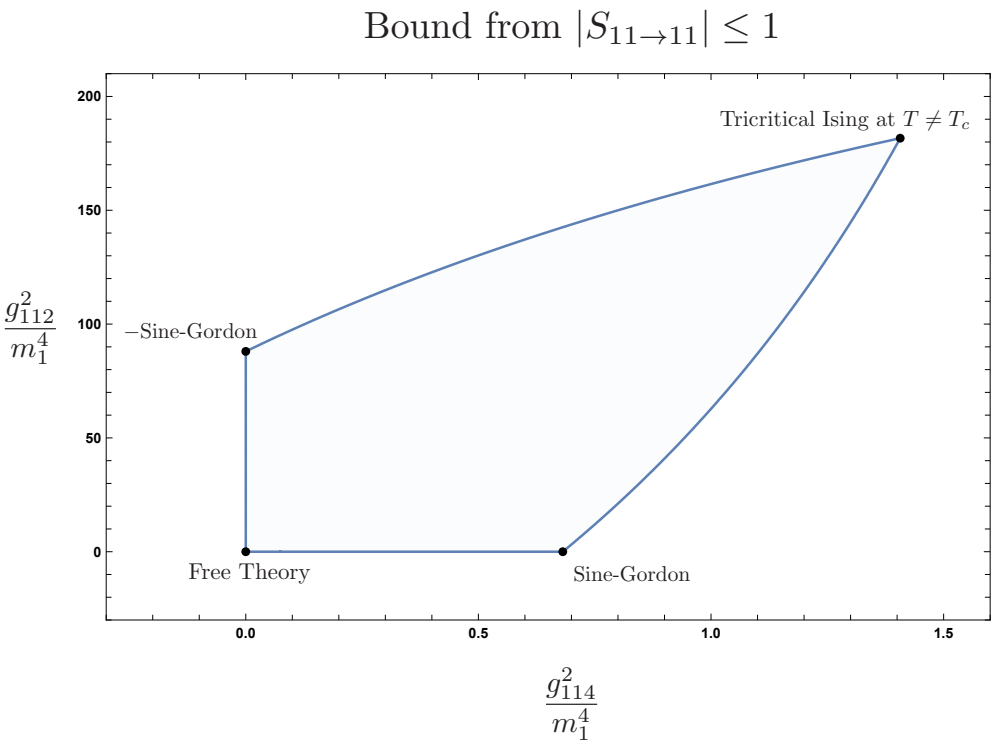

Figure A.10: Space of allowed couplings compatible with $|S_{11\to 11}| \leq 1$ and spectrum according to table (A.1). This space has kinks that are related to integrable theories.

g_{112}^2 is given by the solution of the following algebraic equation on $S_{11\to 11}$:

$$w_4 = \frac{f(z(w_4)) - \alpha}{1 - \alpha f(z(w_4))}. \tag{A.73}$$

After performing the equivalent exercise for the maximisation of g_{114}^2 under $g_{112}^2 = \beta(g_{112}^{max})^2$, where $\beta \in [0, 1]$, we obtain the allowed space of (g_{112}^2, g_{114}^2) as depicted in the figure A.10.

One can play the same game for the $S_{12\to 12}^{\text{Forward}}$ matrix element, which contains bound state poles corresponding to particles m_1 and m_3 (and therefore constrain the space (g_{112}^2, g_{123}^2). One can then combine both results into a $3D$ plot of allowed triplets $(g_{112}^2, g_{114}^2, g_{123}^2)$ compatible with $|S_{11\to 11}| \leq 1$ and $|S_{12\to 12}| \leq 1$. This is figure A.11.

It would be interesting to perform a multiple amplitudes analysis for this setup and explore the space of masses (m_1, m_2, m_3, m_4) in the vicinity of the values of table A.1. Notice that in such an analysis, the values in table A.1 would be single out by the condition that the multiple amplitude bounds saturate the single amplitude bounds of figure A.11 at the tip of the spear. That is because only for those particular masses can the multiple poles in the off-diagonal channels coincide and cancel (à la integrable bootstrap), allowing for the off-diagonal amplitudes to vanish and for the diagonal processes to saturate unitarity, as in the boundary of the yellow surface in figure A.11. It would also be interesting to see if the sub-leading (non-integrable) deformation τ' of the tricritical Ising model leads to any

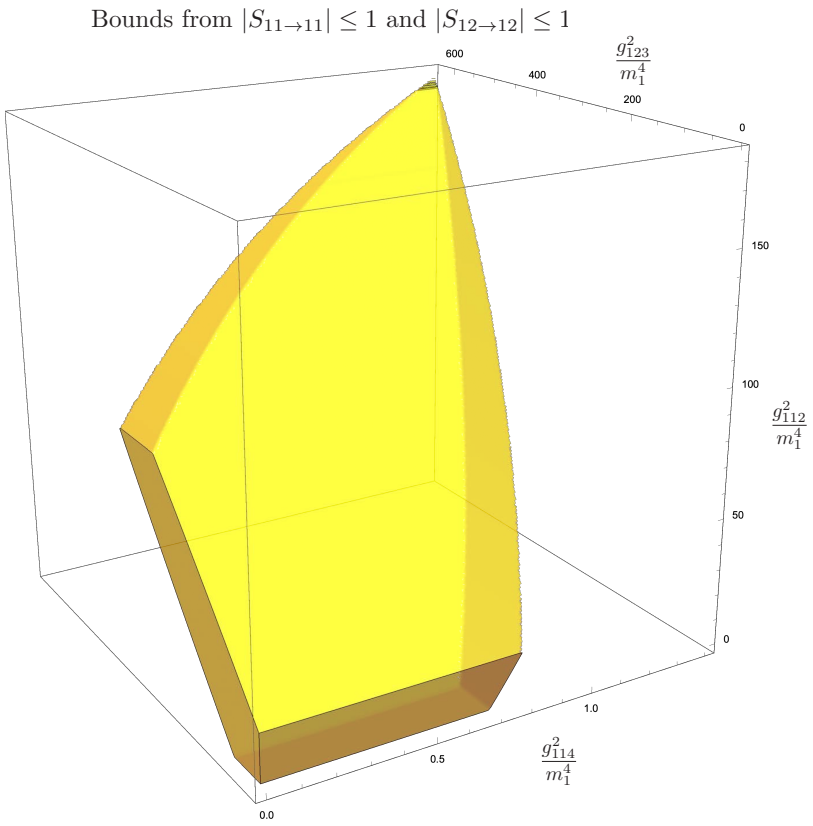

Figure A.11: Space of allowed couplings compatible with $|S_{11\to11}| \leq 1$ and $|S_{12\to12}| \leq 1$ and spectrum as in table (A.1). The tip of this spear is the thermal deformation of the Tricritical Ising Model.

feature of the bounds.

A.9 Numerical optimization as a SDP

As discussed in section 2.3.1, once we fix $\alpha = \frac{g_{222}}{g_{112}}$, our discretised ansatz for the amplitudes depends only on the variables $\vec{\eta} = \{g_{112}^2, C_{a\to b}, \sigma_{a\to b}(x_i)\}$. To reduce the maximisation problem to an SDP, all we need to do is to write the extended unitarity constraint (2.27) as a semidefinite constraint linear on $\vec{\eta}$, as in (2.33). The purpose of this appendix is to prove the equivalence of (2.27) and (2.33) or, explicitly,

$$\begin{pmatrix} \mathbb{I} & \rho\mathbb{M} \\ (\rho\mathbb{M})^\dagger & 2\text{Im }\mathbb{M} \end{pmatrix} \succeq 0 \iff 2\text{Im}\mathbb{M} \succeq \mathbb{M}^\dagger\rho^2\mathbb{M}. \tag{A.74}$$

Proof of $\Rightarrow$:

$$\begin{pmatrix} \mathbb{I} & \rho\mathbb{M} \\ (\rho\mathbb{M})^\dagger & 2\text{Im }\mathbb{M} \end{pmatrix} \succeq 0 \Rightarrow \begin{pmatrix} \vec{v} \\ \vec{w} \end{pmatrix}^\dagger \begin{pmatrix} \mathbb{I} & \rho\mathbb{M} \\ (\rho\mathbb{M})^\dagger & 2\text{Im }\mathbb{M} \end{pmatrix} \begin{pmatrix} \vec{v} \\ \vec{w} \end{pmatrix} \geq 0, \qquad \forall \vec{v}, \vec{w} \in \mathbb{C}^2 \tag{A.75}$$

This becomes the r.h.s of (A.74) if we pick $\vec{v} = -\rho\mathbb{M}\vec{w}$.

Proof of $\Leftarrow$:

$$\begin{aligned} 0 &\leq (\vec{v} + \rho\mathbb{M}\vec{w})^\dagger(\vec{v} + \rho\mathbb{M}\vec{w}) = \vec{v}^\dagger\vec{v} + \vec{v}^\dagger\rho\mathbb{M}\vec{w} + \vec{w}^\dagger\mathbb{M}^\dagger\rho\vec{v} + \vec{w}^\dagger\mathbb{M}^\dagger\rho^2\mathbb{M}\vec{w} \qquad (A.76) \\ &\leq \vec{v}^\dagger\vec{v} + \vec{v}^\dagger\rho\mathbb{M}\vec{w} + \vec{w}^\dagger\mathbb{M}^\dagger\rho\vec{v} + \vec{w}^\dagger\text{Im}\mathbb{M}\vec{w} \iff \begin{pmatrix} \mathbb{I} & \rho\mathbb{M} \\ (\rho\mathbb{M})^\dagger & 2\text{Im }\mathbb{M} \end{pmatrix} \succeq 0 \end{aligned}$$

where we used the r.h.s. of (A.74) in the second inequality.

A.10 Elliptic Deformation

Bellow one can find the definition of the supersymmetric sine-Gordon elliptic deformation S-matrix in `Mathematica` friendly notation.

```
w = EllipticK[k]/\[Pi];
e = 1;
g = 2 \[Pi]/3;

ED = {{JacobiDN[g w, k] - (JacobiDN[I q w, k] JacobiSN[g w, k])/(e
JacobiCN[I q w, k] JacobiSN[I q w, k]), 0, 0,
(JacobiDN[I q w, k] JacobiSN[g w, k])/(e JacobiCN[I q w, k])},
{0, 1, -(JacobiSN[g w, k]/(e JacobiSN[I q w, k])), 0},
{0, -(JacobiSN[g w, k]/(e JacobiSN[I q w, k])), 1, 0},
{(JacobiDN[I q w, k] JacobiSN[g w, k])/(e JacobiCN[I q w, k]), 0, 0, -JacobiDN[g w, k]
- (JacobiDN[I q w, k] JacobiSN[g w, k])/(e JacobiCN[I q w, k] JacobiSN[I q w, k])}};

IntR[x_, k_] := 1/(2 \[Pi] I)Block[{w = (EllipticK[k]/\[Pi])},
 (NIntegrate[Log[((1 - JacobiSN[g w, k]^2/JacobiSN[I q w, k]^2)^ -1)
/Sinh[q]^2]/Sinh[q - x], {q, -Infinity, Infinity}])];

U[x_, k_] := -I Sinh[x] Exp[IntR[x, k]];
CDDPole[q_] := (Sinh[q] + I Sin [g])/(Sinh[q] - I Sin[g])

SED[Q_, K_] := U[Q, K] CDDPole[Q] ((ED /. w -> EllipticK[k]/\[Pi])
 /. {k -> K, q -> Q});
```

Note that to compute the S-matrix for physical $\theta \in \mathbb{R}$, one must be careful and take the appropriate principal value around the singularity at $\theta = x$ in the integrand of `IntR`.

A.11 Conformal computations

A.11.1 Crossing symmetry in one dimension

We consider correlation functions of primary operators $\phi_i(x_i)$ in a one-dimensional boundary field theory. The weight of the operator ϕ_i will be denoted as Δ_i. We will work in the Euclidean theory on $\mathbb{R} \cup \{\infty\}$. The conformal group is a two-fold cover of $PSL(2,\mathbb{R})$; its elements act by the usual fractional linear transformations on the positions,

$$x \to x' = \frac{ax+b}{cx+d} \tag{A.77}$$

with $ad - bc = \pm 1$. The elements with negative determinant involve the parity transformation $x \to -x$. The Jacobian of this transformation is $(ad-bc)(cx+d)^{-2}$ and the fields transform as

$$\phi(x) \to \phi'(x') = (ad-bc)^{P_\phi} |cx+d|^{2h} \phi(x) \tag{A.78}$$

with $P_\phi \in \{0,1\}$ dictated by the parity of ϕ.[9] In a correlation function we should remember that the parity operation also reverses the operator ordering.

In a suitable basis the two-point functions take the familiar form

$$\langle \phi(x)\phi(0)\rangle = \frac{(-1)^{P_\phi}}{|x|^{2\Delta_\phi}} \tag{A.79}$$

The two-point function of a parity odd operator is negative, so the associated norm $\langle\phi|\phi\rangle$ is positive.[10]

The operator product expansion reads

$$\phi_1(x)\phi_2(0) = \frac{C_{12}{}^k}{|x|^{\Delta_1+\Delta_2-\Delta_k}}\phi_k(0) + \dots \tag{A.80}$$

where we assume that $x < 0$. If we act with the parity operator on both sides then we find

$$(-1)^{P_1+P_2}\phi_2(0)\phi_1(-x) = (-1)^{P_k}\frac{C_{12}{}^k}{|x|^{\Delta_1+\Delta_2-\Delta_k}}\phi_k(0) + \dots \tag{A.81}$$

and therefore the reflected OPE coefficients between primaries are

$$C_{21}{}^k = (-1)^{\sigma_{12k}} C_{12}{}^k \tag{A.82}$$

with

$$\sigma_{12k} := P_1 + P_2 + P_k \bmod 2\,. \tag{A.83}$$

[9] The parity operator is unitary and its square is an internal symmetry transformation. Up to a well-known caveat [236, section 3.3] we can always redefine the parity operator so it squares to 1 and its eigenvalues are then ± 1 as we assumed.

[10] It may help the reader that parity odd operators are the same as one-dimensional vectors $\phi_\mu(x)$. The reflection-positive two-point function is then $\langle\phi_\mu(x)\phi_\nu(0)\rangle = |x|^{-2\Delta_\phi}\left(\delta_{\mu\nu} - 2\frac{x_\mu x_\nu}{x^2}\right) = -|x|^{-2\Delta_\phi}$, in one dimension.

The previous relation in particular implies that parity odd operators can never appear in the OPE of two identical operators. We will work in a basis where two-point functions are diagonal. The structure of three-point functions then dictates that

$$C_{12k} = (-1)^{\sigma_{12k}} C_{k21} \tag{A.84}$$

and so the OPE coefficients transform either in the trivial representation (if $\sigma_{12k} = 0$) or the sign representation (if $\sigma_{12k} = 1$) of the permutation group S_3. Notice that, even if parity is broken, the cyclic symmetry is always preserved. This for example means that $C_{12k} = C_{k12}$, whereas C_{12k} and C_{21k} are not always the same.

We will be specifically interested in four-point functions,

$$\langle \phi_1(x_1)\phi_2(x_2)\phi_3(x_3)\phi_4(x_4)\rangle = \left|\frac{x_{14}}{x_{24}}\right|^{\Delta_{21}} \left|\frac{x_{14}}{x_{13}}\right|^{\Delta_{34}} \frac{\mathcal{G}_{1234}(x)}{|x_{12}|^{\Delta_1+\Delta_2}|x_{34}|^{\Delta_3+\Delta_4}} \tag{A.85}$$

with, as usual, $(\cdot)_{ij} = (\cdot)_i - (\cdot)_j$ and

$$x := \frac{x_{12}x_{34}}{x_{13}x_{24}}\,. \tag{A.86}$$

If $x_i < x_{i+1}$ for $i = 1, 2, 3$ then $0 < x < 1$. The s-channel conformal block decomposition reads

$$\mathcal{G}_{1234}(x) = \sum_k C_{12}{}^k C_{34k}\, g(\Delta_{21}, \Delta_{34}; \Delta_k; x) \tag{A.87}$$

with the conformal blocks

$$g(a, b; \Delta; z) := |z|^{\Delta}{}_2F_1(\Delta + a, \Delta + b; 2\Delta; z)\,. \tag{A.88}$$

where we added an absolute value sign so the expression is unambiguous also for negative values of its argument.

Let us briefly discuss operator ordering. Correlation functions with operator orderings that are cyclic permutations of each other are directly related, as follows from covariance under the (orientation-preserving) inversion $x_i \to -1/x_i$. Furthermore, parity symmetry dictates that

$$\mathcal{G}_{1234}(x) = \mathcal{G}_{4321}(x)(-1)^{\sigma_{1234}} \tag{A.89}$$

To see the complications that arise if we just swap two adjacent operators, let us swap operators 1 and 2. A simple relabeling leads to the block decomposition

$$\mathcal{G}_{2134}(x) = \sum_k C_{21}{}^k C_{34k} g(\Delta_{12}, \Delta_{34}; \Delta_k; x) \tag{A.90}$$

and assuming a parity invariant theory this is equal to

$$\mathcal{G}_{2134}(x) = (1-x)^{\Delta_{34}} \sum_k C_{12}{}^k C_{34k} (-1)^{\sigma_{12k}}\, g\left(\Delta_{21}, \Delta_{34}; \Delta_k; \frac{x}{x-1}\right) \tag{A.91}$$

where we used a standard hypergeometric transformation formula, valid for $x < 1$. The

factor $(-1)^{P_k}$ and the absolute value sign in the definition (A.88) imply that $\mathcal{G}_{2134}$ and $\mathcal{G}_{1234}$ are not, in general, related in an obvious manner. The symmetries and non-symmetries altogether leave us with three independent four-point functions from which the others follow. We can take these to be $\langle 2134\rangle$, $\langle 1234\rangle$, and $\langle 1324\rangle$, which respectively correspond to $x<0$, $0<x<1$, and $1<x$. We will here be interested in just the second of these correlators.

With the ordering fixed there are only two OPE channels. For the $\langle 1234\rangle$ ordering we gave the first one above; the crossed channel OPE reads

$$\mathcal{G}_{2341}(y)=\sum_p C_{23}{}^p C_{p41}\, g(\Delta_{32},\Delta_{41};h;y) \tag{A.92}$$

with $y=x_{23}x_{41}/x_{24}x_{31}=1-x$. Crossing symmetry then takes the form[11]

$$\mathcal{G}_{1234}(x)=\frac{|x|^{\Delta_3+\Delta_4}}{|1-x|^{\Delta_2+\Delta_3}}\mathcal{G}_{2341}(1-x) \tag{A.93}$$

Let us consider all correlation functions of two parity-even operators ϕ_1 and ϕ_2. We then find, in a diagonal operator basis, the following set of non-trivial crossing equations:

$$\begin{aligned}
0&=\sum_k C_{11k}^2\, g(0,0;\Delta_k;x)-\frac{|x|^{2\Delta_1}}{|1-x|^{2\Delta_1}}\sum_k C_{11k}^2 g(0,0;\Delta_k;1-x)\\
0&=\sum_k C_{22k}^2\, g(0,0;\Delta_k;x)-\frac{|x|^{2\Delta_2}}{|1-x|^{2\Delta_2}}\sum_k C_{22k}^2 g(0,0;\Delta_k;1-x)\\
0&=\sum_k C_{22k}C_{12k}\, g(0,\Delta_{21};\Delta_k;x)-\frac{|x|^{2\Delta_2}}{|1-x|^{2\Delta_2}}\sum_k C_{22k}C_{12k}\, g(0,\Delta_{12};\Delta_k,1-x)\\
0&=\sum_k C_{11k}C_{12k}\, g(0,\Delta_{12};\Delta_k;x)-\frac{|x|^{2\Delta_1}}{|1-x|^{2\Delta_1}}\sum_k C_{11k}C_{12k}\, g(0,\Delta_{21};\Delta_k,1-x)\\
0&=\sum_p (-1)^{P_p}C_{12p}^2\, g(\Delta_{21},\Delta_{12};\Delta_p;x)-\frac{|x|^{\Delta_1+\Delta_2}}{|1-x|^{\Delta_1+\Delta_2}}\sum_p (-1)^{P_p}C_{12p}^2\, g(\Delta_{12},\Delta_{21};\Delta_p;1-x)\\
0&=\sum_k C_{11k}C_{22k}\, g(0,0;\Delta_k;x)-\frac{|x|^{2\Delta_2}}{|1-x|^{\Delta_1+\Delta_2}}\sum_p C_{12p}^2\, g(\Delta_{21},\Delta_{21};\Delta_p;1-x)
\end{aligned} \tag{A.94}$$

where the operators labeled k are parity even, whereas the operators labeled p can be either parity even or parity odd.

[11] One foolproof way to obtain this expression is to relabel the operators in the original expression (A.85) and then use a conformal transformation to relate $\langle 2341\rangle$ to $\langle 1234\rangle$. To verify that directly fusing operators 2 and 3 together in (A.85) gives the same OPE limit requires that $C_{1p4}=C_{p41}$ which we proved previously.

A.11.2 Transition to convex optimization

In matrix form, the I'th crossing symmetry equation can be written as:

$$\sum_{p,P_p=1} C_p^t M_p^I C_p + \sum_{p,P_p=-1} C_p^t N_p^I C_p = 0 \tag{A.95}$$

with

$$C_p^t = \begin{pmatrix} C_{11p} & C_{12p} & C_{22p} \end{pmatrix}^t \tag{A.96}$$

and with

$$\begin{aligned}
M_p^1 &= \begin{pmatrix} F_p^1(x) & 0 & 0 \\ 0 & 0 & 0 \\ 0 & 0 & 0 \end{pmatrix} & N_p^1 &= 0 \\
M_p^2 &= \begin{pmatrix} 0 & 0 & 0 \\ 0 & 0 & 0 \\ 0 & 0 & F_p^2(x) \end{pmatrix} & N_p^2 &= 0 \\
M_p^3 &= \begin{pmatrix} 0 & 0 & 0 \\ 0 & 0 & F_p^3(x) \\ 0 & F_p^3(x) & 0 \end{pmatrix} & N_p^3 &= 0 \\
M_p^4 &= \begin{pmatrix} 0 & F_p^4(x) & 0 \\ F_p^4(x) & 0 & 0 \\ 0 & 0 & 0 \end{pmatrix} & N_p^4 &= 0 \\
M_p^5 &= \begin{pmatrix} 0 & 0 & 0 \\ 0 & F_p^5(x) & 0 \\ 0 & 0 & 0 \end{pmatrix} & N_p^5 &= -M_p^5 \\
M_p^6 &= \begin{pmatrix} 0 & 0 & F_p^6(x) \\ 0 & G_p^6(x) & 0 \\ F_p^6(x) & 0 & 0 \end{pmatrix} & N_p^6 &= \begin{pmatrix} 0 & 0 & 0 \\ 0 & G_p^6(x) & 0 \\ 0 & 0 & 0 \end{pmatrix}
\end{aligned} \tag{A.97}$$

where

$$\begin{aligned}
F_p^1(x) &= |1-x|^{2\Delta_1} g(0,0;\Delta_p;x) - |x|^{2\Delta_1} g(0,0;\Delta_p;1-x) \\
F_p^2(x) &= |1-x|^{2\Delta_2} g(0,0;\Delta_p;x) - |x|^{2\Delta_2} g(0,0;\Delta_p;1-x) \\
F_p^3(x) &= |1-x|^{2\Delta_2} g(0,\Delta_{21};\Delta_p;x) - |x|^{2\Delta_2} g(0,\Delta_{12};\Delta_p,1-x) \\
F_p^4(x) &= |1-x|^{2\Delta_1} g(0,\Delta_{12};\Delta_p;x) - |x|^{2\Delta_1} g(0,\Delta_{21};\Delta_p,1-x) \\
F_p^5(x) &= |1-x|^{\Delta_1+\Delta_2} g(\Delta_{12},\Delta_{21};\Delta_p;x) - |x|^{\Delta_1+\Delta_2} g(\Delta_{12},\Delta_{21};\Delta_p;1-x) \\
F_p^6(x) &= \frac{1}{2}|1-x|^{\Delta_1+\Delta_2} g(0,0;\Delta_p;x) \\
G_p^6(x) &= -|x|^{2\Delta_2} g(\Delta_{21},\Delta_{21};\Delta_p;1-x)
\end{aligned} \tag{A.98}$$

We can act with a functional on each equation, and then add all of them. This yields

$$\sum_{p,P_p=1} C_p^t \begin{pmatrix} F_p^1 & F_p^4 & F_p^6 \\ F_p^4 & G_p^6+F_p^5 & F_p^3 \\ F_p^6 & F_p^3 & F_p^2 \end{pmatrix} C_p + \sum_{p,P_p=-1} C_p^t \begin{pmatrix} 0 & 0 & 0 \\ 0 & G_p^6-F_p^5 & 0 \\ 0 & 0 & 0 \end{pmatrix} C_p = 0 \tag{A.99}$$

where F_p^I (without an argument) is shorthand for the function of Δ_p obtained by acting with the corresponding component of the functional.

If we single out the identity (with $C_{110} = C_{220} = 1$ and $C_{120} = 0$) and the external operators from the sums then we obtain

$$\begin{aligned} 0 &= F_0^1 + 2F_0^6 + F_0^2 \\ &+ \begin{pmatrix} C_{111} & C_{112} & C_{122} & C_{222} \end{pmatrix} \begin{pmatrix} F_1^1 & F_1^4 & F_1^6 & 0 \\ F_1^4 & G_1^6+F_1^5+F_2^1 & F_1^3+F_2^4 & F_2^6 \\ F_1^6 & F_1^3+F_2^4 & F_1^2+G_2^6+F_2^5 & F_2^3 \\ 0 & F_2^6 & F_2^3 & F_2^2 \end{pmatrix} \begin{pmatrix} C_{111} \\ C_{112} \\ C_{122} \\ C_{222} \end{pmatrix} \\ &+ \sum_{p,P_p=1} C_p^t \begin{pmatrix} F_p^1 & F_p^4 & F_p^6 \\ F_p^4 & G_p^6+F_p^5 & F_p^3 \\ F_p^6 & F_p^3 & F_p^2 \end{pmatrix} C_p \\ &+ \sum_{p,P_p=-1} C_p^t \begin{pmatrix} 0 & 0 & 0 \\ 0 & G_p^6-F_p^5 & 0 \\ 0 & 0 & 0 \end{pmatrix} C_p \end{aligned} \tag{A.100}$$

For a feasibility study we can normalize the functionals on the unit operators, giving

$$F_0^1 + 2F_0^6 + F_0^2 = 1 \tag{A.101}$$

and furthermore demand positive semidefiniteness of the three square matrices listed above. We can also get bounds on products of OPE coefficients. For example, if we set

$$F_1^1 = 1 \qquad F_1^4 = F_1^6 = 0 \tag{A.102}$$

and then maximize/minimize $F_0^1 + 2F_0^6 + F_0^2$, we obtain a lower/upper bound on C_{111}^2. More precisely, if we extremize and the result is positive then crossing cannot be solved. If the result is negative then the absolute value of the result is our upper (for minimization) or lower (for maximization) bound.

A.11.3 Setup with $\mathbb{Z}_2$ symmetry

In the previous section we discussed the general one-dimensional conformal bootstrap analysis for two operators. Let us now specialize to the case discussed in the main text, so we consider a QFT in AdS_2 with a $\mathbb{Z}_2$ symmetry and only two stable parity even particles; a $\mathbb{Z}_2$ odd one created by an operator ϕ_1 and a $\mathbb{Z}_2$ even one created by an operator ϕ_2.

With this additional symmetry $F^3 = F^4 = 0$ automatically which leaves four non-trivial correlation functions of ϕ_1 and ϕ_2. In these correlators we should also label the internal operators with an even/odd quantum number depending on the OPE channel in which they appear. Our notation above is already adapted to this situation: in equation (A.94) the operators labeled k are necessarily parity and $\mathbb{Z}_2$ even, whereas the operators labeled p are parity even or odd but always $\mathbb{Z}_2$ odd. (Operators that are $\mathbb{Z}_2$ even but parity odd do not feature in this set of correlation functions.) With the exception of ϕ_1 and ϕ_2 themselves we take their dimensions to lie above the following 'gap' values:

$\mathbb{Z}_2$	P	gap	index in (A.103)
even	even	$\min(2\Delta_1, 2\Delta_2)$	k
odd	even	$\Delta_1 + \Delta_2$	$p, P_p = 1$
odd	odd	$\Delta_1 + \Delta_2$	$p, P_p = -1$

These gaps are precisely the two-particle values for a QFT in AdS, reflecting our assumption that there are no further stable single-particle states.

Going then through the same logic as before we write the crossing equations in matrix form as

$$\sum_{p,P_p=1} C_p^2 M_p^I + \sum_{p,P_p=-1} C_p^2 N_p^I + \sum_k C_k^t Q_k^I C_k = 0\,, \tag{A.103}$$

with (note some redefinitions with respect to the previous formulae)

$$C_k = \begin{pmatrix} C_{11k} & C_{22k} \end{pmatrix}^t \qquad C_p = C_{12p} \tag{A.104}$$

and with

$$\begin{aligned}
M_p^1 &= 0 \qquad N_p^1 = 0 \qquad Q_k^1 = \begin{pmatrix} F_k^1(x) & 0 \\ 0 & 0 \end{pmatrix} \\
M_p^2 &= 0 \qquad N_p^2 = 0 \qquad Q_k^2 = \begin{pmatrix} 0 & 0 \\ 0 & F_k^2(x) \end{pmatrix} \\
M_p^5 &= F_p^5(x) \qquad N_p^5 = -F_p^5(x) \qquad Q_p^5 = 0 \\
M_p^6 &= G_p^6(x) \qquad N_p^6 = G_p^6(x) \qquad Q_k^6 = \begin{pmatrix} 0 & F_k^6(x) \\ F_k^6(x) & 0 \end{pmatrix}
\end{aligned} \tag{A.105}$$

After acting with the functional and singling out the important operators again we find

$$\begin{aligned}
0 = {} & F_0^1 + 2F_0^6 + F_0^2 + \begin{pmatrix} C_{112} & C_{222} \end{pmatrix} \begin{pmatrix} G_1^6 + F_1^5 + F_2^1 & F_2^6 \\ F_2^6 & F_2^2 \end{pmatrix} \begin{pmatrix} C_{112} \\ C_{222} \end{pmatrix} \\
& + \sum_{p,P_p=1} C_p^2 (G_p^6 + F_p^5) + \sum_{p,P_p=-1} C_p^2 (G_p^6 - F_p^5) + \sum_k \begin{pmatrix} C_{11k} & C_{22k} \end{pmatrix} \begin{pmatrix} F_k^1 & F_k^6 \\ F_k^6 & F_k^2 \end{pmatrix} \begin{pmatrix} C_{11k} \\ C_{22k} \end{pmatrix}
\end{aligned} \tag{A.106}$$

If we want to find bounds in the (C_{112}, C_{222}) plane we can set $C_{222} = \beta C_{112}$ and set a

normalization

$$1 = G_1^6 + F_1^5 + F_2^1 + 2\beta F_2^6 + \beta^2 F_2^2 \tag{A.107}$$

With this normalization our problem takes the form of a semidefinite program and we can proceed using the well-known numerical bootstrap methods of [107,108] and the specialized solver of [112]. Further technical details are available upon request from the authors.

A.11.4 Functionals and derivative combinations

As in previous works, our choice of functionals are linear combinations of derivatives of the crossing equations at $z = 1/2$, so our functionals α can be written as

$$\alpha[F(z)] = \sum_{n=0}^{\Lambda} \alpha_n \frac{d^n F}{dz^n}(1/2). \tag{A.108}$$

The coefficients α_n should be thought of as the main degrees of freedom to be fixed by the optimization procedure. Furthermore, in a multi-correlator study we can act with a different functional on each of the crossing equations in (A.94), so the degrees of freedom are

$$\alpha_n^I, \qquad I \in \{1, 2, 5, 6\}, \qquad n \in \{0, 1, 2, \dots \Lambda\}\,. \tag{A.109}$$

where, as before, I denotes the different crossing equations and we used that the third and fourth equation are identically zero by our $\mathbb{Z}_2$ symmetry assumptions.

Of course the functions that are odd around $z = 1/2$, like the first and second crossing equation in (A.94), contribute only about $\Lambda/2$ non-trivial degrees of freedom since the α_n for odd n are meaningless (and in fact should be set to zero to prevent numerical instabilities). This reduces the scaling of the number of components to 3Λ rather than 4Λ.

In our earliest attempts we thought it unfair to first two crossing equations that they could only contribute half as many functional components as the fifth and sixth equation. Therefore we decided to cut off the sum in (A.108) at $\Lambda/2$ for the fifth and sixth equation but at Λ for the first and second equation. Such an egalitarian approach, however, would have led to completely different and incorrect results. To illustrate this we plot in figure A.12 the upper bound on the coupling as a function of $\Lambda^5 = \Lambda^6$, i.e. the cutoffs for the fifth and sixth equation, whilst holding fixed every other parameter, including the cutoffs $\Lambda^1 = \Lambda^2$ for the first and second equation. Clearly for $\Lambda^5 = \Lambda^1/2$ the multi-correlator bound offers exactly no improvement over the single-correlator bound. So, if we had continued to work with the egalitarian cutoffs then we would erroneously conclude that no improvement would have been possible over the single-correlator bound! Only when increasing Λ^5 beyond $\Lambda^1/2$ do we begin to see a gradual improvement, which stops as abruptly as it started at $\Lambda^5 = \Lambda^1$.

Notice that the plot is drawn for the △ data point in figure 2.11, which has the special property that the multi-correlator bound turns out to be exactly half that of the single-correlator bound. We however observed very similar behavior, including the kinks and stabilization, also for other data points where the final multi-correlator bound is completely non-trivial.

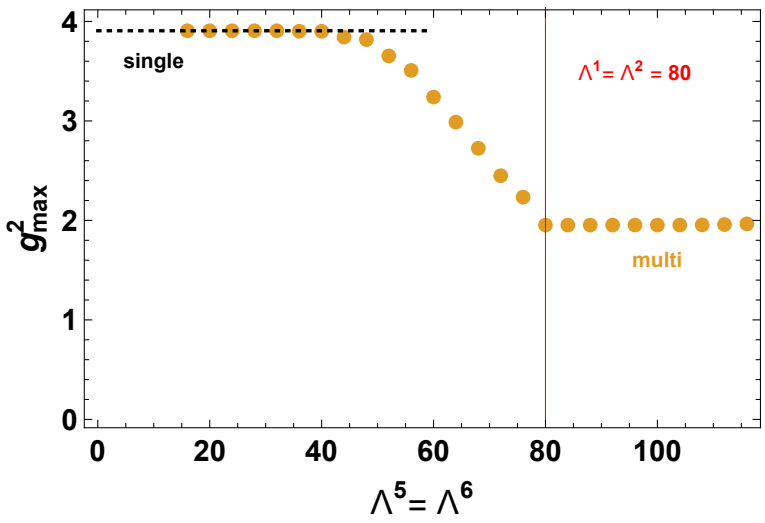

Figure A.12: Bound on the maximal coupling (without any extrapolations) as a function of $\Lambda^5 = \Lambda^6$ for fixed $\Lambda^1 = \Lambda^2 = 80$. We see that the multi-correlator bound does not improve over the single-correlator bound (in black) for a range of values of $\Lambda^5 = \Lambda^6$, and this may lead one to believe that no improvement is possible whatsoever. On the other hand, increasing $\Lambda^5 = \Lambda^6$ above the natural value given by $\Lambda^1 = \Lambda^2$ does not seem to lead to further improvements for the range of values that we tested. The case shown here has $\Delta_1 = \Delta_2 = 6.58895$ and $g_{222}/g_{112} = 1$, but other cases look similar: we start with a plateau, then a kink (not necessarily at $\Lambda^1/2$) marks the start of a downward trajectory (which is not necessarily this linear), and then another kink at $\Lambda^5 = \Lambda^1$ leads to a second plateau where the bound is constant.

A.11.5 Extrapolations

An example of the extrapolation procedure outlined in section 2.4.1 is shown in figure A.13. One important subtlety not mentioned in the main text is that we extrapolate the log-ratio of the multi-correlator and the single-correlator result. That is, for every multi-correlator optimization run we also ran a single-correlator optimization run (for either $\langle 1111 \rangle$ or $\langle 2222 \rangle$) and so we get raw data that we can denote $(g^2_{112})^{\text{max,multi}}[\mu, \alpha, \Delta_1, \Lambda]$ and $(g^2_{112})^{\text{max,single}}[\mu, \alpha, \Delta_1, \Lambda]$. We found that direct extrapolation of the multi-correlator bounds led to a relatively large dependence on our fitting procedure, whereas extrapolation of the log-ratio

$$\log(g^2_{112})^{\text{max,multi}}[\mu, \alpha, \Delta_1, \Lambda] - \log(g^2_{112})^{\text{max,single}}[\mu, \alpha, \Delta_1, \Lambda] \tag{A.110}$$

could, as shown, be done with relatively low-degree fits. Since we know that the single-correlator bounds match the analytic single-amplitude bounds with large accuracy [104], we can add (the logarithm of) this known answer to our extrapolated log-ratio to obtain a better estimate of the flat-space multi-correlator bound.

The first 8 plots show the raw data and subsequent extrapolations to infinite Λ. The three curves correspond to fits with a polynomial in Λ^{-1} of degree 3 (in blue), degree 4 (in orange, mostly coinciding with blue), and degree 2 (in green). In the fits we did not include the (three) data points with $\Lambda < 60$. We observe a rather small difference between the different extrapolations, and we have checked that these fits give good predictions for

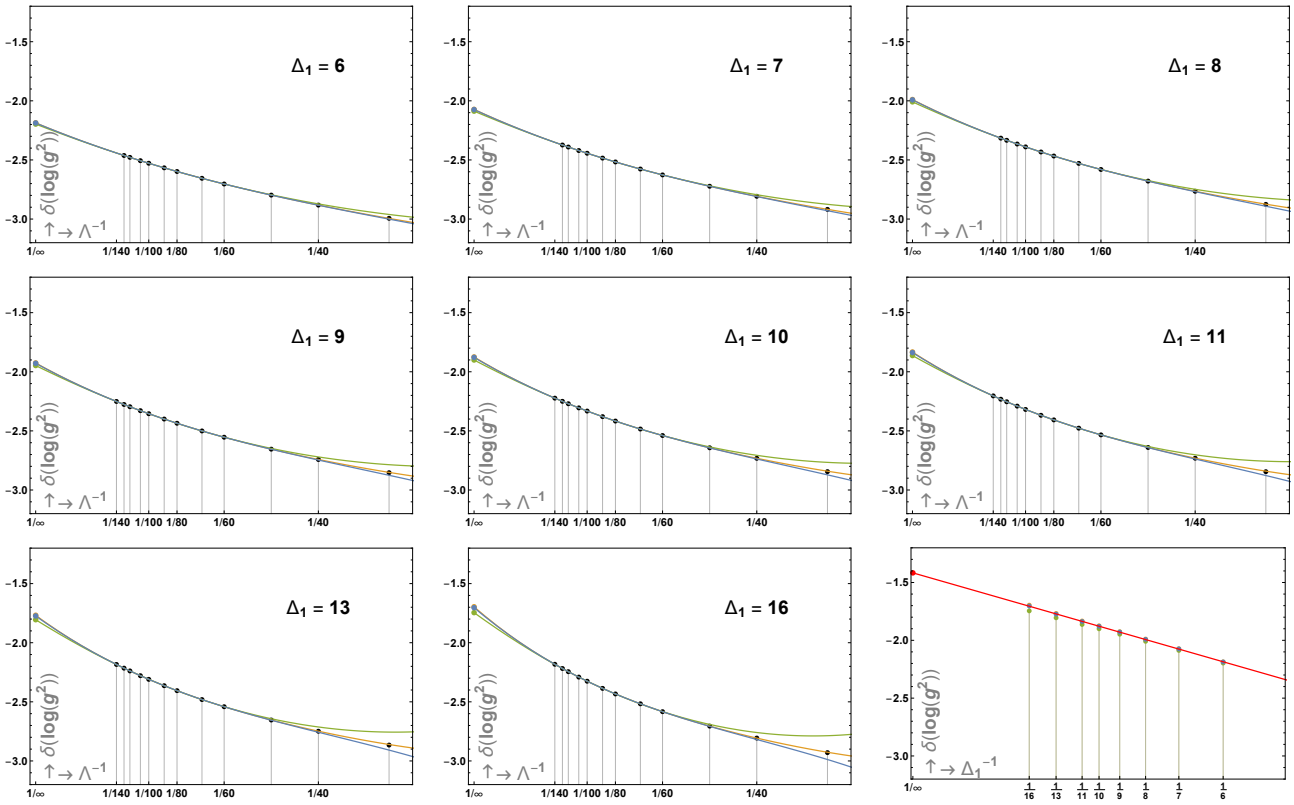

Figure A.13: The double extrapolation for the data point with $m_2/m_1 = 1.15$ in figure 2.12. Vertically we plot the logarithm of the maximal coupling, but with the logarithm of the single-correlator bound subtracted, so $\delta(\log(g^2_{\text{max}})) = \log(g^2_{\text{max,multi}}) - \log(g^2_{\text{max,single}})$. In the first 8 plots we show our raw data in black, and the curves correspond to three different extrapolations to infinite Λ. In the final plot we collected the $\Lambda \to \infty$ extrapolations and the single red line represents our $\Delta_1 \to \infty$ extrapolation. Our final answer gives $\delta(\log(g^2_{\text{max}})) \approx -1.446$ in the flat-space limit, and adding the single-correlator bound 3.673 gives the 2.226 plotted in figure 2.12.

the high Λ raw data points if we exclude one or more of them by hand.

The final plot in figure A.13 collects all the extrapolated points to infinite Λ. The data points line up nicely, providing evidence for a small non-systematic error in our first extrapolation. We have fitted a linear function in Δ^{-1} to the degree 3 (in blue) points, leading to the extrapolated value of -1.446 for the log-ratio of this data point. From this plot it is clear that there is no meaningful difference if we had extrapolated the degree 4 (in orange) points instead.

We employed exactly the same extrapolation procedure, including the choice of the degree of the fitting functions, for all the other data points shown in the main text.

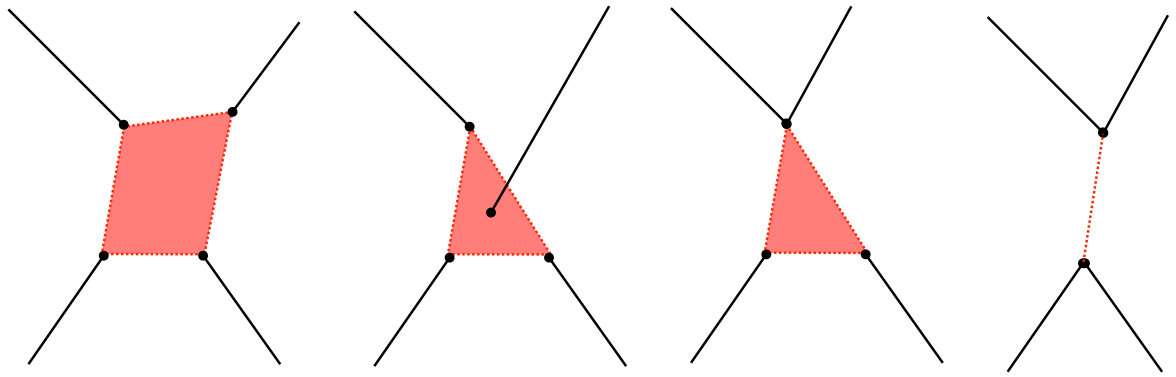

Figure A.14: An on-shell scattering process must lie inside the convex hull defined by the vertices attached to external lines. This is due to momentum conservation: an on-shell internal particle that wandered outside the convex hull would never be able to move back inside, since there would be no external momentum available to kick it back in. There are 3 possible convex hulls for $2 \to 2$ amplitudes: a quadrilateral, a triangle, or a line.

A.12 Landau Singularities in $12 \to 12$ Scattering

Landau singularities are associated to diagrams representing particle interactions with all lines on-shell and momentum conservation at each vertex [109, 111]. We claimed in the text that for the forward $12 \to 12$ scattering there ought to be no new such singularities (to be added to the bound state poles already there) whereas for the $12 \to 12$ backward component we claimed that when $m_2 > \sqrt{2}m_1$ we do find such new on-shell processes. It is easy to convince oneself of that with a few pictures. For that purpose, we adapt here some beautiful discussion in chapter 18 of the book [235] by Bjorken and Drell, translating it to our two dimensional case of interest.

Start with a diagram representing a two-to-two on-shell process. Each of the four external particles eventually encounter a vertex (several can meet at the same vertex). Consider those vertices containing an external line. They define a convex hull which can be a quadrilateral, a triangle or a line as shown in figure A.14. Next we draw all other internal lines to complete the Landau diagram. The first important claim is that all those lines must lie inside the convex hulls just defined. That is simply because of momentum conservation: if they got out of the convex hull there would be no external particle to kick them back in (and the diagram would never close)! With this in mind we can go on to analyse the three possible convex hulls in turn.

Consider first the quadrilateral case and assume first that at each of the four external vertices we have a cubic vertex. Then, momentum conservation and on-shellness constrains the angles at those cubic vertices[12]. For example, for the case at hand with two particles of

[12]In this appendix we assume that the diagrams and four-momenta are euclidean. This is the case in-between two-particle cuts, since then all spatial momenta can be chosen to be purely imaginary, making the lorentzian metric effectively euclidean. The absence of Landau diagrams in the full physical sheet

$$x = 2\arccos\frac{m_2}{2m_1} < \frac{\pi}{2} \text{ if } m_2 > \sqrt{2}m_1$$

Figure A.15: On-shellness and energy-momentum conservation fix angles in cubic vertices. Importantly, when $m_2 > m_1\sqrt{2}$ there are acute angles in cubic couplings and the analysis of Landau singularities becomes more intricate.

different masses we have the angles in figure A.15. For $m_2 < \sqrt{2}m_1$ we realize right away that the angles are obtuse so it is generically impossible to form a quadrilateral! What about using other vertices when particles first interact? Well, that would be even worse as the total opening angles would be even greater in that case. If $m_2 > \sqrt{2}m_1$ then one of the angles is smaller than $\pi/2$ so we have a better chance of finding extra singularities and, indeed, we can sometimes form such diagrams, as the one in figure 2.13, but not if two external particles are of type 2 and two particles are of type 1 as illustrated in figure A.16(a). Hence, there are no "quadrilateral convex hull" Landau diagrams for $12 \to 12$ scattering.

What about "triangular convex hull" singularities? When $m_2 > \sqrt{2}m_1$, as explained in figure A.16(b), those are indeed present in the backward component, but not in the forward one. So the backward amplitude should have extra Landau poles but the forward amplitude should not. As such, the bound on g^2_{112} derived from the forward component should hold even for $m_2 > \sqrt{2}m_1$. As discussed in the main text, this bound is not captured by the QFT in AdS bootstrap, see figure 2.12.

We did not discuss the case where the convex hull is the line: those are just the usual singularities such as the bound state poles and all the production cuts which open for multi-particles at rest, and thus moving parallel to each other, along the convex hull line.

follows from their absence in the euclidean region after a causality argument, as detailed in [235].

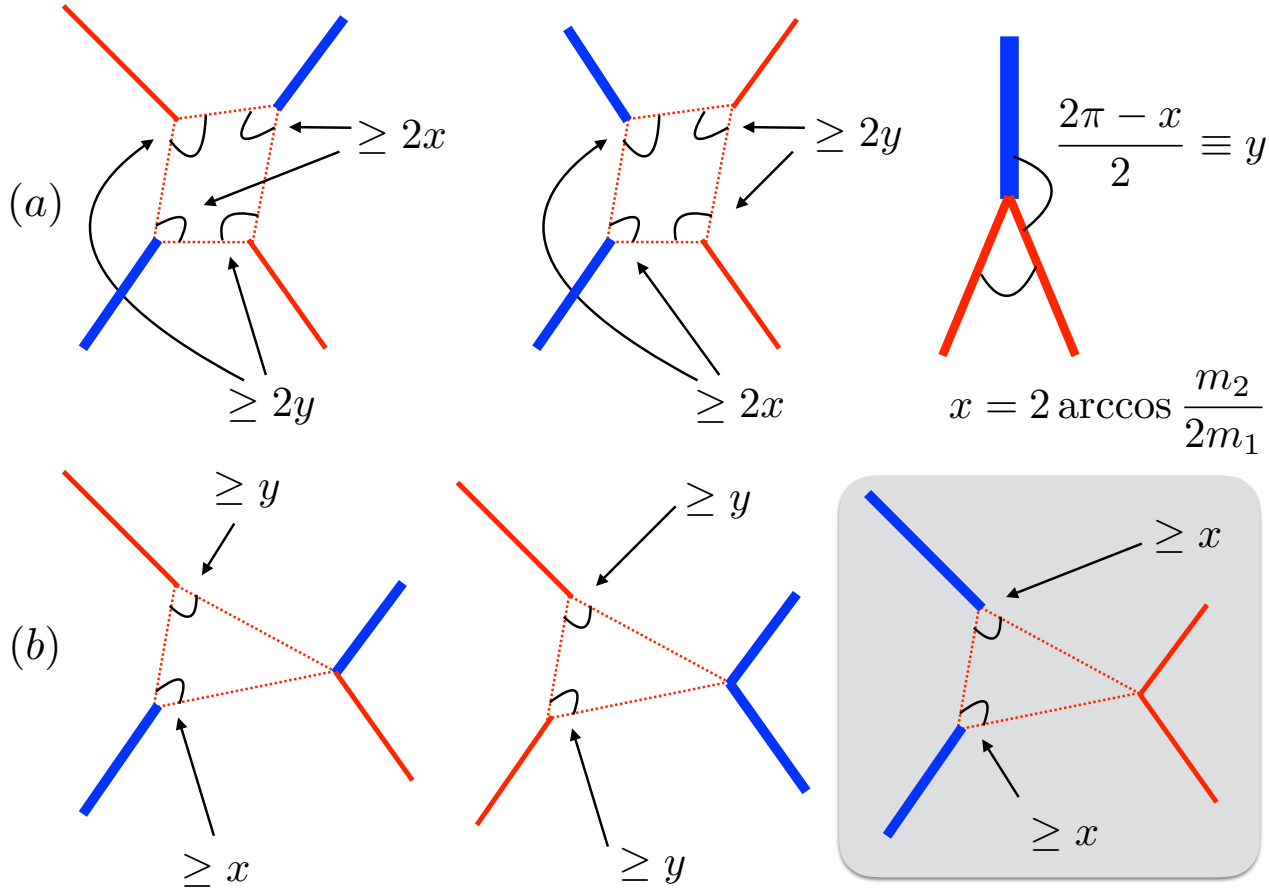

Figure A.16: (a) There are no possible "quadrilateral convex hull" Landau singularities in the $12 \to 12$ amplitude even when $m_2 > \sqrt{2}m_1$. To understand this, consider a vertex with an external leg attached. The total opening between internal edges on such vertex must be greater than x (y) for an external even (odd) leg. Hence, for the $12 \to 12$ process, the total internal angles at the four external vertices must be greater than $2(x + y) \geq 2\pi$, so that it is inconsistent to have a closed singular diagram inside the convex hull. (b) The same is true for "triangular convex hull" diagrams unless two odd particles meet at the same external vertex, as on the bottom right diagram - as in other cases the total opening at external vertices would be greater than π. For the forward component there would be no momentum transfer through such vertex, so that by on-shellness and energy-momentum conservation the internal opening at this vertex would be at least π, once again making it impossible to have a singular Landau diagram. For the backward component, on the other hand, the momentum transfer through the vertex, and hence the opening angle, can be arbitrary. In turn, this amplitude will have extra Landau singularities for $m_2 > \sqrt{2}m_1$.

Appendix B

Appendix: The S-matrix Bootstrap: SUSY, $\mathbb{Z}_2$ and $\mathbb{Z}_4$ symmetry

B.1 Parity and signs

In this appendix we formally review the relation between parity and the signs of residues appearing in the S-matrix [239].

Consider a diagonal scattering process in which a particle a collides against a particle b where both have mass m. If ab can form a bound state c of mass m_c, the S-matrix S_{ab}^{ab} will contain a pole at $s = m_c^2$:

$$S_{ab}^{ab}(s \to m_c^2) \sim -\mathrm{J}_c \frac{{}_{\text{out}}\langle ab|c\rangle^*_{\text{in}} {}_{\text{out}}\langle c|ab\rangle_{\text{in}}}{s - m_c^2},$$

where $\mathrm{J}_c = m^4/(2m_c\sqrt{4m^2 - m_c^2})$ is a Jacobian factor relating the free and interacting parts of the S-matrix.

We can use a PT transformation to rewrite the first three point function as[1]

$${}_{\text{out}}\langle ab|c\rangle_{\text{in}} = {}_{\text{in}}\langle ab|c\rangle_{\text{out}} \eta_a^* \eta_b^* \sigma_{ab} \eta_c,$$

where $\sigma_{ab} = -1$ if a and b are fermions, one otherwise, and η_x is the intrinsic parity of x. Therefore the sign of the residue of the s-channel pole is given by $-\eta_a^* \eta_b^* \sigma_{ab} \eta_c$.

Let's compare the general result above with some familiar examples. Recall that bosons may have intrinsic parity ± 1 while Majorana fermions may have intrinsic parity $\pm i$. If we scatter two identical bosons or Majorana fermions, the s-channel residue is always negative, since $\eta_a^* \eta_b^* \sigma_{ab} = 1$ in these cases (as is η_c from parity conservation).

Next suppose that we scatter a parity even boson and a Majorana fermion of parity i. If they form as a bound state a Majorana fermion with the same parity as the external fermion, then the residue in the s-channel will be negative as well. On the other hand, if the bound state fermion has parity $-i$ the residue will be positive. The same would occur when

[1] Our discussion is formal because this bound state production process happens for unphysical values of s, and so the two-particle states $|ab\rangle_{\text{in/out}}$ are schematic.

scattering two non-identical even bosons which produce a pseudo-scalar as a bound state. These unusual signs are relevant for the SUSY setup with an anti-fundamental bound state considered in section 3.1.1, see also appendix B.3.

B.2 Selection rules and crossing

In the main text we considered three two-particle scattering scenarios. The SUSY setup, in which we scatter a $\mathcal{N}=1$ supermultiplet against itself, is discussed in detail in appendix B.3. In this appendix we spell out the selection rules imposed by symmetry and the constraints from crossing in the two remaining cases: the $\mathbb{Z}_2$ setup, where we consider the scattering of two particle states formed out of a degenerate boson and fermion pair, (ϕ,ψ), and the $\mathbb{Z}_4$ setup, where we scatter all two particle states formed out of a particle of unit charge under $\mathbb{Z}_4$, **1**, together with its antiparticle, **3**. In all cases we assume that the scattered particles are the lightest in the (gapped) spectrum.

In the $\mathbb{Z}_2$ setup, fermion number symmetry together with parity and time-reversal symmetry impose that the two-to-two S-matrix, in the $\{|\phi\phi\rangle,|\phi\psi\rangle,|\psi\phi\rangle,|\psi\psi\rangle\}$ basis, is of the form

$$\mathbb{S}_{\mathbb{Z}_2}(\theta)=\begin{pmatrix} S^{\phi\phi}_{\phi\phi}(\theta) & 0 & 0 & S^{\psi\psi}_{\phi\phi}(\theta) \\ 0 & S^{\phi\psi}_{\phi\psi}(\theta) & S^{\psi\phi}_{\phi\psi}(\theta) & 0 \\ 0 & S^{\psi\phi}_{\phi\psi}(\theta) & S^{\phi\psi}_{\phi\psi}(\theta) & 0 \\ S^{\psi\psi}_{\phi\phi}(\theta) & 0 & 0 & S^{\psi\psi}_{\psi\psi}(\theta) \end{pmatrix},$$

where as usual, the rapidity θ is related to the center of mass energy squared s through $s=4m^2\cosh^2(\theta/2)$.

Crossing symmetry relates the scattering amplitudes at different channels through analytic continuation. The diagonal elements are self-crossing and the annihilation and reflection amplitudes, cross into each other: $S^{\psi\psi}_{\phi\phi}(\theta)=S^{\psi\phi}_{\phi\psi}(i\pi-\theta)$.

The bound state spectrum in each setup is implemented through the presence of single poles in each S-matrix element. For example, in the $\mathbb{Z}_2$ setup, assuming the presence of a degenerate boson and fermion pair (b,f) of mass $m_{\rm bs}$ as bound states, we have

$$S^{\psi\psi}_{\phi\phi}(s)=-\mathrm{J}_{\rm bs}\frac{g_{\phi\phi b}g_{\psi\psi b}}{s-m^2_{\rm bs}}-\mathrm{J}_{\rm bs}\frac{g^2_{\phi\psi f}}{t-m^2_{\rm bs}}+\ \textit{regular}$$

where *regular* correspond to analytic terms away from the unitarity cuts at $s<0$ or $s>4m^2$ and $\mathrm{J}_{\rm bs}=m^4/(2m_{\rm bs}\sqrt{4m^2-m^2_{\rm bs}})$ is a Jacobian factor.

In the $\mathbb{Z}_4$ setup, the selection rules from charge conservation combined with parity, time-reversal and charge conjugation symmetry constrain the S-matrix to be

$$\mathbb{S}_{\mathbb{Z}_4}(\theta)=\begin{pmatrix} S^{11}_{11}(\theta) & 0 & 0 & S^{33}_{11}(\theta) \\ 0 & S^{13}_{13}(\theta) & S^{31}_{13}(\theta) & 0 \\ 0 & S^{31}_{13}(\theta) & S^{13}_{13}(\theta) & 0 \\ S^{33}_{11}(\theta) & 0 & 0 & S^{11}_{11}(\theta) \end{pmatrix} \tag{B.1}$$

in the $\{|11\rangle, |13\rangle, |31\rangle, |33\rangle\}$ basis. Crossing symmetry acts as $S_{ab}^{cd}(\theta) = S_{a(4-d)}^{c(4-b)}(i\pi - \theta)$ and thus relates the transmission amplitudes as $S_{11}^{11}(\theta) = S_{13}^{13}(i\pi - \theta)$ while the annihilation and reflection amplitudes, $S_{11}^{33}(\theta)$ and $S_{13}^{31}(\theta)$, are now self crossing symmetric.

Given a solution of the $\mathbb{Z}_4$ bootstrap setup, i.e. an S-matrix with the correct analytic structure, satisfying unitarity and crossing, one can generate extra solutions by applying independently the following set of transformations:

$$\begin{aligned} \mathbb{S}_{\mathbb{Z}_4} &\to -\mathbb{S}_{\mathbb{Z}_4}, \\ S_{11}^{33} &\to -S_{11}^{33}, \\ S_{13}^{31} &\to -S_{13}^{31}, \\ \begin{pmatrix} S_{11}^{11} \\ S_{11}^{33} \\ S_{13}^{13} \\ S_{13}^{31} \end{pmatrix} &\to \begin{pmatrix} 0 & 0 & 1 & 0 \\ 0 & 0 & 0 & 1 \\ 1 & 0 & 0 & 0 \\ 0 & 1 & 0 & 0 \end{pmatrix} \begin{pmatrix} S_{11}^{11} \\ S_{11}^{33} \\ S_{13}^{13} \\ S_{13}^{31} \end{pmatrix}. \end{aligned} \tag{B.2}$$

The last transformation can be understood as a conjugation of the S-matrix by the operator $\mathbb{1} \otimes \mathcal{C}$, each factor acting on a single asymptotic particle, with particles being ordered in two particle states by their rapidities, and $\mathcal{C}$ denoting charge conjugation. The other transformations are trivial or unphysical modifications.

B.3 Supersymmetry algebra and representations

The $\mathcal{N} = 1$ superalgebra can be written in light-cone coordinates as

$$\{Q_-, Q_+\} = 0\,,\ Q_+^2 = P_+\,,\ Q_-^2 = P_-\,,$$

where $P_\pm = me^{\pm\theta}$ are the light-cone momenta. We realize the algebra as follows

$$\begin{aligned} Q_+|\phi\rangle &= \epsilon\sqrt{m}e^{\theta/2}|\psi\rangle \\ Q_+|\psi\rangle &= \epsilon^*\sqrt{m}e^{\theta/2}|\phi\rangle \\ Q_-|\phi\rangle &= \epsilon^*\sqrt{m}e^{-\theta/2}|\psi\rangle \\ Q_-|\psi\rangle &= \epsilon\sqrt{m}e^{-\theta/2}|\phi\rangle \end{aligned}$$

where θ is the rapidity of the state it acts on and ϵ is a phase conventionally chosen to be $\epsilon = e^{-i\pi/4}$ so that crossing is implemented without extra phases, see [240].

Requiring that the $\mathbb{Z}_2$ S-matrix (B.1) further commutes with the supercharges [116,241], constrains the S-matrix $\mathbb{S}_{\text{SUSY}}$ to take the form

$$\mathbb{S}_{\text{SUSY}} = \begin{pmatrix} S_{\phi\phi}^{\phi\phi} & 0 & 0 & \frac{i(S_{\phi\psi}^{\phi\psi} - S_{\phi\phi}^{\phi\phi})}{\operatorname{csch}(\theta/2)} \\ 0 & S_{\phi\psi}^{\phi\psi} & \frac{S_{\phi\phi}^{\phi\phi} - S_{\phi\psi}^{\phi\psi}}{\operatorname{sech}(\theta/2)} & 0 \\ 0 & \frac{S_{\phi\phi}^{\phi\phi} - S_{\phi\psi}^{\phi\psi}}{\operatorname{sech}(\theta/2)} & S_{\phi\psi}^{\phi\psi} & 0 \\ \frac{i(S_{\phi\psi}^{\phi\psi} - S_{\phi\phi}^{\phi\phi})}{\operatorname{csch}(\theta/2)} & 0 & 0 & S_{\phi\phi}^{\phi\phi} - 2S_{\phi\psi}^{\phi\psi} \end{pmatrix} \tag{B.3}$$

which we can also write as $\mathbb{S}_{\text{SUSY}} = \sigma_+ \mathbb{T}_+ + \sigma_- \mathbb{T}_-$ with

$$\mathbb{T}_- = \begin{pmatrix} \frac{\sinh(\theta/4)^2}{\cosh(\theta/2)} & 0 & 0 & \frac{i\tanh(\theta/2)}{2} \\ 0 & \frac{1}{2} & -\frac{1}{2} & 0 \\ 0 & -\frac{1}{2} & \frac{1}{2} & 0 \\ \frac{i\tanh(\theta/2)}{2} & 0 & 0 & -\frac{\cosh^2(\theta/4)}{\cosh(\theta/2)} \end{pmatrix}$$

and

$$\mathbb{T}_+ = \begin{pmatrix} \frac{\cosh^2(\theta/4)}{\cosh(\theta/2)} & 0 & 0 & -\frac{i\tanh(\theta/2)}{2} \\ 0 & \frac{1}{2} & \frac{1}{2} & 0 \\ 0 & \frac{1}{2} & \frac{1}{2} & 0 \\ -\frac{i\tanh(\theta/2)}{2} & 0 & 0 & -\frac{\sinh(\theta/4)^2}{\cosh(\theta/2)} \end{pmatrix}.$$

The tensors $\mathbb{T}_i$ are invariant under supersymmetry and are constructed such that

$$\mathbb{T}_i(\theta)\mathbb{T}_j(-\theta) = \delta_{ij}\mathbb{P}_i(\theta)\,,$$

where $\mathbb{P}_i$ are orthonormal projectors:

$$\begin{aligned} &\mathbb{P}_i(\theta)\mathbb{P}_j(\theta) = \delta_{ij}\mathbb{P}_i(\theta)\,, \\ &\mathbb{P}_-(\theta) + \mathbb{P}_+(\theta) = \mathbb{1}\,. \end{aligned}$$

Using these properties we can simply write

$$S(\theta)S(-\theta) = |\sigma_-(\theta)|^2\mathbb{P}_-(\theta) + |\sigma_+(\theta)|^2\mathbb{P}_+(\theta)\,.$$

In sum, the advantage of this parametrization is that it trivializes unitarity to

$$|\sigma_+(\theta)|^2 \leq 1 \;\text{ and }\; |\sigma_-(\theta)|^2 \leq 1\,.$$

At this point unitarity is cast in the same spirit of previous S-matrix bootstrap works [11, 15]. As in those works, we are splitting the symmetry group into irreducible representations associated with the projectors $\mathbb{P}_+$ and $\mathbb{P}_-$ corresponding to the fundamental and anti-fundamental representations of the supersymmetry algebra. Within each channel, unitarity is as straightforward as for a single component scattering.

To put a bound state excitation in a particular representation we must put a single pole in the correspondent σ_i function, or conversely, require that the residue of the other representation is zero. If we let $\theta_* = i\gamma$ be the position of the bound state pole in the θ-plane, we have the following relations between the coupling strenghts[2]:

$$\begin{aligned} &\text{fundamental}: g^2_{\phi\phi b} = g^2_{\phi\psi f}\left(1 + \sec\left(\tfrac{\gamma}{2}\right)\right), \\ &\text{anti-fundamental}: g^2_{\phi\phi b} = g^2_{\phi\psi f}\left(-1 + \sec\left(\tfrac{\gamma}{2}\right)\right). \end{aligned} \tag{B.4}$$

[2]We can also arrive at the coupling relations by writing the residues as three point functions and use supersymmetric Ward identities.

The difference in the signs of residues in each case can be interpreted as a difference in the parities of the bound states, see appendix B.1. In both scenarios the boson is parity even, but the fermionic bound state differs. It has the same parity as the external fermion when the multiplet is in the fundamental representation and the opposite parity when it is in the anti-fundamental representation.

B.4 Exact S-matrices

In this appendix we briefly review the exact S-matrices and related field theories showing up in chapter 3. These include the regular sine-Gordon model (SG) [238], the supersymmetric sine-Gordon model (SSG) [116], the restricted sine-Gordon model (RSG) [242,243], Zamolodchikov's $\mathbb{Z}_4$ S-matrix [114] and, so far as we are aware, a novel elliptic deformation of the SSG breathers S-matrix [1], and a new non-factorizable deformation of SSG. The relations between the various S-matrices are summarised in section 3.2.

B.4.1 Sine-Gordon

We begin with the regular sine-Gordon theory, whose action is

$$A_{\text{SG}} = \frac{(\gamma+\pi)}{8\pi\gamma}\int d^2x\left(\frac{\partial_\mu\phi\,\partial^\mu\phi}{2}+m^2\left(\cos\phi-1\right)\right),$$

where γ is the effective coupling. For $\gamma \geq \pi$ the spectrum consists of solitons $\{|+\rangle,|-\rangle\}$ carrying $U(1)$ topological charges. Their exact scattering [238] matrix $S_{\text{SG}_{\text{kinks}}}(\theta)$, in the $\{|++\rangle,|+-\rangle,|-+\rangle,|--\rangle\}$ basis, is equal to

$$\mathcal{U}(\theta)\times\begin{pmatrix}\sinh\frac{\pi(i\pi-\theta)}{\gamma} & 0 & 0 & 0\\ 0 & \sinh\frac{\pi\theta}{\gamma} & i\sin\frac{\pi^2}{\gamma} & 0\\ 0 & i\sin\frac{\pi^2}{\gamma} & \sinh\frac{\pi\theta}{\gamma} & 0\\ 0 & 0 & 0 & \sinh\frac{\pi(i\pi-\theta)}{\gamma}\end{pmatrix} \tag{B.5}$$

where $\mathcal{U}(\theta)=\frac{\Gamma\left(\frac{\pi}{\gamma}\right)\Gamma\left(1+i\frac{\theta}{\gamma}\right)\Gamma\left(1-\frac{\pi}{\gamma}-i\frac{\theta}{\gamma}\right)}{i\pi}\prod_{n=1}^{\infty}\frac{F_n(\theta)F_n(i\pi-\theta)}{F_n(0)F_n(i\pi)}$ with $F_n(\theta)=\frac{\Gamma\left(\frac{2n\pi+i\theta}{\gamma}\right)\Gamma\left(1+\frac{2n\pi+i\theta}{\gamma}\right)}{\Gamma\left(\frac{(2n+1)\pi+i\theta}{\gamma}\right)\Gamma\left(1+\frac{(2n-1)\pi+i\theta}{\gamma}\right)}$.

The S-matrix (B.5) corresponds to the green edge along the boundary of the $\mathbb{Z}_4$ symmetric S-matrices of figure 3.3. The edge is parameterized by $\gamma\in(\pi,\infty)$, with $\gamma=\pi$ corresponding to free field theory.

For $\gamma<\pi$ the solitons can form bound-states called breathers. In integrable theories, the bound states S-matrix can be obtained from the fusion of the S-matrices of their constituents, figure B.1. For the lightest breather of sine-Gordon this gives

$$S_{\text{SG}_{\text{breathers}}}(\theta)=\frac{\sinh\theta+i\sin\gamma}{\sinh\theta-i\sin\gamma},$$

which appeared in the S-matrix bootstrap context in [9]. There it was shown (both analytically and numerically) that this S-matrix has the biggest coupling between the external

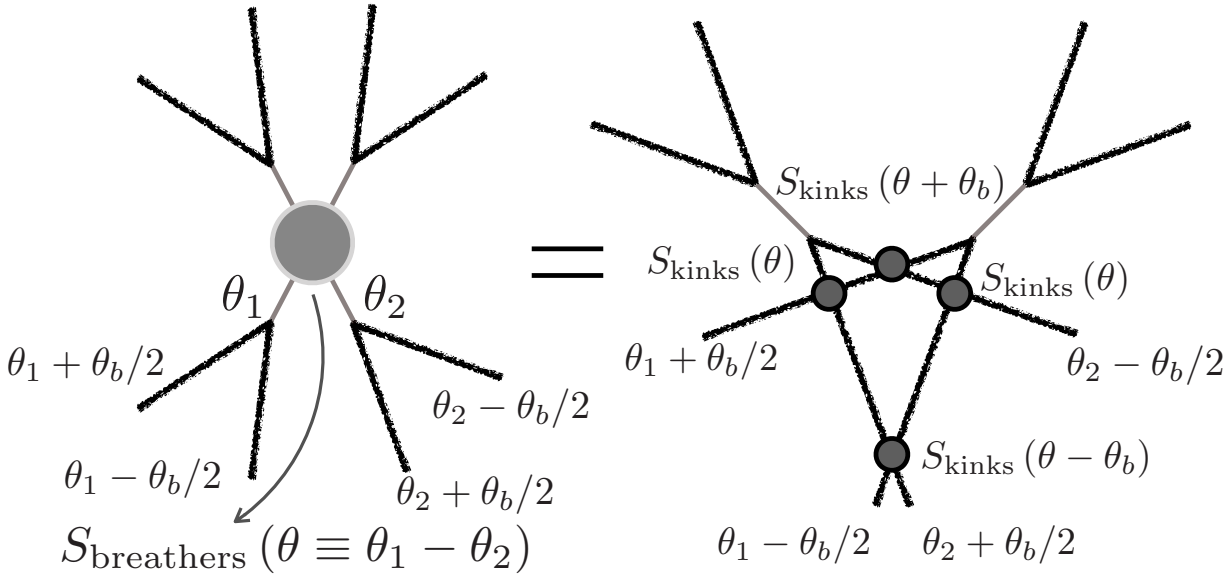

Figure B.1: Suppose we scatter two pairs of kinks, the constituents of each pair having the precise relative rapidity θ_b so as to form a breather. We then let this bound states collide and later decay. That will correspond to a double pole of the $4 \to 4$ kink S-matrix whose coefficient is proportional to the breather-breather S-matrix of the theory. This is the process described in the left hand side of the picture. From integrability, we can rearrange the incoming wave packets so that the kinks scatter before fusing into bound states, as in the right hand side of the figure. In this way, we relate the breathers S-matrix to a factorised product of four two-to-two kinks S-matrix. For simplicity, we omitted quantum numbers that would be relevant in the sine-Gordon or supersymmetric sine-Gordon theories, such as topological or SUSY charges. The fusing angle is fixed both in SG and SSG to be $\theta_b = i\gamma$.

particles (lightest breather) and their bound state (second-lightest breather).

B.4.2 Restricted sine-Gordon

The sine-Gordon theory possess $U_q(\mathfrak{sl}(2))$ quantum symmetry with $q = -e^{-i\pi^2/\gamma}$. The physics of the model is drastically modified when q is a root of identity, *i.e.*, for $\gamma = \pi p$, with $p \geq 3$ and $p \in \mathbb{Z}$. For this values some multi-soliton states decouple and the spectrum can be restricted. It is then useful to introduce a new basis of particles, as described in figure B.2, each carrying a rapidity and two $U_q(\mathfrak{sl}(2))$ spin quantum numbers.

The S-matrix between these new excitations is obtained from the fundamental solitons S-matrix (B.5) through an interaction-round-a-face to vertex transformation. For a given

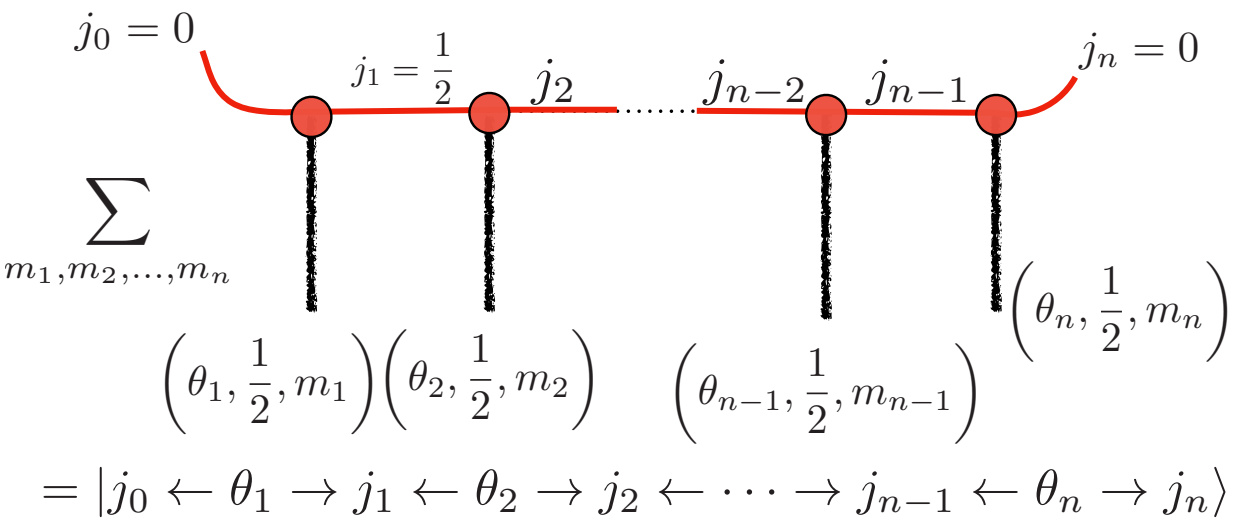

Figure B.2: Consider an n-soliton state in sine-Gordon theory. Each soliton carries a rapidity θ_i and a spin 1/2 index m_i. To construct a basis of $U_q(\mathfrak{sl}(2))$ invariant states we order the solitons in a comb-like structure and project into intermediate $U_q(\mathfrak{sl}(2))$ partial-waves at each vertex by contracting the incoming $U_q(\mathfrak{sl}(2))$ indices with some appropriately normalised $3j$-symbols, see [242] for details. Here we omit and sum over the spin indices of the intermediate states, as well as sum over external indices m_i. The state is invariant if we require that the final symbol projects the state into the spin 0 representation. The invariant subspace is spanned by different decomposition histories $(0, 1/2, j_2, \ldots, j_{n-2}, 1/2, 0)$. In this basis, it is useful to think of each rapidity θ_i as carrying two quantum numbers (j_{i-1}, j_i), see figure B.3.

p, the RSG kinks S-matrix is defined by

$$
\begin{aligned}
&|j_0 \leftarrow \theta_1 \rightarrow j_1 \ldots j_{i-1} \leftarrow \theta_i \rightarrow j_i \leftarrow \theta_{i+1} \rightarrow j_{i+1} \ldots j_n\rangle = \\
&\sum_{j_i} S^{(p)}_{\mathrm{RSG}_{\mathrm{kinks}}}\left(\begin{array}{cc} j_{i-1} & j_i' \\ j_i & j_{i+1} \end{array}\middle| \theta \equiv \theta_i - \theta_{i+1}\right) \qquad \text{(B.6)} \\
&|j_0 \leftarrow \theta_1 \rightarrow j_1 \ldots j_{i-1} \leftarrow \theta_i \rightarrow j_i \leftarrow \theta_{i+1} \rightarrow j_{i+1} \ldots j_n\rangle.
\end{aligned}
$$

As explained in figure B.3, one can then determine this S-matrix in terms of $S_{\mathrm{SG}_{\mathrm{kinks}}}$ and the $U_q(\mathfrak{sl}(2))$ $3j$-symbols [243], to be

$$
S^{(p)}_{\mathrm{RSG}_{\mathrm{kinks}}}\left(\begin{array}{cc} a & b \\ c & d \end{array}\middle| \theta\right) = \frac{\mathcal{U}(\theta)}{2}\left(\frac{[2a+1][2b+1]}{[2c+1][2d+1]}\right)^{\frac{i\theta}{2\pi}} \mathcal{R}^{ab}_{cd}
$$

$$
\mathcal{R}^{ab}_{cd} = \sqrt{\frac{[2a+1][2b+1]}{[2c+1][2d+1]}}\sinh\left(\frac{\pi\theta}{\gamma}\right)\delta_{ad} + \sinh\left(\frac{i\pi-\theta}{\gamma}\right)\delta_{cb}\,,
$$

$$
[x] = \frac{q^x - q^{-x}}{q - q^{-1}}\,,
$$

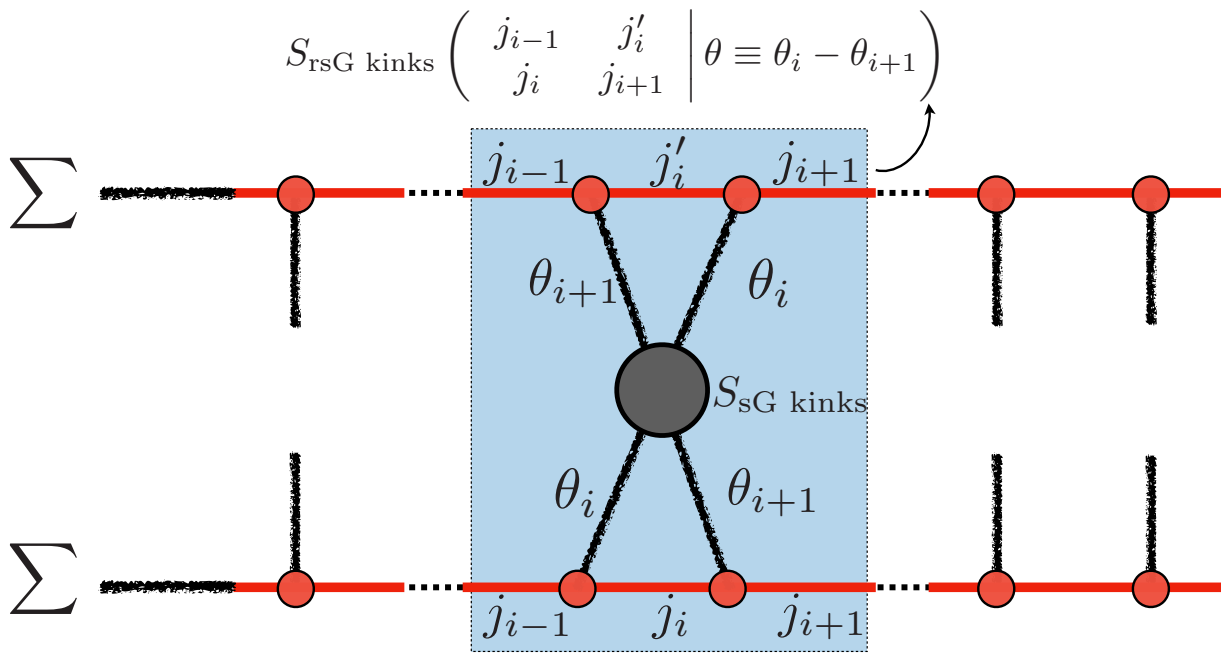

Figure B.3: Each RSG kink carries a rapidity θ_i and quantum numbers (j_{i-1}, j_i) associated to the neighbouring intermediate spins. Their S-matrix is defined by equation (B.6) in terms of the states described in figure B.2, and its relation to the regular SG kinks' S-matrix is illustrated above. As before, spin indexes are summed over and ommited. Note that the incoming and outgoing kinks must share the j_{i-1} and j_{i+1} quantum numbers: this is an IRF type S-matrix.

where $\mathcal{U}(\theta)$ has the same form as in $S_{\text{SG}_{\text{kinks}}}$.

As a consistency check on the restriction one can use this explicit form to verify that the RSG scattering amplitudes vanish whenever $a, c, d \leq p/2 - 1 < b$. For $p = 4$ the quantum group charges act on the scattering states described in figure B.2 as $\mathcal{N} = 1$ supersymmetry[3].

B.4.3 Zamolodchikov's $\mathbb{Z}_4$ S-matrix

It turns out that for $\gamma > \pi$ the sine-Gordon kinks' S-matrix admits a one-parameter deformation which preserves integrability. This is the $\mathbb{Z}_4$-symmetric elliptic S-matrix of Zamolodchikov [114], and is the basic building block to construct the full boundary of the space considered in figure 3.3. It describes the two-to-two scattering in a theory with two particles $\{|1\rangle, |3\rangle\}$. These form a particle-antiparticle pair with charges one and three under $\mathbb{Z}_4$, respectively. The explicit S-matrix $S_{\mathbb{Z}_4}(\theta)$ in the $\{|11\rangle, |13\rangle, |31\rangle, |33\rangle\}$ basis is

[3]Strictly speaking one has to do a change of basis on this states to define a canonical basis that transforms appropriately under supersymmetry as detailed in [116].

equal to

$$\mathcal{U}(\theta)\times\begin{pmatrix}\frac{\mathrm{sn}_{(\pi+i\theta)\alpha}}{\mathrm{sn}_{\pi\alpha}} & 0 & 0 & \frac{\mathrm{sn}_{(\pi+i\theta)\alpha}\mathrm{sn}_{i\theta\alpha}}{k}\\ 0 & -\frac{\mathrm{sn}_{i\theta\alpha}}{\mathrm{sn}_{\pi\alpha}} & 1 & 0\\ 0 & 1 & -\frac{\mathrm{sn}_{i\theta\alpha}}{\mathrm{sn}_{\pi\alpha}} & 0\\ \frac{\mathrm{sn}_{(\pi+i\theta)\alpha}\mathrm{sn}_{i\theta\alpha}}{k} & 0 & 0 & \frac{\mathrm{sn}_{(\pi+i\theta)\alpha}}{\mathrm{sn}_{\pi\alpha}}\end{pmatrix}$$

where $k=-1/\sqrt{\kappa}$ and where here

$$\mathcal{U}(\theta)=\exp\sum_{n=1}^{\infty}\frac{4\sinh^2(2\pi n(\pi-\beta)/\beta')\sin(2\pi n(i\pi-\theta)/\beta')}{n\csc(2\pi n\theta/\beta')\sinh(4\pi n\beta/\beta')\cosh(2\pi^2 n/\beta')}\,,$$

$$\beta=2K(\kappa)/\alpha\,,\quad \beta'=2K(1-\kappa)/\alpha\,,\quad \mathrm{sn}_x\equiv\mathrm{sn}(x,\kappa)\,,$$

with $K(\kappa)$ denoting the complete elliptic integral of the first kind and sn the Jacobi elliptic sine and $\alpha=\pi/\gamma$.

From real analyticity the deformation parameter κ must takes values in $[0,1)$ while α must be either purely imaginary or real. In the $\kappa\to 0$ limit we recover the sine-Gordon kinks S-matrix. It turns out that due to periodicity on the θ-plane the coupling value must be further constrained by $\alpha\in i\left(0,\frac{K(1-\kappa)}{\pi}\right)$ or $\alpha\in\left(0,\frac{2K(\kappa)}{\pi}\right)$ to prevent unphysical poles from coming into the physical sheet. Applying transformations (B.2) to Zamolodchikov's $\mathbb{Z}_4$ S-matrix the full boundary of the space described in figure 3.3 is obtained.

B.4.4 Minimal supersymmetric sine-Gordon

The $\mathcal{N}=1$ supersymmetric sine-Gordon action is given by

$$A_{\mathrm{SSG}}=\frac{(\gamma+2\pi)}{4\pi\gamma}\int d^2x\Bigg(\frac{\partial_\mu\phi\,\partial^\mu\phi}{2}+\frac{i}{2}\bar{\psi}\partial\!\!\!/\psi+$$
$$+\frac{m^2}{4}\cos\phi^2-\frac{m}{2}\bar{\psi}\psi\cos\phi\Bigg).$$

Just as sine-Gordon, for $\gamma<\pi$, the spectrum contains bound states (breathers). And by the same process of fusion, described in figure B.1, we obtain the S-matrix of the lightest breather supermultiplet, [116]. In the $\{|\phi\phi\rangle,|\phi\psi\rangle,|\psi\phi\rangle,|\psi\psi\rangle\}$ basis it is given by

$$S_{\mathrm{SSG}_{\mathrm{breather}}}(\theta)=S_{\mathrm{SG}_{\mathrm{breather}}}(\theta)\mathcal{U}(\theta)\times \tag{B.7}$$
$$\begin{pmatrix}\frac{2i\sin(\gamma/2)}{\sinh(\theta)}+1 & 0 & 0 & \frac{\sin(\gamma/2)}{\cosh\left(\frac{\theta}{2}\right)}\\ 0 & 1 & \frac{i\sin(\gamma/2)}{\sinh\left(\frac{\theta}{2}\right)} & 0\\ 0 & \frac{i\sin(\gamma/2)}{\sinh\left(\frac{\theta}{2}\right)} & 1 & 0\\ \frac{\sin(\gamma/2)}{\cosh\left(\frac{\theta}{2}\right)} & 0 & 0 & \frac{2i\sin(\gamma/2)}{\sinh(\theta)}-1\end{pmatrix}$$

where

$$\mathcal{U}(\theta) =$$
$$\left[\frac{\Gamma(-i\theta/2\pi)}{\Gamma(1/2-i\theta/2\pi)}\prod_{n=1}^{\infty}\left(\frac{\Gamma(\gamma/2\pi-(i\theta/2\pi)+n)}{\Gamma(\gamma/2\pi-(i\theta/2\pi)+n+1/2)}\times\right.\right.$$
$$\left.\left.\frac{\Gamma(-\gamma/2\pi-(i\theta/2\pi)+n-1)\,\Gamma^2(-(i\theta/2\pi)+n-1/2)}{\Gamma(-\gamma/2\pi-(i\theta/2\pi)+n-1/2)\,\Gamma^2(-(i\theta/2\pi)+n-1)}\right)\right]\times$$
$$[\theta\to i\pi-\theta]$$

The poles in the lightest breather S-matrix correspond to the second-lightest breather supermultiplet of the spectrum.

It turns out that the supersymmetric sine-Gordon S-matrix is completely fixed by supersymmetry and Yang-Baxter [240, 241]. Indeed, requiring that the general SUSY S-matrix (B.3) satisfies the Yang-Baxter condition implies that $S^{\phi\phi}_{\phi\phi}/S^{\phi\psi}_{\phi\psi} = 1 + i\alpha/\sinh\theta/2$ with α a constant. The overall factor is then fixed by unitarity up to CDD ambiguities. Furthermore, by requiring that the residues in different matrix elements are consistent with a bound state in the fundamental representation we fix α and obtain the matrix structure of the SSG breathers S-matrix (B.7). For a bound state in the anti-fundamental representation, the S-matrix is similarly fixed to be $S_{\mathrm{SSG}_{\mathrm{breathers}}}$ analytically continued to $\gamma\to\gamma+2\pi$.

B.4.5 Elliptic deformation of the supersymmetric sine-Gordon

In [1] a Yang-Baxter preserving but supersymmetry breaking deformation of (B.7) was obtained. The S-matrix is

$$S_{\mathrm{ED}}(\theta) = S_{\mathrm{SG}_{\mathrm{breathers}}}(\theta)\mathcal{U}(\theta)\times$$
$$\begin{pmatrix} \frac{\mathrm{dn}_{\theta\omega}\mathrm{sn}_{i\gamma\omega}}{\mathrm{cn}_{\theta\omega}\mathrm{sn}_{\theta\omega}}+\mathrm{dn}_{i\gamma\omega} & 0 & 0 & \frac{\mathrm{dn}_{\theta\omega}\mathrm{sn}_{i\gamma\omega}}{\mathrm{cn}_{\theta\omega}} \\ 0 & 1 & \frac{\mathrm{sn}_{\gamma\omega}}{\mathrm{sn}_{\theta\omega}} & 0 \\ 0 & \frac{\mathrm{sn}_{\gamma\omega}}{\mathrm{sn}_{\theta\omega}} & 1 & 0 \\ \frac{\mathrm{dn}_{\theta\omega}\mathrm{sn}_{i\gamma\omega}}{\mathrm{cn}_{\theta\omega}} & 0 & 0 & \frac{\mathrm{dn}_{\theta\omega}\mathrm{sn}_{i\gamma\omega}}{\mathrm{cn}_{\theta\omega}\mathrm{sn}_{\theta\omega}}-\mathrm{dn}_{i\gamma\omega} \end{pmatrix}$$

where

$$\mathcal{U}(\theta) = -i\sinh(\theta)\exp\left(\int_{-\infty}^{\infty}\frac{d\theta'}{2\pi i}\frac{\log\left(g(\theta')/\sinh(\theta')^2\right)}{\sinh(\theta-\theta'+i\epsilon)}\right)$$

$$\omega = -\tfrac{i}{\pi}K(\kappa)\,,\quad g(\theta) = 1-\tfrac{\mathrm{sn}(i\gamma\omega,\kappa)^2}{\mathrm{sn}(\theta\omega,\kappa)^2}\,,$$

$$\mathrm{sn}_x = \mathrm{sn}(x,\kappa)\,,\quad \mathrm{dn}_x = \mathrm{dn}(x,\kappa)\,,\quad \mathrm{cn}_x = \mathrm{cn}(x,\kappa)\,.$$

The deformation parameter κ is constrained to the interval $(-\infty,1)$ due to real analyticity, with the SSG breathers S-matrix being recovered in the $\kappa\to 0$ limit. The residues of

this S-matrix as a function of κ correspond to the solid line in figure 3.3.

B.4.6 Non factorizable deformation of supersymmetric sine-Gordon

Following the steps described in appendix B.5 we were able to obtain an analytical expression for the supersymmetric S-matrices that lies along boundary of the space described in figure 3.1:

$$S_{\rm NF}(\theta) = S_{\rm SSG_{breathers}}(\theta)\,\mathcal{U}(\theta)\times$$

$$\begin{pmatrix} r(\theta) & 0 & 0 & \frac{i(1-r(\theta))}{\operatorname{csch}(\theta/2)} \\ 0 & 1 & \frac{r(\theta)-1}{\operatorname{sech}(\theta/2)} & 0 \\ 0 & \frac{r(\theta)-1}{\operatorname{sech}(\theta/2)} & 1 & 0 \\ \frac{i(1-r(\theta))}{\operatorname{csch}(\theta/2)} & 0 & 0 & r(\theta)-2 \end{pmatrix}, \tag{B.8}$$

where

$$\mathcal{U}(\theta) = \pm\left(\frac{\sinh\theta - i\sqrt{t}}{\sinh\theta + i\sqrt{t}}\right)^{\Theta(t)}$$
$$\times \exp\left(-\int_{-\infty}^{\infty}\frac{d\theta'}{2\pi i}\frac{\log\left(1-\cosh^2(\theta'/2)\,(1-r(\theta'))^2\right)}{\sinh(\theta'-\theta+i\epsilon)}\right),$$

with $r(\theta)$ being the ratio function found in (B.10).

By varying the parameter $t \in \mathbb{R}$ and the overall signs in $\mathcal{U}$ we parametrize the full boundary of figure 3.1. The CDD-zero only makes sense for positive t. Negative values of this parameter would break real analyticity and introduce poles in physical of scattering energies, hence the presence of the step function. The reader can see that $t = 0$ yields the SSG model.

B.5 More on the ratio function

The S-matrices on the boundary of the supersymmetric bootstrap are unitary. This constrains the S-matrices to be on the form (B.8) with the condition that

$$r(\theta) + r(-\theta) = 2 \tag{B.9}$$

where r is simply the ratio between the two independent S-matrices elements ($r = S^{\phi\phi}_{\phi\phi}/S^{\phi\psi}_{\phi\psi}$).

Using crossing symmetry in the relation above, is easy to see that this ratio function is $2\pi i$-periodic. This allows us to look only at two sheets of the θ-plane. It turns out that on the boundary the ratio has a very simple analytical structure. In the first sheet the numerical solutions have a pole at $\theta = i\delta_1$, a zero at $\theta = i\delta_2$ and their corresponding crossing symmetric partners. On the second sheet they have the same poles plus an extra zero at $\theta = i\pi + \delta_3$ and its crossing symmetric partner[4].

[4]Numerically we observe that the δ's belong to $(0, \pi)$ or

We start with an ansatz manifestly crossing symmetric and with the correct analytic structure

$$r(\theta) = A\left(\frac{\sinh\left(\frac{1}{2}(\theta-i\delta_2)\right)\sinh\left(\frac{1}{2}(\theta-i\delta_3)\right)}{\sinh(\theta-i\delta_1)}\right)\times(\delta_j\to\pi-\delta_j)\ .$$

The unitarity constraint (B.9) fixes δ_3 as a function of δ_1 and δ_2, leaving two free parameters. Let $\theta_* = i\gamma$ be the position of the bound state pole. The fact that the residues of the supersymmetric S-matrix elements are related by (B.4) gives another constraint,

$$r(i\gamma) = 1 \pm \sec(\gamma/2)\,,$$

where the sign reflects which representation one chooses. This relation fixes δ_2 as a function of δ_1.

At the SSG point (or at its equivalent for the anti-fundamental representation) we have $\delta_1 = 0$ and therefore

$$r(\theta)|_{\delta_1=0} = 1 \pm \frac{2i\sin(\gamma/2)}{\sinh\theta}\,,$$

which fixes the overall constant A.

The final solution then depends on two parameters: $t = \sin^2\delta_1$ and γ that determines the bound state mass,

$$r(\theta) = 1 \pm i\left(2\sin\left(\frac{\gamma}{2}\right) - \frac{t}{\sin\gamma\cos\left(\frac{\gamma}{2}\right)}\right)\frac{\sinh(\theta)}{t+\sinh(\theta)^2}\,. \tag{B.10}$$

Note that when $t = 0$ we recover the SSG model as expected and when $t = \sin(\gamma)^2$ we reach the free theories points.

B.6 Numerics

Our numerics follow verbatin the algorithms in [1, 9, 13]. In short we first propose a very general ansatz for the S-matrix elements in terms of a large linear combination of basis functions as (here the index a labels all possible scattering channels)

$$S_a(s) = \texttt{poles}_a + \texttt{regular}_a = \sum_{n=1}^{N} c_a^{(n)} f_n(s)\,.$$

with N as large as our computers allow. What are these functions f_n? They can be any basis which spans the full space of possible S-matrices – with their required analytic properties – as $N\to\infty$. Common examples are Fourier series, Taylor expansions, (discretized) dispersion relations etc. We use the latter for the plots in chapter 3.

Note that both the S-matrix elements at some off-shell value, $S_a(s_*)$, as well as the residues of the poles of the S-matrix elements are then explicit linear combinations of the $c_a^{(n)}$. These linear combinations are what we want to maximize or minimize to determine

$\{\pi/2 + i\tau | \tau \in \mathbf{R}\}$.

the boundary of the allowed S-matrix space.

So all we have to do is to maximize these linear combinations subject to the two relevant physical constraints which are crossing and unitarity. Crossing $S_a(4-s) = C_{ab}S_b(s)$ is a simple linear constraints on the $c_a^{(n)}$'s. We can use it to simply eliminate some of these constants in terms of the others. Unitarity is more interesting. In terms of probability conservation it reads as $|S_a(s)|^2 \leq 1$ for any real s above the two-particle production threshold. This condition can be trivially linearized as the statement that the matrix

$$\begin{pmatrix} 1 & S_a(s) \\ S_a(s)^* & 1 \end{pmatrix}$$

is positive semi-definite in that same range of s. In practice we impose this condition in a grid in s starting from threshold and going to some large energy value. For each s we get a positive semi-definite condition, all of which linear in all the parameters $c_a^{(n)}$. Hence our maximization problem is nothing but what is called a semidefinite programming (SDP) problem for which we can use the very powerful `sdpb` software developed by Simons-Duffin [112]. That is what we did.

Appendix C

Appendix: The S-matrix Bootstrap: 2D Dual Theory

C.1 Strong Duality

Assume M_* solves the primal problem (4.19) with optimal coupling g_*^2, and note that there are some amplitudes do not saturate unitarity since we could always cook up models with other particles also with mass m_1 and m_2 so that probability could leak into those *hidden* sectors and manifest itself as non-saturation of unitarity in our truncated Hilbert space.[1] This means that

Inner point property

$$\text{There exists an } M_i \text{ such that } \mathbb{U}(M_i) \succ 0 \text{ and } \mathbb{A}(M_i) = 0. \tag{C.1}$$

In this appendix we argue that this implies strong duality [135–137]. Consider the following auxiliary convex set in the space of real $\mathcal{G}$, symmetric $\mathcal{A}(s)$ and hermitian $\mathcal{U}(s)$:

$$\textbf{Aux} = \{(\mathcal{G}, \mathcal{A}(s), \mathcal{U}(s)) \text{ s.t. } \mathcal{G} \leq g^2, \mathcal{A}(s) = \mathbb{A}(M(s)), \mathcal{U}(s) \preceq \mathbb{U}(M(s)) \text{ for some analytic M}\}.$$

The point $\textbf{bp} \equiv \{g_*^2, 0, 0\}$ is at the boundary of **Aux**. Since **Aux** has an interior point, the supporting hyperplane theorem[2] guarantees that there exists a hyperplane (i.e. a linear functional on the $(\mathcal{G}, \mathcal{A}(s), \mathcal{U}(s))$ space) containing **bp** so that the set **Aux** is to one side of it. In equations, there exists real γ, symmetric $\mathbb{w}_c(s)$ and hermitian $\mathbb{\Lambda}_c(s)$, not all simultaneously zero, such that

$$\gamma\mathcal{G} + \int_{4m_1^2}^{\infty} ds \ \text{Tr}(\mathbb{w}_c \cdot \mathcal{A}(s) + \mathbb{\Lambda}_c \cdot \mathcal{U}(s)) \leq \gamma g_*^2 \qquad \text{for all } (\mathcal{G}, \mathcal{A}(s), \mathcal{U}(s)) \text{ in } \textbf{Aux}. \tag{C.2}$$

Note that, due to the definition of $\mathcal{A}$, this is only possible if $\gamma \geq 0$ and $\mathbb{\Lambda} \succeq 0$.[3]

[1] Here unitarity refers to both unitarity and extended unitarity.

[2] In the infinite dimensional case, this is a consequence of Hahn-Banach's theorem.

[3] To see explicitly, assume $\mathbb{\Lambda}_c(s)$ isn't positive semidefinite. Then there exists $\vec{x}$ such that $\vec{x}^\dagger \mathbb{\Lambda}_c \vec{x} < 0$. In turn, this implies that $\text{Tr}(\mathbb{\Lambda}_c \cdot (\mathcal{U} + r\vec{x}\vec{x}^\dagger))$ could become arbitrarily negative as we take $r \to \infty$. Note,

Equation (C.2) should hold in particular when the inequalities in (C.2) are saturated, in which case it reduces to

$$\gamma g^2 + \int_{4m_1^2}^{\infty} ds\ \mathrm{Tr}(\mathbb{w}_c \cdot \mathbb{A} + \mathbb{\Lambda}_c \cdot \mathbb{U}) \leq \gamma g_*^2 \qquad \text{for all } M. \tag{C.3}$$

Next, we need to argue that $\gamma \neq 0$. First note that, if that were the case, then, after renormalizing $\mathbb{w}_c \to \gamma \mathbb{w}_c$ and $\mathbb{\Lambda}_c \to \gamma \mathbb{\Lambda}_c$, we would conclude that

$$\mathcal{L}(M, \mathbb{w}_c, \mathbb{\Lambda}_c) = g^2 + \int_{4m_1^2}^{\infty} ds\ \mathrm{Tr}(\mathbb{w}_c \cdot \mathbb{A} + \mathbb{\Lambda}_c \cdot \mathbb{U}) \leq g_*^2 \qquad \text{for all } M,$$

which, paired with weak duality, leads to strong duality:

$$g_*^2 \leq d(\mathbb{w}_c, \mathbb{\Lambda}_c) \equiv \sup_{\mathbb{M}} \mathcal{L}(\mathbb{M}, \mathbb{w}_c, \mathbb{\Lambda}_c) \leq g_*^2 \implies d(\mathbb{w}_c, \mathbb{\Lambda}_c) = g_*^2.$$

In particular this implies that unless $\mathbb{\Lambda}_c$ has a zero eigenvalue, $\mathbb{U} = 0$, i.e. unitarity is saturated. This is the matrix version counterpart of the argument in [12] for unitarity saturation.

To prove that $\gamma > 0$, assume $\gamma = 0$ and look for a contradiction. Plugging M_i from (C.1) into (C.3) would show that $\mathbb{\Lambda}_c = 0$. This in turns would lead, using (C.2), to

$$\int_{4m_1^2}^{\infty} ds\ \mathrm{Tr}(\mathbb{w}_c \cdot \mathcal{A}(s)) \leq 0 \qquad \text{for all } (\mathcal{G}, \mathcal{A}(s), \mathcal{U}(s)) \text{ in } \textbf{Aux}.,$$

which can only be true for a symmetric $\mathbb{w}$ if $\mathbb{w}_c = 0$. But $\gamma, \mathbb{w}_c(s), \mathbb{\Lambda}_c(s)$ are not all zero by the supporting hyperplane theorem, which shows that $\gamma = 0$ is a contradiction. This concludes the argument.

C.2 More on dispersion relations

C.2.1 Subtracted dispersions

The construction of the dual problem starts with the dispersive representation of the amplitude, see for instance eq. (4.2). In order to allow the most general behavior compatible with polynomial boundedness, one introduces subtractions.

Here we show that for the case of $M = M_{11\to 11}$ scattering, our derivation is compatible with one-subtracted dispersions. Let us start from the identity (we set the units by the mass of the external particle $m = 1$)

$$M(s) - M(2) = \int_{\mathcal{C}_\varepsilon(s)} \frac{M(z)}{z - s} dz - \int_{\mathcal{C}_\varepsilon(2)} \frac{M(z)}{z - 2} dz, \tag{C.4}$$

however, that $(\mathcal{G}, \mathcal{A}, \mathcal{U} + r\vec{x}\vec{x}^\dagger)$ is in $\mathcal{A}$ for all $r > 0$ provided $(\mathcal{G}, \mathcal{A}, \mathcal{U})$ is. These two facts together are in contradiction with (C.2).

where $\mathcal{C}_\varepsilon(s_0)$ is a circular path around s_0 of radius ε and we can imagine there always exist a path connecting them. The amplitude $M(s)$, by physical assumptions, can only have poles on the real axis in the segment $0 < s < 4$.[4]

Blowing up the contour in eq. (C.4) we get

$$\begin{aligned}
0 = \mathcal{A}(s) = M(s) - M(2) &- \sum_i g_i^2 (s-2) \left(\frac{1}{(m_i^2 - s)(m_i^2 - 2)} - \frac{1}{(t(m_i^2) - s)(t(m_i^2) - 2)} \right) \\
&- \frac{1}{\pi} \int_4^\infty \operatorname{Im} M(z) \left(\frac{s-2}{(z-s)(z-2)} + \frac{t(s) - t(2)}{(z - t(s))(z - t(2))} \right) dz \\
&= M(s) - M(2) + \sum_i g_i^2 \left(\frac{1}{s - m_i^2} + \frac{1}{t(s) - m_i^2} - \frac{2}{m_i^2 - 2} \right) \\
&- \frac{1}{\pi} \int_4^\infty \operatorname{Im} M(z) \frac{2(s-2)^2}{(z-s)(z-2)(z+s-4)} dz. \qquad \text{(C.5)}
\end{aligned}$$

The last line of equation above shows that the imaginary part of the amplitude can grow as $\operatorname{Im} M(z) \sim z$ for large z.

We want to integrate (C.5) against the Lagrange multiplier $w(s)$. Now, note that a new primal variable we have now is the constant $M(2)$ in (C.5); when we construct the Lagrangian by integrating (C.5) agains $w(s)$, that constant term will be multiplied by the integral of $w(s)$ and thus its equations of motion will lead to $\int_4^\infty w(s) ds = 0$ which we assume henceforth. Then, it is easy to show that

$$\begin{aligned}
\int_4^\infty w(s) \mathcal{A}(s) ds = \int_4^\infty M(s) w(s) &+ \sum_i g_i^2 \int_4^\infty w(s) \left(\frac{1}{s - m_i^2} + \frac{1}{t(s) - m_i^2} \right) ds \\
&- \frac{1}{\pi} \int_4^\infty dz \operatorname{Im} M(z) \int_4^\infty w(s) \frac{2(s-2)^2}{(z-s)(z-2)(z+s-4)}.
\end{aligned}$$

If we decompose the subtracted integration kernel in partial fractions

$$\frac{2(s-2)^2}{(z-s)(z-2)(z+s-4)} = \frac{1}{z-s} + \frac{1}{z+s-4} - \frac{2}{z-2}$$

the integration against the Lagrange multiplier nicely yields[5]

$$\int_4^\infty w(s) \frac{2(s-2)^2}{(z-s)(z-2)(z+s-4)} ds = - \int_4^\infty w(s) \left(\frac{1}{s-z} - \frac{1}{s - t(z)} \right) ds.$$

Following the logic outlined in Sec. 4.2, we introduce the anti-crossing analytic function,

[4] We chose $s = 2$ as a subtraction point for convenience: the only dangerous situation is when the mass of the bound state is $m_b^2 = 2$. However, in that case the s and t-channel poles would collide canceling each other, therefore we can avoid this situation and always assume $m_b^2 \neq 2$ without loosing generality.

[5] In all these manipulations we are assuming that $w(s)$ decays fast enough to justify the integration exchanges.

holomorphic in the complex-plane without the normal unitarity cuts

$$W(z) = \frac{1}{\pi}\int_4^\infty \mathrm{Im}\, W(s)\left(\frac{1}{s-z} - \frac{1}{s-t(z)}\right) ds,$$

such that $\mathrm{Im}\, W(s) = w(s)$ for $s > 4$. At the end we get the useful identity

$$\int_4^\infty w(s)\mathcal{A}(s)ds = \int_4^\infty \mathrm{Im}\,(W(s)M(s))ds + \pi\sum_i g_i^2 W(m_i^2),$$

that we have used, for instance, to get eq. (4.11).

C.2.2 The $11 \to 12$ functional.

The analysis leading to the dispersion relation (4.44) arises from the analysis of the term

$$\int_{4m_1^2}^\infty \mathcal{A}_{11\to 12} w_2 = \mathrm{Res}_{m_1^2}(M_{11\to 12})\int_{4m_1^2}^\infty w_2\left(\frac{1}{s-m_1^2}+\frac{1}{t-m_1^2}+\frac{1}{u-m_1^2}\right)ds+$$
$$+\int_{4m_1^2}^\infty \mathrm{Re}\, M_{11\to 12} w_2\, ds - \frac{1}{\pi}\int_{4m_1^2}^\infty dz \mathrm{Im}\, M_{11\to 12}(z)\int_{4m_1^2}^\infty w_2(s)\left(\frac{1}{z-s}+\frac{1}{z-t(s)}+\frac{1}{z-u(s)}\right). \tag{C.6}$$

once we use the dispersion relation (4.38).

The second line suggests that we could define an analytic function W_2 such that $w_2 = \mathrm{Im}\, W_2$, in particular

$$\mathrm{Re}\, W_2(z) = -\frac{1}{\pi}\int_{4m_1^2}^\infty \mathrm{Im}\, W_2(s)\left(\frac{1}{z-s}+\frac{1}{z-t(s)}+\frac{1}{z-u(s)}\right) ds.$$

It is interesting to notice that while $M_{11\to 12}$ is manifestly crossing invariant in s, t, u because the integration kernel is, the crossing properties of W_2 are now implicitly defined and we need to invert the relation between $t(s)$, $u(s)$ and z. Some simple algebra shows that

$$\mathrm{Re}\, W_2(z) = \frac{1}{\pi}\int_{4m_1^2}^\infty \mathrm{Im}\, W_2(s)\left(\frac{1}{s-z}+\frac{J_t(z)}{s-t(z)}+\frac{J_u(z)}{s-u(z)}\right) ds, \tag{C.7}$$

with $J_t = dt/ds$ and $J_u = du/ds$. In other words, we can define an analytic function which is *dual crossing* symmetric in the sense that when we cross we pick a jacobian factor. Notice that this definition is compatible with (4.10) as for single component $J_t = dt/ds = -1$ and $J_u = 0$. The standard anti-crossing case thus follows as a particular case from this general rule. From eq. (C.7) we immediately recover

$$\int_{4m_1^2}^\infty \mathrm{Im}\, W_2(s)\left(\frac{1}{s-m_1^2}+\frac{1}{t(s)-m_1^2}+\frac{1}{u(s)-m_1^2}\right) ds = \pi W_2(m_1^2).$$

In practice, we have shown that eq. (C.6) can be reduced to

$$\int_{4m_1^2}^{\infty} \mathcal{A}_{11\to 12} w_2 = \int_{4m_1^2}^{\infty} \mathrm{Im}\,(W_2 M_{11\to 12})\, ds + \mathrm{Res}_{m_1^2}(M_{11\to 12}) W_2(m_1^2).$$

The analysis of the $12 \to 12$ component follows straightforwardly and is analogous to the $11 \to 11$ case.

C.3 Dual Lagrangian for multiple components

Here we present some of the algebra manipulations pertaining to section 4.3.4. In particular, the final expressions in this appendix contain the optimal phase shifts in terms of the critical dual functionals. Varying the Lagrangian

$$\mathcal{L}(\mathbb{M}, \mathbb{W}, \mathbb{\Lambda}) = \int_{4m_1^2}^{\infty} ds\, \mathrm{tr}\Big(\underbrace{\frac{\mathbb{W}\cdot\mathbb{M} - \overline{\mathbb{M}}\cdot\overline{\mathbb{W}}}{2i}}_{\mathrm{Im}(\mathbb{W}\,\mathbb{M})} + \underbrace{\mathbb{\Lambda}\cdot\big(2\frac{\mathbb{M}-\overline{\mathbb{M}}}{2i} - \mathbb{M}\cdot\rho\cdot\overline{\mathbb{M}}\big)}_{\mathbb{\Lambda}\cdot\mathbb{U}(\mathbb{M}))} \Big). \tag{C.8}$$

with respect to $\mathbb{M}$ and its conjugate[6]

$$0 = \int_{4m_1^2}^{\infty} ds\, \mathrm{tr}\, \Big(\delta\mathbb{M}\cdot\Big[\frac{\mathbb{W}}{2i} + \frac{\mathbb{\Lambda}}{i} - \rho\cdot\overline{\mathbb{M}}\cdot\mathbb{\Lambda}\Big] + \delta\overline{\mathbb{M}}\cdot\Big[\frac{\overline{\mathbb{W}}}{-2i} + \frac{\mathbb{\Lambda}}{-i} - \mathbb{\Lambda}\cdot\mathbb{M}\cdot\rho\Big]\Big)$$

Now, since δM (and its hermitian conjugate) are expressed in a basis of pauli matrices $\sigma_0(=\mathbb{I}), \sigma_1, \sigma_3$ but *not* $\sigma_2 \equiv \sigma$ we can only say that each term in square brackets is zero up to a term proportional to σ which will always vanish under the trace,

$$\frac{\overline{\mathbb{W}}}{-2i} + \frac{\mathbb{\Lambda}}{-i} - \mathbb{\Lambda}\cdot\mathbb{M}\cdot\rho = \mathbf{a}\,\sigma\,. \tag{C.9}$$

At this junction we will split the analysis into the extended and regular unitarity region for the simple reason that ρ is invertible only in the regular unitarity region.

Let us first focus on the regular unitarity region. Dotting (C.9) with $\sigma\cdot\rho\cdot\mathbb{\Lambda}^{-1}$ from the left and taking the trace kills the last two terms on the left hand side and leads to a simple expression for $\mathbf{a}$. Next, armed with $\mathbf{a}$ we can simply multiply the equation by $\mathbb{\Lambda}^{-1}$ and ρ^{-1} from the left/right respectively to get $\mathbb{M}$,

$$\mathbb{M} = \frac{i}{2}\mathbb{\Lambda}^{-1}\cdot\Big(2\mathbb{\Lambda} + \overline{\mathbb{W}} + \sigma\,\underbrace{\frac{\mathrm{tr}\,(\sigma\cdot\mathbb{W}\cdot\mathbb{\Lambda}^{-1}\cdot\rho)}{\mathrm{tr}\,(\mathbb{\Lambda}^{-1}\cdot\rho)}}_{\mathbf{a}}\Big)\cdot\rho^{-1}$$

We could still simplify this expression a bit more noting that $\rho^{-1} = \sigma\cdot\rho\cdot\sigma/\det(\rho)$ and $\mathbb{\Lambda}^{-1} = \sigma\cdot\mathbb{\Lambda}\cdot\sigma/\det(\mathbb{\Lambda})$ to get rid of the some inverses. Finally, we can plug this expression

[6]Note that for the symmetric matrices $\mathbb{M}$ and $\mathbb{W}$ in (4.35) and (4.42) hermitian conjugation is the same as conjugation hence the absence of daggers in these expressions.

into the Lagrangian (C.8) to obtain a beautiful compact matrix form for the dual objective in the regular unitarity region:

$$d^{\text{regular}}(\mathbb{W},\mathbb{\Lambda})=\int\limits_{4m_1^2}^{\infty} ds\,\mathrm{tr}\Big(\rho^{-1}\cdot\Big(\mathbb{\Lambda}+\frac{\mathbb{W}}{2}\Big)\cdot\mathbb{\Lambda}^{-1}\cdot\Big(\mathbb{\Lambda}+\frac{\overline{\mathbb{W}}}{2}\Big)\Big)+\frac{\mathrm{tr}\big(\rho^{-1}\cdot\mathbb{W}\cdot\sigma\cdot\mathbb{\Lambda}\big)\mathrm{tr}\big(\rho^{-1}\cdot\overline{\mathbb{W}}\cdot\mathbb{\Lambda}^{-1}\cdot\sigma\big)}{4\,\mathrm{tr}\big(\rho^{-1}\cdot\mathbb{\Lambda}\big)}\,.$$

Nicely, note how one can formally reduce it to a single component by replacing σ by zero (thus killing the second term), dot products by simple products and matrices by functions; then this Lagrangian would precisely reduce to the single component expression (4.13).

Next we consider the extended unitarity region. An annoying feature is now that ρ is not invertible. On the other hand, the reason why ρ is not invertible is precisely because it becomes full of zeros and hence extremely simple:

$$\rho\to\begin{pmatrix}\rho_{11}^2 & 0\\ 0 & 0\end{pmatrix}$$

which renders the analysis of the extremization of (C.8) in components a straightforward task. We obtain

$$\begin{aligned}d^{\text{extended}}(\mathbb{W},\mathbb{\Lambda}) = \frac{1}{2\rho_{11}^2(\lambda_2^2-4\lambda_1\lambda_3)}\Big(&-8\lambda_3\lambda_1\mathrm{Re}\,(w_1)-4\lambda_2\lambda_1\mathrm{Re}\,(w_2)+4\lambda_2^2\,\mathrm{Re}\,(w_1)-8\lambda_3\lambda_1^2\\ &-2\lambda_1 w_2\,(w_2)^{\,*}+\lambda_2 w_2\,(w_1)^{\,*}-2\lambda_3 w_1\,(w_1)^{\,*}+\lambda_2 w_1\,(w_2)^{\,*}\Big)\,.\end{aligned}$$

It is possible to minimize analytically the dual functional $d(\mathbb{W},\mathbb{\Lambda})$ with respect to $\mathbb{\Lambda}$. The resulting dual objective has been already shown in eq. (4.49). Here we shall report the expressions for the critical amplitudes as function of $\mathbb{W}$ only.

In the extended unitarity region $4<s<(m_1+m_2)^2$ the critical amplitudes are given by

$$\begin{aligned}M_{11\to 11} &= \frac{i}{\rho_{11}^2}\left(1+\frac{(W_2^2-4W_1W_3)^*}{|W_2^2-4W_1W_3|}\right),\\ M_{11\to 12} &= \frac{i}{2\rho_{11}^2}\frac{4W_1^*W_2W_3-|W_2|^2-|W_2^2-4W_1W_3|}{W_3|W_2^2-4W_1W_3|},\\ \mathrm{Im}\,M_{12\to 12} &= \frac{|W_2|^4+|W_2|^2|W_2^2-4W_1W_3|-4W_3\,\mathrm{Re}\,(W_2^2W_1^*)}{4\rho_{11}^2|W_2^2-4W_1W_3|W_3^2}.\end{aligned}\tag{C.10}$$

Notice that we cannot have direct access to $\mathrm{Re}\,M_{12\to 12}$, but we can reconstruct it from its imaginary part. This is of course related to the fact that our equations in the extended unitarity region, with ρ non-invertible, are a bit more degenerate.

In the unitarity region, $s>(m_1+m_2)^2$, the expressions of the critical amplitudes are

much more involved. It is convenient to introduce the two auxiliary functions

$$\alpha = \frac{1}{2\rho_{11}^2}\sqrt{\rho_{12}^4|W_1|^2 + \rho_{11}^4|W_3|^2 + \frac{1}{2}\rho_{11}^2\rho_{12}^2(|W_2|^2 + |W_2^2 - 4W_1W_3|)},$$
$$\beta = \frac{\alpha}{2i}\,\frac{4W_2W_1^*|W_3|^2 + W_3W_2^*(|W_2^2 - 4W_1W_3| - |W_2|^2)}{2\mathrm{Im}\,W_2\,\mathrm{Re}\,W_2\,\mathrm{Re}\,(W_1W_3) - \mathrm{Re}\,(W_2^2)\mathrm{Im}\,(W_1W_3)}.$$

The amplitudes can then compactly written as

$$\begin{aligned} M_{11\to 11} &= \frac{i}{2\alpha}\left(\frac{2\alpha + W_1^*}{\rho_{11}^2} - \frac{W_3^*\beta}{\rho_{12}^2\beta^*}\right), \\ M_{11\to 12} &= \frac{i}{\rho_{12}^2}\frac{W_3^*}{\beta^*}, \\ M_{12\to 12} &= -\frac{i}{2\alpha|\beta|^2\rho_{12}^4}(W_3^*(4\alpha^2\rho_{12}^2 - |\beta|^2\rho_{11}^2) + \rho_{12}^2\beta^*(W_1^*\beta^* - 2\alpha(\beta + W_2^*))). \end{aligned} \tag{C.11}$$

Quite non-trivially, relations (C.10) and (C.11) manifestly saturate extended and regular unitarity in our truncated space.

C.4 Dual $\mathbb{Z}_2$ bootstrap

C.4.1 Setup the primal problem

Here we consider a simple application of the dual technology developed in Sec. 4.2 to the scattering of equal mass particles with different field parity: 1 odd and 2 even. Defining the S-matrix element for the process $ij \to kl$ as $S_{ij}^{kl} = {}_{\rm out}\langle kl|ij\rangle_{\rm in}$, we can group the even and odd scattering processes into two 2×2 matrices[7]

$$\mathbb{S}^{\rm even} = \begin{pmatrix} S_{11\to 11} & S_{11\to 22} \\ S_{11\to 22} & S_{22\to 22} \end{pmatrix} \qquad \mathbb{S}^{\rm odd} = \begin{pmatrix} S_{12\to 12} & S_{12\to 21} \\ S_{12\to 21} & S_{12\to 12} \end{pmatrix}. \tag{C.12}$$

Unitarity is simply given by the two positivity constraints

$$\mathbb{U}^{\rm even} = \mathbb{1} - \mathbb{S}^{\rm even}(\mathbb{S}^{\rm even})^\dagger \succeq 0, \qquad \mathbb{U}^{\rm odd} = \mathbb{1} - \mathbb{S}^{\rm odd}(\mathbb{S}^{\rm odd})^\dagger \succeq 0, \qquad s \geq 4m^2. \tag{C.13}$$

Analyticity and crossing properties are encoded into the dispersion relations

$$\mathcal{A}_a(s) = S_a(s) - S_a(\infty) + \frac{Jg_a^2}{s-m^2} + \frac{J\mathcal{C}_{ab}g_b^2}{t(s)-m^2} - \frac{1}{\pi}\int_{4m^2}^{\infty}\left(\frac{\mathrm{Im}\ S_a(z)}{z-s} + \frac{\mathcal{C}_{ab}\mathrm{Im}\ S_b(z)}{z-t(s)}\right)dz = 0, \tag{C.14}$$

[7]Recall that in $1+1$ dimensions forward $12\to 12$ and backward $12\to 21$ scattering of non-identical particles are independent processes.

where $J = 1/2\sqrt{m^2(4-m^2)}$ and $a, b = \{11 \to 11, 22 \to 22, 12 \to 12, 11 \to 22, 12 \to 21\}$. In this basis the crossing matrix is simply

$$\mathcal{C} = \begin{pmatrix} 1 & 0 & 0 & 0 & 0 \\ 0 & 1 & 0 & 0 & 0 \\ 0 & 0 & 1 & 0 & 0 \\ 0 & 0 & 0 & 0 & 1 \\ 0 & 0 & 0 & 1 & 0 \end{pmatrix}. \tag{C.15}$$

The processes $\{11 \to 11, 22 \to 22, 12 \to 12\}$ are invariant under crossing $s \to t = 4m^2 - s$. The last two processes $11 \to 22$ and $12 \to 21$ are crossed of each other.

Because of $\mathbb{Z}_2$ symmetry there are only two independent couplings that we call g_{112} and g_{222}. They show up in the different processes as follows

Amplitude	Exchange of particle 1	Exchange of particle 2
$11 \to 11$	0	g_{112}^2
$22 \to 22$	0	g_{222}^2
$12 \to 12$	g_{112}^2	0
$11 \to 22$	0	$g_{112}g_{222}$
$12 \to 21$	g_{112}^2	0

One way to explore the space of allowed couplings is to formulate the problem in a radial form. We define

$$g_{112} = R\cos\theta, \qquad g_{222} = R\sin\theta,$$

and the vector $v(\theta) = \{\cos^2\theta, \sin^2\theta, \cos^2\theta, \sin\theta\cos\theta, \cos^2\theta\}$. Then for each fixed θ we solve:

Primal $\mathbb{Z}_2$ Problem

$$\begin{aligned}
&\underset{\text{in } \{R^2, S_a\}}{\text{maximize}} && R^2 && \\
&\text{constr. by} && \text{Res}_{m^2}(S_a) = v_a(\theta) R^2 && \text{for } a = 1, \dots, 5 && \text{(C.16)} \\
& && \mathcal{A}_a(s) = 0 && \text{for } s > 4m^2, \quad \text{for } a = 1, \dots, 5 && \\
& && \mathbb{U}^{\text{even}}(s) \succeq 0, \quad \mathbb{U}^{\text{odd}}(s) \succeq 0 && \text{for } s > 4m^2. && \text{(C.17)}
\end{aligned}$$

This problem and therefore the space of the allowed couplings $\{g_{112}, g_{222}\}$ has been already determined in [1]. Our aim is to give an equivalent dual formulation which makes the problem so simple that can be ran in few minutes using `Mathematica` on a standard laptop.

C.4.2 Dual construction I: residue constraints

As explained in Sec. 4.2, the construction of the dual problem starts with the introduction of Lagrange multipliers for any constraint given in the primal problem (C.17). The first set of linear constraints (C.16) defines what we call "radial problem" – see also [12]. They can be easily taken into account introducing the Lagrangian

$$\mathcal{L}(R^2, S, \nu) = R^2 + \sum_a \nu_a (\text{Res}_{m^2}(S_a) - v_a(\theta) R^2) = R^2 \left(1 - \sum_a \nu_a v_a(\theta)\right) + \sum_a \nu_a \text{Res}_{m^2}(S_a).$$

The Lagrange equation for R^2 yields simply the condition

$$1 - \sum_a \nu_a v_a(\theta) = 0,$$

and the problem can be cast in a simpler equivalent form

$$\begin{aligned}
&\min_{\nu_a} && \left\{ \max_{S_a} && \sum_a \nu_a \text{Res}_{m^2}(S_a) && \text{constrained by} \right. \\
& && && \mathcal{A}_a(s) = 0, \qquad s \geq 4m^2, \quad a = 1, \dots, 5 && \\
& && && \left. \mathbb{U}^{\text{even}}(s) \succeq 0, \quad \mathbb{U}^{\text{odd}}(s) \succeq 0, \quad s \geq 4m^2 \right\} && \\
&\text{constrained by} && 1 - \sum_a \nu_a v_a(\theta) = 0. && && \text{(C.18)}
\end{aligned}$$

C.4.3 Dual construction II: analyticity and crossing

All crossing and analyticity properties of the various S-matrices involved in the $\mathbb{Z}_2$ system can be derived from the dispersion relations in eq. (C.14). Indeed, for each s they can be viewed as a set of linear constraints enforcing a precise relation among the $\text{Re}\, M(s)$ and $\text{Im}\, M(s)$, otherwise independent.

For each component we introduce a dual scattering function w_a and replace the objective in (C.18) by

$$\mathcal{L}(S,\nu,w) = \sum_a \nu_a \mathrm{Res}_{m^2}(S_a) + \sum_a \int_{4m^2}^{\infty} w_a(s)\mathcal{A}_a(s)\,ds. \tag{C.19}$$

The $w_a(s)$ are real functions in general. However, it is often useful to define analytic functions starting from $w_a(s)$ to simplify the analyticity and crossing constraint. It can be shown that if we introduce a *dual crossing* function $W_a(4m^2 - s) = -\mathcal{C}_{ab}W_b(s)$ such that

$$W_a(s) = \frac{1}{\pi}\int_{4m^2}^{\infty}\left(\frac{\mathrm{Im}\ W_a(z)}{z-s} - \frac{\mathcal{C}_{ab}\mathrm{Im}\ W_b(z)}{z-t(s)}\right)dz$$

and identify

$$w_a(s) = \mathrm{Im}\ W_a(s), \qquad \text{for } s > 4m^2,$$

the last term in eq. (C.19) becomes

$$\sum_a \int_{4m^2}^{\infty} w_a(s)\mathcal{A}_a(s)\,ds = \pi J \sum_a \mathrm{Res}_{m^2}(S_a)W_a(m^2) + \sum_a \int_{4m^2}^{\infty} \mathrm{Im}\,(W_a S_a)\,ds. \tag{C.20}$$

Substituting eq. (C.20) into the Lagrangian (C.19) allows us to maximize in the $\mathrm{Res}_{m^2}(S_a)$ variables

$$\frac{\partial}{\partial \mathrm{Res}_{m^2}(S_a)}\mathcal{L}(S,\nu,w) = \nu_a + \pi J W_a(m^2) = 0, \qquad \text{for } a = 1,\ldots,5,$$

and use these 5 equations to eliminate the Lagrange multipliers setting $\nu_a = -\pi J W_a(m^2)$. The radial constraint translates into a condition on the W_a dual scattering functions

$$\begin{aligned} \min_{\nu_a, W_a} \quad & \left\{ \max_{S_a} \quad \sum_a \int_{4m^2}^{\infty} \mathrm{Im}\,(W_a S_a)\,ds \qquad \text{constrained by} \right. \\ & \qquad\qquad \left. \mathbb{U}^{\mathrm{even}}(s) \succeq 0, \quad \mathbb{U}^{\mathrm{odd}}(s) \succeq 0, \quad s \geq 4m^2 \right\} \\ \text{constrained by} \quad & 1 + \pi J \sum_a v_a(\theta) W_a(m^2) = 0. \end{aligned} \tag{C.21}$$

C.4.4 Dual construction III: unitarity

The last constraint to add to the dual Lagrangian is unitarity. This can be elegantly done if we cast the problem (C.21) into a matrix form. If we define the symmetric matrices

$$\mathbb{W}^{\mathrm{even}} = \begin{pmatrix} 2W_1 & W_4 \\ W_4 & 2W_2 \end{pmatrix}, \qquad \mathbb{W}^{\mathrm{odd}} = \begin{pmatrix} W_3 & W_5 \\ W_5 & W_3 \end{pmatrix}. \tag{C.22}$$

the objective of (C.21) is just

$$\sum_a \int_{4m^2}^{\infty} \text{Im}\,(W_a S_a)\, ds = \int_{4m^2}^{\infty} ds \left(\frac{1}{2}\text{Im}\,(\text{tr}\ \mathbb{W}^{\text{even}}\mathbb{S}^{\text{even}}) + \frac{1}{2}\text{Im}\,\left(\text{tr}\ \mathbb{W}^{\text{odd}}\mathbb{S}^{\text{odd}}\right)\right),$$

recalling $\mathbb{S}^{\text{even/odd}}$ were introduced in (C.12). It is then natural to introduce the semidefinite-positive matrix Lagrange multipliers $\mathbb{\Lambda}^{\text{even}}$ and $\mathbb{\Lambda}^{\text{odd}}$

$$\mathcal{L}(\mathbb{S},\mathbb{W},\Lambda)= \int_{4m^2}^{\infty} ds \left(\frac{1}{2}\text{Im}\,\left(\text{tr}\ \mathbb{W}^{\text{even}}\mathbb{S}^{\text{even}} + \text{tr}\ \mathbb{W}^{\text{odd}}\mathbb{S}^{\text{odd}}\right) + \frac{1}{2}\text{tr}\ \mathbb{\Lambda}^{\text{even}}\mathbb{U}^{\text{even}} + \frac{1}{2}\text{tr}\ \mathbb{\Lambda}^{\text{odd}}\mathbb{U}^{\text{odd}}\right), \tag{C.23}$$

So that

$$\delta_{\mathbb{S}}\mathcal{L}= \int_{4m^2}^{\infty} ds \sum_{\eta=\text{even,odd}} \text{tr}\ \left[\left(\frac{-\overline{\mathbb{W}}^{\eta}}{4i} - \frac{1}{2}\mathbb{\Lambda}^{\eta}\cdot\mathbb{S}^{\eta}\right)\delta\bar{\mathbb{S}}^{\eta} + \texttt{conjugate}\right] \tag{C.24}$$

Since $0 = \text{tr}\ (\sigma_y\cdot\bar{\mathbb{S}}) = \text{tr}\ (\sigma_y\cdot\mathbb{S}) = \text{tr}\ (\sigma_y\cdot\delta\bar{\mathbb{S}}) = \text{tr}\ (\sigma_y\cdot\delta\mathbb{S})$ the parentheses does not need to vanish. It does need to be proportional to σ_y with a proportionality constant which we can easily find by dotting it with the appropriate matrices:

$$\frac{-\overline{\mathbb{W}}}{4i} - \frac{1}{2}\mathbb{\Lambda}\cdot\mathbb{S} = -\frac{1}{4i}\frac{\text{tr}(\mathbb{\Lambda}^{-1}\cdot\overline{\mathbb{W}}\cdot\sigma_y)}{\text{tr}(\mathbb{\Lambda}^{-1})}\sigma_y \tag{C.25}$$

where we dropped the implicit label η. For $\eta = \text{odd}$ this equation simplifies dramatically because[8]

$$\mathbb{\Lambda}^{\text{odd}} = \begin{pmatrix} \lambda_3 & \lambda_5 \\ \lambda_5 & \lambda_3. \end{pmatrix}$$

and the right hand side of (C.25) vanishes once we use (C.22). In that case we therefore obtain the critical S-matrix in the odd sector as compactly given by $\mathbb{S}^{\text{odd}} = \frac{i}{4}(\mathbb{\Lambda}^{\text{odd}})^{-1}\overline{\mathbb{W}}^{\text{odd}}$. Furthermore, minimizing the dual functional over $\mathbb{\Lambda}$ is equivalent to solving the constraint equation $\mathbb{1} = \mathbb{S}^{\text{odd}}(\mathbb{S}^{\text{odd}})^{\dagger}$ which determines[9]

$$\mathbb{\Lambda}^{\text{odd}} = \frac{1}{2}\sqrt{\overline{\mathbb{W}}^{\text{odd}}\cdot\mathbb{W}^{\text{odd}}}. \tag{C.26}$$

Plugging eq. (C.26) into the dual functional we finally get

$$\inf_{\mathbb{\Lambda}} d(\mathbb{W},\mathbb{\Lambda})^{\text{odd}} = D^{\text{odd}}(\mathbb{W}) = \frac{1}{2}\int_{4m^2}^{\infty} \text{tr}\ \left(\sqrt{\overline{\mathbb{W}}\cdot\mathbb{W}}\right)^{\text{odd}} ds. \tag{C.27}$$

In the even sector case such an honest explicit derivation is not available because of the very non-linear appearance of $\mathbb{\Lambda}$. Inspired by the simplicity of (C.27) we guessed the matrix

[8]Notice $\mathbb{U}^{\text{odd}}$ is real and symmetric, we can take $\mathbb{\Lambda}^{\text{odd}}$ real and symmetric as well without loss of generality.

[9]The square root of a matrix is not uniquely defined in general. Here we should pick the positive-semidefinite solution.

formulation of the dual problem

Dual $\mathbb{Z}_2$ Problem

$$\begin{aligned} &\underset{\text{in } \{\mathbb{W}^{\text{even}},\mathbb{W}^{\text{odd}}\}}{\text{minimize}} && \frac{1}{2}\int_{4m^2}^{\infty} \text{tr}\left(\sqrt{\overline{\mathbb{W}}\cdot\mathbb{W}}\right)^{\text{odd}} + \text{tr}\left(\sqrt{\overline{\mathbb{W}}\cdot\mathbb{W}}\right)^{\text{even}} ds, \\ &\text{constr. by} && 1 + \pi J \sum_a v_a(\theta) W_a(m^2) = 0. \end{aligned} \tag{C.28}$$

This guess is correct. We checked it numerically and also derived it by brute force going to components.

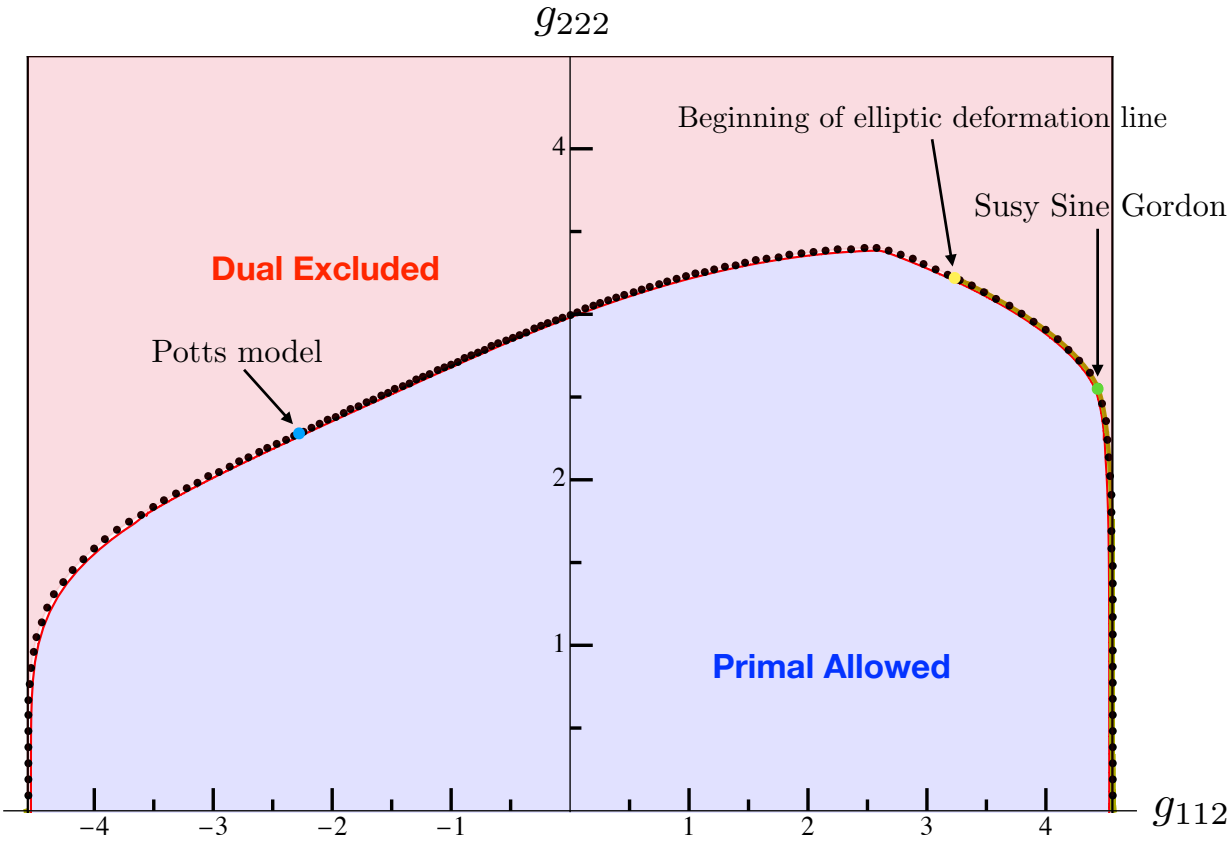

Figure C.1: Space of the $\mathbb{Z}_2$ symmetric coupling constants $\{g_{222}, g_{112}\}$. We restrict to the UHP due to $g \leftrightarrow -g$ symmetry. The black dots are obtained minimizing the objective in (C.29). The red solid line was obtained in [1] running the primal problem. The dual data have been obtained with very little effort: in this plot $N_{\text{max}} = 5$ for all dual scattering functions ansatz. The blue and green dots mark respectively the well known integrable 3-states Potts and supersymmetric Sine-Gordon. We recall that starting at $\theta = \pi/4$, the yellow dot, and all the way to $\theta = \pi/2$ the S-matrix saturating the boundary is known analytically and correspond to the elliptic deformation of supersymmetric Sine-Gordon – see [1, 2] for details.

Despite the simplicity of the matrix formulation, it is convenient to go back to components when performing numerical explorations. The matrix $\overline{\mathbb{W}}\cdot\mathbb{W}$ for both odd and even

sectors is a 2×2 hermitian matrix. We can therefore use the general formula

$$M = \begin{pmatrix} A & B \\ B^* & D \end{pmatrix} \qquad \to \qquad \text{tr } \sqrt{M} = \sqrt{A + D + 2\sqrt{AD - |B|^2}}$$

to derive the explicit form of the functional. Applying this formula we get pretty straightforwardly that the first line in (C.28) is given by

$$\frac{1}{\sqrt{2}} \int_{4m^2}^{\infty} ds \left(\sqrt{|W_3|^2 + |W_5|^2 + |W_3^2 - W_5^2|} + \sqrt{|W_4|^2 + 2|W_1|^2 + 2|W_2|^2 + |W_4^2 - 4W_1 W_2|} \right), \tag{C.29}$$

which is the objective we minimize in practice.

C.4.5 Dual problem numerics

For the dual scattering functions associated to the crossing invariant processes $11 \to 11, 22 \to 22$, and $12 \to 12$ we can simply write the following anti-crossing ansatz

$$W_a(s) = \frac{1}{\sqrt{s(4m^2 - s)}} (\rho(s) - \rho(t(s))) \left(\sum_{n=0}^{N_{\max}^{(a)}} \alpha_n^{(a)} (\rho(s)^n + \rho(t(s))^n) \right), \quad a = 1, 2, 3.$$

For the objective functional (C.29) we must require that $W_a \sim s^{-3/2}$ for $s \to \infty$. Our ansatz for these components has automatically the right behavior since $\rho(s) - \rho(t) \sim s^{-1/2}$.

We can package the $11 \to 22$ and $12 \to 12$-backward into a single scattering function not symmetric under crossing

$$W_4(s) = \frac{1}{\sqrt{s(4m^2 - s)}} \left(\sum_{n=0}^{N_{\max}^{(4)}} \beta_n^{(1)} \rho(s)^n + \beta_n^{(2)} \rho(t(s))^n \right).$$

However, such an ansatz does not automatically decay with the right power and one must tune one of the free parameters. The numerical results for the dual radial problem (C.28) are shown in figure C.1.

Appendix D

Appendix: The Wilson-Loop – Large Spin OPE dictionary

D.1 Spinors

Equation (5.3) provides a manifestly covariant expression for the three point function. However, with the prospects of fitting chapter 5 in the context of $\mathcal{N}=4$ integrability, it is useful to express the three point function in a convenient conformal frame following [246]. In $-+++$ signature we choose

$$x_1 = (0,0,0,0)\,, \qquad x_2 = (0,0,1,0)\,, \qquad x_3 = (0,0,\mathcal{L},0) \tag{D.1}$$

and consider the rescaled correlator

$$\mathbb{C}(\epsilon_1,\epsilon_2,\epsilon_3) \equiv \lim_{\mathcal{L}\to\infty} \mathcal{L}^{2\Delta_3}\langle \mathcal{O}_1(x_1,\epsilon_1),\mathcal{O}_2(x_2,\epsilon_2),\mathcal{O}_3(x_3,\epsilon_3)\rangle. \tag{D.2}$$

Besides choosing a frame, in the context of integrability, it is useful to express the correlator in terms of polarization spinors. That is, to each operator $\mathcal{O}_i$ we assign auxiliary spinors $L_i{}^{\alpha}$ and $R_{i\dot\beta}$. These are related to the polarization vectors by

$$\epsilon_i^{\mu} = R_{i\dot\beta}\bar\sigma^{\mu\dot\beta\alpha}L_{i\alpha}, \tag{D.3}$$

where in our conventions the sigma matrices $\sigma^{\mu}_{\alpha\dot\alpha}$, $\bar\sigma^{\mu\dot\alpha\alpha}$ are given by

$$\sigma^0 = \begin{pmatrix} -1 & 0 \\ 0 & -1 \end{pmatrix}, \qquad \sigma^1 = \begin{pmatrix} 0 & 1 \\ 1 & 0 \end{pmatrix}, \qquad \sigma^2 = \begin{pmatrix} 0 & -i \\ i & 0 \end{pmatrix}, \qquad \sigma^3 = \begin{pmatrix} 1 & 0 \\ 0 & -1 \end{pmatrix}, \tag{D.4}$$

$\bar\sigma = (\sigma_0, -\sigma_1, -\sigma_2, -\sigma_3)$, and indices are raised and lowered with

$$-\epsilon_{\alpha\beta} = \epsilon^{\alpha\beta} = -\epsilon_{\dot\alpha\dot\beta} = \epsilon^{\dot\alpha\dot\beta} = \begin{pmatrix} 0 & 1 \\ -1 & 0 \end{pmatrix}. \tag{D.5}$$

One of the very nice features of this conformal frame is how clean the invariant structures H and V in (5.3) become. In terms of the left and right spinors they simply read

$$H_{ij} = \langle L_i, R_j\rangle\langle L_j, R_i\rangle, \qquad V_{i,jk} = \langle L_i, R_i\rangle, \qquad \langle L_i, R_j\rangle \equiv iR_{j\dot\alpha}\bar\sigma_2^{\dot\alpha\alpha}L_{i\alpha}\,. \tag{D.6}$$

A general spinning three point function can then be cast as linear combination of monomials made out of these brackets. For instance, translating the results of appendix D.6 for the case of three spinning operators with spin $2, 4, 6$ respectively we can write

$$\begin{aligned}
C^{\bullet\bullet\bullet}_{246} = \left(\tfrac{1}{84\sqrt{55}}\right)\Big(&\langle 11\rangle\langle 13\rangle\langle 22\rangle^2\langle 23\rangle^2\langle 31\rangle\langle 32\rangle^2\langle 33\rangle^3\left(720-\tfrac{2480321}{1155}g^2\right)+\langle 11\rangle\langle 12\rangle\langle 21\rangle\langle 22\rangle^3\langle 33\rangle^6\left(8-\tfrac{1202701}{17325}g^2\right)+\\
&+\langle 11\rangle\langle 13\rangle\langle 22\rangle^3\langle 23\rangle\langle 31\rangle\langle 32\rangle\langle 33\rangle^4\left(240-\tfrac{600189}{385}g^2\right)+\langle 11\rangle^2\langle 22\rangle^2\langle 23\rangle^2\langle 32\rangle^2\langle 33\rangle^4\left(90-\tfrac{822427}{1155}g^2\right)+\\
&+\langle 12\rangle\langle 13\rangle\langle 21\rangle\langle 22\rangle\langle 23\rangle^2\langle 31\rangle\langle 32\rangle^2\langle 33\rangle^3\left(1440-\tfrac{811882}{1155}g^2\right)+\langle 11\rangle\langle 12\rangle\langle 21\rangle\langle 22\rangle^2\langle 23\rangle\langle 32\rangle\langle 33\rangle^5\left(144-\tfrac{1335487}{1925}g^2\right)+\\
&+\langle 12\rangle\langle 13\rangle\langle 21\rangle\langle 22\rangle^2\langle 23\rangle\langle 31\rangle\langle 32\rangle\langle 33\rangle^4\left(720-\tfrac{179332}{385}g^2\right)+\langle 11\rangle\langle 12\rangle\langle 21\rangle\langle 22\rangle\langle 23\rangle^2\langle 32\rangle^2\langle 33\rangle^4\left(360-\tfrac{433393}{1155}g^2\right)+\\
&+\langle 11\rangle^2\langle 22\rangle^3\langle 23\rangle\langle 32\rangle\langle 33\rangle^5\left(24-\tfrac{694912}{1925}g^2\right)+\langle 11\rangle\langle 13\rangle\langle 22\rangle^4\langle 31\rangle\langle 33\rangle^5\left(12-\tfrac{716273}{5775}g^2\right)+\\
&+\langle 11\rangle^2\langle 22\rangle^4\langle 33\rangle^6\left(1-\tfrac{814939}{34650}g^2\right)+\langle 12\rangle\langle 13\rangle\langle 21\rangle\langle 22\rangle^3\langle 31\rangle\langle 33\rangle^5\left(48+\tfrac{36268}{5775}g^2\right)+\\
&+\langle 13\rangle^2\langle 23\rangle^4\langle 31\rangle^2\langle 32\rangle^4\left(15+\tfrac{4261}{231}g^2\right)+\langle 12\rangle^2\langle 21\rangle^2\langle 22\rangle^2\langle 33\rangle^6\left(6+\tfrac{219941}{5775}g^2\right)+\\
&+\langle 13\rangle^2\langle 22\rangle^4\langle 31\rangle^2\langle 33\rangle^4\left(15+\tfrac{25231}{462}g^2\right)+\langle 11\rangle^2\langle 22\rangle\langle 23\rangle^3\langle 32\rangle^3\langle 33\rangle^3\left(80+\tfrac{670748}{3465}g^2\right)+\\
&+\langle 12\rangle^2\langle 21\rangle^2\langle 22\rangle\langle 23\rangle\langle 32\rangle\langle 33\rangle^5\left(72+\tfrac{572534}{1925}g^2\right)+\langle 12\rangle^2\langle 21\rangle^2\langle 23\rangle^2\langle 32\rangle^2\langle 33\rangle^4\left(90+\tfrac{422663}{1155}g^2\right)+\\
&+\langle 12\rangle\langle 13\rangle\langle 21\rangle\langle 23\rangle^3\langle 31\rangle\langle 32\rangle^3\langle 33\rangle^2\left(480+\tfrac{433666}{1155}g^2\right)+\langle 13\rangle^2\langle 22\rangle\langle 23\rangle^3\langle 31\rangle^2\langle 32\rangle^3\langle 33\rangle\left(240+\tfrac{97282}{231}g^2\right)+\\
&+\langle 13\rangle^2\langle 22\rangle^3\langle 23\rangle\langle 31\rangle^2\langle 32\rangle\langle 33\rangle^3\left(240+\tfrac{33146}{77}g^2\right)+\langle 11\rangle^2\langle 23\rangle^4\langle 32\rangle^4\langle 33\rangle^2\left(15+\tfrac{520958}{1155}g^2\right)+\\
&+\langle 13\rangle^2\langle 22\rangle^2\langle 23\rangle^2\langle 31\rangle^2\langle 32\rangle^2\langle 33\rangle^2\left(540+\tfrac{53288}{77}g^2\right)+\langle 11\rangle\langle 12\rangle\langle 21\rangle\langle 23\rangle^3\langle 32\rangle^3\langle 33\rangle^3\left(160+\tfrac{2899591}{3465}g^2\right)+\\
&+\langle 11\rangle\langle 13\rangle\langle 23\rangle^4\langle 31\rangle\langle 32\rangle^4\langle 33\rangle\left(60+\tfrac{984272}{1155}g^2\right)+\langle 11\rangle\langle 13\rangle\langle 22\rangle\langle 23\rangle^3\langle 31\rangle\langle 32\rangle^3\langle 33\rangle^2\left(480+\tfrac{1301071}{1155}g^2\right)\Big)
\end{aligned} \tag{D.7}$$

where $\langle ij\rangle = \langle L_i, R_j\rangle$.

Note that by simply looking at the various homogeneous degrees in L_i and R_i we can automatically infer the three spins of this correlator. A very concrete test of the spinning hexagonalization cleaned up in [4] is to reproduce this equation from the hexagon formalism.

D.2 The $\ell(\epsilon)$ map

In the limit of large spin the structure constants $C^{\bullet\bullet\bullet}$ are exponentially small. However, as remarked in section 5.5, $\hat{C}^{\bullet\bullet\bullet}$ suffers from a Stokes-like phenomenon: in the space-like region it is of order one, while in the time-like region it diverges exponentially. These leads to a dramatic simplification in the sum of (5.3) in the large spin limit. Provided the tree-level decay combined with the chemical potentials $T_{i,jk} \equiv \frac{H_{jk}}{V_{j,ki}V_{k,ij}}$ are enough to suppress the contribution from the time-like regions, (5.3) reduces to a saddle point computation

governed by tree-level[1]. The loop corrections are then simply evaluated *at* the saddle location, in which they are of order one.[2]

In this regime, we thus conclude that

$$\frac{\langle \mathcal{O}_{J_1}(x_1,\epsilon_1)\mathcal{O}_{J_2}(x_2,\epsilon_2)\mathcal{O}_{J_3}(x_3,\epsilon_3)\rangle}{\langle \mathcal{O}_{J_1}(x_1,\epsilon_1)\mathcal{O}_{J_2}(x_2,\epsilon_2)\mathcal{O}_{J_3}(x_3,\epsilon_3)\rangle_{\text{tree level}}} = \hat{C}^{\bullet\bullet\bullet} \qquad \text{evaluated at } \ell_i \text{ given by} \qquad \frac{\partial W}{\partial \ell_i} = 0$$

where

$$e^W \equiv \left(C^{\bullet\bullet\bullet}_{\text{tree level}} \simeq \prod_i \frac{\left(J_i + \ell_i - \sum_k \ell_k\right)^{\sum_k \ell_k - J_i - \ell_i - \frac{1}{2}}}{\pi^{\frac{3}{4}} \ell_i^{2\ell_i+1}\, e^{\sum_k \ell_k - 3\ell_i}\, 2^{J_i+1} J_i^{-J_i-\frac{3}{4}}} \right) V_{1,23}^{J_1-l_2-l_3} V_{2,31}^{J_2-\ell_3-\ell_1} V_{3,12}^{J_3-\ell_1-\ell_2} H_{23}^{\ell_1} H_{31}^{\ell_2} H_{12}^{\ell_3}\,.$$

The critical points of the potential W in the large spin limit take a remarkably simple form

$$\begin{aligned} \frac{H_{2,3}}{V_{2,31}V_{3,1,2}} &= \frac{\ell_1^2}{(J_3-\ell_1-\ell_2)(J_2-\ell_1-\ell_3)} \\ \frac{H_{3,1}}{V_{3,12}V_{1,23}} &= \frac{\ell_2^2}{(J_1-\ell_2-\ell_3)(J_3-\ell_2-\ell_1)} \\ \frac{H_{1,2}}{V_{1,23}V_{2,31}} &= \frac{\ell_3^2}{(J_2-\ell_3-\ell_1)(J_1-\ell_3-\ell_2)} \end{aligned} \tag{D.8}$$

where J_i and ℓ_i are both large and of the same order. This constitutes the sought after $\epsilon(\ell)$ map.[3] We emphasize this map should be understood to hold in the space-like region corresponding to the image covered by positive U's through the $\ell(U)$ map (5.14). To access the time-like regions, one must analytically continue away from the well controlled Euclidean region.

Combining (D.8) with (5.14) we can also translate our map into spinor variables. We get

$$\frac{\langle L_{i+1}, R_{i+1}\rangle\langle L_{i+2}, R_{i+2}\rangle}{\langle L_{i+1}, R_{i+2}\rangle\langle L_{i+2}, R_{i+1}\rangle} = \left(R_{i+1;i+2\,i} - \frac{1+R_{i+1;i+2\,i}}{1+R_{i;i+2\,i+1}}\right)\left(R_{i+2;i+1\,i} - \frac{1+R_{i+2;i+1\,i}}{1+R_{i;i+1\,i+2}}\right) \tag{D.9}$$

[1] In the toy model case of two spinning operators at one-loop discussed in the previous section, the sum over tensor structures also simplifies to a saddle computation under the same conditions. There, the chemical potential can suppress the exponential divergences of the one-loop structure constants provided $T_{3,12} < 1$.

[2] We verified this statement numerically in perturbation theory.

[3] Of course, we can not fix the polarization themselves but only meaningful conformal invariant combinations in the left hand side of relation (D.8). In practice we can however pick a particular conformal frame and use (D.8) to define a realization $\epsilon_i(\ell_1,\ell_2,\ell_3)$. This particular realization is what is most convenient when dealing with these structure constants from an integrability perspective as explained in [4].

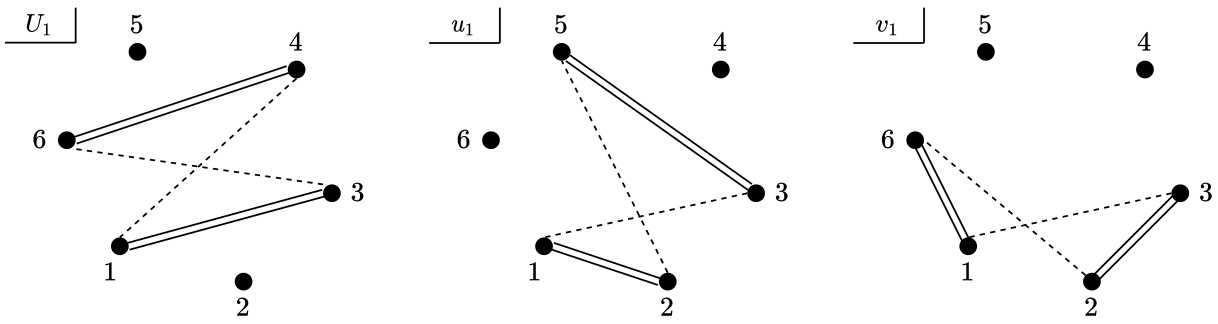

Figure D.1: The six point function has nine independent cross-ratios. We pick three of them to be U_1, represented here, plus its two cyclic images and the remaining six are either the u_1 plus its cyclic images or v_1 and its cyclic images, both represented above. We convert these pictures into the formulae in the text by writing the cross-ratio as the (product of the square of the) distances represented by the solid lines divided by the ones associated with the dashed lines.

with $i = 1, 2, 3$, all indices taken modulo 3 and where

$$R_{a;b\,c} = \frac{\frac{J_b}{J_a} + \frac{J_c}{J_a}\sqrt{\frac{\tilde{U}_c}{\tilde{U}_a\tilde{U}_b}}}{\frac{J_c}{J_a} + \frac{J_b}{J_a}\sqrt{\frac{\tilde{U}_b}{\tilde{U}_a\tilde{U}_c}}}, \qquad \tilde{U}_1 = U_2, \qquad \tilde{U}_2 = U_1, \qquad \tilde{U}_3 = U_3. \tag{D.10}$$

Note that there are more variables in the three point function side of the duality so we have some freedom on how to approach the duality. Only ratios matter: We can take the large spin limit of the three point function with all spins (approximately) equal, for instance. Then all the (red) ratios of spins evaluate to 1 and this already simple relation simplifies even more.

D.3 Cross-ratios

The cross-ratios used to write the six point correlation function are presented in figure D.1. We have

$$u_1 = \frac{x_{12}^2 x_{35}^2}{x_{13}^2 x_{25}^2}, \quad u_2 = \frac{x_{23}^2 x_{46}^2}{x_{24}^2 x_{36}^2}, \quad u_3 = \frac{x_{34}^2 x_{51}^2}{x_{35}^2 x_{41}^2}, \quad u_4 = \frac{x_{45}^2 x_{62}^2}{x_{46}^2 x_{52}^2}, \quad u_5 = \frac{x_{56}^2 x_{13}^2}{x_{51}^2 x_{63}^2}, \quad u_6 = \frac{x_{61}^2 x_{24}^2}{x_{62}^2 x_{14}^2} \tag{D.11}$$

with $x_{ij}^2 = (x_i - x_j)^2$. This set of cross-ratios u_i has a single null distance in the numerator when we send $x_{i,i+1}^2 \to 0$. This is quite convenient for taking one null limit at a time.

For instance, if we take 12, 34 and 56 to become null that sets the odd cross-ratios $u_1, u_3, u_5 \to 0$. That is represented in figure 5.1a. This is a so-called single light-like OPE. In this null limit we have $(x_1 - x_2)^2 \to 0$ since x_1 and x_2 are becoming null separated without necessarily colliding with each other. We could make this distance zero with the stronger condition $x_2 \to x_1$ corresponding to the euclidean OPE. If we take all pairs 12, 34 and 56 to collide in this Euclidean sense we set not only the odd cross-ratios to zero, $u_1, u_3, u_5 \to 0$, but we should expand the even ones around one, $u_2, u_4, u_6 \to 1$, as

represented in figure 5.1b. A very different limit we could take is to keep 12, 34 and 56 null and then send the remaining consecutive pairs of points 23, 45 and 61 to be null so that in total all consecutive points are null drawing a full closed polygon as represented in figure 5.1c. In that case we set all the odd and even cross-ratios to zero $u_i \to 0$. This very Lorentzian limit is also called a double light-like OPE limit.

In this appendix and respective chapter we always take u_1, u_3, u_5 to zero first. This projects into leading twist operators in the corresponding three OPE channels as represented in figure 5.1a. In the main text we then take the remaining u_2, u_4, u_6 to zero to construct a full null polygonal configuration. This projects further into large spin exchanges. In appendix D.5.1, instead, we expand around the Euclidean limit where $u_2, u_4, u_6 \to 1$ to extract OPE data for finite spins.

Another important set of cross-ratios is

$$v_1 = \frac{x_{61}^2 x_{23}^2}{x_{62}^2 x_{13}^2}\,, \quad v_2 = \frac{x_{12}^2 x_{34}^2}{x_{13}^2 x_{24}^2}\,, \quad v_3 = \frac{x_{23}^2 x_{45}^2}{x_{24}^2 x_{35}^2}\,, \quad v_4 = \frac{x_{34}^2 x_{56}^2}{x_{35}^2 x_{46}^2}\,, \quad v_5 = \frac{x_{45}^2 x_{61}^2}{x_{46}^2 x_{51}^2}\,, \quad v_6 = \frac{x_{56}^2 x_{12}^2}{x_{51}^2 x_{62}^2}\,, \tag{D.12}$$

which have two vanishing distances in the null limit. Because of these two distances, taking (either Euclidean or Lorentzian) OPE limits in a sequential way as discussed above is murkier in the v_j language. They have, however, the big advantage of being very local and symmetric, more so that the u_j as can be clearly seen in figure D.1. It is in these local variables that the important recoil effect introduced in [101] is expressed. We will thus use the u_j's for most derivations but switch to the v_j's when imposing the required symmetries of the final results to bootstrap the correlators.

The remaining three cross-ratios (U_1, U_2, U_3) which parametrize the six point function are

$$U_1 = \frac{x_{13}^2 x_{46}^2}{x_{14}^2 x_{36}^2}\,, \qquad U_2 = \frac{x_{24}^2 x_{51}^2}{x_{25}^2 x_{41}^2}\,, \qquad U_3 = \frac{x_{35}^2 x_{62}^2}{x_{36}^2 x_{52}^2}\,. \tag{D.13}$$

These cross-ratios remain finite in the double light-cone limit. They parametrize the resulting null hexagons. (In the triple Euclidean OPE we have $U_i \to 1$.)

D.4 Conformal block integrand $\mathcal{F}$

The light cone six point snowflake conformal block governing the exchange of leading twist single trace operators and all its descendents admits a simple triple integral representa-

tion [144] which we quote here for completeness. The integrand $\mathcal{F}$ in (5.6) reads

$$\begin{aligned}\mathcal{F} = &\frac{\Gamma\left(2J_1+\gamma_1+2\right)}{\Gamma\left(J_1+\frac{\gamma_1}{2}+1\right)^2}\frac{\Gamma\left(2J_2+\gamma_2+2\right)}{\Gamma\left(J_2+\frac{\gamma_2}{2}+1\right)^2}\frac{\Gamma\left(2J_3+\gamma_3+2\right)}{\Gamma\left(J_3+\frac{\gamma_3}{2}+1\right)^2}\frac{u_2u_4u_6}{u_1u_3u_5}U_1U_2U_3\,u_1{}^{\frac{\gamma_1}{2}}u_3{}^{\frac{\gamma_2}{2}}u_5{}^{\frac{\gamma_3}{2}}\\
&\times(U_1-u_2)^{\ell_3}(U_2-u_6)^{\ell_2}(U_3-u_4)^{\ell_1}U_1{}^{J_2+\frac{\gamma_1}{2}+\frac{\gamma_2}{2}-\frac{\gamma_3}{2}}U_2{}^{J_1+\frac{\gamma_1}{2}-\frac{\gamma_2}{2}+\frac{\gamma_3}{2}}U_3{}^{J_3-\frac{\gamma_1}{2}+\frac{\gamma_2}{2}+\frac{\gamma_3}{2}}\\
&\times(y_1(1-y_1))^{J_1+\frac{\gamma_1}{2}}(U_1(1-y_1)+u_2U_2(1-y_2)y_1+U_1U_2y_1y_2)^{-1-J_1-J_2+\ell_1+\ell_2+\frac{\gamma_3}{2}-\frac{\gamma_2}{2}-\frac{\gamma_1}{2}}\\
&\times(y_2(1-y_2))^{J_2+\frac{\gamma_2}{2}}(U_2(1-y_3)+u_6U_3(1-y_1)y_3+U_2U_3y_1y_3)^{-1-J_1-J_3+\ell_1+\ell_3+\frac{\gamma_2}{2}-\frac{\gamma_1}{2}-\frac{\gamma_3}{2}}\\
&\times(y_3(1-y_3))^{J_3+\frac{\gamma_3}{2}}(U_3(1-y_2)+u_4U_1(1-y_3)y_2+U_1U_3y_2y_3)^{-1-J_2-J_3+\ell_2+\ell_3+\frac{\gamma_1}{2}-\frac{\gamma_2}{2}-\frac{\gamma_3}{2}}\\
&\times(U_1-u_2U_2+U_2(u_2-U_1)y_2-U_1(U_3-1)y_3+(U_2-u_6U_3)(U_1y_2y_3+u_2(1-y_2)y_3))^{J_1-\ell_2-\ell_3}\\
&\times(U_3-u_4U_1+U_1(u_4-U_3)y_3-U_3(U_2-1)y_1+(U_1-u_2U_2)(U_3y_1y_3+u_4(1-y_3)y_1))^{J_2-\ell_1-\ell_3}\\
&\times(U_2-u_6U_3+U_3(u_6-U_2)y_1-U_2(U_1-1)y_2+(U_3-u_4U_1)(U_2y_1y_2+u_6(1-y_1)y_2))^{J_3-\ell_1-\ell_2}\,.\end{aligned}$$

D.5 Decomposition through Casimirs

The snowflake light-cone blocks

$$\mathbb{F}_{J_1,J_2,J_3,\ell_1,\ell_2,\ell_3}\equiv\int_0^1 dy_1\int_0^1 dy_2\int_0^1 dy_3\,\mathcal{F}\tag{D.14}$$

obey three important Casimir equations:

$$\left(\widehat{C}_{12}-\mathcal{C}_{\Delta_{J_1},J_1}\right)\cdot\mathbb{F}_{J_1,J_2,J_3,\ell_1,\ell_2,\ell_3}=0\,,\tag{D.15}$$

$$\left(\widehat{C}_{34}-\mathcal{C}_{\Delta_{J_2},J_2}\right)\cdot\mathbb{F}_{J_1,J_2,J_3,\ell_1,\ell_2,\ell_3}=0\,,\tag{D.16}$$

$$\left(\widehat{C}_{56}-\mathcal{C}_{\Delta_{J_3},J_3}\right)\cdot\mathbb{F}_{J_1,J_2,J_3,\ell_1,\ell_2,\ell_3}=0,\tag{D.17}$$

where $\mathcal{C}_{\Delta,J}=J(-2+d+J)+\Delta(\Delta-d)$ is the Casimir eigenvalue[4] and $\widehat{C}_{ij}$ represents the light-cone Casimir operator which we can obtain from

$$\widehat{C}_{ij}f\left(u_1,\ldots,U_3\right)=(x_{12}^2x_{34}^2x_{56}^2)^{\Delta_\phi}\left[\frac{1}{2}(L_{AB,i}+L_{AB,j})^2\right]\frac{1}{(x_{12}^2x_{34}^2x_{56}^2)^{\Delta_\phi}}f\left(u_1,\ldots,U_3\right)\Big|_{u_{2i-1}\to 0}\tag{D.18}$$

[4]We are in four dimensions so that $d=4$ however the leading twist expansion is known to be dimension independent since the kinematics of the OPE is governed by two dimensional light-cone plane. It is still convenient for debugging purposes to leave d unevaluated in all intermediate steps and check that the d dependence drops out in the end.

where the $L_{AB,i}$ is a generator of the conformal group and $u_{2i-1} \to 0$ stands for the leading term in this limit. It is convenient to introduce yet another set of cross ratios given by

$$u_2 = \frac{(1-z_2)\,(1-z_1 z_2 \hat{z}_3)}{1-z_2 z_3 \hat{z}_1}, \qquad u_4 = \frac{(1-z_3)\,(1-z_2 z_3 \hat{z}_1)}{1-z_1 z_3 \hat{z}_2}, \qquad u_6 = \frac{(1-z_1)\,(1-z_1 z_3 \hat{z}_2)}{1-z_1 z_2 \hat{z}_3},$$
$$U_1 = \frac{1-z_2}{1-z_2 z_3 \hat{z}_1}, \qquad U_2 = \frac{1-z_1}{1-z_1 z_2 \hat{z}_3}, \qquad U_3 = \frac{1-z_3}{1-z_1 z_3 \hat{z}_2}. \tag{D.19}$$

The first few terms of the Casimir differential operator $\widehat{C}_{12}$, in these new variables, reads

$$\frac{\widehat{C}_{12}}{2} = u_1^2\,(z_1-2)\,\partial_{u_1}^2 z_1^2 z_3 \hat{z}_2^2 u_5 \partial_{u_5}\partial_{\hat{z}_2} + \frac{z_1^2\,(z_2\hat{z}_3-1)^{\,2}}{(z_1-1)\,(z_1 z_2 \hat{z}_3-1)} u_3 \hat{z}_3 \partial_{u_3}\partial_{\hat{z}_3} + \dots\,. \tag{D.20}$$

We like these new variables because of the most transparent OPE ($z_i, \hat{z}_i \to 0$) boundary conditions:

$$\mathbb{F}_{J_1,J_2,J_3,\ell_1,\ell_2,\ell_3} \simeq \frac{1}{2^{\sum_i (J_i-l_i)}} z_1^{J_1} z_2^{J_2} z_3^{J_3} \hat{z}_1^{l_1} \hat{z}_2^{l_2} \hat{z}_3^{l_3} \tag{D.21}$$

Given a perturbative data `data` (see next subsection (D.25)) we can then extract any OPE data using the projections (D.15,D.16,D.17) as

$$\sum_{\ell_1,\ell_2,\ell_3} P_{123}^{\bullet\bullet\bullet}(J_1,J_2,J_3,\ell_1,\ell_2,\ell_3)\hat{z}_1^{\ell_1}\hat{z}_1^{\ell_2}\hat{z}_3^{\ell_3} = \lim_{z_{1,2,3}\to 0} \frac{1}{z_1^{J_1} z_2^{J_2} z_3^{J_3}}\, \texttt{data}_{J_1,J_2,J_3}$$

where

$$\texttt{data}_{J_1,J_2,J_3} \equiv \prod_{j_3<J_3} \frac{\widehat{C}_{56}-\mathcal{C}_{\Delta_{j_3},j_3}}{\mathcal{C}_{\Delta_{J_3},J_3}-\mathcal{C}_{\Delta_{j_3},j_3}} \cdot \prod_{j_2<J_2} \frac{\widehat{C}_{34}-\mathcal{C}_{\Delta_{j_2},j_2}}{\mathcal{C}_{\Delta_{J_2},J_2}-\mathcal{C}_{\Delta_{j_2},j_2}} \cdot \prod_{j_1<J_1} \frac{\widehat{C}_{12}-\mathcal{C}_{\Delta_{j_1},j_1}}{\mathcal{C}_{\Delta_{J_1},J_1}-\mathcal{C}_{\Delta_{j_1},j_1}} \cdot \texttt{data} \tag{D.22}$$

is the perturbative data with spins smaller than J_1, J_2, J_3 projected out. Every time we act with Casimir on the conformal block we get back the block times its Casimir eigenvalue. The denominator in (D.22) is chosen such that the coefficient multiplying power of $z_i^i \hat{z}_i^{\ell_i}$ is the OPE coefficient.

This way of extracting is very convenient. The data itself is organized in a simple manner, for given power of $z_i^{a_i}$ the $\hat{z}_i^{l_i}$ powers are such that $l_1 + l_2 \leq J_3$ is satisfied and analogously for the others l_i and at one loop these powers can be dressed by $\ln u_i$. An efficient way to do this extraction is transform the Casimir into a matrix that acts on a vector space created powers of $z_i, \hat{z}_i$ and $\ln u_i$ which then makes (D.22) into a matrix multiplication problem, see figure D.2. Obviously we need to consider finite dimensional vector spaces so we take a cut off $(\Lambda_i, \hat{\Lambda}_i)$ in the powers of $z_i, \hat{z}_i$. This allows to extract OPE coefficients up to spin $J_i = \Lambda_i, \ell_i = \hat{\Lambda}_i$. With this we manage to extract around three hundred thousand OPE coefficients at one loop order which we will analyze in the next section.

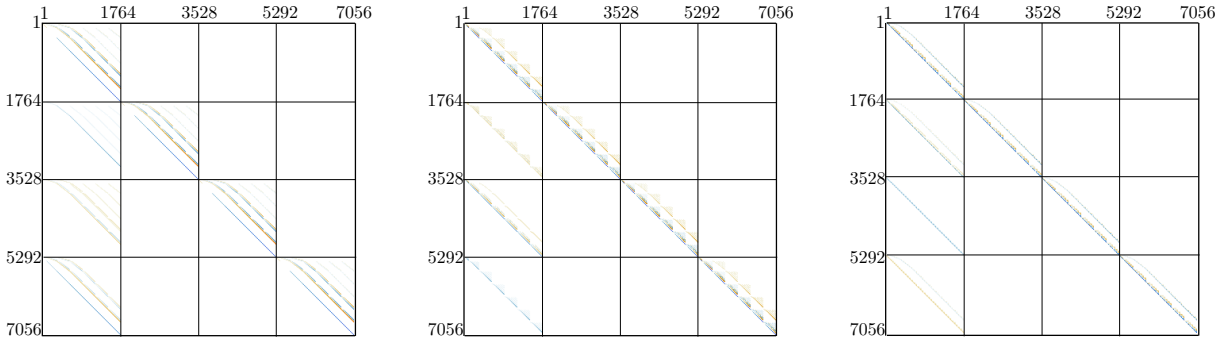

Figure D.2: The six point function in the snowflake OPE limit (z_i, $\hat{z}_i \to 0$) can be expressed as a sum of monomials $\prod_i z_i^{a_i} \hat{z}_i^{l_i}$ which in perturbation theory can be dressed by $\log(u_i)$. The action of the Casimir operators in this base of dressed monomials can be represented as sparse matrices which are plotted here for $a_i \leq 6$, $l_i \leq 2$. The basis is restricted to $l_1 + l_2 \leq a_3$ and similar for the other a_i as discused in the main text. At one loop, the basis can be divided into terms with no logs, or a single $\log(u_1)$, $\log(u_2)$ or $\log(u_3)$, leading to the 4×4 block structure. The Casimir can remove *log*s but never generate them, justifying the absence of off diagonal terms in the last three columns.

D.5.1 Data

Perturbative results for three point functions with more than one spinning operator are considerably more complicated to compute than with just one operator with spin. While three point functions with one spinning operator have been computed, in $\mathcal{N} = 4$ SYM, up to three loops [247], three point functions with two spinning operators have only been computed up to one loop [5]. In the following we will compute these three point functions at one loop for both one, two and three spinning operators by doing conformal block decomposition decomposition of a one loop six point function.

The starting point is the six point function of $20'$ operators

$$\mathcal{O}_2(x) = y^I y^J \mathrm{Tr}(\phi^I(x)\phi^J), \quad y^2 = 0, \quad I = 1, \dots 6 \tag{D.23}$$

which has been computed at one loop in [147] and it is expressed as a simple linear combination of one loop four point integrals $I_{i_1 i_2 i_3 i_4}$(see eq. (32,60-61) of [147] for the precise definition of the six point function)

$$I_{i_1 i_2 i_3 i_4} = \int \frac{d^4 x_0}{x_{i_1 0}^2 x_{i_2 0}^2 x_{i_3 0}^2 x_{i_4 0}^2} \tag{D.24}$$

which can be easily computed in terms of cross ratios.

[5] There are some results for low spinning operators up to two loops [158].

We are interested in obtaining three point functions in the $[0,2,0]$ representation of $SO(6)$ in the OPE. This can be achieved by projecting appropriately the null polarization vectors y into this particular representation (see appendix B of [244] for details). Then we take the light-cone limits $x_{12}^2, x_{34}^2, x_{56}^2 \to 0$ to focus on leading twist operators. At the end of this procedure we arrive at the (tree level plus one loop) expression (D.25), where the two permutations are just given by $u_i, U_i \to u_{i+2}, U_{i+2}; u_{i+4}, U_{i+4}$ and where the dots in the last line stand for higher order powers in z_i. This is precisely the object that enters in (D.22) and that can be used to extract OPE coefficients of three spinning operators at one loop. The last line is transformed into a vector of the monomials and logs which is then acted by the Casimir matrix of figure D.2 to efficiently extract all the needed OPE data.

Through this method we extracted over three hundred thousand OPE coefficients. Both the notebook used for extraction as well as a sample of the result are presented in the attached `Mathematica` notebooks. Our goal now is to write such data as an expression analytically both in spins and polarizations. In the next three sections we display the structure constant for one, two and three spinning operators.

$$\texttt{data} = (x_{12}^2 x_{34}^2 x_{56}^2)^2 \langle \mathcal{O}_2(x_1) \dots \mathcal{O}_2(x_6) \rangle \Big|_{\substack{\text{projection on } [0,2,0] \\ x_{12}^2, x_{34}^2, x_{56}^2 \to 0}} . \tag{D.25}$$

$$\begin{aligned}
&= \prod_{i=1}^{3} \frac{u_{2i-1}}{u_{2i} U_i} \Bigg[\frac{3 u_2 u_4 U_1 U_2 (1+u_6) + U_1 U_2 U_3 (1 + u_2 u_4 u_6)}{24} + \\
&- \frac{\lambda}{4} \Bigg(\ln u_1 \big[U_3 \ln u_2 (u_4 u_6 (U_1 - u_2 U_2) + U_2 (U_1 - u_2 u_6)) \\
&+ U_2 \ln u_6 (u_2 (u_4 (1-u_6) U_1 - u_6 U_3) + U_1 U_3) + u_4 u_6 U_3 \ln U_2 ((1+u_2) U_1 - u_2 (1+U_1) U_2) \\
&+ U_3 \ln U_1 (U_2 (u_2 u_6 - U_1) + u_4 u_6 (u_2 U_2 - U_1)) \big] + \ln u_2 \big[u_2 u_6 U_3 \ln U_3 (U_2 - u_4 U_1) \\
&+ U_1 \ln U_2 (u_2 u_4 (U_2 + u_6 U_3) - U_3 (U_2 + u_4 u_6)) \big] + U_2 \ln U_1 \ln U_2 (U_1 U_3 + u_2 u_6 (u_4 U_1 - (1+u_4) U_3)) \\
&+ u_6 (u_4 U_1 U_3 + u_2 (U_2 U_3 - u_4 U_1 (U_2 + U_3))) \texttt{Li}_2 (1 - u_2) \\
&+ U_2 (U_1 U_3 - u_2 u_4 (U_1 + u_6 U_3 (U_1 - 1))) \texttt{Li}_2 (1 - U_1) \\
&+ \big(U_1 U_3 (u_4 u_6 + U_2) + u_2 (u_4 U_1 U_2 (u_6 - 1) + u_6 U_3 (U_2 (u_4 (U_1 - 1) - 1) - U_1 u_4)) \big) \texttt{Li}_2 \left(1 - \frac{u_2}{U_1} \right) \\
&+ U_2 (U_1 U_3 - u_2 u_4 (U_1 + u_6 U_3 (U_1 - 1))) \texttt{Li}_2 \left(1 - \frac{u_2 u_4}{U_3} \right) \\
&+ u_4 (u_6 U_1 U_3 - u_2 U_2 (u_6 U_3 + U_1 (u_6 - 1))) \texttt{Li}_2 \left(1 - \frac{u_2 U_2}{U_1} \right) \Bigg) + \texttt{two permutations} \Bigg] \\
&= \prod_{i=1}^{3} u_{2i-1} \Bigg[1 + \frac{\sum_i (z_i + z_i^2)}{2} + \frac{z_1 z_2 + z_1 z_3 + z_2 z_3}{4} - \frac{z_2 z_3 \hat{z}_1 + z_1 z_3 \hat{z}_2 + z_1 z_2 \hat{z}_3}{4} + \\
&+ \lambda \big(z_1^2 (\ln u_1 - 2) + z_2^2 (\ln u_3 - 2) + z_3^2 (\ln u_5 - 2) \big) + \dots \Bigg]
\end{aligned} \tag{D.26}$$

D.6 One Loop Explorations

D.6.1 One spinning operator

The structure constants for one spinning operator have been studied extensively in the literature. The first non trivial computation of these three point functions in $\mathcal{N} = 4$ was done at one loop level in [248] via conformal block decomposition of a four point function. It is the most efficient way of computing these three point function. Using this method the structure constants with one spinning operator have been computed up to three loops for any spin in [247] and is known up to five loops for spin two [245].

The one loop structure constant simply reads

$$\hat{C}^{\circ\circ\bullet}_{\texttt{1-loop}} = 4 S_1(J)^2 - 4 S_1(J) S_1(2J) - 2 S_2(J) \tag{D.27}$$

where S_i are the harmonic functions.

To set the coupling convention let us quote here the dimension of these operators

$$\Delta_J = 2 + J + 8\lambda S_1(J) + O(\lambda^2) \tag{D.28}$$

so that from large spin we read

$$f = 8\lambda + O(\lambda^2)\,, \quad \text{and} \quad g = 8\lambda\gamma_E + O(\lambda^2)\,. \tag{D.29}$$

D.6.2 Two spinning operators

Here we complete Bianchi's computation [158] for the one loop structure constant

$$\hat{C}^{\circ\bullet\bullet}_{\texttt{1-loop}} = 4\left(S_1(J_1) + S_1(J_2)\right)\sum_{i=1}^{\ell}\frac{\binom{J_1+J_2+1}{i}\binom{\ell}{i}}{i\binom{J_1}{i}\binom{J_2}{i}} - 4\frac{(J_1+1)(J_2+1)}{J_1+J_2+2}\sum_{i=1}^{\ell}\frac{\binom{J_1+J_2+2}{i}a_i^\ell}{i\binom{J_1}{i}\binom{J_2}{i}} +$$
$$+\sum_{i=1}^{2} 4S_1(J_i)^2 - 4S_1(J_i)S_1(2J_i) - 2S_2(J_i) \tag{D.30}$$

where the constants a_i^ℓ were only known in special limiting cases. They are given by

$$a_i^\ell = \frac{(-1)^i}{2}\left(-S_1(\ell)^2 - S_2(\ell) + 2\sum_{k=2}^{i}\frac{(-1)^k\binom{l}{k-1}}{k-1}\left(S_1(k-2) + S_1(\ell)\right)\right)\,. \tag{D.31}$$

For $i = 1$ and for $i = \ell$ it simplifies to the two previously known special cases (4.5) and (4.6) in [158]. This one loop structure constant can also be rewritten as (D.33), where

$$\mathbb{B}(j,l) = (-1)^l\binom{j}{l}\,. \tag{D.32}$$

Having the full expression for the structure constant at one loop in the form of (D.33) allow us to study the physics of this correlator at large spin and polarizations, with $\frac{\ell}{J_i}$ fixed. As discussed in section 5.5, this serves as a toy model for the large spin limit of three point functions of spinning operators and its relation to the null hexagonal Wilson loops.

$$\begin{aligned}\hat{C}^{\circ\bullet\bullet}_{\texttt{1-loop}} &= 8S_1(J_1)^2 - 4S_1(J_1)S_1(2J_1) + 8S_1(J_1)S_1(J_2) + 8S_1(J_2)^2 - 4S_1(J_2)S_1(2J_2) + \\ &- 4S_1(J_1)S_1(J_1-\ell) - 4S_1(J_2)S_1(J_1-\ell) - 4S_1(J_1)S_1(J_2-\ell) - 4S_1(J_2)S_1(J_2-\ell) + \\ &- 4S_1(J_1)S_1(\ell) - 4S_1(J_2)S_1(\ell) + 4S_1(J_1-\ell)S_1(\ell) + 4S_1(J_2-\ell)S_1(\ell) - 2S_1(\ell)^2 + \\ &- 2S_2(J_1) - 2S_2(J_2) - 2S_2(\ell) - 4\sum_{p=1}^{\infty}\Bigg(\left(\frac{\mathbb{B}(J_1,\ell-p)}{\mathbb{B}(J_1,\ell)} + \frac{\mathbb{B}(J_2,\ell-p)}{\mathbb{B}(J_2,\ell)}\right)\frac{S_1(p-1)}{p} + \\ &+ 4(S_1(J_1)+S_1(J_2)-S_1(\ell))\frac{\mathbb{B}(J_1,\ell-p)}{\mathbb{B}(J_1,\ell)}\frac{\mathbb{B}(J_2,\ell-p)}{\mathbb{B}(J_2,\ell)}\frac{1}{p} - 4\frac{\mathbb{B}(J_1,\ell-p)}{\mathbb{B}(J_1,\ell)}\times \\ &\times\frac{\mathbb{B}(J_2,\ell-p)}{\mathbb{B}(J_2,\ell)}\frac{S_1(p)+S_1(\ell-p)-S_1(\ell)}{p} + \sum_{q=1}^{p-1}\frac{\mathbb{B}(J_1,\ell-p)}{\mathbb{B}(J_1,\ell)}\frac{\mathbb{B}(J_2,\ell-q)}{\mathbb{B}(J_2,\ell)}\frac{1}{(p-q)p} \\ &+ \sum_{q=p+1}^{\infty}\frac{\mathbb{B}(J_1,\ell-p)}{\mathbb{B}(J_1,\ell)}\frac{\mathbb{B}(J_2,\ell-q)}{\mathbb{B}(J_2,\ell)}\frac{1}{(q-p)q}\Bigg).\end{aligned} \tag{D.33}$$

There are two regimes of interest, depending on whether ℓ is before or after $\ell_* \equiv \frac{J_1 J_2}{(J_1+J_2)}$.[6] Before ℓ_* we obtain the order one result

$$\begin{aligned}\hat{C}^{\bullet\bullet\circ}_{\texttt{1-loop}} \xrightarrow{J_1,J_2,\ell\to\infty} &-\pi^2 - 4\log(2)\log\left(J_1J_2e^{2\gamma_E}\right) - 2\log^2\left(\ell e^{\gamma_E}\right) \\ &- 2\log\left(1-\frac{\ell}{J_1}-\frac{\ell}{J_2}\right)\log\left(\frac{e^{2\gamma_E}J_1^2J_2^2}{\ell^2}\left(1-\frac{\ell}{J_1}-\frac{\ell}{J_2}\right)\right)\end{aligned} \tag{D.34}$$

while after ℓ_* we obtain the exponentially large expression

$$\begin{aligned}\hat{C}^{\bullet\bullet\circ}_{\texttt{1-loop}} \xrightarrow{J_1,J_2,\ell\to\infty} &\frac{J_1^{-2J_1-1}J_2^{-2J_2-1}\left(J_1+J_2\right)^{J_1+J_2+\frac{3}{2}}\ell^{2\ell+1}\left(J_1-\ell\right)^{J_1-\ell+\frac{1}{2}}\left(J_2-\ell\right)^{J_2-\ell+\frac{1}{2}}}{J_1J_2-J_1\ell-J_2\ell}\times \\ &\times 4\sqrt{2\pi}\log\left(\frac{\ell}{J_1}+\frac{\ell}{J_2}-1\right).\end{aligned} \tag{D.35}$$

Note that the singular point ℓ_* is reminiscent of the singularities encountered in the $U(\ell)$ map, equation (5.16). The log singularities at ℓ_* in (D.34) should therefore be compared with the log singularities of the hexagonal Wilson loop at $U_i = 0$, see (5.30). This justifies treating $C^{\bullet\bullet\circ}$ as a toy model for the transition in behaviour of $C^{\bullet\bullet\bullet}$ from the space-like region to the time-like region in section 5.5.

Lets comment on how these results can be derived. The only non-trivial pieces in (D.33)

[6] Note that the tree level three point function, given by

$$C^{\bullet\bullet\circ}_{\text{tree}} = \frac{\Gamma(J_1+1)\Gamma(J_2+1)}{\sqrt{\Gamma(2J_1+1)\Gamma(2J_2+1)}\Gamma(J_1-\ell+1)\Gamma(J_2-\ell+1)\Gamma(\ell+1)},$$

approaches a gaussian centered at ℓ_* in the large spin limit.

are the sums, of which there are two types, that with a single ratio of binomials, as in the third line, and those with a product of ratio of binomials, as in the last three lines. First we analyze the latter.

Binomials $\binom{j}{l}$, in the large j limit with $\frac{\ell}{j}$ fixed approach gaussians with mean $j/2$ and standard deviation $\sqrt{j}/2$. The product of binomials in the denominators therefore approach gaussians[7] with mean $\ell_* = \frac{J_1 J_2}{J_1+J_2}$ and standard deviation $O(\sqrt{J})$. Similar happens in the numerators only that arguments are shifted. The sum indices p and q being positive, we see that if $\ell < \ell_*$ so that the denominator is evaluated to the left of the maximum, large p and q are exponentially suppressed relative to p, q of order one. In this limit, the sums are easily evaluated. For example, in the fifth line we have the simplification

$$\sum_{p=1}^{l} \left(\frac{\mathbb{B}(J_1, \ell-p)}{\mathbb{B}(J_1,\ell)} \frac{\mathbb{B}(J_2,\ell-p)}{\mathbb{B}(J_2,\ell)} \frac{1}{p} \to \left(\frac{\ell^2}{(J_1-\ell)(J_2-l)} \right)^p \frac{1}{p} \right) = -\log\left(\frac{\ell(J_1+J_2)-J_1J_2}{(J_1-\ell)(J_2-\ell)} \right). \tag{D.36}$$

On the other hand, if $\ell > \ell_*$, provided p and q are $O(J)$, we can tune the indices so that the numerator sits at the top of the gaussian. The sums are therefore evaluated by saddle point and we obtain the exponential expression in (D.35).

For the summand with a single ratio of binomials, for similar reasons, p of order one dominates when $\ell < \ell_*$ and logs are generated. However, for this term there are no exponential contributions when $\ell > \ell_*$ due to the oscillating phase in (D.32). Therefore this term can be neglected in the $\ell > \ell_*$ regime.

Finally, we note a sum rule for the one-loop sum of structure constants, valid at finite J_1 and J_2:

$$\sum_{\ell} C^{\bullet\bullet\circ}_{\texttt{1-loop}} = 4\left(S_1(J_1)+S_1(J_2)\right) S_1(J_1+J_2) - \sum_{i=1}^{2} 4S_1(J_i)S_1(2J_i) + 2S_2(J_i)\,, \tag{D.37}$$

note that this sums is for the full one loop correction to the structure constants ($C = C_{\texttt{tree}} + C_{\texttt{1-loop}}$) and *not* the correction normalized by tree level ($\hat{C}$).

D.6.3 Three spinning operators

For three spinning operators we were not able to find an expression analogous (D.30) or (D.33), which is analytical both in spin and polarizations. In this section we present a general expression for the one-loop structure constant in terms of unknown coefficients that we could not fix entirely. However, when considering small polarizations (where we have abundant perturbative data) we were able to fix such coefficients and arrive in an analytic expression for the structure constant in terms of the spins J_i, such as (D.43).

We start by parametrizing the one-loop structure constant as the sum of three terms

$$\hat{C}^{J_1,J_2,J_3}_{\ell_1,\ell_2,\ell_3} = \mathcal{X}^{J_1,J_2,J_3} + \mathcal{Y}^{J_1,J_2,J_3}_{\ell_1,\ell_2,\ell_3} + \mathcal{Z}^{J_1,J_2,J_3}_{\ell_1,\ell_2,\ell_3} \tag{D.38}$$

The first term of (D.38) is a generalization of the one spin structure constant (D.27),

[7] The product of gaussians is a gaussian.

and it is simply given by

$$\mathcal{X}^{J_1,J_2,J_3} = 4S_1(J_1)^2 - 4S_1(J_1)S_1(2J_1) - 2S_2(J_1) + 4S_1(J_2)^2 - 4S_1(J_2)S_1(2J_2) + \\ - 2S_2(J_2) + 4S_1(J_3)^2 - 4S_1(J_3)S_1(2J_3) - 2S_2(J_3) \tag{D.39}$$

this term gives the one-loop structure constants for vanishing polarizations ($\ell_i = 0$).

The second term of (D.38) is inspired in the two spin structure constants (D.30), which reads

$$\mathcal{Y}^{J_1,J_2,J_3}_{\ell_1,\ell_2,\ell_3} = 4\left(S_1(J_1)+S_1(J_2)\right)\sum_{i=1}^{\ell_3}\left(\frac{\binom{J_1+J_2+1}{i}\binom{\ell_3}{i}}{i\binom{J_1}{i}\binom{J_2}{i}}\right) - 4\frac{(J_1+1)(J_2+1)}{J_1+J_2+2}\sum_{i=1}^{\ell_3}\left(\frac{\binom{J_1+J_2+2}{i}a_i^{\ell_3}}{i\binom{J_1}{i}\binom{J_2}{i}}\right) + \\ + 4\left(S_1(J_1)+S_1(J_3)\right)\sum_{i=1}^{\ell_2}\left(\frac{\binom{J_1+J_3+1}{i}\binom{\ell_2}{i}}{i\binom{J_1}{i}\binom{J_3}{i}}\right) - 4\frac{(J_1+1)(J_3+1)}{J_1+J_3+2}\sum_{i=1}^{\ell_2}\left(\frac{\binom{J_1+J_3+2}{i}a_i^{\ell_2}}{i\binom{J_1}{i}\binom{J_3}{i}}\right) + \\ + 4\left(S_1(J_2)+S_1(J_3)\right)\sum_{i=1}^{\ell_1}\left(\frac{\binom{J_2+J_3+1}{i}\binom{\ell_1}{i}}{i\binom{J_2}{i}\binom{J_3}{i}}\right) - 4\frac{(J_2+1)(J_3+1)}{J_2+J_3+2}\sum_{i=1}^{\ell_1}\left(\frac{\binom{J_2+J_3+2}{i}a_i^{\ell_1}}{i\binom{J_2}{i}\binom{J_3}{i}}\right) + \\ + 4\sum_{i=1}^{3}S_1(\ell_i)S_1(j_i). \tag{D.40}$$

This expression is a simple symmetrization of (D.30), except the last line, which does not exist in the context of two spinning operators. When combined with $\mathcal{X}^{J_1,J_2,J_3}$ it gives the structure constants with two vanishing polarizations ($\hat{C}^{J_1,J_2,J_3}_{0,0,\ell}$).

Through lengthy explorations of the extracted one loop data and inspired by [158] we were able to parametrize any one-loop structure constant via the following ansatz

$$\mathcal{Z}^{J_1,J_2,J_3}_{\ell_1,\ell_2,\ell_3} = q\left(J_1,J_2,J_3,\ell_1,\ell_2\right) + q\left(J_2,J_3,J_1,\ell_2,\ell_3\right) + q\left(J_3,J_1,J_2,\ell_3,\ell_1\right) \tag{D.41}$$

where

$$\frac{q\left(j_1,j_2,j_3,l_1,l_2\right)}{(1+j_1)(1+j_2)} = (1+j_3)\sum_{n=1}^{l_2}\sum_{m=1}^{l_1}\sum_{p=1}^{l_1+l_2}\beta^{n,m,p}_{l_1,l_2}\frac{\mathbb{B}(j_1,l_2-n)}{\mathbb{B}(j_1,l_2)}\frac{\mathbb{B}(j_2,l_1-m)}{\mathbb{B}(j_2,l_1)}\frac{\mathbb{B}(j_3,l_1+l_2-p)}{\mathbb{B}(j_3,l_1+l_2)} + \\ \sum_{n=1}^{l_2}\sum_{m=1}^{l_1}\sum_{p=n+m}^{l_1+l_2}\gamma^{n,m,p}_{l_1,l_2}\frac{\mathbb{B}(j_1,l_2-n)}{\mathbb{B}(j_1,l_2)}\frac{\mathbb{B}(j_2,l_1-m)}{\mathbb{B}(j_2,l_1)}\frac{\mathbb{B}(j_3,l_1+l_2-p)}{\mathbb{B}(j_3,l_1+l_2)}S_1(j_3) \tag{D.42}$$

with $\mathbb{B}$, defined in (D.32) and being $\beta^{n,m,p}_{l_i,l_j}$ and $\gamma^{n,m,p}_{l_i,l_j}$ unknown coefficients. We were able to fix all $\gamma^{n,m,p}_{l_i,l_j}$ coefficients and a large portion of the $\beta^{n,m,p}_{l_i,l_j}$, by comparing this ansatz with perturbative data and large spin expansions.

By matching with the extracted perturbative data we were able to fix all the $\gamma^{n,m,p}_{l_i,l_j}$ coefficients for polarizations up to $\ell_{\text{max}} = 5$ and all the $\beta^{n,m,p}_{l_1,l_2}$ for polarizations up to $\ell_{\text{max}} = 3$, being expression (D.43) below an explicit example with polarizations $\{\ell_1 =$

$1, \ell_2 = 2, \ell_3 = 3\}$.

$$\hat{C}^{J_1,J_2,J_3}_{1,2,3} = \mathcal{X}^{J_1,J_2,J_3} + \mathcal{Y}^{J_1,J_2,J_3}_{1,2,3} + \left(\frac{(1+J_2)(1+J_3)S_1(J_1)}{\mathbb{B}(J_2,3)\mathbb{B}(J_3,2)\mathbb{B}(J_1,5)}\right)\left(\frac{4}{5} - \frac{8J_2}{15} + \frac{13J_1J_2}{30} + \right.$$
$$- \frac{J_1^2J_2}{30} + \frac{2J_2^2}{15} - \frac{2J_1J_2^2}{15} + \frac{J_1^2J_2^2}{30} - \frac{2J_3}{5} + \frac{J_1J_3}{5} + \frac{4J_2J_3}{15} - \frac{31J_1J_2}{60} + \frac{J_1^2J_2J_3}{5} +$$
$$\left.\frac{J_1^3J_2J_3}{60} - \frac{J_2^2J_3}{15} + \frac{J_1J_2^2J_3}{6} - \frac{J_1^2J_2^2J_3}{10} + \frac{J_1^3J_2^2J_3}{60}\right) +$$
$$+ \left(\frac{(1+J_1)(1+J_3)S_1(J_2)}{\mathbb{B}(J_1,3)\mathbb{B}(J_3,1)\mathbb{B}(J_2,4)}\right)\left(1 - \frac{2J_1}{3} + \frac{J_1^2}{6} + \frac{3J_1J_2}{4} - \frac{J_1^2J_2}{4} - \frac{J_1J_2^2}{12} + \frac{J_1^2J_2^2}{12}\right) +$$
$$+ \left(\frac{(1+J_1)(1+J_2)S_1(J_3)}{\mathbb{B}(J_1,2)\mathbb{B}(J_2,1)\mathbb{B}(J_3,3)}\right)\left(\frac{4}{3} - \frac{2J_1}{3} + \frac{2J_1J_3}{3}\right) +$$
$$+ \left(\frac{(1+J_1)(1+J_2)(1+J_3)}{\mathbb{B}(J_1,5)\mathbb{B}(J_2,4)\mathbb{B}(J_3,3)}\right)\left(- \frac{17}{60} - \frac{29J_1}{720} + \frac{71J_1^2}{864} - \frac{61J_1^3}{2160} + \frac{13J_1^4}{4320} + \right.$$
$$+ \frac{13J_2}{120} + \frac{623J_1J_2}{4320} - \frac{5269J_1^2J_2}{25920} + \frac{877J_1^3J_2}{12960} - \frac{187J_1^4J_2}{25920} - \frac{7J_2^2}{270} - \frac{41J_1J_2^2}{405} + \frac{859J_1^2J_2^2}{6480} +$$
$$- \frac{1177J_1^3J_2^2}{25920} + \frac{25J_1^4J_2^2}{5184} + \frac{J_2^3}{270} + \frac{119J_1J_2^3}{6480} - \frac{103J_1^2J_2^3}{4320} + \frac{227J_1^3J_2^3}{25920} - \frac{5J_1^4J_2^3}{5184} + \frac{29J_3}{120} +$$
$$+ \frac{167J_1J_3}{1440} - \frac{173J_1^2J_3}{960} + \frac{83J_1^3J_3}{1440} - \frac{17J_1^4J_3}{2880} + \frac{37J_2J_3}{240} - \frac{153J_1J_2J_3}{320} + \frac{2393J_1^2J_2J_3}{5760} +$$
$$- \frac{569J_1^3J_2J_3}{4320} + \frac{239J_1^4J_2J_3}{17280} - \frac{73J_2^2J_3}{540} + \frac{215J_1J_2^2J_3}{648} - \frac{1399J_1^2J_2^2J_3}{5184} + \frac{1103J_1^3J_2^2J_3}{12960} +$$
$$- \frac{47J_1^4J_2^2J_3}{5184} + \frac{13J_2^3J_3}{540} - \frac{49J_1J_2^3J_3}{810} + \frac{1277J_1^2J_2^3J_3}{25920} - \frac{83J_1^3J_2^3J_3}{5184} + \frac{23J_1^4J_2^3J_3}{12960} - \frac{J_3^2}{15} +$$
$$- \frac{11J_1J_3^2}{288} + \frac{125J_1^2J_3^2}{1728} - \frac{209J_1^3J_3^2}{8640} + \frac{11J_1^4J_3^2}{4320} - \frac{53J_2J_3^2}{720} + \frac{5J_1J_2J_3^2}{27} - \frac{4199J_1^2J_2J_3^2}{25920}$$
$$+ \frac{173J_1^3J_2J_3^2}{3240} - \frac{149J_1^4J_2J_3^2}{25920} + \frac{31J_2^2J_3^2}{540} - \frac{53J_1J_2^2J_3^2}{405} + \frac{1807J_1^2J_2^2J_3^2}{17280} - \frac{3487J_1^3J_2^2J_3^2}{103680} +$$
$$\left. + \frac{127J_1^4J_2^2J_3^2}{34560} - \frac{11J_2^3J_3^2}{1080} + \frac{623J_1J_2^3J_3^2}{25920} - \frac{31J_1^2J_2^3J_3^2}{1620} + \frac{43J_1^3J_2^3J_3^2}{6912} - \frac{73J_1^4J_2^3J_3^2}{103680}\right). \quad \text{(D.43)}$$

We now consider the large spin expansion, i.e. $J_i \to \infty$ with ℓ_i finite. It is easy to expand the ansatz above (D.42) up to some arbitrary order Λ. The ratio of binomials has a simple large spin limit, which allow us to truncate the sums up to Λ. This means we can trade our knowledge of knowing the $\gamma^{n,m,p}_{l_i,l_j}$ and $\beta^{n,m,p}_{l_i,l_j}$ up to some $\ell_{\max}$ to knowing the large spin expansion up to some order $\mathcal{O}(1/J^{\ell_{\max}})$.

Furthermore, in this large spin limit is easy to disentangle the terms that are associated with the coefficients $\gamma^{n,m,p}_{l_i,l_j}$ and $\beta^{n,m,p}_{l_1,l_2}$, since the first one multiplies $S_1(J_i)$ and will come together with a $\ln J_i$ factor. Therefore, using our perturbative data we can write the large spin expansion for the one-loop structure constant for arbitrary polarizations, up to order $\mathcal{O}(1/J^5)$ for the terms with logs and up to order $\mathcal{O}(1/J^3)$ for the rest (which are simple

polynomials in polarizations and harmonic numbers), for example at order $\mathcal{O}(1/J^1)$ it reads

$$\begin{aligned}\hat{C}^{J_1,J_2,J_3}_{\ell_1,\ell_2,\ell_3} &= -\pi^2 - 2S_1(\ell_1)^2 - 2S_1(\ell_1)S_1(\ell_2) - 2S_1(\ell_2)^2 - 2S_1(\ell_1)S_1(\ell_3) - 2S_1(\ell_2)S_1(\ell_3) + \\ &- 2S_1(\ell_3)^2 - 2S_2(\ell_1) - 2S_2(\ell_2) - 2S_2(\ell_3) + 4(\ln J_1 + \gamma_E)(S_1(\ell_1) - \ln 2) + \\ &+ 4(\ln J_2 + \gamma_E)(S_1(\ell_2) - \ln 2 + 4(\ln J_3 + \gamma_E)(S_1(\ell_3) - \ln 2) + \frac{2}{J_1} + \frac{2}{J_2} + \frac{2}{J_3} + \\ &- \frac{2\ln 2}{J_1} - \frac{2\ln 2}{J_2} - \frac{2\ln 2}{J_3} + (\ln J_1 + \gamma_E)\Big(\frac{1}{J_1} + \frac{4\ell_2}{J_1} + \frac{4\ell_2}{J_3} + \frac{4\ell_3}{J_1} + \frac{4\ell_3}{J_2}\Big) + \\ &+ (\ln J_2 + \gamma_E)\Big(\frac{1}{J_2} + \frac{4\ell_1}{J_2} + \frac{4\ell_1}{J_3} + \frac{4\ell_3}{J_1} + \frac{4\ell_3}{J_2}\Big) + (\ln J_3 + \gamma_E)\Big(\frac{1}{J_3} + \frac{4\ell_1}{J_2} + \\ &+ \frac{4\ell_1}{J_3} + \frac{4\ell_2}{J_1} + \frac{4\ell_2}{J_3}\Big) + S_1(\ell_1)\Big(\frac{2}{J_1} - \frac{4\ell_1}{J_2} - \frac{4\ell_1}{J_3} - \frac{2\ell_2}{J_1} - \frac{2\ell_2}{J_3} - \frac{2\ell_3}{J_1} - \frac{2\ell_3}{J_2}\Big) + \\ &+ S_1(\ell_2)\Big(\frac{2}{J_2} - \frac{4\ell_2}{J_1} - \frac{4\ell_2}{J_3} - \frac{2\ell_1}{J_2} - \frac{2\ell_1}{J_3} - \frac{2\ell_3}{J_1} - \frac{2\ell_3}{J_2}\Big) + S_1(\ell_3)\Big(\frac{2}{J_3} - \frac{4\ell_3}{J_1} + \\ &- \frac{4\ell_3}{J_1} - \frac{2\ell_1}{J_2} - \frac{2\ell_1}{J_3} - \frac{2\ell_2}{J_1} - \frac{2\ell_2}{J_3}\Big) + O(1/J_i^2) \end{aligned} \tag{D.44}$$

where γ_E is the Euler's constant.

Our goal now is to use the large spin expansion to write the one-loop structure constant using the basis of binomials akin to (D.33). We again divide the structure constant expression in three factors

$$\hat{C}^{J_1,J_2,J_3}_{\ell_1,\ell_2,\ell_3} = X^{J_1,J_2,J_3}_{\ell_1,\ell_2,\ell_3} + Y^{J_1,J_2,J_3}_{\ell_1,\ell_2,\ell_3} + Z^{J_1,J_2,J_3}_{\ell_1,\ell_2,\ell_3} \tag{D.45}$$

The first factor corresponds to terms which in the large spin limit come multiplying logs. These terms are easier to obtain for two reasons. The first one is simply that we have more data in the large spin expansion for them ($O(1/J^5)$). The second is transcendentality: the harmonic numbers account for transcendentality one so the factors that come multiplying them turned out to be simpler than one naively would expect for the full one-loop structure constant.

Here the big advantage of the binomials representation comes to play. We can parametrize families of terms in the large spin expansion using a basis of the binomials $\mathbb{B}$. For example, when expanding in large spin we find the following factors

$$\hat{C}^{J_1,J_2,J_3}_{\ell_1,\ell_2,\ell_3} = \cdots + 4\ln J_1\left(\frac{\ell_2^2}{J_1 J_3} - \frac{\ell_2^2}{J_1 J_3^2} - \frac{\ell 2^2}{J_1^2 J_3} + \frac{\ell_1 \ell_2^2}{J_1 J_3^2} + \frac{\ell_2^3}{J_1 J_3^2} + \frac{\ell_2^3}{J_1^2 J_3} + O(J^3)\right) + \ldots \tag{D.46}$$

so we consider a linear combination of sums involving ratios of the binomials $\mathbb{B}(J_1,\ell_2)$, $\mathbb{B}(J_3,\ell_2)$, $\mathbb{B}(J_1,\ell_1)$, $\mathbb{B}(J_1-\ell_1)$, $\mathbb{B}(J_3-\ell_1,\ell_2)$ and fix their coefficients by matching with the large spin expansion (D.46). For this piece of the one-loop structure constant, we obtain

the following expression

$$\hat{C}^{J_1,J_2,J_3}_{\ell_1,\ell_2,\ell_3} = \cdots + 4S_1(J_1)\left(\sum_{p=1}^{\infty}\frac{\mathbb{B}(J_1,\ell_2-p)}{\mathbb{B}(J_1,\ell_2)}\frac{\mathbb{B}(J_3-\ell_1,\ell_2-p)}{\mathbb{B}(J_3-\ell_1,\ell_2)}\frac{1}{p}\right)+\dots \tag{D.47}$$

a simple check of this expression is to expand it in the large spin limit and recover (D.46).

By following these procedure we were able to write the first factor in (D.45) of the one-loop structure constant, it reads

$$\begin{aligned}
X^{J_1,J_2,J_3}_{\ell_1,\ell_2,\ell_3} = &\Big(8S_1(J_1)^2 - 4S_1(J_1)S_1(2J_1) + 4S_1(J_1)S_1(J_2) + 4S_1(J_1)S_1(J_3) + 2S_1(\ell_1)S_1(J_1-\ell_2)+\\
&- 4S_1(J_1)S_1(J_3-\ell_2) - 4S_1(J_1)S_1(\ell_2) + 2S_1(J_1-\ell_2)S_1(\ell_2) - S_1(\ell_2)^2 + 2S_1(\ell_1)S_1(J_1-\ell_3)+\\
&- 4S_1(J_1)S_1(J_2-\ell_3) - 4S_1(J_1)S_1(J_1-\ell_2-\ell_3) + 2S_1(\ell_2)S_1(J_1-\ell_2-\ell_3) - 4S_1(J_1)S_1(\ell_3)+\\
&- 2S_1(\ell_2)S_1(\ell_3) + 2S_1(J_1-\ell_3)S_1(\ell_3) + 2S_1(J_1-\ell_2-\ell_3)S_1(\ell_3) - S_1(\ell_3)^2 - 2S_2(J_1) - S_2(\ell_2)+\\
&- S_2(\ell_3)\Big) + 4\Big(S_1(J_1) - \frac{S_1(\ell_2)}{2} - \frac{S_1(\ell_3)}{2}\Big)\left(\sum_{p=1}^{\infty}\sum_{q=1}^{\infty}\frac{\mathbb{B}(J_2,\ell_3-p)}{\mathbb{B}(J_2,\ell_3)}\frac{\mathbb{B}(J_3,\ell_2-q)}{\mathbb{B}(J_3,\ell_2)}\frac{\mathbb{B}(\ell_2,p)\mathbb{B}(\ell_3,q)}{B^{(1+J_1-\ell_2-\ell_3)}_{(p+q)}}+\right.\\
&\left.+\sum_{p=1}^{\infty}\frac{\mathbb{B}(J_2,\ell_3-p)}{\mathbb{B}(J_2,\ell_3)}\frac{\mathbb{B}(J_1-\ell_2,\ell_3-p)}{\mathbb{B}(J_1-\ell_2,\ell_3)}\frac{1}{p}+\sum_{p=1}^{\infty}\frac{\mathbb{B}(J_3,\ell_2-p)}{\mathbb{B}(J_3,\ell_2)}\frac{\mathbb{B}(J_1-\ell_3,\ell_2-p)}{\mathbb{B}(J_1-\ell_3,\ell_2)}\frac{1}{p}\right)+\\
&(\{J_1,\ell_1\}\longleftrightarrow\{J_2,\ell_2\}) + (\{J_1,\ell_1\}\longleftrightarrow\{J_3,\ell_3\})
\end{aligned} \tag{D.48}$$

where $B^{(b)}_{(a)}$ is the inverse of the Euler's beta function, $B^{(b)}_{(a)} = 1/B(a,b)$.

With this factors fully fixed we can turn now to the match with the Wilson loop. In order to compare with the Wilson loop we will consider the expansion around the origin limit of (5.32). The factor (D.48) written above encodes all the contributions proportional to logs, therefore it is precisely this factor that should reproduce the $\mathcal{A}_i$ factor of (5.30). And indeed, up to order $O(1/J^{10})$ in the origin expansion we find a perfect match between the structure constant and the Wilson loop for the terms linear in logs. For finite J_i/ℓ_j ratio, we can perform the sums akin to (D.36) and use the (5.14) to write the combinations of spins and polarizations in terms of cross-ratios recovering precisely that $\mathcal{A}_i = 2\ln(1-U_i)$, in perfect agreement with the Wilson loop (5.30).

The second term of (D.45) in the large spin limit is given only by powers of the polarizations ℓ_i. By transcendentality the combination of binomials appearing here can be more complicated than before, as happens in the two spins case of (D.33). This expansion is again separated in various families depending in the J_i and ℓ_i that they display, which then we try to match with a linear combination of sum of ratio of binomials. However, we were not able to fix all the combinations of $\mathbb{B}$ in a close form like (D.48), these partial

results we display below

$$
\begin{aligned}
Y^{J_1,J_2,J_3}_{\ell_1,\ell_2,\ell_3} = 4\Bigg(& \sum_{p=1}^{\infty} \frac{\mathbb{B}(J_1,\ell_2-p)}{\mathbb{B}(J_1,\ell_2)} \frac{\mathbb{B}(J_3,\ell_2-p)}{\mathbb{B}(J_3,\ell_2)} \frac{S_1(\ell_2)-S_1(p)-S_1(\ell_2-p)}{p} - \sum_{p=1}^{\infty} \frac{\mathbb{B}(J_3,\ell_1-p)}{\mathbb{B}(J_3,\ell_1)} \frac{S_1(p-1)}{p} + \\
& + \sum_{p=1}^{\infty} \sum_{q=1}^{p-1} \frac{\mathbb{B}(J_1,\ell_2-p)}{\mathbb{B}(J_1,\ell_2)} \frac{\mathbb{B}(J_3,\ell_2-q)}{\mathbb{B}(J_3,\ell_2)} \frac{1}{(p-q)p} + \sum_{p=1}^{\infty} \sum_{q=p+1}^{\infty} \frac{\mathbb{B}(J_1,\ell_2-p)}{\mathbb{B}(J_1,\ell_2)} \frac{\mathbb{B}(J_3,\ell_2-q)}{\mathbb{B}(J_3,\ell_2)} \frac{1}{(q-p)q} + \\
& - \sum_{p=1}^{\infty} \sum_{q=1}^{\infty} \frac{\mathbb{B}(J_1,\ell_3-p)}{\mathbb{B}(J_1,\ell_3)} \frac{\mathbb{B}(J_3,\ell_1-p)}{\mathbb{B}(J_3,\ell_1)} \frac{1}{2pq} - \sum_{p=1}^{\infty} \frac{\mathbb{B}(J_1,\ell_3-p)}{\mathbb{B}(J_1,\ell_3)} \frac{S_1(p-1)}{p} \Bigg) + \\
& + (\{J_1,\ell_1\} \longleftrightarrow \{J_2,\ell_2\}) + (\{J_3,\ell_3\} \longleftrightarrow \{J_1,\ell_2\})
\end{aligned}
\tag{D.49}
$$

More precisely, we were not able to fix the combinations of binomials in a close form, for factors that in the large spin expansion mix the following spins and polarizations $\frac{\ell_{i-1}\ell_{i+1}}{J_i}$, $\frac{\ell_{i-1}\ell_{i+1}}{J_i J_{i+1}}$ and $\frac{\ell_{i-1}\ell_{i+1}}{J_{i+1} J_i J_{i+1}}$. The last term in (D.45) accounts for that

$$
Z^{J_1,J_2,J_3}_{\ell_1,\ell_2,\ell_3} = q\left(J_1,J_2,J_3,\ell_1,\ell_2\right) + q\left(J_2,J_3,J_1,\ell_2,\ell_3\right) + q\left(J_3,J_1,J_2,\ell_3,\ell_1\right) \tag{D.50}
$$

where

$$
q\left(j_1,j_2,j_3,l_1,l_2\right) = \sum_{n=0}^{l_2} \sum_{m=0}^{l_1} \sum_{p=0}^{l_1+l_2} \beta^{n,m,p}_{l_1,l_2} \frac{\mathbb{B}(j_1,l_2-n)}{\mathbb{B}(j_1,l_2)} \frac{\mathbb{B}(j_2,l_1-m)}{\mathbb{B}(j_2,l_1)} \frac{\mathbb{B}(j_3,l_1+l_2-p)}{\mathbb{B}(j_3,l_1+l_2)} \tag{D.51}
$$

but now it has no $\gamma^{n,m,p}_{l_i,l_j}$ since the coefficients of the logs were already fixed. The remaining unknown coefficients $\beta^{n,m,p}_{l_i,l_j}$ are all fixed for $\ell_{\max} = 4$ and only six remain unfixed for $\ell_{\max} = 5$. These fixed $\beta^{n,m,p}_{l_i,l_j}$ are a set of simple numbers,

$$
\begin{aligned}
& \beta^{0,0,0}_{0,0} = 0, \quad \beta^{0,0,0}_{0,1} = 0, \quad \beta^{0,0,0}_{0,2} = 0, \quad \beta^{0,0,0}_{0,3} = 0, \qquad \beta^{0,0,0}_{0,3} = 0, \qquad \beta^{0,0,1}_{0,1} = 0, \\
& \beta^{0,0,1}_{0,2} = 1, \quad \beta^{0,0,1}_{0,3} = \tfrac{2}{3}, \quad \beta^{1,0,1}_{0,1} = 0, \quad \beta^{1,0,1}_{0,2} = -1, \quad \beta^{1,0,1}_{0,3} = -\tfrac{2}{3}, \quad \ldots
\end{aligned}
\tag{D.52}
$$

which we were not able to find a pattern for. This and the other fixed coefficients are in the attached `Mathematica` notebook.

Finally, let's consider the relation with the Wilson loop. The only factor left to match in (5.30) is $\mathcal{B}$. Since we lack a close expression for the $\beta^{n,m,p}_{l_i,l_j}$ we cannot recover the full $\mathcal{B}$ in terms of cross-ratios, however using the $\beta^{n,m,p}_{l_i,l_j}$ fixed through data we were able to match the Wilson Loop expansion up to order six, meaning we matched the first 873 terms of the origin expansion.

Appendix E

Appendix: Spinning Hexagons

E.1 Spinors

In section 6.3 we parametrize spinning operators through their left- and right-handed polarization spinors $L_{i\alpha}$ and $R_{i\dot{\alpha}}$. These are related to the polarization vectors by

$$\epsilon_i^\mu = R_{i\dot{\beta}} \, (\bar{\sigma}^\mu)^{\dot{\beta}\alpha} \, L_{i\alpha}. \tag{E.1}$$

In our conventions the sigma matrices $\sigma^\mu_{\alpha\dot{\alpha}}$, $\bar{\sigma}^{\mu\dot{\alpha}\alpha}$ are given by

$$\sigma^0 = -\begin{pmatrix} 1 & 0 \\ 0 & 1 \end{pmatrix}, \qquad \sigma^1 = \begin{pmatrix} 0 & 1 \\ 1 & 0 \end{pmatrix}, \qquad \sigma^2 = \begin{pmatrix} 0 & -i \\ i & 0 \end{pmatrix}, \qquad \sigma^3 = \begin{pmatrix} 1 & 0 \\ 0 & -1 \end{pmatrix}, \tag{E.2}$$

$\bar{\sigma} = (\sigma_0, -\sigma_1, -\sigma_2, -\sigma_3)$. Indices are raised and lowered with

$$\epsilon^{\alpha\beta} = \epsilon^{\dot{\alpha}\dot{\beta}} = -\epsilon_{\alpha\beta} = -\epsilon_{\dot{\alpha}\dot{\beta}} = \begin{pmatrix} 0 & 1 \\ -1 & 0 \end{pmatrix}. \tag{E.3}$$

The structures $\langle i, j\rangle \equiv iR_{j\dot{\alpha}}(\bar{\sigma}_2)^{\dot{\alpha}\alpha}L_{i\alpha}$ are preserved by the residual symmetry of the conformal frame chosen along the x_2 direction. Due to this it is useful to define, when working in the conformal frame, left-handed spinors $R^\alpha = iR_{\dot{\alpha}}(\bar{\sigma}_2)^{\dot{\alpha}\alpha} = \epsilon^{\alpha\dot{\alpha}}R_{\dot{\alpha}}$. These can now be straightforwardly contracted with the L_i spinors to form invariants, as is used in section 6.2 to define the hexagon partition function (6.7).

The $\langle i, j\rangle$ structures are related to the canonical covariant V_i, H_{ij} structures used in the literature [146] through

$$\langle i, j\rangle\langle j, i\rangle \equiv H_{ij}, \qquad \langle i, i\rangle \equiv V_i. \tag{E.4}$$

E.2 Frames, Vertex, and Markers

The integrability description of $\mathcal{N} = 4$ SYM requires a choice of a frame, i.e. a representation for the single-trace operators in terms of magnons on top of a spin chain. Two

choices are common: the string and spin-chain frame [66]. For most of chapter 6 we use the spin-chain frame, in which a single trace operator made out of L fundamental fields is assigned to a spin chain of length L. Clearly the number of fields composing an operator is not a non-perturbative notion. Moreover, it is not preserved by the dynamics: the scattering between excitations on top of the vacuum can change the chain length, deleting or introducing additional sites $\mathcal{Z}$ in the chain. These are represented by the $\mathcal{Z}^{\mp}$ markers. The spin-chain frame is nevertheless useful to compare with previous weak coupling results available in the literature.

The S-matrix for excitations in the spin chain frame is given by

$$
\begin{aligned}
S|\phi^a(x)\phi^b(y)\rangle &= \mathcal{A}(x,y)|\phi^{\{a}(y)\phi^{b\}}(x)\rangle + \mathcal{B}(x,y)|\phi^{[a}(y)\phi^{b]}(x)\rangle + \frac{1}{2}\mathcal{C}(x,y)\Sigma^{ab}\epsilon_{cd}|\mathcal{Z}^{-}\psi^c(y)\psi^d(x)\rangle \\
S|\psi^a(x)\psi^b(y)\rangle &= \mathcal{D}(x,y)|\psi^{\{a}(y)\psi^{b\}}(x)\rangle + \mathcal{E}(x,y)|\psi^{[a}(y)\psi^{b]}(x)\rangle + \frac{1}{2}\mathcal{F}(x,y)\epsilon^{ab}\Sigma_{cd}|\mathcal{Z}^{+}\phi^c(y)\phi^d(x)\rangle \\
S|\phi^a(x)\psi^b(y)\rangle &= \mathcal{G}(x,y)|\psi^b(y)\phi^a(x)\rangle + \mathcal{H}(x,y)|\phi^a(y)\psi^b(x)\rangle \\
S|\psi^a(x)\phi^b(y)\rangle &= \mathcal{K}(x,y)|\psi^a(y)\phi^b(x)\rangle + \mathcal{L}(x,y)|\phi^b(y)\psi^a(x)\rangle.
\end{aligned}
\tag{E.5}
$$

The S-matrix elements are expressed in terms of the Zhukovsky variables as [59, 159]

$$
\begin{aligned}
\mathcal{A}(x,y) &= \frac{x^+(y)-x^-(x)}{x^-(y)-x^+(x)}, \\
\mathcal{B}(x,y) &= -1+\frac{\left(x^+(x)-x^+(y)\right)\left(x^-(x)\left(x^-(y)-2x^+(y)\right)+x^+(x)x^+(y)\right)}{\left(-1+x^-(x)x^-(y)\right)\left(x^-(y)-x^+(x)\right)x^+(x)x^+(y)}, \\
\mathcal{C}(x,y) &= \frac{2\gamma(x)\gamma(y)\left(x^+(x)-x^+(y)\right)}{\left(1-x^-(x)x^-(y)\right)\left(x^-(y)-x^+(x)\right)}, \\
\mathcal{D}(x,y) &= -1, \\
\mathcal{E}(x,y) &= \frac{x^+(y)-x^-(x)}{x^-(y)-x^+(x)}+\frac{\left(x^+(x)-x^+(y)\right)\left(x^-(x)x^-(y)+x^+(x)\left(x^+(y)-2x^-(y)\right)\right)}{\left(1-x^-(x)x^-(y)\right)\left(x^-(y)-x^+(x)\right)x^+(x)x^+(y)}, \\
\mathcal{F}(x,y) &= \frac{2x^-(x)x^-(y)\left(x^-(x)-x^+(x)\right)\left(x^-(y)-x^+(y)\right)\left(x^+(x)-x^+(y)\right)}{\gamma(x)\gamma(y)\left(-1+x^-(x)x^-(y)\right)\left(x^-(y)-x^+(x)\right)x^+(x)x^+(y)}, \\
\mathcal{G}(x,y) &= \frac{x^+(y)-x^+(x)}{x^-(y)-x^+(x)}, \\
\mathcal{H}(x,y) &= \frac{\gamma(x)\left(x^+(y)-x^-(y)\right)}{\gamma(y)\left(x^-(y)-x^+(x)\right)}, \\
\mathcal{L}(x,y) &= \frac{x^-(y)-x^-(x)}{x^-(y)-x^+(x)}, \\
\mathcal{K}(x,y) &= \frac{\gamma(y)\left(x^+(x)-x^-(x)\right)}{\gamma(x)\left(x^-(y)-x^+(x)\right)},
\end{aligned}
\tag{E.6, E.7}
$$

where

$$\gamma(x) = \sqrt{x^-(x) - x^+(x)}.$$

In computing the hexagon form factors we cross all $\mathcal{D}^{\alpha\dot{\alpha}}$ excitations to the **u** edge, figure (6.9), break them into left- and right- fermions, and then scatter all left components with the $PSU(2|2)$ S-matrix described above. Finally we project the scattering result into the final state of right-fermions. When fermions scatter they may produce markers according to the $\mathcal{C}$ and $\mathcal{F}$ elements in (E.5). Our computation scheme is then to, as soon as a $\mathcal{Z}$ marker is created in this chain of scatterings, move it immediately to the extreme left side of the spin chain. This amounts to a translation by unit on the asymptotic wavefunctions of the excitations [59, 159]

$$|\psi(u)\mathcal{Z}\rangle = \frac{\chi^+(u)}{\chi^-(u)}|\mathcal{Z}\psi(u)\rangle. \tag{E.8}$$

Once on the left side of the chain, it can be ignored for the rest of the computation. The result is an extra factor in the matrix elements corresponding to the product of momentas $\frac{x^+(z)}{x^-(z)}$ for all fermions to the left of those being scattered. The result are the cumulative $\mathcal{Z}$ marker factors

$$\phi_{\mathcal{Z}}(v_i, u_j) = \prod_{a=1}^{i-1}\prod_{b=j+1}^{J_1}\frac{x^+(v_a)}{x^-(v_a)}\frac{x^-(u_b)}{x^+(u_b)}, \quad \phi_{\mathcal{Z}}(v_i, w_j) = \prod_{a=1}^{i-1}\prod_{b=k+1}^{J_3}\frac{x^+(v_a)}{x^-(v_a)}\frac{x^+(w_b)}{x^-(w_b)},$$

$$\phi_{\mathcal{Z}}(u_j, w_k) = \prod_{a=j+1}^{J_1}\prod_{b=1}^{J_2}\prod_{c=k+1}^{J_3}\frac{x^-(u_a)}{x^+(u_a)}\frac{x^+(v_b)}{x^-(v_b)}\frac{x^+(w_c)}{x^-(w_c)}.$$

in equation (6.3).

Once the $\mathcal{Z}$ marker is removed in this way, we proceed with the remaining scatterings. Note that the $x(v)$, $x(w)$ factors are inverted with respect to the $\chi(u)$ factors due to the crossed kinematics, equation (6.5).

In the string frame the length of the spin-chain is well defined non-perturbatively, corresponding to the R-charge of the dual single-trace operator. As a consequence, the S-matrix in the string frame does not produce $\mathcal{Z}$ markers and non-perturbative crossing transformations are simple. For a PSU(2|2)^2 bifundamental magnon excitation $\eta^{A\dot{B}}(z)$ crossing in the string frame simply amounts to

$$\eta^{A\dot{B}}(z) \overset{\circlearrowleft}{\to} -\eta^{B\dot{A}}(z^{\circlearrowleft}), \qquad \eta^{A\dot{B}}(z) \overset{\circlearrowleft}{\to} -\eta^{B\dot{A}}(z^{\circlearrowleft}). \tag{E.9}$$

Crossing in the spin-chain frame is in general complicated, requiring one to map the spin-chain frame magnons to the string frame, use (E.9), and convert back. For our purposes the procedure is trivial, since in the SL$(2,\mathbb{R})$ sector we just need to cross covariant derivatives and $\mathcal{D}^{\alpha\dot{\alpha}}_{\text{spin-chain}} = \mathcal{D}^{\alpha\dot{\alpha}}_{\text{string}}$.

E.3 σ crossing

The crossing transformations are implemented through analytic continuation on the rapidities around the $u = \pm\frac{i}{2} + 2g$ branch points. The S-matrix elements (E.6-E.7) have simple transformation rules under these monodromies, as follows from (6.4). Clockwise $z^{\circlearrowleft}$ and anti-clockwise $z^{\circlearrowright}$ crossings are equivalent for these factors.

The dynamical factor $h(z, z')$, on the other hand, transforms non-trivially [66]. The necessary formulae can be derived as a consequence of the crossing equation for the BES factor,

$$\sigma(z^{\circlearrowleft}, z')\sigma(z, z') = \frac{(1 - 1/x^+y^+)(1 - x^-/y^+)}{(1 - x^-/y^-)(1 - 1/x^+y^-)} \tag{E.10}$$

combined with unitarity, $\sigma(z, z')\sigma(z', z) = 1$. We use x and y to denote the Zhukovsky variable associated to z and z' respectively. Some of the most useful equations are

$$h(z^{\circlearrowleft}, z') = h(z, z'^{\circlearrowleft}) = \frac{1 - 1/x^+y^-}{1 - 1/x^-y^+}\sigma(z, z') \tag{E.11}$$

$$h(z^{\circlearrowleft}, z'^{\circlearrowleft}) = \frac{y^- - x^+}{y^- - x^-}\frac{1 - 1/y^+x^+}{1 - 1/y^-x^+}\frac{1}{\sigma(z, z')} \tag{E.12}$$

which in particular imply the simplified unitarity equations referred to in figure 6.4.

E.4 Equal spins operators

When two or more operators have the same spin the hexagon form factors can have off-shell singularities which display an order of limits issue when going on-shell [249].

For two spinning operators (consider $J_1 = J_2 = J$ and $J_3 = 0$), this can be easily avoided via two operations. First we cross the v rapidities twice $v \to v^{\pm 4\gamma}$, which makes the matrix part of the hexagon form factor invariant and makes the kinematic pole of the diagonal limit appear only in the dynamical part. Second we use Bethe equations in the splitting factors of the u particles

$$\omega_{\ell_{13}}(a, \bar{a}) = (-1)^{\bar{a}} \prod_{u_j \in \bar{a}} e^{-ip(u_j)\ell_{12}} \prod_{\substack{u_i \in a \\ i<j}} S^{-1}(u_j, u_i) \tag{E.13}$$

which eliminates ℓ_{13} for ℓ_{12}. As worked out in [249], after summing over partitions the diagonal poles cancel resulting in the well-defined off-shell object.

Turning on the third operator, provided that it is not equal to the other two, does not introduce new poles, so again we have well-defined off-shell object. However, for three spinning operators of equal spins ($J_1 = J_2 = J_3 = J$) we cannot choose crossing and splitting factors in such a way that all the sets of particles satisfy the two criteria above. In other words, there is no choice of crossing and weights for the excitations w that make the glued hexagon free of off-shell poles. However when going on-shell these poles must cancel with zeros coming from the matrix part and yield the physical three-point function.

We were not able to come with a correct prescription for the glued hexagons that deals with the order of limit issue, therefore we avoided equal three spinning operators such as the seemingly harmless $J_1 = J_2 = J_3 = 2$ case. We believe that understanding the correct prescription is another interesting question for the hexagon formalism.

E.5 From C to H's

In this section we explain how to express the structure constant in terms of hexagon components. Our starting point is (6.31), which we rewrite here as

$$\sum_{\ell_1,\ell_2,\ell_3} C^{J_1,J_2,J_3}_{\ell_1,\ell_2,\ell_3} \left(\frac{\langle 1,1\rangle^{J_1-\ell_2-\ell_3}\langle 2,2\rangle^{J_2-\ell_1-\ell_3}\langle 3,3\rangle^{J_3-\ell_1-\ell_2}}{\langle 2,3\rangle^{-\ell_1}\langle 3,2\rangle^{-\ell_1}\langle 1,3\rangle^{-\ell_2}\langle 3,1\rangle^{-\ell_2}\langle 1,2\rangle^{-\ell_3}\langle 2,1\rangle^{-\ell_3}} \right) =$$

$$= L_{1,\vec{\alpha}_1} L_{2,\vec{\alpha}_2} L_{3,\vec{\alpha}_3} R_{1,\vec{\beta}_1} R_{2,\vec{\beta}_2} R_{3,\vec{\beta}_3} \mathcal{H}_G^{\vec{\alpha}_1\vec{\beta}_1;\vec{\alpha}_2\vec{\beta}_2;\vec{\alpha}_3\vec{\beta}_3}(\mathbf{u},\mathbf{v},\mathbf{w}) \tag{E.14}$$

where $\mathcal{H}_G$ are the glued hexagons.

By expanding in components and taking derivatives with respect to the spinors in both sides of the expression above we can construct a matrix M that writes the polarized glued hexagons in terms of structure constants

$$\mathcal{H}_G^{(\vec{\alpha}_1\vec{\beta}_1);(\vec{\alpha}_2\vec{\beta}_2);(\vec{\alpha}_3\vec{\beta}_3)} = M^{(\vec{\alpha}_1\vec{\beta}_1);(\vec{\alpha}_2\vec{\beta}_2);(\vec{\alpha}_3\vec{\beta}_3)}_{\ell_1,\ell_2,\ell_3} C^{J_1,J_2,J_3}_{\ell_1,\ell_2,\ell_3}\,, \tag{E.15}$$

where we emphasize that the indices of $\mathcal{H}_G$ are completely symmetrized, in accordance with the symmetric traceless nature of the operators we are considering.

Notice that the rectangular matrix M has linearly independent columns, so that $M^T M$ is invertible (since it is a grammiam matrix of linearly independent vectors). Therefore we can act on the LHS of equation (E.15) with the left inverse $M^+ = (M^T M)^{-1} M^T$ and find the inverted relation

$$C^{\ell_1,\ell_2,\ell_3}_{J_1,J_2,J_3} = \left(M^{\ell_1,\ell_2,\ell_3}_{(\vec{\alpha}_1\vec{\beta}_1);(\vec{\alpha}_2\vec{\beta}_2);(\vec{\alpha}_3\vec{\beta}_3)} \right)^+ \mathcal{H}_G^{(\vec{\alpha}_1\vec{\beta}_1);(\vec{\alpha}_2\vec{\beta}_2);(\vec{\alpha}_3\vec{\beta}_3)} \tag{E.16}$$

which writes the structure constants as combinations of hexagons. Note also that the $O(3)$ invariance implies several identities between the hexagon components. These identities are simply the vanishing of the null vectors of M^+.

E.6 Abelian $C^{\bullet\bullet\bullet}$ and Pfaffians

In section (6.3.3) we presented a determinant formula for structure constants of three non protected spinning operators polarized so that two are parallel and orthogonal to the third. Here we make explicit some of the formulas and detail some steps.

First we discuss the pfaffian identity. As derived in [69],

$$\sum_{\bar{a}\subset\mathbf{u}} (-1)^{|\bar{a}|} w'(u_{\bar{a}}) H(u_{\bar{a}}, u_{\bar{a}}) = pf(I - \mathcal{K})_{2J_1\times 2J_1}.$$

where the matrix $\mathcal{K}$ is defined as

$$\mathcal{K} = \begin{pmatrix} K_{11}(u,u) & K_{12}(u,u) \\ K_{21}(u,u) & K_{22}(u,u) \end{pmatrix} \tag{E.17}$$

with

$$K_{11}(a,b)_{ij} \equiv g_i^a / k(x^+(a_i), x^-(b_j)), \qquad K_{12}(a,b)_{ij} \equiv -g_i^a k(x^+(a_i), x^+(b_j))/(x^+(a_i)x^+(b_j))^2,$$
$$K_{21}(a,b)_{ij} \equiv g_i^a k(x^-(a_i), x^-(b_j))/(x^-(a_i)x^-(b_j))^2, \qquad K_{22}(a,b)_{ij} \equiv -g_i^a / k(x^-(a_i), x^+(b_j)),$$

and where

$$g_i^u = k(x^+(u_i), x^-(u_i))\omega'(u_i), \qquad k(x,y) = \frac{x-y}{1-1/xy}. \tag{E.18}$$

As previously emphasized, this formula holds for any factorized function of the rapidities $w'(u_{\bar{a}}) = \prod_{i\in\bar{a}} w'(u_i)$.

The next point we would like to clarify in this appendix is the sequence of manipulations leading to the pfaffian representation of the blue terms. The starting point is equation (6.40) which reads

$$\text{blue} = \sum_{\substack{b\cup\bar{b}\subset\mathbf{v} \\ c\cup\bar{c}\subset\mathbf{w}}} (-1)^{|\bar{b}|+|\bar{c}|} e_{\bar{b}}^v e_{\bar{c}}^w H(v_{\bar{b}}, v_{\bar{b}}) H(w_{\bar{c}}, w_{\bar{c}}) h(v_b^{\circlearrowleft}, \hat{u}) h(\hat{u}, w_c^{\circlearrowleft}) h(v_b^{\circlearrowleft}, w_c^{\circlearrowleft}) h(w_{\bar{c}}^{\circlearrowleft}, v_{\bar{b}}^{\circlearrowleft}).$$

We then write

$$h(v_b^{\circlearrowleft}, w_c^{\circlearrowleft}) = \frac{h(\hat{v}^{\circlearrowleft}, \hat{w}^{\circlearrowleft}) h(v_{\bar{b}}^{\circlearrowleft}, w_{\bar{c}}^{\circlearrowleft})}{h(v_{\bar{b}}^{\circlearrowleft}, w_{\bar{c}}^{\circlearrowleft}) h(v_{\bar{b}}^{\circlearrowleft}, w_c^{\circlearrowleft}) h(v_b^{\circlearrowleft}, w_{\bar{c}}^{\circlearrowleft}) h(v_{\bar{b}}^{\circlearrowleft}, w_{\bar{c}}^{\circlearrowleft})}, \quad h(v_b^{\circlearrowleft}, \hat{u}) = \frac{h(\hat{v}^{\circlearrowleft}, \hat{u})}{h(v_{\bar{b}}^{\circlearrowleft}, \hat{u})}, \quad h(\hat{u}, w_c^{\circlearrowleft}) = \frac{h(\hat{u}, \hat{w}^{\circlearrowleft})}{h(\hat{u}, w_{\bar{c}}^{\circlearrowleft})}$$

to end up with

$$\text{blue} = h(\hat{v}^{\circlearrowleft}, \hat{w}^{\circlearrowleft}) h(\hat{v}^{\circlearrowleft}, \hat{u}) h(\hat{u}, \hat{w}^{\circlearrowleft}) \sum_{\substack{b\cup\bar{b}\subset\mathbf{v} \\ c\cup\bar{c}\subset\mathbf{w}}} (-1)^{|\bar{b}|+|\bar{c}|} \underbrace{\left(\frac{e_{\bar{b}}^v}{h(v_{\bar{b}}^{\circlearrowleft}, \hat{w}^{\circlearrowleft}) h(v_{\bar{b}}^{\circlearrowleft}, \hat{u})} \right)}_{\equiv \omega'(v_{\bar{b}}^{\circlearrowleft})} \underbrace{\left(\frac{e_{\bar{c}}^w}{h(\hat{u}, w_{\bar{c}}^{\circlearrowleft}) h(\hat{v}^{\circlearrowleft}, w_{\bar{c}}^{\circlearrowleft})} \right)}_{\equiv \omega'(w_{\bar{c}})}$$
$$\times H(v_{\bar{b}}, v_{\bar{b}}) H(w_{\bar{c}}, w_{\bar{c}}) h(v_{\bar{b}}^{\circlearrowleft}, w_{\bar{c}}^{\circlearrowleft}) h(w_{\bar{c}}^{\circlearrowleft}, v_{\bar{b}}^{\circlearrowleft}).$$

Here, as before, we interpret the effect of O_1 on operators O_2 and O_3 as a background that corrects their propagation but does not affect their interactions. Next, we use the identity $h(v_{\bar{b}}^{\circlearrowleft}, w_{\bar{c}}^{\circlearrowleft}) h(w_{\bar{c}}^{\circlearrowleft}, v_{\bar{b}}^{\circlearrowleft}) = h(v_{\bar{b}}^{\circlearrowleft}, w_{\bar{c}}) h(w_{\bar{c}}, v_{\bar{b}}^{\circlearrowleft})$ to obtain the result from the main text (6.41),

$$\text{blue} = h(\hat{v}^{\circlearrowleft}, \hat{w}^{\circlearrowleft}) h(\hat{v}^{\circlearrowleft}, \hat{u}) h(\hat{u}, \hat{w}^{\circlearrowleft}) \sum_{\substack{b\cup\bar{b}\subset\mathbf{v} \\ c\cup\bar{c}\subset\mathbf{w}}} (-1)^{|\bar{b}|+|\bar{c}|} \omega'(v_{\bar{b}}^{\circlearrowleft}) \omega'(w_{\bar{c}}) H(v_{\bar{b}}^{\circlearrowleft}, v_{\bar{b}}^{\circlearrowleft}) H(w_{\bar{c}}, w_{\bar{c}}) H(v_{\bar{b}}^{\circlearrowleft}, w_{\bar{c}}).$$

The next step is to recognize the sum over partitions for the effective operator $O_2 \cup O_3$

as a pfaffian,

$$\sum_{d\cup\bar{d}\subset\mathbf{z}}(-1)^{|\bar{d}|}\omega'(z_{\bar{d}})H(z_{\bar{d}},z_{\bar{d}})=pf(I-\mathcal{K}')_{2(J_2+J_3)\times 2(J_2+J_3)}.$$

Comparing with the definition $(E.17)$, $\mathcal{K}'$ is defined in terms of the functions $K_{x,y}(a,b)$ as

$$\mathcal{K}'=-\begin{pmatrix} K_{11}(v^{\circlearrowleft},v^{\circlearrowleft}) & K_{12}(v^{\circlearrowleft},v^{\circlearrowleft}) & K_{11}(v^{\circlearrowleft},w) & K_{12}(v^{\circlearrowleft},w)\\ K_{21}(v^{\circlearrowleft},v^{\circlearrowleft}) & K_{22}(v^{\circlearrowleft},v^{\circlearrowleft}) & K_{21}(v^{\circlearrowleft},w) & K_{22}(v^{\circlearrowleft},w)\\ K_{11}(w,v^{\circlearrowleft}) & K_{12}(w,v^{\circlearrowleft}) & K_{11}(w,w) & K_{12}(w,w)\\ K_{21}(w,v^{\circlearrowleft}) & K_{22}(w,v^{\circlearrowleft}) & K_{21}(w,w) & K_{22}(w,w)\end{pmatrix}.$$

where $g_i^{v^{\circlearrowleft}}=k(x^+(v_i^{\circlearrowleft}),x^-(v_i^{\circlearrowleft}))\omega'(v_i^{\circlearrowleft})$ and $g_i^{w}=k(x^+(w_i),x^-(w_i))\omega'(w_i)$.

A last comment regards the choice of splitting factors in (6.39). There we chose to cross all three sets of magnons from the front to the back hexagon through the right boundary of the cut chain. Alternative pfaffian representations can be obtained in an analogous manner for all other possible choices[1] of splitting factor provided one replaces (6.39) by the appropriate expression. The only difference is the final result is the replacement of the original splitting factors $e^a_{\bar{x}}$ by their left alternatives in the pfaffian formula. As usual, the expressions differ off-shell but reproduce the same structure constants.

E.6.1 A two loop check

An important question is if the asymptotic part is sufficient to capture the leading contribution, in the large spin limit, of three point functions with more than one non-BPS operator. The goal of this section is to lay out the main ingredients that are necessary to compute the first correction to the asymptotic part of the OPE coefficient in the Abelian polarization. Most of the discussion is valid for operators with any spin but we compute explicitly only the finite size correction of the OPE coefficient of two Konishi operators and one BPS leaving a more general analysis(including the large spin limit mentioned above) to the future. These new effects are obtained by gluing the two hexagons along the three seams (from now on referred to as mirror edges) to form a pair of pants. The gluing procedure is achieved by dressing the mirror edges with multiparticle states and integrating over their rapidities. The multiparticle states are labeled by boundstate number n as explained [66, 69, 170, 171].

One crucial but important detail is that the bound state particles live in the mirror edges. This might seem innocuous but is the reason why their contribution only starts at two loops. To have a better grasp on this matter let us look at the integrand of just one

[1] e.g. left-left-left, right-right-left, etc.

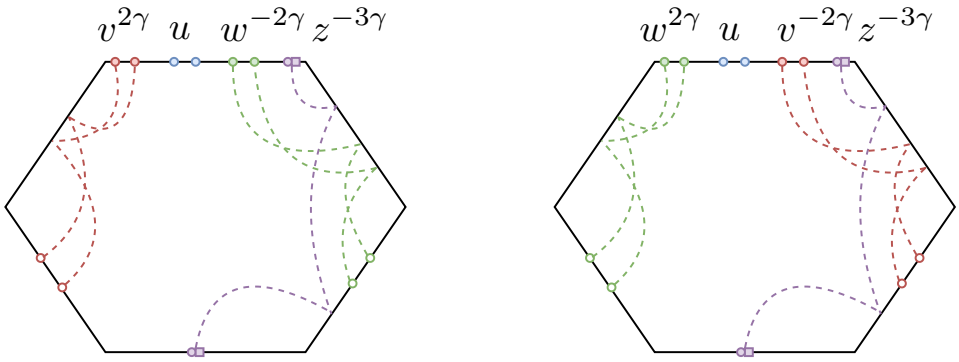

Figure E.1: Single mirror particle contribution to a three point function with three spinning operators. The mirror particle would correspond to a bottom contribution (in the notation of [66]) if the operators $2,3$ were BPS and adjacent if the the 1 and 2 or 3 were absent.

boundstate particle in the hexagon formalism

$$\text{int} = \sum_{\substack{a\cup\bar{a}=\mathbf{u}\\ b\cup\bar{b}=\mathbf{v}\\ c\cup\bar{c}=\mathbf{w}\\ X}} \mu(z^\gamma)e^{ip_z^\gamma}\omega_{l_{13}}(a,\bar{a})\omega_{l_{23}}(c,\bar{c})\omega_{l_{12}}(b,\bar{b})\mathcal{H}(b^{2\gamma},a,c^{-2\gamma},z^{-3\gamma})\mathcal{H}(\bar{c}^{2\gamma},\bar{a},\bar{b}^{-2\gamma},z^{-3\gamma}) \tag{E.19}$$

where X is a particle in the mirror theory with rapidity z and

$$\mu(z^\gamma) = \frac{n(x^{[+n]}x^{[-n]})^2}{g^2(x^{[+n]}x^{[-n]}-1)^2((x^{[+n]})^2-1)(1-(x^{[-n]})^2)}, \quad e^{ip_{u^\gamma}} = \frac{1}{x^{[n]}x^{[-n]}}, \tag{E.20}$$

with n being the boundstate number. Since the boundstate particle lives in the mirror edge we need to do an odd number of γ rotations. In this case the expressions for $\mu(z^\gamma)$ and $e^{ip_{u^\gamma}}$ start with g^2 at weak coupling. Physically, this is just saying that we pay a coupling for the mirror particle to travel from the front hexagon to the back. For this reason the finite size correction for twist two operators only makes an appearance at the two loop level. Fortunately there is perturbative data computed using traditional Feynman integrals that we can compare against [158]. The rest of this section is devoted to obtain the finite size correction at two loops and for two spin two operators and match it with the result obtained in [158].

The integrand (E.19) is very similar to the hexagon partition function, as it is the scattering of three sets of particles in a pairwise fashion, but now with an additional bound state particle arising from the mirror contributions.

There are several simplifications for the Abelian polarization, for example the scattering

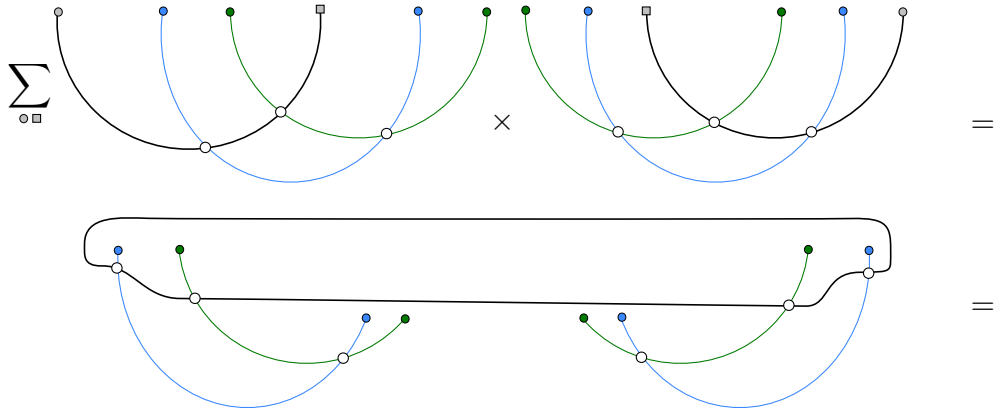

Figure E.2: The sum over the flavour indices of the mirror particle states in the matrix part of the hexagon form factor is proportional to a transfer matrix. This is precisely the same mechanism present in the OPE with just one spinning operator.

between the three sets of particles **u**, **v** and **w** is simple. If it was not for the boundstate particles, the whole matrix part would be trivial. However, as depicted in figure E.2, in this abelian configuration the boundstate scattering can be recasted as a transfer matrix [66],

$$T_a(z) = \sum_{n=-1}^{1} (3n^2-2) \prod_{m=0}^{n} \frac{R^{(+)}(z^{[2m-a]})}{R^{(-)}(z^{[2m-a]})} \sum_{j=\frac{2-a}{2}}^{\frac{a-2n}{2}} \prod_{k=j+n}^{\frac{a-2}{2}} \frac{R^{(+)}(z^{[2n-2k]})B^{(+)}(z^{[-2k]})}{R^{(-)}(z^{[2n-2k]})B^{(-)}(z^{[-2k]})}\,, \tag{E.21}$$

where

$$R^{(\pm)}(z) = \prod_j (x(z) - x_j^{\mp})\,, \quad B^{(\pm)}(z) = \prod_j \left(\frac{1}{x(z)} - x_j^{\mp}\right)\,. \tag{E.22}$$

and the product in j should be taken over all physical particles. Notice that some of these particles are mirror rotated as can be seen in figure E.1 and for this reason the transfer matrix that shows up in the integrand (E.19) is not exactly (E.21). Instead, the integrand will be written in term of $T_n^{\circlearrowleft\circlearrowleft}(z)$ which is defined by

$$T_n^{\circlearrowleft\circlearrowleft}(z) = T_n(z)\Big|_{x^{[-a]}\to\frac{1}{x^{[-a]}},\, x_j^{\pm}\to\frac{1}{x_j^{\pm}}} \qquad j \in \mathbf{v}\cup\mathbf{w}. \tag{E.23}$$

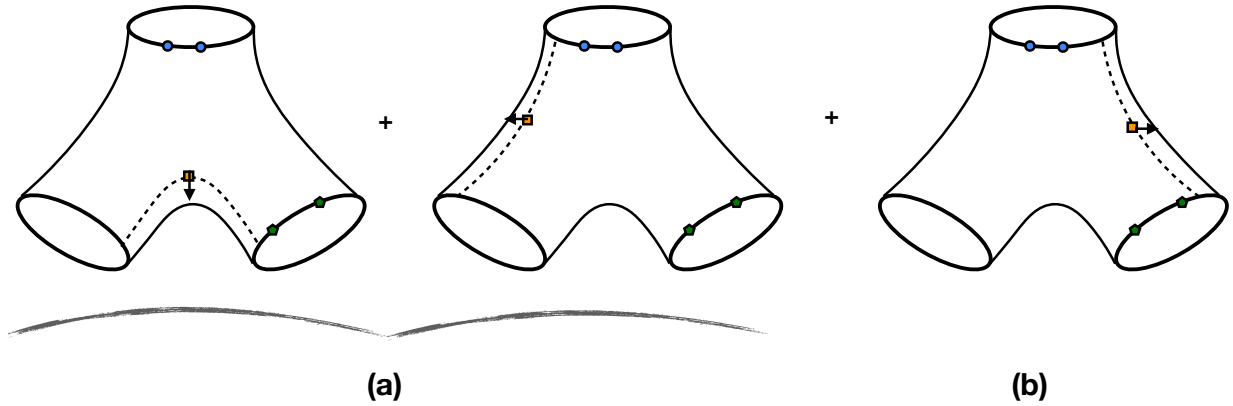

Figure E.3: For two non-BPS operators there is one mirror edge that is distinct from the other two. It turns out that up to two loops only the finite size corrections (a) contribute while the finite size correction (b) will only starts at three loop order.

The integrand (E.19) can then be written in a compact form as

$$\text{int}(z) = \frac{T_n^{\circlearrowleft\circlearrowleft}(z)\mu(z^\gamma)e^{ip_z^\gamma}}{h_n(z^{-\gamma},\mathbf{v})h_n(z^\gamma,\mathbf{u})} h_n(\mathbf{w},z^{-\gamma}) \sum_{\substack{a\cup\bar{a}=\mathbf{u}\\ b\cup\bar{b}=\mathbf{v}\\ c\cup\bar{c}=\mathbf{w}}} \omega'_{l_{23}}(c,\bar{c})\omega_{l_{13}}(a,\bar{a})\omega'_{l_{12}}(b,\bar{b})\times$$

$$\times\, h(b^{2\gamma},a)h(b^{4\gamma},c)h(a,c^{-2\gamma})h(\bar{c}^{2\gamma},\bar{a})h(\bar{c}^{4\gamma},\bar{b}_2)h(\bar{a},\bar{b}^{-2\gamma})\prod_{i=1}^{3} h(w_i,w_i)h(\bar{w}_i,\bar{w}_i), \qquad \text{(E.24)}$$

with ω', p_n and h_n defined by

$$\omega'_{\ell_{23}}(c,\bar{c}) = \omega_{\ell_{23}}(c,c)p_n\left(\bar{c}^{4\gamma},z^{-\gamma}\right)\ , \quad \omega'_{\ell_{12}}(b,\bar{b}) = \omega_{\ell_{12}}(b,b)p_n\left(\bar{b},z^{-\gamma}\right)\ , \qquad \text{(E.25)}$$

$$p_n(u,v) = h_n(u,v)h_n(v,u) = \frac{(u-v)^2+\frac{(n-1)^2}{4}}{(u-v)^2+\frac{(n+1)^2}{4}}\left(\frac{1-\frac{1}{y^-x^{[+n]}}}{1-\frac{1}{y^-x^{[-n]}}}\frac{1-\frac{1}{y^+x^{[-n]}}}{1-\frac{1}{y^+x^{[+n]}}}\right)^2, \qquad \text{(E.26)}$$

$$S_n(u,v) = \frac{1}{\sigma_n^2(u,v)}\frac{(u-v+i\frac{n-1}{2})(u-v+i\frac{n+1}{2})}{(u-v-i\frac{n-1}{2})(u-v-i\frac{n+1}{2})}\prod_{k=-\frac{n-1}{2}}^{\frac{n-1}{2}}\left(\frac{1-\frac{1}{y^+x^{[-2k-1]}}}{1-\frac{1}{y^-x^{[+2k+1]}}}\right)^2 \qquad \text{(E.27)}$$

and $\sigma_n(u,v)$ is the (fused) BES dressing phase [60]. Let us remark that these formulas should be valid for operators with any spin but only in the Abelian polarization.

For simplicity we focus on three point functions with two spinning operators $J_1 = J_2 = 2$ and one BPS and compare it with perturbative results obtained in [158]. Obviously, this choice breaks the symmetry between the mirror edges since one of them will be between the two non-BPS operators, as can be seen in figure E.3. It is straightforward to check by expanding at weak coupling that we only need to take into consideration the finite size corrections represented in E.3.a.

The building blocks to get this contribution are very explicit and now it is just a matter

of evaluating them at weak coupling after taking the appropriate monodromies. After doing this we obtain

$$\text{int}(z) = \frac{55296(-1)^{2/3}n^2g^4\left(12z^2-n^2\right)\left(3n^2+12z^2-4\right)}{(n^2+4z^2)^3\left(216n^6(6z^2-1)+432n^4(18z^4-2z^2+1)+384n^2(54z^6+9z^4-15z^2-1)+81n^8+256(9z^4+3z^2+1)^2\right)} \tag{E.28}$$

where we used the Konishi Bethe roots for the two spinning operators

$$\mathbf{u} = \mathbf{v} = \left(-\frac{1}{2\sqrt{3}}, \frac{1}{2\sqrt{3}}\right) . \tag{E.29}$$

The OPE coefficient[2] for two spin two operators is given by at two loops

$$\sum_{\ell=0}^{2} C^{\ell}_{2,2,0} = \mathcal{N}(2)\mathcal{N}(2)\left(\textbf{asymptotic}_{\ \textbf{Abelian}} + 2\sum_{n=1}^{\infty}\int dz \text{int}(z)\right) . \tag{E.30}$$

where **asymptotic** are the abelian structures given by the hexagon partition function (6.37) or by the pfaffian (6.42) and the factor of two in front of the integral takes into account the two possibilities to add mirror particles as shown in figure E.3.a.

The integral over the rapidity z, that can be done by picking residues and the sum over the boundstate n can be evaluated without much effort. After adding everything up we obtain

$$\sum_{\ell=0}^{2} C^{\ell}_{2,2,0} = \frac{1}{6}\left(1 - 12g^2 + 147g^4\right) \tag{E.31}$$

which matches exactly the result obtained in [158].

It should be possible to obtain the finite size correction for other spins (in the Abelian polarization). The only issue that might occur is that the integral/sum needs to be regularized. However, we expect that the HPL method of [170] can be used to regularize efficiently the sums in a similar fashion as in one spinning case. Along these lines it would be interesting to extend the results of [186] to our setting.

Obtaining finite size corrections for other polarizations is somewhat harder but should be doable at least at leading order in the coupling and for small spins. The main issue is that the sum over mirror particles in (E.19) is more involved.

[2]One might be worried about the $(-1)^{\frac{2}{3}}$ in (E.28) because it can give rise to an imaginary part in the structure constant. However this does not pose an issue since this factor is removed with the normalization factor $\mathcal{N}(2)^2 = \frac{(-1)^{-\frac{2}{3}}}{54}$.

Appendix F

Appendix: Structure Constants in $\mathcal{N}=4$ SYM and Separation of Variables

F.1 Notation

F.1.1 Roots and Charges

Up to at least 4 loops, the Bethe roots v_k are the solutions to the asymptotic Bethe equations [184, 252]

$$1 = \left(\frac{x_k^+}{x_k^-}\right)^L \prod_{j\neq k}\left(\frac{x_j^- - x_k^+}{x_j^+ - x_k^-}\right)^\eta \frac{1-g^2/(x_j^- x_k^+)}{1-g^2/(x_j^+ x_k^-)}\sigma(v_k,v_j)^2$$

for the simplest SU(2) and SL(2) rank one sectors where $\eta = \pm 1$ respectively. Here the Zhukowsky variables

$$x_k^\pm = x(v_k \pm \tfrac{i}{2}) \text{ with } x(u) = \frac{u+\sqrt{u^2-4g^2}}{2} \simeq u - \frac{g^2}{u} + \dots$$

where $g^2 = \lambda/(4\pi)^2$ is the coupling. (For three point functions g^{2k} effects are $N^k LO$ effects while for the quantum anomalous dimensions they are $N^{k-1}LO$ effects.) We sometimes also use $x^{[\pm a]} \equiv x(u \pm ia/2)$. Finally the dressing phase starts only at very high loop order, $\sigma = 1 + O(g^6)$ and we will not use its explicit expression in this appendix. Generating Bethe roots for SL(2) is simple since they are real; for SU(2) we used [250] to produce tree level solutions and then we found the loop corrections by linearizing Bethe equations around these seed values.

We also define the auxiliary real functions

$$q_k^+(u) = i^{k+0}(x^+(u))^{-k} + (-i)^{k+0}(x^-(u))^{-k}\,, \tag{F.1}$$

$$q_k^-(u) = i^{k-1}(x^+(u))^{-k} + (-i)^{k-1}(x^-(u))^{-k}\,, \tag{F.2}$$

which can be used to construct the conserved charges

$$Q_k^{\pm} = \sum_{i=1}^{J} q_k^{\pm}(v_j)\,. \tag{F.3}$$

The Q_k^+ are even and Q_k^- are odd functions of the Bethe roots. The anomalous dimension of an operator is nothing by $\gamma = 2g^2 Q_1^+$ for instance.

We can also package the Bethe roots into Baxter polynomials $\mathbb{Q}(u) \equiv \prod_{k=1}^{J}(u - v_k)$ or dressed Baxter functions as in (7.1) or (7.25). Then these charges can be extracted by simple contour integrals as well. For instance:

$$Q_1^+ = \oint \frac{u\,du}{4\pi g^2\sqrt{u^2-4g^2}} \log\frac{\mathbb{Q}(u+i/2)}{\mathbb{Q}(u-i/2)} \tag{F.4}$$

where the contour encircles the Zhukowsky cut $u \in [-2g, 2g]$. This is an interesting definition since it now applies to any function $\mathbb{Q}$, be it a polynomial or not. We can use such definitions to pair up arbitrary functions in scalar products such as (7.3).

The concept of transcendentality is often useful. At loop order n we expect functions of uniform transcendentality n to show up once properly counted. It is tempting to assign transcendentality k to the charges $q_k^{\pm}$. Some identities like $(q_1^+)^2 - (q_1^-)^2 = 2q_2^+$ nicely preserve this counting but others such as $(q_1^+)^2 + (q_1^-)^2 = 4q_1^+ + O(g^2)$ can lead to ambiguities in perturbation theory. In the $SL(2)$ sector Harmonic numbers H_k of transcendentality k often show up. We use the `mathematica` notation $H_k(x) = \texttt{HarmonicNumber}(x,k)$ and

$$H_n^+(u) \equiv H_n(-1/2+iu) + H_n(-1/2-iu)\,, \tag{F.5}$$

$$iH_n^-(u) \equiv H_n(-1/2+iu) - H_n(-1/2-iu)\,. \tag{F.6}$$

F.1.2 Structure Constants and Hexagons

The hexagon formalism [66] is a non-perturbative integrability framework developed to evaluate structure constants in planar $\mathcal{N} = 4$ SYM. It was used throughout chapter 7 to generate a myriad of perturbative data. This formalism entails two main components: asymptotic sums and mirror corrections, as depicted in figure F.1.

When we cut the three point function pair of pants into two hexagons the excitations on each operator can end up on either hexagon so we must sum over the ways of partitioning such excitations. In the end when we glue back the hexagons into a pair of pants we must sum over all possible quantum states along each edge where we glue. In this appendix we ignore these second effect, focusing only in the asymptotic contributions.

The three point function depicted in figure 7.1 in the hexagon formalism is given by the ratio of two quantities

$$\left(C^2_{\bullet\circ\circ}\right)_\ell = \frac{\mathcal{A}_\ell^2}{\mathcal{B}}\,. \tag{F.7}$$

The numerator entering the ratio above is the central object of the hexagons approach. In

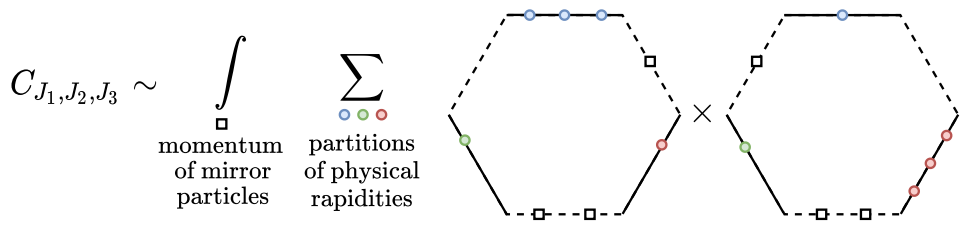

Figure F.1: Each closed spin chain operator is split into two open chain operators. We sum over all the ways its excitations can end up in either one of the chains. Gluing the hexagons together amounts to integrating over all possible mirror states.

the asymptotic regime

$$\mathcal{A}_\ell^{\texttt{asymptotic}} = \mathbb{N}_{J,\ell} \sum_{\alpha\cup\bar{\alpha}=\mathbf{v}} (-1)^{|\bar{\alpha}|} \frac{e^{-ip_{\bar{\alpha}}\ell}}{h_{\bar{\alpha}\alpha}} \tag{F.8}$$

where p is the momentum of the excitation

$$p_{\bar{\alpha}} = \sum_{v_i\in\bar{\alpha}} p(v_i) \quad \text{where} \quad e^{ip(u)} = x^+(u)/x^-(u) \tag{F.9}$$

and the so-called dynamical factor $h_{\bar{\alpha}\alpha} = \prod_{\substack{v_i\in\bar{\alpha}\\ v_j\in\alpha}} h(v_i,v_j)\,,$

$$h(u,v) = \left(\frac{x^-(u)-x^+(v)}{x^+(u)-x^-(v)}\right)^\eta \frac{x^-(u)-x^-(v)}{x^-(u)-x^+(v)} \frac{1-\frac{1}{x^-(u)x^+(v)}}{1-\frac{1}{x^+(u)x^+(v)}} \frac{1}{\sigma(u,v)} \tag{F.10}$$

with $\eta = 0$ for SL(2) and $\eta = 1$ for SU(2).

The denominator of (F.7) is the normalization of the three point function by its two point function constituents

$$\mathcal{B} = \frac{|\mathbb{N}_J|^2 \det(\partial_{v_i}\phi_j)}{\prod_{i=1}^J \mu(v_i) \prod_{i\neq j}^J h(v_i,v_j)} \tag{F.11}$$

where $e^{i\phi_j} \equiv e^{ip(v_j)L} \prod_{k\neq j} S(v_j,v_k)$ and

$$\mu(u) = \left(1-g^2/(x^+x^-)\right)^2 \left(1-g^2/(x^+)^2\right)^{-1} \left(1-g^2/(x^-)^2\right)^{-1}$$

is the hexagon measure, not to be confused with the various SoV measures. The factor $|\mathbb{N}_J^2|$ is the (ℓ-independent) absolute value of $\mathbb{N}_{J,\ell}$. The normalization cancels when evaluating the physical three point function but matters when comparing with the SoV formalism. It

is given by

$$\mathbb{N}_{J,\ell} = \Big(\prod_{i,j}\big(1-\frac{g^2}{x_i^+ x_j^-}\big)\Big)^{-\eta}\binom{\mathbb{J}}{\mathbb{J}-J}^{\eta-1} \times \frac{i^{2\ell+J+1}}{J!}\times$$
$$\times \prod_{i=1}^{J}\sqrt{x_i^+ x_i^-}\times e^{-\frac{i}{2}p(v_i)\ell} \tag{F.12}$$

where $\eta = 0$ for SL(2) and $\eta = 1$ is for SU(2).

Similar to the hexagon formalism, our SoV expressions for the three point functions are also given by the ratio of two quantities. We were able to directly match each one of the inner products entering the SoV with its hexagon formalism counter parts. For SL(2) it is simply

$$\mathcal{A}_\ell = \langle \mathcal{Q}, \mathbf{1}\rangle_\ell\,, \qquad \mathcal{B} = \frac{(2\mathbb{J})!}{(\mathbb{J}!)^2}\langle \mathcal{Q}, \mathcal{Q}\rangle_L\,, \tag{F.13}$$

and for SU(2) it reads

$$\mathcal{A}_\ell = \Lambda_{\mathcal{A}}\langle\!\langle \mathcal{Q}, \mathbf{1}\rangle\!\rangle_{\ell,L}\,, \quad \mathcal{B} = \Lambda_{\mathcal{B}}\frac{(2J)!}{(J!)^2}\langle\!\langle \mathcal{Q}, \mathcal{Q}\rangle\!\rangle_{L,L}\,. \tag{F.14}$$

where

$$\Lambda_{\mathcal{A}} = e^{g^4\left(\alpha-\delta_{\ell=2}\pi^2\right)\left((Q_1^-)^2+Q_2^+\right)} \tag{F.15}$$
$$\Lambda_{\mathcal{B}} = \prod_{i,j}^{J}\Big(1-\tfrac{g^2}{x^+(v_i)x^+(v_j)}\Big)\prod_{i,j}^{J}\Big(1-\tfrac{g^2}{x^-(v_i)x^-(v_j)}\Big)$$

The normalization factor in (7.19) is then $\Lambda_\ell(Q) = \Lambda_{\mathcal{A}}^2/\Lambda_{\mathcal{B}}$.

F.2 SL(2) material

F.2.1 Hahn Polynomials and Measures

A Hahn polynomial $p_J(x|a,b,c,d)$ is given by

$${}_3F_2\left(\begin{matrix} a+ix\,,\ a+b+c+d-1+J\,,\ -J \\ a+c\,,\ a+d\end{matrix}\,\middle|\,1\right) \tag{F.16}$$

and admits a simple orthogonality relation

$$\int dx\,\mu_{\text{Hahn}}(x)\,p_J(x|a,b,c,d)p'_J(x|a,b,c,d) \propto \delta_{JJ'} \tag{F.17}$$

with

$$\mu_{\text{Hahn}}(x) = \Gamma(a+ix)\Gamma(b+ix)\Gamma(c-ix)\Gamma(d-ix)\,. \tag{F.18}$$

At LO the twist-2 Baxter functions are given by these polynomials with $a, b, c, d = \frac{1}{2}$ so that the measure becomes $\Gamma(\frac{1}{2}+ix)^2\Gamma(\frac{1}{2}-ix)^2 \propto \text{sech}^2(\pi x)$ as quoted in (7.5).

At loop level the corrections to 1/2 for the coefficients a, b, c, d depend on J albeit mildly, through the Harmonic number $H_1(J)$, so that (F.16) reads

$$ {}_3F_2\left(\begin{matrix} \frac{1}{2} + i\sqrt{2}g + 2g^2 H_1 + iu\,,\; J+1+8g^2H_1\,,\; -J \\ 1+4g^2H_1\,,\; 1+2i\sqrt{2}g+4g^2H_1 \end{matrix} \middle| 1 \right) $$

where we highlighted the NLO corrections in magenta. If we plug the J dependent one loop values for a, b, c, d in (F.18) we would obtain

$$ \mu_{\text{Hahn}}(x) \propto \frac{1}{\cosh^2(\pi x)} \Big(1 + 2\pi^2 g^2 \alpha \tanh^2(\pi x) + 4g^2 H_1(J) H_1^+(x) + O(g^4) \Big) \,. \tag{F.19} $$

where $\alpha = 1$. This is unsatisfactory as it is J dependent. To fix this we tried to absorb the second line into the definition of $\mathcal{Q}_J$; recalling that these Harmonic numbers are nothing but the energy Q_1^+ of these twist-two operators we end up with the correction in the first line in (7.1). (We can not derive the second line with this simple derivation since the odd charge Q_1^- vanishes for the operators in this leading Regge trajectory.) What we did is then absorb this second line of (F.19) into the Baxter functions and look for an orthogonal measure for these *no longer polynomial* Baxter functions of the form of the first line of (F.19). It exists with $\alpha = 3/2$. In (7.5) we fixed the overall normalization of the measure so that the vacuum ($Q_0 = 1$) is unit normalized.

There are still interesting open problems to pursue along these lines. NNLO corrections to twist-two Baxter polynomials are also known [177, 251]. Can we use them to infer the next correction to the measure? Some twist three families are also known [251, 253–255]. Can we use them to shed light on the multi-particle measure μ_2?

F.2.2 SL(2) Baxter and Measure

It is easy[1] to check that for on-shell solutions of the one-loop twist 2 Baxter equation (7.9) the dressed polynomials (7.1) solve the simplified difference equation

$$ \tilde{B} \circ \mathcal{Q}(u) = T(u)\mathcal{Q}(u) \tag{F.20} $$

with $\tilde{B} \equiv (x^+)^2 e^{i\partial_u} + c.c.$ without any charge dependence in contradistinction with the original $\mathcal{B}$.

From this is easy to build a one loop orthogonal inner product for the twist 2 solutions.

[1] One simply use the Baxter equation (7.9) to solve for $\mathbb{Q}^{[+2]}$ in terms of $\mathbb{Q}$ and $\mathbb{Q}^{[-2]}$, plug the result in (F.20), use recurrence identities to cancel the Harmonic functions and note that that what is left is zero provided $\mathbb{Q}$ is an even function. This is the case for twist 2 Bethe states.

We look for a measure so that $\tilde{B}$ is self adjoint in the inner product

$$\langle \mathcal{Q}_i, \mathcal{Q}_j \rangle \equiv \int dx\, \mu_1(x) \mathcal{Q}_i \mathcal{Q}_j \tag{F.21}$$

on the space of dressed polynomials (7.1). Deforming the contours in $\langle \tilde{B} \circ \mathcal{Q}_1, \mathcal{Q}_2 \rangle$ as done in section 7.2 shows that it is enough to consider a periodic measure with fast enough decay at infinity provided all poles of the integrand – which now receive contributions from μ_1, $\mathcal{Q}$ and $\tilde{B}$ – have vanishing combined residue. See [94] for similar ideas applied to SL(N) spin chains. Writing an ansatz

$$\mu_1(x) = \frac{\pi/2}{\cosh^2(\pi x)} \left(a_1 + g^2 \left[a_2 \tanh^2(\pi u) + a_3\right]\right) \tag{F.22}$$

and requiring the cancelation of poles combined with the requirement that the vacuum ($\mathcal{Q}_0 = 1$) is normalized to one in (F.21) fix $a_1 = 1$, $a_2 = 3\pi^2$, $a_3 = -1$. This is (7.5).

F.2.3 Hexagons $\mathcal{A}$ at $\ell = 1$

For minimal left bridge length $\ell = 1$ the hexagon sum over partitions simplifies dramatically. We thank Frank Coronado for highlighting this and for help in establishing the asymptotic formulae (F.23) a few years ago.

The asymptotic result (F.8) for $\ell = 1$ simplifies to

$$(\mathcal{A}_{\ell=1}^{\texttt{asymptotic}})^2 = 1 + g^4 \sum_{k=3}^{S} \sum_{i_1<\cdots<i_k} \frac{i^k (4-k) B_{3-k}}{\prod_{l=1}^{k} \left(v_{i_l} + \frac{i}{2}\right)} + \, c.c.$$

plus $O(g^6)$. Here B_n are the Bernouli numbers.

Since the roots v_i that appear in the denominator product never appear repeated we can cast the sum as

$$1 + g^4 \frac{P(v_j)}{Q(-i/2)} + c.c. \tag{F.23}$$

where $P(v_k)$ is a polynomial *linear* in each of the Bethe roots v_j, just like the Baxter polynomial $Q(u) \equiv \prod(u - v_k) = \sum_n c_n u^n$ is. We can thus look for a linear integral operator acting on Q and producing such $P(v_j)$,

$$\langle Q(u) \rangle = \sum_{n=0}^{S} c_n(v_j) \langle u^n \rangle = P(v_j)\,. \tag{F.24}$$

(It is not granted that such operation exists for all S.) We imposed it spin by spin and observed that we can indeed satisfy (F.24) as long as we fix the linear map moments as

$$\langle 1 \rangle = \langle u \rangle = \langle u^2 \rangle = 0\,, \langle u^3 \rangle = \tfrac{i}{2}\,, \langle u^4 \rangle = 1\,, \langle v^5 \rangle = -\tfrac{7i}{6}\,, \ldots$$

We computed the first few dozens such moments from which we guessed that they can be generated from

$$\langle F\rangle \equiv \tfrac{\pi^2}{15}F(\tfrac{-i}{2}) + 3i\zeta_3 F'(\tfrac{-i}{2}) - \tfrac{\pi^4}{12}F''(\tfrac{-i}{2}) + \int du\, \nu(u) F(u)$$

where the measure

$$\nu(u) = \frac{i\pi - i(u+\frac{i}{2})\pi^2 \tanh(\pi u)}{2\left(u+\frac{i}{2}\right)^3 \cosh^2(\pi u)}\,. \tag{F.25}$$

This came as a surprise as this very same measure arose before in a very different context. Once we use that $Q(\frac{i}{2}) = Q(-\frac{i}{2})$ for physical states to combine both terms in (F.23) we see that (the real part of) this measure is nothing but the measure which arose when computing the first wrapping correction when the bottom bridge $\ell_B = 1$, see equations (44),(55) in [66]! We conclude that we can not only cast the two loop asymptotic contribution (F.23) as a simple SoV looking integral but we can also trivially incorporate the bottom wrapping effects:

$$\begin{aligned}\left(\mathcal{A}_{\ell=1}^{\texttt{asymptotic + bottom wrapping}}\right)^2 &= 1+ \\ &+ g^4\Big(\eta\tfrac{\pi^2}{12}Q_1^+ - \eta\tfrac{\pi^2}{6}Q_2^+ - 6(2-\eta)\zeta(3)Q_1^+ + \eta\tfrac{4\pi^4}{15} + \\ &+ 16\pi\eta\int \tfrac{1-12u^2+2\pi u(1+4u^2)\tanh(\pi u)}{(1+4u^2)^3\cosh^2(\pi u)}\tfrac{Q(u)}{Q(i/2)}\,du\Big) + \dots\end{aligned} \tag{F.26}$$

where $\eta = 1$ for $\ell_B > 1$ and $\eta = 2$ for $\ell_B = 1$[2].

Do we continue to have identical formulas with and without wrapping at higher loops? The NNNLO effective wrapping measure correction was nicely worked out in appendix B of [171] (in appendix E of [170] an equivalent representation – a sort of Fourier transform – was derived). Can the next loop order asymptotic result still be neatly combined with the wrapping correction?

At higher loops we will get more mirror corrections which we might be able to cast as SoV like integrals. We should probably expect a similar growth in the number of integrals for the asymptotic part of the result as well. Ultimately, at finite coupling, the distinction between the two should fade away as in the spectrum problem.

[2]For $\ell_B > 1$ the right hand side of (F.26) is a rational number; the π's and the $\zeta(3)$ in the second line are simply cancelling the π's and the $\zeta(3)$ generated by the integral. For $\ell_B = 1$ the π's still cancel but there is no $\zeta(3)$ in the second line. (In that sense the expression is even simpler in this case when wrapping is present!) A $\zeta(3)$ term is generated by the integral so that the rhs of (F.26) is of the form $\texttt{rational} + \texttt{rational}'\zeta(3)$ as it should.

F.3 SU(2) material

F.3.1 θ-morphism at NNLO

The morphism operator $\mathcal{M}$ performs a "Zhukowskization" of the rational propagation of magnons in the $XXX_{1/2}$ through the action on background inhomogeneities. From our perspective $\mathcal{M}$ is defined by equation (7.17). We write an ansatz and fix it by requiring the match of the RHS of (7.17) with $C^2_{\bullet\circ\circ}$ which can be computed from hexagons. It can be divided into a *closed* part and a *boundary* part,

$$\mathcal{M} = \mathcal{M}_{\rm c} \cdot \mathcal{M}_{\rm b} + O(g^6). \tag{F.27}$$

At NLO we recover the result in [183]; at NNLO we obtain

$$\mathcal{M}_{\rm c} = \exp\Big(\sum_{i=1}^{L}\Big(g^2(\partial_{i,i+1})^2 - \frac{1}{4}g^4(\partial_{i,i+1})^2(\partial_{i+1,i+2})^2\Big)\Big)\,,$$

and

$$\mathcal{M}_b = \exp\big(-ig^2Q_1^+(\partial_1-\partial_L) + g^4\delta\mathcal{M}_{\text{NNLO-b}}\big), \tag{F.28}$$

with

$$\begin{aligned}\mathcal{M}_{\text{NNLO-b}} &= \tfrac{1}{2}\left(2(Q_1^+)^2 - iQ_2^- - Q_1^-Q_1^+\right)\partial_1^2 + iQ_1^+\partial_1^3 + \\ &\tfrac{1}{2}\left(Q_1^-Q_1^+ - (Q_1^+)^2\right)\partial_2^2 - \tfrac{1}{2}iQ_1^+\partial_2^3 - \tfrac{i}{2}Q_1^+\partial_1\partial_2^2 + \\ &\tfrac{1}{2}(iQ_2^- - (Q_1^+)^2)\partial_1\partial_2 - (\partial_1 \leftrightarrow \partial_L, \partial_2 \leftrightarrow \partial_{L-1})\,.\end{aligned} \tag{F.29}$$

It would be interesting to re-derive $\mathcal{M}_c$ and $\mathcal{M}_b$ along the lines of [183].

The *closed* action satisfies the *morphism* property when acting on symmetric functions $f_{\rm sym}(\theta)$ of the inhomogeneities θ_j:

$$\mathcal{M}_{\rm c} \circ (f_{\rm sym}\, g) = (\mathcal{M}_{\rm c} \circ f_{\rm sym})\,(\mathcal{M}_{\rm c} \circ g) \tag{F.30}$$

for a generic function g. It also satisfies the "Zhukowskization" property

$$\mathcal{M}_{\rm c} \circ \prod_{i=1}^{L}(u-\theta_i \pm i/2)^k = \left(x^{\pm}\right)^{kL}. \tag{F.31}$$

The inhomogeneous Gaudin norm (7.16) is given in the SOV representation, see [89] for details, by

$$\mathcal{B}_\theta = f_{\rm sym}(\theta) \times \oint d\tilde{\mu}\mu_\theta \prod_{j=1}^{L-1}\mathcal{Q}(u_j)^2 \tag{F.32}$$

with the θ dependence entering only through the symmetric normalization function $f_{\rm sym}(\theta)$

and the measure

$$\mu_\theta = \prod_{i=1}^{L-1}\prod_{j=1}^{L}((u_i-\theta_j)^2+1/4)^{-1}. \tag{F.33}$$

Combining (F.30), (F.31) we get the NNLO Gaudin measure

$$d\mu_{L,L} = d\tilde{\mu} \times \left(\mathcal{M}_c \circ \mu_\theta = (x_j^+ x_j^-)^{-L}\right) \tag{F.34}$$

as in (7.21,7.22,7.23). The same measure is derived from a orthogonality principle in section (F.3.2). Comparison with the NNLO gaudin determinant fixes the conversion factor $\Lambda_{\mathcal{B}}$ to (F.15), so that in the end we are left with

$$|\Lambda_{\mathcal{B}}\mathcal{M} \circ \mathcal{B}_\theta| = \mathcal{B},$$

with $\mathcal{B}$ given in (F.14) [3]. Note that $\mathcal{M}_b$, (F.28), acts trivialy in $\mathcal{B}_\theta$ since it is a symmetric function of θ_i.

Having fixed the morphism operator through hexagons, the SOV result (7.19) then follows[4] from the action of the morphism operator (F.27) on the inhomogeneous $XXX_{1/2}$ spin chain SOV overlaps [89, 91, 93].

F.3.2 SU(2) orthogonality

The *Gaudin* measure defining $\langle \mathcal{Q}, \mathcal{Q}\rangle_{L,L}$ was derived in sections 7.3, F.3.1 from the θ-morphism action. Here we show it also defines an orthogonal scalar product for NNLO Baxter polynomials $\mathbb{Q}$, meaning

$$\langle \mathbb{Q}_1, \mathbb{Q}_2\rangle_{L,L} = \mathcal{N}_1\delta_{12} \tag{F.35}$$

if $\mathbb{Q}_1, \mathbb{Q}_2$ are solutions to the Baxter equation $\mathcal{B}\circ\mathbb{Q} = T(u)\mathbb{Q}(u)$ with

$$\mathcal{B} = (x^+)^L e^{-i\partial_u} + (x^-)^L e^{i\partial_u}\,. \tag{F.36}$$

What follows is a simple loop generalization of the XXX case [93]. Consider the pairing

$$\langle f, g\rangle_\mu \equiv \oint_\gamma du\, \mu(u) f(u) g(u) \tag{F.37}$$

with the γ countour being the boundary of the $[-3g, 3g]\times[-2i, 2i]$ square. Inserting $\mathcal{B}$,

$$\langle \left((x^+)^L e^{-i\partial_u} + (x^-)^L e^{i\partial_u}\right)\circ f, g\rangle_\mu, \tag{F.38}$$

[3] In writing (7.19), (F.14) we introduced the vacuum integrals $\langle \mathbf{1}, \mathbf{1}\rangle_{\ell,L}$ relative to the naive θ-morphism action in order to simplify the resulting measure and normalizations factors. We also massaged the expression into a manifestly real form.

[4] In writing (7.19), (F.14) we introduced the vacuum integrals $\langle \mathbf{1}, \mathbf{1}\rangle_{\ell,L}$ relative to the naive θ-morphism action in order to simplify the resulting measure and normalizations factors. We also massaged the expression into a manifestly real form.

and shifting contours down by i in the first term and up by i in the second term, as done below equation (7.11), we find that $\mathcal{B}$ is self-adjoint with respect to (F.37) provided

$$\mu^{[2]}/\mu = (x^{[-1]}/x^{[3]})^L, \tag{F.39}$$

so that $\mu = (x^+x^-)^{-L}\mu_{\rm p}$ with $\mu_{\rm p}$ an $i-$periodic factor.

Note that $T(u)$ is polynomial for physical zero-momentum states at NNLO

$$T(u) = 2u^L + \sum_{i=0}^{L-2} c_i(\mathbb{Q})u^i \tag{F.40}$$

with $c_i(\mathbb{Q})$ being the state-dependent integrals of motion. Consider the family of measures

$$\mu_j = \frac{\sinh(2\pi u)}{(x^+x^-)^L} \times \exp[2\pi u(2j-L)] \tag{F.41}$$

with $j = 1, \dots, L-1$. Let $\mathbb{Q}_1, \mathbb{Q}_2$ be solutions of the Baxter equation. We then have, from self-adjointness,

$$\sum_{i=0}^{L-2}(c_i(\mathbb{Q}_1) - c_i(\mathbb{Q}_2))\langle \mathbb{Q}_1, u^i\mathbb{Q}_2\rangle_{\mu_j} = 0 \tag{F.42}$$

since the LHS is simply $\langle \mathcal{B}\circ\mathbb{Q}_1, \mathbb{Q}_2\rangle_{\mu_j} - \langle \mathbb{Q}_1, \mathcal{B}\circ\mathbb{Q}_2\rangle_{\mu_j} = 0$. The integrals of motion c_i are generic and therefore the linear system (F.42) should be non degenerate, implying

$$\det\left[\langle \mathbb{Q}_1, u^{i-1}\mathbb{Q}_2\rangle_{\mu_j}\right] = \mathcal{N}_1\delta_{12}. \tag{F.43}$$

with $i, j = 1, \dots, L-1$. Our claim is that expanding the Vandermonde-like determinant (F.43)into a $L-1$ dimensional integral reproduces the main text result (7.21,7.22,7.23) for $\ell = L$ up to a combinatorial normalization factor,

$$\det\left[\langle \mathbb{Q}_1, u^{i-1}\mathbb{Q}_2\rangle_{\mu_j}\right] \propto \oint_\gamma d\mu_{L,L}\prod_{i=1}^{L-1}\mathcal{Q}_1(u_i)\mathcal{Q}_2(u_i).$$

We conclude that the *Gaudin* measure defines and orthogonal scalar product and, more over, the *Gaudin* norm takes determinant form in the SOV representation.

For $\mathcal{A}$ things are more involved as explained in the main text with the additional exponential dressings in (7.22,7.23) kicking in.

F.3.3 SU(2) structure constants at finite volume

At leading order mirror particles have infinite energy and vanishing phase space, and therefore can be ignored. Their contribution, which starts at NNLO, is however crucial. It is only when they are taken into account that selection rules are realized for instance. In this appendix, we review how the first mirror contributions are computed in the hexagon formalism, adapting the SL(2) computations of [69, 170, 171] to the SU(2) case. We then

discuss how these virtual effects are taken into account in the SOV approach by appropriately dressing the Q-functions.

Part I: mirror particles on the hexagon

When gluing hexagons together to reconstruct the closed string geometry one must insert a complete basis of states along the seams $(\ell_{12}, \ell_{31}, \ell_{23})$. This complete set of states is given by the Fock space of mirror particles labeled by their rapidities v and bound state index a. The contribution from terms with n_{ij} particles on edge ℓ_{ij} is

$$\mathcal{A}(n_{ij}) = \sum_{\{\mathbf{a}\}} \int d\mu(\mathbf{v}) e^{-\tilde{E}(\mathbf{v}_{ij})\ell_{ij}} \mathcal{H}^2(\mathbf{v}, \mathbf{a})$$

where $\{\mathbf{a}\} = \{a_k^{ij}\}$ is a collective index for the bound state label a_k^{ij} of particle k on edge (ij) and similar for the mirror rapidities v_k^{ij}. Above $\mu(v)$ and $\tilde{E}$ are respectively the phase space measure and the energy of the mirror particle and $\mathcal{H}^2(\mathbf{v}, \mathbf{a})$ are the glued hexagon form factors with mirror particles labeled by $(\mathbf{v}, \mathbf{a})$ inserted along the seams, the dependence on the external operators being left implicit. Below we provide explicit expressions for the case of interest, see [69, 170] for general expressions.

At weak coupling multiparticle mirror states are suppressed, both the energies and the measure being of $O(g^2)$. Mirror contributions are also suppressed for large geometries so that at NNLO only edges with bridge length $\ell_{ij} = 1$ can support mirror excitations. Moreover, at this order only one edge can be excited at a time: we may have an excitation in the adjacent or in the opposite edge to the non BPS operator.

Adjacent virtual corrections in the SU(2) sector provide an example of the selection rules restoration aforementioned. We now delve into this in detail to understand what is expected from the SOV formulas at NNLO. Structure constants in the SU(2) sector for states with R-charge M when an adjacent bridge length $\ell < M$ vanish. At the classical level ($g = 0$) this is simply the statement that we cannot contract J scalars through a bridge of length ℓ [66, 168, 183]. The asymptotic contribution $n_{ij} = 0$ correctly reproduce this selection rule at LO and NLO, but at NNLO a non-zero contribution is obtained when $\ell_{12} = 1$. The claim is that the mirror factor cancels this contribution and restore the symmetry[5]. This reads

$$\mathcal{A}_\ell^{\texttt{asymptotic}} = -\mathcal{A}(n_{12} = 1), \tag{F.44}$$

with

$$\begin{aligned}\mathcal{A}(n_{12} = 1) =& \mathbb{N}_{J,\ell} \int \frac{dv}{2\pi} \frac{ag^4}{(v^2 + a^2/4)^3} \vec{\tau}_{SU(2)}(v^\gamma, \mathcal{O}_1) \times \\ & \sum_{\alpha \cup \bar{\alpha}} (-1)^{|\bar{\alpha}|} \frac{e^{-ip_{\bar{\alpha}}} h_a(v^\gamma, \alpha)}{h^{SU(2)}_{\bar{\alpha},\alpha} h_a(\bar{\alpha}, v^\gamma)}.\end{aligned} \tag{F.45}$$

where h_a are the fused hexagon dynamical factors, v^γ denotes analytic continuation to mirror kinematics across the $x_v^{[+a]}$ cuts, $h^{SU(2)}_{\bar{\alpha},\alpha}$ are the SU(2) dynamical factors (F.10) and

[5]Note that primary SU(2) operators have $M \geq 2$ and therefore all structure constants for $\ell_{12} = 1$ vanish.

$\vec{\tau}_{SU(2)}(v^\gamma, \mathcal{O}_1)$ is the forward SU(2) transfer-matrix eigenvalue for the Bethe state describing operator $\mathcal{O}_1$. We sum over partitions of the bethe state $\mathbf{u} = \alpha \cup \bar{\alpha}$, and use the short hand notation $h_a(\bar{\alpha}, v^\gamma) = \prod_{u_i \in \bar{\alpha}} h_a(u_i, v^\gamma)$ and similar for $h_a(v^\gamma, \alpha)$. To leading order the objects in (F.45) read

$$h_a(v^\gamma, u_j) = \frac{u_j + i/2}{u_j + i/2 - v + ai/2}$$

$$h_a(u_j, v^\gamma) = \frac{-g_j^2}{u_j + i/2} \frac{(v-u_j)^2 + (a-1)^2/4}{(v-u_j) + i(a+1)/2}$$

and $\vec{\tau}_{SU(2)}(v^\gamma, \mathcal{O}_1)$ is given by

$$(a+1)\prod_{j=1}^{J} f_j^- + a\prod_{j=1}^{J} f_j^+ + a\prod_{j=1}^{J} g_j f_j^- + (a-1)\prod_{j=1}^{J} g_j f_j^+$$

where $g_j = (u_j - v - \frac{i}{2}(a+1))(u_j + \frac{i}{2})/((u_j - v - \frac{i}{2}(a-1))(u_j - \frac{i}{2}))$ and $f_j^\pm = (u_j - v + \frac{i}{2}(a \pm 1))/(u_j - \frac{i}{2}a)$. Equation (F.44) holds off-shell. The LHS is a rational function of the rapidities u_k. The RHS integral can be evaluated by residues. Poles at $v = u_k \pm \frac{i}{2}(a-1)$ cancel after summing over the bound-state index while those at $v = \pm\frac{i}{2}a$ sum to a rational function matching the LHS.

Performing an R-symmetry transformation permuting the polarizations of operators $\mathcal{O}_2 \leftrightarrow \mathcal{O}_3$ should leave the structure constant invariant. In the integrability description this amounts to the replacement $\ell \leftrightarrow L - \ell$. The structure constant must therefore also vanish when $\ell = L - 1$. The story in this case is more interesting. First, the LO and NLO asymptotic contributions only vanish on-shell, since after all the expression (F.8) only knows that the right bridge $\ell_{31} = 1$ through the Bethe roots which solve Bethe equations on a chain of size $L = \ell_{12} + \ell_{31}$. At the NNLO the rational result is non-zero on-shell. The mirror contribution $\mathcal{A}(n_{31} = 1)$ is now given by an expression identical to (F.45) with the last line replaced by

$$\sum_{\alpha \cup \bar{\alpha}} (-1)^{|\bar{\alpha}|} \frac{e^{-ip_{\bar{\alpha}}} h_a(v^\gamma, \bar{\alpha})}{h^{SU(2)}_{\bar{\alpha},\alpha} h_a(\alpha, v^\gamma)}. \tag{F.46}$$

After summing over the bound state index in the wrapping corrections we now obtain a complicated expression full of ζ and Polygamma functions whose coefficients vanish on-shell so that in the end the we are left with simple algebraic numbers that cancel the asymptotic result, reproducing the selection rule.

Part II: dressing the Q-functions

Wrapping effects at NNLO are due to virtual particles propagating over bridges of size one. Since nontrivial SU(2) operators have R-charge $M \geq 2$, NNLO wrapping effects are only present when restoring the selection rules discussed in Part I of F.3.3. There are two cases to consider in the SOV proposal: $\ell_{12} \equiv \ell = 1$ and $\ell_{31} = 1$ i.e. $\ell = L - 1$. The selection rules are realized trivially for $\ell = 1$ simple due to the binomials in (7.20). This

holds off-shell, as in the hexagon method. We henceforth focus on the nontrivial case. In other words, we seek to restore the important $\ell \leftrightarrow L-\ell$ symmetry for any possible lengths.

The NNLO SOV expression for structure constants in the SU(2) sector (7.19) was derived from the morphism action, (7.17). Note that $\mathcal{A}_\theta$ depends only on θ_i with $i \leq \ell$. One might therefore naively think that the method is unaware of ℓ_{31} being short or long and therefore cannot distinguish when mirror corrections are relevant. The solution is provided by the *right boundary* terms, i.e. terms with explicit ∂_L and ∂_{L-1} dependence in the second line of (7.18)[6]. These can be ignored whenever $\ell < L-1$. Equation (7.17) then reproduces the asymptotic structure constants. However, when $\ell = L-1$ the right boundary acts non-trivially. Its action generates the extra terms proportional to $\delta_{\ell,L-1}$ in (7.25). Once these terms are properly taken into account, the selection rules are correctly reproduced when (7.19) is evaluated on-shell. Note that this corresponds to an infinite number of constrains on the on-shell action of the right boundary terms, and therefore the match is quite non-trivial.

[6]The action of ∂_L boundary terms is irrelevant for the non-extremal correlators considered here.

Appendix G

Appendix: Complex Spin: The Missing Zeroes and Newton's Dark Magic

G.1 Structure Constants From Integrability

Local operators in $\mathcal{N}=4$ SYM are described by $\mathcal{Q}$-functions. For SL(2) operators such as (8.2) the $\mathcal{Q}$-functions reduce, at leading order, to the Baxter polynomials $Q(x)=\prod_{j=1}^{S}(x-u_j)$. Structure constants between such operators and BPS scalars are given by simple overlaps between the polynomials Q,

$$\frac{C(S)^2}{C_{\rm BPS}^2}=\frac{(S!)^2}{(2S)!}\frac{\langle Q,\mathbf{1}\rangle_\ell^2}{\langle Q,Q\rangle_L} \tag{G.1}$$

where $C_{\rm BPS}^2$ is the (protected) structure constant between the 2 fixed BPS scalars and the BPS operator given by (8.2) with $S=0$.

The case we are interested is $L=3$, $\ell=1$, corresponding to the twist 3 operators (8.2). For $\ell=1$ the numerator overlap trivializes, $\langle Q,\mathbf{1}\rangle_\ell^2=1$, while the *norm* $\langle Q,Q\rangle_L$ is non-trivial. It is given in terms of the roots $\{u_1,\ldots,u_S\}$ through a determinant [174]

$$\langle Q,Q\rangle_L=\frac{\det\left(\partial_{u_i}\phi_j\right)Q(i/2)Q(-i/2)}{(2S)!\prod_{i\neq j}^{S}\frac{u_i-u_j}{u_i-u_j-i}}, \tag{G.2}$$

with $e^{i\phi_j}=(\frac{u_j+i/2}{u_j-i/2})^L\prod_{k\neq j}\frac{u_j-u_k+i}{u_j-u_k-i}$, or through the Separation of Variables integrals [6, 88, 91, 94]

$$\langle Q,Q\rangle_L=\binom{2S+L-1}{L-1}\int_{\mathbb{R}^{L-1}}\mu_L\prod_{i=1}^{L-1}Q(x_i)^2, \tag{G.3}$$

with factorized measure

$$d\mu_L=\prod_{i=1}^{L-1}dx_i\,\mu_1(x_i)\prod_{i=1}^{L-2}\prod_{j=i+1}^{L-1}\mu_2(x_i,x_j)$$

where

$$\mu_1(u)=\frac{\pi}{2\cosh(\pi u)^2},\quad \mu_2(u,v)=\frac{\pi(u-v)\sinh(\pi(u-v))}{\cosh(\pi u)\cosh(\pi v)}.$$

Once the roots are determined through (8.3), either (G.2) or (G.3) can be used to generate the figure 8.1 data.

G.2 Twist 3 Lowest Family

At leading order the Baxter functions are polynomials. These polynomials are known analytically in the cases of the twist 2 and lowest twist 3 trajectories. They are given [177, 208] by

$$\mathcal{Q}_2(u,S) = {}_3F_2\left(1+S,-S,1/2+iu;1,1|1\right), \tag{G.4}$$

$$\mathcal{Q}_3^{\texttt{lowest}}(u,S) = {}_4F_3\left(-\tfrac{S}{2},1+\tfrac{S}{2},\tfrac{1}{2}+iu,\tfrac{1}{2}-iu;1,1,1|1\right). \tag{G.5}$$

In this section we use this result to determine the structure constants for these trajectories in closed form. Note that naively these Q-functions are not appropriate to describe the trajectory at non-(even-)integer values of spin. For example, $\mathcal{Q}_3^{\text{lowest}}(u,S)$ has a symmetry $S\to -2-S$ which is not a symmetry of the anomalous dimension $\gamma_3^{\text{lowest}}=8H(S/2)$. This will be reflected in the analytic structure constant obtained.

We are therefore interested in the structure constants described in (G.1) in the case $L=3$ and $\ell=1$. For $\ell=1$ the numerator in (G.1) trivializes since there are no integrals to be performed. Only the denominator is non-trivial. The SOV integrals (G.3) simplify in the tree-level approximation and acquire determinant form. In the case of interest we have

$$\langle \mathcal{Q}_3^{\texttt{lowest}},\mathcal{Q}_3^{\texttt{lowest}}\rangle_3 = \binom{2S+2}{2}\det\left[\int d\mu_{i,j}(u)\mathcal{Q}_3^{\texttt{lowest}}\right]$$

with

$$d\mu_{i,j}(u) = u^i\pi\cosh(\pi u)^{-2}\tanh(\pi u)^j,\qquad i,j=0,1.$$

Moreover, since the lowest trajectory $\mathcal{Q}_3^{\text{lowest}}$ is an even polynomial at even spins, the off-diagonal integrals vanish. We therefore have

$$\det\left[\int d\mu_{i,j}(u)\mathcal{Q}_3^{\texttt{lowest}}\right] = \left(\mathcal{I}_1\equiv\int du\frac{\pi}{2}\frac{(\mathcal{Q}_3^{\texttt{lowest}})^2}{\cosh(\pi u)^2}\right)\left(\mathcal{I}_2\equiv\int du\frac{\pi^2 u\tanh(\pi u)(\mathcal{Q}_3^{\texttt{lowest}})^2}{\cosh(\pi u)^2}\right).$$

The integral $\mathcal{I}_2$ is simple. One can check that it evaluates to $\mathcal{I}_2=(S+1)^{-1}$. This is shown in appendix G.2.1. We are thus left with the evaluation of $\mathcal{I}_1$. We do so through two observations. First, note that $\mathcal{I}_1$ measure is an orthogonal measure for the twist 2 Q-functions (see [6, 88, 94]):

$$\int du\frac{\pi}{2}\frac{\mathcal{Q}_2(u,S)\mathcal{Q}_2(u,S')}{\cosh(\pi u)^2} = \delta_{S,S'}(-1)^S(2S+1)^{-1}.$$

We also derive this integral in appendix G.2.1. Second, note that, for even spin S, the

Q-functions (G.4, G.5) are even polynomials of degree S. One can therefore decompose the twist 3 polynomials (G.5) in a basis of twist 2 polynomials (G.4). The result is

$$\mathcal{Q}_3^{\texttt{lowest}}(u,S) = \sum_{j=0}^{S/2} \mathcal{Q}_2(u,2j)\times$$
$$\left(\frac{i^{2j+S}(1+4j)\Gamma\left(\frac{1}{2}+j\right)^2\Gamma\left((1+\frac{S}{2}+j)\right)/\Gamma\left(1+j\right)^2}{2\Gamma\left(\frac{1}{2}-\frac{S}{2}+j\right)\Gamma\left(1+\frac{S}{2}-j\right)\Gamma\left(\frac{3}{2}+\frac{S}{2}+j\right)}\right)$$

We can therefore combine these two observations to write

$$\mathcal{I}_1 = \sum_{j=0}^{S/2}\left(\frac{\sqrt{1+4j}\Gamma\left(\frac{1}{2}+j\right)^2\Gamma\left(1+\frac{S}{2}+j\right)/\Gamma\left(1+j\right)^2}{2\Gamma\left(\frac{1}{2}-\frac{S}{2}+j\right)\Gamma\left(1+\frac{S}{2}-j\right)\Gamma\left(\frac{3}{2}+\frac{S}{2}+j\right)}\right)^2, \tag{G.6}$$

The sum (G.6) can be extended to infinity. Combining with (G.3) leads to the final result (8.6) which holds for any even integer S.

G.2.1 Hypergeometric integrals, orthogonality and recursions

In this subsection we compute the integrals

$$\mathcal{I}_A(S) = \int du \frac{\pi}{2}\frac{\mathcal{Q}_2(S)^2}{\cosh(\pi u)^2}, \tag{G.7}$$

$$\mathcal{I}_B(S) = \int du \frac{\pi^2 u\tanh(\pi u)\mathcal{Q}_3^{\text{lowest}}(S)^2}{\cosh(\pi u)^2}. \tag{G.8}$$

Key are the recursion relations satisfied by the Hahn polynomials (G.4,G.5),

$$(S+2)^2\mathcal{Q}_2^{[2]} + 2i(3+2S)u\mathcal{Q}_2^{[1]} = (S+1)^2\mathcal{Q}_2^{[0]}, \tag{G.9}$$

$$(S+2)^3\mathcal{Q}_3^{[2]} + S^3\mathcal{Q}_3^{[-2]} = 2(1+S)(2+2S+S^2-8u^2)\mathcal{Q}_3^{[0]}. \tag{G.10}$$

with $\mathcal{Q}_2^{[a]} \equiv \mathcal{Q}_2(S+a)$ and $\mathcal{Q}_3^{[a]} \equiv \mathcal{Q}_3^{\texttt{lowest}}(S+a)$. As follows from the SOV methods of [6], the kernels of (G.7, G.8) define orthogonal scalar products for the trajectories under consideration:

$$\int du \frac{\pi}{2}\frac{\mathcal{Q}_2(S)\mathcal{Q}_2(S')}{\cosh(\pi u)^2} \propto \delta_{SS'}, \tag{G.11}$$

$$\int du \frac{\pi^2 u\tanh(\pi u)\mathcal{Q}_3^{\texttt{lowest}}(S)\mathcal{Q}_3^{\texttt{lowest}}(S')}{\cosh(\pi u)^2} \propto \delta_{SS'}. \tag{G.12}$$

To compute $\mathcal{I}_A(S)$, integrate equation (G.9) against $\mathcal{Q}_2(S)\frac{\pi}{2}\cosh(\pi u)^{-2}$. Using the

decomposition

$$u\mathcal{Q}_2(S) = i\frac{(1+S)^2}{2+4S}\mathcal{Q}_2(S+1) + \sum_{k=0}^{S} c_k \mathcal{Q}_2(k),$$

which follows from matching asymptotics, and the orthogonality relation (G.11), we obtain the recursion

$$\frac{3+2S}{1+2S}\mathcal{I}_A(S+1) + \mathcal{I}_A(S) = 0$$

whose solution is

$$\mathcal{I}_A(S) = \frac{(-1)^S}{2S+1}\,. \tag{G.13}$$

Similarly, to compute $\mathcal{I}_B(S)$, integrate (G.10) against $\pi^2 u \tanh(\pi u)\mathcal{Q}_3^{\texttt{lowest}}(S-2)\cosh(\pi u)^{-2}$. Using the decomposition

$$u^2\mathcal{Q}_3^{\texttt{lowest}}(S-2) = \tfrac{16(1-S)}{S^3}\mathcal{Q}_3^{\texttt{lowest}}(S) + \sum_{k=0}^{\frac{S}{2}-1} c_{2k}\mathcal{Q}_3^{\texttt{lowest}}(2k)$$

and the orthogonality relation (G.12) we obtain

$$\frac{1+S}{1-S}\mathcal{I}_B(S) + \mathcal{I}_B(S-2) = 0$$

from which follows

$$\mathcal{I}_B(S) = \frac{1}{S+1}\,. \tag{G.14}$$

The derivation in this section is a bit of an overkill given the simplicity of the final results. It would be much simpler to evaluate the integrals (G.7) and (G.8) for the first few physical spins S and immediately recognize (G.13) and (G.14). (This was of course how we first found them.)

G.3 Baxter at Complex Spin

Analysis of the asymptotics of (8.9) determine that the leading power-law behaviour of Q can be either u^S or u^{-2-S}. In [215] Janik proposed, in the case of twist 2 operators, that it is the second class of solutions which control the correct analytic continuation in spin of the physical data. Note: as one approach integer spin, Q must approach point-wise the polynomial solutions with u^S asymptotics describing the local operators while decaying (in the RHP) as u^{-2-S} when $u \to +\infty$! Once the decaying Q is known, the energy can be extracted from

$$\gamma = 2i \oint \frac{du}{2\pi i}\frac{1}{u^2}\log\left(\frac{Q(u+i/2)}{Q(u-i/2)}\right), \tag{G.15}$$

which generalize (8.4) to the non-polynomial case.

Baxter equation, being a finite difference equation, admits a gauge redundancy $Q(u) \to$

$Q(u)p(u)$ for any i-periodic p. The energy is invariant under this transformation[1]. This gauge invariance is crucial for the method proposed here. Solutions with leading power-law asymptotics have poles at $u = \frac{i}{2} + ik$, $k \in \mathbb{Z}$. These poles can be removed through multiplication by $\sinh(2\pi u)$ factors so that we are left with an entire solution normalizable at $i/2$. This does not fix the gauge freedom completely as we can still multiply Q by, say, $\cosh(\pi u)^2$ factors. These would increase the exponential rate of Q as $u \to \infty$. We therefore look for the slowest growing entire solutions to (8.9). In section 8.4 we propose a numerical algorithm that determines this solution and computes the correct continuation of the energies.

G.4 Twist 2, Newton Series and Integrability

The analytically solvable twist 2 trajectory

$$\mathrm{Tr}\left(ZD_+^S Z\right) + \texttt{permutations} \tag{G.16}$$

serves as the perfect toy model to test the ideas presented in chapter 8. Its anomalous dimension $\gamma_2(S) = 8H(S)$ and structure constant (with two BPS operators) $C(S)^2_{\texttt{twist-2}LO} = \frac{2(S!)^2}{(2S)!}$ can be extracted from the four point correlator and are given by [180, 214].

Alternatively, it can be computed from integrability through the twist 2 Baxter equation

$$\begin{aligned}(u+i/2)^2 Q(u+i) + (u-i/2)^2 Q(u-i) \\ = (2u^2 - S(S+1) - 1/2) Q(u),\end{aligned}$$

whose solution at integer spin is given by Hahn polynomials $\mathcal{Q}_2(u, S)$, equation (G.4).

Newton series can be used to reproduce γ_2 and $C(S)^2_{\texttt{twist-2}LO}$ everywhere in the complex plane provided one subtracts singularities. In the case of the structure constant it is important to subtract the exponential behaviour through multiplication by $e^{(2\log(2)S)}$ before applying the interpolation method.

One can also extract the energies directly at complex spin, as proposed by Janik in [215], through the slow-growing solution described in section 8.4. In this case the slow-growing Q-function can be written analytically as

$$\begin{aligned}\mathcal{Q}_{\texttt{slow}} = \frac{i\sinh(2\pi u)}{2\sin(\pi S)} \Bigg(\left(1 - i\tan(\pi\tfrac{S}{2})\coth(\pi u)\right) \mathcal{Q}_2(u, S) - \\ \left(1 + i\tan(\pi\tfrac{S}{2})\coth(\pi u)\right) \mathcal{Q}_2(-u, S) \Bigg)\end{aligned} \tag{G.17}$$

[1]The asymptotics condition can also be expressed in an invariant form as the requirement that $\log\left(Q(u+i)/Q(u-i)\right) \sim i(M+2)/u$ as $u \to \infty$.

from which one reads the energy

$$\gamma = 2i\left(\frac{\mathcal{Q}'_{\texttt{slow}}(\frac{i}{2})}{\mathcal{Q}_{\texttt{slow}}(\frac{i}{2})} - \frac{\mathcal{Q}'_{\texttt{slow}}(-\frac{i}{2})}{\mathcal{Q}_{\texttt{slow}}(-\frac{i}{2})}\right) = 8H(S). \tag{G.18}$$

As mentioned in section 8.5 there are currently no available integrability methods to extract structure constants directly at complex spin. On the other hand, in the case of twist 2 the light-ray operators that physically realize the complex spin data $\{\gamma_2, C(S)^2_{\texttt{twist-2}LO}\}$ can be constructed explicitly [52], providing a direct method to extract the data. This is reviewed in section G.5.

G.5 Twist 2 and Light-ray operators

In this appendix we review how the matrix elements of the explicit leading order twist 2 light-ray operators constructed in [52] encode the complex spin structure constants.

The leading order twist 2 local (even S) primary operators are given by

$$\mathcal{O}_S(x) = \frac{1}{\sqrt{2(2S)!}}\sum_i \psi_i \,\mathrm{Tr}\left(D_+^i Z D_+^{S-i} Z\right)(x),$$

where $\psi_i = (-1)^i\binom{S}{i}^2$ is completely fixed by the primary condition $[K_-, O_S(0)] = 0$. The operators are unit-normalized so that

$$\langle \bar{\mathcal{O}}_S(x)\mathcal{O}_S(0)\rangle = \frac{(x^-)^{2S}}{(x^2)^\Delta}.$$

The three point function between $\mathcal{O}_S$ and $\frac{1}{2}$-BPS operators [2] $O^{(2)}$ and $O^{(3)}$ is then given by

$$\langle O^{(2)}(x_2)\mathcal{O}_S(x_1)O^{(3)}(x_3)\rangle = \frac{\sqrt{2}(S!)}{\sqrt{(2S)!}}\frac{\left(x_{13}^- x_{12}^2 - x_{12}^- x_{13}^2\right)^S}{x_{12}^{2+2S}x_{13}^{2+2S}x_{23}^2}, \tag{G.19}$$

from which one reads $C(S)^2 = \frac{2(S!)^2}{(2S)!}$. We assumed the insertions were space-like separated.

The operators $\mathcal{O}_S$ only make sense at integer spin. Our goal is to construct operators in continuous spin representations whose matrix-elements at integer S reproduce the local operator data $C(S)$. These are necessarily non-local [52, 259]. With that purpose in mind, consider the light-transform of operator $\mathcal{O}_S$

$$L[\mathcal{O}_S] = \int_{-\infty}^{\infty} d\alpha\, \mathcal{O}_S(\alpha n^+). \tag{G.20}$$

In [52] it was shown that these operators transform as primaries with dimension $\Delta_L = 1 - S$

[2] Explicitly, consider $O^{(2)} = \mathrm{Tr}(\bar{Z}\bar{X})$ and $O^{(3)} = \mathrm{Tr}(\bar{Z}X)$.

and spin $S_L = 1 - \Delta$ inserted at past-null infinity (at $(0, -\infty, 0)$ in light-cone coordinates $(x_-, x_+, \vec{x})$).

Indeed, fixing the insertions as in figure G.1 and acting with the transform on (G.19) while being careful with implicit $i\epsilon$s we obtain[3]

$$\langle \Omega | O^{(2)} L[\mathcal{O}_S] O^{(3)} | \Omega \rangle = \frac{C(S) f(S)}{x_2^- x_3^- x_{23}^2} \left(\frac{x_3^2}{x_3^-} - \frac{x_2^2}{x_2^-} \right)^{-1-S}, \tag{G.21}$$

with $f(S) = 2\pi i \Gamma(2S+1)/\Gamma(S+1)^2$. This is precisely the structure of a correlator of two BPS scalars and a primary with quantum numbers (Δ_L, S_L).

So far, all we did was to perform an integral transform. However, we are rewarded once we realize (G.20) belong to a continuous family of *light-ray* operators

$$\mathbb{O}(S) = \frac{i}{4\pi} \frac{\sqrt{2}\sqrt{\Gamma(2S+1)}}{\Gamma(S+1)} \times \tag{G.22}$$
$$\int_{-\infty}^{\infty} d\alpha d\beta \left(\frac{1}{(\alpha - \beta + i\epsilon)^{S+1}} + (\alpha \leftrightarrow \beta) \right) \mathrm{Tr}\left(Z(\alpha) Z(\beta) \right).$$

which transform as primaries with quantum numbers (Δ_L, S_L) for *arbitrary* values of S [52]! Indeed, at even S we have

$$\left(\frac{1}{(\alpha - \beta + i\epsilon)^{S+1}} + (\alpha \leftrightarrow \beta) \right) = -\frac{2\pi i}{\Gamma(S+1)} \delta^{(S)}(\alpha - \beta),$$

so that in this case

$$\mathbb{O}(S) = \frac{\sqrt{\Gamma(2S+1)}}{\sqrt{2}\Gamma(S+1)^2} \int d\alpha \, \mathrm{Tr}\left(Z \mathcal{D}_+^S Z \right)(\alpha) = L[\mathcal{O}_S].$$

where we used integration by parts to act with all derivatives inside $\mathcal{O}_S$ on the second field. Hence, at the even integers the partons must move together along the light-ray and we recover the (correctly normalized) light-transform of the local operator.

For non-integer S, $\mathbb{O}$ provides a physical realization of the structures $C(S)$. To see that, compute through Wick contractions the matrix element

$$\langle \Omega | O^{(2)} \mathbb{O}_S O^{(3)} | \Omega \rangle = \frac{i}{4\pi} \frac{\sqrt{2}\sqrt{\Gamma(2S+1)}}{\Gamma(S+1)} \int \frac{d\alpha d\beta}{(\alpha - \beta + i\epsilon)^{S+1}}$$
$$\times \frac{2}{\alpha x_2^- + x_2^2 - i\epsilon} \frac{1}{\beta x_3^- + x_3^2 - i\epsilon} \frac{1}{x_{23}^2} + (\beta \leftrightarrow \alpha). \tag{G.23}$$

The $i\epsilon$s are crucial and follow from the operator ordering. Since $x_2^- > 0$ and $x_3^- < 0$, see figure G.1, only the first term contributes since otherwise the contours can be deformed to infinity and the integral vanishes. For the first term, the integral in pinched by the

[3] As usual, when inserting the operator at past null infinity we rescale the correlator by a factor $(x_1^+)^{\Delta_L + S_L}$ before taking the $x_1^+ \to \infty$ limit.

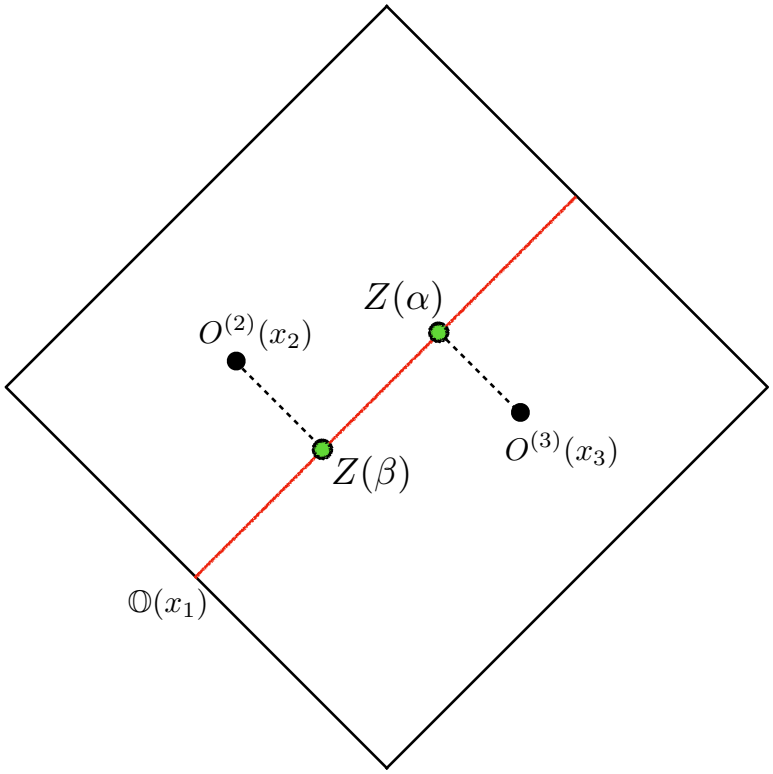

Figure G.1: We insert the operators at $x_1^- = 0$, $x_2^- > 0$ and $x_3^- < 0$. When computing the matrix element $\langle\Omega|O^{(2)}\mathbb{O}_S O^{(3)}|\Omega\rangle$ the green partons are integrated along the light-ray, equation (G.23). The integral is evaluated by picking residues that localize the partons on the null-cone of the BPS insertions.

singularities. Picking the residues from the propagators, see figure G.1, we obtain

$$\langle\Omega|O^{(2)}\mathbb{O}_S O^{(3)}|\Omega\rangle = \frac{f(S)C(S)}{x_2^- x_3^- x_{23}^2}\left(\frac{x_3^2}{x_3^-} - \frac{x_2^2}{x_2^-}\right)^{-S-1},$$

which match (G.21) exactly.

The anomalous dimension can be read off similarly. The one-loop dilatation action on the Wilson line insertions is given by [178, 256, 257]

$$\mathcal{D} \circ \mathrm{Tr}\,(Z(\alpha)Z(\beta)) = 4g^2 \int_0^1 \frac{d\tau}{\tau}\Big(\mathrm{Tr}\,(Z(\alpha)Z(\beta)) - \mathrm{Tr}\,(Z(\alpha(1-\tau)+\beta\tau)Z(\beta)) + (\alpha \leftrightarrow \beta)\Big). \tag{G.24}$$

Acting with $\mathcal{D}$ on (G.22) and changing variables to transpose the convolution from the

fields to the wavefunction, we readily obtain

$$\mathcal{D}\circ\mathbb{O}(S)=\left(8g^2\underbrace{\int_0^1\frac{d\tau}{\tau}\left(1-(1-\tau)^S\right)}_{H(S)}\right)\mathbb{O}(S).$$

Thus, we are able to reconstruct the complex spin data $\{\gamma(S), C(S)\}$ from the explicit wavefunctions of the light-ray operators. In the twist 2 case the computation is sort of trivial: $C(S)$, for example, is essentially encoded in the normalization of the operator so that when computing the matrix elements all the integrals do is reproduce the correct tensor structures. This is not a surprise as both the twist 2 local operators and light-rays have their wavefunctions completely fixed by conformal symmetry.

It is an important open problem to generalize this construction to higher-twist operators. There we do not expect such trivialities to occur, and the structure of the wavefunction should contribute non-trivially to the complex spin structure constants. Besides giving direct access to the complex spin data, such construction should clarify a number of puzzles regarding the higher-twist trajectories. See further discussion in section 8.5.